Section 2 Contents

2. Design Data for Waste Forms

The purpose of this chapter is to collect the data which are presently available from several sources on all the types of radioactive wastes which must be disposed of in accordance with 10 CFR 60.113.

The data are presented so that they are as much as possible directly usable as design criteria and design constraints for the containment and EBR design tasks.

The information as presented has been taken directly from the references so as to prevent introduction of errors. If further information on a given subject is necessary, it may be found in the appropriate reference.

By arranging the data in this manner, we have made it easier to update the document as new data become available.

2.1 Spent-Fuel Waste Form

The spent fuel referred to in this section consists of irradiated fuel discharged from a light-water moderated nuclear reactor (LWR). All such spent fuels are assumed to be permanently discharged and eligible for repository disposal.

2.1.1 Radionuclide Content

Knowledge of radionuclide content of the spent fuel is important to all aspects of the design of nuclear waste repositories as well as in the performance appraisal of the finished system design.

The radionuclide content is determined by the initial fuel composition, the fuel's irradiation history measured by the burnup, and the time the spent fuel has been stored out of the reactor core whether in wet or in dry storage.

The heat generated in the spent fuel, usually given as the linear heat generation rate, is a direct function of the radionuclide content. From the linear heat generation rate for the spent fuel assemblies we can calculate the total heat generation in a disposal container. Fuel assemblies or fuel elements can thus be selected for individual containers to give a desired heat distribution within the repository.

The radionuclide content also determines the radiation spectrum and the intensity which emanates from an assembly. This determines the radiation field which exists around any given container at any given time. From this we can determine the amount of shielding necessary during handling, transportation and interment.

There is a relationship between radionuclide content and fission gas release, in the sense that the amount of gas released is a function of both the burnup and of the centerline temperatures which existed in the fuel during its life in the reactor.

Fission gas release into the space between the cladding and the fuel is of importance to the designers because it may influence the failure rate of the cladding in the repository. A knowledge of the release makes possible the calculation of pressure which, combined with the temperature of the elements in the repository must be analyzed together with the properties of the materials as they are at a given time in the repository.

The fragment size distribution and grain size distributions in spent fuel as a function of burnup and other significant parameters influence fission gas release, and potentially, dissolution behavior. A more detailed knowledge of these parameters is needed.

The fission product inventory is also used to model the radionuclide transport which may take place through various modes out of the container and through the EBS in the event that the cladding and container should both fail.

Because the radionuclide inventory in the spent fuel decreases as a function of time, prediction of release rates becomes a very complicated function of a large number of variables.

2.1.1.1 Present Inventory

Table 2.1.1.1-1   Historical quantities of spent fuel by assembly class (reproduced from the LWR Quantities Database) (Table 3.1 of K.J. Notz, T.D. Welch, R.S. Moore, and W.J. Reisch, *Preliminary Waste Form Characteristics,* ORNL-TM-11681 [draft], Sept. 1990)

LWR QUANTITIES DATABASE
Historical Data
Discharged Assemblies by Assembly Class

ASSEMBLY CLASS	FUEL ASSEMBLIES	FUEL RODS	DEFECTIVE ASSEMBLIES	AVERAGE BURNUP (MWd/MT)	TOTAL WEIGHT (MT)	AVERAGE INITIAL ENRICH.
B&W 15 X 15	3,564	740K	67	28,004	1654.8	2.815
CE 14 X 14	3,329	551K	6	29591	1271.5	2.865
CE 16 X 16	1,231	238K	23	24884	512.5	2.554
CE 16 X 16 SYSTEM 80	188	41K	0	17699	78.8	2.137
GE BWR/2,3	14,809	827K	1478	21493	2762.1	2.384
GE BWR/4-6	20,470	1,194K	949	21233	3795.0	2.307
WE 14 X 14	2,949	520K	80	32309	1146.1	3.150
WE 15 X 15	5,557	1,133K	132	30127	2507.2	2.926
WE 17 X 17	5,873	1,552K	100	27835	2670.1	2.833
Big Rock Point	315	29K	52	19339	41.6	3.490
Dresden-1	891	32K	159	16227	90.8	2.166
Ft. Calhoun	426	73K	0	30549	154.0	2.912
Haddam Neck	734	150K	43	31320	303.2	3.819
Humboldt Bay	390	15K	1	14936	28.9	2.351
Indian Point	160	28K	0	16715	30.6	4.111
Lacrosse	333	33K	104	14708	38.0	3.727
Palisades	597	126K	21	22720	239.3	2.640
St. Lucie-2	236	84K	0	23626	88.9	2.347
San Onofre-1	468	53K	7	29029	171.4	3.792
Yankee Rowe	417	102K	0	28285	100.6	3.949
— GRAND TOTALS	62,749	7,521K	3222	25950	17606.6	2.718

Table 2.1.1.1-2   Quantities of domestic LWR spent fuel (Table 2.2 from K.J. Notz, T.D. Welch, R.S. Moore, and W.J. Reisch, *Preliminary Waste Form Characteristics,* ORNL-TM-11681 [draft], Sept. 1990)

BWR Assembly Class	Historical Quantities as of Dec. 31, 1988 (MTIHM)
GE BWR/4,5,6	3795
GE BWR/2,3	2762
Dresden 1	91
Humboldt Bay	29
Big Rock Point	42
Lacrosse	38
Elk River (reprocessed)	5

PWR Assembly Class	Historical Quantities as of Dec. 31, 1988 (MTIHM)
WE 15x15	2507
WE 17x17	2670
BW 15x15	1655
CE 14x14	1272
WE 14x14	1146
CE 16x16	512
CE 16x16 System 80	79
South Texas	0
Haddam Neck	303
Palisades	239
San Onofre 1	171
Fort Calhoun	154
Yankee Rowe	101
Saint Lucie 2	89
Indian Point 1	31
BW 17x17	0

---

[a]   R. S. Moore, D. A. Williamson, and K. J. Notz, A Classification Scheme for LWR Fuel Assemblies, ORNL/TM-10901, Oak Ridge National Laboratory, November 1988.
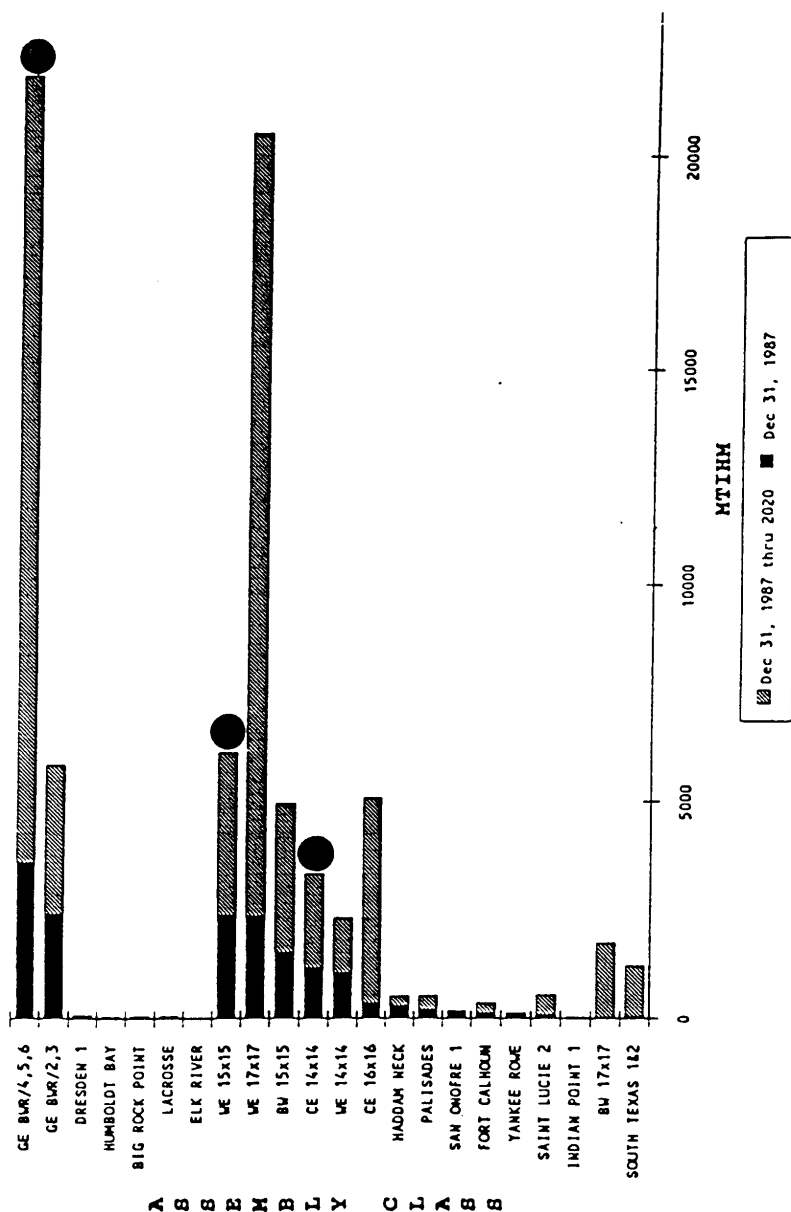
Figure 2.1.1.1-1 **Quantities of domestic LWR spent fuel (Figure 1 from K.J. Notz, T.D. Welch, R.S. Moore, and W.J. Reisch,** *Preliminary Waste Form Characteristics,* **ORNL-TM-11681 [draft], Sept. 1990)**
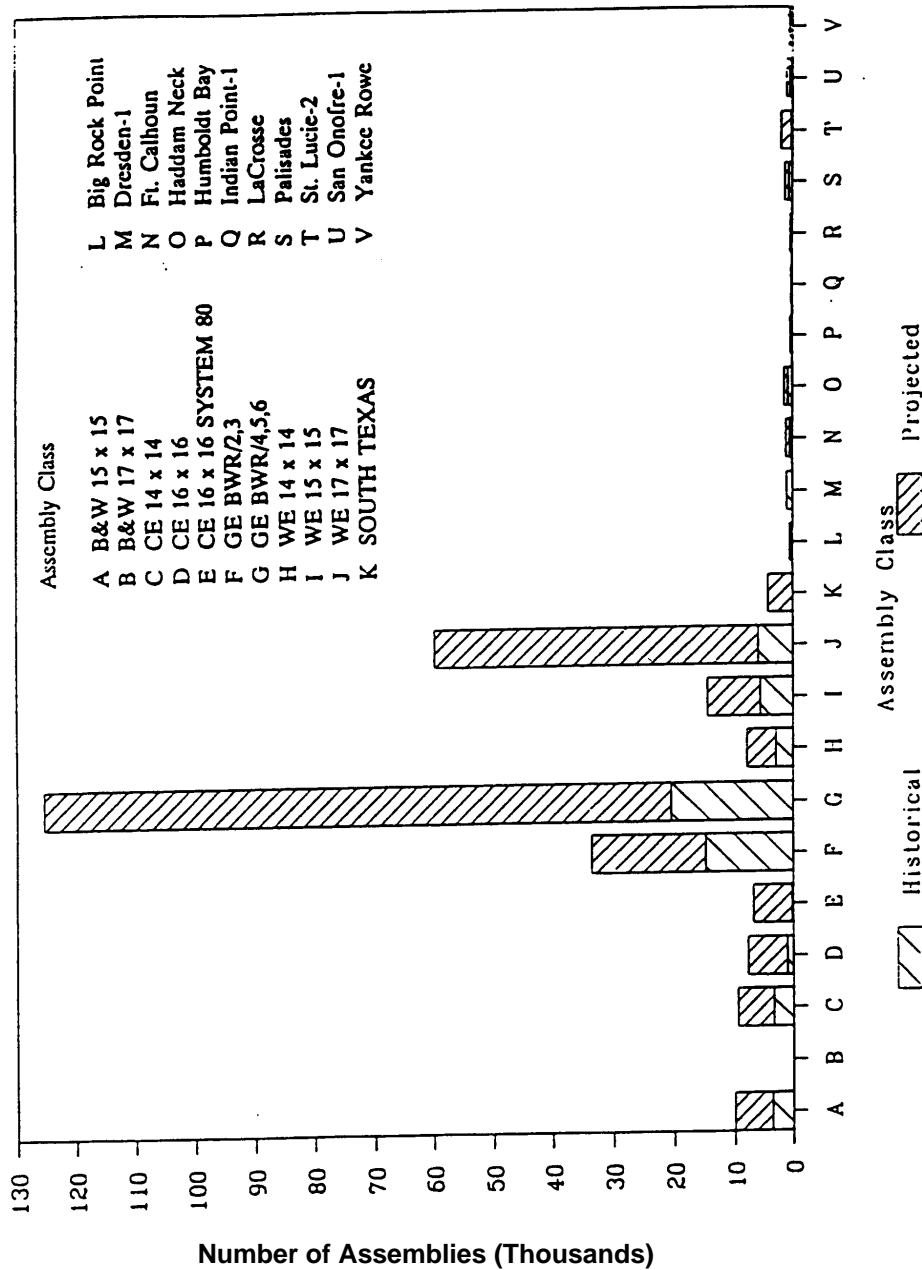
**Figure 2.1.1.1-2   Assembly by assembly class (1988 EIA data) (Figure 3.1
from K.J. Notz, T.D. Welch, R.S. Moore, and W.J. Reisch,
Preliminary Waste Form Characteristics, ORNL-TM-11681
[draft], Sept. 1990)**
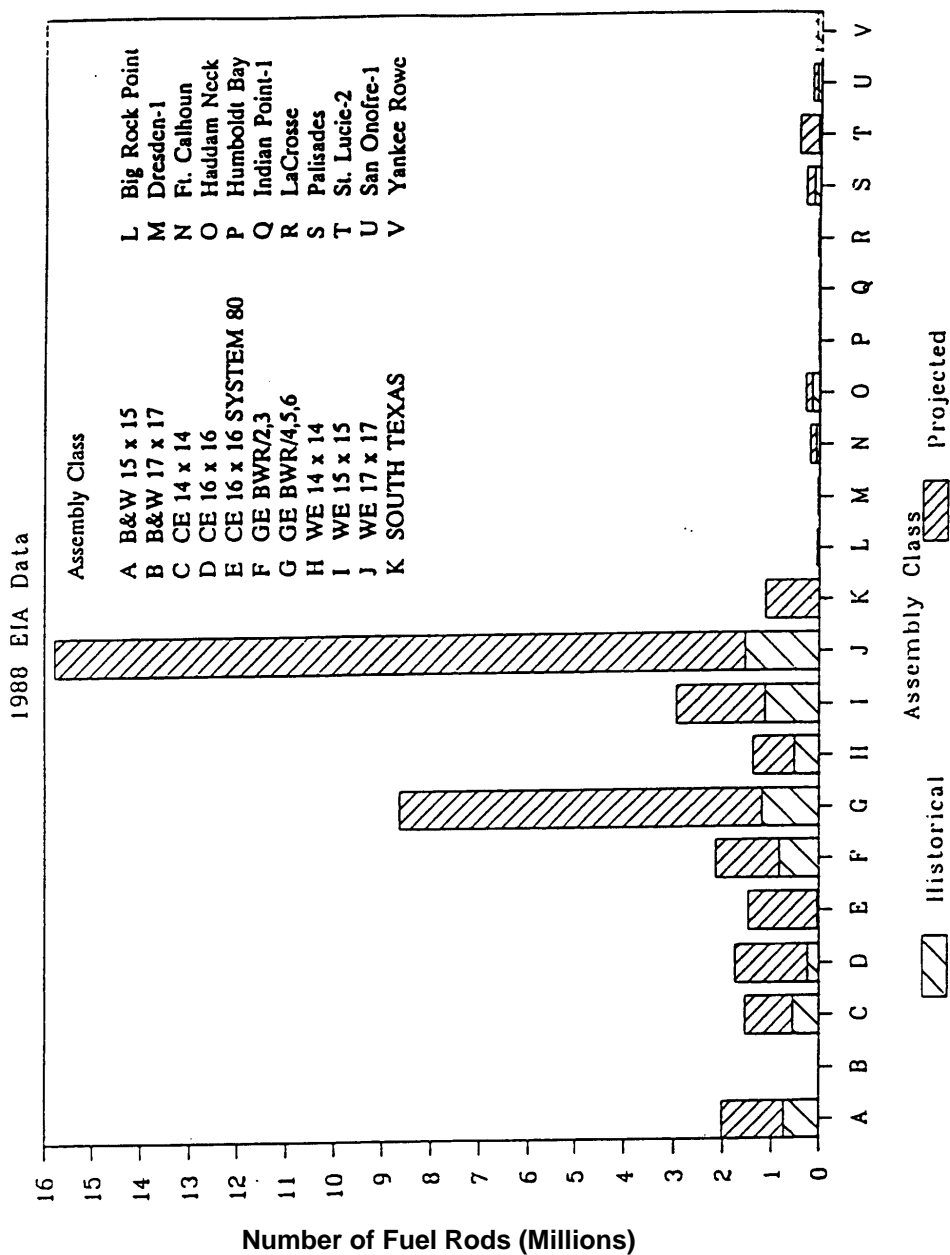
Figure 2.1.1.1-3   Fuel rods by assembly class (1988 EIA data) (Figure 3.2 from K.J. Notz, T.D. Welch, R.S. Moore, and W.J. Reisch, *Preliminary Waste Form Characteristics*, ORNL-TM-11681 [draft], Sept. 1990)

Table 2.1.1.1-3   Spent-fuel distribution by discharge year, based on 1988 EIA data
(Table 3.4 from K.J. Notz, T.D. Welch, R.S. Moore, and W.J. Reisch,
Preliminary Waste Form Characteristics, ORNL-TM-11681 [draft], Sept.
1990)

| Discharge Year	BWR Assemblies	BWR Metric Tons	PWR Assemblies	PWR Metric Tons
		HISTORICAL		
1968	5	0.6	0	0.0
1969	96	9.7	0	0.0
1970	29	5.6	99	39.0
1971	408	64.0	64	26.5
1972	771	141.5	331	117.9
1973	577	95.2	165	67.1
1974	1314	244.6	574	207.3
1975	1170	215.0	797	321.8
1976	1584	298.6	920	396.6
1977	2045	382.7	1087	457.7
1978	2239	383.2	1661	696.7
1979	2131	399.9	1658	719.4
1980	3330	619.8	1469	624.0
1981	2467	458.7	1610	686.3
1982	1951	357.2	1519	652.8
1983	2698	491.3	1763	764.5
1984	2623	462.2	1953	848.2
1985	2674	485.2	2045	867.1
1986	2583	464.0	2365	1030.2
1987	3506	632.2	2715	1162.1
1988	3008	545.2	2746	1165.4

Table 2.1.1.1-4 Historical spent-fuel distribution by discharge burnup, based on 1988 EIA data (Table 3.5 from K.J. Notz, T.D. Welch, R.S. Moore, and W.J. Reisch, *Preliminary Waste Form Characteristics,* ORNL-TM-11681 [draft], Sept. 1990)

Burnup (GWd/MTIHM)	BWR Assemblies	BWR Metric Tons	PWR Assemblies	PWR Metric Tons
0	30	5.6	0	0.0
1	46	8.5	0	0.0
2	178	34.3	0	0.0
3	432	79.7	1	0.4
4	899	164.0	7	2.6
5	70	5.9	40	7.2
6	189	35.5	9	4.1
7	334	62.4	0	0.0
8	182	30.7	29	12.1
9	680	124.2	109	43.6
10	1348	254.9	5	2.3
11	426	77.8	133	54.9
12	760	136.7	191	75.8
13	493	81.8	234	86.6
14	804	144.8	305	129.8
15	421	73.6	315	137.6
16	1090	196.7	512	220.8
17	1569	276.6	958	430.2
18	857	133.0	429	183.0
19	1970	366.4	568	246.0
20	1372	248.5	342	151.9
21	1413	258.4	378	168.5
22	1726	309.1	232	96.6
23	2390	444.8	345	139.7
24	2637	488.5	526	237.6
25	3215	592.4	922	377.1
26	2131	389.5	1013	446.9
27	1832	334.2	1367	573.3
28	3181	576.2	1088	460.6
29	1569	284.5	1308	550.5
30	2340	424.2	1395	588.4
31	475	85.8	1957	840.9
32	89	16.3	1460	626.0
33	31	5.6	1993	859.6
34	10	1.7	1956	840.6
35	4	0.7	1200	502.6

Table 2.1.1.1-4 (continued)

HISTORICAL DATA

Burnup (GWd/MTIHM)	BWR Assemblies	Metric Tons	PWR Assemblies	Metric Tons
36	0	0.0	1229	515.9
37	4	0.7	969	417.8
38	2	0.4	698	289.0
39	3	0.6	612	249.8
40	0	0.0	245	100.7
41	2	0.4	148	56.5
42	1	0.2	124	47.1
43	4	0.7	142	55.9
44	0	0.0	4	1.6
45	0	0.0	18	8.1
46	0	0.0	4	1.7
47	0	0.0	0	0.0
48	0	0.0	6	2.5
49	0	0.0	0	0.0
50	0	0.0	0	0.0
51	0	0.0	2	0.8
52	0	0.0	2	0.8
53	0	0.0	2	0.8
54	0	0.0	0	0.0
55	0	0.0	4	1.8
56	0	0.0	4	1.5
57	0	0.0	1	0.4

Figure 2.1.1.1-4   BWR discharges by year (1988 EIA data) (Figure 3.3 from K.J. Notz, T.D. Welch, R.S. Moore, and W.J. Reisch, *Preliminary Waste Form Characteristics,* ORNL-TM-11681 [draft], Sept. 1990)
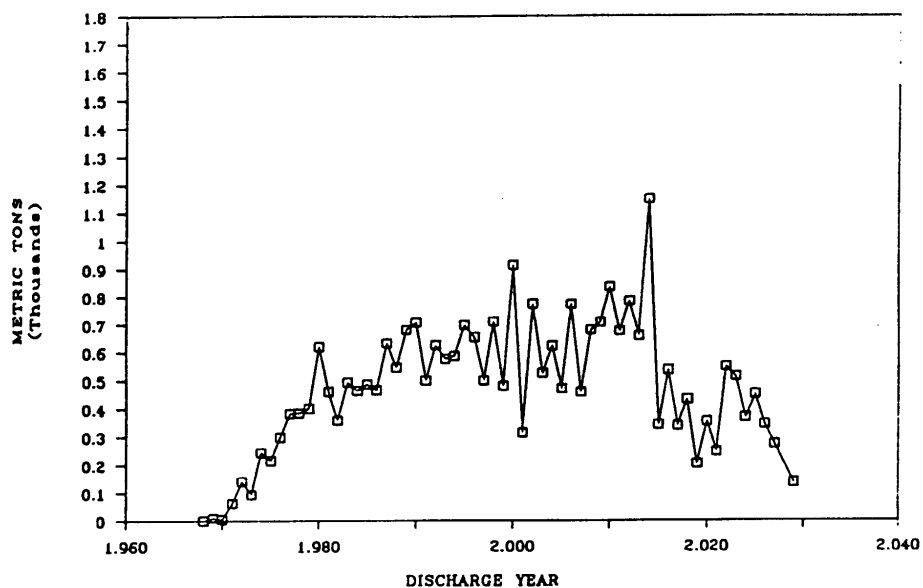

Figure 2.1.1.1-5   PWR discharges by year (1988 EIA data) (Table 3.4 from K.J. Notz, T.D. Welch, R.S. Moore, and W.J. Reisch, *Preliminary Waste Form Characteristics,* ORNL-TM-11681 [draft], Sept. 1990)

Figure 2.1.1.1-6 BWR discharges by burnup (historical) (Figure 3.5 from K.J. Notz, T.D. Welch, R.S. Moore, and W.J. Reisch, Preliminary Waste Form Characteristics, ORNL-TM-11681 [draft], Sept. 1990)
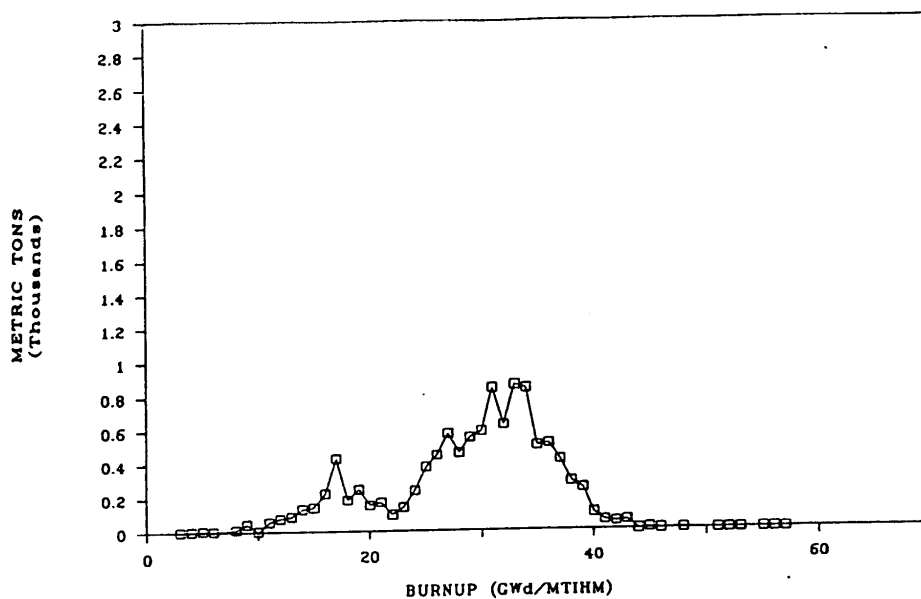
Figure 2.1.1.1-7 PWR discharges by burnup (historical) (Figure 3.7 from K.J. Notz, T.D. Welch, R.S. Moore, and W.J. Reisch, Preliminary Waste Form Characteristics, ORNL-TM-11681 [draft], Sept. 1990)

Table 2.1.1.1-5   Summary of the quantities of LWR spent fuel (Table 4.1
from K.J. Notz, T.D. Welch, R.S. Moore, and W.J. Reisch,
Preliminary Waste Form Characteristics, ORNL-TM-11681
[draft], Sept. 1990)

		Historical or Projected					
		Through 1988			Projected		
		Reactor Type			Reactor Type		
		BWR	PWR	Summary	BWR	PWR	Summary
No. of Assemblies	Total	37124	25540	62664	123822	101952	225774
Mass, Mtihm	Total	6741	10850	17590	22100	44217	66317

Table 2.1.1.1-6   Summary of the quantities of
LWR spent fuel (Table 4.2 from
K.J. Notz, T.D. Welch, R.S. Moore,
and W.J. Reisch, Preliminary
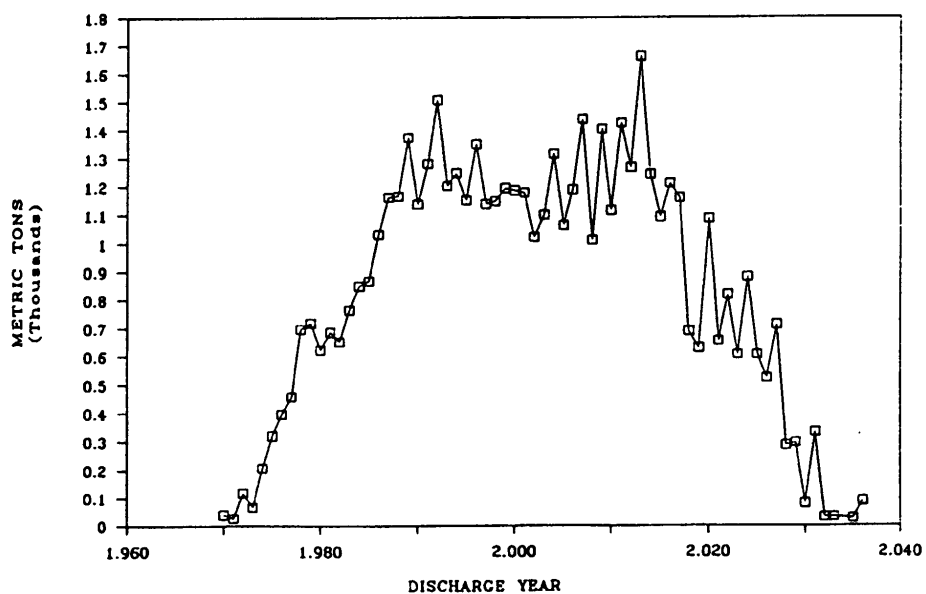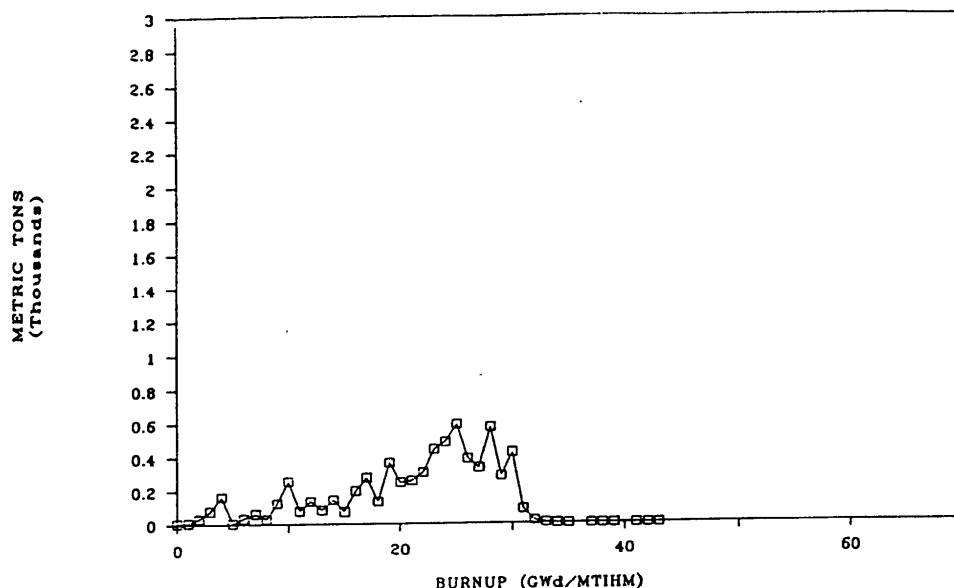Waste Form Characteristics,
ORNL-TM-11681 [draft], Sept. 1990)

		Summary		
		Reactor Type		
		BWR	PWR	Summary
No. of Assemblies	Total	160946	127492	288438
Mass, Mtihm	Total	28841	55067	83908

Table 2.1.1.1-7   Summary LWR spent-fuel burnup, enrichment, and age
(Table 4.3 from K.J. Notz, T.D. Welch, R.S. Moore, and
W.J. Reisch, Preliminary Waste Form Characteristics,
ORNL-TM-11681 [draft], Sept. 1990)

| | | Historical or Projected | | | | | |
		Through 1988			Projected		
		Reactor Type			Reactor Type		
		BWR	PWR	Summary	BWR	PWR	Summary
Burnup, MWd/Mt	Minimum	0	3000	0	3000	5000	3000
	MEAN	21213	28908	25959	32904	41987	38960
	Maximum	43000	57000	57000	47000	67000	67000
	Standard Deviation	19979	20181	22679	30273	28528	32518
Enrichment	Minimum	0.0	0.7	0.0	0.7	1.3	0.7
	MEAN	2.3	2.9	2.7	3.2	3.9	3.7
	Maximum	3.9	4.9	4.9	3.9	5.2	5.2
	Standard Deviation	1.4	1.5	1.7	1.5	1.5	1.9
Discharge Date	Minimum	1968	1970	1968	1989	1989	1989
	MEAN	1981	1982	1982	2007	2007	2007
	Maximum	1988	1988	1988	2029	2036	2036

Table 2.1.1.1-8   Summary of LWR spent-fuel burnup, enrichment, and age (Table 4.4 from K.J. Notz, T.D. Welch, R.S. Moore, and W.J. Reisch, Preliminary Waste Form Characteristics, ORNL-TM-11681 [draft], Sept. 1990)

| | | Summary | | |
| | | Reactor Type | | Summary |
		BWR	PWR	
Burnup, MWd/Mt	Minimum	0	3000	0
	MEAN	30172	39410	36234
	Maximum	47000	67000	67000
	Standard Deviation	32110	31340	34685
Enrichment	Minimum	0.0	0.7	0.0
	MEAN	3.0	3.7	3.5
	Maximum	3.9	5.2	5.2
	Standard Deviation	1.9	2.0	2.3
Discharge Date	Minimum	1968	1970	1968
	MEAN	2001	2002	2002
	Maximum	2029	2036	2036

Table 2.1.1.1-9   Total quantitites (historical and projected) of spent fuel by assembly class (reproduced from the LWR quantities database) (Table 3.3 from K.J. Notz, T.D. Welch, R.S. Moore, and W.J. Reisch, Preliminary Waste Form Characteristics, ORNL-TM-11681 [draft], Sept. 1990)

LWR QUANTITIES DATABASE
Totals - Historical and Projected Data
Discharged Assemblies by Assembly Class

ASSEMBLY CLASS	FUEL ASSEMBLIES	FUEL RODS	AVERAGE BURNUP (MWd/MT)	TOTAL WEIGHT (MT)	AVERAGE INITIAL ENRICH.
B&W 15 X 15	9,892	2,031K	36230	4586.4	3.446
CE 14 X 14	9,391	1,545K	39547	3554.5	3.726
CE 16 X 16	7,898	1,758K	41118	3234.1	3.926
CE 16 X 16 SYSTEM 80	6,715	1,477K	43186	2795.7	3.951
GE BWR/2,3	33,403	2,147K	27220	5998.2	2.838
GE BWR/4-6	125,409	8,645K	31091	22621.3	3.039
WE 14 X 14	7,818	1,392K	37910	2899.3	3.538
WE 15 X 15	14,451	2,947K	36967	6559.3	3.482
WE 17 X 17	59,759	15,778K	40767	26472.7	3.807
South Texas	4,258	1,124K	34904	2303.7	3.264
Big Rock Point	604	63K	20611	79.3	3.464
Dresden-1	891	32K	16227	90.8	2.166
Ft. Calhoun	1,094	191K	37237	391.6	3.549
Haddam Neck	1,407	287K	33892	548.7	3.833
Humboldt Bay	390	15K	14936	28.9	2.351
Indian Point	160	28K	16715	30.6	4.111
Lacrosse	333	33K	14708	38.0	3.727
Palisades	1,285	275K	32638	513.6	3.368
St. Lucie-2	1,911	459K	44725	741.1	4.260
San Onofre-1	964	142K	30434	354.4	3.988
Yankee Rowe	678	162K	29684	160.9	3.950
— GRAND TOTALS	288,523	40,531K	36234	83924.2	3.477

Figure 2.1.1.1-8   Enrichment as a function of burnup for BWRs (Figure 4.5 from K.J. Notz, T.D. Welch, R.S. Moore, and W.J. Reisch, Preliminary Waste Form Characteristics, ORNL-TM-11681 [draft], Sept. 1990)
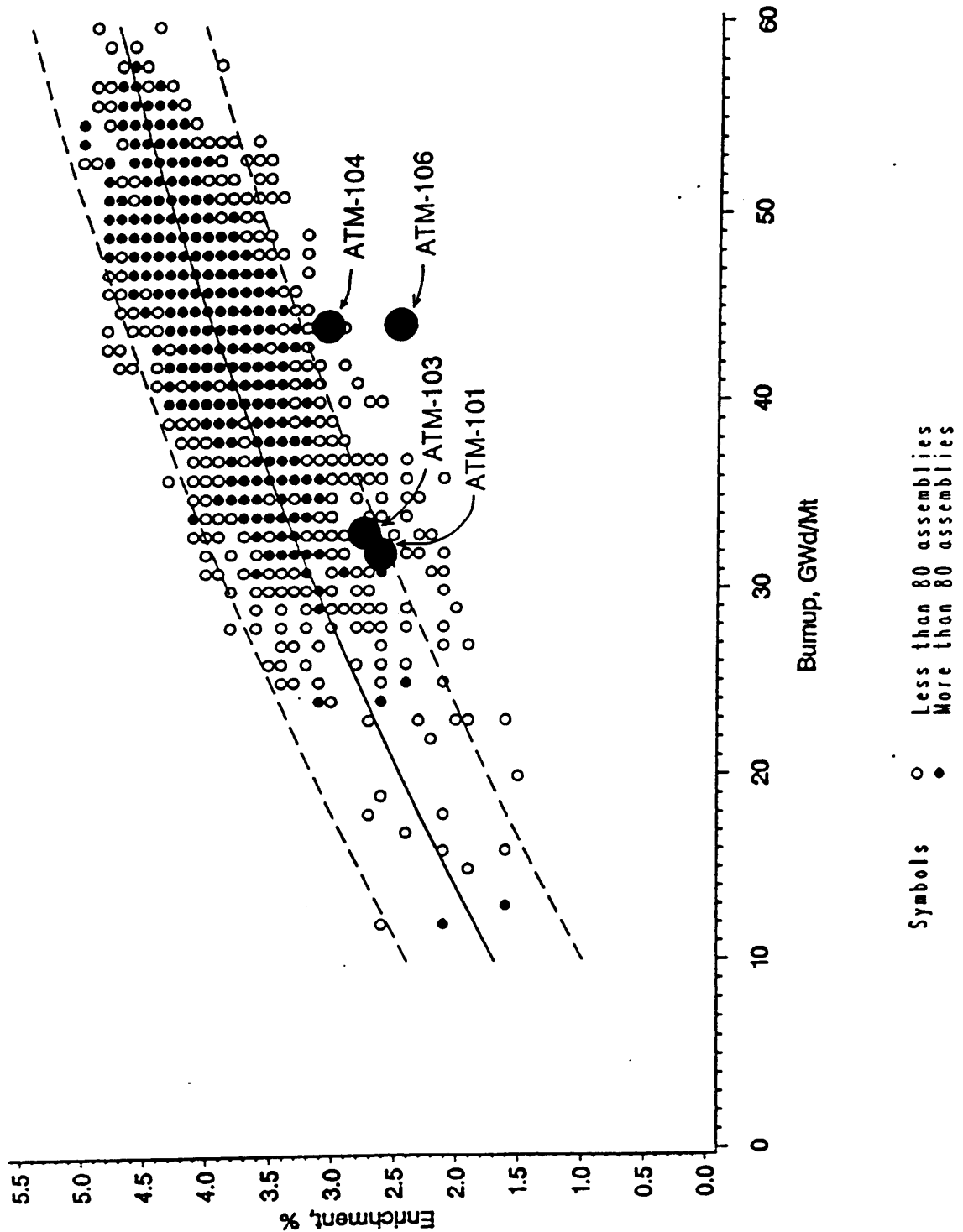
Figure 2.1.1.1-9   Enrichment as a function of burnup for PWRs (Figure 4.6 from
                   K.J. Notz, T.D. Welch, R.S. Moore, and W.J. Reisch, Preliminary
                   Waste Form Characteristics, ORNL-TM-11681 [draft], Sept. 1990)

Figure 2.1.1.1-10 Cumulative increase in all PWR spent-fuel assemblies with time (Figure 4 from R.E. Woodley, *The Characteristics of Spent LWR Fuel Relevant to its Storage in Geologic Repositories*. HEDL-TME 83-28, Oct. 1983)
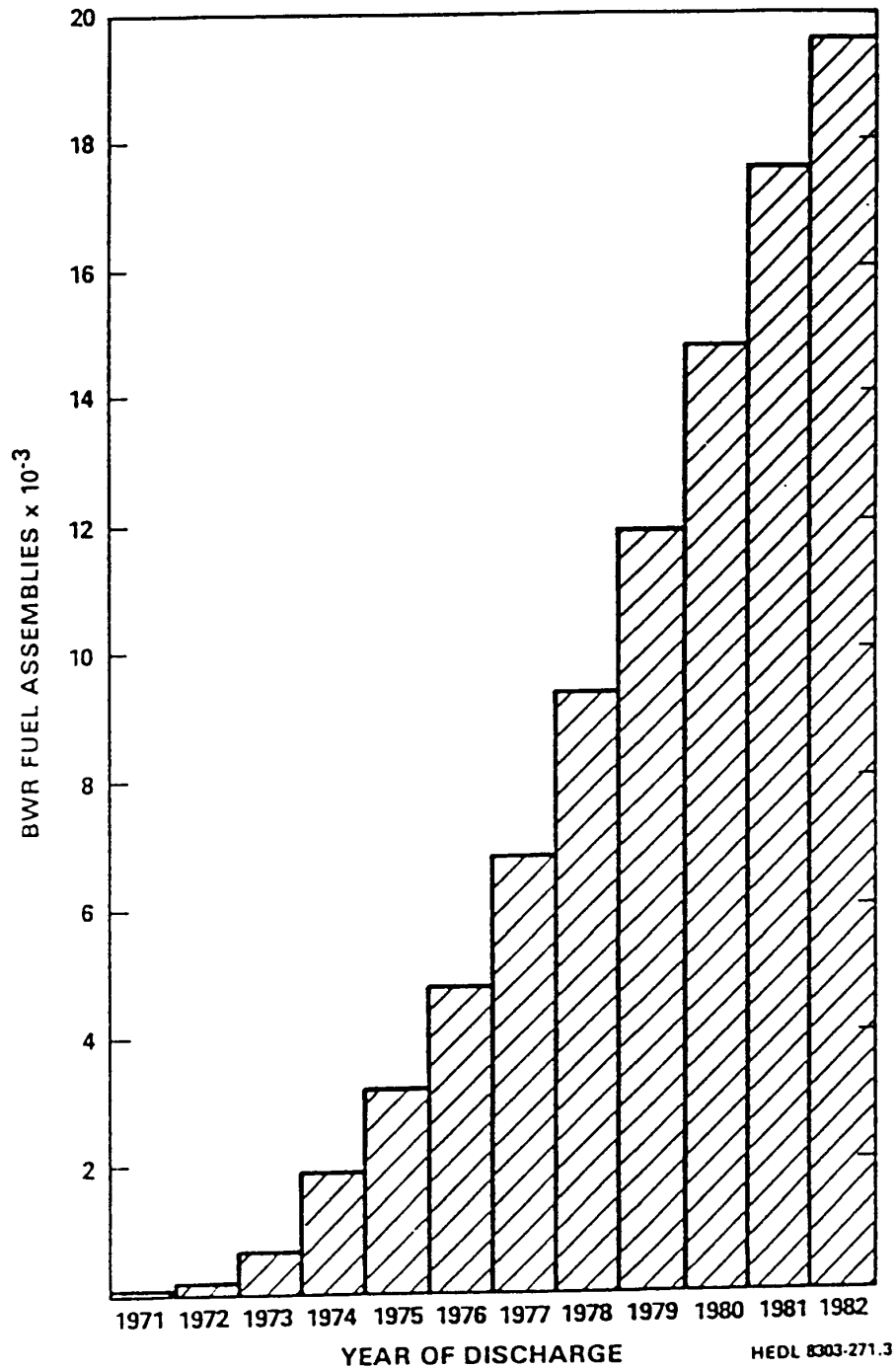
Figure 2.1.1.1-11 Cumulative increase in all BWR spent-fuel assemblies with time (Figure 5 from R.E. Woodley, *The Characteristics of Spent LWR Fuel Relevant to its Storage in Geologic Repositories.* HEDL-TME 83-28, Oct. 1983)
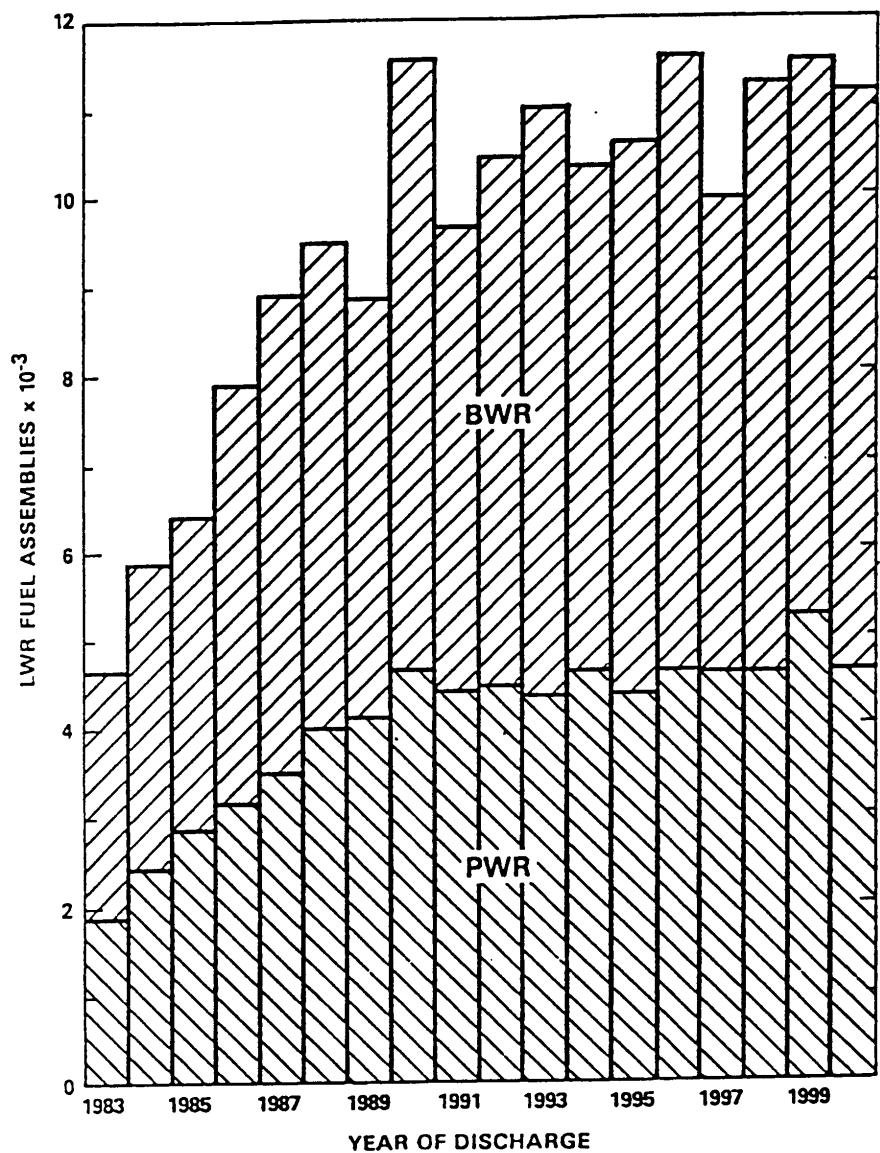
HEDL 8303-271.10

Figure 2.1.1.1-12 Projected annual discharges of spent LWR fuel assemblies (Figure 6 from R.E. Woodley, *The Characteristics of Spent LWR Fuel Relevant to its Storage in Geologic Repositories.* HEDL-TME 83-28, Oct. 1983)

HEDL 8303-271.11
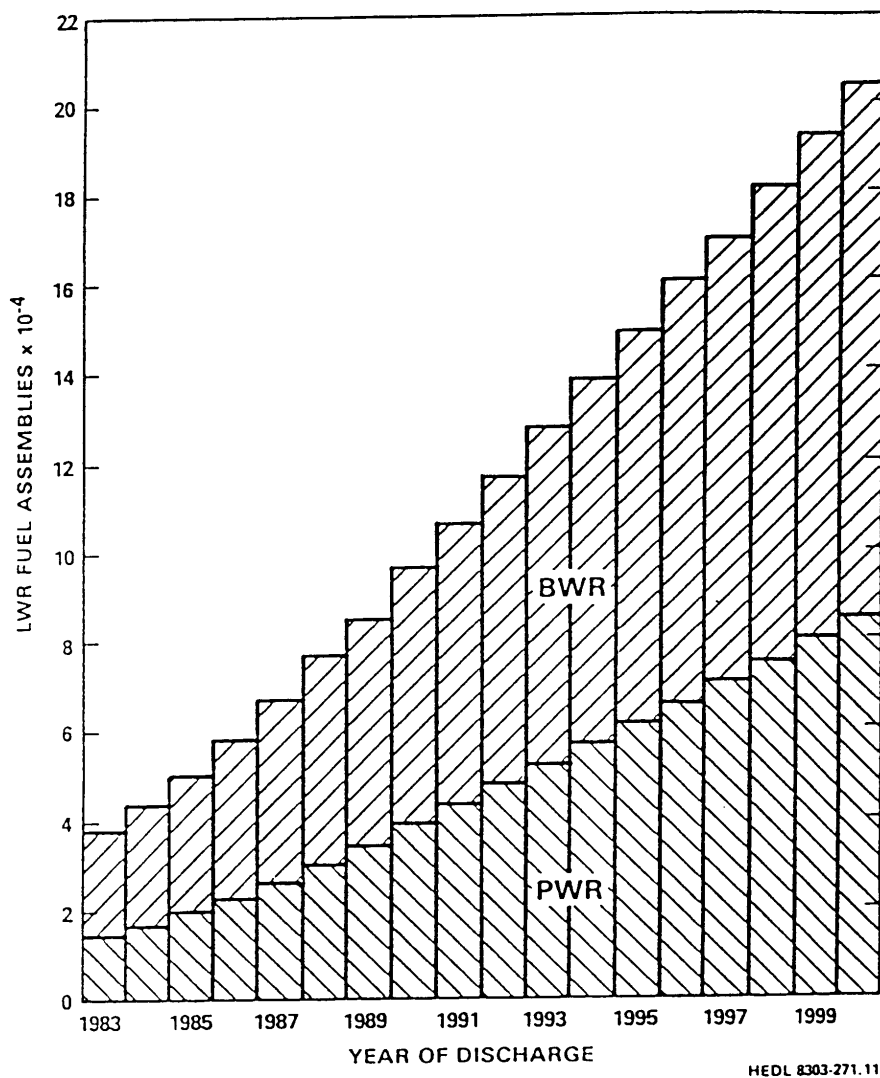
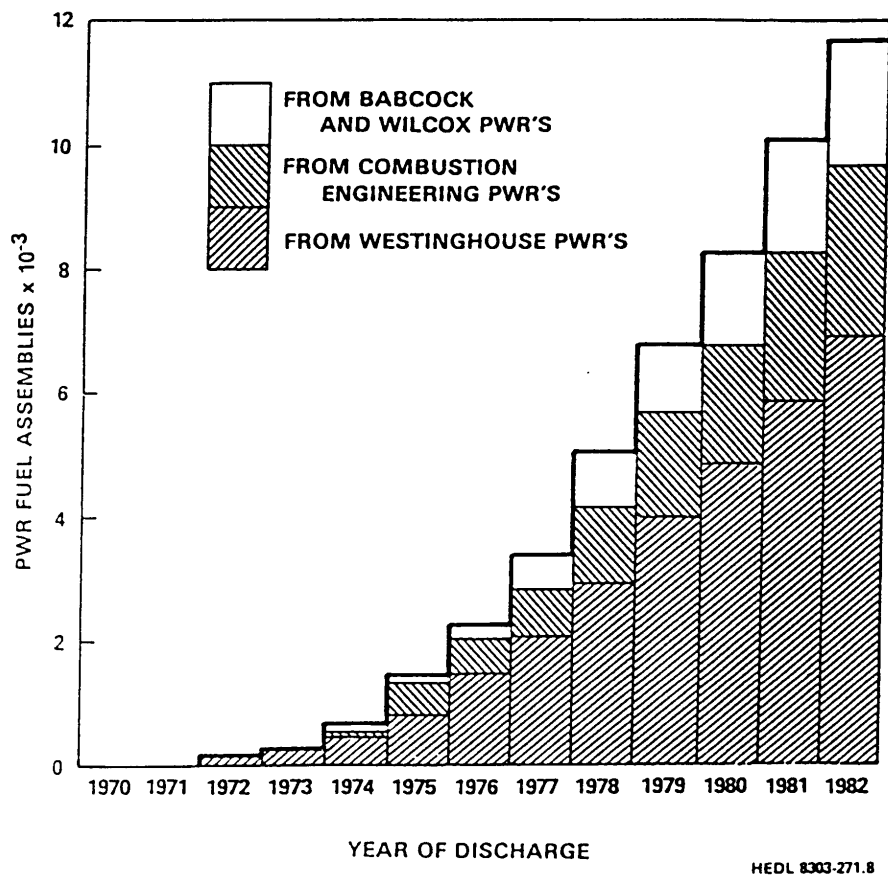**Figure 2.1.1.1-13 Cumulative discharges of spent LWR fuel assemblies (Figure 7 from R.E. Woodley, *The Characteristics of Spent LWR Fuel Relevant to its Storage in Geologic Repositories.* HEDL-TME 83-28, Oct. 1983)**

BU = 14,162 + 1196 (YEAR-1969)

SPREAD IN ANNUAL DATA =
1 STANDARD DEVIATION

HEDL 8303-271.7
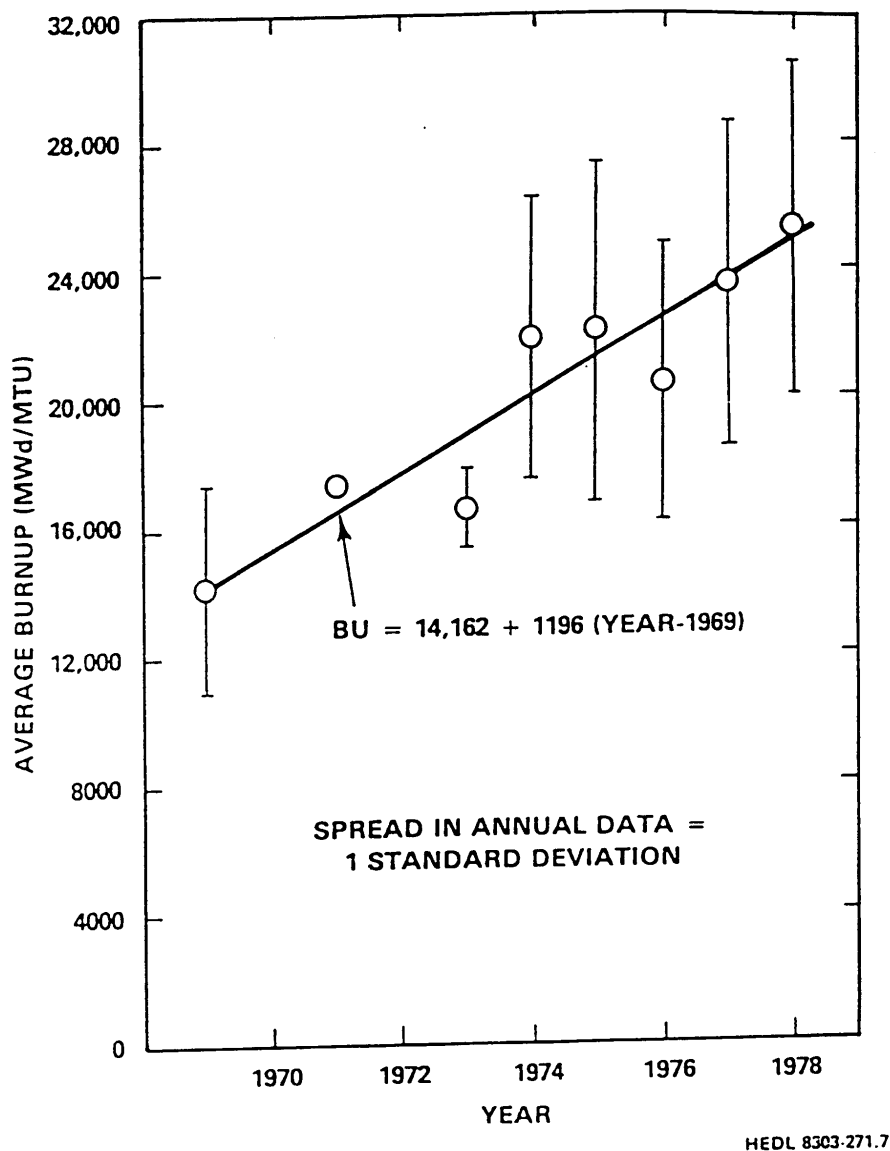
**Figure 2.1.1.1-14 Temporal variation in the burnup of fuel discharged
from LWRs (adapted from Reference 26) (Figure 12
from R.E. Woodley,** *The Characteristics of Spent LWR
Fuel Relevant to its Storage in Geologic Repositories.*
HEDL-TME 83-28, Oct. 1983)

DATA POINTS ARE UNSCREENED, UNWEIGHTED EXPOSURES OF DISCHARGED FUEL, REGARDLESS OF AMOUNT OF FUEL INVOLVED.

HEDL 8303-271.12
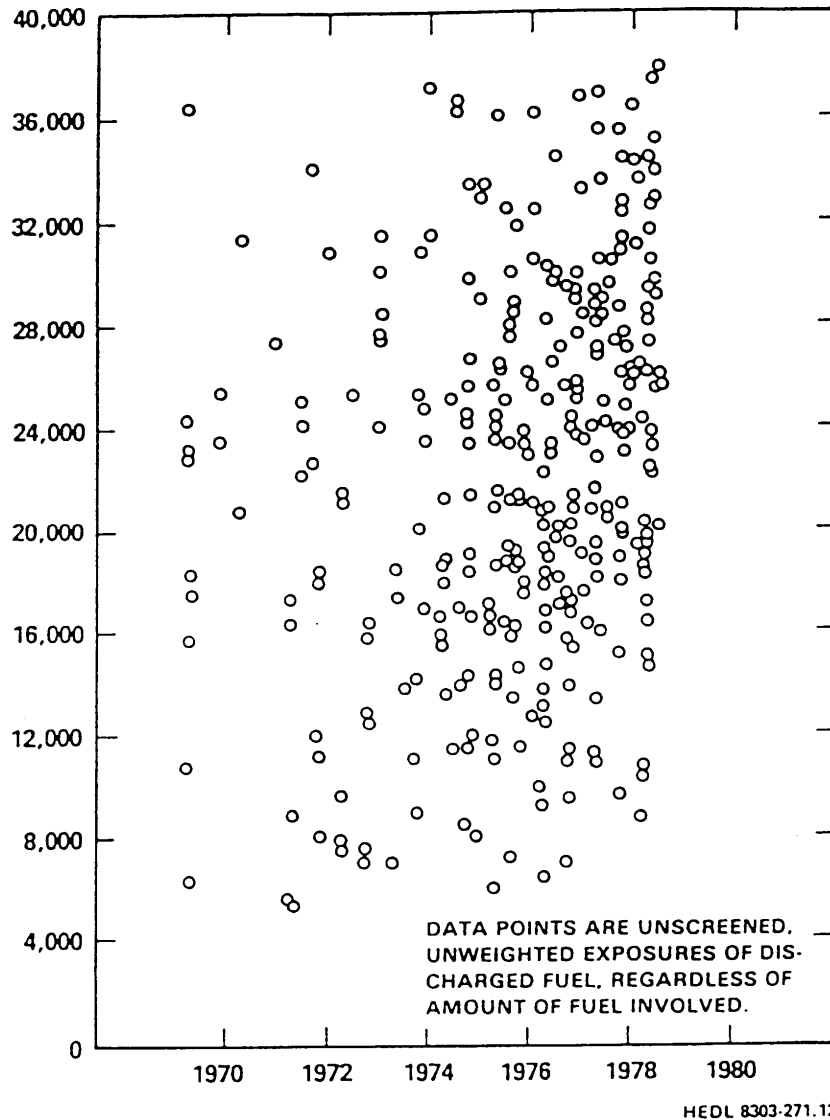
Figure 2.1.1.1-15 Average burnup of fuel discharged from LWRs (adapted from Reference 26) (Figure 13 from R.E. Woodley, *The Characteristics of Spent LWR Fuel Relevant to its Storage in Geologic Repositories.* **HEDL-TME 83-28, Oct. 1983)**

Table 2.1.1.1-10 Summary of burnup distribution percentiles (Table 4.22a from K.J. Notz, *Characteristics of Potential Repository Waste,* DOE/RW-0184-R1, V.1 [draft] July 1990)

Reactor Type	Age Group	Minimum 0%	1%	5%	10%	25%	Median 50%	Mode	75%	90%	95%	99%	Maximum 100%
BWR	Historical	0	2000	7000	10000	16000	21000	23000	26000	29000	30000	35000	43000
PWR	Historical	3000	9000	15000	18000	25000	30000	31000	35000	38000	40000	48000	57000

Table 2.1.1.1-11   Summary of enrichment distribution percentiles (Table 4.22b from K.J. Notz, *Characteristics of Potential Repository Waste,* DOE/RW-0184-R1, V.1 [draft] July 1990)

Reactor Type	Age Group	Minimum 0%	1%	5%	10%	25%	Median 50%	Mode	75%	90%	95%	99%	Maximum 100%
BWR	Historical	0.0	0.7	1.8	2.1	2.2	2.5	2.5	2.8	3.3	3.6	3.9	3.9
PWR	Historical	0.7	1.9	2.0	2.1	2.6	3.1	3.2	3.3	3.6	3.8	4.0	4.9

2.1.1.2 Projected Inventory

Table 2.1.1.2-1   Quantities of domestic LWR spent fuel (Table 2.2
from R.S. Moore, D.A. Williamson, and K.J. Notz,
A Classification Scheme for LWR Fuel Assemblies,
ORNL/TM-10901, Oak Ridge National Laboratory,
November 1988)

BWR Assembly Class		Projected Quantities from 1989 to 2036 (MTIHM)
GE BWR/4,5,6		18826
GE BWR/2,3		3236
Dresden 1		0
Humboldt Bay		0
Big Rock Point		38
Lacrosse		0
Elk River (reprocessed)		0
PWR Assembly Class		**Projected Quantities from 1989 to 2036 (MTIHM)**
WE 15x15		4052
WE 17x17		23803
BW 15x15		2932
CE 14x14		2283
WE 14x14		1753
CE 16x16		2722
CE 16x16 System 80		2716
South Texas		2304
Haddam Neck		246
Palisades		274
San Onofre 1		183
Fort Calhoun		238
Yankee Rowe		60
Saint Lucie 2		652
Indian Point 1		0
BW 17x17		0
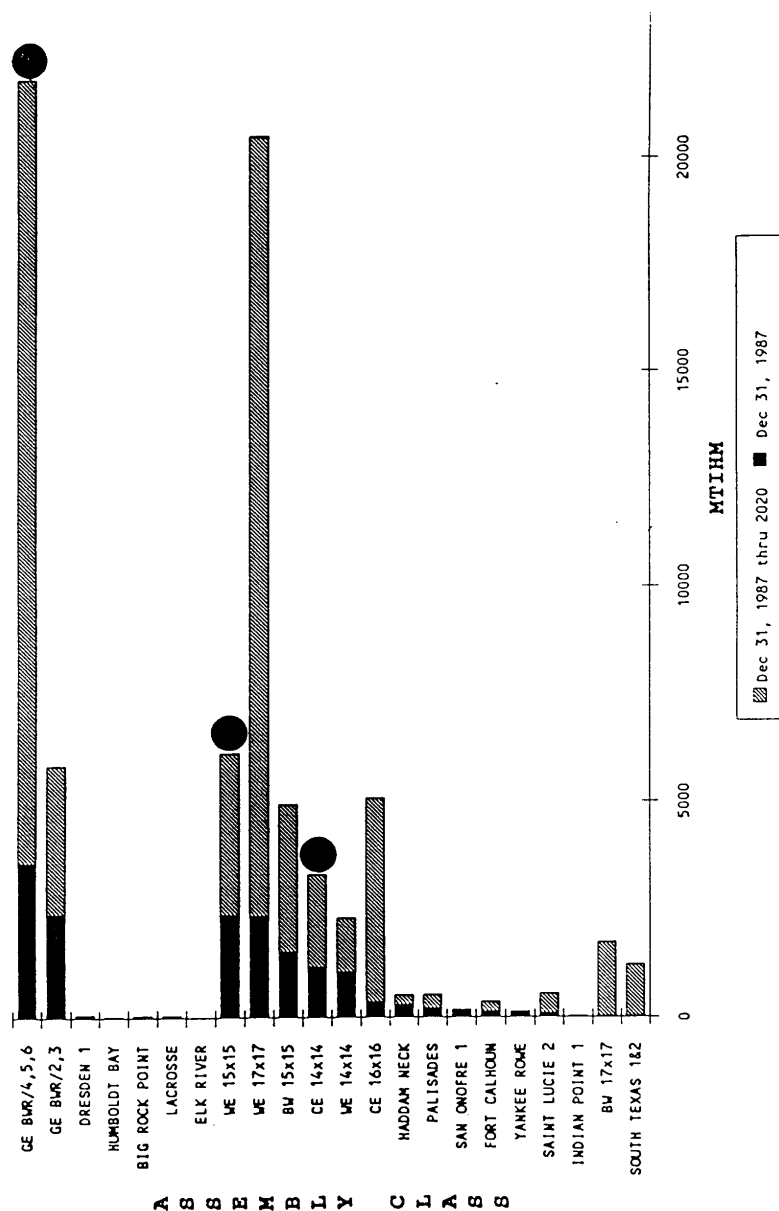
Figure 2.1.1.2-1   Quantities of domestic LWR spent fuel (Figure 1
from K.J. Notz, T.D. Welch, R.S. Moore, and W.J.
Reich, *Preliminary Waste Form Characteristics,*
ORNL-TM-11681 [draft] September 1990)

Table 2.1.1.2-2 **Summary of burnup distribution percentiles (Table 4.22a from K.J. Notz, *Characteristics of Potential Repository Waste*, DOE/RW-0184-R1, V.1 [draft], July 1990)**

Reactor Type	Age Group	Minimum 0%	1%	5%	10%	25%	Median 50%	Mode	75%	90%	95%	99%	Maximum 100%
BWR	Projected	3000	10000	16000	23000	29000	34000	33000	37000	40000	42000	45000	47000
BWR	Projected	5000	16000	27000	32000	38000	44000	46000	49000	52000	55000	60000	67000

Table 2.1.1.2-3 Summary of enrichment distribution percentiles (Table 4.22b from K.J. Notz, *Characteristics of Potential Repository Waste*, DOE/RW-0184-R1, V.1 [draft], July 1990)

Reactor Type	Age Group	Minimum 0%	1%	5%	10%	25%	Median 50%	Mode	75%	90%	95%	99%	Maximum 100%
BWR	Projected	0.7	1.8	2.6	2.8	3.0	3.2	3.3	3.4	3.5	3.6	3.8	3.9
BWR	Projected	1.3	2.1	3.0	3.3	3.6	4.0	4.0	4.2	4.5	4.7	4.9	5.2

Table 2.1.1.2-4   Projected quantities of spent fuel by assembly class (reproduced from the LWR quantities database) (Table 3.2 from K.J. Notz, T.D. Welch, R.S. Moore, and W.J. Reich, *Preliminary Waste Form Characteristics,* ORNL-TM-11681 [draft] September 1990)

LWR QUANTITIES DATABASE
Projected Data: No New Orders Case with Extended Burnup
Projected Assemblies by Assembly Class through 2036

ASSEMBLY CLASS	FUEL ASSEMBLIES	FUEL RODS	AVERAGE BURNUP (MWd/MT)	TOTAL WEIGHT (MT)	AVERAGE INITIAL ENRICH.
B&W 15 X 15	6,328	1,291K	40874	2931.6	3.802
CE 14 X 14	6,062	994K	45092	2283.0	4.205
CE 16 X 16	6,667	1,520K	44175	2721.6	4.184
CE 16 X 16 SYSTEM 80	6,527	1,436K	43925	2716.9	4.004
GE BWR/2,3	18,594	1,320K	32108	3236.1	3.226
GE BWR/4-6	104,939	7,451K	33078	18826.3	3.187
WE 14 X 14	4,869	872K	41571	1753.2	3.791
WE 15 X 15	8,894	1,814K	41199	4052.1	3.826
WE 17 X 17	53,886	14,226K	42218	23802.6	3.916
South Texas	4,258	1,124K	34904	2303.7	3.264
Big Rock Point	289	34K	22015	37.7	3.435
Ft. Calhoun	668	118K	41572	237.6	3.962
Haddam Neck	673	137K	37068	245.5	3.851
Palisades	688	149K	41290	274.3	4.004
St. Lucie-2	1,675	375K	47601	652.2	4.521
San Onofre-1	496	89K	31755	183.0	4.171
Yankee Rowe	261	60K	32018	60.3	3.953
--- GRAND TOTALS	225,774	33,010K	38964	66317.6	3.678

Table 2.1.1.2-5   Total quantitites (historical and projected) of spent fuel by assemby class (reproduced from the LWR quantities database) (Table 3.3 from K.J. Notz, T.D. Welch, R.S. Moore, and W.J. Reich, *Preliminary Waste Form Characteristics*, ORNL-TM-11681 [draft] September 1990)

LWR QUANTITIES DATABASE
Totals - Historical and Projected Data
Discharged Assemblies by Assembly Class

ASSEMBLY CLASS	FUEL ASSEMBLIES	FUEL RODS	AVERAGE BURNUP (MWd/MT)	TOTAL WEIGHT (MT)	AVERAGE INITIAL ENRICH.
B&W 15 X 15	9,892	2,031K	36230	4586.4	3.446
CE 14 X 14	9,391	1,545K	39547	3554.5	3.726
CE 16 X 16	7,898	1,758K	41118	3234.1	3.926
CE 16 X 16 SYSTEM 80	6,715	1,477K	43186	2795.7	3.951
GE BWR/2,3	33,403	2,147K	27220	5998.2	2.838
GE BWR/4-6	125,409	8,645K	31091	22621.3	3.039
WE 14 X 14	7,818	1,392K	37910	2899.3	3.538
WE 15 X 15	14,451	2,947K	36967	6559.3	3.482
WE 17 X 17	59,759	15,778K	40767	26472.7	3.807
South Texas	4,258	1,124K	34904	2303.7	3.264
Big Rock Point	604	63K	20611	79.3	3.464
Dresden-1	891	32K	16227	90.8	2.166
Ft. Calhoun	1,094	191K	37237	391.6	3.549
Haddam Neck	1,407	287K	33892	548.7	3.833
Humboldt Bay	390	15K	14936	28.9	2.351
Indian Point	160	28K	16715	30.6	4.111
Lacrosse	333	33K	14708	38.0	3.727
Palisades	1,285	275K	32638	513.6	3.368
St. Lucie-2	1,911	459K	44725	741.1	4.260
San Onofre-1	964	142K	30434	354.4	3.988
Yankee Rowe	678	162K	29684	160.9	3.950
— GRAND TOTALS	288,523	40,531K	36234	83924.2	3.477

Table 2.1.1.2-6   Spent-fuel distribution by discharge year, based on 1988 EIA data (Table 3.4 from K.J. Notz, T.D. Welch, R.S. Moore, and W.J. Reich, *Preliminary Waste Form Characteristics*, ORNL-TM-11681 [draft] September 1990)

Discharge Year	BWR Assemblies	BWR Metric Tons	PWR Assemblies	PWR Metric Tons
		PROJECTED		
1989	3810	680.9	3160	1372.0
1990	3972	707.2	2707	1136.6
1991	2804	498.1	2942	1279.4
1992	3496	625.1	3526	1507.2
1993	3240	575.6	2774	1201.3
1994	3296	586.0	2903	1247.3
1995	3928	696.4	2669	1151.8
1996	3658	653.2	3138	1350.4
1997	2802	498.8	2656	1138.6
1998	3954	709.3	2663	1148.8
1999	2702	478.1	2775	1194.5
2000	5116	913.5	2789	1185.8
2001	1762	312.3	2694	1179.1
2002	4338	772.2	2381	1022.3
2003	2939	523.8	2549	1100.3
2004	3479	622.1	3025	1316.0
2005	2626	468.6	2467	1063.5
2006	4311	772.0	2738	1188.8
2007	2561	455.6	3373	1439.1
2008	3807	678.3	2342	1011.9
2009	3984	707.2	3267	1404.2
2010	4695	834.9	2573	1116.1
2011	3814	675.3	3320	1425.4
2012	4379	783.4	2917	1267.1
2013	3686	658.1	3814	1662.2
2014	6381	1149.8	2855	1244.1
2015	1886	340.4	2509	1092.7
2016	2966	534.9	2784	1211.9
2017	1878	337.6	2639	1161.3
2018	2392	429.9	1560	691.1
2019	1125	202.2	1445	631.5
2020	1979	352.2	2452	1087.2
2021	1363	246.0	1475	654.8
2022	3086	545.7	1889	819.3
2023	2857	511.3	1406	607.6
2024	2065	366.3	2025	882.2
2025	2489	449.5	1380	607.5
2026	1884	341.4	1190	525.1
2027	1548	271.9	1597	712.8
2028	0	0.0	622	287.7
2029	764	135.4	625	296.9
2030	0	0.0	177	81.3
2031	0	0.0	772	333.8
2032	0	0.0	68	31.4
2033	0	0.0	68	31.4
2034	0	0.0	0	0.0
2035	0	0.0	59	27.1
2036	0	0.0	193	89.1

Table 2.1.1.2-7   Projected spent-fuel distribution by discharge burnup, based on 1988 EIA data (Table 3.6 from K.J. Notz, T.D. Welch, R.S. Moore, and W.J. Reich, *Preliminary Waste Form Characteristics*, ORNL-TM-11681 [draft] September 1990)

Burnup (GWd/MTIHM)	BWR Assemblies	BWR Metric Tons	PWR Assemblies	PWR Metric Tons
0	0	0.0	0	0.0
1	0	0.0	0	0.0
2	0	0.0	0	0.0
3	76	14.1	0	0.0
4	276	48.7	0	0.0
5	4	0.5	20	7.6
6	16	2.1	24	9.2
7	0	0.0	0	0.0
8	112	19.1	0	0.0
9	317	56.1	128	64.8
10	1020	181.1	0	0.0
11	446	79.5	63	29.1
12	872	156.6	392	164.0
13	1659	302.0	480	202.2
14	1623	289.4	211	89.6
15	1428	254.4	178	77.8
16	756	131.3	521	220.5
17	812	143.1	225	98.0
18	184	32.9	512	211.1
19	348	61.3	449	195.5
20	631	112.9	377	175.6
21	590	104.1	439	201.3
22	1524	268.6	567	256.9
23	511	88.5	458	203.7
24	594	104.7	492	210.5
25	1749	310.8	637	277.0
26	2378	431.2	519	225.9
27	3658	655.3	434	190.9
28	2233	402.7	471	199.1
29	4389	788.4	794	360.3
30	5443	976.1	456	214.6
31	5442	977.4	1126	508.3
32	7084	1273.6	1537	671.4
33	8321	1497.1	1889	856.6
34	7643	1371.4	2545	1199.8
35	7300	1314.6	1892	848.9

Table 2.1.1.2-7 (continued)

| Burnup (GWd/MTIHM)	BWR Assemblies	Metric Tons	PWR Assemblies	Metric Tons
36	9028	1615.0	3249	1437.5
37	8714	1548.7	2560	1131.9
38	8035	1429.8	3712	1647.9
39	8510	1508.5	3221	1356.9
40	8707	1524.5	6448	2728.7
41	4199	738.5	4222	1818.2
42	2137	379.9	5029	2157.6
43	2326	413.5	4792	2076.0
44	1535	275.8	4744	2069.9
45	956	174.4	5719	2433.0
46	173	31.0	6911	2901.4
47	63	11.1	5825	2539.2
48	0	0.0	4710	2080.0
49	0	0.0	4848	2126.7
50	0	0.0	5029	2187.4
51	0	0.0	3114	1316.1
52	0	0.0	2765	1177.5
53	0	0.0	2401	1008.4
54	0	0.0	1204	487.8
55	0	0.0	1406	605.9
56	0	0.0	897	390.9
57	0	0.0	557	242.5
58	0	0.0	332	149.0
59	0	0.0	129	55.0
60	0	0.0	46	20.5
61	0	0.0	8	2.8
62	0	0.0	61	24.2
63	0	0.0	74	30.0
64	0	0.0	70	29.2
65	0	0.0	4	1.8
66	0	0.0	0	0.0
67	0	0.0	29	13.5
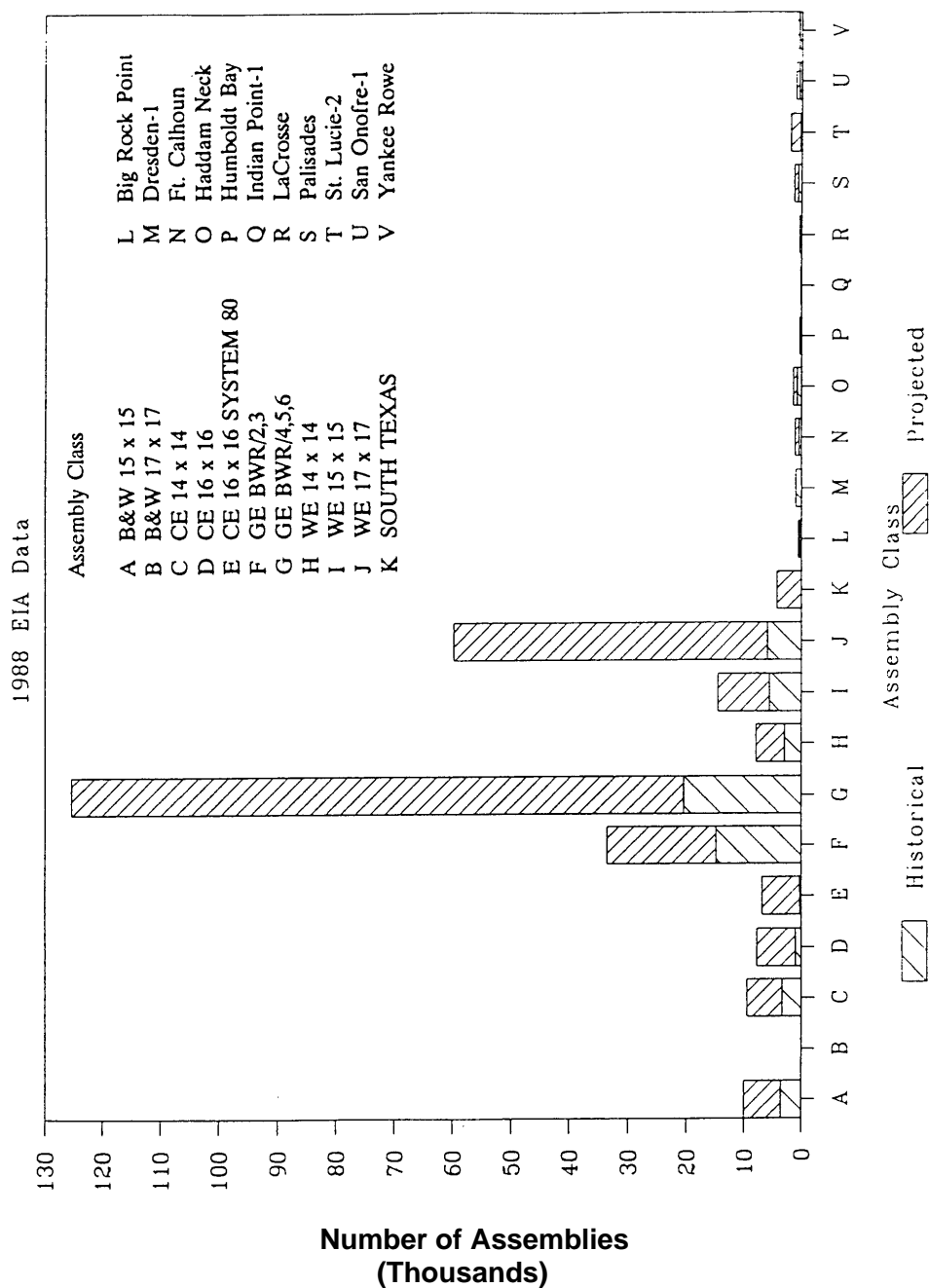
**Figure 2.1.1.2-2   Assemblies by assembly class (Figure 3.1 from K.J. Notz,
T.D. Welch, R.S. Moore, and W.J. Reich, *Preliminary Waste
Form Characteristics,* ORNL-TM-11681 [draft] September 1990)**
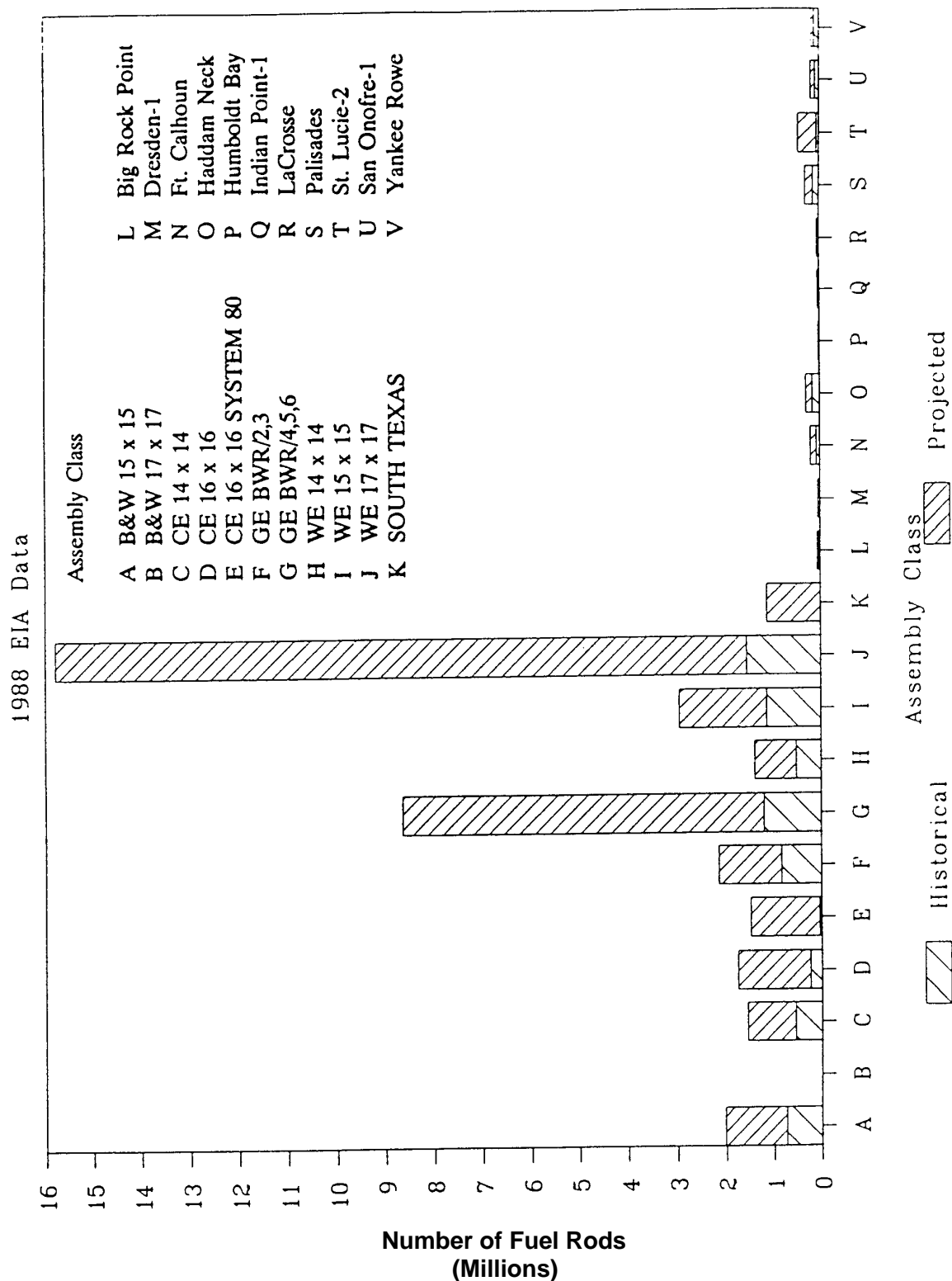
Figure 2.1.1.2-3 Fuel rods by assembly class (Figure 3.2 from K.J. Notz, T.D. Welch, R.S. Moore, and W.J. Reich, *Preliminary Waste Form Characteristics*, ORNL-TM-11681 [draft] September 1990)
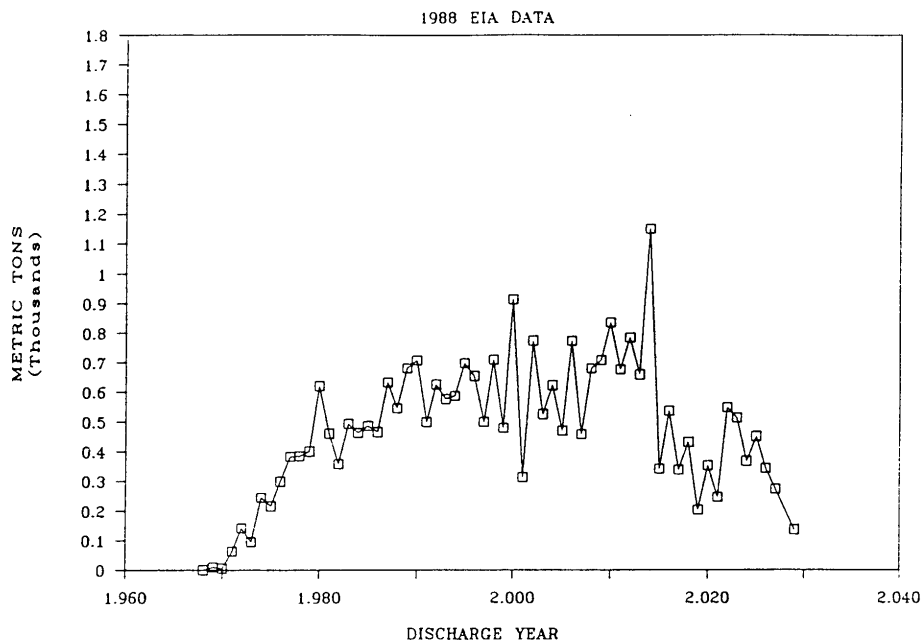
Figure 2.1.1.2-4   BWM discharges by year (Figure 3.3 from K.J. Notz, T.D. Welch, R.S. Moore, and W.J. Reich, *Preliminary Waste Form Characteristics,* ORNL-TM-11681 [draft] September 1990)

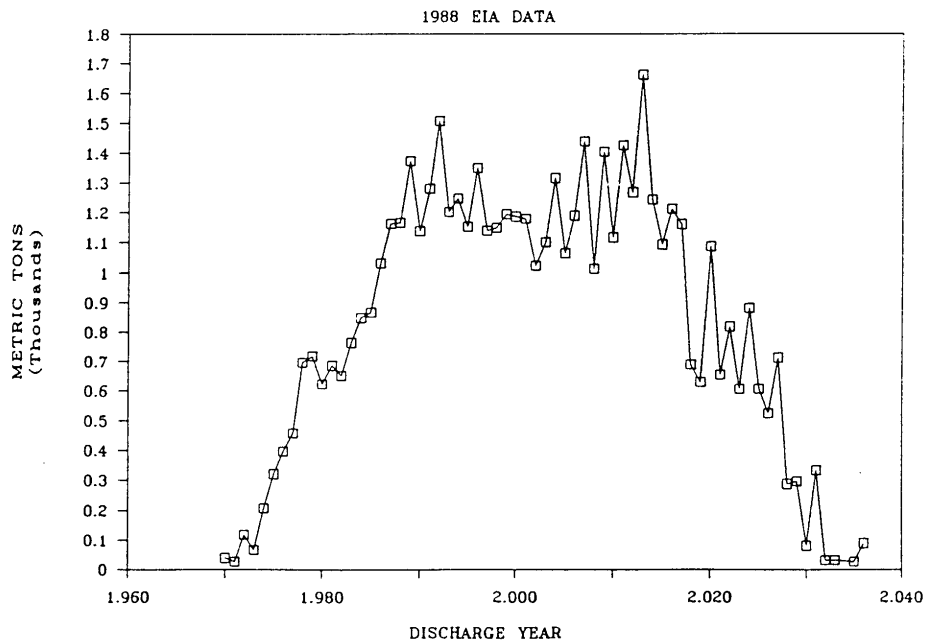**Figure 2.1.1.2-5   PWR discharges by year (Figure 3.4 from K.J. Notz, T.D. Welch, R.S. Moore, and W.J. Reich, *Preliminary Waste Form Characteristics,* ORNL-TM-11681 [draft] September 1990)**

Figure 2.1.1.2-6   BWR dischrages by burnup (Figure 3.6 from K.J. Notz, T.D. Welch, R.S. Moore, and W.J. Reich, *Preliminary Waste Form Characteristics,* **ORNL-TM-11681 [draft] September 1990)**
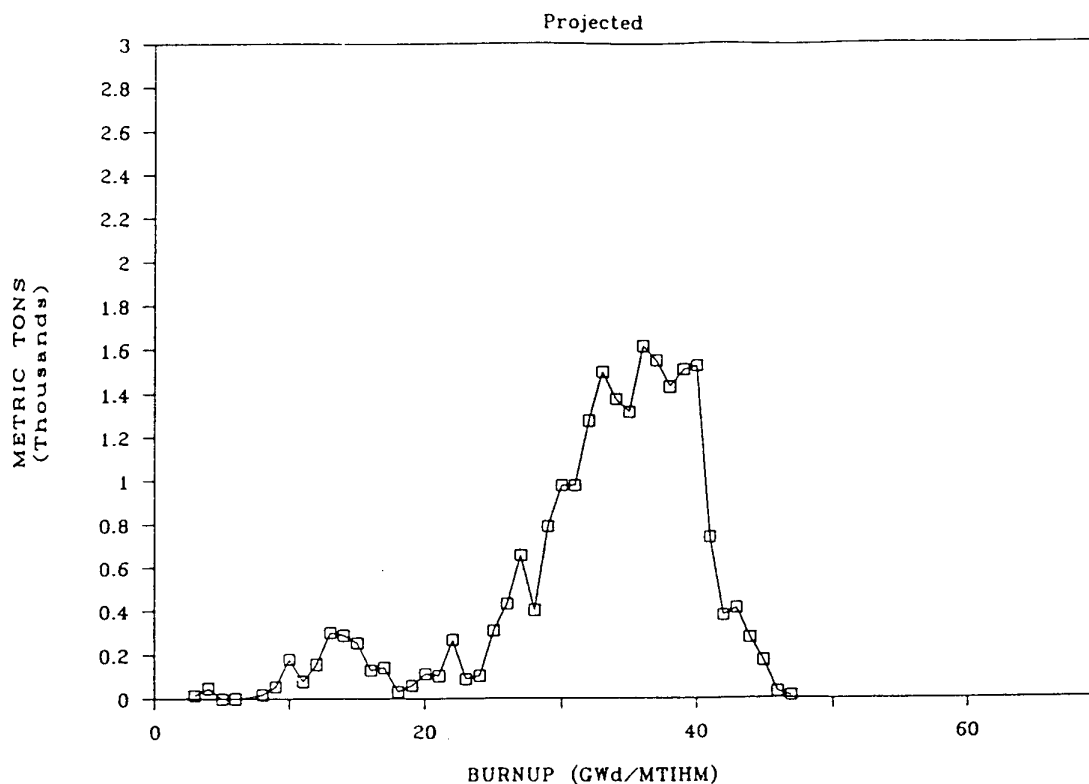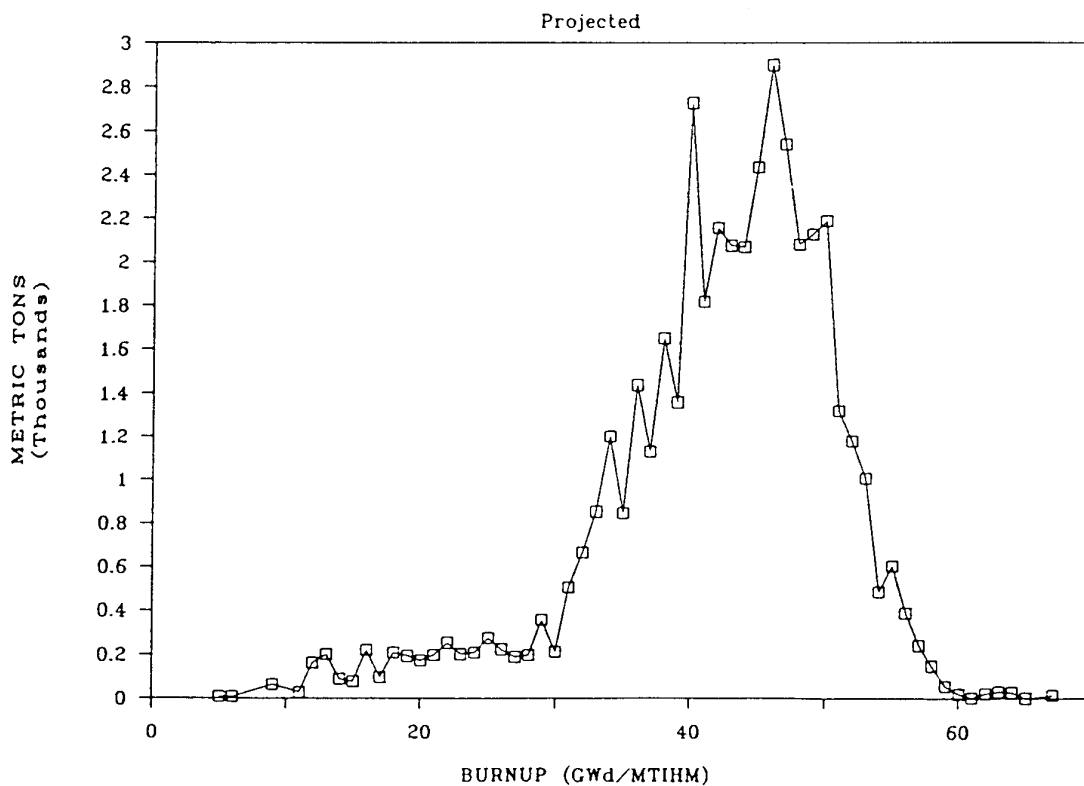
Figure 2.1.1.2-7 **PWR discharges by burnup (Figure 3.8 from K.J. Notz, T.D. Welch, R.S. Moore, and W.J. Reich,** *Preliminary Waste Form Characteristics,* **ORNL-TM-11681 [draft] September 1990)**

Table 2.1.1.2-8   Summary of the quantities of LWR spent fuel (Table 4.1 from K.J. Notz, T.D. Welch, R.S. Moore, and W.J. Reich, *Preliminary Waste Form Characteristics,* ORNL-TM-11681 [draft] September 1990)

		Historical or Projected					
		Through 1988			Projected		
		Reactor Type			Reactor Type		
		BWR	PWR	Summary	BWR	PWR	Summary
No. of Assemblies	Total	37124	25540	62664	123822	101952	225774
Mass, Mtihm	Total	6741	10850	17590	22100	44217	66317

Table 2.1.1.2-9   Summary of the quantities of LWR spent fuel (Table 4.2 from K.J. Notz, T.D. Welch, R.S. Moore, and W.J. Reich, *Preliminary Waste Form Characteristics,* ORNL-TM-11681 [draft] September 1990)

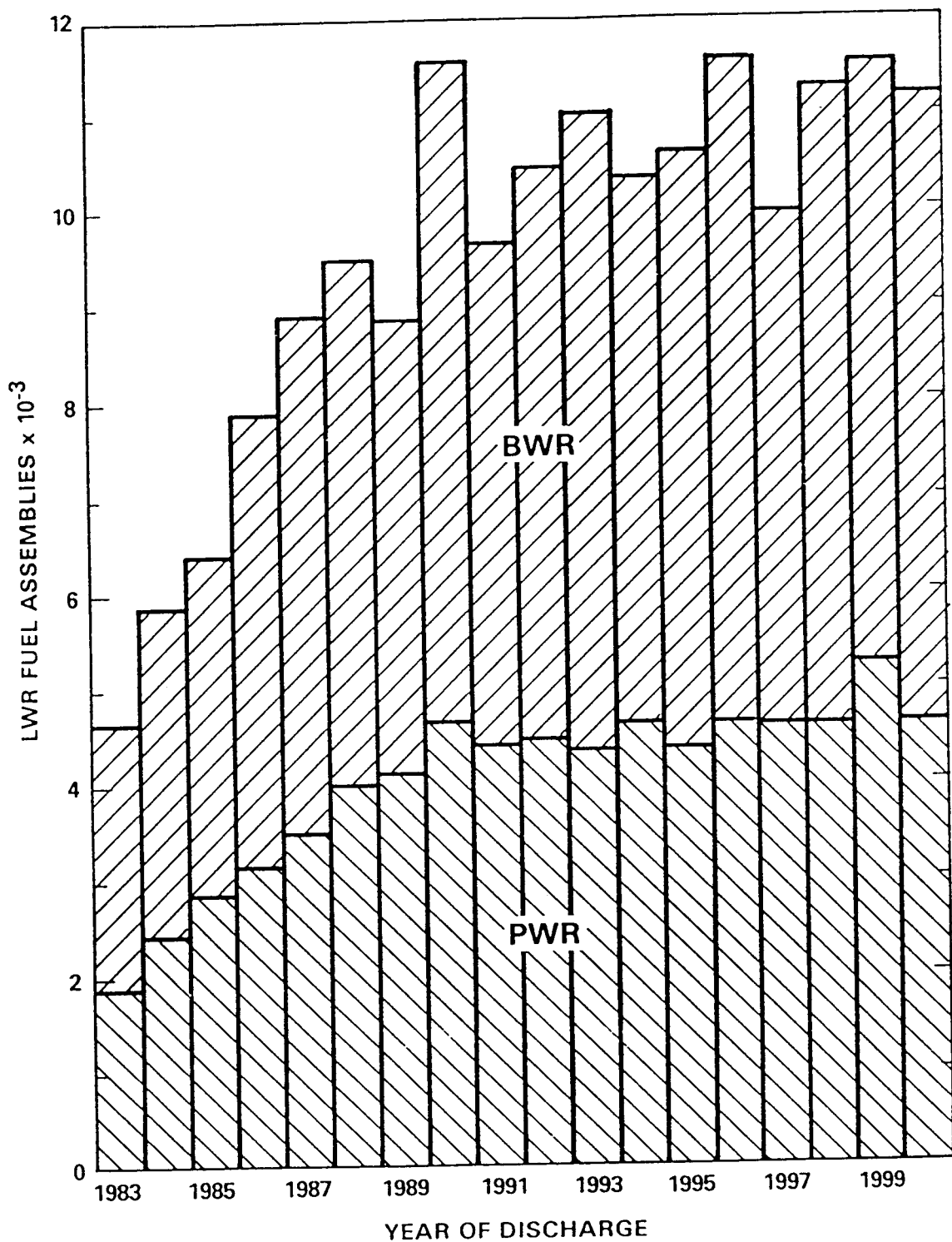| | | Summary | | |
		Reactor Type		
		BWR	PWR	Summary
No. of Assemblies	Total	160946	127492	288438
Mass, Mtihm	Total	28841	55067	83908

Table 2.1.1.2-10 Summary of LWR spent-fuel burnup, enrichment, and age (Table 4.3 from K.J. Notz, T.D. Welch, R.S. Moore, and W.J. Reich, *Preliminary Waste Form Characteristics,* ORNL-TM-11681 [draft] September 1990)

		Historical or Projected					
		Through 1988			Projected		
		Reactor Type			Reactor Type		
		BWR	PWR	Summary	BWR	PWR	Summary
Burnup, MWd/Mt	Minimum	0	3000	0	3000	5000	3000
	MEAN	21213	28908	25959	32904	41987	38960
	Maximum	43000	57000	57000	47000	67000	67000
	Standard Deviation	19979	20181	22679	30273	28528	32518
Enrichment	Minimum	0.0	0.7	0.0	0.7	1.3	0.7
	MEAN	2.3	2.9	2.7	3.2	3.9	3.7
	Maximum	3.9	4.9	4.9	3.9	5.2	5.2
	Standard Deviation	1.4	1.5	1.7	1.5	1.5	1.9
Discharge Date	Minimum	1968	1970	1968	1989	1989	1989
	MEAN	1981	1982	1982	2007	2007	2007
	Maximum	1988	1988	1988	2029	2036	2036

Table 2.1.1.2-11   Summary of LWR spent-fuel burnup, enrichment, and age (Table 4.4 from K.J. Notz, T.D. Welch, R.S. Moore, and W.J. Reich, *Preliminary Waste Form Characteristics, ORNL-TM-11681* [draft] September 1990)

| | | Summary | | |
| | | Reactor Type | | Summary |
		BWR	PWR	
Burnup, MWd/Mt	Minimum	0	3000	0
	MEAN	30172	39410	36234
	Maximum	47000	67000	67000
	Standard Deviation	32110	31340	34685
Enrichment	Minimum	0.0	0.7	0.0
	MEAN	3.0	3.7	3.5
	Maximum	3.9	5.2	5.2
	Standard Deviation	1.9	2.0	2.3
Discharge Date	Minimum	1968	1970	1968
	MEAN	2001	2002	2002
	Maximum	2029	2036	2036

HEDL 8303-271.10

Figure 2.1.1.2-8   Projected annual discharges of spent LWR fuel assemblies (Figure 6 from R.E. Woodley, *The Characteristics of Spent LWR Fuel Relevant to its Storage in Geologic Repositories.* **HEDL-TME 83-28, Oct. 1983.)**
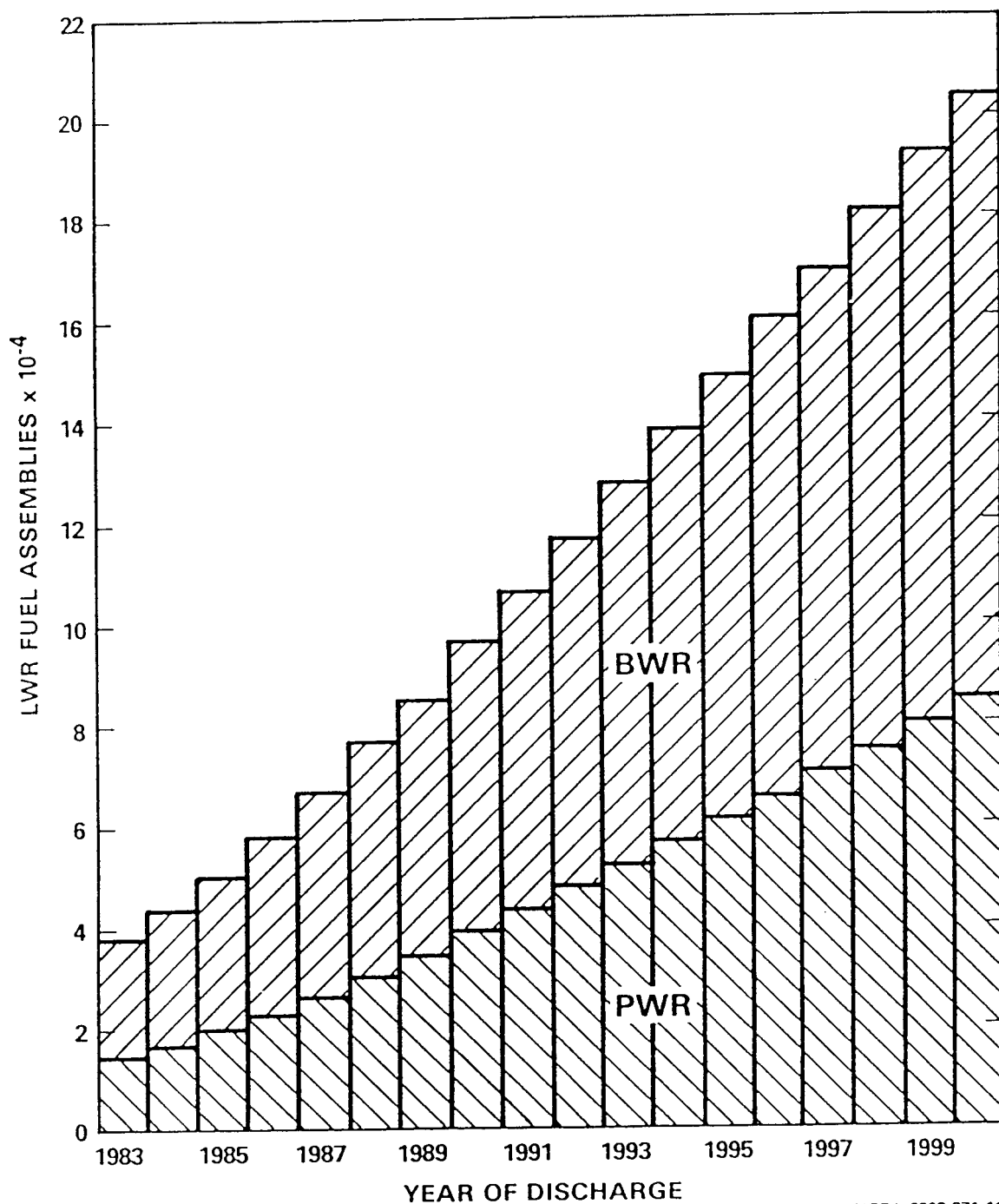
Figure 2.1.1.2-9   Cumulative discharges of spent LWR fuel assemblies (Figure 7 from R.E. Woodley, *The Characteristics of Spent LWR Fuel Relevant to its Storage in Geologic Repositories.* HEDL-TME 83-28, Oct. 1983.)

2.1.1.3 Radionuclide Activity vs. History

Table 2.1.1.3-1   Summary of radioactivity (curies/MTIHM) of BWR spent fuel as a function of burnup, initial enrichment, and decay time (Table 4.6 from K.J. Notz, T.D. Welch, R.S. Moore, and W.J. Reich, *Preliminary Waste Form Characteristics*, ORNL-TM-11681 [draft], September 1990)

Initial Enrichment, %	Years After Discharge					
	1	10	100	1000	10k	100k
BURNUP = 7,500 MWd/MTIHM						
0.72	1.055E+06	1.316E+05	1.202E+04	1.066E+03	2.767E+02	2.624E+01
1.05	9.523E+05	1.137E+05	1.076E+04	8.601E+02	2.531E+02	2.489E+01
1.75	8.879E+05	1.004E+05	1.005E+04	6.233E+02	2.192E+02	2.449E+01
BURNUP = 15,000 MWd/MTIHM						
1.09	1.445E+06	2.153E+05	2.038E+04	1.467E+03	3.405E+02	3.532E+01
1.79	1.366E+06	2.040E+05	1.999E+04	1.228E+03	3.155E+02	3.477E+01
2.49	1.310E+06	1.939E+05	1.958E+04	1.014E+03	2.911E+02	3.467E+01
BURNUP = 22,500 MWd/MTIHM						
1.72	1.696E+06	2.911E+05	2.881E+04	1.675E+03	3.933E+02	4.434E+01
2.42	1.631E+06	2.849E+05	2.880E+04	1.482E+03	3.694E+02	4.393E+01
3.12	1.575E+06	2.774E+05	2.858E+04	1.291E+03	3.466E+02	4.371E+01
BURNUP = 30,000 MWd/MTIHM						
2.23	1.890E+06	3.628E+05	3.706E+04	1.859E+03	4.525E+02	5.361E+01
2.93	1.828E+06	3.595E+05	3.727E+04	1.692E+03	4.265E+02	5.309E+01
3.63	1.773E+06	3.543E+05	3.721E+04	1.519E+03	4.022E+02	5.266E+01
BURNUP = 40,000 MWd/MTIHM						
2.74	2.396E+06	5.132E+05	5.357E+04	2.530E+03	6.400E+02	7.804E+01
3.44	2.338E+06	5.121E+05	5.410E+04	2.382E+03	6.079E+02	7.771E+01
4.14	2.280E+06	5.092E+05	5.432E+04	2.224E+03	5.780E+02	7.694E+01
BURNUP = 50,000 MWd/MTIHM						
3.04	2.383E+06	5.601E+05	5.953E+04	2.677E+03	7.018E+02	8.697E+01
3.74	2.332E+06	5.593E+05	6.013E+04	2.531E+03	6.675E+02	8.675E+01
4.44	2.279E+06	5.571E+05	6.041E+04	2.375E+03	6.349E+02	8.591E+01

Table 2.1.1.3-2   Summary of radioactivity (curies/MTIHM) of PWR spent fuel as a function of burnup, initial enrichment, and decay time (Table 4.10 from K.J. Notz, T.D. Welch, R.S. Moore, and W.J. Reich, *Preliminary Waste Form Characteristics*, ORNL-TM-11681 [draft], September 1990)

Initial Enrichment, %	Years After Discharge					
	1	10	100	1000	10k	100k

BURNUP = 10,000 MWd/MTIHM

0.99	1.295E+06	1.542E+05	1.450E+04	1.133E+03	3.071E+02	2.952E+01
1.69	1.191E+06	1.360E+05	1.346E+04	8.422E+02	2.703E+02	2.854E+01
2.39	1.145E+06	1.266E+05	1.300E+04	6.459E+02	2.389E+02	2.852E+01

BURNUP = 20,000 MWd/MTIHM

1.74	1.828E+06	2.634E+05	2.597E+04	1.527E+03	3.862E+02	4.132E+01
2.44	1.756E+06	2.550E+05	2.578E+04	1.310E+03	3.600E+02	4.095E+01
3.14	1.701E+06	2.466E+05	2.547E+04	1.110E+03	3.341E+02	4.090E+01

BURNUP = 30,000 MWd/MTIHM

2.41	2.180E+06	3.629E+05	3.719E+04	1.799E+03	4.660E+02	5.298E+01
3.11	2.110E+06	3.589E+05	3.732E+04	1.619E+03	4.388E+02	5.254E+01
3.81	2.051E+06	3.533E+05	3.722E+04	1.436E+03	4.125E+02	5.225E+01

BURNUP = 40,000 MWd/MTIHM

3.02	2.501E+06	4.735E+05	4.926E+04	2.297E+03	5.977E+02	7.035E+01
3.72	2.435E+06	4.703E+05	4.949E+04	2.125E+03	5.677E+02	6.973E+01
4.42	2.374E+06	4.656E+05	4.948E+04	1.948E+03	5.392E+02	6.903E+01

BURNUP = 50,000 MWd/MTIHM

3.56	2.789E+06	5.668E+05	6.033E+04	2.559E+03	7.020E+02	8.391E+01
4.26	2.723E+06	5.652E+05	6.073E+04	2.395E+03	6.677E+02	8.330E+01
4.96	2.658E+06	5.620E+05	6.087E+04	2.223E+03	6.347E+02	8.239E+01

BURNUP = 60,000 MWd/MTIHM

4.03	3.045E+06	6.552E+05	7.114E+04	2.817E+03	8.217E+02	9.817E+01
4.73	2.981E+06	6.548E+05	7.174E+04	2.658E+03	7.829E+02	9.784E+01
5.43	2.916E+06	6.532E+05	7.204E+04	2.487E+03	7.448E+02	9.690E+01

Table 2.1.1.3-3   Radioactivity (in curies/MTIHM) by radionuclide (contributing ≥1% of total) for BWR spent fuel as a function of initial enrichment and decay time for a burnup of 30,000 MWd/MTIHM (Table 4.14 from K.J. Notz, T.D. Welch, R.S. Moore, and W.J. Reich, *Preliminary Waste Form Characteristics*, ORNL-TM-11681 [draft], September 1990)

Nuclide	Enrichment					
	2.23%		2.93%		3.63%	
	Radio-activity	Percent of Total	Radio-activity	Percent of Total	Radio-activity	Percent of Total

Decay Time = 1 Year

Nuclide	Radio-activity	Percent of Total	Radio-activity	Percent of Total	Radio-activity	Percent of Total
Sr 90	5.69E+04	3.01	6.28E+04	3.44	6.76E+04	3.81
Y 90	5.69E+04	3.01	6.28E+04	3.44	6.76E+04	3.81
Zr 95	2.13E+04	1.13	2.19E+04	1.20	2.25E+04	1.27
Nb 95	4.80E+04	2.54	4.93E+04	2.70	5.05E+04	2.85
Ru106	2.46E+05	13.01	2.09E+05	11.43	1.77E+05	9.97
Rh106	2.46E+05	13.01	2.09E+05	11.43	1.77E+05	9.97
Cs134	1.07E+05	5.66	9.71E+04	5.31	8.73E+04	4.92
Cs137	9.09E+04	4.81	9.09E+04	4.97	9.08E+04	5.12
Ba137m	8.60E+04	4.55	8.59E+04	4.70	8.59E+04	4.84
Ce144	3.07E+05	16.26	3.20E+05	17.53	3.32E+05	18.74
Pr144	3.07E+05	16.26	3.20E+05	17.53	3.32E+05	18.73
Pm147	7.86E+04	4.16	8.59E+04	4.70	9.39E+04	5.29
Pu241	1.38E+05	7.32	1.24E+05	6.76	1.07E+05	6.06

Decay Time = 10 Years

Nuclide	Radio-activity	Percent of Total	Radio-activity	Percent of Total	Radio-activity	Percent of Total
Kr 85	3.90E+03	1.08	4.23E+03	1.18	4.49E+03	1.27
Sr 90	4.59E+04	12.66	5.07E+04	14.10	5.45E+04	15.39
Y 90	4.59E+04	12.66	5.07E+04	14.10	5.45E+04	15.39
Cs134	5.19E+03	1.43	4.71E+03	1.31	4.24E+03	1.20
Cs137	7.39E+04	20.36	7.38E+04	20.53	7.38E+04	20.82
Ba137m	6.99E+04	19.27	6.98E+04	19.43	6.98E+04	19.70
Pm147	7.29E+03	2.01	7.97E+03	2.22	8.70E+03	2.46
Eu154	4.34E+03	1.20	3.73E+03	1.04	3.19E+03	0.90
Pu241	8.97E+04	24.73	8.01E+04	22.29	6.96E+04	19.66

Decay Time = 100 Years

Nuclide	Radio-activity	Percent of Total	Radio-activity	Percent of Total	Radio-activity	Percent of Total
Sr 90	5.39E+03	14.55	5.95E+03	15.97	6.40E+03	17.21
Y 90	5.39E+03	14.55	5.95E+03	15.98	6.41E+03	17.22
Cs137	9.23E+03	24.91	9.22E+03	24.75	9.22E+03	24.77
Ba137m	8.73E+03	23.57	8.73E+03	23.42	8.72E+03	23.44
Pu238	1.40E+03	3.77	1.22E+03	3.28	1.03E+03	2.75
Pu240	4.70E+02	1.27	4.38E+02	1.18	4.04E+02	1.09
Pu241	1.18E+03	3.18	1.05E+03	2.82	9.15E+02	2.46
Am241	4.38E+03	11.83	3.92E+03	10.52	3.41E+03	9.16

Table 2.1.1.3-3 (continued)

Decay Time = 1000 Years

Np239	2.75E+01	1.48	1.76E+01	1.04	1.10E+01	0.73
Pu239	2.98E+02	16.02	2.93E+02	17.30	2.86E+02	18.84
Pu240	4.27E+02	22.98	3.98E+02	23.54	3.67E+02	24.19
Am241	1.05E+03	56.24	9.34E+02	55.21	8.13E+02	53.50
Am243	2.75E+01	1.48	1.76E+01	1.04	1.10E+01	0.73

Decay Time = 10,000 Years

Tc 99	1.14E+01	2.52	1.16E+01	2.72	1.18E+01	2.93
Np239	1.18E+01	2.61	7.57E+00	1.77	4.74E+00	1.18
Pu239	2.34E+02	51.70	2.28E+02	53.57	2.23E+02	55.32
Pu240	1.64E+02	36.35	1.53E+02	35.97	1.41E+02	35.17
Am243	1.18E+01	2.61	7.57E+00	1.77	4.74E+00	1.18

Decay Time = 100,000 Years

Ni 59	8.12E−01	1.52	7.04E−01	1.33	6.12E−01	1.16
Zr 93	2.14E+00	3.99	2.13E+00	4.02	2.12E+00	4.03
Nb 93m	2.03E+00	3.79	2.03E+00	3.82	2.02E+00	3.83
Tc 99	8.52E+00	15.88	8.66E+00	16.31	8.78E+00	16.68
Pb210	9.53E−01	1.78	1.03E+00	1.94	1.12E+00	2.13
Pb214	9.54E−01	1.78	1.03E+00	1.95	1.12E+00	2.13
Bi210	9.54E−01	1.78	1.03E+00	1.95	1.12E+00	2.13
Bi214	9.54E−01	1.78	1.03E+00	1.95	1.12E+00	2.13
Po210	9.54E−01	1.78	1.03E+00	1.95	1.12E+00	2.13
Po214	9.53E−01	1.78	1.03E+00	1.95	1.12E+00	2.13
Po218	9.54E−01	1.78	1.03E+00	1.95	1.12E+00	2.13
Rn222	9.54E−01	1.78	1.03E+00	1.95	1.12E+00	2.13
Ra226	9.54E−01	1.78	1.03E+00	1.95	1.12E+00	2.13
Th230	9.45E−01	1.76	1.02E+00	1.93	1.11E+00	2.11
Pa233	1.26E+00	2.35	1.17E+00	2.21	1.06E+00	2.01
U234	1.45E+00	2.70	1.56E+00	2.94	1.69E+00	3.21
Np237	1.26E+00	2.35	1.17E+00	2.21	1.06E+00	2.01
Pu239	1.79E+01	33.40	1.73E+01	32.68	1.68E+01	31.92
Pu242	1.97E+00	3.67	1.47E+00	2.77	1.07E+00	2.03

Table 2.1.1.3-4   Radioactivity (in curies/MTIHM) by radionuclide (contributing ≥1% of total) for PWR spent fuel as a function of initial enrichment and decay time for a burnup of 40,000 MWd/MTIHM (Table 4.17 from K.J. Notz, T.D. Welch, R.S. Moore, and W.J. Reich, *Preliminary Waste Form Characteristics*, ORNL-TM-11681 [draft], September 1990)

Nuclide	Enrichment					
	3.02%		3.72%		4.42%	
	Radio-activity	Percent of Total	Radio-activity	Percent of Total	Radio-activity	Percent of Total
Decay Time = 1 Year						
Sr 90	7.76E+04	3.10	8.39E+04	3.44	8.91E+04	3.75
Y 90	7.77E+04	3.11	8.39E+04	3.44	8.92E+04	3.76
Zr 95	2.74E+04	1.10	2.82E+04	1.16	2.89E+04	1.22
Nb 95	6.18E+04	2.47	6.34E+04	2.60	6.50E+04	2.74
Ru106	3.21E+05	12.84	2.81E+05	11.55	2.45E+05	10.33
Rh106	3.21E+05	12.84	2.81E+05	11.55	2.45E+05	10.33
Cs134	1.65E+05	6.59	1.53E+05	6.28	1.41E+05	5.93
Cs137	1.21E+05	4.84	1.21E+05	4.97	1.21E+05	5.10
Ba137m	1.15E+05	4.58	1.14E+05	4.70	1.14E+05	4.82
Ce144	4.16E+05	16.61	4.30E+05	17.65	4.43E+05	18.65
Pr144	4.16E+05	16.62	4.30E+05	17.65	4.43E+05	18.65
Pm147	9.10E+04	3.64	9.84E+04	4.04	1.07E+05	4.49
Pu241	1.62E+05	6.48	1.48E+05	6.07	1.32E+05	5.57
Decay Time = 10 Years						
Kr 85	5.31E+03	1.12	5.66E+03	1.20	5.95E+03	1.28
Sr 90	6.27E+04	13.23	6.77E+04	14.39	7.19E+04	15.45
Y 90	6.27E+04	13.24	6.77E+04	14.40	7.20E+04	15.45
Cs134	8.00E+03	1.69	7.42E+03	1.58	6.83E+03	1.47
Cs137	9.83E+04	20.77	9.82E+04	20.89	9.82E+04	21.10
Ba137m	9.30E+04	19.65	9.30E+04	19.77	9.29E+04	19.96
Pm147	8.44E+03	1.78	9.12E+03	1.94	9.90E+03	2.13
Eu154	6.36E+03	1.34	5.70E+03	1.21	5.08E+03	1.09
Pu241	1.05E+05	22.18	9.57E+04	20.36	8.57E+04	18.40
Cm244	4.75E+03	1.00	2.88E+03	0.61	1.72E+03	0.37
Decay Time = 100 Years						
Sr 90	7.36E+03	14.93	7.95E+03	16.06	8.45E+03	17.07
Y 90	7.36E+03	14.94	7.95E+03	16.06	8.45E+03	17.07
Cs137	1.23E+04	24.96	1.23E+04	24.83	1.23E+04	24.82
Ba137m	1.16E+04	23.61	1.16E+04	23.49	1.16E+04	23.47
Pu238	2.27E+03	4.62	2.07E+03	4.19	1.83E+03	3.70
Pu240	6.22E+02	1.26	5.84E+02	1.18	5.44E+02	1.10
Pu241	1.38E+03	2.80	1.26E+03	2.54	1.13E+03	2.27
Am241	5.13E+03	10.41	4.68E+03	9.45	4.19E+03	8.47

Table 2.1.1.3-4 (continued)

Decay Time = 1000 Years

Np239	3.57E+01	1.55	2.52E+01	1.19	1.75E+01	0.90
Pu239	3.93E+02	17.13	3.87E+02	18.22	3.80E+02	19.49
Pu240	5.66E+02	24.64	5.31E+02	24.99	4.95E+02	25.41
Am241	1.22E+03	53.21	1.11E+03	52.46	9.98E+02	51.24
Am243	3.57E+01	1.55	2.52E+01	1.19	1.75E+01	0.90

Decay Time = 10,000 Years

Tc 99	1.48E+01	2.48	1.50E+01	2.65	1.53E+01	2.83
Np239	1.53E+01	2.56	1.08E+01	1.91	7.50E+00	1.39
Pu239	3.09E+02	51.70	3.03E+02	53.29	2.96E+02	54.82
Pu240	2.18E+02	36.47	2.05E+02	36.03	1.91E+02	35.34
Am243	1.53E+01	2.56	1.08E+01	1.91	7.50E+00	1.39

Decay Time = 100,000 Years

Ni 59	1.31E+00	1.86	1.18E+00	1.69	1.06E+00	1.53
Zr 93	2.36E+00	3.35	2.41E+00	3.45	2.45E+00	3.54
Nb 93m	2.24E+00	3.18	2.29E+00	3.28	2.32E+00	3.37
Tc 99	1.10E+01	15.69	1.12E+01	16.09	1.14E+01	16.49
Pb210	1.38E+00	1.97	1.44E+00	2.07	1.50E+00	2.18
Pb214	1.38E+00	1.97	1.44E+00	2.07	1.50E+00	2.18
Bi210	1.38E+00	1.97	1.44E+00	2.07	1.50E+00	2.18
Bi214	1.38E+00	1.97	1.44E+00	2.07	1.50E+00	2.18
Po210	1.38E+00	1.97	1.44E+00	2.07	1.50E+00	2.18
Po214	1.38E+00	1.97	1.44E+00	2.07	1.50E+00	2.18
Po218	1.38E+00	1.97	1.45E+00	2.07	1.50E+00	2.18
Rn222	1.38E+00	1.97	1.45E+00	2.07	1.50E+00	2.18
Ra226	1.38E+00	1.97	1.45E+00	2.07	1.50E+00	2.18
Th230	1.37E+00	1.95	1.43E+00	2.05	1.49E+00	2.16
Pa233	1.60E+00	2.27	1.52E+00	2.18	1.41E+00	2.05
U234	2.08E+00	2.96	2.17E+00	3.11	2.26E+00	3.27
Np237	1.60E+00	2.27	1.52E+00	2.18	1.41E+00	2.05
Pu239	2.36E+01	33.59	2.30E+01	32.99	2.24E+01	32.40
Pu242	2.27E+00	3.23	1.81E+00	2.59	1.41E+00	2.04

Table 2.1.1.3-5 Activity of selected radionuclides in a PWR fuel assembly irradiated to an average burnup of 33,000 MWd/MTU* (Table 6 from R.E. Woodley, *The Characteristics of Spent LWR Fuel Relevant to its Storage in Geologic Repositories.* **HEDL-TME 83-28, Oct. 1983.)**

Radionuclide	Activity (curies)						
	Discharge	1 yr	10 yr	100 yr	300 yr	1000 yr	10,000 yr
Americium-241	5.015E 01	1.397E-02	7.740E-02	1.731E-03	1.269E-03	4.139E-02	4.734E-03
Americium-243	7.621E 00	7.631E 00	7.625E 00	7.563E 00	7.427E 00	6.971E 00	3.084E 00
Carbon-14	6.853E-01	6.852E-01	6.844E-01	6.770E-01	6.608E-01	6.072E-01	2.044E-01
Cesium-135	1.711E-01	1.714E-01	1.714E-01	1.714E-01	1.714E-01	1.714E-01	1.709E-01
Cesium-137	4.786E 04	4.677E 04	3.801E 04	4.785E 03	4.783E 01	4.777E-06	0.0
Neptunium-237	1.403E-01	1.436E-01	1.450E-01	1.914E-01	2.883E-01	4.613E-01	5.435E-01
Plutonium-238	9.832E 02	1.054E 03	1.001E 03	4.970E 02	1.052E 02	4.867E-01	6.144E-20
Plutonium-239	1.400E 02	1.424E 02	1.424E 02	1.421E 02	1.413E 02	1.387E 02	1.084E 02
Plutonium-240	2.358E 02	2.358E 02	2.361E 02	2.352E 02	2.305E 02	2.145E 02	8.525E 01
Plutonium-242	8.294E-01	8.295E-01	8.295E-01	8.294E-01	8.291E-01	8.281E-01	8.147E-01
Radium-226	5.867E-09	1.104E-08	1.457E-07	1.145E-05	1.142E-04	1.336E-03	5.733E-02
Strontium-90	3.493E 04	3.408E 04	2.729E 04	2.964E 03	2.138E 01	6.780E-07	0.0
Technecium-99	6.095E 00	6.124E 00	6.124E 00	6.122E 00	6.118E 00	6.104E 00	5.927E 00
Tin-126	3.577E-01	3.577E-01	3.577E-01	3.575E-01	3.570E-01	3.553E-01	3.338E-01

*The fuel assembly initially contained 0.461 MTU, enriched to 3.2% in ^{235}U. (Adapted from Reference 3.)
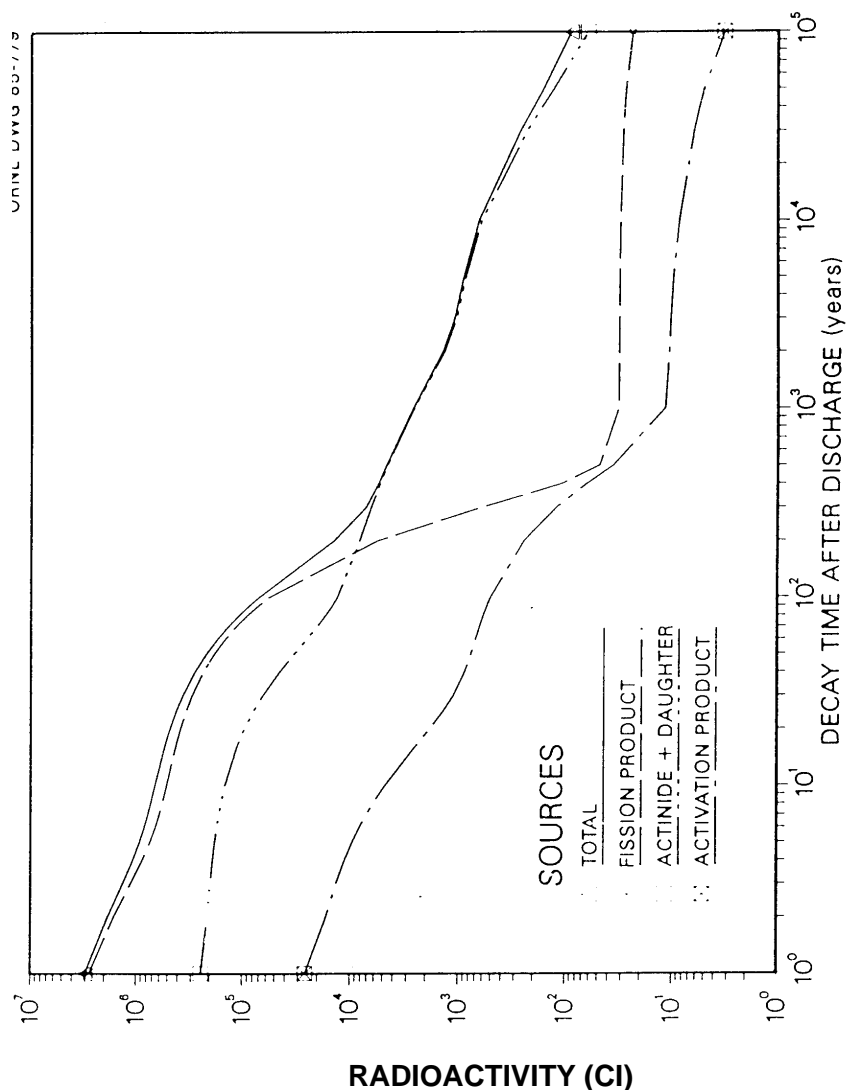
Initial enrichment ~4.1–4.15% U-235 for PWR 60,000 MWd/MT data

Figure 2.1.1.3-1   Radioactivity produced by 1 metric ton of initial heavy metal: PWR; 60,000 MWd (Figure 3.1 from J.W. Roddy, H.C. Claiborne, R.C. Ashline, P.T. Johnson, and B.T. Rhyne, *Physical and Decay Characteristics of Commercial LWR Spent Fuels,* **ORNL/TM-9591/V.1, October, 1985)**
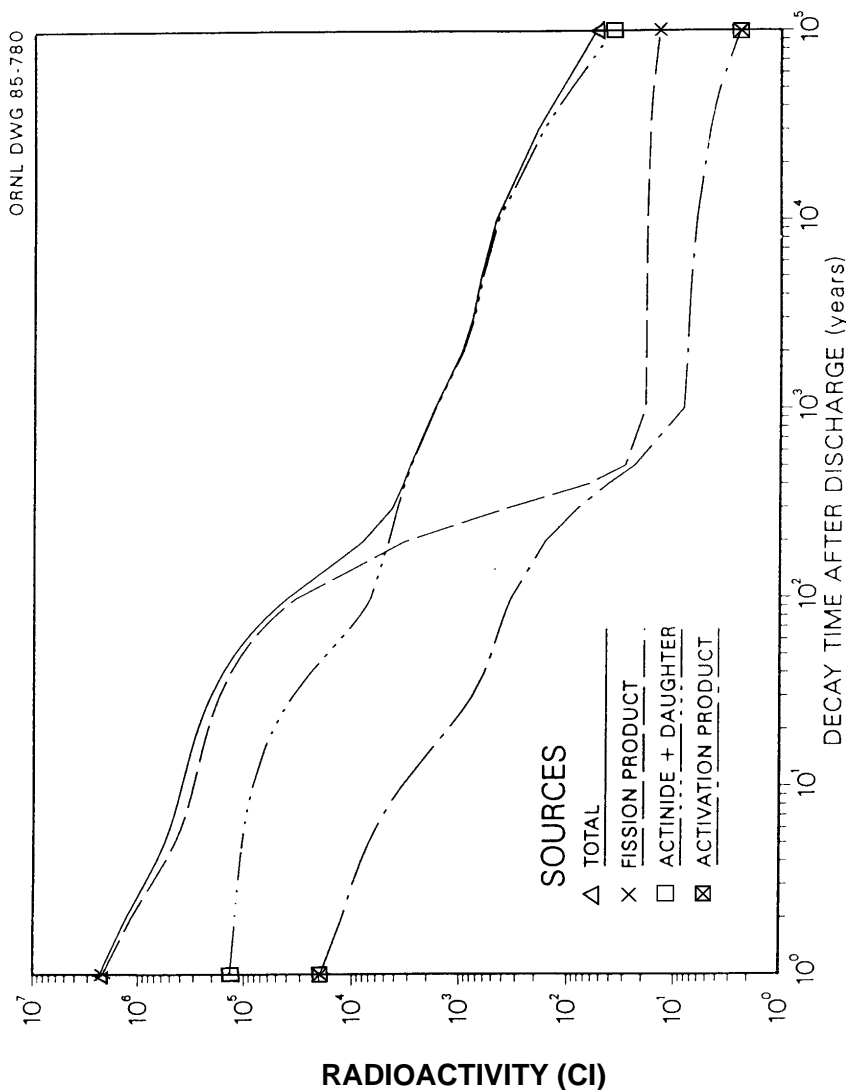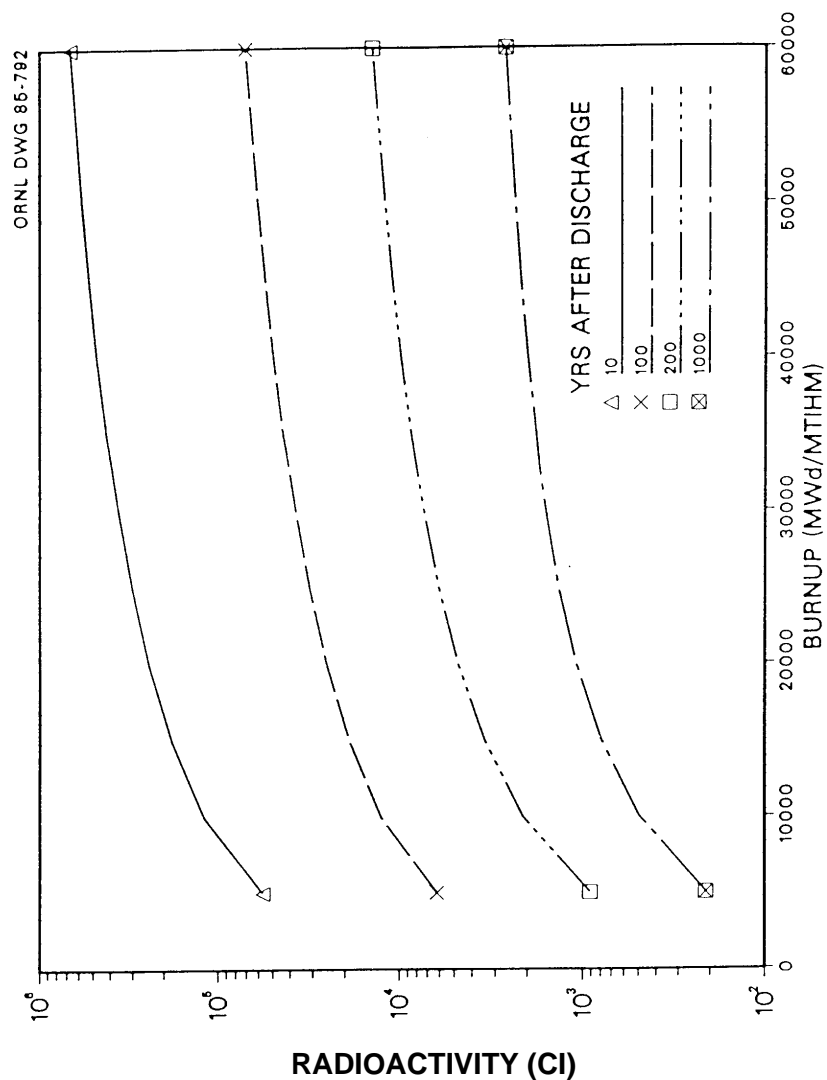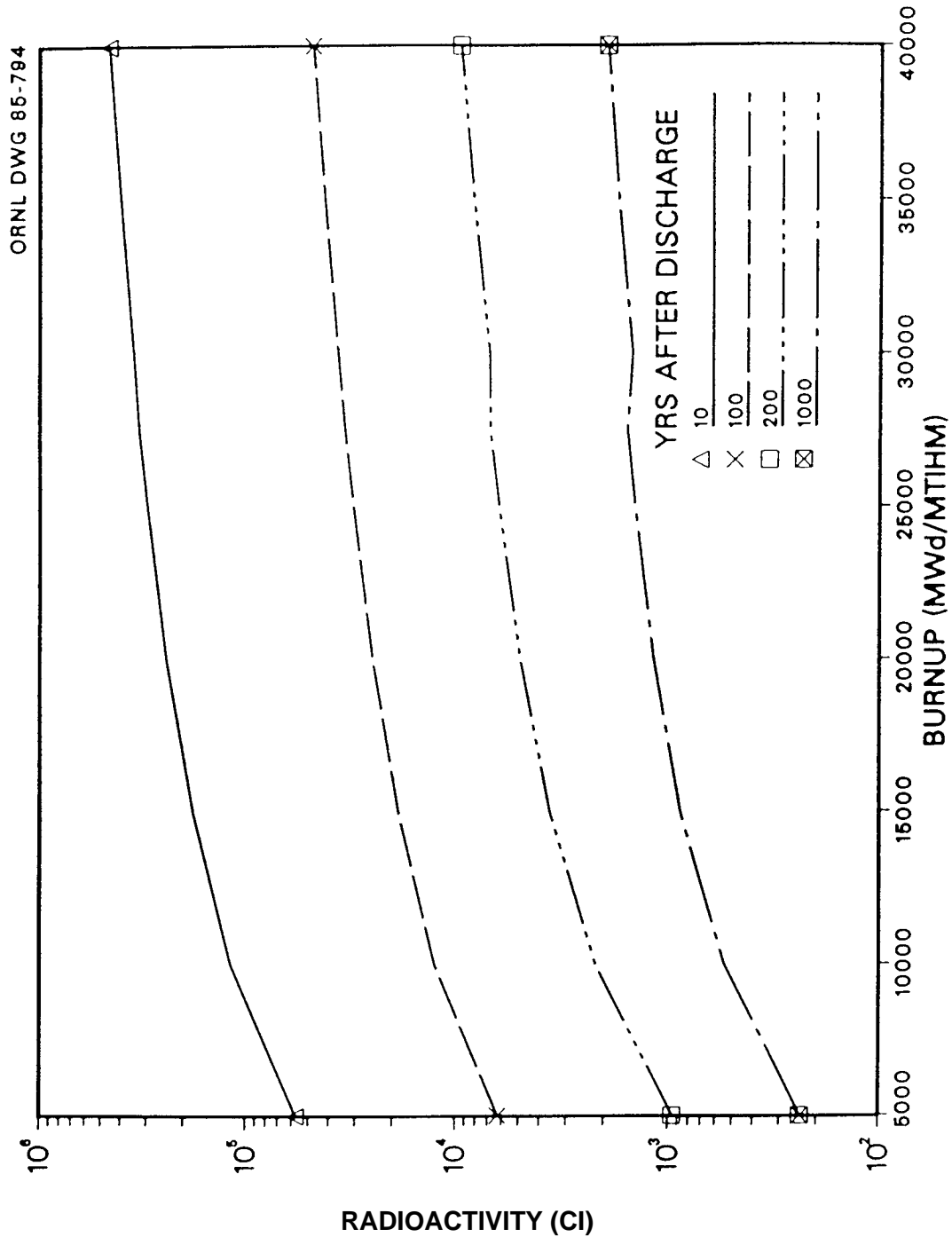
Initial enrichment ~3.2% U-235 for PWR 33,000 MWd/MT data

Figure 2.1.1.3-2 **Radioactivity produced by 1 metric ton of initial heavy metal: PWR; 33,000 MWd (Figure 3.2 from J.W. Roddy, H.C. Claiborne, R.C. Ashline, P.T. Johnson, and B.T. Rhyne,** *Physical and Decay Characteristics of Commercial LWR Spent Fuels,* **ORNL/TM-9591/V.1, October, 1985)**

ORNL DWG 85-781
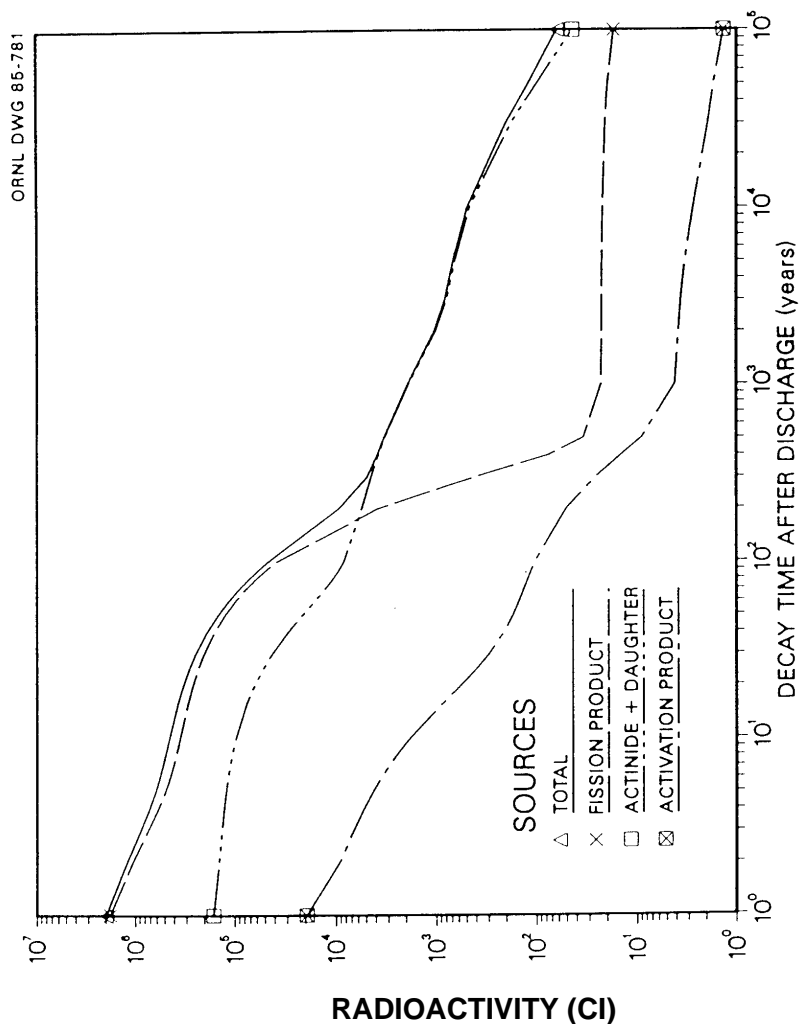
RADIOACTIVITY (CI)

Initial enrichment ~3.5% U-235 for BWR 40,000 MWd/MT data

Figure 2.1.1.3-3   Radioactivity produced by 1 metric ton of initial heavy metal: BWR; 40,000 MWd (Figure 3.3 from J.W. Roddy, H.C. Claiborne, R.C. Ashline, P.T. Johnson, and B.T. Rhyne, *Physical and Decay Characteristics of Commercial LWR Spent Fuels,* **ORNL/TM-9591/V.1, October, 1985)**
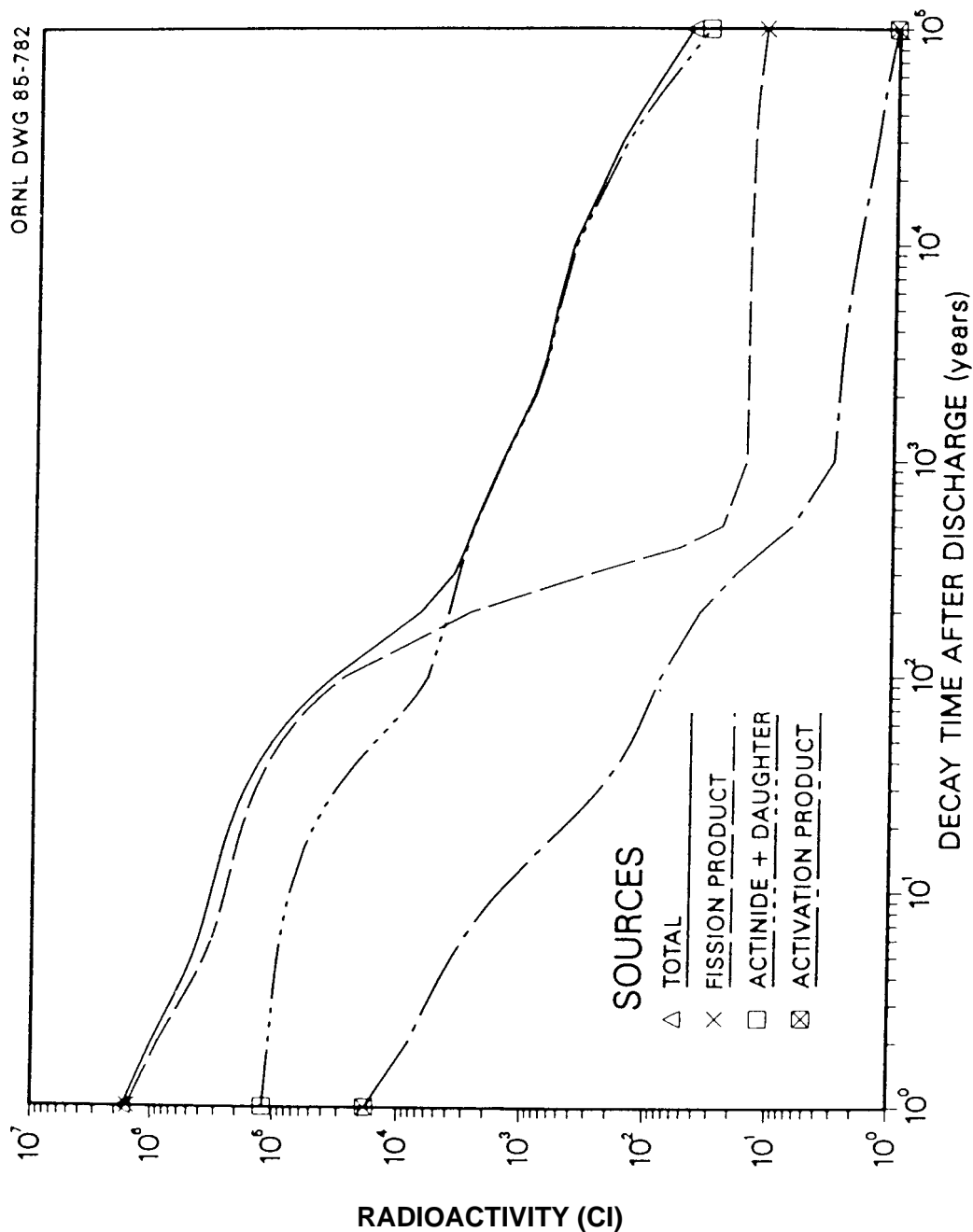
Initial enrichment ~2.75% U-235 for BWR 27,500 MWd/MT data

Figure 2.1.1.3-4   Radioactivity produced by 1 metric ton of initial heavy metal: BWR;
27,500 MWd (Figure 3.4 from J.W. Roddy, H.C. Claiborne, R.C. Ashline,
P.T. Johnson, and B.T. Rhyne, *Physical and Decay Characteristics of
Commercial LWR Spent Fuels*, ORNL/TM-9591/V.1, October, 1985)

Initial enrichment ~4.15% U-235 for PWR 60,000 MWd/MT data

Figure 2.1.1.3-5   Radioactivity produced by 1 metric ton of initial heavy metal for a PWR (Figure 3.14 from J.W. Roddy, H.C. Claiborne, R.C. Ashline, P.T. Johnson, and B.T. Rhyne, *Physical and Decay Characteristics of Commercial LWR Spent Fuels,* ORNL/TM-9591/V.1, October, 1985)

Initial enrichment ~3.5% U-235 for BWR 40,000 MWd/MT data

Figure 2.1.1.3-6   **Radioactivity produced by 1 metric ton of initial heavy metal for a BWR (Figure 3.16 from J.W. Roddy, H.C. Claiborne, R.C. Ashline, P.T. Johnson, and B.T. Rhyne,** *Physical and Decay Characteristics of Commercial LWR Spent Fuels,* **ORNL/TM-9591/V.1, October, 1985)**

Table 2.1.1.3-6 Variation of radioactivity (Ci/MTIHM) for significant actinides as a function of time since discharge from a 60,000-MWd/MTIHM PWR (includes all structural material) (Table 3.9 from J.W. Roddy, H.C. Claiborne, R.C. Ashline, P.T. Johnson, and B.T. Rhyne, *Physical and Decay Characteristics of Commercial LWR Spent Fuels,* ORNL/TM-9591/V.1, October, 1985)

Isotope[a]	Time since discharge (years)					
	1.0E+0	1.0E+1	1.0E+2	1.0E+3	1.0E+4	1.0E+5
Ra-226	—	—	3.32E-5	5.81E-3	2.68E-1	2.12E+0
U-234	—	—	—	4.08E+0	3.99E+0	3.16E+0
Np-237	—	—	—	1.74E+0	2.03E+0	1.97E+0
Np-239	7.22E+1	7.21E+1	7.15E+1	6.57E+1	2.82E+1	—
Pu-238	8.56E+3	8.10E+3	3.98E+3	3.60E+0	—	—
Pu-239	3.67E+2	3.67E+2	3.66E+2	3.59E+2	2.87E+2	2.24E+1
Pu-240	6.78E+2	6.90E+2	7.13E+2	6.49E+2	2.50E+2	—
Pu-241	1.88E+5	1.22E+5	1.61E+3	1.74E+0	—	—
Pu-242	—	—	—	4.53E+0	4.47E+0	3.80E+0
Am-241	5.77E+2	2.76E+3	5.98E+3	1.43E+3	—	—
Am-243	7.22E+1	7.21E+1	7.15E+1	6.57E+1	2.82E+1	—
Cm-242	2.75E+4	1.40E+1	9.25E+0	—	—	—
Cm-243	9.13E+1	7.34E+1	8.22E+0	—	—	—
Cm-244	1.55E+4	1.10E+4	3.51E+2	—	—	—
OTHER	6.47E+1	4.16E+1	3.03E+1	5.84E+0	—	3.07E+1[b]
TOTAL	2.42E+5	1.45E+5	1.32E+4	2.59E+3	6.13E+2	6.20E+1

[a]Nuclides contributing >0.1% are listed.

[b]The following isotopes contribute 2.12 Ci each: Pb-210, Pb-214, Bi-210, Bi-214, Po-210, Po-214, Po-218, and Rn-222. Others contributing 0.64 Ci each include: Pb-209, Bi-213, At-217, Fr-221, Ra-225, Ac-225, and Th-229.

Table 2.1.1.3-7 Variation of radioactivity (Ci/MTIHM) for significant actinides as a function of time since discharge from a 33,000-MWd/MTIHM PWR (includes all structural material) (Table 3.10 from J.W. Roddy, H.C. Claiborne, R.C. Ashline, P.T. Johnson, and B.T. Rhyne, *Physical and Decay Characteristics of Commercial LWR Spent Fuels,* ORNL/TM-9591/V.1, October, 1985)

Isotope[a]	Time since discharge (years)					
	1.0E+0	1.0E+1	1.0E+2	1.0E+3	1.0E+4	1.0E+5
Ra-226	—	—	2.66E-5	3.12E-3	1.34E-1	1.07E+0
U-234	—	—	—	2.03E+0	1.99E+0	1.61E+0
Np-237	—	—	—	9.99E-1	1.18E+0	1.14E+0
Np-239	1.71E+1	1.71E+1	1.69E+1	1.56E+1	6.68E+0	—
Pu-238	2.45E+3	2.33E+3	1.15E+3	1.08E+0	—	—
Pu-239	3.13E+2	3.13E+2	3.12E+2	3.05E+2	2.37E+2	1.80E+1
Pu-240	5.26E+2	5.27E+2	5.26E+2	4.78E+2	1.84E+2	—
Pu-241	1.20E+5	7.76E+4	1.02E+3	—	—	—
Pu-242	—	—	—	1.72E+0	1.69E+0	1.44E+0
Am-241	3.08E+2	1.69E+3	3.75E+3	8.93E+2	—	—
Am-243	1.71E+1	1.71E+1	1.69E+1	1.56E+1	6.68E+0	—
Cm-242	1.04E+4	5.72E+0	3.78E+0	—	—	—
Cm-243	2.06E+1	1.66E+1	1.86E+0	—	—	—
Cm-244	1.86E+3	1.32E+3	4.21E+1	—	—	—
OTHER	2.74E+2	2.60E+1	1.56E+1	2.68E+0	4.30E+0	1.68E+1[b]
TOTAL	1.36E+5	8.39E+4	6.85E+3	1.72E+3	4.44E+2	3.90E+1

[a]Nuclides contributing >0.1% are listed.

[b]The following isotopes contribute 1.07 Ci each: Pb-210, Pb-214, Bi-210, Bi-214, Po-210, Po-214, Po-218, and Rn-222. Others contributing 0.37 Ci each include: Pb-209, Bi-213, At-217, Fr-221, Ra-225, Ac-225, and Th-229.

Table 2.1.1.3-8 Variation of radioactivity (Ci/MTIHM) for significant actinides as a function of time since discharge from a 40,000-MWd/MTIHM BWR (includes all structural material) (Table 3.11 from J.W. Roddy, H.C. Claiborne, R.C. Ashline, P.T. Johnson, and B.T. Rhyne, *Physical and Decay Characteristics of Commercial LWR Spent Fuels,* ORNL/TM-9591/V.1, October, 1985)

Isotope[a]	Time since discharge (years)					
	1.0E+0	1.0E+1	1.0E+2	1.0E+3	1.0E+4	1.0E+5
Ra-226	–	–	2.94E-5	3.85E-3	1.70E-1	1.35E+0
U-234	–	–	–	2.58E+0	2.52E+0	2.02E+0
Np-237	–	–	–	1.21E+0	1.42E+0	1.38E+0
Np-239	2.83E+1	2.83E+1	2.80E+1	2.58E+1	1.11E+1	–
Pu-238	4.06E+3	3.85E+3	1.90E+3	1.82E+0	–	–
Pu-239	3.06E+2	3.06E+2	3.06E+2	2.98E+2	2.34E+2	1.79E+1
Pu-240	5.63E+2	5.65E+2	5.67E+2	5.16E+2	1.98E+2	–
Pu-241	1.37E+5	8.87E+4	1.17E+3	–	–	–
Pu-242	–	–	–	2.37E+0	2.33E+0	1.98E+0
Am-241	4.36E+2	2.02E+3	4.36E+3	1.04E+3	–	–
Am-243	2.83E+1	2.83E+1	2.80E+1	2.58E+1	1.11E+1	–
Cm-242	1.60E+4	1.09E+1	7.22E+0	–	–	–
Cm-243	3.64E+1	2.92E+1	3.28E+0	–	–	–
Cm-244	3.75E+3	2.66E+3	8.48E+1	–	–	–
OTHER	1.08E+2	6.23E+1	1.27E+1	3.56E+0	5.33E+0	2.06E+1[b]
TOTAL	1.62E+5	9.83E+4	8.47E+3	1.92E+3	4.66E+2	4.38E+1

aNuclides contributing >0.1% are listed.

bThe following isotopes contribute 1.35 Ci each: Pb-210, Pb-214, Bi-214, Po-210, Po-214, Po-218, and Rn-222. Others contributing 0.45 Ci each include: Pb-209, Bi-213, At-217, Fr-221, Ra-225, Ac-225, and Th-229.

Table 2.1.1.3-9 Variation of radioactivity (Ci/MTIHM) for significant actinides as a function of time since discharge from a 27,500-MWd/MTIHM PWR (includes all structural material) (Table 3.12 from J.W. Roddy, H.C. Claiborne, R.C. Ashline, P.T. Johnson, and B.T. Rhyne, *Physical and Decay Characteristics of Commercial LWR Spent Fuels,* ORNL/TM-9591/V.1, October, 1985)

Time since discharge (years)

Isotope[a]	1.0E+0	1.0E+1	1.0E+2	1.0E+3	1.0E+4	1.0E+5
Ra-226	–	–	2.32E-5	2.60E-3	1.11E-1	8.86E-1
U-234	–	–	–	1.68E+0	1.64E+0	1.34E+0
Np-237	–	–	–	8.64E-1	1.02E+0	9.95E-1
Np-239	1.29E+1	1.29E+1	1.28E+1	1.18E+1	5.06E+0	–
Pu-238	1.86E+3	1.78E+3	8.77E+2	8.87E-1	–	–
Pu-239	3.00E+2	3.00E+2	3.00E+2	2.92E+2	2.27E+2	1.72E+1
Pu-240	4.78E+2	4.78E+2	4.76E+2	4.33E+2	1.67E+2	–
Pu-241	1.07E+5	6.95E+4	9.13E+2	–	–	–
Pu-242	–	–	–	1.42E+0	1.39E+0	1.19E+0
Am-241	3.15E+2	1.56E+3	3.39E+3	8.07E+2	–	–
Am-243	1.29E+1	1.29E+1	1.28E+1	1.18E+1	5.06E+0	–
Cm-242	9.42E+3	6.87E+0	4.54E+0	–	–	–
Cm-243	1.67E+1	1.34E+1	1.50E+0	–	–	–
Cm-244	1.25E+3	8.86E+2	2.83E+1	–	–	–
OTHER	3.05E+1	2.29E+1	1.61E+1	2.00E+0	3.90E+0	1.44E+1[b]
TOTAL	1.21E+5	7.45E+4	6.03E+3	1.56E+3	4.12E+2	3.51E+1

[a] Nuclides contributing >0.1% are listed.

[b] The following isotopes contribute 0.89 Ci each: Pb-210, Pb-214, Bi-210, Bi-214, Po-210, Po-214, Po-218, and Rn-222. Others contributing 0.33 Ci each include: Pb-209, Bi-213, At-217, Fr-221, Ra-225, Ac-225, and Th-229.

2.1.1.4 Decay Heat vs. Time

Table 2.1.1.4-1   Summary of thermal output (watts/MTIHM) of BWR spent fuel as a function of burnup, initial enrichment, and decay time (Table 4.7 from K.J. Notz, T.D. Welch, R.S. Moore, and W.J. Reich, *Preliminary Waste Form Characteristics,* ORNL-TM-11681 [draft], September 1990)

Initial Enrichment, %	Years After Discharge					
	1	10	100	1000	10k	100k
BURNUP = 7,500 MWd/MTIHM						
0.72	4.081E+03	2.887E+02	1.258E+02	3.404E+01	8.278E+00	5.958E-01
1.05	3.656E+03	2.602E+02	1.002E+02	2.737E+01	7.587E+00	5.676E-01
1.75	3.385E+03	2.475E+02	7.416E+01	1.969E+01	6.561E+00	5.527E-01
BURNUP = 15,000 MWd/MTIHM						
1.09	5.818E+03	5.277E+02	1.954E+02	4.669E+01	1.002E+01	7.455E-01
1.79	5.359E+03	5.055E+02	1.670E+02	3.904E+01	9.321E+00	7.299E-01
2.49	5.046E+03	4.921E+02	1.420E+02	3.212E+01	8.602E+00	7.231E-01
BURNUP = 22,500 MWd/MTIHM						
1.72	7.089E+03	8.003E+02	2.483E+02	5.301E+01	1.142E+01	8.879E-01
2.42	6.606E+03	7.670E+02	2.250E+02	4.696E+01	1.077E+01	8.733E-01
3.12	6.223E+03	7.442E+02	2.012E+02	4.082E+01	1.012E+01	8.640E-01
BURNUP = 30,000 MWd/MTIHM						
2.23	8.221E+03	1.105E+03	3.021E+02	5.843E+01	1.299E+01	1.038E+00
2.93	7.694E+03	1.050E+03	2.812E+02	5.331E+01	1.231E+01	1.019E+00
3.63	7.245E+03	1.011E+03	2.583E+02	4.786E+01	1.164E+01	1.003E+00
BURNUP = 40,000 MWd/MTIHM						
2.74	1.136E+04	1.908E+03	4.644E+02	7.880E+01	1.814E+01	1.512E+00
3.44	1.075E+04	1.784E+03	4.469E+02	7.443E+01	1.733E+01	1.495E+00
4.14	1.018E+04	1.687E+03	4.244E+02	6.963E+01	1.654E+01	1.469E+00
BURNUP = 50,000 MWd/MTIHM						
3.04	1.173E+04	2.227E+03	5.197E+02	8.301E+01	1.984E+01	1.675E+00
3.74	1.113E+04	2.080E+03	5.028E+02	7.874E+01	1.896E+01	1.660E+00
4.44	1.055E+04	1.959E+03	4.802E+02	7.408E+01	1.811E+01	1.632E+00

Table 2.1.1.4-2 Summary of thermal output (watts/MTHIM) of PWR spent fuel as a function of burnup, initial enrichment, and decay time) (Table 4.11 from K.J. Notz, T.D. Welch, R.S. Moore, and W.J. Reich, *Preliminary Waste Form Characteristics*, ORNL-TM-11681 [draft], September 1990)

Initial Enrichment, %	Years After Discharge					
	1	10	100	1000	10k	100k
BURNUP = 10,000 MWd/MTIHM						
0.99	5.071E+03	3.593E+02	1.368E+02	3.605E+01	9.161E+00	6.615E-01
1.69	4.603E+03	3.359E+02	1.035E+02	2.666E+01	8.069E+00	6.355E-01
2.39	4.390E+03	3.268E+02	8.283E+01	2.030E+01	7.111E+00	6.278E-01
BURNUP = 20,000 MWd/MTIHM						
1.74	7.430E+03	6.915E+02	2.143E+02	4.838E+01	1.132E+01	8.504E-01
2.44	6.974E+03	6.707E+02	1.894E+02	4.148E+01	1.058E+01	8.369E-01
3.14	6.634E+03	6.554E+02	1.661E+02	3.502E+01	9.817E+00	8.302E-01
BURNUP = 30,000 MWd/MTIHM						
2.41	9.270E+03	1.068E+03	2.838E+02	5.656E+01	1.347E+01	1.036E+00
3.11	8.728E+03	1.028E+03	2.624E+02	5.095E+01	1.272E+01	1.018E+00
3.81	8.281E+03	9.992E+02	2.398E+02	4.517E+01	1.198E+01	1.005E+00
BURNUP = 40,000 MWd/MTIHM						
3.02	1.117E+04	1.539E+03	3.938E+02	7.196E+01	1.717E+01	1.381E+00
3.72	1.058E+04	1.467E+03	3.720E+02	6.672E+01	1.637E+01	1.358E+00
4.42	1.006E+04	1.412E+03	3.479E+02	6.119E+01	1.559E+01	1.333E+00
BURNUP = 50,000 MWd/MTIHM						
3.56	1.299E+04	2.032E+03	4.778E+02	7.961E+01	2.005E+01	1.622E+00
4.26	1.235E+04	1.926E+03	4.569E+02	7.469E+01	1.915E+01	1.597E+00
4.96	1.175E+04	1.843E+03	4.325E+02	6.941E+01	1.825E+01	1.566E+00
BURNUP = 60,000 MWd/MTIHM						
4.03	1.479E+04	2.582E+03	5.664E+02	8.705E+01	2.342E+01	1.886E+00
4.73	1.411E+04	2.441E+03	5.476E+02	8.232E+01	2.239E+01	1.866E+00
5.43	1.346E+04	2.324E+03	5.233E+02	7.720E+01	2.135E+01	1.831E+00

Table 2.1.1.4-3   Decay heat (watts/MTHIM) by radionuclide (contributing ≥1% of total) for BWR spent fuel as a function of initial enrichment and decay time for a burnup of 30,000 MWd/MTHIM (Table 4.15 from K.J. Notz, T.D. Welch, R.S. Moore, and W.J. Reich, *Preliminary Waste Form Characteristics*, ORNL-TM-11681 [draft], September 1990)

Nuclide	Enrichment					
	2.23%		2.93%		3.63%	
	Decay heat	Percent of Total	Decay heat	Percent of Total	Decay heat	Percent of Total
Decay Time = 1 Year						
Co 60	9.86E+01	1.20	8.58E+01	1.11	7.46E+01	1.03
Sr 90	6.60E+01	0.80	7.29E+01	0.95	7.84E+01	1.08
Y 90	3.16E+02	3.84	3.48E+02	4.52	3.75E+02	5.17
Zr 95	1.08E+02	1.31	1.11E+02	1.44	1.14E+02	1.57
Nb 95	2.30E+02	2.80	2.36E+02	3.07	2.42E+02	3.35
Rh106	2.36E+03	28.69	2.00E+03	26.04	1.70E+03	23.41
Cs134	1.09E+03	13.24	9.88E+02	12.85	8.88E+02	12.26
Cs137	1.01E+02	1.22	1.00E+02	1.31	1.00E+02	1.39
Ba137m	3.38E+02	4.11	3.37E+02	4.39	3.37E+02	4.65
Ce144	2.04E+02	2.48	2.13E+02	2.76	2.20E+02	3.04
Pr144	2.26E+03	27.48	2.35E+03	30.61	2.44E+03	33.69
Pu238	9.84E+01	1.20	8.61E+01	1.12	7.24E+01	1.00
Cm242	4.87E+02	5.93	3.81E+02	4.95	2.88E+02	3.97
Cm244	1.52E+02	1.85	8.09E+01	1.05	4.24E+01	0.58
Decay Time = 10 Years						
Co 60	3.02E+01	2.73	2.63E+01	2.50	2.28E+01	2.26
Sr 90	5.33E+01	4.82	5.88E+01	5.60	6.33E+01	6.26
Y 90	2.55E+02	23.04	2.81E+02	26.77	3.02E+02	29.90
Cs134	5.28E+01	4.78	4.80E+01	4.57	4.31E+01	4.27
Cs137	8.17E+01	7.40	8.16E+01	7.77	8.16E+01	8.07
Ba137m	2.74E+02	24.84	2.74E+02	26.12	2.74E+02	27.11
Eu154	3.88E+01	3.51	3.34E+01	3.18	2.86E+01	2.82
Pu238	9.38E+01	8.49	8.19E+01	7.80	6.87E+01	6.80
Pu240	1.45E+01	1.31	1.36E+01	1.30	1.26E+01	1.25
Am241	6.71E+01	6.08	6.01E+01	5.72	5.23E+01	5.18
Cm244	1.08E+02	9.77	5.73E+01	5.46	3.00E+01	2.97
Decay Time = 100 Years						
Sr 90	6.26E+00	2.07	6.91E+00	2.46	7.43E+00	2.88
Y 90	2.99E+01	9.90	3.30E+01	11.74	3.55E+01	13.75
Cs137	1.02E+01	3.38	1.02E+01	3.63	1.02E+01	3.95
Ba137m	3.43E+01	11.35	3.43E+01	12.19	3.42E+01	13.26
Pu238	4.63E+01	15.34	4.05E+01	14.39	3.40E+01	13.15
Pu239	9.40E+00	3.11	9.24E+00	3.29	9.04E+00	3.50
Pu240	1.46E+01	4.84	1.36E+01	4.85	1.26E+01	4.87
Am241	1.46E+02	48.21	1.30E+02	46.32	1.13E+02	43.85
Cm244	3.45E+00	1.14	1.83E+00	0.65	9.58E-01	0.37

Table 2.1.1.4-3 (continued)

Decay Time = 1000 Years

Pu239	9.18E+00	15.71	9.02E+00	16.92	8.82E+00	18.43
Pu240	1.33E+01	22.77	1.24E+01	23.26	1.14E+01	23.91
Am241	3.47E+01	59.44	3.10E+01	58.21	2.70E+01	56.41
Am243	8.84E-01	1.51	5.66E-01	1.06	3.55E-01	0.74

Decay Time = 10,000 Years

Pu239	7.21E+00	55.50	7.04E+00	57.20	6.86E+00	58.91
Pu240	5.12E+00	39.43	4.78E+00	38.80	4.41E+00	37.84
Am243	3.80E-01	2.92	2.43E-01	1.98	1.52E-01	1.31

Decay Time = 100,000 Years

Bi214	1.22E-02	1.18	1.32E-02	1.30	1.44E-02	1.43
Po210	3.06E-02	2.94	3.31E-02	3.25	3.59E-02	3.58
Po213	2.04E-02	1.97	1.90E-02	1.86	1.71E-02	1.71
Po214	4.43E-02	4.26	4.80E-02	4.71	5.20E-02	5.18
Po218	3.46E-02	3.33	3.74E-02	3.67	4.06E-02	4.05
At217	1.76E-02	1.69	1.64E-02	1.61	1.48E-02	1.47
Rn222	3.16E-02	3.04	3.42E-02	3.36	3.71E-02	3.70
Fr221	1.59E-02	1.53	1.48E-02	1.45	1.34E-02	1.33
Ra226	2.75E-02	2.65	2.98E-02	2.93	3.23E-02	3.22
Ac225	1.44E-02	1.39	1.34E-02	1.31	1.21E-02	1.21
Th229	1.26E-02	1.21	1.17E-02	1.15	1.06E-02	1.06
Th230	2.68E-02	2.58	2.90E-02	2.84	3.14E-02	3.13
U233	1.31E-02	1.27	1.22E-02	1.20	1.10E-02	1.10
U234	4.16E-02	4.01	4.50E-02	4.42	4.87E-02	4.85
U236	8.59E-03	0.83	9.64E-03	0.95	1.05E-02	1.04
Np237	3.86E-02	3.71	3.58E-02	3.52	3.24E-02	3.23
Pu239	5.52E-01	53.15	5.35E-01	52.47	5.18E-01	51.65
Pu242	5.81E-02	5.60	4.34E-02	4.26	3.16E-02	3.15

Table 2.1.1.4-4   Decay heat (watts/MTHIM) by radionuclide (contributing ≥1% of total) for PWR spent fuel as a function of initial enrichment and decay time for a burnup of 40,000 MWd/MTHIM (Table 4.18 from K.J. Notz, T.D. Welch, R.S. Moore, and W.J. Reich, *Preliminary Waste Form Characteristics*, ORNL-TM-11681 [draft], September 1990)

| Nuclide | Enrichment | | | | | |
| | 3.02% | | 3.72% | | 4.42% | |
	Decay heat	Percent of Total	Decay heat	Percent of Total	Decay heat	Percent of Total
			Decay Time = 1 Year			
Co 60	1.44E+02	1.29	1.29E+02	1.22	1.16E+02	1.15
Sr 90	9.01E+01	0.81	9.73E+01	0.92	1.03E+02	1.03
Y 90	4.30E+02	3.85	4.65E+02	4.39	4.94E+02	4.91
Zr 95	1.39E+02	1.24	1.43E+02	1.35	1.46E+02	1.45
Nb 95	2.96E+02	2.65	3.04E+02	2.87	3.12E+02	3.10
Rh106	3.08E+03	27.57	2.70E+03	25.49	2.35E+03	23.38
Cs134	1.68E+03	15.03	1.56E+03	14.72	1.43E+03	14.24
Cs137	1.34E+02	1.20	1.34E+02	1.26	1.34E+02	1.33
Ba137m	4.50E+02	4.03	4.49E+02	4.25	4.49E+02	4.47
Ce144	2.76E+02	2.47	2.85E+02	2.70	2.94E+02	2.92
Pr144	3.05E+03	27.35	3.16E+03	29.86	3.25E+03	32.35
Eu154	1.17E+02	1.05	1.05E+02	1.00	9.39E+01	0.93
Pu238	1.61E+02	1.45	1.47E+02	1.39	1.30E+02	1.29
Cm242	5.82E+02	5.21	4.78E+02	4.52	3.84E+02	3.81
Cm244	2.35E+02	2.10	1.42E+02	1.34	8.50E+01	0.85
			Decay Time = 10 Years			
Co 60	4.41E+01	2.86	3.96E+01	2.70	3.54E+01	2.51
Sr 90	7.27E+01	4.73	7.86E+01	5.35	8.35E+01	5.91
Y 90	3.48E+02	22.58	3.75E+02	25.58	3.99E+02	28.24
Cs134	8.14E+01	5.29	7.56E+01	5.15	6.95E+01	4.92
Cs137	1.09E+02	7.07	1.09E+02	7.41	1.09E+02	7.70
Ba137m	3.65E+02	23.74	3.65E+02	24.89	3.65E+02	25.84
Eu154	5.69E+01	3.69	5.10E+01	3.48	4.54E+01	3.22
Pu238	1.53E+02	9.93	1.39E+02	9.49	1.23E+02	8.71
Pu240	1.92E+01	1.25	1.81E+01	1.24	1.70E+01	1.20
Am241	7.83E+01	5.09	7.15E+01	4.88	6.41E+01	4.54
Cm244	1.66E+02	10.80	1.01E+02	6.87	6.02E+01	4.27
			Decay Time = 100 Years			
Sr 90	8.54E+00	2.17	9.22E+00	2.48	9.80E+00	2.82
Y 90	4.08E+01	10.36	4.40E+01	11.84	4.68E+01	13.46
Cs137	1.36E+01	3.45	1.36E+01	3.65	1.36E+01	3.90
Ba137m	4.57E+01	11.59	4.56E+01	12.27	4.56E+01	13.11
Pu238	7.54E+01	19.14	6.87E+01	18.46	6.06E+01	17.42
Pu239	1.24E+01	3.15	1.22E+01	3.29	1.20E+01	3.45
Pu240	1.94E+01	4.92	1.82E+01	4.89	1.70E+01	4.87
Am241	1.70E+02	43.24	1.55E+02	41.76	1.39E+02	40.00
Cm244	5.30E+00	1.35	3.22E+00	0.86	1.92E+00	0.55

Table 2.1.1.4-4 (continued)

Decay Time = 1000 Years

Pu239	1.21E+01	16.85	1.19E+01	17.88	1.17E+01	19.12
Pu240	1.76E+01	24.49	1.65E+01	24.79	1.54E+01	25.18
Am241	4.06E+01	56.42	3.70E+01	55.51	3.32E+01	54.18
Am243	1.15E+00	1.59	8.10E−01	1.21	5.61E−01	0.92

Decay Time = 10,000 Years

Pu239	9.52E+00	55.46	9.32E+00	56.95	9.11E+00	58.43
Pu240	6.79E+00	39.53	6.37E+00	38.91	5.93E+00	38.06
Am243	4.93E−01	2.87	3.48E−01	2.12	2.41E−01	1.55

Decay Time = 100,000 Years

Bi214	1.77E−02	1.28	1.85E−02	1.36	1.93E−02	1.45
Po210	4.43E−02	3.21	4.63E−02	3.41	4.82E−02	3.62
Po213	2.58E−02	1.87	2.46E−02	1.81	2.29E−02	1.72
Po214	6.42E−02	4.65	6.71E−02	4.94	6.98E−02	5.24
Po218	5.01E−02	3.63	5.24E−02	3.86	5.45E−02	4.09
At217	2.23E−02	1.61	2.12E−02	1.56	1.97E−02	1.48
Rn222	4.59E−02	3.32	4.79E−02	3.53	4.99E−02	3.74
Fr221	2.01E−02	1.46	1.92E−02	1.41	1.78E−02	1.34
Ra226	4.00E−02	2.89	4.17E−02	3.07	4.34E−02	3.26
Ac225	1.82E−02	1.32	1.73E−02	1.28	1.62E−02	1.21
Th229	1.60E−02	1.16	1.52E−02	1.12	1.41E−02	1.06
Th230	3.88E−02	2.81	4.05E−02	2.98	4.22E−02	3.17
U233	1.66E−02	1.20	1.58E−02	1.16	1.47E−02	1.11
U234	5.99E−02	4.34	6.25E−02	4.60	6.50E−02	4.88
U236	1.16E−02	0.84	1.27E−02	0.93	1.36E−02	1.02
Np237	4.88E−02	3.53	4.64E−02	3.42	4.32E−02	3.24
Pu239	7.28E−01	52.73	7.09E−01	52.20	6.89E−01	51.71
Pu242	6.72E−02	4.86	5.34E−02	3.93	4.16E−02	3.12

Table 2.1.1.4-5 **Decay heat distribution parameters for greate than 5-year-old fuel in 1998 (Table 4.20 from K.J. Notz, T.D. Welch, R.S. Moore, and W.J. Reich,** *Preliminary Waste Form Characteristics,* **ORNL-TM-11681 [draft], September 1990)**

| | | Reactor Type | | Aggregate |
		BWR	PWR	
Decay Heat, Watts	Minimum	11	47	11
	MEAN	804	1148	1022
	Maximum	1792	2586	2586
	Standard Deviation	1132	1335	1357

ORNL DWG 85-784
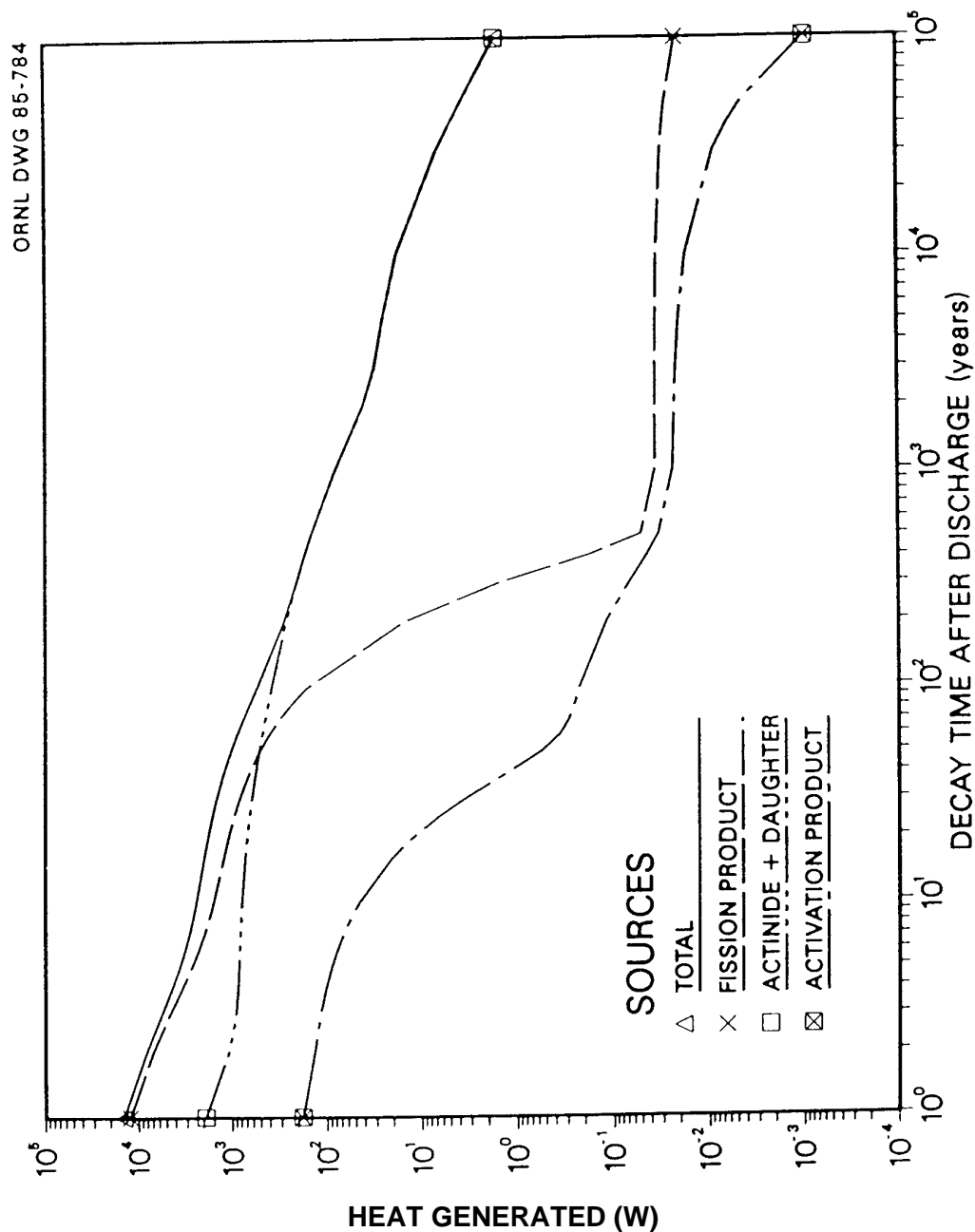
HEAT GENERATED (W)

Initial enrichment ~4.15% U-235 for PWR 60,000 MWd/MT data

Figure 2.1.1.4-1   Heat generated by 1 metric ton of initial heavy metal: PWR; 60,000 MWd
(Figure 3.6 from J.W. Roddy, H.C. Claiborne, R.C. Ashline, P.T. Johnson,
and B.T. Rhyne, *Physical and Decay Characteristics of Commercial LWR*
***Spent Fuels*, ORNL/TM-9591/V.1, October, 1985)**
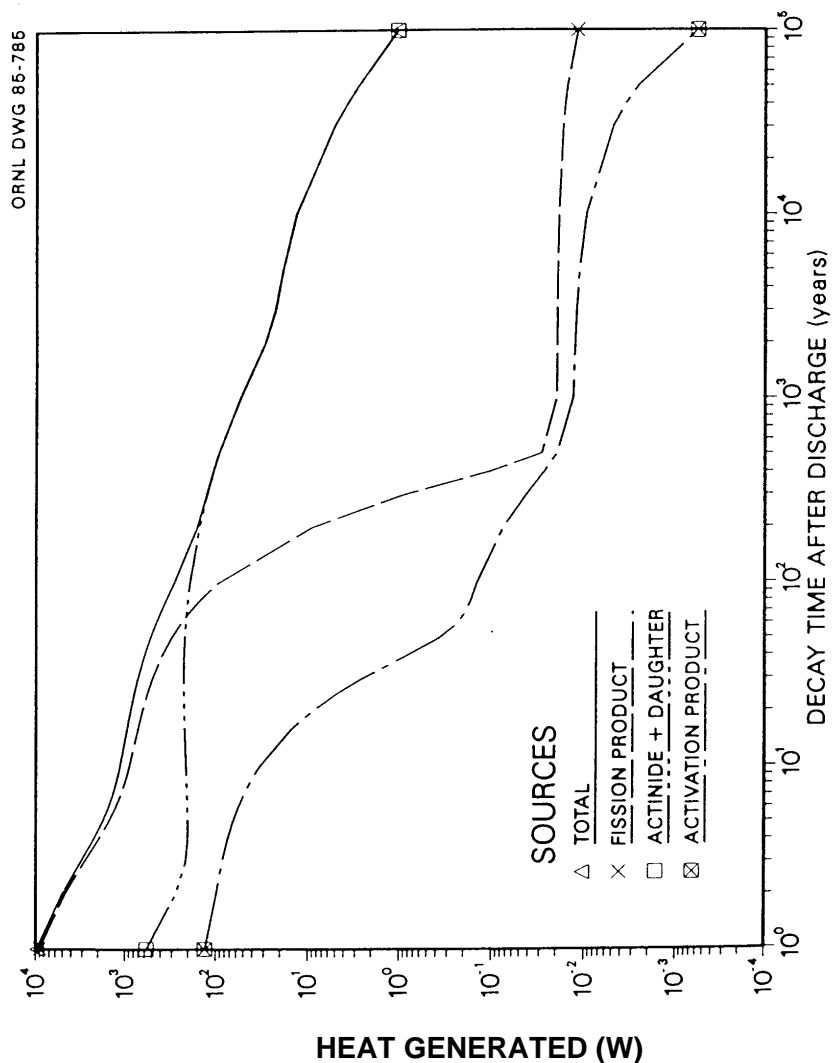
HEAT GENERATED (W)

Initial enrichment ~3.2% U-235 for PWR 33,000 MWd/MT data

Figure 2.1.1.4-2   Heat generated by 1 metric ton of initial heavy metal: PWR; 33,000 MWd
(Figure 3.7 from J.W. Roddy, H.C. Claiborne, R.C. Ashline, P.T. Johnson,
and B.T. Rhyne, *Physical and Decay Characteristics of Commercial LWR*
Spent Fuels, **ORNL/TM-9591/V.1, October, 1985)**
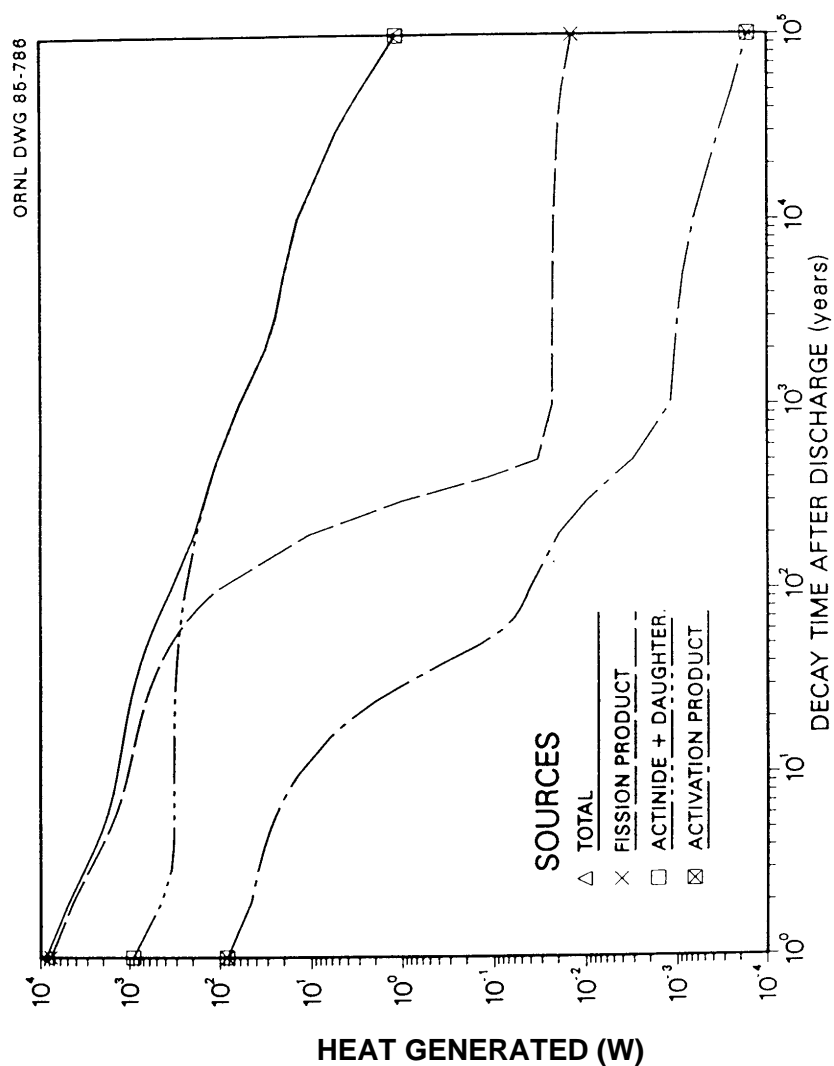
HEAT GENERATED (W)

Initial enrichment ~3.5% U-235 for BWR 40,000 MWd/MT data

Figure 2.1.1.4-3 **Heat generated by 1 metric ton of initial heavy metal: BWR; 40,000 MWd (Figure 3.8 from J.W. Roddy, H.C. Claiborne, R.C. Ashline, P.T. Johnson, and B.T. Rhyne,** *Physical and Decay Characteristics of Commercial LWR Spent Fuels,* **ORNL/TM-9591/V.1, October, 1985)**
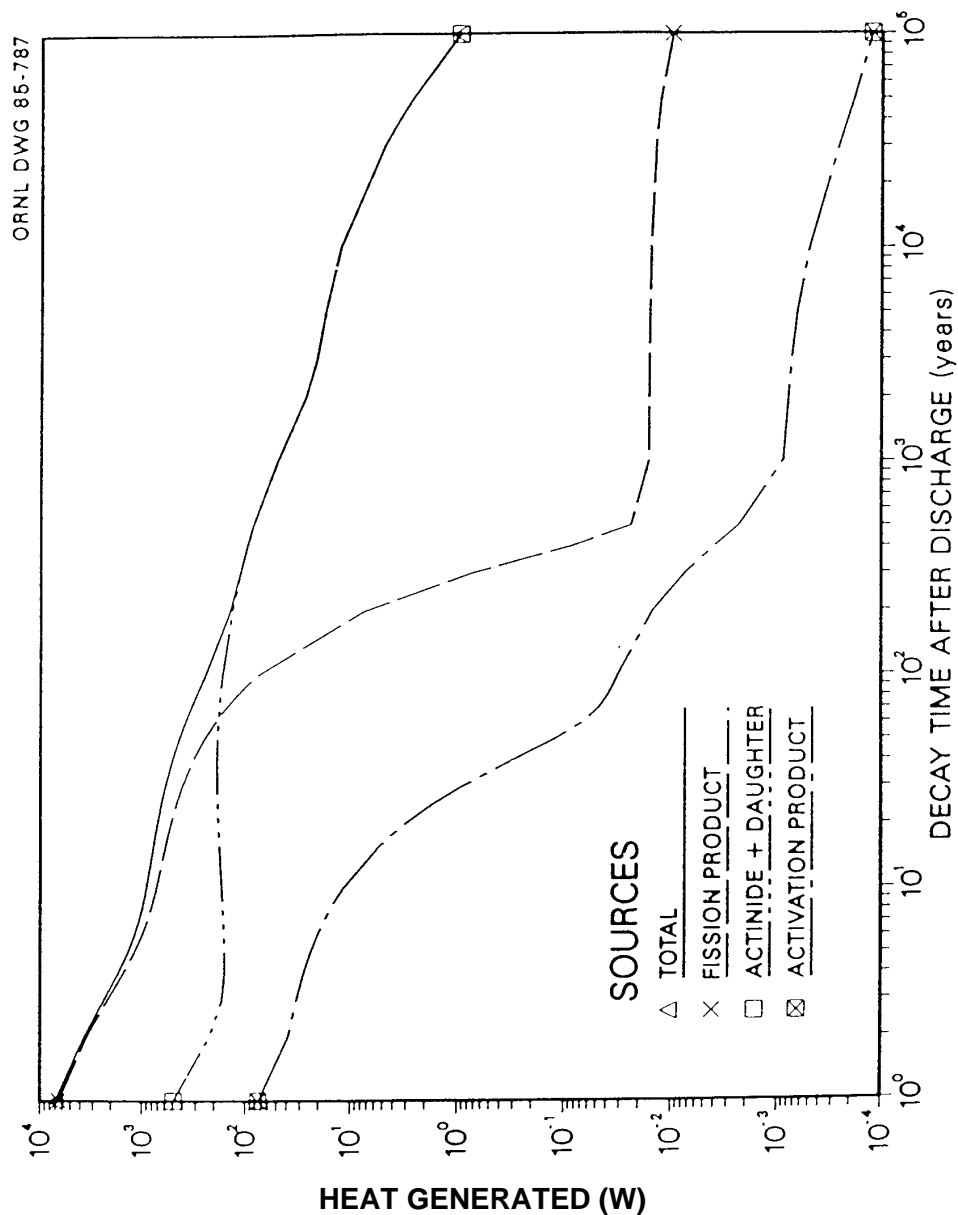
Initial enrichment ~2.75% U-235 for BWR 27,500 MWd/MT data

**Figure 2.1.1.4-4   Heat generated by 1 metric ton of initial heavy metal:
BWR; 27,500 MWd (Figure 3.9 from J.W. Roddy, H.C.
Claiborne, R.C. Ashline, P.T. Johnson, and B.T. Rhyne,
*Physical and Decay Characteristics of Commercial
LWR Spent Fuels*, ORNL/TM-9591/V.1, October, 1985)**
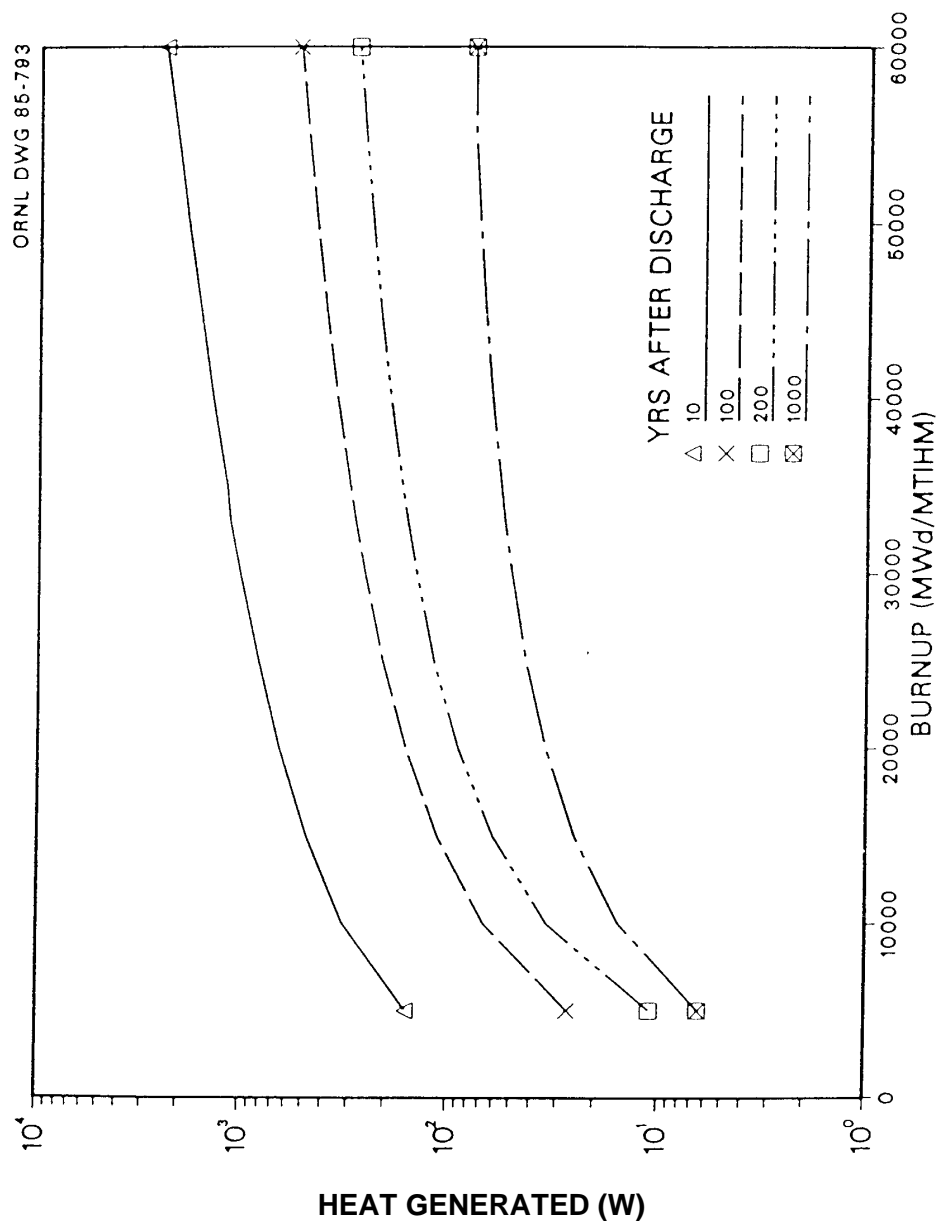
Initial enrichment ~4.15% U-235 for PWR 60,000 MWd/MT data

Figure 2.1.1.4-5   Heat generated by 1 metric ton of initial heavy metal for a PWR (Figure 3.15 from J.W. Roddy, H.C. Claiborne, R.C. Ashline, P.T. Johnson, and B.T. Rhyne, *Physical and Decay Characteristics of Commercial LWR Spent Fuels,* ORNL/TM-9591/V.1, October, 1985)
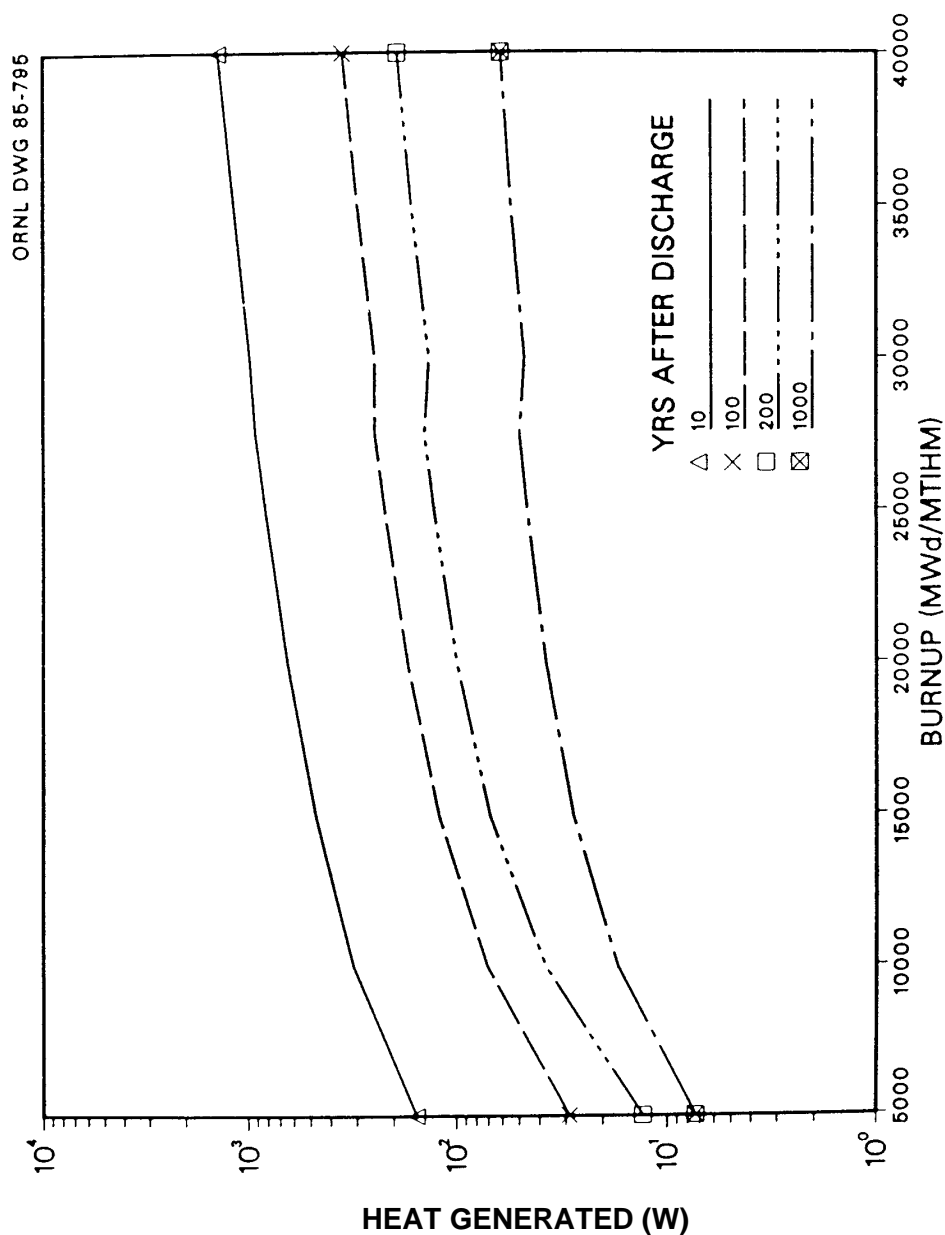
Initial enrichment ~3.5% U-235 for BWR 40,000 MWd/MT data

Figure 2.1.1.4-6   Heat generated by 1 metric ton of initial heavy metal for a BWR (Figure 3.17 from J.W. Roddy, H.C. Claiborne, R.C. Ashline, P.T. Johnson, and B.T. Rhyne, *Physical and Decay Characteristics of Commercial LWR Spent Fuels*, ORNL/TM-9591/V.1, October, 1985)

Table 2.1.1.4-6   Variation in thermal power (W/MTIHM) for significant nuclides as a function of time since discharge from a 60,000-MWd/MTIHM PWR (includes all structural material) (Table 3.13 from J.W. Roddy, H.C. Claiborne, R.C. Ashline, P.T. Johnson, and B.T. Rhyne, *Physical and Decay Characteristics of Commercial LWR Spent Fuels,* ORNL/TM-9591/V.1, October, 1985)

Isotope[a]	Time since discharge (years)					
	1.0E+0	1.0E+1	1.0E+2	1.0E+3	1.0E+4	1.0E+5
Co-60[b]	1.47E+2	4.50E+1	–	–	–	–
Kr-85	2.00E+1	1.12E+1	–	–	–	–
Sr-89	1.57E+1	–	–	–	–	–
Sr-90	1.32E+2	1.06E+2	–	–	–	–
Y-90	6.29E+2	5.08E+2	5.96E+1	–	–	–
Y-91	4.38E+1	–	–	–	–	–
Zr-95[c]	1.48E+2	–	–	–	–	–
Nb-95[c]	3.16E+2	–	–	–	–	–
Ru-106	2.28E+1	–	–	–	–	–
Rh-106	3.68E+3	7.56E+0	–	–	–	–
Ag-110m	6.21E+1	–	–	–	–	–
Sb-125[c]	5.63E+1	5.34E+0	–	–	–	–
Cs-134	2.66E+3	1.29E+2	–	–	–	–
Cs-137	1.97E+2	1.60E+2	2.00E+1	–	–	–
Ba-137m	6.60E+2	5.36E+2	6.71E+1	–	–	–
Ce-144	2.84E+2	–	–	–	–	–
Pr-144	3.15E+3	–	–	–	–	–
Pm-147	3.37E+1	3.12E+0	–	–	–	–
Eu-154[c]	2.09E+2	1.01E+2	–	–	–	–
U-233	–	–	–	–	–	2.05E-2
U-234	–	–	–	1.18E-1	1.15E-1	9.10E-2
U-236	–	–	–	–	–	1.55E-2
Np-237	–	–	–	–	–	6.02E-2
Pu-238	2.84E+2	2.68E+2	1.32E+2	–	–	–
Pu-239	1.13E+1	1.13E+1	1.13E+1	1.10E+1	8.84E+0	6.90E-1
Pu-240	2.11E+1	2.15E+1	2.22E+1	2.02E+1	7.78E+0	–
Pu-241	5.84E+0	3.79E+0	–	–	–	–
Pu-242	–	–	–	1.34E-1	1.32E-1	1.12E-1
Am-241	1.92E+1	9.16E+1	1.98E+2	4.74E+1	–	–
Am-243	2.32E+0	2.32E+0	2.30E+0	2.11E+0	9.07E-1	–
Cm-242	1.01E+3	–	–	–	–	–
Cm-243	3.35E+0	2.69E+0	–	–	–	–
Cm-244	5.44E+2	3.85E+2	1.23E+1	–	–	–
OTHER	7.25E+1	7.00E+0	8.50E+0	5.18E-1	3.42E-1	6.44E-1
SUBTOTAL						
A.P.[d]	1.80E+2	4.61E+1	2.23E-1	2.35E-2	1.69E-2	9.54E-4
F.P.[e]	1.23E+4	1.57E+3	1.59E+2	3.62E-2	3.43E-2	2.10E-2
A.+D.[f]	1.90E+3	7.88E+2	3.80E+2	8.14E+1	1.81E+1	1.61E+0
TOTAL	1.44E+4	2.41E+3	5.39E+2	8.15E+1	1.81E+1	1.63E+0

[a] Nuclides contributing >0.1% of total are listed.
[b] Only activation products contribute to this nuclide.
[c] Both activation and fission products contribute to this nuclide.
[d] A.P. = Activation products.
[e] F.P. = Fission products.
[f] A.+D. = Actinides plus daughters.

Table 2.1.1.4-7 Variation in thermal power (W/MTIHM) for significant nuclides as a function of time since discharge from a 33,000-MWd/MTIHM PWR (includes all structural material) (Table 3.14 from J.W. Roddy, H.C. Claiborne, R.C. Ashline, P.T. Johnson, and B.T. Rhyne, *Physical and Decay Characteristics of Commercial LWR Spent Fuels,* ORNL/TM-9591/V.1, October, 1985)

Isotope[a]	Time since discharge (years)					
	1.0E+0	1.0E+1	1.0E+2	1.0E+3	1.0E+4	1.0E+5
Co-60[b]	1.07E+2	3.28E+1	–	–	–	–
Kr-85	1.30E+1	7.27E+1	–	–	–	–
Sr-89	1.98E+1	–	–	–	–	–
Sr-90	8.22E+1	6.63E+1	7.79E+0	–	–	–
Y-90	3.93E+2	3.17E+2	3.72E+1	–	–	–
Y-91	5.34E+1	–	–	–	–	–
Zr-95[c]	1.59E+2	–	–	–	–	–
Nb-95[c]	3.39E+2	–	–	–	–	–
Ru-106	1.60E+1	–	–	–	–	–
Rh-106	2.57E+3	5.28E+0	–	–	–	–
Ag-110m	2.54E+1	–	–	–	–	–
Sb-125[c]	3.82E+1	4.02E+0	–	–	–	–
Cs-134	1.10E+3	5.31E+1	–	–	–	–
Cs-137	1.12E+2	9.08E+1	1.14E+1	–	–	–
Ba-137m	3.76E+2	3.05E+2	3.81E+1	–	–	–
Ce-144	2.99E+2	–	–	–	–	–
Pr-144	3.31E+3	–	–	–	–	–
Pm-147	3.67E+1	3.40E+0	–	–	–	–
Eu-154[c]	8.67E+1	4.20E+1	–	–	–	–
U-233	–	–	–	–	–	1.19E-2
U-234	–	–	–	5.84E-2	5.72E-2	4.64E-2
U-236	–	–	–	–	–	1.09E-2
Np-237	–	–	–	–	–	3.49E-2
Pu-238	8.13E+1	7.74E+1	3.71E+1	–	–	–
Pu-239	9.65E+0	9.64E+0	9.62E+0	9.39E+0	7.32E+0	5.54E-1
Pu-240	1.64E+1	1.64E+1	1.64E+1	1.49E+1	5.73E+0	–
Pu-241	3.71E+0	2.41E+0	–	–	–	–
Pu-242	–	–	–	5.08E-2	5.00E-2	4.25E-2
Am-241	1.02E+1	5.63E+1	1.24E+2	2.97E+1	–	–
Am-243	5.49E-1	5.49E-1	5.44E-1	5.00E-1	2.15E-1	–
Cm-242	3.83E+2	–	–	–	–	–
Cm-243	7.56E-1	6.08E-1	–	–	–	–
Cm-244	6.51E+1	4.62E+1	1.47E+0	–	–	–
OTHER	4.96E+1	4.70E+0	1.60E+0	1.65E-1	1.40E-1	3.57E-1
SUBTOTAL						
A.P.[d]	1.30E+2	3.35E+1	1.46E-1	1.34E-2	9.66E-3	5.64E-4
F.P.[e]	9.04E+3	8.96E+2	9.46E+1	2.01E-2	1.91E-2	1.18E-2
A.+D.[f]	5.71E+2	2.10E+2	1.91E+2	5.47E+1	1.35E+1	1.03E+0
TOTAL	9.74E+3	1.14E+3	2.86E+2	5.47E+1	1.35E+1	1.05E+0

[a] Nuclides contributing >0.1% of total are listed.
[b] Only activation products contribute to this nuclide.
[c] Both activation and fission products contribute to this nuclide.
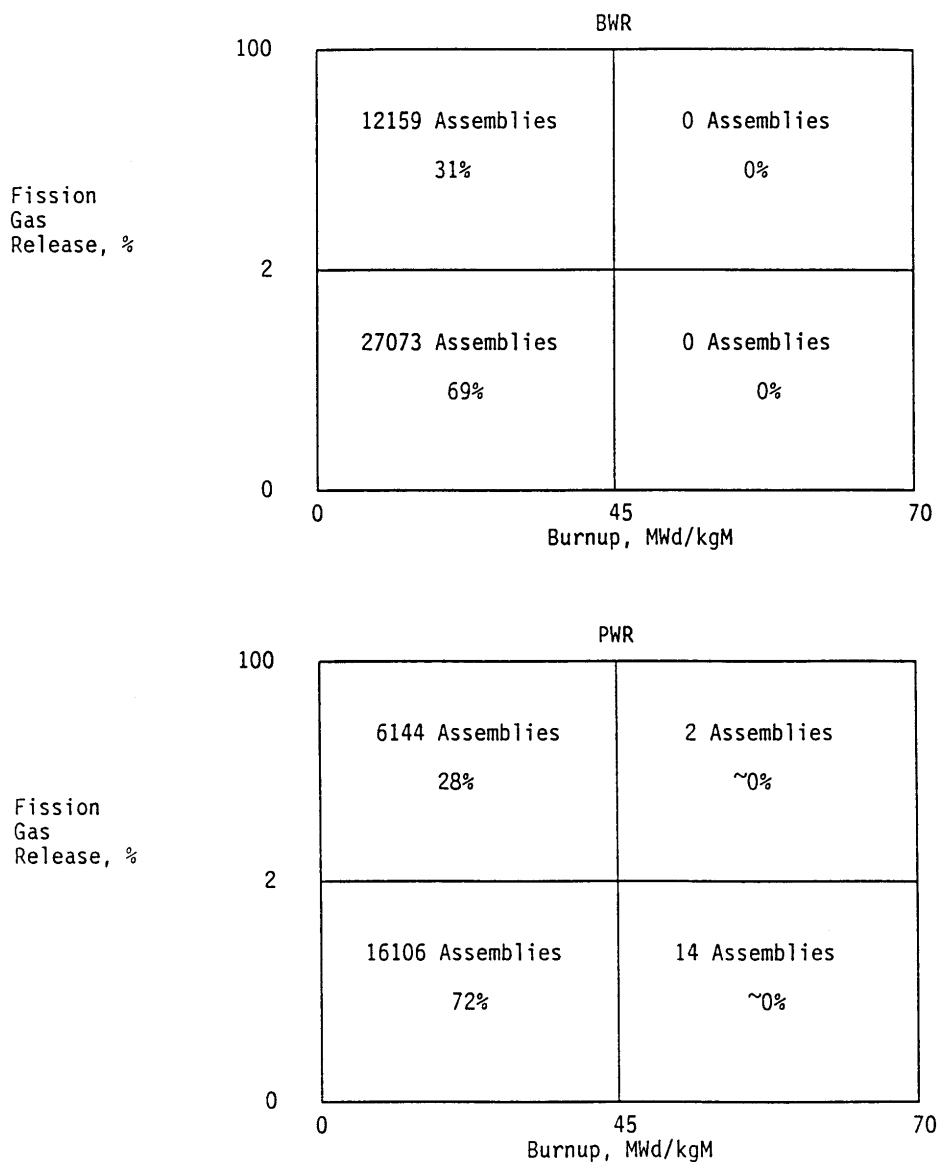[d] A.P. = Activation products.
[e] F.P. = Fission products.
[f] A.+D. = Actinides plus daughters.

Table 2.1.1.4-8   Variation in thermal power (W/MTIHM) for significant nuclides as a function of time since discharge from a 40,000-MWd/MTIHM BWR (includes all structural material) (Table 3.15 from J.W. Roddy, H.C. Claiborne, R.C. Ashline, P.T. Johnson, and B.T. Rhyne, *Physical and Decay Characteristics of Commercial LWR Spent Fuels,* ORNL/TM-9591/V.1, October, 1985)

Isotope[a]	Time since discharge (years)					
	1.0E+0	1.0E+1	1.0E+2	1.0E+3	1.0E+4	1.0E+5
Co-60[b]	4.04E+1	1.24E+1	–	–	–	–
Kr-85	1.43E+1	7.97E+0	–	–	–	–
Sr-89	1.24E+1	–	–	–	–	–
Sr-90	9.51E+1	7.68E+1	9.01E+0	–	–	–
Y-90	4.54E+2	3.67E+2	4.30E+1	–	–	–
Y-91	3.38E+1	–	–	–	–	–
Zr-95[c]	1.10E+2	–	–	–	–	–
Nb-95[c]	2.35E+2	–	–	–	–	–
Ru-106	1.35E+1	–	–	–	–	–
Rh-106	2.18E+3	4.48E+0	–	–	–	–
Ag-110m	2.72E+1	–	–	–	–	–
Sb-125[c]	3.90E+1	4.10E+0	–	–	–	–
Cs-134	1.29E+3	6.26E+1	–	–	–	–
Cs-137	1.32E+2	1.07E+2	1.34E+1	–	–	–
Ba-137m	4.42E+2	3.59E+2	4.49E+1	–	–	–
Ce-144	2.03E+2	–	–	–	–	–
Pr-144	2.25E+3	–	–	–	–	–
Pm-147	3.17E+1	2.94E+0	–	–	–	–
Eu-154[c]	1.17E+2	5.64E+1	–	–	–	–
U-233	–	–	–	–	–	1.44E-2
U-234	–	–	–	7.43E-2	7.26E-2	5.83E-2
U-236	–	–	–	–	–	1.23E-2
Np-237	–	–	–	–	–	4.22E-2
Pu-238	1.34E+2	1.28E+2	6.29E+1	–	–	–
Pu-239	9.44E+0	9.44E+0	9.41E+0	9.20E+0	7.22E+0	5.51E-1
Pu-240	1.75E+1	1.76E+1	1.76E+1	1.60E+1	6.18E+0	–
Pu-241	4.24E+0	2.75E+0	–	–	–	–
Pu-242	–	–	–	6.99E-2	6.88E-2	5.85E-2
Am-241	1.45E+1	6.71E+1	1.45E+2	3.45E+1	–	–
Am-243	9.10E-1	9.09E-1	9.02E-1	8.28E-1	3.56E-1	–
Cm-242	5.91E+2	–	–	–	–	–
Cm-243	1.34E+0	1.07E+0	–	–	–	–
Cm-244	1.31E+2	9.30E+1	2.97E+0	–	–	–
OTHER	1.24E+1	7.85E+0	8.00E-1	2.96E-1	1.75E-1	4.25E-1
SUBTOTAL						
A.P.[d]	8.28E+1	1.40E+1	4.18E-2	1.20E-3	6.64E-4	1.64E-4
F.P.[e]	7.66E+3	1.05E+3	1.10E+2	2.34E-2	2.22E-2	1.38E-2
A.+D.[f]	9.05E+2	3.20E+2	2.39E+2	6.09E+1	1.40E+1	1.15E+0
TOTAL	8.65E+3	1.38E+3	3.50E+2	6.09E+1	1.41E+1	1.16E+0

[a]Nuclides contributing >0.1% of total are listed.
[b]Only activation products contribute to this nuclide.
[c]Both activation and fission products contribute to this nuclide.
[d]A.P. = Activation products.
[e]F.P. = Fission products.
[f]A.+D. = Actinides plus daughters.

Table 2.1.1.4-9   Variation in thermal power (W/MTIHM) for significant nuclides as a function of time since discharge from a 27,500-MWd/MTIHM BWR (includes all structural material) (Table 3.16 from J.W. Roddy, H.C. Claiborne, R.C. Ashline, P.T. Johnson, and B.T. Rhyne, *Physical and Decay Characteristics of Commercial LWR Spent Fuels*, ORNL/TM-9591/V.1, October, 1985)

Isotope[a]	Time since discharge (years)					
	1.0E+0	1.0E+1	1.0E+2	1.0E+3	1.0E+4	1.0E+5
Co-60[b]	3.36E+1	1.03E+1	–	–	–	–
Kr-85	1.05E+1	5.88E+0	–	–	–	–
Sr-89	1.35E+1	–	–	–	–	–
Sr-90	6.76E+1	5.45E+1	6.40E+0	–	–	–
Y-90	3.23E+2	2.60E+2	3.06E+1	–	–	–
Y-91	3.63E+1	–	–	–	–	–
Zr-95[c]	1.14E+2	–	–	–	–	–
Nb-95[c]	2.42E+2	–	–	–	–	–
Ru-106	1.17E+1	–	–	–	–	–
Rh-106	1.89E+3	3.87E+0	–	–	–	–
Ag-110m	1.76E+1	–	–	–	–	–
Sb-125[c]	3.28E+1	3.45E+0	–	–	–	–
Cs-134	7.78E+2	3.78E+2	–	–	–	–
Cs-137	9.25E+1	7.52E+1	9.40E+0	–	–	–
Ba-137m	3.11E+2	2.52E+2	3.16E+1	–	–	–
Ce-144	2.06E+2	–	–	–	–	–
Pr-144	2.28E+3	–	–	–	–	–
Pm-147	3.12E+1	2.89E+0	–	–	–	–
Eu-154[c]	6.83E+1	3.31E+1	–	–	–	–
U-233	–	–	–	–	–	1.04E-2
U-234	–	–	–	4.83E-2	4.73E-2	3.87E-2
U-236	–	–	–	–	–	9.42E-3
Np-237	–	–	–	–	–	3.04E-2
Pu-238	6.18E+1	5.90E+1	2.91E+1	–	–	–
Pu-239	9.26E+0	9.26E+0	9.23E+0	9.01E+0	7.00E+0	5.29E-1
Pu-240	1.49E+1	1.49E+1	1.48E+1	1.35E+1	5.19E+0	–
Pu-241	3.32E+0	2.15E+0	–	–	–	–
Pu-242	–	–	–	4.18E-2	4.12E-2	3.50E-2
Am-241	1.05E+1	5.17E+1	1.12E+2	2.68E+1	–	–
Am-243	4.16E-1	4.15E-1	4.12E-1	3.78E-1	1.62E-1	–
Cm-242	3.47E+2	–	–	–	–	–
Cm-243	6.12E-1	4.92E-1	–	–	–	–
Cm-244	4.37E+1	3.10E+1	9.89E-1	–	–	–
OTHER	2.47E+1	6.32E+0	6.00E-1	1.25E-1	1.14E-1	2.92E-1
SUBTOTAL						
A.P.[d]	7.42E+2	1.19E+1	3.18E-2	8.92E-4	5.02E-4	1.24E-4
F.P.[e]	6.50E+3	7.30E+2	7.80E+1	1.65E-2	1.57E-2	9.78E-3
A.+D.[f]	4.92E+2	1.69E+2	1.68E+2	4.99E+1	1.25E+1	9.35E-1
TOTAL	7.07E+3	9.11E+2	2.46E+2	4.99E+1	1.26E+1	9.45E-1

[a] Nuclides contributing >0.1% of total are listed.
[b] Only activation products contribute to this nuclide.
[c] Both activation and fission products contribute to this nuclide.
[d] A.P. = Activation products.
[e] F.P. = Fission products.
[f] A.+D. = Actinides plus daughters.

2.1.1.5 Fission Gas Release Distribution
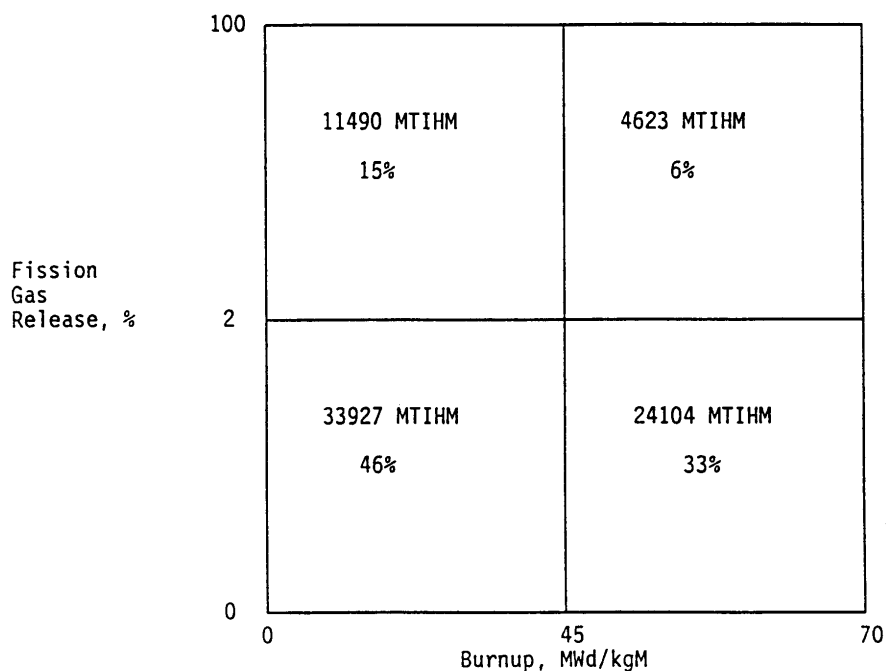
Figure 2.1.1.5-1 **Burnup and fission gas release distribution of spent fuel inventory projected through 2020 (Figure 2.1 from M.E. Cunningham, et al.,** *The Impact of Burnup and Fission Gas Release Distributions of the U.S. LWR Spent Fuel Inventory on the Selection of Spent Fuel Test Materials for the U.S. Geological Repository Project,* **Pacific Northwest Laboratory Report [Draft] 1991)**

BWR

```
      100 ┌─────────────────────┬─────────────────────┐
          │                     │                     │
          │   12159 Assemblies  │    0 Assemblies     │
 Fission  │        31%          │        0%           │
 Gas      │                     │                     │
 Release, %  2 ├─────────────────────┼─────────────────────┤
          │                     │                     │
          │   27073 Assemblies  │    0 Assemblies     │
          │        69%          │        0%           │
          │                     │                     │
        0 └─────────────────────┴─────────────────────┘
          0                     45                    70
                    Burnup, MWd/kgM
```

PWR

```
      100 ┌─────────────────────┬─────────────────────┐
          │                     │                     │
          │    6144 Assemblies  │    2 Assemblies     │
 Fission  │        28%          │       ~0%           │
 Gas      │                     │                     │
 Release, %  2 ├─────────────────────┼─────────────────────┤
          │                     │                     │
          │   16106 Assemblies  │   14 Assemblies     │
          │        72%          │       ~0%           │
          │                     │                     │
        0 └─────────────────────┴─────────────────────┘
          0                     45                    70
                    Burnup, MWd/kgM
```

Figure 2.1.1.5-2   Distribution summary for spent fuel discharged through 1987 (Figure 7.3 from M.E. Cunningham, et al., *The Impact of Burnup and Fission Gas Release Distributions of the U.S. LWR Spent Fuel Inventory on the Selection of Spent Fuel Test Materials for the U.S. Geological Repository Project,* Pacific Northwest Laboratory Report [Draft] 1991)

BWR

Fission
Gas
Release, %

100

6032 MTIHM 23%	836 MTIHM 3%
17025 MTIHM 64%	2648 MTIHM 10%

2

0

0   45   70

Burnup, MWd/kgM

PWR

Fission
Gas
Release, %

100

5458 MTIHM 11%	3787 MTIHM 8%
16902 MTIHM 36%	21456 MTIHM 45%

2

0

0   45   70
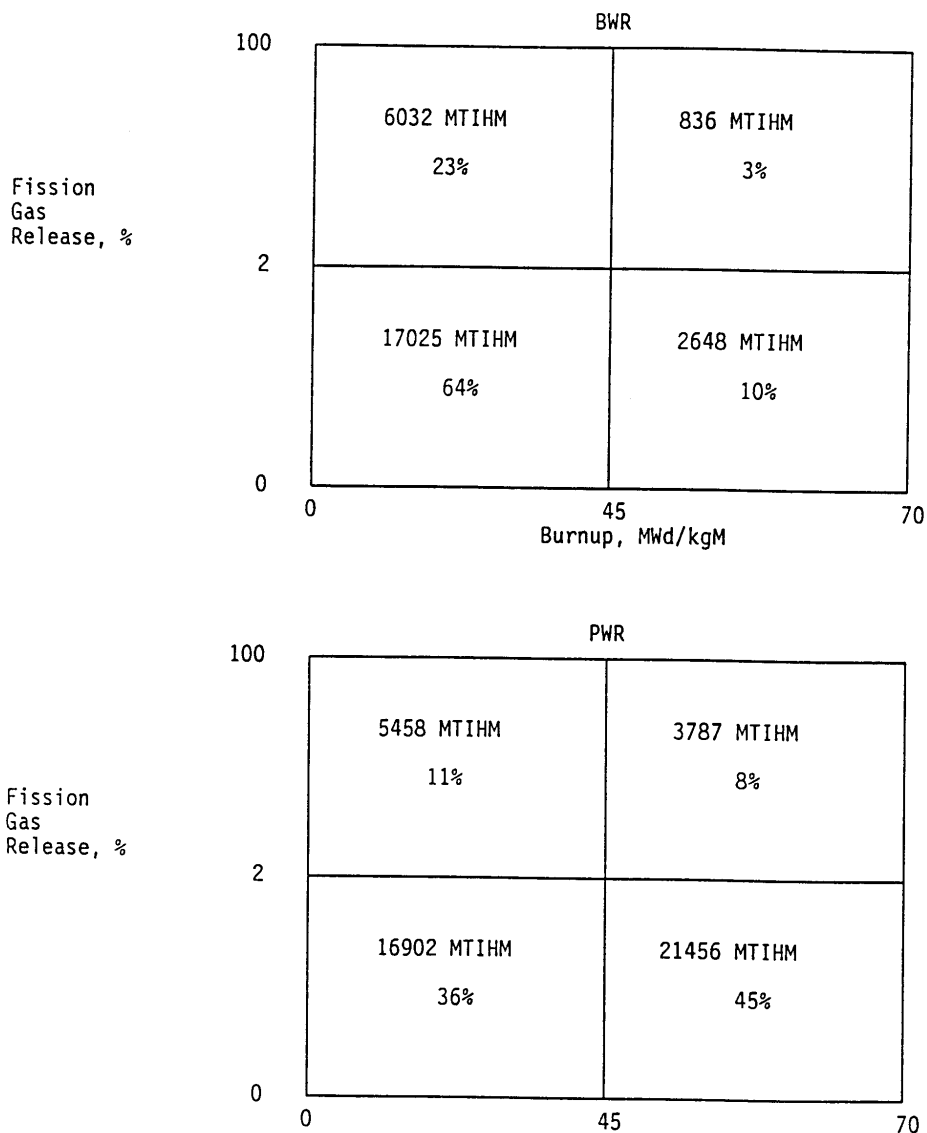
Figure 2.1.1.5-3   Distribution summary for projected spent-fuel inventory (Figure 7.4 from M.E. Cunningham, et al., *The Impact of Burnup and Fission Gas Release Distributions of the U.S. LWR Spent Fuel Inventory on the Selection of Spent Fuel Test Materials for the U.S. Geological Repository Project,* Pacific Northwest Laboratory Report [Draft] 1991)
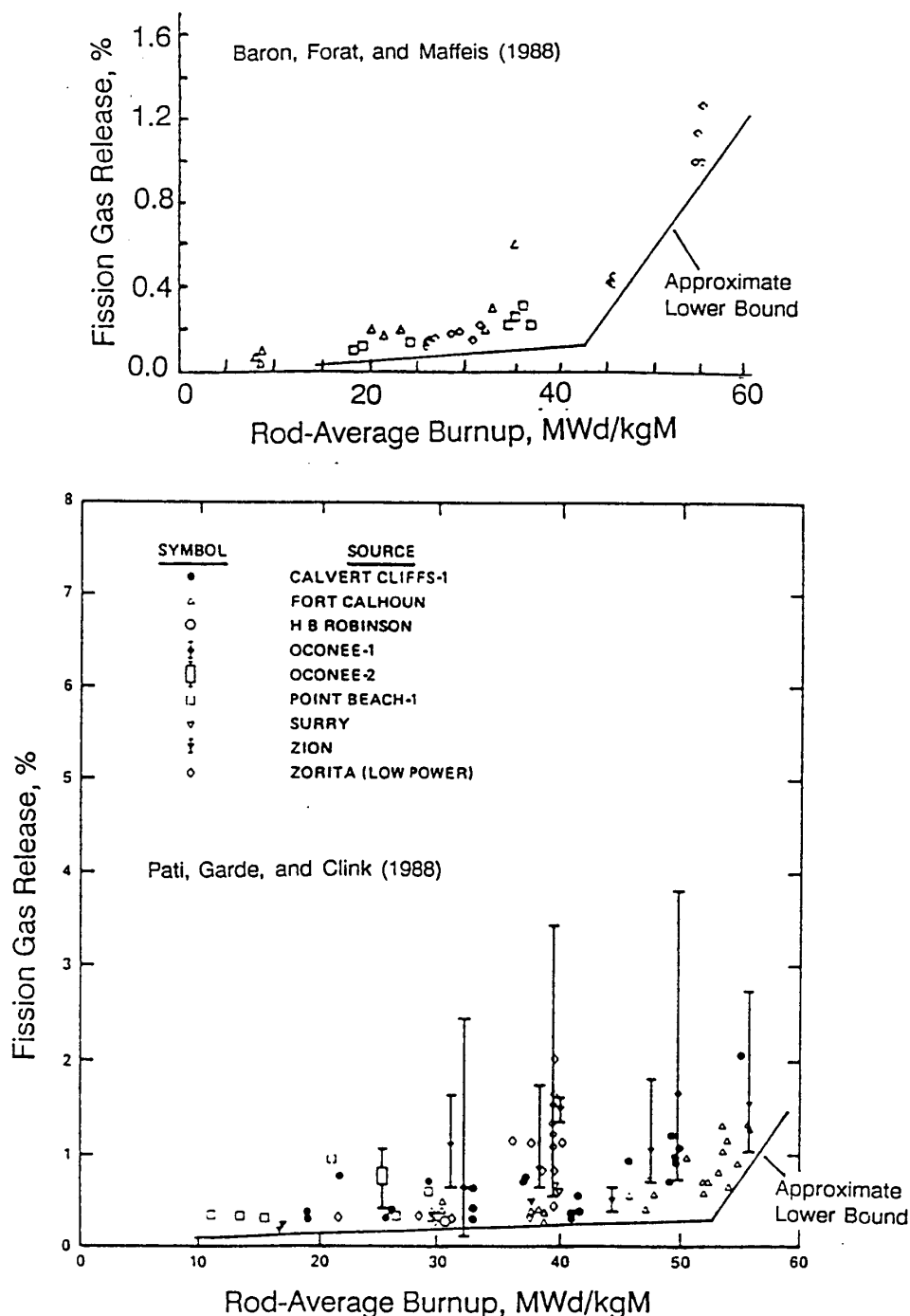
Figure 2.1.1.5-4   **Exsample of indicated burnup dependency of fission gas release at low temperature (Figure 7.1 from M.E. Cunningham, et al.,** *The Impact of Burnup and Fission Gas Release Distributions of the U.S. LWR Spent Fuel Inventory on the Selection of Spent Fuel Test Materials for the U.S. Geological Repository Project,* **Pacific Northwest Laboratory Report [Draft] 1991)**
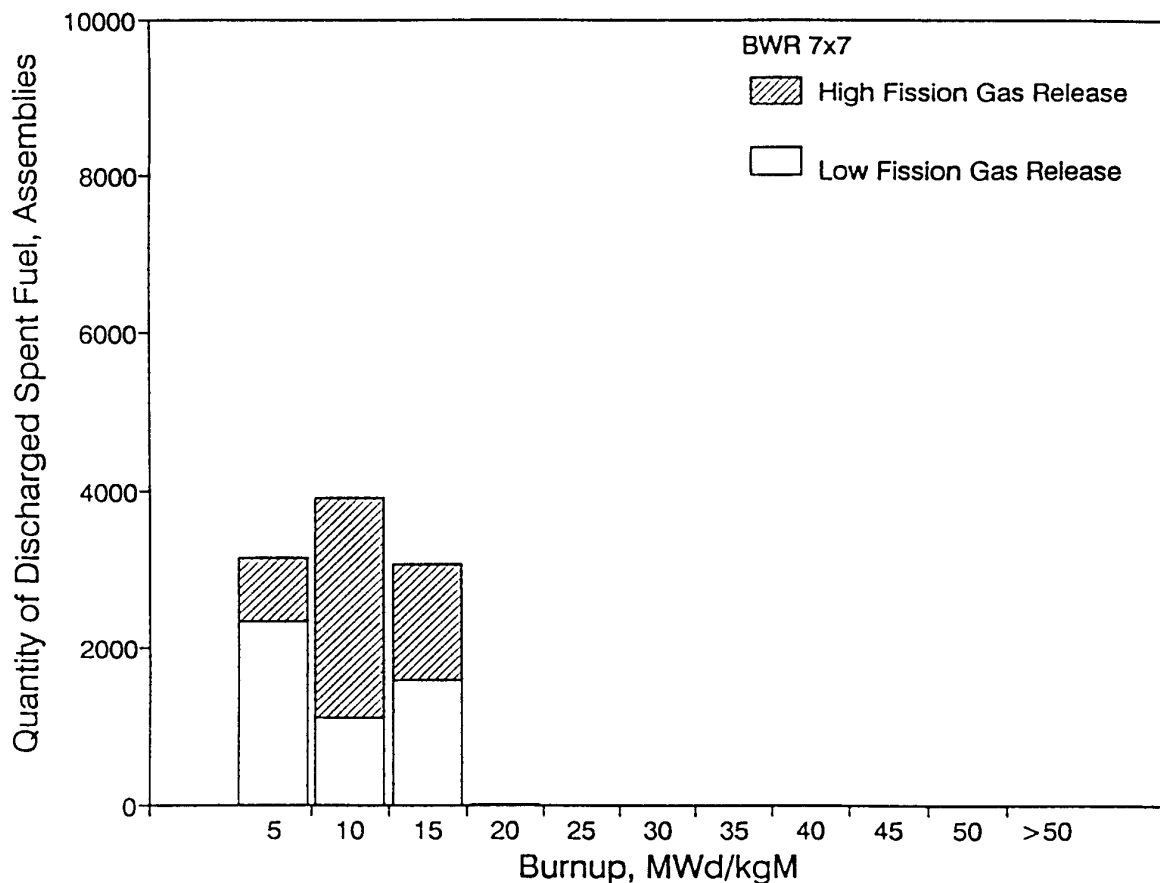
Figure 2.1.1.5-5   **Fission gas release distribution for 7 × 7 BWR rod group through 1987 (High and low fission gas release are greater than 2% and less than 2%, respectively.) (Figure 6.7 from M.E. Cunningham, et al.,** *The Impact of Burnup and Fission Gas Release Distributions of the U.S. LWR Spent Fuel Inventory on the Selection of Spent Fuel Test Materials for the U.S. Geological Repository Project,***Pacific Northwest Laboratory Report [Draft] 1991)**
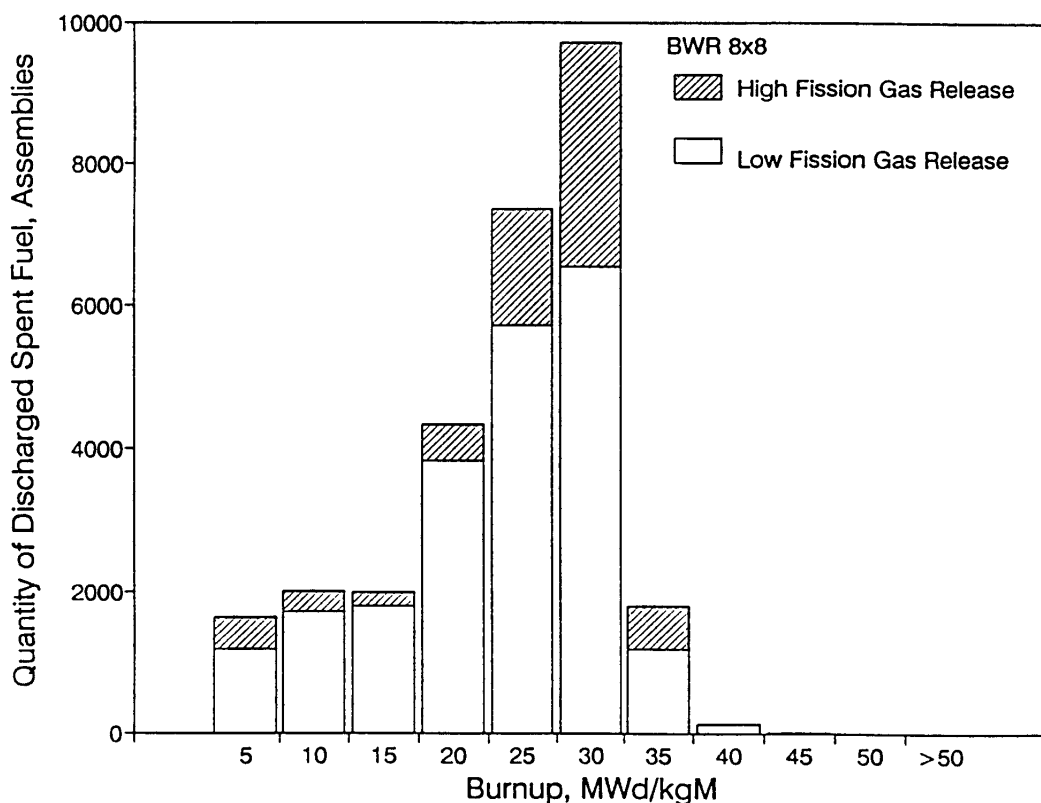
Figure 2.1.1.5-6 **Fission gas release distribution for 8 × 8 BWR rod group through 1987 (High and low fission gas release are greater than 2% and less than 2%, respectively.) (Figure 6.8 from M.E. Cunningham, et al.,** *The Impact of Burnup and Fission Gas Release Distributions of the U.S. LWR Spent Fuel Inventory on the Selection of Spent Fuel Test Materials for the U.S. Geological Repository Project,* **Pacific Northwest Laboratory Report [Draft] 1991)**

No 9 $\times$ 9 Fuel Discharged Through 1987; No Data in the CDB.

**Figure 2.1.1.5-7   Fission gas release distribution for 9 $\times$ 9 BWR rod group through 1987
(Figure 5.9 from M.E. Cunningham, et al., *The Impact of Burnup and
Fission Gas Release Distributions of the U.S. LWR Spent Fuel Inventory on
the Selection of Spent Fuel Test Materials for the U.S. Geological
Repository Project,*Pacific Northwest Laboratory Report [Draft] 1991)**
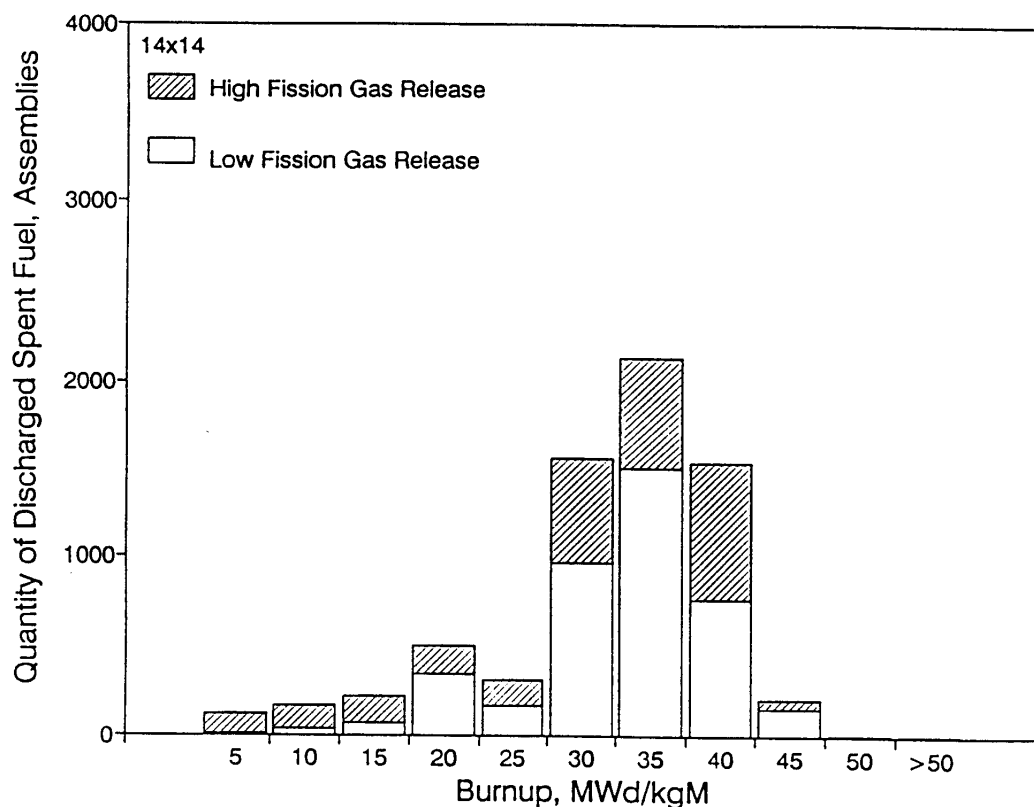
Figure 2.1.1.5-8   Fission gas release distribution for 14 × 14 PWR rod group through
1987 (High and low fission gas release are greater than 2% and less
than 2%, respectively.) (Figure 6.10 from M.E. Cunningham,
et al., *The Impact of Burnup and Fission Gas Release Distributions
of the U.S. LWR Spent Fuel Inventory on the Selection of Spent
Fuel Test Materials for the U.S. Geological Repository Project,*
Pacific Northwest Laboratory Report [Draft] 1991)
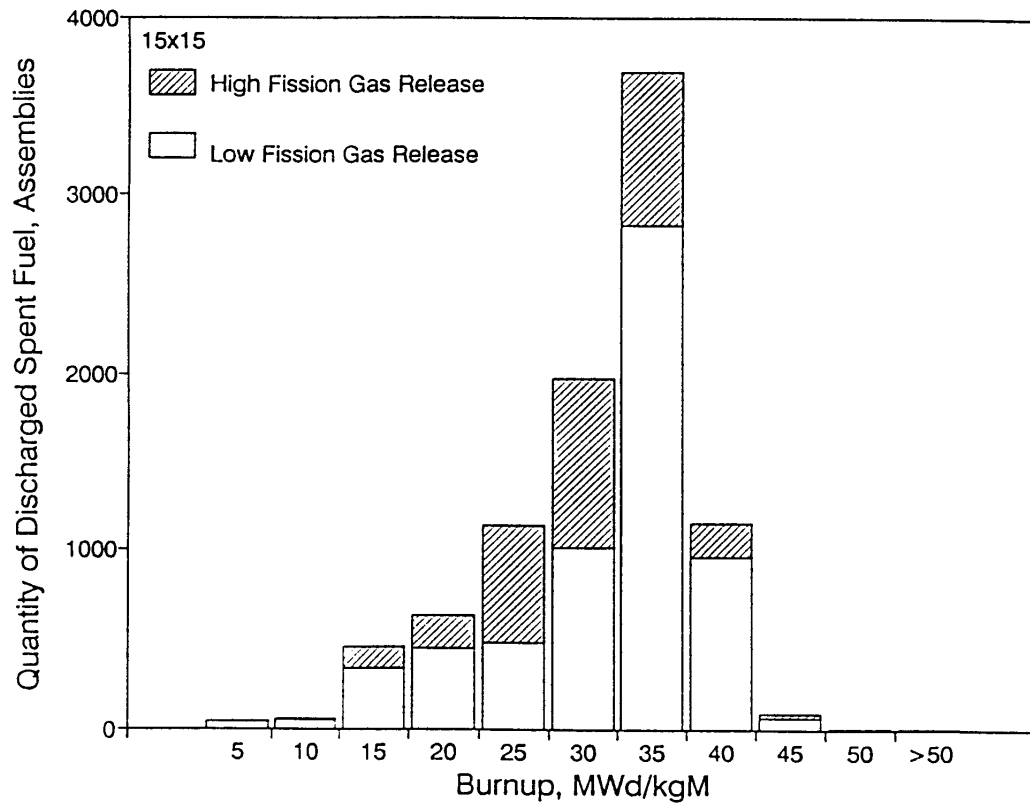
Figure 2.1.1.5-9   **Fission gas release distribution for 15 × 15 PWR rod group through 1987 (High and low fission gas release are greater than 2% and less than 2%, respectively.) (Figure 6.11 from M.E. Cunningham, et al.,** *The Impact of Burnup and Fission Gas Release Distributions of the U.S. LWR Spent Fuel Inventory on the Selection of Spent Fuel Test Materials for the U.S. Geological Repository Project,* **Pacific Northwest Laboratory Report [Draft] 1991)**
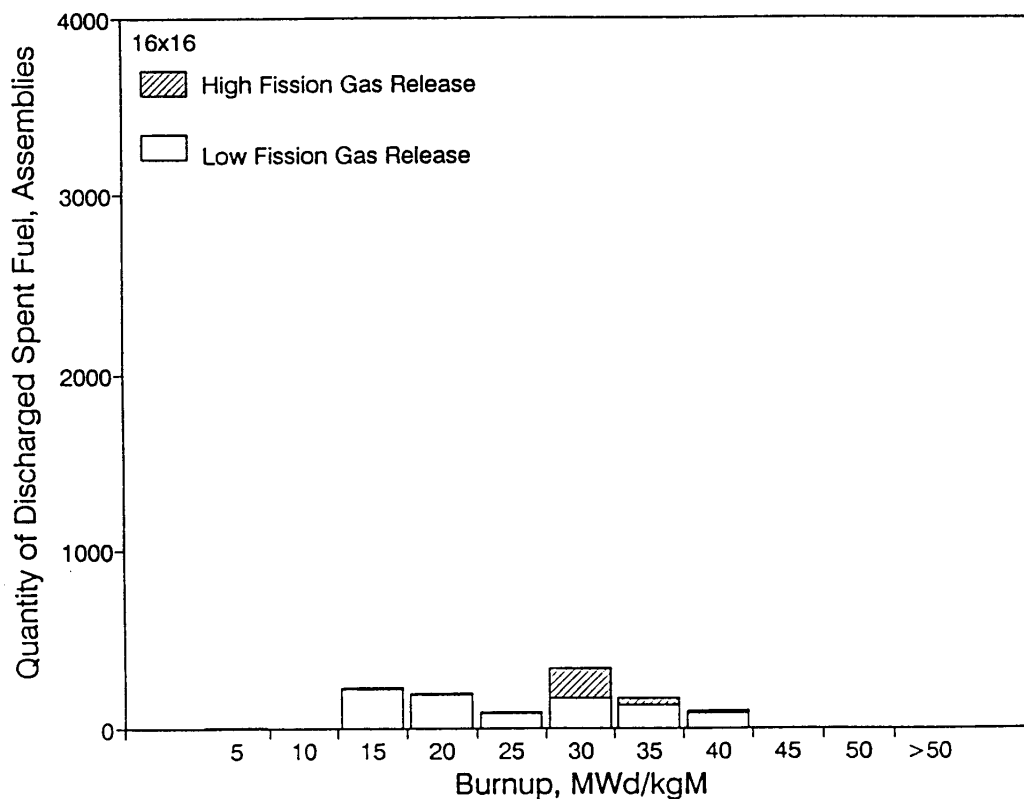
Figure 2.1.1.5-10 Fission gas release distribution for 16 × 16 PWR rod group through
1987 (High and low fission gas release are greater than 2% and less
than 2%, respectively.) (Figure 6.12 from M.E. Cunningham,
et al., *The Impact of Burnup and Fission Gas Release Distributions
of the U.S. LWR Spent Fuel Inventory on the Selection of Spent
Fuel Test Materials for the U.S. Geological Repository Project,*
Pacific Northwest Laboratory Report [Draft] 1991)
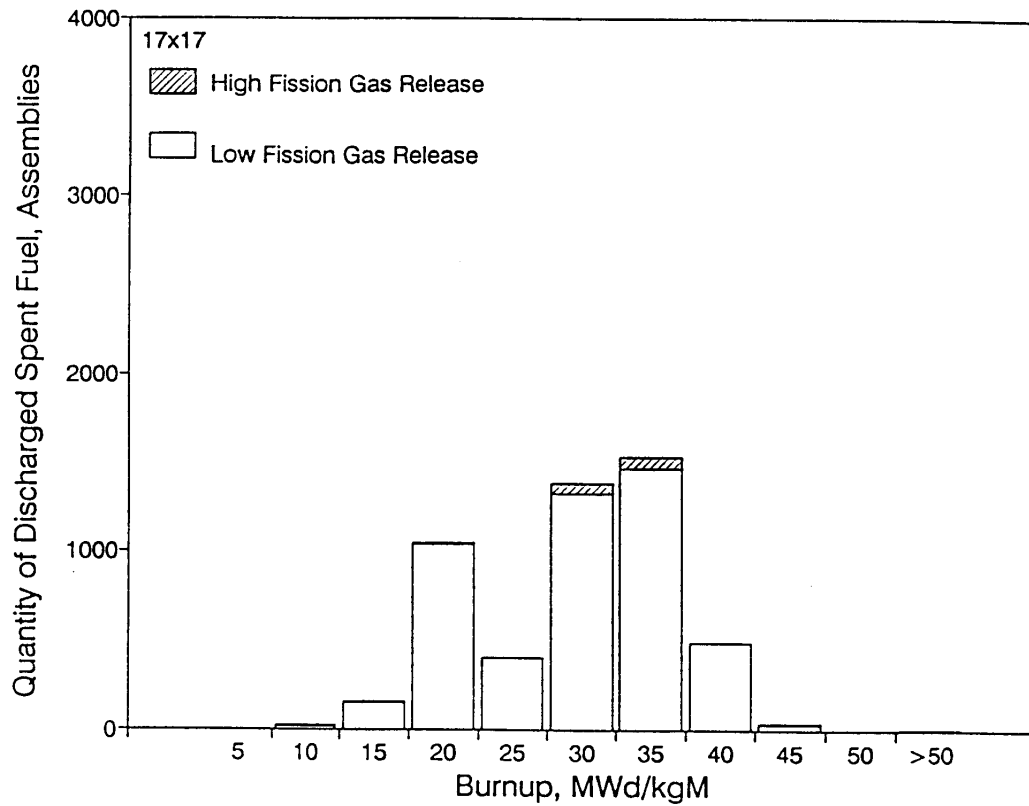
Figure 2.1.1.5-11 Fission gas release distribution for 17 × 17 PWR rod group through 1987 (High and low fission gas release are greater than 2% and less than 2%, respectively.) (Figure 6.13 from M.E. Cunningham, et al., *The Impact of Burnup and Fission Gas Release Distributions of the U.S. LWR Spent Fuel Inventory on the Selection of Spent Fuel Test Materials for the U.S. Geological Repository Project,* **Pacific Northwest Laboratory Report [Draft] 1991)**
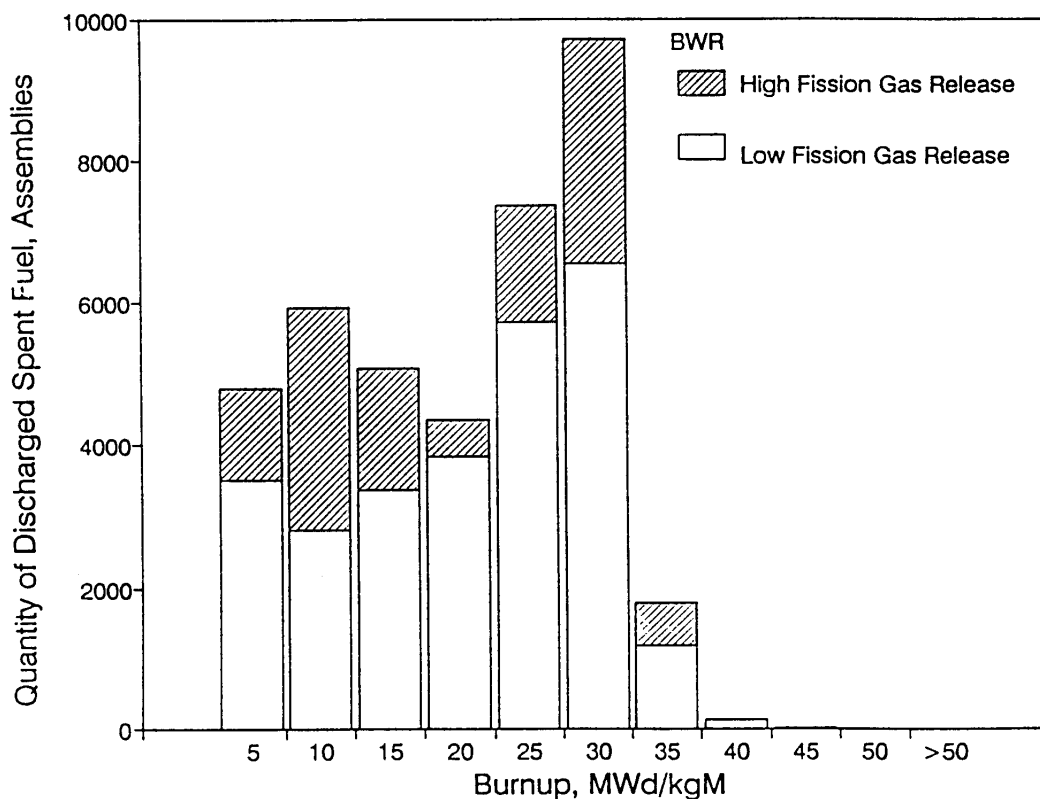
Figure 2.1.1.5-12 **Fission gas release distribution for BWR spent fuel discharged through 1987 (High and low fission gas release are greater than 2% and less than 2%, respectively.) (Figure 6.14 from M.E. Cunningham, et al.,** *The Impact of Burnup and Fission Gas Release Distributions of the U.S. LWR Spent Fuel Inventory on the Selection of Spent Fuel Test Materials for the U.S. Geological Repository Project,* **Pacific Northwest Laboratory Report [Draft] 1991)**
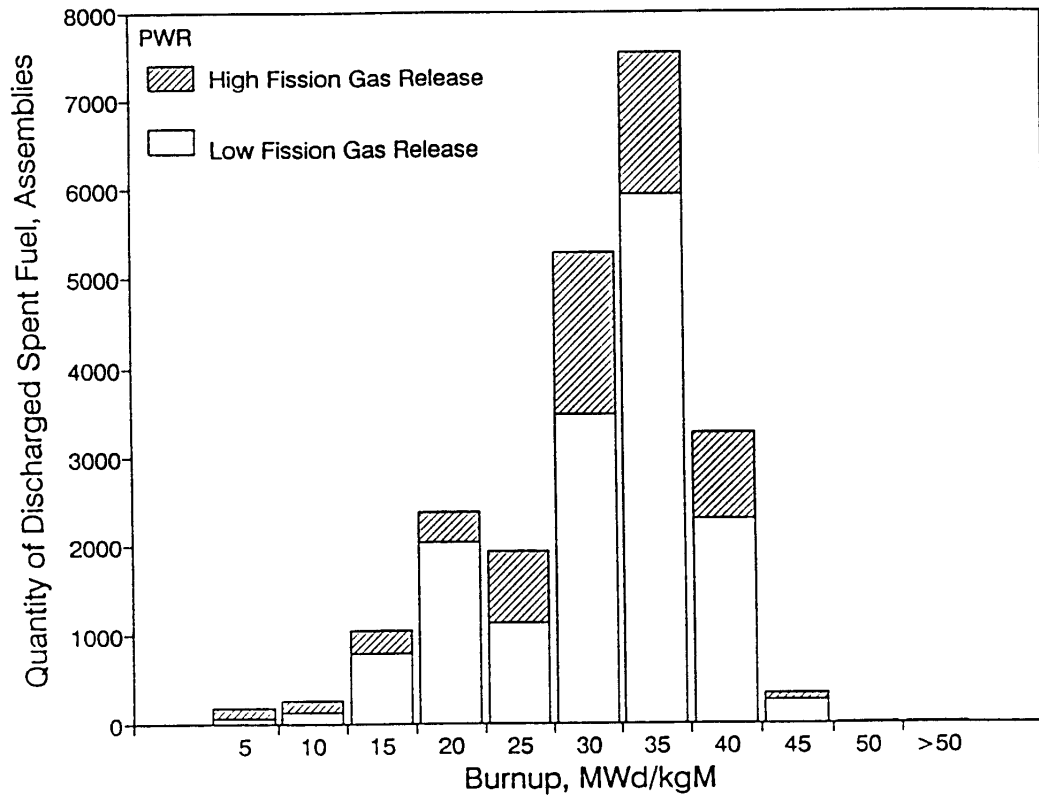
Figure 2.1.1.5-13 Fission gas release distribution for PWR spent fuel discharged through 1987 (High and low fission gas release are greater than 2% and less than 2%, respectively.) (Figure 6.15 from M.E. Cunningham, et al., *The Impact of Burnup and Fission Gas Release Distributions of the U.S. LWR Spent Fuel Inventory on the Selection of Spent Fuel Test Materials for the U.S. Geological Repository Project,*Pacific Northwest Laboratory Report [Draft] 1991)
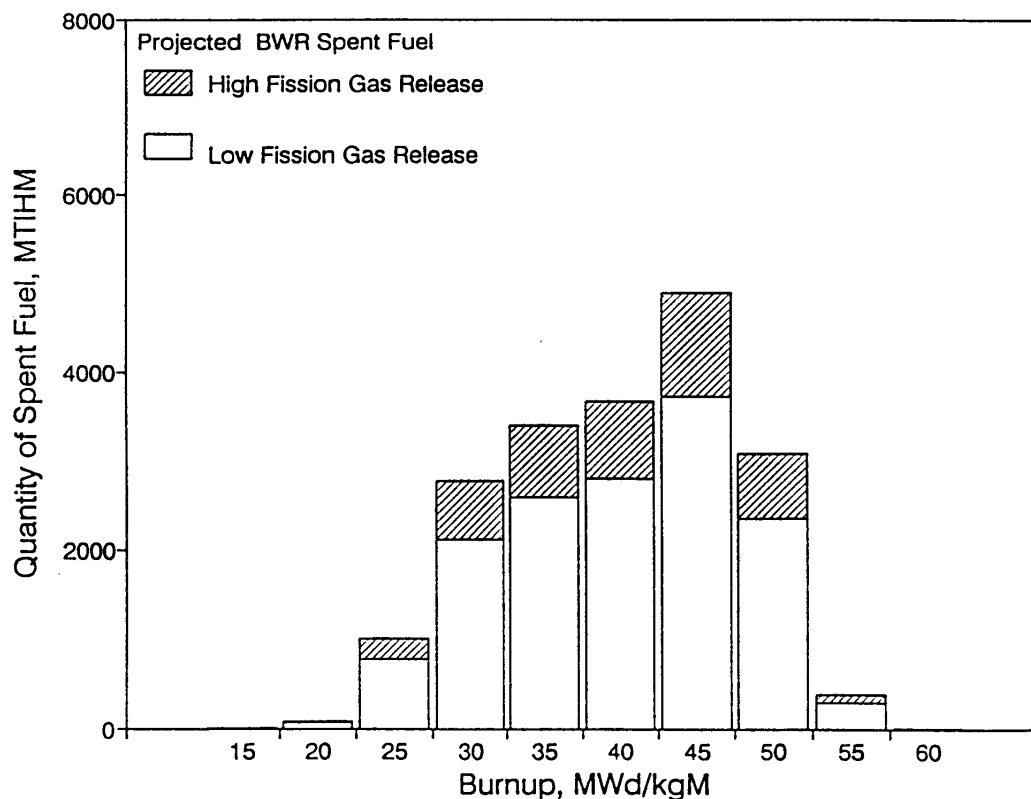
Figure 2.1.1.5-14 Projected fission gas release distribution for BWR spent fuel
discharged 1989 through 2020 (High and low fission gas release
are greater than 2% and less than 2%, respectively.) (Figure 6.16
from M.E. Cunningham, et al., *The Impact of Burnup and Fission
Gas Release Distributions of the U.S. LWR Spent Fuel Inventory
on the Selection of Spent Fuel Test Materials for the U.S. Geological
Repository Project,*Pacific Northwest Laboratory Report [Draft] 1991)
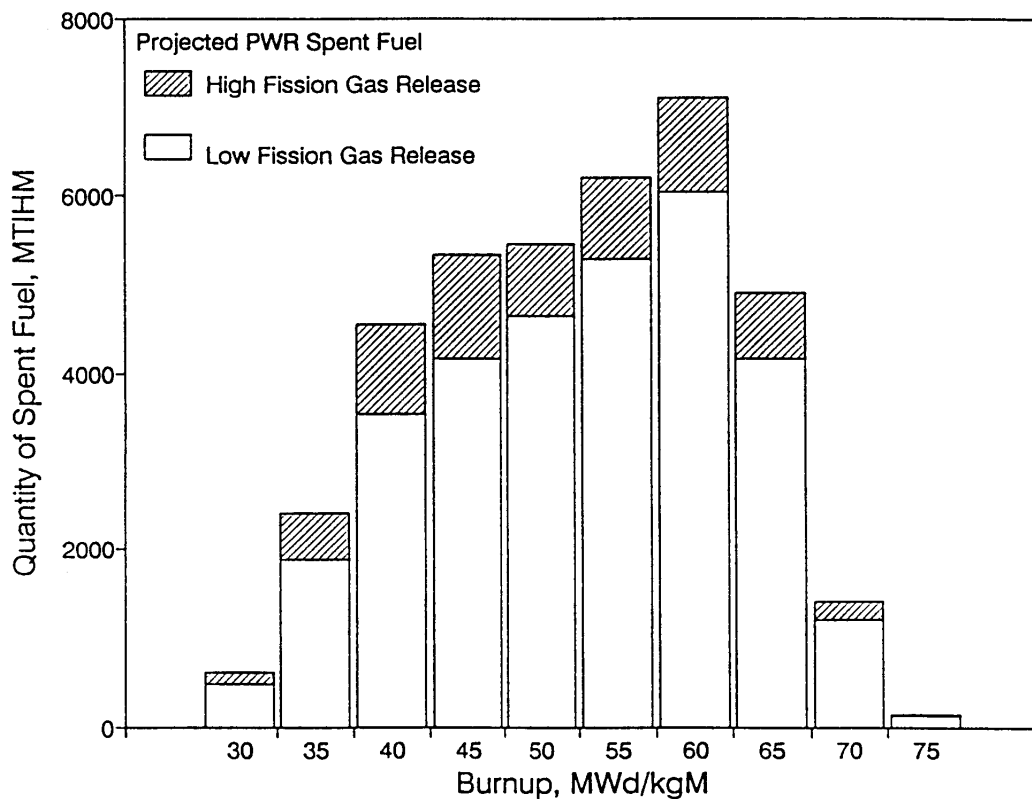
Figure 2.1.1.5-15 Projected fission gas release distribution for PWR spent fuel discharged 1989 through 2020 (High and low fission gas release are greater than 2% and less than 2%, respectively.) (Figure 6.17 from M.E. Cunningham, et al., *The Impact of Burnup and Fission Gas Release Distributions of the U.S. LWR Spent Fuel Inventory on the Selection of Spent Fuel Test Materials for the U.S. Geological Repository Project,*Pacific Northwest Laboratory Report [Draft] 1991)

UNPRESSURIZED RODS
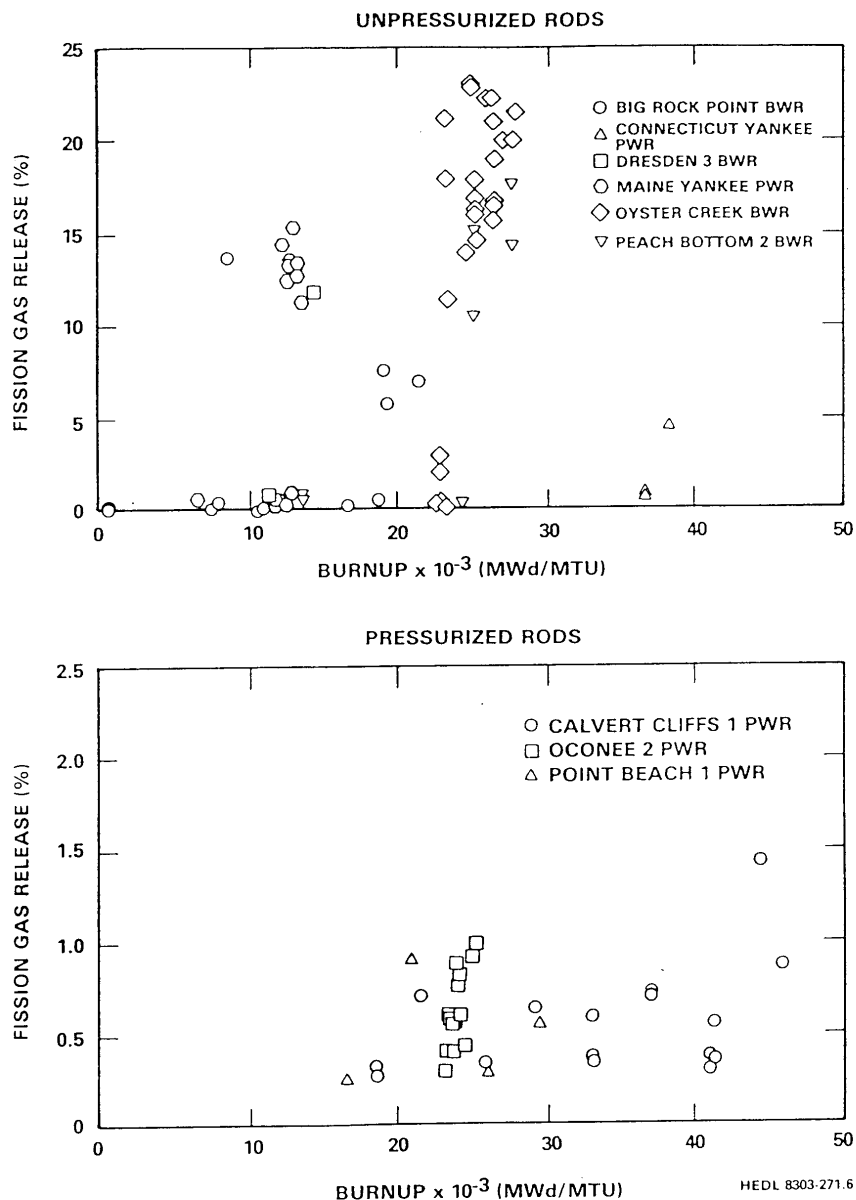
PRESSURIZED RODS

Figure 2.1.1.5-16 Comparison of fission gas release from unpressurized and pressurized LWR fuel rods (Figure 14 from R.E. Woodley, *The Characteristics of Spent LWR Fuel Relevant to its Storage in Geologic Repositories*, HEDL-TME 83-28, October, 1983)
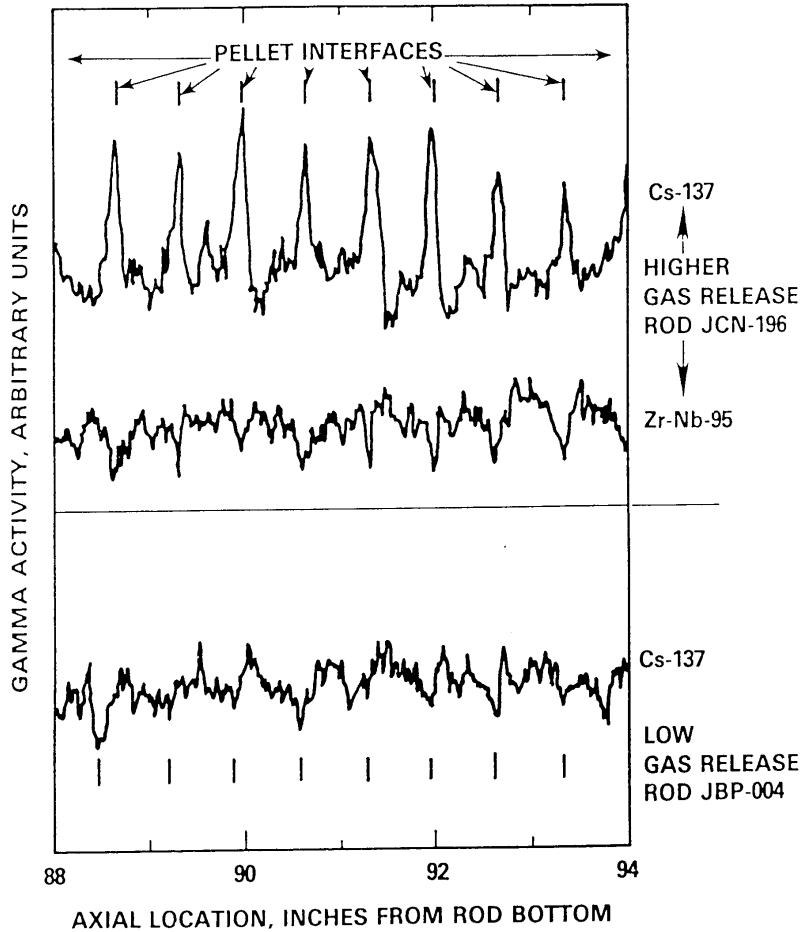
HEDL 8303-271.2

Figure 2.1.1.5-17 Portions of ^{137}Cs gamma scans from the peak power position (88 in. to 94 in.) of high- and low-gas-release fuel rods from the Maine Yankee PWR (This graph is illustrative only, and readers are advised to consult the reference for discussion of variability.) (Figure 15 from R.E. Woodley, *The Characteristics of Spent LWR Fuel Relevant to its Storage in Geologic Repositories,* HEDL-TME 83-28, October, 1983)
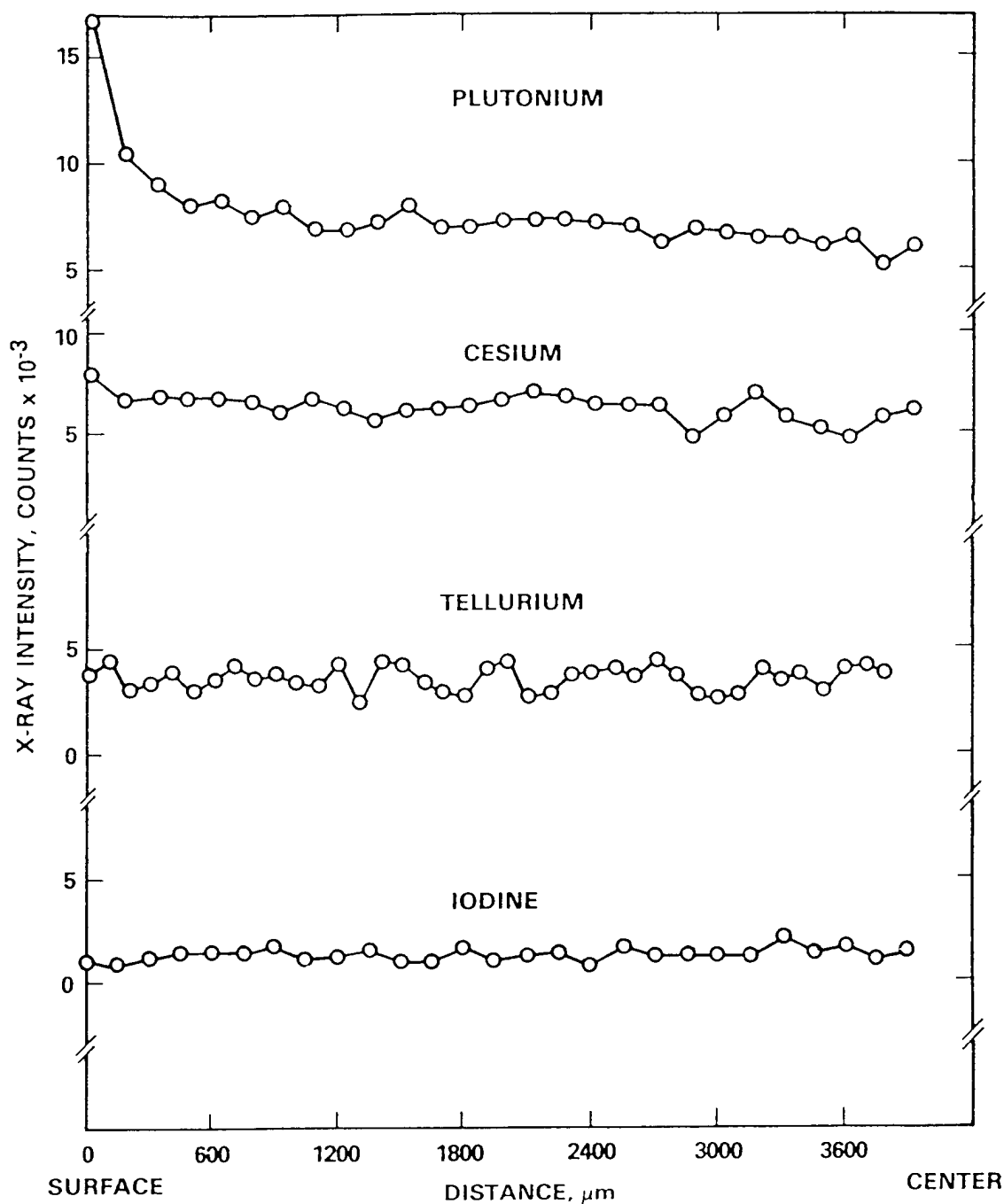
HEDL 8303-271.4

Figure 2.1.1.5-18 Microprobe-measured X-ray intensities for plutonium, cesium, tellurium, and iodine (adapted from Reference 40) (This graph is illustrative only, and readers are advised to consult the reference for discussion of variability across radius of a pellet.) (Figure 16 from R.E. Woodley, The Characteristics of Spent LWR Fuel Relevant to its Storage in Geologic Repositories, HEDL-TME 83-28, October, 1983.)

2.1.2 Structural Characteristics and Dimensions

Spent fuel elements may exist in several physical forms depending on the type of reactor from which they came and who was the manufacturer of the fuel. This has typically resulted in a division of fuel elements into classes.

Several types of spent fuel do not fall into the general classification; these include fuels for unusual, one-of-a-kind reactors, fuel assemblies which have been dismantled, etc.

In order to have the smallest number of standard designs of disposal containers, designers must know the dimensions, weights, shapes and material compositions, as well as the amounts of spent fuels which are intended for disposal in the repository.

It must also be known what special handling devices must be used in order to pick up and handle the many types of fuel and if they must be supported during handling, transportation, and after internment.

This section presents those properties which are most obviously necessary to the designers, although not all have been presented here. Some are not readily available and others, such as assembly drawings of fuel elements can be obtained from the complete report on characteristics of spent fuel, DOE/RW-0184. It should be noted that all "as manufactured dimensions" of Zircaloy will be altered due to stress-induced and irradiation growth-induced strain field during reactor operation. For the long fuel rods, the irradiation growth-induced strain and total length increase in the axial direction must be considered in dimensional tolerances of spent fuel rod and spent fuel assembly containers and handling techniques. A discussion of available models to predict irradiation growth induced strain can be found in an ASTM STP-824 publication (D.G. Franklin and R.B. Adamson, eds., "Zirconium in the Nuclear Industry," Sixth Int. Symposium, Vancouver, B.C., pp. 343–382, 1984.)

2.1.2.1 Fuel Assemblies

Table 2.1.2.1-1   Characteristics of CDB assembly classes (Table 5.1 from K.J. Notz, T.D. Welch, R.S. Moore, and W.J. Reich, *Preliminary Waste Form Characteristics,* ORNL-TM-11681 [draft] September, 1990)

Assembly Class	Reactor Type	Assembly Length	Assembly Width	Array Size(s) Used
Multi-reactor classes				
GE BWR/2,3	BWR	171.2	5.44	7 x 7, 8 x 8, 9 x 9
GE BWR/4-6	BWR	176.2	5.44	7 x 7, 8 x 8, 9 x 9
B&W 15 X 15	PWR	165.7	8.54	15 x 15
B&W 17 X 17	PWR	165.7	8.54	17 x 17
CE 14 X 14	PWR	157.	8.1	14 x 14
CE 16 X 16	PWR	176.8	8.1	16 x 16
CE 16 X 16 System 80	PWR	178.3	8.1	16 x 16
WE 14 X 14	PWR	159.8	7.76	14 x 14
WE 15 X 15	PWR	159.8	8.44	15 x 15
WE 17 X 17	PWR	159.8	8.44	17 x 17
SOUTH TEXAS	PWR	199.	8.43	17 x 17
Single-reactor classes				
BIG ROCK POINT	BWR	84.0	6.52	12 x 12, 11 x 11, 9 x 9, 8 x 8, 7 x 7
DRESDEN 1	BWR	134.4	4.28	6 x 6, 7 x 7, 8 x 8
ELK RIVER	BWR	81.6	3.5	5 x 5
HUMBOLDT BAY	BWR	95.	4.67	6 x 6, 7 x 7
LACROSSE	BWR	102.5	5.62	10 x 10
FT. CALHOUN	PWR	146.	8.1	14 x 14
HADDAM NECK	PWR	137.1	8.42	15 x 15
INDIAN POINT	PWR	138.8	6.27	13 x 14 (14 x 14)
PALISADES	PWR	147.5	8.2	15 x 15
PATHFINDER	BWR			
ST. LUCIE 2	PWR	158.2	8.1	16 x 16
SAN ONOFRE 1	PWR	137.1	7.76	14 x 14
YANKEE ROWE	PWR	111.8	7.62	15 x 16 (16 x 16), 17 x 18 (18 x 18)

Dimensions are nominal before irradiation. All dimension are in inches. Lengths are rounded to the next higher tenth of an inch. Lengths of some newer fuel assemblies use slightly (0.1 in.) longer fuel designs. Widths are rounded to the next higher hundredth of an inch. Fuel assembly widths for GE BWR/2,3 and GE BWR.4,5,6 classes include 80-mil fuel channels. Assemblies with thicker channels (100 and 120 mil) have larger widths.

Table 2.1.2.1-2   Summary of fuel-design usage (Table 5.2 from K.J. Notz, T.D. Welch, R.S. Moore, and W.J. Reich, *Preliminary Waste Form Characteristics,* ORNL-TM-11681 [draft] September, 1990)

Name	Year Introduced	Where Used	Brief Description
		WESTINGHOUSE FUEL DESIGNS Westinghouse-Built Reactors	
St. Steel	First Use:	San Onofre-1 Haddam Neck	Stainless steel cladding and guide tubes, inconel grid spacers.
Standard		WE 14 x 14 WE 15 x 15	Zircaloy cladding introduced; inconel grid spacers, stainless steel guide tubes.
LOPAR		WE 14 x 14 WE 15 x 15 WE 17 x 17 SOUTH TEXAS	Inconel grid spacers, Zircaloy guide tubes.
OFA	First Use: 1979 Farley 1, Point Beach 2 Beaver Valley 1	WE 14 x 14 WE 15 x 15 WE 17 x 17	Zircaloy intermediate grid spacers, optimized fuel rod diameter.
Vantage 5	First Use: 1984 V.C. Summer	WE 14 x 14 WE 15 x 15 WE 17 x 17	OFA fuels features, plus 5 options: 1)integral fuel burnable absorbers, 2) intermediate flow mixer grids, 3) natural uranium axial blankets, 4) increased discharge burnups, and 5) reconstitutable top nozzles. Options are available separately or in combination.
Vantage 5H	First Use: Unknown	WE 17 x 17	VANTAGE 5H (or Hybrid) fuel combines the features available with VANTAGE 5 fuel with Zircaloy grids spacers, but utilizes the larger fuel rod diameters of the STANDARD and LOPAR designs.
Vantage +	First Use: 1987 North Anna-1	WE 17 x 17	VANTAGE + fuel features ZIRLO cladding. ZIRLO is an advanced zirconium-niobium alloy with additional resistance to corrosion at high temperatures and burnups.
		WESTINGHOUSE FUEL DESIGNS Other Reactor Vendors	
Model C	First Use: 1980 Millstone 2	CE 14 x 14 Fort Calhoun	Fuel designed for use in CE-built reactors.
B&W	First Use: 1991 (proj) Three Mile Island-1	B&W 15 x 15	Fuel designed for use in B&W-built reactors.
QUAD+	First Use: 1987 Fitzpatrick	GE BWR/4,5,6	BWR fuel design utilizing four 4 x 4 minibundles and Zircaloy water cross.

Table 2.1.2.1-2 (continued)

GENERAL ELECTRIC FUEL DESIGNS
General Electric Built Reactors

Early Fuels (GE-1)	First Use: 1959 Continuing at Big Rock Point	Dresden-1 Humboldt Bay Big Rock Point	Fuels for BWR/1 reactors
GE-2	First Use: 1969 Last Discharge: 1979	GE BWR/2,3 GE BWR/4,5,6	Original 7 x 7 Array
GE-3	First Use: 1972 Last Discharge: 1983	GE BWR/2,3 GE BWR/4,5,6	Improved 7 x 7 Array - thicker cladding, hydrogen getter chamfered pellets.
GE-4	First Use: 1974 Last Discharge: 1986	GE BWR/2,3 GE BWR/4,5,6	Original 8 x 8 Array - introduction of water rod.
GE-5	First Use: 1975 Last Discharge:	GE BWR/2,3 GE BWR/4,5,6	8 x 8 Retrofit fuel - two water rods, axial natural uranium blankets, longer active fuel rod length.
Prepressurized (GE-6 and GE-7)	First Use: 1977 Peach Bottom-2	GE BWR/2,3 GE BWR/4,5,6	Retrofit fuel with fuel rods prepressurized to 3 atm helium.
Barrier (GE-6 and GE-7)	First Use: 1979 Quad Cities-1	GE BWR/2,3 GE BWR/4,5,6	Pressurized Retrofit fuel with pure zirconium barrier on cladding interior.
GE-8	First Use: 1981 Brown's Ferry-3	GE BWR/2,3 GE BWR/4,5,6	Increased number of water rods (3-6), larger diameter fuel pellets, higher stack density, axial gadolinia distribution, improved upper tie plate, prepressurization increase to 5 atms in BWR/3-6 reactors.
GE-9	First Use: 1987 Hatch-1	GE BWR/2,3 GE BWR/4,5,6	Single large water rod, possibly ferrule-type spacers.
GE-10	First Use: 1988(?) Cooper Station (?)	GE BWR/4,5,6	
GE-11	First Use: 1990 WNP-2, Fitzpatrick	GE BWR/4,5,6	9 x 9 fuel rod array with 74 fuel rods and two large-diameter water rods.

BABCOCK & WILCOX FUEL DESIGNS
Babcock & Wilcox Reactors

Mark B2	First Use: Oconee 2	B&W 15 x 15	
Mark B3	First Use: Oconee 2	B&W 15 x 15 Increased fuel pellet density and changed spacer from corrugated to spring type.	
Mark B4	First Use: 1975 Oconee 1	B&W 15 x 15	Introduced fuel rod prepressurization; modified end fitting reduced fuel assembly pressure drop.

Table 2.1.2.1-2 (continued)

BABCOCK & WILCOX FUEL DESIGNS (cont.)

Mark B5	First Use: 1982 Rancho Seco	B&W 15 x 15	Eliminated the use of retainers for burnable absorber holddown by using modified end fitting. Inconel 718 holddown spring.
Mark BxZ	First Use: 1979 Oconee 1	B&W 15 x 15	Mark B4 and B5 fuels with Zircaloy intermediate grid spacers.
Mark B6	First Use: 1988 Ark. Nuclear One-1	B&W 15 x 15	Zircaloy intermediate spacers grids; skirtless upper end grid, and removable upper end fitting.
Mark B7	First Use: 1988 Oconee 3	B&W 15 x 15	Mark B6 features plus slightly shorter lower end fitting, slightly longer fuel rod, and increased plenum volume.
Mark B8	First Use: 1989 Oconee 3	B&W 15 x 15	Debris fretting resistent fuel rod design, reduced prepressurization.
Mark C	First Use: 1976 Oconee 2	B&W 15 x 15	Four demonstration assemblies of fuel design intended for B&W 17 x 17 class reactors.

BABCOCK & WILCOX FUEL DESIGNS
Other Reactor Vendors

St. Steel	First Use: Haddam Neck	Haddam Neck	Stainless steel clad assemblies for use at WE-built reactors.
Westinghouse	First Use: 1974 Ginna	WE 14 x 14	Demonstration assemblies for use at WE-built reactors.
Mark BW	First Use: 1989 McGuire 1	WE 17 x 17	Lead test assemblies under irradiation; full core reload scheduled for 1991.

ADVANCED NUCLEAR FUELS, INC.
PWR Fuels

Westinghouse	First Use: 1974 Ginna	WE 14 x 14 WE 15 x 15 WE 17 x 17	Fuels designed for use at WE-built reactors.
Toprod	First Use: 1981 Prairie Island-1	WE 14 x 14	Fuels for use at WE 14 x 14 plants; fueled rods containing Gadolinia.
Part Length	First Use: 1986 (?) Robinson-2	WE 15 x 15	Fuel for use at WE-built reactors; bottom 42 in. of fuel rod contains stainless steel inserts.
Comb. Eng.	First Use: 1980 Fort Calhoun	CE 14 x 14 Fort Calhoun	Fuels designed for use at CE-built reactors.

Table 2.1.2.1-2 (continued)

ADVANCED NUCLEAR FUELS, INC. (cont.)

| Palisades | First Use: 1975 Palisades | Palisades | Fuel designed for use at Palisades reactor. |
| Yankee Rowe | First Use: 1975 Yankee Rowe | Yankee Rowe | Fuel designed for use at Yankee Rowe. |

ADVANCED NUCLEAR FUELS, INC.
BWR Fuels

Early BWR Fuels	First Use: 1977 1974 1972	Dresden 1 Humboldt Bay Big Rock Point	Fuels designed for GE BWR/1 reactors.
7 x 7 Arrays	First Use: 1972 Oyster Creek	GE BWR/2,3	7 x 7 array designed for use at GE-built reactors.
8 x 8 Arrays	First Use: 1975 Oyster Creek	GE BWR/2,3 GE BWR/4,5,6	8 x 8 array designed for use at GE-built reactors.
9x9	First Use: 1983 Dresden-2	GE BWR/2,3 GE BWR/4,5,6	9 x 9 fuel array for GE-built reactors; 2 water rods.
9x9-5	First Use: Unknown	GE BWR/4,5,6	9 x 9 fuel array for GE-built reactors; 5 water rods.
9x9-IX	First Use: 1989 WNP-2	GE BWR/4,5,6	9 x 9 fuel array for GE-built reactors; 72 fuel rods; Zirconium barrier used on all rods except Gadolinia rods; 1.65" square water channel.
9x9-9X	First Use: 1989 WNP-2	GE BWR/4,5,6	9 x 9 fuel array for GE-built reactors; 72 fuel rods; 1.65" square water channel.

COMBUSTION ENGINEERING FUEL DESIGNS

Standard	First Use:	CE 14 x 14 CE 16 x 16 CE 16 x 16 System 80 Fort Calhoun St. Lucie 2	
Palisades	First Use:	Palisades	
Yankee Rowe	First Use:	Yankee Rowe	

Table 2.1.2.1-3   Listing of assembly types by assembly class (Table 5.3 from K.J. Notz, T.D. Welch, R.S. Moore, and W.J. Reich, *Preliminary Waste Form Characteristics,* ORNL-TM-11681 [draft] September, 1990)

Assembly Class Assembly Type	Rodarray Code	Assemblies In Storage	Status	Comments
BABCOCK & WILCOX 15 X 15				
B&W 15 X 15 B&W Mark B	B1515B	567	Discharged	
B&W 15 X 15 B&W Mark B2	B1515B2	92		
B&W 15 X 15 B&W Mark B3	B1515B3	615	Discharged	
B&W 15 X 15 B&W Mark B4	B1515B4	2071	Incore	
B&W 15 X 15 B&W Mark B4Z	B1515B4Z	36	Incore	
B&W 15 X 15 B&W Mark B5	B1515B5	56	Incore	
B&W 15 X 15 B&W Mark B5Z	B1515B5Z	43	Incore	
B&W 15 X 15 B&W Mark B6	B1515B6	0	Incore	
B&W 15 X 15 B&W Mark B7	B1515B7	0	Incore	
B&W 15 X 15 B&W Mark B8	B1515B8	68	Incore	
B&W 15 X 15 B&W Mark BGd	B1515BG	4	Discharged	Lead Assembly
B&W 15 X 15 WE	B1515W	0	Projected	Lead Assembly in 1991.
BABCOCK & WILCOX 17 X 17				
B&W 17 X 17 B&W Mark C	B1717B	4	Discharged	Lead Assembly
COMBUSTION ENGINEERING 14 X 14				
CE 14 X 14 CE	C1414C	2810	Incore	
CE 14 X 14 ANF	C1414A	323	Incore	
CE 14 X 14 WE	C1414W	189	Incore	
COMBUSTION ENGINEERING 16 X 16				
CE 16 X 16 CE San Onofre	C1616C	1043	Incore	
CE 16 X 16 CE ANO2	C1616C		Incore	
COMBUSTION ENGINEERING 16 X 16 SYSTEM 80				
CE 16 X 16 CE System 80	C1616CS8	188	Incore	
GENERAL ELECTRIC BWR/2,3				
GE BWR/2,3 7 X 7 GE-2a	G2307G2A	1672	Discharged	
GE BWR/2,3 7 X 7 GE-2b	G2307G2B	5047	Discharged	
GE BWR/2,3 7 X 7 GE-3	G2307G3	394	Discharged	
GE BWR/2,3 7 X 7 ANF	G2307A	260	Discharged	
GE BWR/2,3 8 X 8 GE-4	G2308G4	3876	Discharged	
GE BWR/2,3 8 X 8 GE-5	G2308G5	792	Incore	
GE BWR/2,3 8 X 8 GE Pressurized	G2308GP	1836	Incore	
GE BWR/2,3 8 X 8 GE Barrier	G2308GB	248	Incore	
GE BWR/2,3 8 X 8 GE-8a	G2308G8A		Incore	
GE BWR/2,3 8 X 8 GE-8b	G2308G8B		Incore	
GE BWR/2,3 8 X 8 GE-9a	G2308G9A		Lead Assembly	
GE BWR/2,3 8 X 8 GE-9b	G2308G9B		Lead Assembly	
GE BWR/2,3 8 X 8 ANF	G2308A	68	Incore	
GE BWR/2,3 8 X 8 ANF Pressurized	G2308AP		Incore	
GE BWR/2,3 9 X 9 ANF	G2309A		Incore	
GE BWR/2,3 9 X 9 ANF 9-5	G2309A5		Unknown	
GE BWR/2,3 9 X 9 ANF IX	G2309AIX		Lead Assembly	
GE BWR/2,3 9 X 9 ANF 9X	G2309A9X		Lead Assembly	

Table 2.1.2.1-3 (continued)

ELECTRIC BWR/4,5,6			
J4-6 7 X 7 GE-2	G4607G2	1142	Discharged
J4-6 7 X 7 GE-3a	G4607G3A	3752	Discharged
J4-6 7 X 7 GE-3b	G4607G3B	1184	Discharged
J4-6 8 X 8 GE-4a	G4608G4A	1784	Discharged
J4-6 8 X 8 GE-4b	G4608G4B	1787	Discharged
J4-6 8 X 8 GE-5	G4608G5	3455	Incore
J4-6 8 X 8 GE Pressurized	G4608GP	6591	Incore
J4-6 8 X 8 GE Barrier	G4608GB	775	Incore
J4-6 8 X 8 GE-8a	G4608G8A		Incore
J4-6 8 X 8 GE-8b	G4608G8B		Incore
J4-6 8 X 8 GE-9a	G4608G9A		Lead Assembly
J4-6 8 X 8 GE-9b	G4608G9B		Lead Assembly
J4-6 8 X 8 GE-10	G4608G10		Lead Assembly
J4-6 9 X 9 GE-11	G4609G11		Future
J4-6 8 X 8 ANF	G4608A		Incore
J4-6 8 X 8 ANF Pressurized	G4608AP		Incore
J4-6 9 X 9 ANF	G4609A		Incore
R/4-6 9 X 9 ANF 9-5	G4609A5		Lead Assembly
R/4-6 9 X 9 ANF IX	G4609AIX		Lead Assembly
R/4-6 9 X 9 ANF 9X	G4609A9X		Lead Assembly
R/4-6 8 X 8 WE	G4608W		Lead Assembly
R/4-6 10 X 10 SVEA 96	*		Future

GHOUSE 14 X 14			
X 14 WE Std	W1414W	581	Incore
X 14 WE LOPAR	W1414WL	1376	Incore
X 14 WE OFA	W1414WO	88	Incore
X 14 WE Vantage 5	W1414WV5		
X 14 ANF	W1414A	559	Incore
X 14 ANF Top Rod	W1414ATR	299	Incore
X 14 B&W	W1414B	2	Discharged

IGHOUSE 15 X 15			
X 15 WE Std	W1515W	1395	Incore
X 15 WE LOPAR	W1515WL	3149	Incore
X 15 WE OFA	W1515WO	266	Incore
X 15 WE Part Length	W1515WPL		Incore
X 15 WE Vantage 5	W1515WV5		
X 15 ANF Westinghouse	W1515A	743	Incore
X 15 B&W Mark BW	W1515B		Future

IGHOUSE 17 X 17			
X 17 WE LOPAR	W1717W	5106	Incore
X 17 WE OFA	W1717WO	628	Incore
X 17 WE Vantage 5	W1717WV5	4	Incore
X 17 WE Vantage +	W1717WV+		Lead Assembly
X 17 WE Vantage H	W1717WVH		Lead Assembly
X 17 ANF Westinghouse	W1717A	139	Incore
X 17 B&W Mark BW	W1717B		Lead Assembly

TEXAS			
I TEXAS 17 X 17 WE	WST17W		Incore

Table 2.1.2.1-3 (continued)

BIG ROCK POINT

BIG ROCK POINT 12 X 12 GE	XBR12G		Reprocessed	
BIG ROCK POINT 11 X 11 GE	XBR11G	6	Discharged	
BIG ROCK POINT 9 X 9 GE	XBR09G	143	Discharged	
BIG ROCK POINT 7 X 7 GE	XBR07G	4	Discharged	Lead Assembly
BIG ROCK POINT 8 X 8 GE	-XBR08G	2	Discharged	Lead Assembly
BIG ROCK POINT 9 X 9 ANF	XBR09A	4	Discharged	
BIG ROCK POINT 11 X 11 ANF	XBR11A	145	Incore	
BIG ROCK POINT 11 X 11 NFS	XBR11N	8	Discharged	

DRESDEN 1

DRESDEN 1 6 X 6 GE Type I	XDR06G1	1	Reprocessed
DRESDEN 1 7 x 7 GE Type II	XDR07G		Reprocessed
DRESDEN 1 6 x 6 GE Type III-B	XDR06G3B	163	Discharged
DRESDEN 1 6 x 6 GE Type III-F	XDR06G3F	96	Discharged
DRESDEN 1 6 x 6 GE Type V	XDR06G5	106	Discharged
DRESDEN 1 7 x 7 GE SA-1	XDR07GSA		Discharged
DRESDEN 1 8 x 8 GE PF Fuels	XDR08G	1	Discharged
DRESDEN 1 6 X 6 UNC	XDR06U	458	Discharged
DRESDEN 1 6 X 6 ANF	XDR06A	66	Discharged

FORT CALHOUN

FT. CALHOUN 14 X 14 CE	XFC14C	290	Incore
FT. CALHOUN 14 X 14 ANF	XFC14A	136	Incore
FT. CALHOUN 14 x 14 WE	XFC14W		Future

HUMBOLDT BAY

HUMBOLDT BAY 7 X 7 GE Type I	XHB07G1		Reprocessed
HUMBOLDT BAY 7 x 7 GE Type II	XHB07G2	88	Discharged
HUMBOLDT BAY 6 X 6 GE	XHB06G	176	Discharged
HUMBOLDT BAY 6 X 6 ANF	XHB06A	126	Discharged

HADDAM NECK

HADDAM NECK 15 X 15	XHN15W	309	Discharged	
HADDAM NECK 15 x 15 NUM Zir	XHN15MZ	2	Discharged	Lead Assembly
HADDAM NECK 15 x 15 NUM SS	XHN15MS	2	Discharged	Lead Assembly
HADDAM NECK 15 x 15 GGA Zir	XHN15IZ	2	Discharged	Lead Assembly
HADDAM NECK 15 x 15 GGA SS	XHN15IS	1	Discharged	Lead Assembly
HADDAM NECK 15 X 15 B&W SS	XHN15B	418	Incore	
HADDAM NECK 15 X 15 B&W Zir	XHN15BZ			Lead Assembly

INDIAN POINT 1

INDIAN POINT 13 X 14 B&W	XIP14B	0	Reprocessed
INDIAN POINT 13 X 14 WE	XIP14W	160	Discharged

Table 2.1.2.1-3 (continued)

Assembly Class Assembly Type	Rodarray Code	Assemblies In Storage	Status	Comments
LACROSSE				
LACROSSE 10 X 10 AC	XLC10L	155	Discharged	
LACROSSE 10 X 10 ANF	XLC10A	178	Discharged	
PALISADES				
PALISADES 15 X 15 CE	XPA15C	273	Discharged	
PALISADES 15 X 15 ANF	XPA15A	324	Incore	
ST.LUCIE 2				
ST. LUCIE 2 16 X 16 CE	XSL16C	236	Incore	
SAN ONOFRE 1				
SAN ONOFRE 1 14 X 14 WE	XSO14W	468	Incore	
YANKEE ROWE				
YANKEE ROWE 17 X 18 WE	XYR18W	76	Discharged	
YANKEE ROWE 15 X 16 UNC	XYR16U	73	Discharged	
YANKEE ROWE 15 X 16 ANF	XYR16A	228	Discharged	
YANKEE ROWE 15 X 16 CE	XYR16C	40	Incore	

Table 2.1.2.1-4   Assumed fuel assembly structural material mass distribution (Table 3.2 from K.J. Notz, T.D. Welch, R.S. Moore, and W.J. Reich, *Preliminary Waste Form Characteristics,* ORNL-TM-11681 [draft] September, 1990)

| | PWR[a] | | | BWR[a] | | |
| | | Mass | | | Mass | |
Fuel Zone	Material	kg/MTHM	kg/assembly	Material	kg/MTHM	kg/assembly
Fuel Zone						
Cladding	Zircaloy-4	223.0	102.9	Zircaloy-2	279.5	51.2
Fuel channel[b]	--	--	--	Zircaloy-4	227.5	41.7
Grid spacers	Inconel 718	12.8	5.9	Zircaloy-4	10.6	1.9
Grid-spacer springs	Inconel 718			Inconel X-750	1.8	0.3
Grid-brazing material	Nicrobraze 50	2.6	1.2	--	--	--
Miscellaneous	SS 304[c]	9.9	4.6	--	--	--
Fuel-gas plenum zone						
Cladding	Zircaloy-4	12.0	5.5	Zircaloy-2	25.4	4.7
Fuel channel[b]	--	--	--	Zircaloy-4	20.7	3.8
Plenum spring	SS 302	4.2	1.9	SS 302	6.0	1.1
End fitting zone						
Top end fitting	SS 304	14.8	6.8	SS 304	10.9	2.0
Bottom end fitting	SS 304	12.4	5.7	SS 304	26.1	4.8
Expansion springs	--	--	--	Inconel X-750	2.1	0.4
Total		291.7	134.5		610.6	111.9

[a]Source: A. G. Croff, M. A. Bjerke, G. W. Morrison, and L. M. Petrie, *Revised Uranium — Plutonium Cycle PWR and BWR Models for the ORIGEN Computer Code*, ORNL/TM-6051, September 1978.

[b]Assumed to be discarded with fuel assembly; channels are often reused with fresh fuel.

[c]Distributed throughout the PWR core in sleeves and so forth.

Table 2.1.2.1-5   Sample physical description report from LWR NFA hardware database
(Table 2.8.1 from K.J. Notz, *Characteristics of Potential Repository Waste,*
DOE/RW-0184-R1, V.1 [draft], July, 1990)

```
Combustion Enigneering SYSTEM80 12-Rod Full-Length Control Element

Composition:
     Material            Total Weight(kg)      Neutron Zone

   St.Steel 304                8.17                 Top
   Inconel 625                53.62                 Top
   Boron Carbide (CE)         20.90                 Top
   St.Steel 304                0.68             Gas Plenum
   Inconel 625                 2.20             Gas Plenum
   Boron Carbide (CE)          1.60             Gas Plenum


Used at the Following Reactors:
     Reactor              Number in Core

   Palo Verde 1                48
   Palo Verde 2                48
   Palo Verde 3                48


Used with the Following Fuel Assembly Types:
     Vendor                   Array      Version

   Combustion Engineering    16 x 16    System 80
```

Table 2.1.2.1-6   Sample radiological description report from the LWR NFA hardware database (Table 2.8.2 from K.J. Notz, *Characteristics of Potential Repository Waste,* DOE/RW-0184-R1, V.1 [draft], July, 1990)

```
Combustion Engineering SYSTEM80 12-Rod Full-Length Control Element
```

```
                       ISOTOPIC COMPOSITION
```

Used for 7 cycles (77,000 MWd/MTIHM)   5 years after discharge
Weight: 97.170 kg   Volume of metal: 0.013289 Cu. Meters

Isotope	Grams	Watts	Curies	Curies/m3	Class C Limit	Class C Ratio
C-14	5.348E-04	6.994E-07	2.384E-05	5.311E-03	80	0.6
Ni-59	2.474E-01	7.447E-07	1.876E-02	4.179E+02	220	1.9
Ni-63	3.583E-02	2.227E-04	2.211E+02	4.926E+04	7000	7.0
Co-60	9.512E-03	1.659E-03	1.068E+01	2.397E+03	N/A	N/A
Nb-94	9.760E-03	1.865E-05	1.831E+00	4.097E+02	0.2	220
Total	5.490E+00	1.535E+00	8.349E+03	2.465E+06	N/A	N/A

Used for 10 cycles (111,000 MWd/MTIHM)   5 years after discharge
Weight: 97.170 kg   Volume of metal: 0.013289 Cu. Meters

Isotope	Grams	Watts	Curies	Curies/m3	Class C Limit	Class C Ratio
C-14	5.348E-04	6.994E-07	2.384E-05	5.311E-03	80	0.6
Ni-59	2.474E-01	7.447E-07	1.876E-02	4.179E+02	220	1.9
Ni-63	3.583E-02	2.227E-04	2.211E+02	4.926E+04	7000	7.0
Co-60	9.512E-03	1.659E-03	1.068E+01	2.397E+03	N/A	N/A
Nb-94	9.760E-03	1.865E-05	1.831E+00	4.097E+02	0.2	220
Total	5.490E+00	1.535E+00	8.349E+03	2.465E+06	N/A	N/A

Table 2.1.2.1-6 (continued)

PHOTON SPECTRA

Mean Energy(MeV)	Photons/second (77,000 MWd/MTIHM)	Photons/second (110,000 MWd/MTIHM)
0.0100	2.162E+10	3.569E+10
0.0250	3.674E+09	6.063E+09
0.0375	2.088E+09	3.444E+09
0.0575	2.397E+09	3.874E+09
0.0850	9.237E+08	1.524E+09
0.1250	3.548E+08	7.851E+08
0.2250	1.167E+08	1.925E+08
0.3750	3.272E+07	5.396E+07
0.5750	1.879E+06	3.099E+06
0.8500	6.411E+08	9.650E+08
1.2500	7.960E+11	1.313E+12
1.7500	2.253E+01	2.768E+01
2.2500	4.219E+06	6.956E+06
2.7500	1.306E+04.	2.152E+04

METALLIC COMPOSITION
(Materials modeled to obtain this report)

Material	Total Weight (kg)	Zone
Inconel 625	53.620	Top
Boron Carbide	20.900	Top
Stainless Steel 304	8.170	Top
Inconel 625	2.200	Gas Plenum
Boron Carbide	1.600	Gas Plenum
Stainless Steel 304	0.680	Gas Plenum

The data presented here are only for the purpose of illustrating the form of the radiological description report. They are not intended to be used for any purpose other than that of illustration.

Table 2.1.2.1-7 **Summary of the quantities of MFA components projected to be available for delivery to the FWMS—for cases where components are delivered as an integral part of the fuel assembly and where they are delivered in either an uncompacted or compacted form.[a,b] (Table 2-1 from E. R. Johnson Associates, Inc. [compilers],** *Acceptance of Non-Fuel Assembly Hardware by the Federal Waste Management System***, ORNL/SUB./86-SA094/8, JAI-328, March, 1990)**

	Total Units	Can Dimensions (in)	Can Capacity	Total No. Cans or Units	Weight of Loaded Can or Unit (lb)
As Integral Part of Fuel Assys					
PWR Control Rod Assemblies	10,000		In Fuel Assy	10,000	149
PWR Burnable Poison Assys (West)	55,000		In Fuel Assy	55,000	156
PWR Burnable Poison Assys (B&W)	6,500		In Fuel Assy	6,500	57
PWR Neutron Source Assemblies	320		In Fuel Assy	320	51
PWR Thimble Plug Assemblies	2,900		In Fuel Assy	2,900	13
BWR Fuel Channels	110,000		In Fuel Assy	110,000	98
BWR Control Assemblies[c]	14,500		No Can	14,500	225
BWR Instrument Assemblies	5,000		In Fuel Assy	5,000	2
BWR Poison Curtains[c]	750	10.5x10.5x176	74	11	2,263
Compacted					
PWR Control Rod Assys – Rod Sets	10,000	9x9x160	15	667	2,437
– Spiders	10,000	9x9x160	20	500	482
PWR Burnable Poison Assys (West)					
– Rod Sets	55,000	9x9x160	15	3,667	2,527
– Spiders	55,000	9x9x160	40	1,375	682
PWR Burnable Poison Assys (B&W)					
– Rod Sets	6,500	9x9x160	19	342	1,253
– Spiders	6,500	9x9x160	26	250	530
PWR Neutron Source Assemblies					
– Rod Sets	320	9x9x160	15	21	967
– Spiders	320	9x9x160	53	6	746
PWR Thimble Plug Assys – Rod Sets	2,900	9x9x160	114	25	778
– Spiders	2,900	9x9x160	40	73	682
BWR Fuel Channels	110,000	6x6x168	7	15,714	909
BWR Control Assemblies[d]	14,500	No Can	No Can	14,500	225
BWR Instrument Assemblies	5,000	6x6x160	47	106	306
BWR Poison Curtains	750	10.5x10.5x176	74	11	2,263
Uncompacted					
PWR Control Rod Assemblies	10,000	9x9x162	1	10,000	475
PWR Burnable Poison Assys (West)	55,000	9x9x160	1	55,000	478
PWR Burnable Poison Assys (B&W)	6,500	9x9x160	1	6,500	379
PWR Neutron Source Assemblies	320	9x9x160	1	320	373
PWR Thimble Plug Assemblies	2,900	9x9x160	13	223	491
BWR Fuel Channels	110,000	No Can	No Can	110,000	98
BWR Control Assemblies	14,500	No Can	No Can	14,500	225
BWR Instrument Assemblies	5,000	6x6x160	47	106	306
BWR Poison Curtains	750	10.5x10.5x176	74	11	2,263

[a] Assumes all NFA components listed are classified as greater-than-Class-C waste
[b] Quantities are estimated to be those equivalent to the production of a nominal 80,000 MTU of SNF assemblies.
[c] Not integral
[d] Uncompacted

Table 2.1.2.1-8   Summary comparison of attributes of control rod assemblies in PWRs.[a] (Table 3-1 from E. R. Johnson Associates, Inc. [compilers], *Acceptance of Non-Fuel Assembly Hardware by the Federal Waste Management System,* **ORNL/SUB./86-SA094/8, JAI-328, March, 1990)**

Fuel Array	Total Length (in)	Spider Length (in)	No. Rods	Total Weight (lb)	Poison	No. Assys in Core
Westinghouse						
14x14	159	8	16	128	Ag-In-Cd	53 Full Length; 8 Part Length[b]
14x14	157	8	16	128	Ag-In-Cd	53 Full Length; 8 Part Length[b]
14x14	134	8	16	109	Ag-In-Cd	53 Full Length; 8 Part Length[b]
15x15	157	8	20	165	Ag-In-Cd	53 Full Length; 8 Part Length[b]
17x17	161	8	24	149	Ag-In-Cd	53 Full Length; 8 Part Length[b]
17x17	161	8	24	180	Hf	53 Full Length; 8 Part Length[b]
17x17	161	8	24	149	Ag-In-Cd	53 Full Length; 8 Part Length[b]
17x17 (Hybrid)	161	8	24	93	B_4C/Ag-In-Cd	53 Full Length; 8 Part Length[b]
17x17	161	8	24	100	Ag-In-Cd	53 Full Length; 8 Part Length[b]
B&W						
15x15	160	4	16	130	Ag-In-Cd	61
Combustion Engineering						
16x16	253	8[c]	4	95	Inconel 625	13
16x16	253	8[c]	12	192	B_4C	48
16x16	181	8[c]	5	92	Inconel 625	8
16x16	181	8[c]	5	72	B_4C	83
16x16	181	8[c]	5	91	Inconel 625	8
16x16	181	8[c]	5	71	B_4C	73
16x16	163	8[c]	5	83	Inconel 625	8
16x16	163	8[c]	5	66	B_4C	83
14x14	161	8[c]	5	105	B_4C	12
14x14	161	8[c]	5	82	B_4C	8
14x14	161	8[c]	5	63	B_4C	12
14x14	161	8[c]	5	77	B_4C	65
14x14	152	8[c]	5	63	B_4C	4
14x14	152	8[c]	5	67	B_4C	45
15x15	151	8[c]	Cruciform	214	Ag-In-Cd	45

[a]   Source: DOE/RW-O184, Vol. 5   [b]   Salem FSAR   [c]   Estimated (assumed)

2.1.2.2 PWR Fuel

Table 2.1.2.2-1   Spent-fuel disassembly hardware for major PWR assembly types (listing by assembly class) (Table 5.9 from K.J. Notz, T.D. Welch, R.S. Moore, and W.J. Reich, *Preliminary Waste Form Characteristics,* ORNL-TM-11681 [draft], September, 1990)

Class Name Assembly Type Name	Hardware Weight	Hardware Composition
B&W 15 x 15 Assembly Class		
B&W 15 x 15 B&W Mark B	35.6 kg	26% Zirc, 25% Inc, 49% SS
B&W 15 x 15 B&W Mark BZ	35.6 kg	40% Zirc, 11% Inc, 49% SS
B&W 17 x 17 Assembly Class		
B&W 17 x 17 B&W Mark C	42.3 kg	28% Zirc, 25% Inc, 47% SS
CE 14 x 14 Assembly Class		
CE 14 x 14 CE	29.8 kg	58% Zirc, 8% Inc, 34% SS
CE 14 x 14 ANF	33.3 kg	45% Zirc, 15% Inc, 40% SS
CE 14 x 14 WE	34.1 kg	32% Zirc, 26% Inc, 42% SS
CE 16 x 16 Assembly Class		
CE 16 x 16 CE ANO2	40.1 kg	50% Zirc, 6% Inc, 44% SS
CE 16 x 16 CE SONGS	42.6 kg	45% Zirc, 14% Inc, 41% SS
CE 16 x 16 System 80 Assembly Class		
CE 16 x 16 CE System 80	44.0 kg	44% Zirc, 13% Inc, 43% SS
WE 14 x 14 Assembly Class		
WE 14 x 14 WE Std	32.0 kg	20% Inc, 80% SS
WE 14 x 14 WE LOPAR	31.8 kg	25% Zirc, 20% Inc, 55% SS
WE 14 x 14 WE OFA	32.1 kg	55% Zirc, 8% Inc, 37% SS
WE 14 x 14 ANF	28.4 kg	49% Zirc, 4% Inc, 47% SS
WE 14 x 14 ANF Toprod	24.6 kg	54% Zirc, 4% Inc, 42% SS
WE 15 x 15 Assembly Class		
WE 15 x 15 WE Std	35.8 kg	24% Inc, 76% SS
WE 15 x 15 WE LOPAR	35.6 kg	26% Zirc, 24% Inc, 50% SS
WE 15 x 15 WE OFA	32.6 kg	53% Zirc, 9% Inc, 38% SS
WE 15 x 15 ANF	27.3 kg	53% Zirc, 4% Inc, 43% SS
WE 17 x 17 Assembly Class		
WE 17 x 17 WE LOPAR	29.6 kg	32% Zirc, 22% Inc, 45% SS
WE 17 x 17 WE OFA	32.3 kg	51% Zirc, 8% Inc, 40% SS
WE 17 x 17 ANF	34.6 kg	59% Zirc, 7% Inc, 34% SS

Table 2.1.2.2-2   Mechanical design parameters of PWR fuel assemblies* (Table 2 from R.E. Woodley, *The Characteristics of Spent LWR Fuel Relevant to its Storage in Geologic Repositories,* HEDL-TME 83-28, October, 1983)

	Westinghouse 15 x 15	Westinghouse 17 x 17	Combustion Engineering 14 x 14	Combustion Engineering 16 x 16	Babcock & Wilcox 15 x 15	Babcock & Wilcox 17 x 17	Exxon 15 x 15
Rod Array	15 x 15	17 x 17	14 x 14	16 x 16	15 x 15	17 x 17	15 x 15
Fuel Assemblies							
Transverse Dimension (in., cm)	8.426(21.402)	8.426(21.402)	7.98(20.27)	7.98(20.27)	8.536(21.681)	8.436(21.427)	
Assembly Weight (lb, kg)	1420(644)	1450(658)	1280(581)	1446(656)			
Overall Assembly Length (in., cm)	161.3(409.7)	161.3(409.7)	156.7(398)	176.8(448.9)		165.6(420.6)	
Fuel Rods							
Number per Assembly	204	264	176	236	.208	264	204
Rod Pitch (in., cm)	0.563(1.430)	0.496(1.260)	0.580(1.473)	0.506(1.285)	0.568(1.443)	0.501(1.273)	0.563(1.430)
Length (in., cm)	149.7(380.2)	151.6(385.1)	145.9(370.6)	161.0(408.9)	153.7(390.4)	152.1(386.4)	152.0(386.1)
Fueled Length (in., cm)	144.0(365.8)	143.7(365.0)	136.7(347.2)	150.0(381.0)	141.8(360.2)	143.0(363.2)	144.0(365.8)
OD (in., cm)	0.422(1.072)	0.374(0.950)	0.440(1.118)	0.382(0.970)	0.430(1.092)	0.379(0.963)	0.424(1.077)
Diametral Gap (in., cm)	0.0075(0.0190)	0.0065(0.0165)	0.0085(0.0216)	0.007(0.0178)	0.0084(0.0213)	0.0078(0.0198)	0.0075(0.0190)
Cladding Thickness (in., cm)	0.0243(0.0617)	0.0225(0.0572)	0.026(0.0660)	0.025(0.0635)	0.0265(0.0673)	0.0240(0.0610)	0.030(0.0762)
Cladding Material	Zircaloy-4ᵇ	Zircaloy-4	Zircaloy-4	Zircaloy-4	Zircaloy-4	Zircaloy-4	Zircaloy-4
Fuel Pellets							
Density (% TD)	95	95	94.75	95	95	95	94
Diameter (in., cm)	0.3659(0.9294)	0.3225(0.8192)	0.3795(0.9639)	0.325(0.8255)	0.3686(0.9362)	0.3232(0.8209)	0.3565(0.9055)
Length (in., cm)	0.600(1.524)	0.530(1.346)	0.650(1.651)	0.390(0.991)	0.600(1.524)	0.375(0.952)	0.273(0.693)
Guide Tubes							
Number	20	24	4	4	16	24	20
Upper OD (in., cm)	0.544(1.382)	0.480(1.219)	1.115(2.832)	1.115(2.832)		0.465(1.181)	
Wall Thickness (in., cm)	0.017(0.043)	0.016(0.041)	0.036(0.091)	0.036(0.091)		0.017(0.043)	
Material	Zircaloy-4	Zircaloy-4	Zircaloy-4	Zircaloy-4	Zircaloy-4	Zircaloy-4	
Instrument Tubes							
Number	1	1	1	1	1	1	1
OD (in., cm)	0.544(1.382)	0.480(1.219)	1.115(2.832)	0.417(1.059)		0.420(1.067)	
Wall Thickness (in., cm)	0.017(0.043)	0.016(0.041)	0.036(0.091)	0.027(0.069)		0.01512(0.0384)	
Material	Zircaloy-4	Zircaloy-4	Zircaloy-4	Zircaloy-4	Zircaloy-4	Zircaloy-4	
Tie Plate							
Material	304 SS	304 SS	304 SS	304 SS	304 SS	304 SS	
Spacers							
Numbers	7	8	9	12	8	8	
Material	Inconel 718ᵇ / Inconel 718	Inconel 718 / Inconel 718	Zircaloy-4 / Zircaloy-4	Zircaloy-4 / Zircaloy-4	Inconel 718 / Inconel 718	Inconel 718 / Inconel 718	
Springs					•		
Plenum Springs							
Working Length	6.80(17.27)	6.70(17.02)	8.60(21.86)	6.48(16.46)			
Material	Inconel 718	Inconel 718	Inconel 718	Inconel 718			

ᵃ   Updated from Reference 3.
ᵇ   Zircaloy™ is a registered trademark of Westinghouse Electric Corp.

Table 2.1.2.2-3   Mechanical design parameters for Westinghouse PWR fuel assemblies.[a] (Table 2.2 from J.W. Roddy, H.C. Claiborne, R.C. Ashline, P.T. Johnson, and B.T. Rhyne, *Physical and Decay Characteristics of Commercial LWR Spent Fuels*, ORNL/TM-9591/V.1, October, 1985)

| | Rod array | | | | | | | |
| Design component | 17 × 17 | | | 15 × 15 | | 14 × 14 | | 16 × 16[b] |
	Standard	OFA	VANTAGE	Standard	OFA	Standard	OFA	Standard
Assembly								
Transverse dimension, in.	8.426	8.426	8.426	8.426	8.426	7.763	7.763	7.763
Assembly weight, lb	1467	1365	1365	1440	1443	1274	1135	1310
Uranium/assembly, lb	1017.23	932.61	932.61	1011.86	1011.86	887.77	786.61	905.32
UO$_2$/assembly, lb	1154.00	1058.00	1058.00	1147.90	1147.90	1007.14	892.37	1027.04
Overall length, in.	159.8	159.8	160.1	159.765	159.765	159.71	159.71	159.8
Rod replacement capabilities	Yes	Yes	Yes	Yes	Yes	Yes	Yes	Yes
Disassembly capabilities	Yes	Yes	Yes	Yes	Yes	Yes	Yes	Yes
Fuel rods								
Date of commercial operation	1975	1984	1987	1967	1983	1969	1984	1981
Number per assembly	264	264	264	204	204	179	179	235
Rod pitch, in.	0.496	0.496	0.496	0.563	0.563	0.556	0.556	0.485
Length, in.	151.635	151.635	152.3	151.83	151.83	151.83	151.83	151.64
Fuel length, in.	144	144	144	144	144	144	144	144
OD, in.	0.374	0.36	0.36	0.422	0.422	0.422	0.400	0.374
Diametral gap, in.	0.0065	0.0062	0.0065	0.0075	0.0075	0.0075	0.0070	0.0065
Clad thickness, in.	0.0225	0.0225	0.0225	0.0243	0.0243	0.0243	0.0243	0.0225
Clad material	Zr-4	Zr-4	Zr-4	Zr-4	Zr-4	Zr-4	Zr-4	Zr-4
Fuel pellets								
Type	UO$_2$	UO$_2$	UO$_2$	UO$_2$	UO$_2$	UO$_2$	UO$_2$	UO$_2$
Density, % TD	95	95	95	95	95	95	95	95
Diameter, in.	0.3225	0.3088	0.3088	0.3659	0.3695	0.3659	0.3444	0.3225
Length, in.	0.53	0.51	0.51	0.60	0.60	0.60	0.565	0.53
Total weight/rod, lb	4.37	4.01	4.01	5.52	5.52	5.63	4.99	4.37
Spacer pellets	None	None	None	None	None	None	None	None
Plenum spring								
Working length, in.	6.90	6.90	7.405	7.136	7.136	7.136	7.158	6.90
Material	SS	SS	SS	SS	SS	SS	SS	SS
Miscellaneous								
Prepressurization, atm	Variable	Variable	Variable	Variable	Variable	Variable	Variable	Variable
Gas used	Helium	Helium	Helium	Helium	Helium	Helium	Helium	Helium
Spacer grids								
Top and bottom grids								
Number/assembly	2	2	2	2	2	2	2	2
Material	Inconel 718	Inconel 718	Inconel 718	Inconel 718	Inconel 718	Inconel 718	Inconel 718	Inconel 718
Intermediate grids								
Number/assembly	6	6	6	5	5	5	5	6
Material	Inconel 718	Zr-4	Zr-4	Inconel 718	Zr-4	Inconel 718	Zr-4	Inconel 718
Intermediate flow mixer								
Number/assembly	None	None	3	None	None	None	None	None
Material			Zr-4					
Guide tubes								
Number/assembly	24	24	24	20	20	16	16	20
OD, in.	0.474	0.474	0.474	0.546	0.532	0.539	0.527	0.471
Wall thickness, in.	0.016	0.016	0.016	0.017	0.017	0.017	0.017	0.016
Material	Zr-4	Zr-4	Zr-4	Zr-4	Zr-4	Zr-4	Zr-4	Zr-4
Instrument tube								
Number/assembly	1	1	1	1	1	1	1	1
OD, in.	0.48	0.476	0.476	0.546	0.533	0.422	0.4019	0.473
Material	Zr-4	Zr-4	Zr-4	Zr-4	Zr-4	Zr-4	Zr-4	Zr-4
Top and bottom nozzles material	SS	SS	SS	SS	SS	SS	SS	SS
Approximate no. of assemblies shipped by Westinghouse	6000	800	0	5200	400	4000	30	400

[a] Source: L. Iyengar, Westinghouse Electric Corporation, letter to J.W. Roddy, Oak Ridge National Laboratory, December 17, 1984

[b] All of these assemblies have been exported.

Table 2.1.2.2-4 **Mechanical design parameters for Combustion Engineering PWR fuel assemblies.**[a] **(Table 2.3 from J.W. Roddy, H.C. Claiborne, R.C. Ashline, P.T. Johnson, and B.T. Rhyne,** *Physical and Decay Characteristics of Commercial LWR Spent Fuels*, **ORNL/TM-9591/V.1, October, 1985)**

Design component	Rod array	
	14 × 14R	16 × 16
Fuel assemblies		
Width dimension, in.	8.12	8.23
Assembly weight, lb (typical)	1204	1435
Overall length, in. (typical)	157	177
Rod replacement capabilities	Yes	Yes
Disassembly capabilities	Yes	Yes
Fuel rods		
Date of introduction (first criticality)	11/3/72	12/6/78
Number per assembly (unshimmed)	176	236
Rod pitch, in.	0.580	0.5063
Rod length, in. (typical)	146	161
Active fuel length, in.	136.7	150
OD, in.	0.440	0.382
Diametral gap, in.	0.0075	0.0070
Clad thickness, in.	0.028	0.025
Clad material (composition)	Zircaloy-4	Zircaloy-4
Total weight/rod, lb	6.7	5.7
Fuel pellets		
Density, % theoretical	95	95
Diameter, in.	0.3765	0.325
Length, in.	0.450	0.390
Total weight/rod, lb	5.4	4.5
Guide tubes[b]		
Number	5	5
OD, in	1.115	0.980
Wall thickness, in.	0.040	0.040
Tie plate		
Material	304 SS	304 SS
Total weight/assembly, lb	NA[c]	NA
Spacers		
Number (top and bottom)	2	2
Material (composition)	Al_2O_3	Al_2O_3
Total weight/rod, lb	0.004	0.005
Plenum springs		
Working length, in.	8.6	10.0
Material (composition)	SS	SS
Total weight/rod, lb	0.05	0.07
Miscellaneous		
Prepressurized to atm (typical)	Variable	Variable
Gas used	100% He	100% He

[a] Source: M.G. Andrews, C-E Power Systems, Combustion Engineering, Inc., letter to J.W. Roddy, Oak Ridge National Laboratory, February 11, 1985

[b] Guide tubes may be used to guide the control-rod assembly or to contain instrumentation that is located in the center guide tube.

[c] Not available

Table 2.1.2.2-5   **Number of Combustion Engineering PWR fuel assemblies active and discharged.[a] (Table 2.4 from J.W. Roddy, H.C. Claiborne, R.C. Ashline, P.T. Johnson, and B.T. Rhyne,** *Physical and Decay Characteristics of Commercial LWR Spent Fuels,* **ORNL/TM-9591/V.1, October, 1985)**

Reactor	Core assemblies per cycle	Total active and discharged		
		14 × 14	16 × 16	15 × 15
Arkansas Nuclear One-2	177	–	345	–
Calvert Cliffs 1	217	693	–	–
Calvert Cliffs 2	217	609	–	–
Fort Calhoun	133	289	–	–
Maine Yankee	217	650	–	–
Millstone 2	217	361	–	–
Palisades	204	–	–	272
St. Lucie-1	217	497	–	–
St. Lucie-2	217	–	297	–
SONGS-2	217	–	217	–
SONGS-3	217	–	217	–

[a]   Source: M.G. Andrews, C-E Power Systems, Combustion Engineering, Inc., letter to J.W. Roddy, Oak Ridge National Laboratory, February 11, 1985

Table 2.1.2.2-6 Mechanical design parameters for Babcock and Wilcox PWR fuel assemblies.[a] (Table 2.5 from J.W. Roddy, H.C. Claiborne, R.C. Ashline, P.T. Johnson, and B.T. Rhyne, *Physical and Decay Characteristics of Commercial LWR Spent Fuels,* ORNL/TM-9591/V.1, October, 1985)

Design component	Rod array		
	15 × 15	17 × 17	15 × 15 SS
Assembly			
Transverse dimension, in.	8.536	8.536	8.466
Assembly weight, lb	1515	1506	NA[b]
Overall length, in.	165–5/8	165–23/32	137.066 + .565 spring protrusion
Rod replacement capabilities	None	None	Grippable top end
Disassembly capabilities	None	None	Locking cups on upper nuts
Fuel rods			
Date of introduction	1971	1976	1976
Number per assembly	208	264	204
Rod pitch, in.	0.568	0.502	0.563
Length, in.	153.68	152.688	126.68
Fueled length, in.	141.8	143.0	120.5
OD, in.	0.430	0.379	0.422
Diametral gap, in.	0.0084	0.0078	0.0065
Clad thickness, in.	0.0265	0.0240	0.0165
Clad material	Zircaloy–4	Zircaloy–4	304 SS
Total weight/rod, lb	7.0	4.9	5.9
Fuel pellets			
Density, % TD	95	95	95
Diameter, in.	0.3686	0.3232	0.3825
Length, in.	0.600	0.375	0.458
Total weight/rod, lb	5.58	Unavailable	Unavailable
Guide tubes			
Number	16	24	20
OD, in.	0.530	0.564	0.543, upper 106.8 in. 0.479, lower 20.95 in.
Wall thickness, in.	0.016	0.0175	0.012
Weight/assembly with end plugs, lb	16.5	24	17
Material	Zircaloy–4	Zircaloy–4	304 SS
Instrument tubes			
Number	1	1	1
OD, in.	0.493	0.420	0.422
Material (composition)	Zircaloy–4	Zircaloy–4	304 SS
Total weight/assembly, lb	0.7	0.7	0.78
Tie plate			
Material	NA	NA	NA
Spacers			
Number	3	3	--
Material (composition)	Zircaloy–4	Zircaloy–4	--
Total weight/rod, lb	.028	Unavailable	--
Plenum springs			
Working length, in.	7.435	5.9735	5.01
Material (composition)	302 SS	302 SS	302 SS
Total weight/rod, lb	Unavailable	Unavailable	Unavailable
Miscellaneous			
Prepressurized to, psig	465	435	40
Gas used	Helium	Helium	Helium

[a] Source: K.O. Stein, Nuclear Power Division, Babcock and Wilcox, letter to J.W. Roddy, Oak Ridge National Laboratory, January 25, 1985

[b] Not available

Table 2.1.2.2-7   Control and burnable poison rods in PWRs used by Babcock and Wilcox.[a]
(Table 2.6 from J.W. Roddy, H.C. Claiborne, R.C. Ashline, P.T. Johnson,
and B.T. Rhyne, *Physical and Decay Characteristics of Commercial LWR
Spent Fuels*, ORNL/TM-9591/V.1, October, 1985)

Design component	Rod array		
	Standard	Long life	
	15 × 15		17 × 17
Control rod assembly			
Clad material	304 SS	UNS N06625[b]	304 SS
Clad length, in.	145.5	147.5	148-7/8
Clad OD, in.	0.440	0.441	0.377
Clad ID, in.	0.398	0.396	0.310
Pellet material	Ag-In-Cd	Ag-In-Cd	B_4C
Pellet OD, in.	0.392	0.386	0.285
Prepressure	1 atm He	465 psig He	1 atm He
Plenum volume, in.^{3}	0.4214	--	0.7075
Assembly weight, lb	130	130	65
Pellet stack length, in.	134	139	139
Burnable poison rod assembly			
Clad material	Zircaloy-4		Zircaloy-4
Clad length, in.	147-1/4		148
Clad OD, in.	0.430		0.371
Clad ID, in.	0.360		0.309
Pellet material	Al_2O_3—B_4C		Al_2O_3—B_4C
Pellet OD, in.	0.340		0.293
Prepressure	1 atm He		1 atm He
Plenum volume, in.^{3}	0.840		0.8774
Assembly weight, lb	57		60
Pellet stack length, in.	126		126

[a]   Source: K.O. Stein, Utility Power Generation Division, Babcock and Wilcox, letter to J.W. Roddy, Oak Ridge
National Laboratory, January 25, 1985
[b]   NiCrMoCb alloy

Table 2.1.2.2-8 **Number of PWR fuel assemblies shipped by Babcock and Wilcox.**[a] (Table 2.7 from J.W. Roddy, H.C. Claiborne, R.C. Ashline, P.T. Johnson, and B.T. Rhyne, *Physical and Decay Characteristics of Commercial LWR Spent Fuels,* ORNL/TM-9591/V.1, October, 1985)

Reactor	Rod array		
	15 × 15	17 × 17	15 × 15 SS
Oconee 1	646	—	—
Oconee 2	533	2 MkC 2 MkCR	—
Oconee 3	521	—	—
ANO-1 Unit 1	493	—	—
Rancho Seco	432	—	—
Davis Besse	317	—	—
Crystal River	437	—	—
TMI-1	385	—	—
Conn Yankee	—	—	368
TVA Bellefonte I	—	205	—
TVA Bellefonte II	—	205	—

[a] Source: K.O. Stein, Nuclear Power Division, Babcock and Wilcox, letter to J.W. Roddy, Oak Ridge National Laboratory, January 25, 1985

Table 2.1.2.2-9 **Mechanical design parameters for Exxon Nuclear PWR fuel assemblies.[a]** (Table 2.8 from J.W. Roddy, H.C. Claiborne, R.C. Ashline, P.T. Johnson, and B.T. Rhyne, *Physical and Decay Characteristics of Commercial LWR Spent Fuels,* ORNL/TM-9591/V.1, October, 1985)

| Design component | Rod array | | | |
	14 × 14	15 × 15	17 × 17	14 × 14[b]
Assembly				
Transverse dimension, in.	7.763	8.426	8.426	8.105
Assembly weight, lb	NA[c]	1425	NA	1280
Overall length, in.	162	162	162	157
Rod replacement capability	Yes	Yes	Yes	Yes
Disassembly capability	Yes	Yes	Yes	Yes
Fuel rods				
Number per assembly	179	204	264	176
Rod pitch, in.	0.556	0.563	0.496	0.580
Length, in.	152	152	152	147
Fueled length, in.	144	144	144	137
OD, in.	0.417/0.424	0.424	0.360/0.376	0.440
Diametral gap, in.				
Clad thickness, in.	0.0295/0.030	0.030	0.025/0.024	0.031
Clad material	Zr-4	Zr-4	Zr-4	Zr-4
Total weight/rod, lb	NA	NA	NA	NA
Fuel pellets				
Type	UO_2	UO_2	UO_2	UO_2
Density, % TD	94	94	94	94
Diameter, in.	0.3505/0.3565	0.3565	0.303/0.321	0.370
Length, in.	NA	NA	NA	NA
Total weight/rod, lb	NA	NA	NA	NA
Spacers				
Number	7	7	7	7
Material	Zr-4/Inconel-718	Zr-4/Inconel-718	Zr-4/Inconel-718	Zr-4/Inconel-718
Total weight/rod, lb	2—3	2—3	2—3	2—3
Plenum springs				
Working length, in.	NA	NA	NA	NA
Material	Inconel-718	Inconel-718	Inconel-718	Inconel-718
Miscellaneous				
Prepressurization, atm	>20	>20	>20	>20
Gas used	Helium	Helium	Helium	Helium
Guide tubes				
Number	16	20	24	5
OD, in.	0.541	0.544	0.480	1.115
Wall thickness, in.	0.017	0.0165	0.016	0.040
Material	Zr-4	Zr-4	Zr-4	Zr-4
Instrument tubes				
Number	1	1	1	NA
OD, in.	NA	NA	NA	NA
Material	Zr-4	Zr-4	Zr-4	Zr-4
Tie plate				
Material	SS 304L, Inconel springs	SS 304L, Inconel springs	SS 304L, Inconel springs	SS 304L, Inconel springs
Total weight/assembly, lb	25	25	25	25

[a]   Source: C.J. Busselman, Exxon Nuclear Company, Inc., letter to J.W. Roddy, Oak Ridge National Laboratory, March 28, 1985 (Note: Exxon Nuclear Company, Inc., has become Advanced Fuels Corp. [Siemens].)

[b]   Produced only for Combustion Engineering

[c]   Not available

2.1.2.3 BWR Fuel

Table 2.1.2.3-1   Spent-fuel disassembly hardware for major BWR assembly types (listing by assembly class) (Table 5.10 from K.J. Notz, T.D. Welch, R.S. Moore, and W.J. Reich, *Preliminary Waste Form Characteristics,* ORNL-TM-11681 [draft] September, 1990)

Class Name Assembly Type Name	Hardware Weight[a]	Hardware Materials	Comments
GE BWR/2,3 Assembly Class			
GE BWR/2,3 7 x 7 GE-2a	8.4 kg	20% Zirc, 4% Inc, 76% SS	b
GE BWR/2,3 7 x 7 GE-2b	8.44 kg	20% Zirc, 4% Inc, 76% SS	
GE BWR/2,3 7 x 7 GE-3	8.3 kg	20% Zirc, 4% Inc, 76% SS	
GE BWR/2,3 8 x 8 GE-4	9.9 kg	28% Zirc, 4% Inc, 68% SS	c
GE BWR/2,3 8 x 8 GE-5	10.9 kg	35% Zirc, 3% Inc, 62% SS	b,c
GE BWR/2,3 8 x 8 GE Prepressurized	10.9 kg	35% Zirc, 3% Inc, 62% SS	b,c
GE BWR/2,3 8 x 8 GE Barrier	10.9 kg	35% Zirc, 3% Inc, 62% SS	b,c
GE BWR/2,3 8 x 8 GE-8	12.7 kg	44% Zirc, 3% Inc, 53% SS	
GE BWR/2,3 7 x 7 ANF	13.6 kg	41% Zirc, 5% Inc, 55% SS	
GE BWR/2,3 8 x 8 ANF	8.1 kg	28% Zirc, 5% Inc, 67% SS	
GE BWR/2,3 9 x 9 ANF	9.3 kg	27% Zirc, 6% Inc, 67% SS	
GE BWR/4,5,6 Assembly Class			
GE BWR/4,5,6 7 x 7 GE-2	8.4 kg	20% Zirc, 4% Inc, 76% SS	
GE BWR/4,5,6 7 x 7 GE-3a	8.4 kg	20% Zirc, 4% Inc, 76% SS	
GE BWR/4,5,6 7 x 7 GE-3b	8.4 kg	20% Zirc, 4% Inc, 76% SS	
GE BWR/4,5,6 8 x 8 GE-4a	10.0 kg	28% Zirc, 4% Inc, 68% SS	c
GE BWR/4,5,6 8 x 8 GE-4b	10.0 kg	28% Zirc, 4% Inc, 68% SS	b,c
GE BWR/4,5,6 8 x 8 GE-5	11.0 kg	35% Zirc, 3% Inc, 62% SS	c
GE BWR/4,5,6 8 x 8 GE Prepressurized	11.0 kg	35% Zirc, 3% Inc, 62% SS	b,c
GE BWR/4,5,6 8 x 8 GE Barrier	11.0 kg	35% Zirc, 3% Inc, 62% SS	b,c
GE BWR/4,5,6 8 x 8 GE-8	12.9 kg	44% Zirc, 3% Inc, 53% SS	b,c,d
GE BWR/4,5,6 8 x 8 ANF	9.0 kg	35% Zirc, 4% Inc, 61% SS	
GE BWR/4,5,6 9 x 9 ANF	9.3 kg	28% Zirc, 6% Inc, 66% SS	

[a]   The weight of fuel channels depends directly on the thickness of the channel. 80, 100, and 120-mil fuel channels weigh approximately 30, 38, and 45 kg, respectively. Because the thickness of the channel is not assembly-type specific, the weight of fuel channels is not included in the SFD hardware weights given.
[b]   Estimated on the basis of similar assemblies
[c]   Estimated on the basis of calculated weights of water rods and water channels
[d]   Four water rods assumed.

Table 2.1.2.3-2   Summary of General Electric BWR fuel designs[a] (Table 1 from R.E. Woodley, *The Characteristics of Spent LWR Fuel Relevant to its Storage in Geologic Repositories,* **HEDL-TME 83-28, October, 1983)**

Fuel Rod Array	7 x 7		7 x 7R	8 x 8	8 x 8R
Introduction Date	1966	1968	1972	1973	1977
Fuel Rod OD (cm)	1.430	1.448	1.430	1.252	1.227
Fuel Rod ID (cm)		1.268	1.242	1.080	1.064
Nominal Cladding Thickness (mil)	32	35.5	37	34	32
Nominal Diametral Gap (mil)	11	12	12	9	9
Pellet Type	long,sharp corners		short, chamfered		
Hydrogen Getter	No		Yes	Yes	Yes
Peak Linear Power (W/cm)		607	607	440	440
Prepressurized to 3 atm		No	No	No	Yes[b]
Cumulative Fuel Assemblies[c]		10,289	5824	10,731	1898
Assemblies Sipped at Least Once[d]		10,289	5793	5698	7
Estimated Rod Failure Rate (%)		0.98	0.04	0.03	0

[a]   Adapted from Reference 6
[b]   Starting with Fall 1979 deliveries
[c]   Fabricated and put into operation as of Spring 1979
[d]   See Section III.A.3.b for an explanation of sipping.

Table 2.1.2.3-3   Mechanical design parameters of BWR fuel assemblies* (Table 3 from R.E. Woodley, *The Characteristics of Spent LWR Fuel Relevant to its Storage in Geologic Repositories,* HEDL-TME 83-28, October, 1983)

	General Electric		Exxon
Rod Array	7 x 7	8 x 8	8 x 8
Fuel Assemblies			
Transverse Dimension (in., cm)	5.518(14.016)	5.518(14.016)	
Assembly Weight (lb, kg)	600(272.16)	600(272.16)	
Overall Assembly Length (in., cm)	171.2(434.8)	171.2-178.5 (434.8-452.6)	
Fuel Rods			
Number per Assembly	49	63	60
Rod Pitch (in., cm)	0.738(1.874)	0.640(1.626)	0.842(2.139)
Length (in., cm)	161.1(409.2)	161.1(409.2)	156.9(398.5)
Fueled Length (in., cm)	144(365.8)	146(370.8)	144(365.8)
OD (in., cm)	0.563(1.430)	0.493(1.252)	0.5015(1.274)
Diametral Gap (in., cm)	0.012(0.0305)	0.009(0.0229)	0.010(0.0254)
Cladding Thickness (in., cm)	0.032(0.0813)	0.034(0.0864)	0.036(0.0914)
Cladding Material	Zircaloy-2	Zircaloy-2	Zircaloy-2
Fuel Pellets			
Density	95	95	95
Diameter (in., cm)	0.487(1.237)	0.416(1.057)	0.4195(1.066)
Length (in., cm)	0.500(1.270)	0.420(1.067)	0.320(0.813)
Tie Plate			
Material	304 SS	304 SS	
Spacers			
Number	7	7	
Material	Zircaloy-4	Zircaloy-4	
Springs	Inconel	Inconel	
Plenum Springs			
Working Length (in., cm)	10.6(26.9)	10.6-16.0 (26.9-30.6)	
Material	Inconel	Inconel	
Compression Springs			
Working Length (in., cm)	0.94(2.39)	0.84(2.13)	
Material	Inconel	Inconel	

* Updated from Reference 3

Table 2.1.2.3-4 General Electric BWR product lines and characteristics[a] (Table 2.9 from J.W. Roddy, H.C. Claiborne, R.C. Ashline, P.T. Johnson, and B.T. Rhyne, *Physical and Decay Characteristics of Commercial LWR Spent Fuels*, ORNL/TM-9591/V.1, October, 1985)

Product line class	Year of introduction	Plants and characteristics
BWR/1	1955	Dresden-1, Big Rock Point, Humboldt Bay, KRB — Initial commercial BWRs — First internal steam separation
BWR/2	1963	Oyster Creek — The first turnkey plant — Elimination of dual cycle
BWR/3	1965	Dresden-2 — The first jet pump application — Improved emergency core cooling system (ECCS)
BWR/4	1966	Browns Ferry — Increased power density 20%
BWR/5	1969	Zimmer — Improved safeguards — Valve flow control
BWR/6	1972	BWR/6 — 8 × 8 fuel bundle — Added fuel bundles, increased output — Improved recirculation system performance — Improved ECCS performance — Reduced fuel duty

[a] Source: E.D. Fuller, J.R. Finney, and H.E. Streeter, *BWR/6 Nuclear System from General Electric—A Performance Description*, NEDO-10569A, April 1972

Table 2.1.2.3-5   Summary of General Electric BWR reactor fuel designs[a] (Table 2.10 from J.W. Roddy, H.C. Claiborne, R.C. Ashline, P.T. Johnson, and B.T. Rhyne, *Physical and Decay Characteristics of Commercial LWR Spent Fuels,* ORNL/TM-9591/V.1, October, 1985)

Design component	Rod array				
	7 × 7		7 × 7R	8 × 8	8 × 8R
Introduction date	1966	1968	1972	1973	1977
Fuel rod OD, in.	0.563	0.570	0.563	0.493	0.483
Fuel rod ID, in.	0.499		0.0489	0.425	0.419
Nominal cladding thickness, mil	32	35.5	37	34	32
Nominal diametral gap, mil	11	12	12	9	9
Pellet type	Long, sharp corners		Short, chamfered		
Hydrogen getter	No		Yes	Yes	Yes
Peak liner power, W/cm	607		607	440	440
Prepressurized to 3 atm	No		No	No	Yes

[a]   Source: R.E. Woodley, *The Characteristics of Spent LWR Fuel Relevant to its Storage in Geologic Formations,* HEDL-TME 83-28, October 1983

Table 2.1.2.3-6   **Mechanical design parameters of BWR fuel assemblies**[a] **(Table 2.11 from J.W. Roddy, H.C. Claiborne, R.C. Ashline, P.T. Johnson, and B.T. Rhyne,** *Physical and Decay Characteristics of Commercial LWR Spent Fuels,* **ORNL/TM-9591/V.1, October, 1985)**

Design component	Rod array		
	BWR/1—5 (General Electric)		QUAD+ (Westinghouse)
	7 × 7	8 × 8	8 × 8
Fuel assemblies			
Transverse dimension, in.	5.518	5.518	5.50
Assembly weight, lb	600	600	600
Overall assembly length, in.	171.2	171.2—178.5	175.5
Fuel rods			
Number per assembly	49	62—63	64
Rod pitch, in.	0.738	0.640	0.609
Length, in.	161.1	161.1	160.6
Fueled length, in.	144—146	144—146	150
OD, in.	0.563—0.570	0.483—0.493	0.458
Diametral gap, in.	0.011—0.012	0.009	0.083
Cladding thickness, in.	0.032—0.037	0.032—0.034	0.029
Cladding material	Zircaloy-2	Zircaloy-2	Zircaloy-2
Fuel pellets			
Density, % TD	95	95	95
Diameter, in.	0.487	0.416	0.3913
Length, in.	0.500	0.420	0.470
Tie plate			
Material	304 SS	304 SS	304 SS
Spacers			
Number	7	7	
Material	Zircaloy-4	Zircaloy-4	Zircaloy-4
Springs	Inconel	Inconel	Zircaloy-4
Plenum springs			
Working length, in.	10.6	10.6-16.0	9.56
Material	Inconel	Inconel	302 SS
Compression springs			
Working length, in.	0.94	0.84	0.84
Material	Inconel	Inconel	Inconel

[a]   Source: R.E. Woodley, *The Characteristics of Spent LWR Fuel Relevant to its Storage in Geologic Formations,* HEDL-TME 83-28, October 1983, and E.M. Greene, *Spent Fuel Data for Waste Storage Programs,* HEDL-TME 79-20, September 1980

Table 2.1.2.3-7 Mechanical design parameters for Exxon Nuclear BWR fuel assemblies[a] (Table 2.12 from J.W. Roddy, H.C. Claiborne, R.C. Ashline, P.T. Johnson, and B.T. Rhyne, *Physical and Decay Characteristics of Commercial LWR Spent Fuels,* ORNL/TM-9591/V.1, October, 1985)

| Design component | Replacement array | | |
| | BWR/1—5 | BWR/2—6 | New |
	7 × 7	8 × 8	9 × 9
Fuel assemblies			
Transverse dimension, in.	5.25	5.25	5.25
Assembly weight, lb	590	580	570
Overall length, in.	174	174	174
Rod replacement capability	Yes	Yes	Yes
Disassembly capability	Yes	Yes	Yes
Fuel rods			
Date of introduction	1971	1974	1981
Number per assembly	49	63	79
Rod pitch, in.	0.73	0.64	0.57
Length, in.	145	145	145
OD, in.	0.59	0.48	0.42
Diametral gap, in.	None at end of life		
Clad thickness, in.	0.03	0.03	0.03
Clad material	Zr-2	Zr-2	Zr-2
Total weight/rod, lb	12.0	9.0	7.0
Fuel pellets			
Type	UO_2	UO_2	UO_2
Density, % TD	94	94	94
Diameter, in.	0.49	0.40	0.36
Length, in.	NA[b]	NA	NA
Total weight/rod, lb	NA	7.0	5.7
Plenum springs			
Working length, in.	10	10	13
Material	Inconel	Inconel	Inconel
Total weight/rod, lb	0.09	0.09	0.09
Compression springs			
Working length, in.	0.8	0.9	1.3
Material	Inconel	Inconel	Inconel
Total weight/rod, lb	0.007	0.007	0.007
Tie plate			
Material	CF-3 (304L)	CF-3 (304L)	CF-3 (304L)
Weight, lb	12	12	12

[a] Source: G.J. Busselman, Exxon Nuclear Company, Inc., letter to J.W. Roddy, Oak Ridge National Laboratory, March 28, 1985

[b] Not available

Table 2.1.2.3-8   Mechanical design parameters for Allis-Chalmers BWR fuel assemblies[a] (Table 2.13 from J.W. Roddy, H.C. Claiborne, R.C. Ashline, P.T. Johnson, and B.T. Rhyne, *Physical and Decay Characteristics of Commercial LWR Spent Fuels,* ORNL/TM-9591/V.1, October, 1985)

Design component	Rod array (10 × 10)
Fuel assemblies	
Transverse dimension, in.	NA[b]
Assembly weight, lb	NA
Overall assembly length, in.	NA
Fuel rods	
Number per assembly	100
Rod pitch, in.	0.565
Length, in.	NA
Fueled length, in.	83
OD, in.	0.396
Diametral gap, in.	0.006
Cladding thickness, in.	0.020
Cladding material	348 H SS
Fuel pellets	
Density, % TD	95
Diameter, in.	0.350
Length, in.	0.350–1.050
Tie plate	
Material	304 SS
Spacers	
Number	NA
Material	NA
Springs	NA
Plenum springs	
Working length, in.	NA
Material	NA
Compression springs	
Working length, in.	NA
Material	NA

[a]   Source: Allis-Chalmers, *Initial Testing of the La Crosse Boiling Water Reactor*, ACNP-67533, December 1967
[b]   Not available

2.1.2.4 Non-Zircaloy Clad Fuel

Table 2.1.2.4-1   Non-Zircaloy clad fuels from commercial LWRs (Table 5.4 from K.J. Notz, T.D. Welch, R.S. Moore, and W.J. Reich, *Preliminary Waste Form Characteristics,* ORNL-TM-11681 [draft] September, 1990.)

Assembly Class	Historical Discharges	Number Reprocessed	Historical (In Storage)	Projected	Total
STAINLESS STEEL CLAD					
Big Rock Point	66	66	0	0	0
Dresden-1	110	109	1 (<1 MT)	0	1 (<1 MT)
Haddam Neck	734	0	734 (303 MT)	673 (246 MT)	1407 (549 MT)
Humboldt Bay	189	189	0	0	0
Indian Point-1	280	120	160 (31 MT)	0	160 (31 MT)
San Onofre-	468	0	468 (171 MT)	496 (183 MT)	964 (354 MT)
Yankee Rowe	438	362	76 (21 MT)	0	76 (21 MT)
BWR TOTALS	365	364	1 (< 1 MT)	0	1 (< 1 MT)
PWR TOTALS	1920	482	1438 (526 MT)	1169 (429 MT)	2607 (955 MT)
GRAND TOTAL	2285	846	1439 (526 MT)	1169 (429 MT)	2608 (955 MT)
ZIRLO CLAD					
WE 15 x 15 North Anna	0	0	0	0	2 + Future Use

Stainless cladding that was not reprocessed is SS 304.

Historical Discharges and Number of Assemblies Reprocessed are estimates, based on continuing investigation into fuels reprocessed at West Valley

2.1.2.5 Hardware

Table 2.1.2.5-1 **Characteristics of reference PWR control rod assemblies. (Table 3-2 from E.R. Johnson Associates, Inc. (compilers),** *Acceptance of Non-Fuel Assembly Hardware by the Federal Waste Management System,* **ORNL/SUB./86-SA094/8, JAI-328, March, 1990.)**

Overall Length (in)	161
Length of Spider (in)	8
Length of Control Rods (in)	153
Diameter of Control Rods (in)	0.385
Overall Weight (lb)	149
Weight of Spider (lb)	8
Weight of Control Rods (lb)	141
No. of Control Rods	24
Weight/Control Rod (lb)	5.9
No. CRAs in Core	61
Lifetime (yrs)	15
	(2 sets for life of reactor)

Table 2.1.2.5-2 **Characteristics of reference PWR burnable poison assemblies (Table 3-4 from E.R. Johnson Associates, Inc. (compilers),** *Acceptance of Non-Fuel Assembly Hardware by the Federal Waste Management System,* **ORNL/SUB./86-SA094/8, JAI-328, March, 1990.)**

	Westinghouse	B&W
Overall Length (in)	156	160
Length of Spider (in)	4	6
Length of Rods (in)	152	154
Diameter of Rods (in)	0.385	0.430
Overall Weight (lb)	156	57
Weight of Spider (lb)	9	8
Weights of Rods (lb)	147	49
No. of Rods	24	16
Weight/Rod (lb)	6.1	3.1
No. BPA + APSA in Core	96	76
Lifetime (yr)	3	3
	(10 sets for life of reactor)	(10 sets for life of reactor)

Table 2.1.2.5-3   Summary comparison of attributes of burnable poison assemblies in PWRs.[a] (Table 3-3 from E.R. Johnson Associates, Inc. (compilers), *Acceptance of Non-Fuel Assembly Hardware by the Federal Waste Management System,* ORNL/SUB./86-SA094/8, JAI-328, March, 1990.)

	Fuel Array	Total Length (in)	Spider Length (in)	Total Weight (lb)	Poison	No. Poison Rods	No. Orifice Rods
Westinghouse							
4-Rod Neutron Poison	14x14	156	6	17	Borosilicate Glass	4	12
12-Rod Neutron Poison	14x14	156	6	32	Borosilicate Glass	12	4
BPA 16-Rod Neutron Poison	14x14	156	6	40	Borosilicate Glass	16	0
WABA 4-Rod Neutron Poison	14x14	154	4	16	B_4C	4	12
WABA 12-Rod Neutron Poison	14x14	154	4	28	B_4C	12	4
WABA 16-Rod Neutron Poison	14x14	154	4	34	B_4C	16	0
WABA 8-Rod Neutron Poison	15x15	154	4	23	B_4C	8	12
WABA 20-Rod Neutron Poison	15x15	154	4	41	B_4C	20	0
WABA 4-Rod Neutron Poison	15x15	147	4	17	B_4C	4	16
WABA 12-Rod Neutron Poison	15x15	147	4	28	B_4C	12	8
BPA 4-Rod Neutron Poison	15x15	156	4	20	Borosilicate Glass	4	16
BPA 10-Rod Neutron Poison	15x15	156	4	34	Borosilicate Glass	10	10
BPA 20-Rod Neutron Poison	15x15	156	4	54	Borosilicate Glass	20	0
WABA 4-Rod Neutron Poison	17x17	154	4	17	B_4C	4	20
WABA 16-Rod Neutron Poison	17x17	154	4	37	B_4C	16	8
WABA 24-Rod Neutron Poison	17x17	154	4	51	B_4C	24	0
BPA 4-Rod Neutron Poison	17x17	156	4	19	Borosilicate Glass	4	20
BPA 10-Rod Neutron Poison	17x17	156	4	28	Borosilicate Glass	10	14
BPA 16-Rod Neutron Poison	17x17	156	4	38	Borosilicate Glass	16	8
BPA 24-Rod Neutron Poison	17x17	157	5	50	Borosilicate Glass	24	0
B&W							
Ax Pwr Shaping Assembly	15x15	160	5	71	Inconel 600	16	0
Ax Pwr Shaping Assembly	15x15	160	4	57	Ag-In-Cd	16	0
Burnable Poison Assembly	15x15	154	6	57	B_4C; Al_2O_3	16	0
Combustion Engineering							
None - Burnable Poison in Fuel							

[a]   Source: DOE/RW-0184, Vol. 5

Table 2.1.2.5-4   **Summary comparison of attributes of neutron source assemblies in PWRs.[a] (Table 3-5 from E.R. Johnson Associates, Inc. (compilers),** *Acceptance of Non-Fuel Assembly Hardware by the Federal Waste Management System,* **ORNL/SUB./86-SA094/8, JAI-328, March, 1990.)**

Type	Fuel Array	Total Length (in)	Spider Length (in)[b]	Total Weight (lb)	Source	Burnable Poison	No. Burnable Poison Rods	No. Orifice Rods	No. Source Rods Primary	No. Source Rods Secondary
Westinghouse										
Version 1	14x14	125	3	48	Cf/Sb-Be	Borosil Glass	12	0	1	3
Version 2	14x14	158	3	48	Cf/Sb-Be	Borosil Glass	12	0	1	3
Version 3	14x14	158	3	48	Pu-Be/Sb-Be	Borosil Glass	12	12	1	3
116-Inch Source	14x14	116	3	22	Sb-Be	N/A	0	12	0	4
137-Inch Source	14x14	138	3	24	Sb-Be	N/A	0	12	0	4
143-Inch Source	14x14	143	3	23	Sb-Be	N/A	0	12	0	4
157-Inch Source	14x14	157	3	28	Sb-Be	N/A	0	4	0	4
Version 1	15x15	158	3	52	Pu-Be/Sb-Be	Borosil Glass	12	4	1	3
Version 2	15x15	158	3	52	Po-Be/Sb-Be	Borosil Glass	12	7	1	0
Version 3	15x15	156	3	34	Cf/Ag-In-Cd	Borosil Glass	12	16	1	4
116-Inch Source	15x15	116	3	28	Sb-Be	N/A	0	16	0	4
143-Inch Source	15x15	143	3	25	Sb-Be	N/A	0	16	0	4
157-Inch Source	15x15	156	3	19	Cf/Sb-Be	N/A	0	8	0	3
Version 1	17x17	156	3	39	Cf	Borosil Glass	12	11	1	0
Version 2	17x17	156	3	34	Cf	Borosil Glass	12	0	1	0
Version 3	17x17	156	3	51	Sb-Be	Borosil Glass	23	20	1	4
On-Spider	17x17	157	3	24	Sb-Be	N/A	0	8	0	4
12 BP Rod	17x17	156	3	39	Sb-Be	Borosil Glass	12	0	0	4
20 BP Rod	17x17	156	3	51	Sb-Be	Borosil Glass	20	0	0	4
B&W										
Primary	15x15	146	4	1	Am-Be	N/A	0	0	1	0
Regenerative	15x15	145	4	46	Sb-Be	N/A	0	0	0	8
Combustion Engineering										
Standard	16x16	99	3	8	Pu-Be/Sb-Be	N/A	0	0	1	1
128-Inch Core	14x14	100	3	11	Pu-Be/Sb-Be	N/A	0	0	1	1
137-Inch Core	14x14	106	3	11	Pu-Be/Sb-Be	N/A	0	0	1	1
Sustaining	15x15	117	3	5	Sb-Be	N/A	0	0	0	1
Startup Source	15x15	117	3	5	Pu-Be/Sb-Be	N/A	0	0	1	1

[a]   Source: DOE/RW-0184, Vol. 5   [b]   Estimated

Table 2.1.2.5-5   Characteristics of reference PWR neutron source assemblies (Table 3-6 from E.R. Johnson Associates, Inc. (compilers), *Acceptance of Non-Fuel Assembly Hardware by the Federal Waste Management System,* **ORNL/SUB./86-SA094/8, JAI-328, March, 1990.)**

Overall Length (in)	157
Length of Spider (in)	3
Length of Rods (in)	154
Diameter of Rods (in)	0.385
Overall Weight (lb)	51
Weight of Spider (lb)	8
Weight of Rods (lb)	43
No. of Rods	24
Weight/Rod (lb)	1.8
No. NSAs in Core	4
Lifetime (yrs)	(1 set for life of reactor)

Table 2.1.2.5-6   Characteristics of reference PWR thimble plug assemblies (Table 3-8 from E.R. Johnson Associates, Inc. (compilers), *Acceptance of Non-Fuel Assembly Hardware by the Federal Waste Management System,* **ORNL/SUB./86-SA094/8, JAI-328, March, 1990.)**

Overall Length (in)	12
Length of Spider (in)	4
Length of Rods (in)	8
Diameter of Rods (in)	0.424
Overall Weight (lb)	13
Weight of Spider (lb)	9
Weight of Rods (lb)	4
No. of Rods	24
Weight/Rod (lb)	0.16
No. TPAs in Core	36
Lifetime (yrs)	Plant Life

Table 2.1.2.5-7 **Summary comparison of attributes of thimble plug assemblies in PWRs.[a]**
(Table 3-7 from E.R. Johnson Associates, Inc. (compilers), *Acceptance of*
Non-Fuel Assembly Hardware by the Federal Waste Management System,
ORNL/SUB./86-SA094/8, JAI-328, March, 1990.)

Fuel Array	Total Length (in)	Spider Length (in)[b]	Total Weight (lb)	No. Orifice Rods
Westinghouse				
Water Displacement 14x14	156	4	21	16
Standard 14x14	12	4	10	16
Standard 15x15	10	4	11	20
Standard 17x17	12	4	13	24
B&W				
Standard 15x15	16	5	16	16
Combustion Engineering				
None Described				

[a]   Source: DOE/RW-0184, Vol. 5
[b]   Estimated

Table 2.1.2.5-8 **Characteristics of reference BWR fuel channel (Table 3-9 from E.R. Johnson Associates, Inc. (compilers),** *Acceptance of Non-Fuel Assembly Hardware by the Federal Waste Management System,* **ORNL/SUB./86-SA094/8, JAI-328, March, 1990.)**

```
Overall Length (in)      167
Wall Thickness (in)        0.120
Inside Width (in)          5.3
Overall Weight (lb)       98
```

Table 2.1.2.5-9 **Characteristics of reference BWR control assembly (Table 3-10 from E.R. Johnson Associates, Inc. (compilers),** *Acceptance of Non-Fuel Assembly Hardware by the Federal Waste Management System,* **ORNL/SUB./86-SA094/8, JAI-328, March, 1990.)**

```
Overall Length (in)                    174

Length of Control Blades (in)          144

Length of Handle (in)                    6

Length of Base (in)                     24

Thickness of Handle & Blades (in)        0.26

Width of Handle & Blades (in)            9.81

Diameter of Base (in)                    9.265 (w/o bearings)
                                        10.182 (at bearing
                                                    locations)

No. of Assemblies in Core              185

Lifetime (yrs)                           3-25
                      (Assumes 2 sets for life of reactor)
```

Table 2.1.2.5-10 **Summary of quantities of NFA components associated with 70,000 MTU SNF (Table 3-11 from E.R. Johnson Associates, Inc. (compilers),** *Acceptance of Non-Fuel Assembly Hardware by the Federal Waste Management System,* **ORNL/SUB./86-SA094/8, JAI-328, March, 1990.)**

Component	Items
PWR – Control Rod Assemblies	10,000
PWR – Burnable Poison Assemblies	61,500
PWR – Neutron Source Assemblies	320
PWR – Thimble Plug Assemblies	2,900
BWR – Fuel Channels	110,000
BWR – Control Assemblies	14,500
BWR – Neutron Sources	Negligible
BWR – Instrumentation Assemblies	5,000
BWR – Poison Curtains	750

Table 2.1.2.5-11   Summary of the quantities of NFA components projected to be available for delivery to the FWMS—for cases where components are delivered as an integral part of the fuel assembly and where they are delivered in either an uncompacted or compacted form.[a,b] (Table 4-1 from E.R. Johnson Associates, Inc. (compilers), *Acceptance of Non-Fuel Assembly Hardware by the Federal Waste Management System,* **ORNL/SUB./86-SA094/8, JAI-328, March, 1990.)**

	Total Units	Can Dimensions (in)	Can Capacity	Total No. Cans or Units	Weight of Loaded Can or Unit (lb)
As Integral Part of Fuel Assys					
PWR Control Rod Assemblies	10,000		In Fuel Assy	10,000	149
PWR Burnable Poison Assys (West)	55,000		In Fuel Assy	55,000	156
PWR Burnable Poison Assys (B&W)	6,500		In Fuel Assy	6,500	57
PWR Neutron Source Assemblies	320		In Fuel Assy	320	51
PWR Thimble Plug Assemblies	2,900		In Fuel Assy	2,900	13
BWR Fuel Channels	110,000		In Fuel Assy	110,000	98
BWR Control Assemblies[c]	14,500		No Can	14,500	225
BWR Instrument Assemblies	5,000		In Fuel Assy	5,000	2
BWR Poison Curtains[c]	750	10.5x10.5x176	74	11	2,263
Compacted					
PWR Control Rod Assys - Rod Sets	10,000	9x9x160	15	667	2,437
- Spiders	10,000	9x9x160	20	500	482
PWR Burnable Poison Assys (West)					
- Rod Sets	55,000	9x9x160	15	3,667	2,527
- Spiders	55,000	9x9x160	40	1,375	682
PWR Burnable Poison Assys (B&W)					
- Rod Sets	6,500	9x9x160	19	342	1,253
- Spiders	6,500	9x9x160	26	250	530
PWR Neutron Source Assemblies					
- Rod Sets	320	9x9x160	15	21	967
- Spiders	320	9x9x160	53	6	746
PWR Thimble Plug Assys - Rod Sets	2,900	9x9x160	114	25	778
- Spiders	2,900	9x9x160	40	73	682
BWR Fuel Channels	110,000	6x6x168	7	15,714	909
BWR Control Assemblies[d]	14,500	No Can	No Can	14,500	225
BWR Instrument Assemblies	5,000	6x6x160	47	106	306
BWR Poison Curtains	750	10.5x10.5x176	74	11	2,263
Uncompacted					
PWR Control Rod Assemblies	10,000	9x9x162	1	10,000	475
PWR Burnable Poison Assys (West)	55,000	9x9x160	1	55,000	478
PWR Burnable Poison Assys (B&W)	6,500	9x9x160	1	6,500	379
PWR Neutron Source Assemblies	320	9x9x160	1	320	373
PWR Thimble Plug Assemblies	2,900	9x9x160	13	223	491
BWR Fuel Channels	110,000	No Can	No Can	110,000	98
BWR Control Assemblies	14,500	No Can	No Can	14,500	225
BWR Instrument Assemblies	5,000	6x6x160	47	106	306
BWR Poison Curtains	750	10.5x10.5x176	74	11	2,263

[a]   Assumes all NFA components listed are classified as greater-than-Class C waste
[b]   Quantities are estimated to be those equivalent to the production of a nominal 70,000 MTU of SNF assemblies
[c]   Not integral
[d]   Uncompacted.

Table 2.1.2.5-12 **Estimated number of from-reactor shipments required for NFA hardware (shipped integral to fuel assembly and separately in both canned and uncompacted and compacted form) (Table 5-1 from E.R. Johnson Associates, Inc. (compilers),** *Acceptance of Non-Fuel Assembly Hardware by the Federal Waste Management System,* **ORNL/SUB./86-SA094/8, JAI-328, March, 1990.)**

	Total Amount (Assys/Units)	Can Dimensions (in)	Can Capacity	Total No. Cans or Uncanned Items	Weight Loaded Can or Unit (lb)	Cask Capacity (Cans/Items) Truck	Cask Capacity (Cans/Items) Rail	Total Additional Shipments[a] Truck	Total Additional Shipments[a] Rail	Added Weight Shipped (CWT)[b] Truck	Added Weight Shipped (CWT)[b] Rail
Integral With Fuel Assemblies											
PWR Control Rod Assemblies	10,000	Integral w/FA	Integral w/FA	10,000	149	Integral	w/FA	Integral	w/FA	6,705	8,195
PWR Burnable Poison Assys (West)	55,000	Integral w/FA	Integral w/FA	55,000	156	Integral	w/FA	Integral	w/FA	38,610	47,190
PWR Burnable Poison Assys (B&W)	6,500	Integral w/FA	Integral w/FA	6,500	57	Integral	w/FA	Integral	w/FA	1,667	2,038
PWR Neutron Source Assemblies	320	Integral w/FA	Integral w/FA	320	51	Integral	w/FA	Integral	w/FA	73	90
PWR Thimble Plug assemblies	2,900	Integral w/FA	Integral w/FA	2,900	13	Integral	w/FA	Integral	w/FA	170	207
BWR Fuel Channels	110,000	Integral w/FA	Integral w/FA	110,000	98	Integral	w/FA	Integral	w/FA	48,510	59,290
BWR Control Assemblies[c]	14,500	No Can	No Can	14,500	225	1	12	6,525	665	14,681	17,944
BWR Instrument Assemblies	5,000	Integral w/FA	Integral w/FA	5,000	2	Integral	w/FA	Integral	w/FA	45	55
BWR Poison Curtains[e]	750	10.5x10.5x176	74	11	2,263	1	12	5	1	112	137
Total								6,530	666	110,573	135,146
Compacted											
PWR Control Rod Assys – Rod Sets	10,000	9x9x160	15	667	2,437	4	21	75	17	7,315	8,940
– Spiders	10,000	9x9x160	20	500	482	4	21	56	13	1,084	1,326
PWR Burnable Poison Assys (West) – Rod Sets	55,000	9x9x160	15	3,667	2,527	4	21	413	96	41,699	50,966
– Spiders	55,000	9x9x160	40	1,375	682	4	21	155	36	4,220	5,158
PWR Burnable Poison Assys (B&W) – Rod Sets	6,500	9x9x160	19	342	1,253	4	21	38	9	1,928	2,357
– Spiders	6,500	9x9x160	26	250	530	4	21	28	7	596	729
PWR Neutron Source Assemblies – Rod Sets	320	9x9x160	15	21	967	4	21	3	1	93	113
– Spiders	320	9x9x160	53	6	746	4	21	1	1	20	25
PWR Thimble Plug Assys – Rod Sets	2,900	9x9x160	114	25	778	4	21	3	1	88	107
– Spiders	2,900	9x9x160	40	73	682	4	21	8	2	224	274
BWR Fuel Channels	110,000	6x6x168	7	15,714	909	9	48	786	180	64,278	78,562
BWR Control Assemblies[d]	14,500	No Can	No Can	14,500	225	1	12	6,525	665	14,681	17,944
BWR Instrument Assemblies	5,000	6x6x160	47	106	306	9	48	5	1	146	178
BWR Poison Curtains[e]	750	10.5x10.5x176	74	11	2,263	1	12	5	1	112	137
Total								8,101	1,030	136,484	166,816
Uncompacted											
PWR Control Rod Assemblies	10,000	9x9x162	1	10,000	475	4	21	1,125	262	21,375	26,125
PWR Burnable Poison Assys (West)	55,000	9x9x160	1	55,000	478	4	21	6,188	1,440	118,305	144,595
PWR Burnable Poison Assys (B&W)	6,500	9x9x160	1	6,500	379	4	21	731	170	11,086	13,549
PWR Neutron Source Assemblies	320	9x9x160	1	320	373	4	21	36	9	537	656
PWR Thimble Plug Assemblies	2,900	9x9x160	13	223	491	4	21	25	6	493	602
BWR Fuel Channels	110,000	No Can	No Can	110,000	98	9	48	5,500	1,260	48,510	59,290
BWR Control Assemblies	14,500	No Can	No Can	14,500	225	1	12	6,525	665	14,681	17,944
BWR Instrument Assemblies	5,000	6x6x160	47	106	306	9	48	5	1	146	178
BWR Poison Curtains	750	10.5x10.5x176	74	11	2,263	1	12	5	1	112	137
Total								20,140	3,814	215,245	263,076

[a]   Number of shipments additional to the shipment of SNF assemblies over a period of 25 years. Assumes 45% of material is shipped by truck and 55% by rail   [b]   Empty can weights used are as follows: 9 × 9 × 162 in—326 lb; 9 × 9 × 160 in—322 lb; 6 × 6 × 160 in—212 lb; 6 × 6 × 168 in—223 lb; 10.5 × 10.5 × 176 in—413 lb

[c]   Cannot be shipped integral with SNF assemblies   [d]   Assumes that it is not compacted at reactor site

[e]   No further compaction possible.

Table 2.1.2.5-13 **Total number of cans and can sizes for repository disposal (for both MRS and no-MRS options) (Table 6-8 from E.R. Johnson Associates, Inc. (compilers),** *Acceptance of Non-Fuel Assembly Hardware by the Federal Waste Management System***, ORNL/SUB./86-SA094/8, JAI-328, March, 1990.)**

Description	Storage and/or Disposal of Reactor-Canned Uncompacted NFA Hardware[a]		Storage and/or Disposal of Reactor-Canned & Compacted NFA Hardware[b]		Storage and/or Disposal of Intact NFA Hardware Received Integral W/SNF Assemblies[c]		Storage and/or Disposal of FWMS-Compacted NFA Hardware Received Integral W/SNF Assemblies[g]		Storage and/or Disposal of FWMS-Compacted NFA Hardware Received In Canned Uncompacted Form[d]	
	Can Dimensions (in)	Total No. Cans	Can Dimensions (in)	Total No. Cans	Can Dimensions (in)	Total No. Cans	Can Dimensions (in)	Total No. Cans	Can Dimensions (in)	Total No. Cans
All PWR Hardware	9x9x160-162	72,043[e]	9x9x160	6,926[f]	-	-	9x9x160	6,926	9x9x160	6,926
BWR Fuel Channels	9x9x168	8,462	6x6x168	15,714[f]	-	-	9x9x168	8,462	9x9x168	8,462
BWR Control Assys	10.5x10.5x176	14,500	10.5x10.5x176	3,038	10.5x10.5x176	14,500	10.5x10.5x176	3,038	10.5x10.5x176	3,038
BWR Instrument Rods	9x9x160	89	6x6x160	106[f]	-	-	9x9x160	89	9x9x160	89
BWR Poison Curtains	10.5x10.5x176	11[f]	10.5x10.5x176	11[f]	10.5x10.5x176	11[f]	10.5x10.5x176	11[f]	10.5x10.5x176	11[f]
Total		95,105		25,795		14,511		18,526		18,526

[a] Assumes BWR fuel channels, and instrument rods are compacted and canned in FWMS facilities; and BWR control assemblies are canned there.   [b] Assumes BWR control assemblies are compacted and canned in FWMS facilities   [c] Assumes BWR control assemblies are canned in FWMS facilities

[d] Assumes all NFA hardware is compacted and canned in FWMS facilities   [e] Received in canned form

[f] Received in compacted and canned form.

Table 2.1.2.5-14 Estimated number of from-MRS shipments required for NFA hardware (for MRS cases only) (Table 7-1 from E.R. Johnson Associates, Inc. (compilers), *Acceptance of Non-Fuel Assembly Hardware by the Federal Waste Management System*, ORNL/SUB./86-SA094/8, JAI-328, March, 1990.)

Hardware	Can Dimensions (in.)	No. Cans	Weight of Loaded Can (lb.)	Cask Capacity (No. Cans)[e]	Total Additional Shipments	Added Weight Shipped (CWT)
Storage and/or Disposal of Reactor-Canned Uncompacted NFA Hardware[a]						
All PWR Hardware	9x9x160-162	72,043	468 Av.	28	2,573	337,323
BWR Fuel Channels	9x9x168	8,462	1,611	28	302	136,323
BWR Control Assemblies	10.5x10.5x176	14,500	638	17	853	92,510
BWR Instrument Assemblies	9x9x160	89	502	28	3	447
BWR Poison Curtains	10.5x10.5x176	11	2,263	17	1	249
Total		95,105			3,732	566,852
Storage and/or Disposal of Reactor-Canned and Compacted NFA Hardware[b]						
All PWR Hardware	9x9x160	6,926	1,837 Av.	28	247	127,262
BWR Fuel Channels	6x6x168	15,714	909	61	258	142,840
BWR Control Assemblies	10.5x10.5x176	3,038	1,487	17	179	45,175
BWR Instrument Assemblies	6x6x160	106	306	61	2	324
BWR Poison Curtains	10.5x10.5x176	11	2,263	17	1	249
Total		25,795			687	315,850
Storage and/or Disposal of Intact NFA Hardware Received Integral With SNF Assemblies[c]						
BWR Control Assemblies	10.5x10.5x176	14,500	638	17	853	92,510
BWR Poison Curtains	10.5x10.5x176	11	2,263	17	1	249
Total		14,511			854	92,759
Storage and/or Disposal of MRS-Compacted NFA Hardware[d]						
All PWR Hardware	9x9x160	6,926	1,837 Av.	28	247	127,262
BWR Fuel Channels	9x9x168	8,462	1,611	28	302	136,323
BWR Control Assemblies	10.5x10.5x176	3,038	1,487	17	179	45,175
BWR Instrument Assemblies	9x9x160	89	502	28	3	447
BWR Poison Curtains	10.5x10.5x176	11	2,263	28	1	249
Total		18,526			732	309,456

[a] Assumes BWR fuel channels, and instrument assemblies are compacted and canned in FWMS facilities; and BWR control assemblies are canned there.

[b] Assumes BWR control assemblies are compacted and canned in FWMS facilities

[c] Assumes BWR control assemblies are canned in FWMS facilities

[d] Assumes all NFA hardware is compacted and canned in FWMS facilities

[e] Capacity of cask described in Section 7.2 for NFA hardware of various forms.

Table 2.1.2.5-15   Assumed elemental compositions (g/ton of metal) of LWR fuel-assembly structural materials.[a] (Table 3.3 from K.J. Notz, T.D. Welch, R.S. Moore, and W.J. Reich, *Preliminary Waste Form Characteristics,* ORNL-TM-11681 [draft] September, 1990.)

Element	Atomic number	Zircaloy-2	Zircaloy-4	Inconel-718	Inconel X-750	Stainless steel 302	Stainless steel 304	Nicrobraze 50
H	1	13	13	0	0	0	0	0
B	5	0.33	0.33	0	0	0	0	50
C	6	120	120	400	399	1,500	800	100
N	7	80	80	1,300	1,300	1,300	1,300	66
O	8	950	950	0	0	0	0	43
Al	13	24	24	5,992	7,982	0	0	100
Si	14	0	0	1,997	2,993	10,000	10,000	511
P	15	0	0	0	0	450	450	103,244
S	16	35	35	70	70	300	300	100
Ti	22	20	20	7,990	24,943	0	0	100
V	23	20	20	0	0	0	0	0
Cr	24	1,000	1,250	189,753	149,660	180,000	190,000	149,709
Mn[b]	25	20	20	1,997	6,984	20,000	20,000	100
Fe	26	1,500	2,250	179,766	67,846	697,740	688,440	471
Co[b]	27	10	10	4,694	6,485	800	800	381
Ni	28	500	20	519,625	721,861	89,200	89,200	744,438
Cu	29	20	20	999	499	0	0	0
Zr[b]	40	979,630	979,110	0	0	0	0	100
Nb	41	0	0	55,458	8,980	0	0	0
Mo	42	0	0	29,961	0	0	0	0
Cd	48	0.25	0.25	0	0	0	0	0
Sn	50	16,000	16,000	0	0	0	0	0
Hf	72	78	78	0	0	0	0	0
W	74	20	20	0	0	0	0	100
U	92	0.2	0.2	0	0	0	0	0
Density, g/cm^3	--	6.56	6.56	8.19	8.30	8.02	8.02	--

[a]   Source: A. G. Croff, M. A. Bjerke, G. W. Morrison, and L. M. Petrie, *Revised Uranium–Plutonium Cycle PWR and BWR Models for the ORIGEN Computer Code,* ORNL/TM-6051, September 1978

[b]   Value used in ORIGEN should be less than this (actual) value if the materials are not in the active fuel zone.

Table 2.1.2.5-16 Fuel assembly materials[a] (Table 2.1 from K.J. Notz, T.D. Welch, R.S. Moore, and W.J. Reich, *Preliminary Waste Form Characteristics, ORNL-TM-11681 [draft] September, 1990.*)

Design component	Subcomponent	Alloy or material
Fuel pellets		Uranium dioxide
Fuel rods		Zircaloy-2 (BWR) Zircaloy-4 (PWR)
		304 SS, 348H
Fuel spacers	Grid	304 SS
		Inconel 718
		Zircaloy-4
	Springs	Inconel 718, 625
		Zircaloy-4
Upper tie plates	Bail/tie plate	304 SS
	Bolts/nuts	304 SS
		Inconel 600
	Springs	Inconel 718, X750
Lower tie plates	Tie plate/nozzle	304 SS, CF-8
Tie rods		Zircaloy-4 304 SS

[a]   Source: E. M. Greene, Spent Fuel Data for Waste Storage Programs, HEDL-TME 79-20, September 1980

Table 2.1.2.5-17   Sample physical description report from LWR NFA hardware
data base (Table 2.8.1 from K.J. Notz, *Characteristics of Potential
Repository Waste,* DOE/RW-0184-R1, V.1 (draft), July, 1990.)

```
Combustion Enigneering SYSTEM80 12-Rod Full-Length Control Element

Designed for:
  Fuel Assembly with array size:  16 x 16
  Pressurized Water Reactor

Dimensions:
  Total Length:          253     inches
  Total Weight:          192.2   pounds

Cladding:
  Material:              Inconel 625
  Outer Diameter:        0.816   inches
  Wall Thickness:        0.035   inches
  Diametral Gap:         0.009   inches

Poison:
  Primary Material:      Boron Carbide (CE)
  Poison Length:         148     inches
  Pellet Diameter:       0.737   inches

Plenum Spring Material:   St. Steel 302

Spider Material:          St. Steel 304

Number of Control Rods:   12

Life Expectancy:          4000    EFPD
```

2.1.3 Repository Response

This section provides preliminary spent fuel information for the response of various components of spent fuel waste forms that may be exposed to the range of different environmental histories arising in the conceptual design process for a geological repository. The information presented is taken from the literature and from ongoing experimental testing and model development activities. The information addresses the response of spent fuel waste forms exposed to temperature, atmospheric, aqueous and solution chemistry function variables. In its present form some of the information is incomplete and it may not be directly applicable for the final repository design process. However, this information can be utilized to establish a basis for preliminary conceptual repository designs.

2.1.3.1 Cladding Degradation

2.1.3.1.1 Introduction

This section on cladding degradation has been taken from the Waste Form Degradation and Radionuclide Mobilization Preliminary Total System Performance Assessment, Section 2.7.2 (Siegmann, 1998).

2.1.3.1.2 Cladding-Failure Process Models

Process models for cladding failure were developed from strain failure, delayed hydride cracking, and mechanical failure from rock drops. In addition, some fuel is received with failed cladding or is made with stainless steel cladding, which is expected to fail soon after the waste package (WP) fails.

2.1.3.1.3 Juvenile Cladding Failures and Stainless Steel Cladding

In this analysis, it is assumed that a small fraction of the fuel (0.1%, median, range 0.01 to 3%) will be received with failed cladding (juvenile cladding failures). A recent survey (Yang, 1997) shows that today's fuel has a pin failure rate of approximately 0.01%, but the historic failure rate is higher (0.1%). Rothman (1984) suggests much less than 0.1% of all fuel that will be accepted will be failed. There have been a few reactor cores with manufacturing defects having failure rates as high as 3%, but these have been rare.

Some early cores were designed with stainless-steel (SS) cladding. This represents about 1.15% of the spent fuel (CRWMS M&O, 1997a). Because the SS cladding has a much higher corrosion rate than does the Zircaloy™ cladding, no credit is taken for SS cladding, and it is assumed to fail when the WP fails, exposing the complete pin to the environment. No range was assigned to the SS fraction.

2.1.3.1.4 Creep (Strain) Failures

A Monte Carlo model was developed to estimate the fraction of spent fuel cladding that becomes perforated from creep (strain). The model analyzes the performance of eight groups of pins, distributed across the WP, as a function of time. It calculates the time in which the pin becomes perforated and the time in which the cladding unzips. The pin properties, initial conditions, and performance correlations are assumed to be described using log-normal distributions. This analysis is repeated 5200 times, and the statistics are collected. The analysis is performed for two groups of WPs: one operating at the average temperature and power and one operating at a hot (design-basis) temperature and power. Both Rothman 1984) and Pescatore (1989; 1994) reviewed other cladding failure mechanisms and concluded that strain failure was the dominant failure mechanism during dry storage.

2.1.3.1.4.1 Pin Temperatures

Pin temperatures were radially distributed across the WP, and time histories were taken from a detailed analysis conducted by the Waste Package Development Department (WPDD) (Bahney, 1995). Temperatures for the average and design-basis WP are both used. The average WP contains 21 assemblies at 445 W/assembly, and the hot (design-basis) WP contains 21 assemblies at 850 W/assembly. In the Monte Carlo analysis, the temperature of an individual pin is sampled by assuming that the pin temperature is log normally distributed about a median temperature. The error factor (EF) is the ratio of the median to

95% quantile. For this analysis, an error factor of 1.25 was used, based on the difference in predicted temperatures for the WPs in different locations in the repository. The median peak temperature of the cladding in the center of the design-basis WP is 327°C (see Figure 2.1.3.1-1).
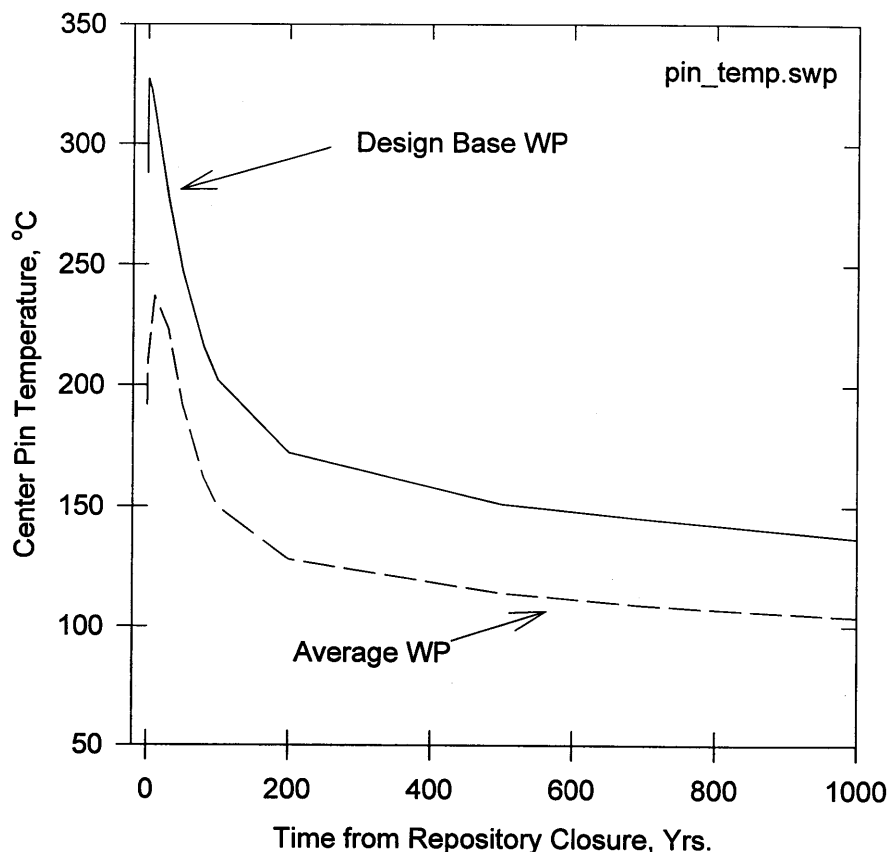
Figure 2.1.3.1-1   Center fuel pin temperature distribution

When considering the temperature uncertainties, the extreme (5%) pins could have a peak temperature as hot as 408°C and could possibly fail from creep. The use of temperatures that are continuously distributed produces this temperature maximum in the tail of the log-normal distribution. These high temperatures are a product of the Monte Carlo simulation and may exceed the design analysis, which has no pins (hottest pin in hottest WP) exceeding the 350°C limit. The average pin in the design-basis (hot) WP has a peak temperature of 289°C. In the design-basis WP, the median pins do not undergo creep failure. The average WP operates at much cooler temperature, with a median peak center pin temperature of only 237°C (see Figure 2.1.3.1-1). The average pin in the average WP has a peak temperature of 220°C. No creep failures are observed with this group. It is assumed that the repository contents comprises 95% average WPs and 5% design-basis WPs.

2.1.3.1.4.2 Pin Stress

For this analysis, the median stress for a Westinghouse 17×17 (W1717WL) assembly of 32 MPa room temperature (Pescatore, 1994) was used. A log-normal distribution is assumed with an EF (ratio of the median to 95% quantile) of 1.4. This represents the observed range for fission gas release reported by Manzel (1997). Fission gas is the principal source of internal

pressure. The stress at any time is calculated using the ideal gas law and the current temperature. In addition, the stress is reduced by adjusting the free volume inside the cladding from the strain that has expanded it outward.

2.1.3.1.4.3 Pin Strain and Failure Limit

The model assumes that the cladding creeps as a function of stress, temperature, and time using the creep correlation developed by Matsuo (1987). Figure 2.1.3.1-2 gives the strain for pins operating at a constant temperature for 10 yr. This figure shows that creep failures might be expected if the cladding operated in a repository for long periods of time at temperatures great than 350°C, the cladding temperature design limit. At the temperatures observed in the average WP, little or no creep is expected. The model presented here assumes that the strain is log-normal distributed with the median value from Matsuo's correlation and an EF (ratio of the median to 95% quantile) of 2.0. This error factor is derived by comparing Matsuo's correlation with experimentally measured strains. The 95% quantile strain is two times greater than the median, as predicted by Matsuo's correlation.

Earlier modeling used creep correlation from Peehs and Fleisch (1986). This model predicted slightly higher creep rates below 300°C and slightly lower creep rates above that temperature. The results are very similar to those using Matsuo's (1987) correlation, and neither model predicts any creep failures for the average WP because of the low cladding temperatures.
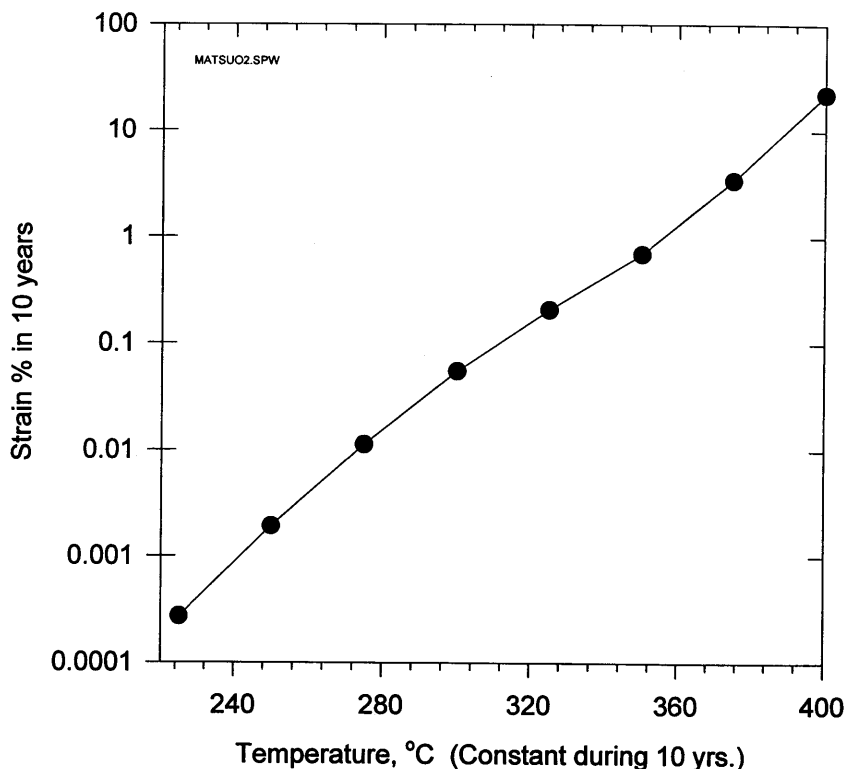
Figure 2.1.3.1-2   Cladding strain vs. temperature

Cladding was assumed to become perforated when a strain limit of 4% was reached. This is the median and mean value of 55 experiments summarized in Table 2.1.3.1-1. The 4% strain failure criteria is also assumed to be a median value for the failure strain, and an EF (ratio of

the median to 95% quantile) of 10.0 was used. This error factor was selected to cover all but one of the experimental values. It permits 5% of the pins to fail with strains less than 0.4%. The 4% strain limit could be conservative. Lowry et al, (1981, p. 219), reports the strength and ductility of spent fuel cladding from three different pressurized water reactors (PWRs). The tests were expanding mandrel tests performed at 371°C. This is a possible temperature for creep failure because the pins that fail in the design-basis WP have temperatures greater than the median. The measured, uniform strains were about 15%, and the ultimate stress was typically above 250 MPa, again higher than expected in the WP.

Table 2.1.3.1-1   Strain limit observed in testing

Source	Stress Temp. (°C)	Ult. Tens Stress (MPa)	Unif. Elong. Strain (%)	Number of Tests	Notes
VanSwam, 1997	25	910	1.50	1	Irrad
VanSwam, 1997	25	775-883	2.00	2	Irrad
VanSwam, 1997	25	660-956	4.00	3	Irrad
VanSwam, 1997	25	710-878	5.00	3	Irrad
VanSwam, 1997	25	840	6.00	1	Irrad
VanSwam, 1997	350	602	3.00	1	Irrad
VanSwam, 1997	350	586-666	4.00	6	Irrad
VanSwam, 1997	350	376-417	4.50	2	Irrad
Puls, 1988	25	625-1079	4.10	3	Unirr, hydrides added
Puls, 1988	25	659-689	4.70	5	Unirr, hydrides added
Puls, 1988	25	698-730	6.00	3	Unirr, hydrides added
Einziger et al., 1982	482	43*	1.70	2	Irrad, no failure
Einziger et al., 1982	510	39*	3.40	5	Irrad, no failure
Einziger et al., 1982	571	23-50*	5.00	3	Irrad, no failure
Einziger et al., 1982	571	33-39*	7.00	5	Irrad, no failure
Chung et al. 1987	325	337	0.40	1	Irrad
Chung et al. 1987	325	344	0.80	1	Irrad
Chung et al. 1987	325	384-498	1.00	3	Irrad
Chung et al. 1987	325	469-545	2.00	2	Irrad
Chung et al. 1987	325	552	11.00	1	Irrad
Yagee et al., 1980	325	275	0.01	1	Irrad
Yagee et al., 1979	360	200	0.40	1	Irrad
Number of Tests				55	
Mean Strain %			4.0		
Median Strain %			4.0		
Standard Deviation			2.1		
Variance			4.2		

*Stress at which creep test was performed.

At a strain of 4%, the cladding is assumed to fail by developing a perforation, relieving the internal pressure and stress. The cladding perforation then permits UO_2 oxidation and cladding unzipping if oxygen is present (i.e., if the WP has been breached). For perforated cladding, it is assumed that the hole developed is 2 mm^2, the observed hole size reported in pin burst tests (Lorenz, 1980).

For the design-basis (hot) WPs, 3% of the pins become perforated by creep strain. No pins in the average WP fail because of the low temperatures in that group of WPs. Assuming that 5% of the WPs operate at the design conditions, 0.15% of the pins are expected to become perforated by strain failure. The range was selected from 0.01%, (representing current pin failure rates) to 1.5% (representing one order of magnitude increase from the median). Figure 2.1.3.1-3 gives the percentage of pins that are simulated to perforate as a function of WP surface temperature for the average WP and for the design-basis WP. WP surface temperatures are affected by location in the repository and by water ingression rates. For the average WP, the figure shows (labeled base case) that the current WP surface temperature is almost 100°C, from where cladding perforation would increase dramatically. The design-basis WP represents a very hot WP, being loaded with 21 assemblies, all of which have the maximum power. It is seen that, for the base case, perforation could increase if the WP surface temperature were increased.
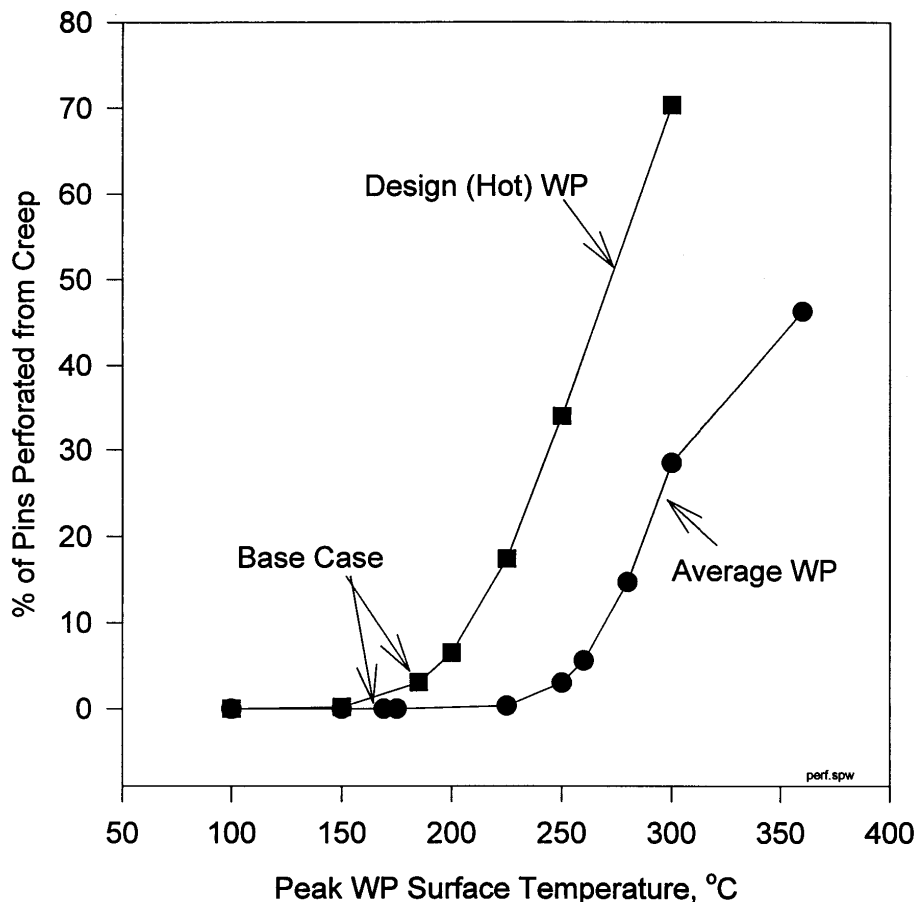
Figure 2.1.3.1-3   Percent cladding perforation due to creep vs WP surface temperature

2.1.3.1.4.4 Zircaloy™ Dry Oxidation

For fuel rods in failed WPs, Zircaloy™ oxidation was modeled using the equations developed by Einziger (1994). The oxidation has the effect of thinning the clad. The thinning is small and increases the stress slightly but has a very small effect on strain failure. The second effect is direct cladding failure. However, no fuel rods were observed to fail directly by dry oxidation through the cladding thickness in these analyses. This is consistent with earlier analysis that showed that this mechanism's unzipping is about four orders of magnitude slower than cladding unzipping and requires 10,000 yr at temperatures greater than 250°C to fail the cladding by this mechanism (CRWMS M&O, 1995). If the cladding were wet, the wet Zircaloy™ oxidation rates would be slightly slower than the dry Zircaloy™ oxidation rates and make little change on the effects of cladding oxidation.

2.1.3.1.4.5 Cladding Unzipping

If both the cladding and WP are penetrated, the UO_2 fuel can oxidize to U_3O_8, increasing the fuel volume and tearing the clad. The model used for cladding unzipping was developed by Einziger (1994). The cladding unzips in two phases: an incubation phase and an unzipping phase. In the incubation phase, the oxidized spent fuel phase builds up just inside the perforation until tearing starts. The time required for crack propagation is small compared with the incubation time and can be ignored.

Figure 2.1.3.1-4 shows the fraction of perforated pins that might unzip using the Einziger model. For the design-basis (hot) WP, all perforated pins would unzip in a juvenile failed WP (open to air at time = 0). If the WP were not breached for 200 yr, very few perforated pins would unzip. For the average WP, only 56% of the perforated pins in a juvenile failed WP would unzip. If the WP were to stay sealed for 50 yr, very few perforated pins would unzip. This analysis shows that cladding unzipping is unlikely for the YMP-designed WPs, which have expected lifetimes of thousands of years.
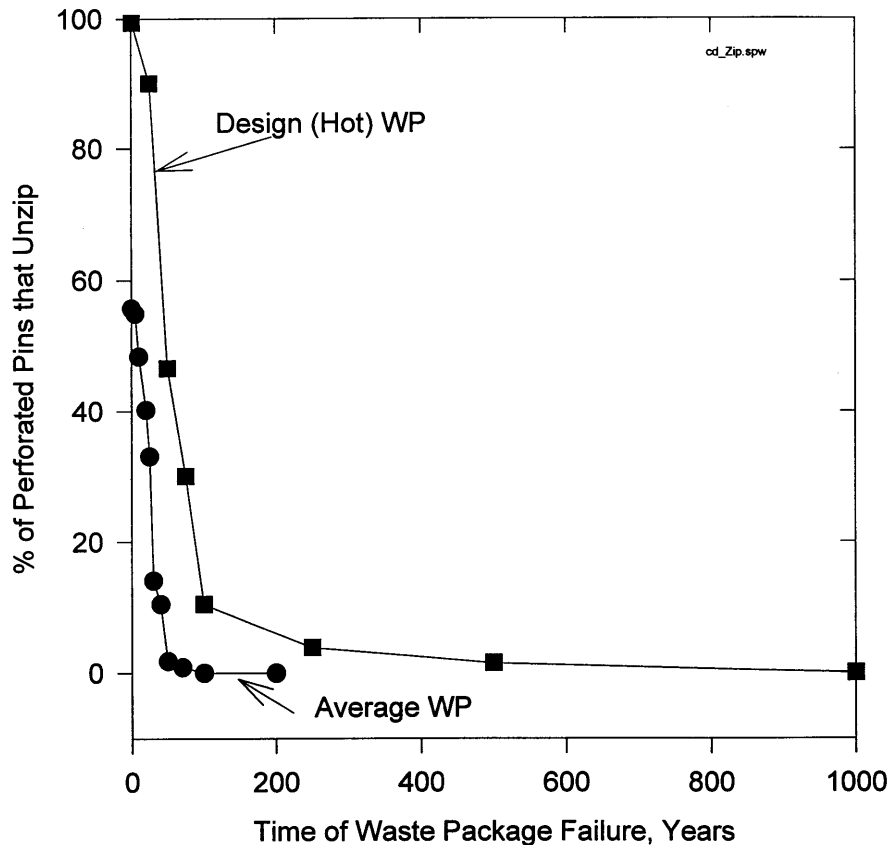
Figure 2.1.3.1-4   Clad unzipping vs WP failure time

2.1.3.1.5 Delayed Hydride Cracking

Delayed hydride cracking (DHC) under repository conditions is another cladding failure mode to consider. A separate analysis was performed and showed that only a very small percentage (< 0.01%) of cladding would fail by this mechanism; therefore, DHC was not incorporated into the cladding Monte Carlo analysis.

At repository closure, the design-basis spent-fuel cladding heats to a maximum of 330°C and then slowly cools over many years (to about 200°C at 100 yr). For DHC, the predicted threshold stress intensity factor for the onset of crack propagation is compared with the stress intensity factor. It is assumed that, if crack propagation starts, there is sufficient time to propagate across the cladding.

Using a model for threshold stress intensity factor (K_{IH})(Shi, 1994), crack propagation would be expected if the stress intensity reached a threshold level of 6.7 MPa·m$^{0.5}$. Stresses for Westinghouse W1717WL fuel are predicted to increase from 66 MPa to 100 MPa as burnup increases from 40 to 60 MWd/kgU (median crack depth, at a peak repository cladding temperature of 350°C). This produces a stress intensity factor of 0.28 to 0.40 MPa·m$^{0.5}$. This stress intensity is a factor of 17 to 24 smaller than the threshold stress intensity limits. Cracks at the largest possible size for surviving reactor operation (28% of wall thickness, probability = 6.8E-5/pin) produce stress intensity factors of 1.39 to 2.00 MPa·m$^{0.5}$, a factor of 2 to 5 smaller than the threshold range. In light of these differences, a statistical model for DHC was not developed because only a very small fraction of pins would fail.

2.1.3.1 Cladding Degradation

A mapping of the temperature and stress field, where hydride reorientation has been observed, and comparison with expected stresses and temperatures suggests that hydride reorientation is not expected under repository conditions. Strain experiments by Puls (1988) using reoriented hydrides suggest that, even if hydride reorientation did occur, the cladding strength would be only marginally affected.

2.1.3.1.6 Mechanical Failure

A preliminary model has been developed for the fraction of fuel rods broken, and fuel exposed, because of mechanical failure of cladding. The repository drifts are assumed to collapse at some time a few hundred years after emplacement, as rubble blocks pile on the intact containers and then crush the containers at some later time when the containers have degraded to the point of losing their mechanical integrity. The sizes of the rubble blocks are derived from information on rock-joint spacings and angles, and the height from which the blocks fall is determined from the design of the WP.

The number of fuel rods that break from the impact of a rubble block is limited by the available energy: breakage stops when the energy of the falling block is consumed. The energy necessary to break a single fuel rod is calculated by using beam theory and an elastic-plastic–stress-strain relation. An approximate method is developed for treating the effects of load sharing when one fuel rod contacts another.

Predicting the loading on the fuel rods is difficult because rubble blocks have irregular bottom faces. As an approximation, the blocks are modeled as having protrusions or "punches" on their bottom faces. Two types of punches are considered: one simulates the vertex of a block, and the other simulates an edge. All of the energy of the falling block is concentrated on the rods under the punches. To estimate the exposure of fuel, the length of each broken rod that lies under the punch is assumed to have its cladding entirely removed.

Previous total system performance assessments (TSPAs) have treated cladding by simply assuming a certain level of cladding performance. This model is the first attempt to quantify the effect of mechanical loading on cladding performance.

2.1.3.1.7 Details of Cladding Mechanical Failure Process Model

Over long times, the WP containment barriers may degrade to the point that they can no longer provide mechanical protection to the spent fuel inside them. The following sequence of events is considered: The ground support for the emplacement drifts is designed to last only until the repository is closed; thus, the emplacement drifts will collapse and be filled with rubble blocks. Some of these blocks will lie on the waste containers. When the containers become sufficiently weak, the blocks will crush the container and impact the fuel assemblies inside it. The blocks will accumulate kinetic energy as they fall, then dissipate the energy in bending and breaking the fuel rods. Breakage stops when all the kinetic energy is dissipated.

The fuel cladding and spacer grids of nuclear fuel are typically made of zirconium alloy and are, thus, extremely resistant to corrosion. Because of this corrosion resistance, the fuel assemblies should maintain their geometry even when the disposal containers are breached. However, when the disposal containers lose their mechanical integrity, blocks of rock can fall on the assemblies and break them.

Because the fuel rods are long and slender, they act as simple beams with supports at the spacer grids. A span of cladding from one spacer grid to the next is taken to be a simple elastic-plastic beam with clamped ends. The spacer grids in fact allow some rotation at the

ends of the span, but the use of clamped ends simplifies the treatment and conservatively reduces the amount of energy the beam can absorb. The cladding is treated as a thin-walled tube with a radius equal to the arithmetic mean of the inner and outer radii. Although the uranium dioxide fuel has negligible flexural strength by itself, it nevertheless contributes to the stiffness of the fuel rod. Because irradiated fuel is in the form of discrete pellets or fragments, the fuel resists compression but can be readily extended. As a result, the neutral axis moves toward the compressive surface of the fuel rod. In this treatment, the neutral axis is taken to lie at the surface of the fuel rod. Note that the neutral axis is on the bottom of the fuel rod near the supports and on the top near the load. This treatment is conservative in that it gives the smallest energy absorption.

The failure behavior of the cladding depends on the stress-strain properties of the cladding. Two types of fuel, with different mechanical properties, were considered. The properties were chosen to simulate typical and high-burnup fuel assemblies. Mechanical failure of fuel rods will occur only long after emplacement, when temperatures in the repository will be low. Accordingly, room-temperature mechanical properties were used. For typical fuel, the yield strength of the cladding is 780 MPa, the ultimate tensile strength is 925 MPa, and the uniform tensile elongation is 3.5% (Lowry et al., 1981, p. 219). For high-burnup fuel, the uniform tensile elongation is 0.15% (Garde, 1986). The elongations listed previously are taken to include the plastic portion only. For both types of fuel, the elastic modulus of the cladding is 99 GPa. For the calculations, the tensile portion of the stress-strain curve is taken to be composed of two line segments; these connect the origin, the tensile yield stress and strain, and the ultimate tensile stress and uniform tensile elongation (elastic plus plastic), respectively. The stress-strain curve is determined by properties for typical fuel. To simplify the treatment, the curve for high-burnup fuel is taken to coincide with that for typical fuel, but it is truncated at a smaller strain.

As is discussed subsequently, the external load from a rubble block is taken to be a point load at midspan. The loading, the geometry of the cladding, and the stress-strain curve of the cladding have been used with standard elastic-plastic beam theory to calculate the midspan displacement as a function of applied force. This model, however, requires substantial amounts of computation. For efficiency, it is replaced by the following empirical force-displacement function (CRWMS M&O, 1997a):

$$D(F) = F\frac{D_y}{F_y} \text{ if } 0 \le F < F_y \tag{2.1.3.1-1}$$

$$D(F) = F\frac{D_y}{F_y} + \left(D_{ut} - F_y\frac{D_y}{F_y}\right)\left(\frac{F - F_y}{F_{ut} - F_y}\right)^{3.468} \text{ if } F_y \le F < F_{ut} \tag{2.1.3.1-2}$$

In Equations 2.1.3.1-1 and 2.1.3.1-2, F and D are the current force and displacement, respectively. F_y and D_y are the force and displacement at the onset of yielding (i.e.,, when the maximum fiber stress reaches the yield stress), and F_{ut} and D_{ut} are the force and displacement when the maximum fiber strain reaches the uniform elongation for typical fuel. Note that positive forces and displacements are downward. For a given assembly design, F_y, D_y, F_{ut}, and D_{ut} are constants. They are calculated with the equations

2.1.3.1 Cladding Degradation

$$F_y = 2.941 \cdot 10^{10} \frac{tR^2}{l} \, , \qquad\qquad (2.1.3.1\text{-}3)$$

$$D_y = 1.636 \cdot 10^{-4} \frac{l^2}{R} \, . \qquad\qquad (2.1.3.1\text{-}4)$$

$$F_{ut} = 4.374 \cdot 10^{10} \frac{tR^2}{l} \, , \text{ and} \qquad\qquad (2.1.3.1\text{-}5)$$

$$D_{ut} = 4.016 \cdot 10^{10^{-4}} \frac{t^2}{R} \, , \qquad\qquad (2.1.3.1\text{-}6)$$

where t is the thickness of the cladding wall, R is the mean cladding radius, and l is the distance between supports. For high-burnup fuel, Equations 2.1.3.1-1 and 2.1.3.1-2 still apply, but the force-displacement curve is truncated at smaller forces and displacements; the force and displacement at failure, F_{uh} and D_{uh}, respectively, are

$$F_{uh} = 3.262 \cdot 10^{10} \frac{tR^2}{l} \text{ and} \qquad\qquad (2.1.3.1\text{-}7)$$

$$D_{uh} = 1.829 \cdot 10^{-4} \frac{t^2}{R} \, . \qquad\qquad (2.1.3.1\text{-}8)$$

Equations 2.1.3.1-1 and 2.1.3.1-2 agree with the beam-theory calculation to within 0.22% of D_{ut} for all applicable values of F.

Data on fuel-assembly design were obtained from qualified references. Data of interest include rod diameter, rod pitch, number of rods per side, cladding thickness, rod length, and maximum distance between spacer grids (CRWMS M&O, 1997a). Numbers of assemblies discharged were also obtained (DOE, 1996). Only pressurized-water reactor (PWR) fuel assemblies were considered because the fuel cladding of boiling-water reactor assemblies is normally protected by the flow channels. Complete data were available for 20 fuel types. These account for 31,931 of the 44,598 PWR fuel assemblies discharged through 1994 and were taken to be representative of all PWR fuel assemblies. No attempt was made to estimate the performance of the remaining assemblies.

A fuel assembly is an array of rods rather than an individual rod. Because the details of loading for individual rods are not known, forces from an impacting block are calculated in a one-dimensional continuum approximation. In this approximation, the array of rods is replaced by a continuum that has the force-displacement behavior that would result if the rods were smeared over space and the continuum responds to the impact by being displaced only in the direction of block motion. As a falling block of rock penetrates an assembly, the fuel rods will be compacted from their original density to a substantially higher density. The compacted region will accumulate ahead of the block. At the same time, the deformed but unbroken fuel rods will exert a retarding force on the block. At first, the force on the block increases as additional rods take up more of the load. At larger penetrations, however, the force becomes constant as rods begin to break and new rods take the place of the broken rods.

The one-dimensional–continuum model is used to calculate the energy absorbed before rods begin to break and to calculate the additional energy per rod needed to break rods.

In developing the one-dimensional–continuum approximation, the block is approximated as a rigid body. Because the rods are light, their mass is neglected. The density of rods in the compacted region is taken to be 90% of the density for closely packed rods with a hexagonal pattern. Although not all fuel-rod positions are fueled, the number of fuel-rod positions is taken to be equal to the square of the number of fuel rods per side.

The standard disposal container for PWR fuel has a capacity of 21 assemblies; these are arranged in three columns of five assemblies and two columns of three assemblies. This arrangement is approximated in the continuum model by a uniform arrangement of assemblies in which each column is 21/5 assemblies tall. Edge effects and end effects are neglected. This is appropriate because blocks that fall near the edge of a WP are expected to strike rubble as well as fuel.

The external loading may be described in terms of the types and sizes of blocks that fall onto the assemblies, the exposure of assemblies to falling blocks, and the response of the assemblies upon impact. Each of these is discussed in the following text.

A distribution of block sizes for the repository rock has been developed from information on joint spacings and angles for the geologic member that would contain the potential repository (CRWMS M&O, 1997b). The block size distribution has been applied in the following way: Blocks are assumed to fall so that they cover the area of the fuel assemblies exactly once. The shape of the blocks is taken to be a right circular cylinder, and the height and diameter are taken to be equal. The axes of the blocks are taken to be vertical, and the blocks are assumed to fall freely onto the fuel assemblies.

In the standard disposal container, a component called a basket side cover, shaped as a segment of a circle, fills the space between the fuel assemblies and the curved wall of the container. Because the basket degrades before the containment barriers fail mechanically, the bottom layer of fuel assemblies can settle into the space originally occupied by the bottom basket side covers, and the overlying assemblies can also settle. Accordingly, the drop height was taken to be twice the height of a basket side cover. For the standard disposal container, the basket side cover is a segment of a circle with radius 711.7 mm and chord length 733 mm. From these dimensions, the height of the side cover is calculated to be 101.6 mm.

If the bottom surface of a falling block is flat, the energy of the block would be spread over as many rods as were exposed to the impact (e.g., the diameter of the block divided by the rod pitch). Because the blocks are irregular, however, this description is not realistic. To provide greater realism, two geometries were considered; both are intended to simulate the effects of irregular block surfaces. In these geometries, the bottom surface of the block is taken to have a rigid, massless protrusion called a punch. The entire energy of the falling block is concentrated onto the rods that lie under the punch. The punch is taken to be sufficiently long that only the punch contacts the fuel; the rods that lie under the remainder of the area of the block are not loaded. For purposes of calculating the amount of fuel exposed, the cladding is taken to be completely removed from the portion of a broken fuel rod that lies under the punch.

Two types of punches are considered: circular and linear. With the circular punch, the ratio of the diameter of the punch to the diameter of the block is called the focusing parameter. To provide maximum energy transfer, the punch may be considered to be coaxial with the block. The second type is a linear punch. Two parallel chords of equal length and the

two arcs that connect them define the outline of a linear punch. A linear punch is defined by two variables: the focusing parameter and the angle. The focusing parameter is the ratio of the distance between the two chords to the block diameter. The angle is simply the angle between a chord and the fuel rods. For both punch types, a focusing parameter of one corresponds to a flat-bottomed block. Focusing parameters near zero describe a block with either a slender pin (circular punch) or a blade (linear punch) on the bottom. The circular and linear punches are intended to simulate blocks that fall on their vertices or their edges, respectively.

When a block strikes the fuel, the number of rod breaks can vary from zero (if there is not enough energy to begin breaking rods) to the number of rods under the punch. The number of breaks is determined as a weighted average over the number of assemblies of each type and the distribution of block sizes.

The number of breaks is calculated by considering the energy of the falling block. The block accumulates kinetic energy as it falls freely toward the fuel rods. It releases additional potential energy as it deforms the fuel rods; at the same time, the deformation of the rods consumes energy. If the block has sufficient energy, it breaks fuel rods. After the first layer of rods is broken, the energy consumed for each additional layer is constant. Again, there is an additional release of potential energy as the block continues to fall. After the number of breaks is determined, the number of broken rods is calculated by a probabilistic approach. These two quantities can differ because a single rod can be broken in several places.

It was mentioned previously that two types of fuel were considered: typical and high-burnup. Burnup is significant because cladding tends to become brittle at high burnups. Because there is a long-term trend toward higher burnups as experience with reactor operations increases, what constitutes high burnup depends on when the fuel was irradiated. However, the continued demand by utilities for good fuel performance should ensure that the strength and ductility of typical fuel assemblies are maintained even though "typical" burnups are increasing.

The typical fuel was taken to represent 95% of the inventory, and the high-burnup fuel was taken to represent 5% of the inventory. The mechanical properties of high-burnup fuel are those for a sample, discharged no later than 1986, with a local burnup of 59.0 GWd/MTU. This is an exceptionally high burnup for fuel that was discharged that early; of the 19,968 PWR fuel assemblies discharged through 1986, only 200 had assembly average burnups of greater than 40.0 GWd/MTU (DOE, 1996).

The fraction of fuel rods broken and the fraction of fuel exposed were calculated for both circular and linear punches with several values, ranging from 1 to 0.01, of the focusing parameter. The results are documented in Tables 2.1.3.1-2 and 2.1.3.1-3. The results of most interest are those in columns labeled "95% typ + 5% hi-burn," which contain arithmetically weighted means for a repository that contains 95% typical fuel and 5% high-burnup fuel. All of the results in the tables account for the block size distribution and the number of assemblies of each type.

Results for blocks with a circular punch are shown in Table 2.1.3.1-2. The number of breaks per rod and the fraction of fuel rods broken increase as the focusing parameter decreases. A smaller punch apparently makes the block more effective in breaking rods. The largest reported values of the number of breaks per rod and the fraction of rods broken are 0.2845 and 0.2341, respectively. Both of these values are reached at a focusing parameter of 0.1. In contrast to these results, the amount of fuel exposed is nearly independent of the focusing parameter over the range 1.0 to 0.4, then decreases at smaller values of the focusing

parameter. The maximum fraction of fuel exposed per waste package is 0.0114 at a focusing parameter of 0.6.

Table 2.1.3.1-2   Amount of fuel damage as a function of the focusing parameter for fuel struck by blocks with a circular punch [LL981106851021.070]

Focus Param.	Average Number of Breaks per Rod			Fraction of Rods Broken			Fraction of Fuel Exposed			Punch Aspect Ratio	
	Typical	Hi-Burn	95% Typ +5% Hi-Burn	Typical	Hi-Burn	95% Typ +5% Hi-Burn	Typical	Hi-Burn	95% Typ +5% Hi-Burn	Typical	Hi-Burn
1.0	0.0325	0.6145	0.0616	0.0142	0.1799	0.0225	0.0060	0.1055	0.0110	0.006	0.045
0.9	0.0386	0.6466	0.0689	0.0175	0.2050	0.0268	0.0064	0.0997	0.0111	0.008	0.058
0.8	0.0463	0.6831	0.0782	0.0217	0.2383	0.0325	0.0068	0.0941	0.0112	0.010	0.077
0.7	0.0568	0.7339	0.0906	0.0273	0.2830	0.0401	0.0073	0.0886	0.0113	0.013	0.106
0.6	0.0700	0.8073	0.1069	0.0345	0.3481	0.0501	0.0076	0.0839	0.0114	0.020	0.156
0.5	0.0853	0.9058	0.1263	0.0441	0.4343	0.0636	0.0076	0.0785	0.0112	0.033	0.248
0.4	0.1032	1.0390	0.1500	0.0576	0.5490	0.0822	0.0073	0.0716	0.0105	0.059	0.440
0.3	0.1264	1.1410	0.1771	0.0784	0.6482	0.1069	0.0067	0.0576	0.0092	0.122	0.868
0.2	0.1650	0.9978	0.2066	0.1174	0.6276	0.1429	0.0058	0.0323	0.0071	0.329	1.770
0.1	0.2682	0.5934	0.2845	0.2229	0.4467	0.2341	0.0046	0.0090	0.0049	1.920	4.620

Another result of interest for calculations with a circular punch is the punch-aspect ratio. This is the ratio of the depth of penetration of the punch to the width of the punch. Here "depth of penetration" is defined as the number of layers of rods broken times the effective rod pitch. Different combinations of block size and assembly type yield different punch-aspect ratios. The values reported in Table 2.1.3.1-2 are arithmetic means for blocks that break rods. (For blocks that do not break rods, the punch-aspect ratio is zero.) Because it is improbable that a block has a very long, slender protrusion on its bottom surface, large punch-aspect ratios indicate an unrealistic focusing of energy onto a few rods. It is seen from Table 2.1.3.1-3 that the punch-aspect ratio increases as the focusing parameter decreases. Because the punch-aspect ratios are fairly large for a focusing parameter of 0.1, it is expected that the actual number of breaks per rod and fraction of rods broken will be smaller than the values reported above.

Table 2.1.3.1-3 Amount of fuel damage as a function of the focusing parameter for fuel struck by blocks with a linear punch (composite of eight punch orientations) [LL981106851021.070]

Focus Param	Average Number of Breaks per Rod			Fraction of Rods Broken			Fraction of Fuel Exposed		
	Typical	Hi-Burn	95% Typ +5% Hi-Burn	Typical	Hi-Burn	95% Typ +5% Hi-Burn	Typical	Hi-Burn	95% Typ. +5% Hi-Burn
1.0	0.0325	0.6145	0.0616	0.0142	0.1799	0.0225	0.0060	0.1055	0.0110
0.9	0.0348	0.6258	0.0643	0.0154	0.1893	0.0241	0.0062	0.1032	0.0110
0.8	0.0377	0.6402	0.0678	0.0170	0.2018	0.0262	0.0063	0.0990	0.0109
0.7	0.0416	0.6593	0.0725	0.0191	0.2186	0.0291	0.0064	0.0940	0.0108
0.6	0.0467	0.6875	0.0787	0.0219	0.2436	0.0329	0.0065	0.0892	0.0106
0.5	0.0528	0.7261	0.0864	0.0257	0.2773	0.0382	0.0066	0.0845	0.0105
0.4	0.0600	0.7787	0.0959	0.0310	0.3225	0.0456	0.0067	0.0797	0.0103
0.3	0.0695	0.8209	0.1071	0.0392	0.3630	0.0554	0.0068	0.0713	0.0100
0.2	0.0852	0.7731	0.1196	0.0545	0.3603	0.0698	0.0072	0.0526	0.0095
0.1	o.1255	0.6296	0.1507	0.0950	0.2995	0.1052	0.0092	0.0267	0.0101

For a linear punch, the results depend on the angle between the punch and the rods. The rubble blocks in a drift are randomly oriented. As a discrete approximation of a random orientation, the fraction of rods broken and the fraction of fuel exposed were calculated for 8 orientations (0 , 22.5 , . . . 157.5), and the arithmetic mean was taken. The results for this composite orientation are shown in Table 2.1.3.1-3. As is the case with a circular punch, the number of breaks per rod and the fraction of rods broken both increase as the focusing parameter decreases from 1 to 0.1. The largest reported values are 0.1507 and 0.1052, respectively. However, the dependence on the focusing parameter is much weaker than it is with a circular punch. The fraction of fuel exposed has a more complicated dependence on the focusing parameter, with a maximum at 1, a minimum near 0.2, and a second maximum at 0.1. The maximum fraction of fuel exposed is 0.0110 at focusing parameters of 0.9 and 1.0.

The two models provide substantially different results for the fraction of rods broken. With a linear punch (Table 2.1.3.1-3), the largest reported value is 0.1052 for a focusing parameter of 0.1; with a circular punch (Table 2.1.3.1-2), the largest reported value is 0.2341, again for a focusing parameter of 0.1. The two models agree more closely at larger focusing parameters. However, it may be that the circular punch simply represents a more severe loading configuration as regards the number of rods broken.

With respect to the amount of fuel exposed per waste package, the agreement between results for a circular punch and a linear punch is much closer. With a linear punch, the maximum fraction of fuel exposed per waste package is 0.0114; with a circular punch, 0.0110 is exposed. These values are reached at fairly large values of the focusing parameter, 0.6 and 0.9 to 1.0, respectively. These results indicate that only a small fraction of fuel will be exposed by mechanical failure.

Energies for breaking fuel rods of boiling-water reactor (BWR) assemblies have not been calculated. For most of these, the fuel rods are protected by the flow channels from impacts and static loads. It would be conservative to assume that the number of breaks per rod and the fraction of fuel exposed are the same for PWR and BWR fuels.

2.1.3.1.7.1 Abstraction of Model

The development of the model is its own abstraction. An elastic-plastic beam theory is used to calculate the force-displacement behavior of a fuel rod. A curve is fitted to those results to provide an empirical force-displacement equation. That equation, in turn, is used to develop a one-dimensional continuum model for the energy absorbed in breaking rods. Finally, the fraction of fuel exposed is calculated by accounting for the distribution of block sizes and the number of fuel assemblies of each type.

2.1.3.1.7.2 Recommended Model

For the geometries considered in this analysis, the maximum fraction of fuel exposed by mechanical loading is 0.0114 per waste package. The uncertainty range for this value has not yet been defined. It is recommended that this value be used for all Zircaloy™-clad, commercial spent nuclear fuel that does not fail by other mechanisms.

The model does not predict the time at which mechanical failure of the container (and thus cladding failure) occurs. If this time cannot be derived from other models, it is recommended that the time of container breach be used as the time of mechanical failure.

The model of dynamic loading contains the following conservatisms:

- The block fall height is essentially an upper limit; there is no accounting for possible deformation of the containment barriers before complete collapse.
- Blocks are assumed to fall freely; there is no accounting for blocks that encounter friction or are partially supported.
- There is no accounting for energy absorbed in deforming the remnants of the containment barriers.
- There is no reduction of block size to account for breakage when the blocks fall onto the intact disposal container or other rubble.
- There is no accounting for energy absorption by crushing of the spacer grids; that process would also increase the flexibility of the rods and thus increase the energy they could absorb before breaking.
- Falling blocks are assumed to cover the entire exposed area of the assemblies.
- Rod breakage is likely to cause only a few guillotine breaks in the cladding, but the amount of fuel exposed is assumed to be that in the entire length of the rod under the block.
- The neutral axis is taken to be at the surface of the rod; this location minimizes energy absorption.
- No credit is taken for the protection of BWR fuel rods by their flow channels.

Because of these conservatisms, the reported values of the number of breaks per rod and the fraction of fuel exposed are believed to be conservative.

2.1.3.1.8 Zircaloy™ Corrosion

The current cladding model accounts for Zircaloy™ cladding failure from strain, oxidation, and mechanical failures. It does not address failure from corrosion. Uhlig, (1985) and Schweitzer (1996) summarized the susceptibility of zirconium to corrosion by common chemicals. They concluded that the material is resistant to corrosion by most basic chemicals but is corroded by ferric chloride and a few other compounds. Cragnolino (Cragnolino and Galvele, 1977) measured anodic behavior of Zircaloy™ in Cl solutions and showed that a pitting potential exists. Maguire's experiments (1984) show that $FeCl_3$ corrosion potentials exist.

In an experiment, Barkatt (1983) showed that gamma radiolysis of 6.2E4 grays (6.2E6 rads) over 3 days at 25°C could produce:

Acid	Concentration	Comment on Formation
Nitric	78E-6 M	pH must be below 4, formed in gas phase.
Formic	46E-6 M	Formed by dissolved CO_2 in liquid phase, pH at or below 4.
Oxalic	30E-6 M	Formed by dissolved CO_2 in liquid phase, pH at or below 4.
H_2O_2	16E-6 M	Formed in liquid phase.

Van Konynenburg (Van Konynenburg and Curtis, 1996) performed accelerated corrosion tests with Zircadyne-702, an unalloyed metal. The test solution contained 0.01M each of sodium formate (NaCOOH), nitric acid (HNO_3), NaCl, H_2O_2, and 0.02M sodium oxalate ($Na_2C_2O_4$). The temperature was 90°C, and the duration was 96 hr. The corrosion rate measured was 0.06 mm/yr (a rate fast enough to be through cladding in 10 yr). The initial pH was 4.06, and final pH was 4.26. The solutions used were three orders of magnitude more concentrated than the acids observed in Barkatt's tests.

Water does not contact the cladding until the WPs have failed. Current analysis predicts that this will not occur for thousands of years. At that time, the gamma dose will have decreased by about three orders of magnitude. Alpha and beta radiation is inside the cladding and will not contribute to the radiolysis on the cladding outer surface. Near-field chemical analysis suggests that the water will be modified by the concrete and will be basic (or at worst, near neutral) for tens of thousands of years. This incoming water should neutralize the production of radiolytic acids. Until the chemical analysis is performed to predict radiolysis, pH, HCO_3^- and $FeCl_3$ in solution, and the composition of the water contacting the cladding, it is assumed that the cladding is not damaged by radiolytically produced acids because the incoming solution is basic from the effects of the concrete. Thus, corrosion of Zircaloy™ is not expected to contribute to significant failures.

2.1.3.1.9 Clad Unzipping

If there is a pinhole crack in the cladding and air is present, the spent fuel inside can oxidize, eventually to U_3O_8, which expands and exerts pressure in its confined space. The pinhole can then be transformed into a longitudinal crack. Because of data variability, it is difficult to put a value on the radius at crack initiation. Rather, model the phenomenon is modeled in net-result form closely following the parameters measured in the experiments.

Later, a radius is estimated at cracking, but that is a check on reasonableness rather than a link in the model. The crack eventually extends along the length of the cladding. The crack propagation velocity depends on the oxidation of additional U_3O_8 along the rod.

Einziger and Strain (1986) have done experiments at 255°C and above on fuel rod sections and on exposed fuel fragments, both from the same batch of spent fuel. They report the oxidation progress curves, the initiation of spalling in the exposed fragments, and the initiation and propagation of cracks in the fuel-rod sections. For the time to initiation of spalling, they find an activation energy of 46.4 kcal/mole. They use this activation energy for the temperature dependence and use an adjustable multiplier to form a lower-bound curve for the initiation-of-rod-splitting data. In both free fragment spalling and rod cracking, sections from near the ends of the rods reach these changes at earlier times, with the difference averaging approximately a factor of five. The data on crack initiation for rod center pieces seem to have a lesser slope with temperature, closer to the activation energy found previously from a number of different experiments. The data on crack initiation for rod end pieces are fewer and do not give much additional information on the temperature dependence. To extrapolate to lower temperatures than the data range covers and to cover end as well as center locations of initial pinholes or pinhole cracks, a Q_0 and a curve anchored in the 283°C data are recommended. The equation for time to initiation of rod splitting is then

$$t_o = c_{S0} \cdot \exp(+Q_{S0} / RT) \tag{2.1.3.1-9}$$

where c_0 = 3.04 e–13 hr with a multiplicative standard deviation of a factor of 5 (i.e., c_0 has a log-normal distribution, and 3.04 e–13 hours is the median) and Q_0 = (38.4 ± 3) kcal/mol, as previously. (This gives t_0 = 385 hr at T = 283°C using the central values of the parameters.)

The subsequent crack propagation velocity has a lower activation energy (i.e., less change with temperature), but the full-rod extension time is fairly short compared with the initiation time. The crack propagation velocity depends on the oxidation of additional U_3O_8. Presumably there is some early fraction oxidized along the interior during the initiation period; hence, the temperature-dependence of the crack extension is not as strong overall as it is for the initiation. Because of the short overall crack extension time, this part of the phenomenon can be considered instantaneous in the model; the time to cracking is the main time in the process.

The reported experiments were done on one series of spent fuel. The activation energy used in the fit is global for U_3O_8; the leading multiplying factor for the crack initiation time should depend on grain size. The uncertainty of a factor of five is large enough to encompass a good fraction of this source of variability.

One can compare (Figure 2.1.3.1-5) the time to initiation of splitting at 255°C (5000 to 10,000 in the data of Einziger and Strain (1986) or 2000 to 10,000 hr using a fit to the data for rod center sections only) to the U_3O_8 oxidation rate data of Einziger et al., reported in 1995 and reproduced in Figures 3.2.2-5 through 3.2.2-8 of this report (*Waste Form Characterization Report* [WFCR]). At 5000 to 10,000 hr, the WFCR data show that the $\Delta(O/M)$ is on the order of one-seventh of the way between U_4O_9 and U_3O_8. The time values in this set of experiments vary with a multiplicative standard deviation of approximately a factor of five. The $\Delta(O/M)$ parallels the change in mass of U oxidized to a higher state and, thus, to the change in volume. A one-seventh change from a base volume to a 30%-increased volume means a 4.3% increase in volume, or a 1.4% increase in radius (assuming that the initial oxidized mass can expand longitudinally in the fuel rod, pushing other spent fuel along the rod and radially

pushing on the cladding). The fuel-cladding gap is essentially gone in spent fuel because of expansion of the matrix during irradiation; hence, the expansion means an expansion (strain) of the cladding circumference of about 1.4%. This seems to be about the right order of magnitude to initiate unzipping, given that there is an initial crack or pinhole to provide an initial crack tip or stress riser. Thus, the time-to-initiation data and the oxidation-rate data at 255°C are plausibly consistent, at least using an order-of-magnitude comparative rationale.
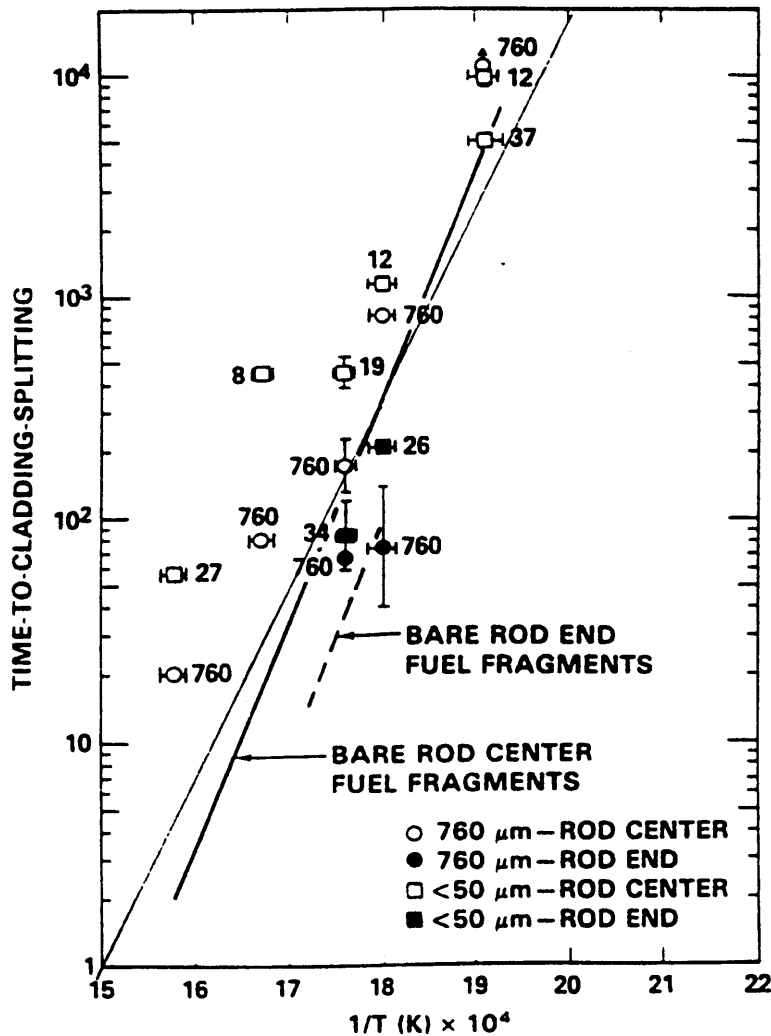
Figure 2.1.3.1-5   Time-to-cladding-splitting from Einziger and Strain (1986), with a more general proposed fit added (the longer, lesser-slope line)

The new fit uses a Q value from other experiments and is a best-estimate fit to rod-end and rod-center data combined. The original fits (shorter lines) were intended to be lower-bound fits for the data sets, treating rod-end and rod-center data groups separately.

Thus, the final model recommended for the time delay in generating a large breach in cladding from a small pinhole breach, when exposed to air, is given by the time to initiation of longitudinal cracking, given by Eq. 2.1.3.1-3. Extrapolating the model to T = 100°C gives the following time t_0, depending on the values of the parameters within their distributions. It gives $t_0 = 9.9e + 9$ hr, or $1.1e + 6$ yr using central values, and $1.7e + 4$ yr using the -1σ value of

Q_0 and the median value of c_0. Using the -1σ value of both Q_0 and c_0, it gives a value $t_0 = 3.4$ e + 3 yr. Thus, there is a substantial time delay from this process, and it is highly variable between a "substantial" delay of the thousands of years and an "extreme" delay in the millions of years and longer.

2.1.3.1.10 References

Bahney, R. H. (1995). *Thermal Calculations in Support of the Thermal Loading Study.* LV.WP.RHB.12/95-392. [MOL.19960611.0506; 237199]

Barkatt, A., A. Barkatt, and W. Sousanpour (1983). "Gamma Radiolysis of Aqueous Media and its Effects on the Leaching Processes of Nuclear Waste Disposal Materials." *Nucl. Technol.* 60(2):218–227. [NNA.19891101.0002]

Chung, H. M., F. L. Yagee, and T. F. Kassner (1987). "Fracture Behavior and Microstructural Characteristics of Irradiated Zircaloy Cladding." *Zirconium in the Nuclear Industry.* (ASTM STP 939) American Society for Testing and Materials. [238255]

Cragnolino, G. A., and J. R. Galvele (1977). "Anodic behavior and pitting of zirconium and Zircaloy-4 in aqueous solutions of sodium chloride." *Passivity of Metals.* R. P. Frankenthal and J. Kruger (eds.). Princeton, NJ: The Electrochemical Society. (pp. 1053–1057) [237155]

CRWMS M&O (1995). *Updated Report on RIP/YMIM Analysis of Designs.* (BBA000000-01717-5705-00002, Rev. 02) Las Vegas, NV: Civilian Radioactive Waste Management System Management and Operating Contractor, TRW Environmental Safety Systems, Inc., for the U.S. Department of Energy. [MOL.19960226.0049]

CRWMS M&O (1997a). *Design Basis Cladding Analysis.* (BBA000000-01717-0200-00054, Rev. 00) Las Vegas, NV: Civilian Radioactive Waste Management System Management and Operating Contractor, TRW Environmental Safety Systems, Inc., for the U.S. Department of Energy. [MOL.19971121.0750]

CRWMS M&O (1997b). *Waste Quantity, Mix and Throughput Study Report.* (B00000000-01717-5705-00059, Rev. 01) Las Vegas, NV: Civilian Radioactive Waste Management System Management and Operating Contractor, TRW Environmental Safety Systems, Inc., for the U.S. Department of Energy. [MOL.19971210.0628]

DOE (1996). *Spent Nuclear Fuel Discharges from U.S. Reactors 1994.* (SR/CNEAF/96-01) Washington, DC: U. S. Department of Energy, Energy Information Administration. [232923]

Einziger, R. E., S. D. Atkin, D. E. Stellrecht, and V. Pasupathi (1982). "High-Temperature Post-Irradiation Materials Performance of Spent Pressurized Water-Reactor Fuel-Rods under Dry Storage-Conditions" *Nucl. Technol.* **57**(1):65–80.

Einziger, R. E. (1994). "Preliminary Spent LWR Fuel Oxidation Source Term Model," in proceedings from High Level Radioactive Waste Management International Conference. Las Vegas, NV: May 1994. p. 554. [MOL.19950517.0141; 233158]

Einziger, R. E., L. E. Thomas, and B. D. Hanson (1995). *Oxidation of Spent LWR Fuel, FY 95 Year end Report.* (MOL212 and MOL213 combined interim report). Richland, WA: Pacific Northwest National Laboratory. [MOL.19960611.0215]

2.1.3.1 Cladding Degradation

Einziger , R. E., and R. V. Strain (1986). "Behavior of Breached Pressurized Water-Reactor Spent-Fuel Rods in an Air Atmosphere Between 250°C and 360°C." *Nucl. Technol.* **75**(1):82–95. [238325]

Garde, A. M. (1986). *Hot Cell Examination of Extended Burnup Fuel from Fort Calhoun*. DOE/ET/34030-11, CEND-427, Combustion Engineering. [NNA.19911017.0103; 237128]

Lorenz, R. A., J. L. Collins, R. L. Towns, A. P. Malinauskas, and O. L. Kirkland (1980). *Fission Product Release for Highly Irradiated LWR Fuel.* (NUREG/CR-0722) Oak Ridge, TN: Oak Ridge National Laboratory. [NNA.19891109.0121; 211434]

Lowry, L. M. A. J. Markworth, J. S. Perrin, and M. P. Landow (1981). *Evaluating Strength and Ductility of Irradiated Zircaloy, Task 5.* (NUREG/CR-1729) Washington, DC: Nuclear Regulatory Commission. [237180]

Maguire, M. (1984). "The Pitting Susceptibility of Zirconium in Aqueous Cl⁻, Br⁻, and I⁻ solutions." In proceedings from Industrial Applications of Titanium and Zirconium: Third Conference. American Society for Testing and Materials. **830:**175–189. [237161]

Manzel, R., and M. Coquerelle (1997). "Fission gas release and pellet structure at extended burnup." In proceedings from International Topical Meeting on LWR Fuel Performance. Portland, OR: March 2–6, 1997. pp. 463–470. [237134]

Matsuo, Y. (1987). "Thermal Creep of Zircaloy-4 Cladding Under Internal Pressure," *J. Nucl. Sci. and Technol.* **24**:111–119. [237137]

Peehs, M., and J. Fleisch (1986). "LWR Spent Fuel Storage Behavior," *J. Nucl. Mat.* **137**:190. [235595]

Pescatore, C., M. G. Cowgill, and T. M. Sullivan (1989). *Zircaloy Cladding Performance Under Spent Fuel Disposal Conditions.* (BNL 52235) Upton, NY: Brookhaven National Laboratory. [NNA.19900710.0055; 200475]

Pescatore, C., and M. Cowgill (1994). *Temperature Limit Determination for the Inert Dry Storage of Spent Nuclear Fuel.* (EPRI TR-103949) Upton, NY: Brookhaven National Laboratory. [102933]

Puls, M. P. (1988). "The influence of hydride size and matrix strength on fracture initiation at hydrides in zirconium alloys." *Met. Trans. A.* **19**(6):1507–1522. [237143]

Rothman, A. J. (1984). *Potential Corrosion and Degradation Mechanisms for Zircaloy Cladding on Spent Nuclear Fuel in a Tuff Repository.* (UCID-20172.) Livermore, CA: Lawrence Livermore National Laboratory. [209058]

Schweitzer, P. A. (1996). *Corrosion Engineering Handbook.* New York, NY: Marcel Dekker, Inc.

Shi, S. -Q., M. P. Puls, (1994). "Criteria for fracture initiation at hydrides in zirconium alloys. 1. Sharp crack-tip." *J. Nucl. Mat.* **208**(3)232–242. [237135]

Siegmann, E. (1998). *Waste Form Degradation and Radionuclide Mobilization Preliminary TSPA, Section 2.7.* Las Vegas, NV: Civilian Radioactive Waste Management System, Management and Operating Contractor. (B00000000-01717-2200-0199)

Uhlig, H. H., and R. W. Revie (1985). *Corrosion and Corrosion Control.* (Third Edition) New York, NY: John Wiley & Sons. [NNA.19891018.0177]

Van Konynenburg, R. A. and P. G. Curtis (1996). *Corrosion test on candidate waste package basket materials for the Yucca Mountain Project.* (UCRL-JC-123236) Livermore, CA: Lawrence Livermore National Laboratory. [MOL.19960417.0256; 237230]

VanSwam, I. F. (1997). "Behavior of Zircaloy-4 and zirconium liner Zircaloy-4 cladding at high burnup." In proceedings from International Topical Meeting on LWR Fuel Performance. Portland, OR: March 2–6, 1997. pp. 421–431. [237262]

Yagee, F. L., R. F. Mattas, and L. A. Neimark (1979). *Characterization of Irradiated Zircaloys: Susceptibility to Stress Corrosion Cracking.* (EPRI NP-1155) Argonne, IL: Argonne National Laboratory. [MOL.19980625.0351]

Yagee, F. L., R. F. Mattas, and L. A. Neimark (1980). *Characterization of Irradiated Zircaloys: Susceptibility to Stress Corrosion Cracking.* (EPRI NP-1557) Argonne, IL: Argonne National Laboratory. [MOL.19980625.0350]

Yang, R. L. (1997). "Meeting the Challenge of Managing Nuclear Fuel in a Competitive Environment." In proceedings from International Topical Meeting on LWR Fuel Performance. Portland, OR: March 2–6, 1997. p. 3. [237148]

2.1.3.2 UO$_2$ Oxidation in Fuel

This section has been reproduced essentially intact from Chapter 3 of Hanson (1998). It details the results of the present oxidation studies, including the burnup and post-oxidation analyses performed. Detailed oxidation curves (oxygen-to-metal ratio as a function of time at operating temperature) for individual samples are presented in Section 2.1.3.2 Appendix.

2.1.3.2.1 Thermal Gravimetric Analysis Oxidation Results

A summary of the experimental conditions and measured parameters for the thermal gravimetric analysis (TGA) tests is presented in Table 2.1.3.2-1. All oxygen-to-metal (O/M) ratios were calculated using Eq. 2.1.3.2-1:

$$\Delta(O/M) = (270/16) \cdot (\Delta M / M_0) \qquad\qquad 2.1.3.2\text{-}1$$

where 270 represents the atomic mass of UO$_2$ (the mass difference due to fission of U and substitution of fission products and higher actinides is ignored), 16 represents the atomic mass of the oxygen taken up by the sample (i.e., assumes that the only mechanism for mass increase is oxygen uptake), DM is the increase in mass, and M0 is the original mass of the specimen.

The O/M ratios were calculated directly from the mass increase of a sample, neglecting any effects due to substitution of two fission products for each fission in the specimen or replacement of a uranium atom by a higher actinide. Further, it was assumed that all specimens had an initial O/M ratio of 2.00. The uncertainty in the calculated O/M ratios is estimated as ±0.01.

Table 2.1.3.2-1   Summary of experimental conditions and measured parameters [LL980608251021.046]

Sample ID#	Oxidation Temperature (°C)	Final O/M Ratio	XRD results	Sample Burnup (MWd/kgM)	
				137Cs[a]	148Nd[b]
105-01	283	2.78	U$_3$O$_8$	c	c
105-02	325	2.73	U$_3$O$_8$	c	c
105-03	305	2.75	U$_3$O$_8$	c	28.1
105-04	270	2.59	c	c	27.5
105-05	255	2.41	U$_4$O$_9$	c	29.2
105-06	283	2.49	U$_3$O$_8$/ U$_4$O$_9$	c	31.5
105-07	283	2.62	U$_3$O$_8$/ U$_4$O$_9$	c	27.6
105-08	283	2.47	U$_3$O$_8$/ U$_4$O$_9$	c	32.5
105-09	305	2.43	c	c	c
105-10	305	2.65≤	c	c	29.8
105-11	305	2.70	c	25.9	29.6
105-12	305	2.73	c	27.9	c
105-13	305	2.71	c	28.3	c

Sample ID#	Oxidation Temperature (°C)	Final O/M Ratio	XRD results	Sample Burnup (MWd/kgM)	
105-14	305	2.73	c	28.1	c
105-15	305	2.73	c	19.1	18.6
105-16	305	2.71	c	18.3	c
105-17	305	2.70	c	16.7	c
105-18	305	2.69	c	16.8	c
104-01	305	2.51	c	42.3	c
104-02	305	2.42	c	42.4	c
108-01	305	2.48	c	17.6	c
108-02	305	2.45	c	34.8	c

[a] Measured by γ-ray energy analysis prior to oxidation
[b] Measured by destructive analysis after oxidation
[c] Measurement/analysis not performed

2.1.3.2.1.1 Doped Fuel

The TGA systems had not been used for two to three years prior to the present tests. New, calibrated pressure transducers were installed, and the sample temperature thermocouples were checked by comparing them with a calibrated thermocouple. The balances and the data-acquisition system were also calibrated. All calibrated standards are traceable to National Institute of Standards and Technology (NIST) standards.

To test one of the TGA systems, a 268.50 mg disk of UO$_2$ doped with 8 wt% Gd$_2$O$_3$ was cut from an unirradiated pellet. The specimen was oxidized in TGA#2 for 454 hr at 283°C. As seen in Figure 2.1.3.2-A-1, the sample reached a plateau at an O/M ratio of approximately 2.35 within about 250 hr. Upon unloading, the disk broke into smaller pieces, which were found to be quite friable. A subsample was taken and analyzed via X-ray powder diffractometry (XRD). The XRD analysis revealed that the sample was entirely converted to a phase that most closely matches U$_4$O$_9$, even though the O/M ratio was significantly higher than the nominal value of 2.25 for U$_4$O$_9$. No other analyses were performed, and the systems were deemed ready for experimental use.

2.1.3.2.1.2 ATM-105 Tests

To minimize the possible influence of factors associated with fuel variability, each fuel specimen (except where noted for samples 105-15 through 105-18) consisted of a single fragment of ATM-105 fuel that came from a 56 cm axial segment from the high-burnup region of the characterized rod ADD2974. The bulk average burnup of this segment, as calculated by correlating the measured [137]Cs γ-ray activity with [148]Nd analyses (Guenther et al., 1991a), ranged from 28.5 to 31.5 MWd/kgM. A radial distribution in burnup was also expected. The fuel had been removed from the clad, and fragments were taken for earlier TGA studies and for the dry-bath tests. The remaining fragments (approximately 90 g from the original 687 g of fuel in this segment) had been placed in a capped storage tube and kept in the hot cell where the dry-baths were located. When a fragment was needed for a test, the tube was opened, and fragments were poured into a petri dish. Once a fragment of ~200 mg

was found, it was placed in a glass vial and transported to the TGA laboratory. The remaining fragments were returned to the storage tube. Thus, the exact radial and axial location of these specimens within the irradiated rod is not known.

Scoping Tests

The first five oxidation tests were run as scoping tests to help determine the time required to oxidize the spent fuel samples to U$_3$O$_8$ (i.e., a second plateau at an O/M ratio of approximately 2.75) as a function of temperature. These results, plotted as the O/M ratio as a function of time (Figure 2.1.3.2-1), were to be used to establish the test matrix to determine the oxidation kinetics and to assist in the development of the mechanism of oxidation of spent fuel to U$_3$O$_8$. The temperatures were chosen to compare the data from the present studies with the previous oxidation data of Einziger and Strain (1986).
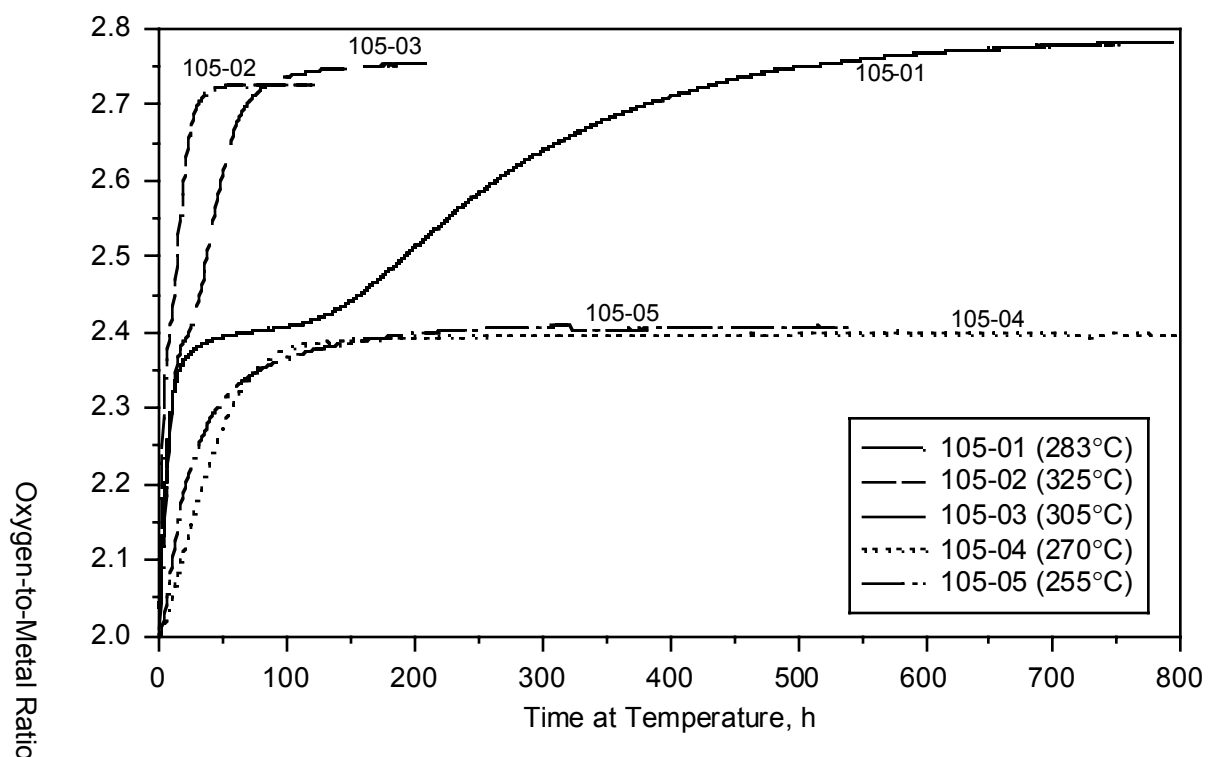
Figure 2.1.3.2-1   Oxygen-to-metal ratio as a function of time for ATM-105 fragments oxidized at various temperatures [LL980601851021.044]

Sample 105-01 (i.e., ATM-105 sample #1) consisted of a 184.63 mg fragment; it was oxidized for 793 hr at 283°C. The first plateau at an O/M ratio of about 2.4 was reached after approximately 55 hr, and a short plateau (although not of zero slope) was observed before the onset of more rapid mass increase resumed. A final bulk O/M ratio of 2.78 was achieved. XRD analysis revealed the sample was converted to U$_3$O$_8$ with minor amounts of U$_4$O$_9$ remaining. Scanning electron microscopy (SEM) revealed that the sample had disintegrated into small clusters of individual grains with a great deal of inter- and intragranular cracking.

Sample 105-02 was a 193.73 mg fragment oxidized at 325°C to a final bulk O/M ratio of approximately 2.73. An O/M ratio of approximately 2.4 was reached after only 8 hr, and no truly identifiable plateau existed, although there was an obvious change in the rate-of-

increase in O/M ratio after this point (see Figure 2.1.3.2-A-3). The only phase detected by XRD was U$_3$O$_8$. SEM revealed even more intragranular cracking than was observed with the first sample; this is consistent with the higher stresses experienced because of the rapid oxidation at higher temperatures.

The third sample, 105-03, consisted of a single 207.11 mg fragment, which was oxidized at 305°C to a final bulk O/M of 2.75. An O/M ratio of 2.4 was reached after approximately 23 hr. Again, a plateau with zero slope did not exist, although there was clearly a different rate of change in O/M ratio after a ratio of approximately 2.39 was reached. XRD of the resultant powder detected only U$_3$O$_8$.

Sample 105-04 was oxidized for 2375 hr at 270°C. This 203.39 mg fragment was the first in this series to exhibit a plateau with zero slope, as seen in Figure 2.1.3.2-A-5. The duration of the plateau was between 700 and 800 hr; mass increase then began again. An eventual final bulk average O/M of 2.59 was reached before the test was terminated. This sample was converted to powder, but no XRD analysis was performed because of the loss of the subsample taken for this purpose. Twice during oxidation of this sample, at 1076 and 1870 hr, power fluctuations caused relays to the furnace to reset, resulting in loss of power to the furnace. Each time, the sample cooled to room temperature before the test was restarted.

Sample 105-05 was oxidized at 255°C to compare with sample 105F-100, which was being oxidized in a dry-bath also operating at 255°C. As can be seen in Figure 2.1.3.2-2, the two oxidation curves agree fairly well over the first 400 hr. A computer malfunction after 322 hr at operating temperature resulted in the sample cooling to room temperature before being reheated to 255°C. Because the data of Einziger and Strain (1986) suggested that the duration of the plateau would be on the order of 10^4 hr, this TGA test was halted after only 544 hr when a bulk O/M ratio of 2.41 had been reached. The sample appeared to be an intact fragment when it was unloaded, and XRD analysis revealed that U$_4$O$_9$ was the only phase present.

Originally, spent fuel fragments were to be oxidized to progressively larger O/M ratios between the plateau (~2.4) and final completion (~2.75) at a fixed temperature. Post-oxidation analyses would then be used to determine the amount of each phase present and to determine the mechanism and kinetics of the transition from UO$_{2.4}$ to U$_3$O$_8$. The tests would then be repeated at different temperatures to determine the temperature dependence of oxidation. From the scoping tests, it was clear that, to perform enough tests to adequately study this transition, the temperatures would need to be in the range of 275° to 305°C. At temperatures less than 275°C, the duration of the plateau was expected to be ≥800 hr; at temperatures greater than 305°C, the plateau is not well defined and oxidation occurs rapidly. It was decided that the first series of tests would be performed at 283°C.
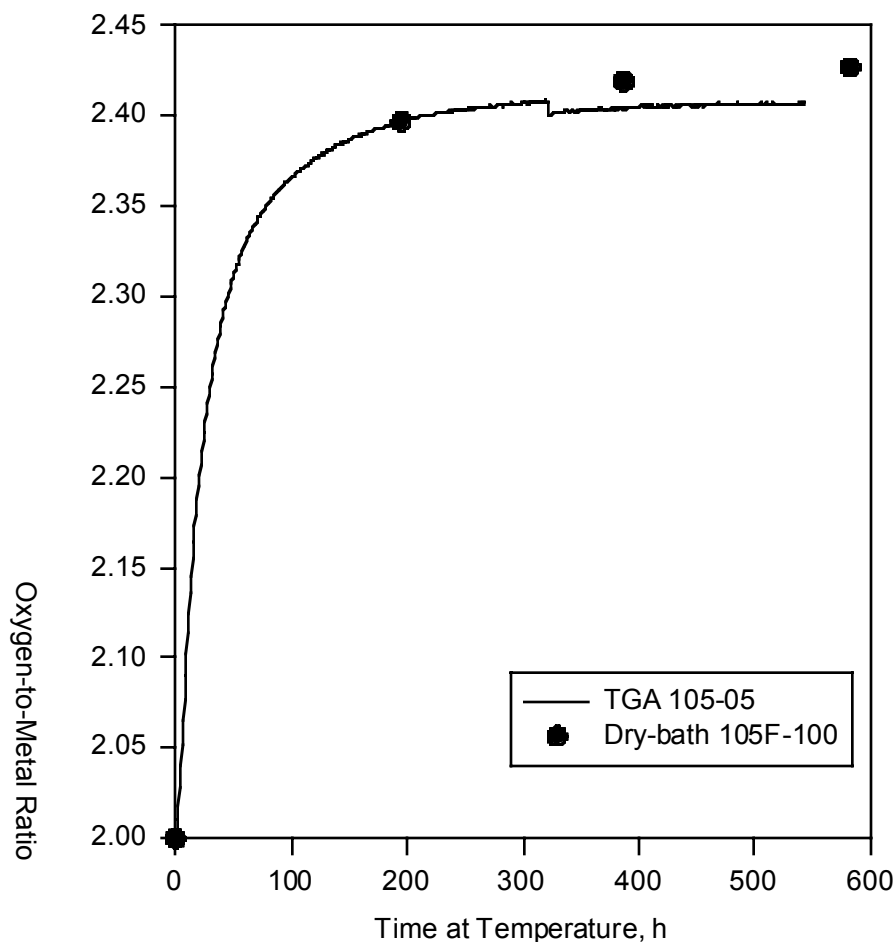
Figure 2.1.3.2-2   Oxidation behavior of ATM-105 fragments in a TGA and dry-bath at 255°C [LL980608251021.046]

2.1.3.2.1.3 283°C Tests

As reported in Section 2.1.3.2.1.2, sample 105-01 had been oxidized at 283°C. Based on the behavior of this sample and the earlier samples of Einziger and Strain (1986), it was expected that a short plateau with non-zero slope would exist for each sample at this temperature. Sample 105-06 was then oxidized at 283°C. It is clearly seen in Figure 2.1.3.2-3 that the oxidation behaviors of samples 105-01 and 105-06 were quite different. Although the time to reach an O/M ratio of 2.4 was similar, and neither specimen exhibited a plateau of zero slope, the time rate of change in O/M for sample 105-06 was much smaller than it was for the previous sample. This 214.06 mg fragment was oxidized for 1125 hr to a final bulk O/M ratio of 2.49. This sample consisted of powder and of a remaining fragment when unloaded from the TGA. XRD was performed, and both U$_3$O$_8$ and U$_4$O$_9$ were detected in the powder; the fragment consisted solely of U$_4$O$_9$. The only known difference between samples 105-01 and 105-06 was that the latter experienced two intermittent power losses to the furnace (at 21 and 816 hr) during which the sample cooled to room temperature before the test was resumed.

Sample 105-07 was then oxidized at 283°C for 743 hr. The oxidation behavior of this 167.37 mg fragment was intermediate to the previous two samples oxidized under identical conditions. The initial rate of O/M increase was less than that of the other samples (Figure 2.1.3.2-3); however, the time to reach an O/M ratio of 2.4 was about the same for all specimens. This sample then exhibited a plateau with near zero slope; once mass increase resumed, it was at a rate intermediate to that of the previous samples. The test was halted when a final bulk O/M ratio of 2.62 was reached. The sample consisted of only powder, which XRD identified as a mixture of U$_3$O$_8$ and U$_4$O$_9$. During oxidation of this specimen, a power outage resulted in the sample cooling to room temperature after 314 hr at operating temperature. A computer malfunction resulted in the loss of data from 356–434 hr, although no other impact on the test was observed.
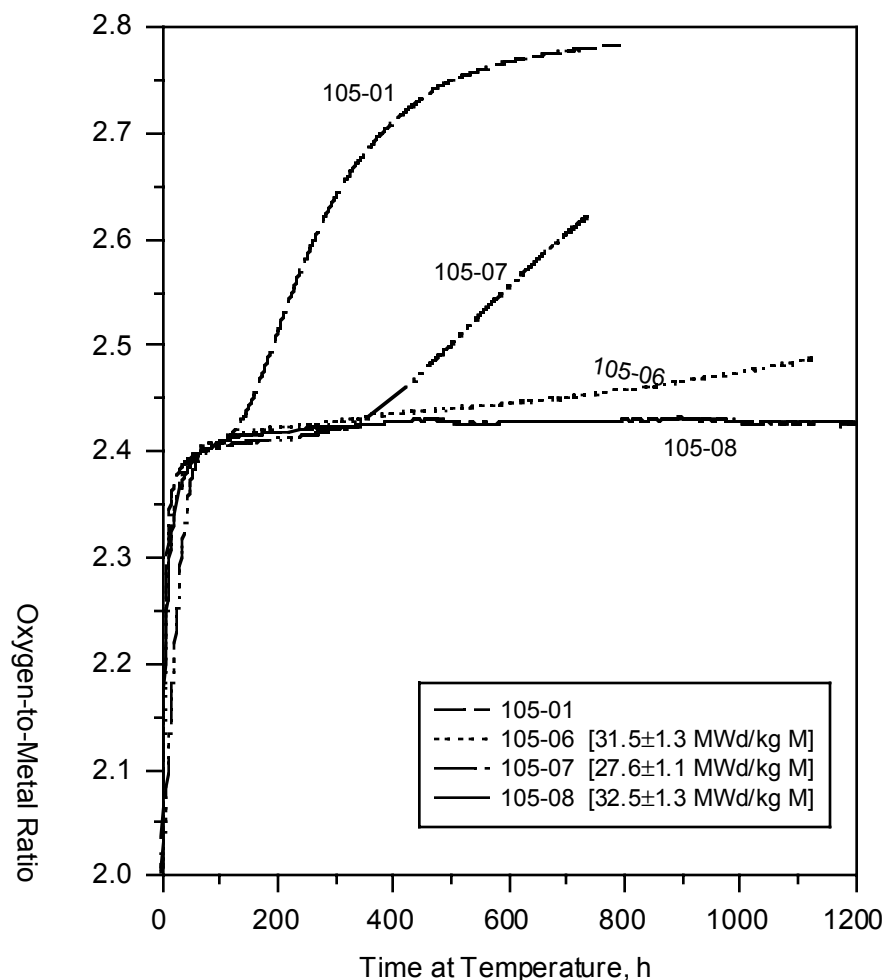
Figure 2.1.3.2-3   Oxidation behavior of ATM-105 fragments oxidized at 283°C [LL980601851021.044]

Both TGA systems were then thoroughly checked using NIST-traceable standards to ensure their proper calibration. Copper wire was oxidized in each TGA to determine if the tare and/or calibration of the balance drifted as a function of time or temperature. No problems were found with the balances or with the calibrated data-acquisition systems. Thus, the observed difference in oxidation behavior for the first three samples oxidized at 283°C

was determined to be real and not due to equipment problems. The furnace-control relays were reconfigured so that power fluctuations or power outages lasting less than 2 min would not cause the relays to reset.

Sample 105-08 was a 195.63 mg fragment that was oxidized at 283°C. Three weeks after this test was initiated, the building where the TGA laboratory is located was placed under a radiologic work stoppage. No entry was allowed to the laboratory, so this system ran virtually unattended for months. Although the system appeared to have operated normally, there are large gaps in the data because no data were recorded once the data disk was full. Still, it is clear that a plateau with zero slope persisted for well over 1000 hr and likely closer to 3000 hr, as observed in Figure 2.1.3.2-A-9. Once mass increase began after this plateau, it was at a very slow rate. This experiment was halted after 5375 hr at constant temperature, and the final bulk average O/M ratio was 2.47. The sample consisted of powder and a remaining fragment. As with earlier samples, XRD detected a mixture of U_3O_8 and U_4O_9 in the powder, whereas only U_4O_9 was detected in the fragment. While the oxidation behavior to an O/M ratio of ~2.4 was rather consistent with earlier observations (Einziger et al. 1992), the duration of the plateau and oxidation behavior to U_3O_8 varied widely among the samples tested.

305°C Tests

A second series of samples from the high-burnup region of the ATM-105 fuel rod was oxidized at 305°C to determine if the variable oxidation behavior after reaching an O/M ratio of ~2.4 persisted at higher temperatures. Sample 105-09 (185.42 mg) was oxidized for about 122 hr, at which time the bulk O/M ratio was 2.43. This sample oxidized at a much slower rate than did sample 105-03, the scoping test specimen also oxidized at 305°C. Oxidation of sample 105-09 was halted because of this marked difference. When unloaded, the sample consisted of powder and a remaining fragment. XRD of the sample is planned for future work.

Sample 105-10 was then oxidized under identical conditions of temperature and ambient atmosphere in the same TGA system that had been used for the oxidation of sample 105-09. As seen in Figure 2.1.3.2-4, the oxidation behavior of this 181.36 mg fragment was intermediate to those of the samples previously oxidized at 305°C. This sample oxidized for 287 hr; however a problem with the balance resulted in no mass data being recorded for the last 60 hr. Prior to this failure, the O/M ratio was calculated as 2.65. It is clear that the variability in oxidation behavior persisted at 305°C.
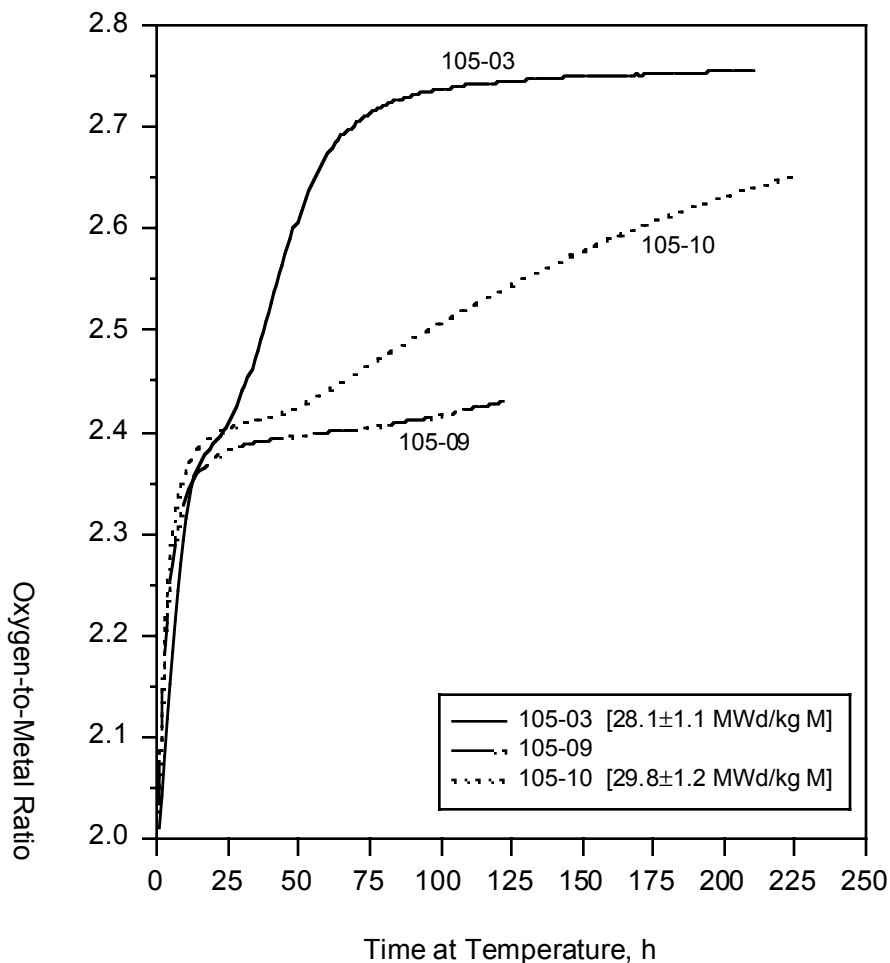
Figure 2.1.3.2-4   Oxidation behavior of ATM-105 fragments oxidized at 305°C [LL980601851021.044]

The only known differences among the first 10 samples oxidized were specimen-to-specimen variations and the intermittent cooling of some specimens to room temperature as a result of power fluctuations or computer failure. To test the effect of these variables, one large fragment from the high-burnup region of the ATM-105 fuel was broken into four smaller fragments. All four (samples 105-11 through 105-14) were oxidized individually at 305°C; the time dependence of their oxidation is shown in Figure 2.1.3.2-5.
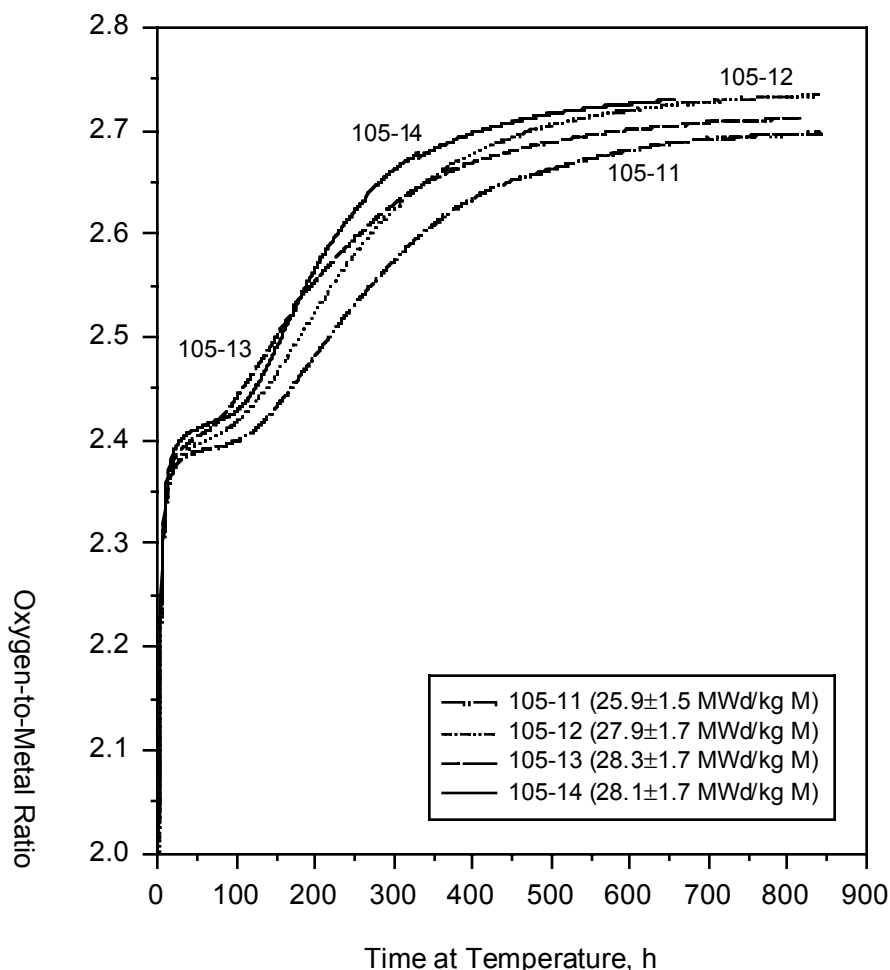
Figure 2.1.3.2-5   **Oxidation behavior of four samples broken from the same fragment of ATM-105 fuel oxidized at 305°C [LL980601851021.044]**

Sample 105-11 (143.37 mg) was oxidized for 843.5 hr to a final bulk O/M ratio of 2.70. Concurrently, sample 105-12 (188.27 mg) was oxidized for 840.5 hr to a final bulk O/M ratio of 2.73. Although some variability in the oxidation kinetics is evident (see Figure 2.1.3.2-5), it is much less than seen in Figure 2.1.3.2-4 for fragments with random locations within the same fuel segment.

Sample 105-13 (238.26 mg) was then oxidized under identical conditions. The furnace was turned off after 170 hr when the O/M ratio was 2.53. A subsequent problem with the balance required that the sample remain at room temperature for one month before testing could be resumed. It was necessary to open the system to temporarily add weight to the tare side of the balance. The system was then sealed, evacuated, and filled with dry air. During this procedure, some of the sample fell from the quartz crucible to the bottom of the reaction tube. This was confirmed by the very high activity measured in this location with a Geiger-Mueller detector. Comparison of the mass before and after this incident indicated that about 22.58 mg of the sample fell from the crucible. Because the entire sample had gained only 7.54 mg, it was assumed that the sample lost included both UO$_{2.4}$ and U$_3$O$_8$ and that the remaining sample had an O/M ratio of 2.53. The test was restarted and continued for a total oxidation time of 819.5 hr, when a final bulk average O/M ratio of 2.71 was achieved.

Sample 105-14 (241.21 mg) was also oxidized at 305°C. For the first 50 hr, the behavior of this sample was nearly identical to that of sample 105-12. Power to the furnace was turned off after 68 hr when the bulk O/M ratio was 2.42. The sample remained at room temperature for one week before being reheated to 305°C. Oxidation continued for a total of 656 hr, at which time the relay for the temperature controller failed, resulting in a slight rise in the sample temperature; this, in turn, resulted in an automatic loss of power to the furnace. The final bulk O/M ratio was 2.73.

Again, Figure 2.1.3.2-5 clearly illustrates some variability in the oxidation kinetics for these four samples broken from the same larger parent fragment; however, the variability is much less than that observed previously for fragments that were probably located at random locations within the segment of the fuel rod taken for study. Based on the comparison of the results of the oxidation of samples 105-11 through 105-14, and on dry-bath data where the samples are intermittently cooled for periodic weighings, it was concluded that temperature cycling had a relatively small or negligible effect on the characteristics of the fuel oxidation and was not the cause of the variability observed.

It is clear that specimen-to-specimen variability is the major cause of the different oxidation behaviors observed. The small sample size (~200 mg) mandated by radiologic dose control ensures that an individual specimen is much too small to sample across the entire fuel radius. The small sample size, coupled with the axial and radial burnup variations in the fuel, was suspected as the cause of the wide variation found in the oxidation kinetics of $UO_{2.4}$ to U_3O_8. To test this hypothesis, two large fragments of ATM-105 fuel from the low-burnup upper-end of the same fuel rod were each broken into two smaller fragments (samples 105-15 through 105-18) and oxidized at 305°C (Guenther et al., 1991a). The bulk average burnup reported for this segment ranged from 13.5 to 17.5 MWd/kgM.

The variation in the O/M ratio dependence on time for samples 105-15 through 105-18 is shown in Figure 2.1.3.2-6. Samples 105-15 (213.20 mg) and 105-16 (138.68 mg) both oxidized rapidly, achieving an O/M ratio of 2.4 within 16 hr. The plateaus at this lower burnup were merely an inflection in the O/M curve. Sample 105-15 reached an O/M of 2.73 in 78.5 hr and remained at this O/M until the test was terminated after 121 hr. Similarly, sample 105-16 obtained an O/M ratio of 2.71 within approximately 100 hr and remained there until the test was terminated after 142 hr. Samples 105-17 (210.49 mg) and 105-18 (161.97 mg) oxidized even faster and reached bulk O/M ratios of 2.70 and 2.69, respectively, within 50 hr. Clearly, the transformation from $UO_{2.4}$ to U_3O_8 occurred much earlier than for the fragments from the high-burnup region.
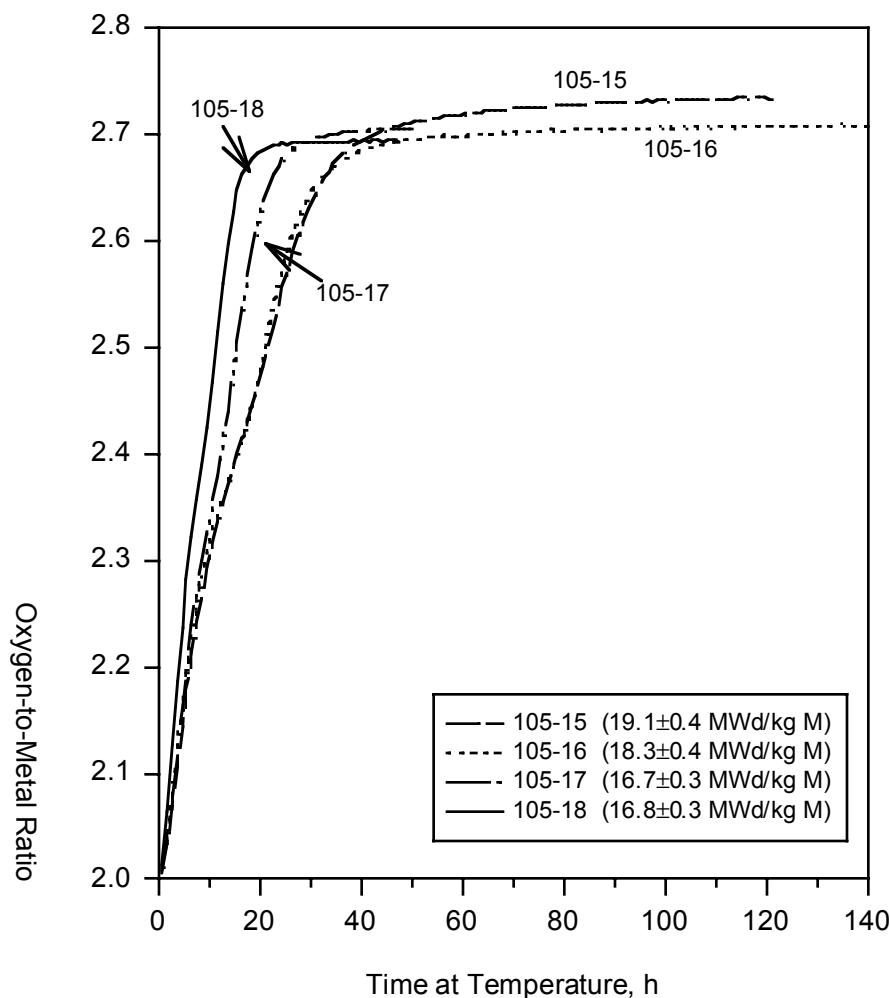
Figure 2.1.3.2-6   Oxidation behavior of low burnup ATM-105 fragments oxidized at 305°C [LL980601851021.044]

2.1.3.2.1.4 ATM-104 Tests

To support the burnup dependence on oxidation rate inferred from measurements on fuel fragments that were randomly distributed axially and radially throughout the ATM-105 (boiling-water reactor [BWR]) fuel segments studied, fuel specimens were taken from a specially cut segment of ATM-104 (pressurized-water reactor[PWR]) fuel in which the fuel had not separated from the cladding.

With a low-speed saw, two fragments were taken from near the centerline of a segment from the high-burnup region of the ATM-104 fuel rod (MKP-109), thus reducing the likelihood that the sample would contain the large burnup gradients and highly restructured microstructure found near the fuel surface. The fuel in this region had an estimated bulk average burnup of 44 MWd/kgM (Guenther et al., 1991b). These two fragments, 104-01 and 104-02, were oxidized individually at 305°C (see Figure 2.1.3.2-7). Sample 104-01 (184.53 mg) was oxidized to an O/M ratio of approximately 2.41 within 100 hr and exhibited a plateau with zero slope for approximately 400 hr before mass increase resumed. The test was terminated after 1201 hr and gave a final O/M ratio of 2.51. Sample 104-02 (213.90 mg)

oxidized to an O/M ratio of about 2.40 within 120 hr and remained on this plateau with no mass increase for more than 500 hr before mass increase resumed, albeit at a much slower rate than with sample 104-01. A final bulk average O/M ratio of 2.42 was reached before the test was terminated after 1200 hr.

Oxidation of these PWR fragments clearly demonstrated much longer plateaus than those observed in oxidation of the lower burnup ATM-105 (BWR) fragments at the same temperature and under similar atmosphere. While further testing should be performed to rule out the possible dependence of the stabilization effect (plateau behavior of the transition from $UO_{2.4}$ to U_3O_8) on reactor type, the data obtained in these measurements strongly suggest similar burnup dependencies for BWR and PWR fuels.
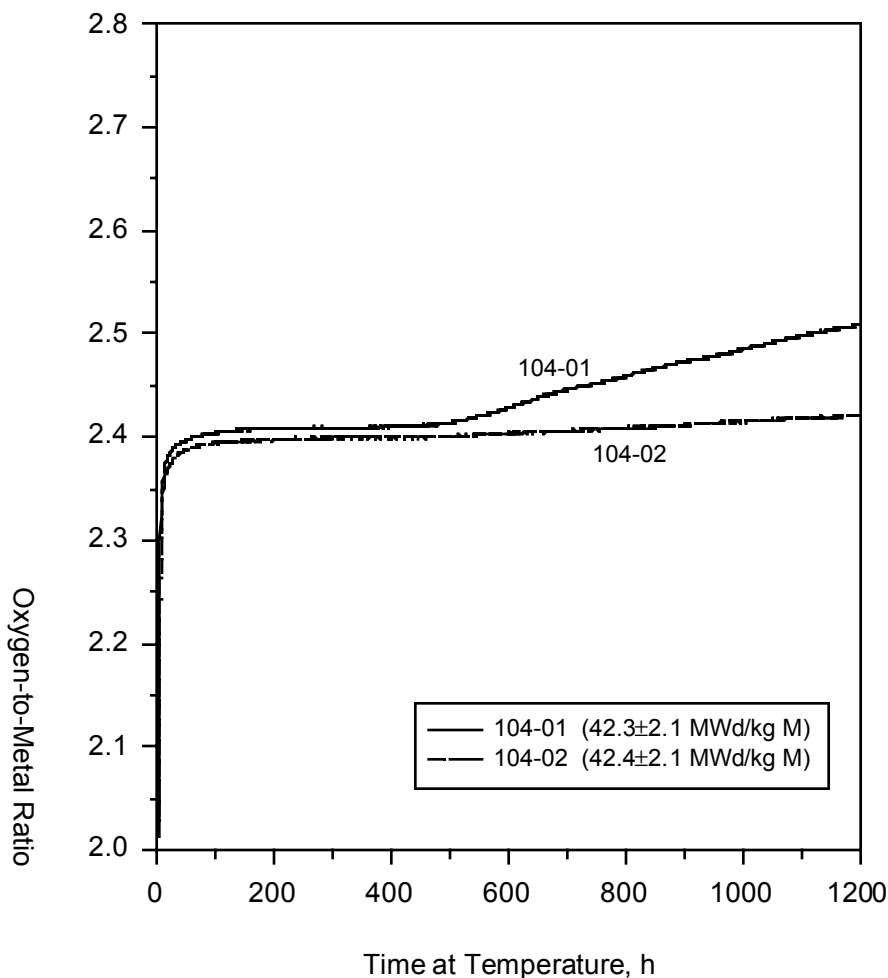
Figure 2.1.3.2-7   Oxidation behavior of ATM-104 fragments at 305°C [LL980601851021.044]

2.1.3.2.1.5 ATM-108 Tests

In this final test, two fragments of fuel from the high-burnup region of ATM-108 were obtained in a manner similar to that for the ATM-104 samples. One fragment (108-01) was cut from near the centerline of a pellet, and a second fragment (108-02) was cut from the pellet surface. ATM-108 is a group of fuel rods from the same assembly as ATM-105; however, the

rods making up ATM-108 contained an initial doping of Gd$_2$O$_3$ to serve as a burnable poison for reactivity control. The rod (ADN0206) from which these samples were cut contained 3 wt% Gd$_2$O$_3$ and the same initial enrichment (2.93 wt%) of ^{235}U as did the ATM-105 rod from which the previous samples were obtained. The burnup of the ATM-108 fuel in this region was expected to be approximately 26-28 MWd/kgM (Guenther et al., 1994), slightly lower than the 28.5 to 31.5 MWd/kgM expected for the ATM-105 high-burnup region (Guenther et al., 1991a).

The initial Gd in the fuel undergoes neutron capture during reactor operations and remains as Gd, although of higher atomic mass number. Both the substitution of U with fission products and actinides and the Gd-doping were expected to stabilize the UO$_{2.4}$ with respect to oxidation to U$_3$O$_8$. The actual distribution of Gd$_2$O$_3$ within the fuel is not known; however, the homogeneity of these early fuels is questionable.

Sample 108-01 (171.01 mg) was cut from near the centerline of the fuel pellet and was oxidized at 305°C for more than 2400 hr. As seen in Figure 2.1.3.2-8, this sample did not exhibit a plateau with zero slope, but exhibited a very slow, continuous increase in the O/M ratio. The time required to oxidize this sample from an O/M of about 2.475 to 2.481 was approximately 1000 hr.

On the other hand, sample 108-02 (232.23 mg) was taken from the higher burnup fuel pellet surface and has exhibited two different plateau behaviors. The first plateau, at an O/M ratio of approximately 2.38, was reached after about 40 hr and had a duration of less than 50 hr before more rapid mass increase resumed. A second plateau at an O/M ratio of 2.45 was reached after about 475 hr and then exhibited a plateau with zero slope for more than 2000 hr. It is believed that those portions of the specimen with lower burnup or lower Gd content have oxidized to U$_3$O$_8$, while the portions with higher substitutional impurities remained at UO$_{2.4}$. This would explain the second plateau at such a low O/M ratio. Post-oxidation analyses are planned to determine the quantity of each phase present. Clearly, these irradiated samples doped with Gd$_2$O$_3$ have exhibited much slower overall oxidation behavior than have any other specimen oxidized at 305°C.
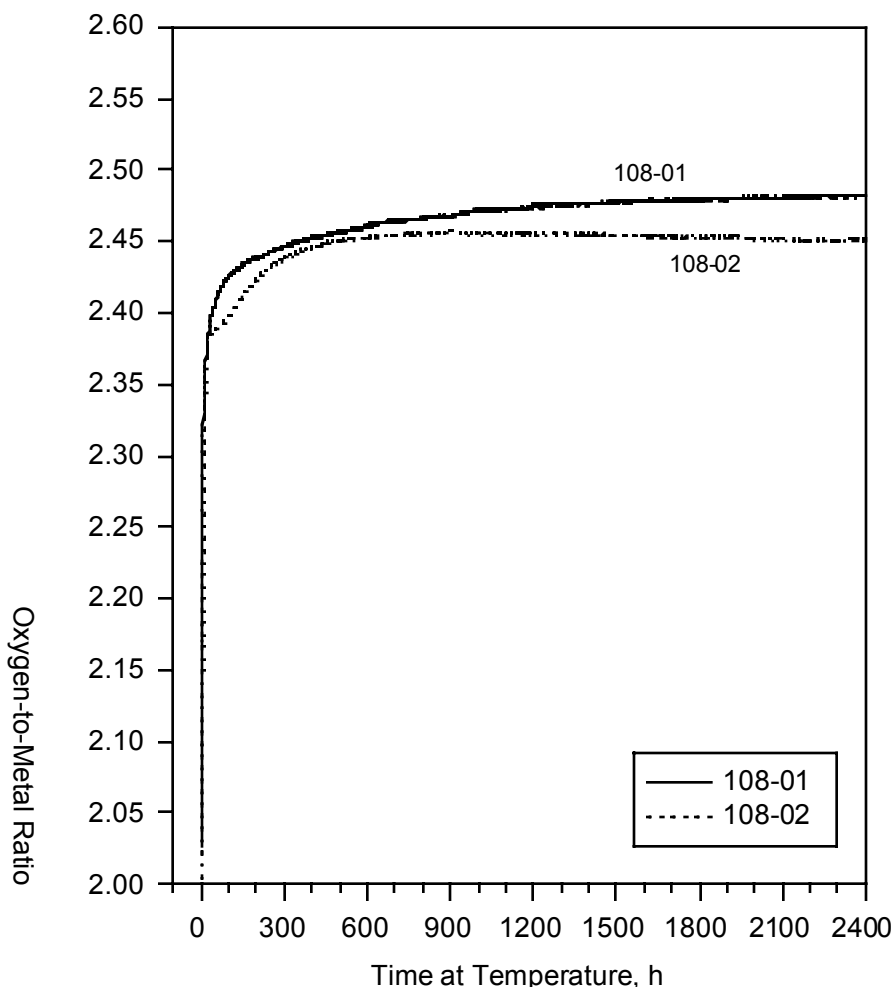
Figure 2.1.3.2-8 **Oxidation behavior of ATM-108 fragments at 305°C**
[LL980601851021.044]

2.1.3.2.2 Burnup Analyses

2.1.3.2.2.1 ^{148}Nd Isotope-Dilution Method

At the end of 1996, authorization and funding were obtained to perform an analysis of the burnup of some of the individual specimens that had been oxidized previously. Nine of the 18 samples oxidized prior to that time were chosen. Samples 105-01 and 105-02 had been disposed of and were unavailable for any further testing. The remaining specimens from the scoping tests (105-03 through 105-05), the 283°C tests (105-6 through 105-08), and three of the 305°C tests (105-10, 105-11, and 105-15), including one of the known low-burnup specimens, were analyzed for burnup using the method essentially equivalent to American Society for Testing and Materials (ASTM) procedure E321 (ASTM, 1990). The results of this analysis are found in Table 2.1.3.2-1 and are identified on the appropriate oxidation curves in square brackets The uncertainty of ±4% accounts for experimental uncertainty and the reported uncertainty in converting atom percent burnup to burnup in units of MWd/kgM (ASTM, 1990). Analysis of other specimens will be performed is planned.

Table 2.1.3.2-2 lists the number of fissions and the total number of uranium and plutonium atoms normalized to the mass of the specimen in the one-tenth mL aliquots analyzed. The atom percent burnup is calculated using

$$\text{atom\% burnup} = \text{Fissions}/(\text{U+Pu+Fissions}) \qquad \qquad 2.1.3.2\text{-}2$$

Also included is the fraction of ^{242}Pu in the total Pu, as determined by thermal ionization mass spectrometry. The amount of ^{242}Pu can be used to qualitatively order the samples with respect to possible higher actinide content. The atom densities reported for sample 105-11 appear very low with respect to the other samples; however, additional calculations (comparing the ratios of the atom densities of this sample to samples of similar burnup) seem to indicate that the burnup results are correct. It is suspected that either the reported mass was incorrect (too large) or that not all of the sample dissolved.

Table 2.1.3.2-2   Atom densities found by mass spectrometry normalized to sample mass [LL980608251021.046]

Sample	Atom Density U	Atom Density Pu	Atom Density Fissions	Percent ^{242}Pu
105-03	8.107×10^{18}	5.583×10^{16}	2.458×10^{17}	8.03
105-04	8.247×10^{18}	5.629×10^{16}	2.445×10^{17}	7.56
105-05	8.234×10^{18}	7.209×10^{16}	2.610×10^{17}	7.79
105-06	8.033×10^{18}	7.104×10^{16}	2.753×10^{17}	9.01
105-07	8.109×10^{18}	5.610×10^{16}	2.414×10^{17}	7.84
105-08	8.069×10^{18}	7.206×10^{16}	2.851×10^{17}	10.44
105-10	7.933×10^{18}	6.548×10^{16}	2.559×10^{17}	8.19
105-11	6.386×10^{18}	5.157×10^{16}	2.048×10^{17}	8.46
105-15	8.343×10^{18}	4.169×10^{16}	1.653×10^{17}	3.17

2.1.3.2.2.2 Gamma Spectrum Analysis

The burnup of all specimens starting with sample 105-11 was determined prior to oxidation by correlating the specific activity of ^{137}Cs with ORIGEN2 predictions. The specific activity for each sample, the uncertainty associated with the combined effects of the γ-ray self-absorption and statistical and calibration uncertainties, and the corresponding burnup range are listed in Table 2.1.3.2-3. Burnups calculated by comparing the measured ^{137}Cs specific activity with ORIGEN2 predictions are also included in parentheses in the corresponding oxidation curves. Included in Table 2.1.3.2-3 are the specific activities for ^{241}Am and the rather large uncertainties associated with this isotope. Although the activity of ^{241}Am is not a good measure of burnup, it is the only higher actinide detected by this method and is the only means of qualitatively determining the relative higher actinide content of samples. Samples from near the pellet surface will have not only higher burnup, but larger concentrations of higher actinides due to the resonance absorption in ^{238}U.

Table 2.1.3.2-3   Burnup as a function of ^{137}Cs specific activity [LL980608251021.046]

Sample	Specific activity of ^{137}Cs (µCi/mg)	Burnup (MWd/kgM)	Specific activity of ^{241}Am (µCi/mg)
105-11	48.3±2.9	25.9±1.5 (3.9)	1.6±0.5
105-12	52.1±3.1	27.9±1.7 (4.2)	1.9±0.6
105-13	52.8±3.2	28.3±1.7 (4.2)	1.1±0.3
105-14	52.5±3.2	28.1±1.7 (4.2)	2.0±0.6
105-15	34.9±0.7	19.1±0.4 (2.9)	1.4±0.4
105-16	33.3±0.7	18.3±0.4 (2.7)	0.8±0.2
105-17	30.3±0.6	16.7±0.3 (2.5)	0.7±0.2
105-18	30.6±0.6	16.8±0.3 (2.5)	1.1±0.3
104-01	80.8±4.0	42.3±2.1 (6.3)	1.8±0.5
104-02	81.1±4.1	42.4±2.1 (6.4)	2.0±0.6
108-01[a]	31.3±3.1	17.6±1.8 (2.6)	Not detected
108-02[a]	63.0±3.2	34.8±1.9 (5.2)	18.0±6.7

(a)   ORIGEN2 runs were performed using the same input parameters as for the ATM-105 samples (i.e., Gd$_2$O$_3$ doping was ignored).

In the present tests, two samples had burnup determined by both the ^{148}Nd and ^{137}Cs methods. ORIGEN2 was run for the burnups found by the ^{148}Nd method for these two samples, and the specific activity of ^{137}Cs predicted by ORIGEN2 was compared with the measured value. Sample 105-15 had a burnup of 18.6 ± 0.7 MWd/kgM measured using the isotope-dilution method. The ^{137}Cs activity predicted for a BWR sample with this burnup was within 3% of the value measured by the γ-ray energy analysis.

Similarly, sample 105-11 had a measured burnup of 29.6 ± 1.2 MWd/kgM. ORIGEN2 predicted a specific activity of 55.5 µCi/mg, which is 13% larger than the experimentally measured value of 48.3 µCi/mg. The deviation of the predicted value from the measured value ranged from 8% (at +1σ of the measured value) to 18% (at–1σ). With the estimated uncertainty of about 4% for the ^{148}Nd analysis and an average difference between the ORIGEN2 burnup prediction for ^{137}Cs activity and experimental values of 13%, it is reasonable to assume an uncertainty in the burnup estimates obtained through γ-ray spectroscopy of approximately ±15%. This 15% uncertainty is expressed in parentheses for the burnups reported in Table 2.1.3.2-3. The smaller uncertainties are those associated with the uncertainty in the specific activity only. It is important to note the marked difference in ^{137}Cs activity and the corresponding difference in local burnup between sample 108-02, which was taken from the pellet surface, and sample 108-01, which was taken from the pellet centerline.

2.1.3.2.3 Dry-Bath Oxidation Results

During the past 10 yr, more than 100 different samples have been oxidized at various temperatures in the dry-baths. A large fraction of the samples has been oxidized at temperatures less than 150°C; even though they had operated for almost 50,000 hr, the bulk

average O/M ratios were less than 2.2. For the purpose of this study, the primary focus was on samples that consisted of fragments (as opposed to fragments crushed to powders) and were oxidized in dry air to an O/M ratio near the plateau. As with the TGA studies, the precise axial and radial location of the fuel samples in the fuel rod segments is not known.

2.1.3.2.3.1 175°C Tests

Multiple samples of each of the fuels have been oxidized at 175°C in two separate dry-baths using a dry-air atmosphere. Overall agreement of the samples for each fuel type has been excellent, with the largest difference in the O/M ratio between samples at any given time being approximately 0.04. Each sample had an initial mass of approximately 10 g; however, the number of fragments required to make up this sample varied greatly. For example, the three different ATM-105 samples contained 15, 22, and 28 fragments, respectively. The number of fragments for a 10 g sample of Turkey Point fuel ranged from 31 to 34, while the range was from 15 to 40 and 35 to 101 for ATM-104 and ATM-106, respectively.

The corresponding variation in surface area exposed to the oxidant is thought to be one reason for the minor differences in the initial mass increase among samples of the same fuel type. Also, fragments from near the pellet surface will have a high concentration of fine fission gas bubbles on the grain boundaries, promoting more rapid oxidation than promoted for the fuel near the center where the bubbles are larger and fewer in number. This hypothesis is substantiated by the fact that the differences among samples decreased with increasing time such that the O/M ratios for samples of each fuel type varied by no more than 0.02 at the end of these experiments. The temperature difference between the two blocks of dry-bath #1 was roughly 7°C, which also contributed to the more rapid mass increase for some of the samples. Figure 2.1.3.2-9 shows the change in the O/M ratio as a function of time for one sample of each of the four fuel types. For each fuel, with the possible exception of ATM-106, it appears that a plateau at an O/M of about 2.4 had been reached, and mass increase was continuing to occur at the end of the measurements.
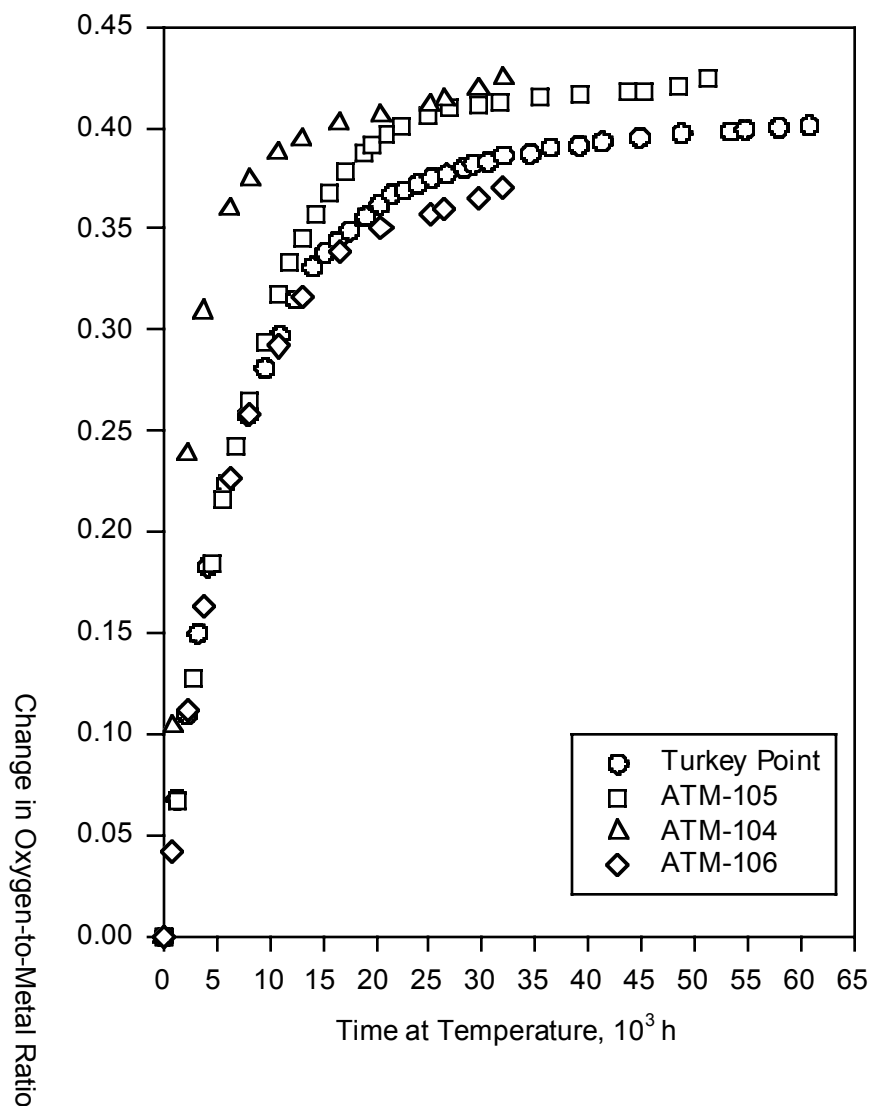
Figure 2.1.3.2-9   Oxidation behavior of light-water reactor (LWR) spent-fuel fragments oxidized in a 175°C dry-bath [LL980608251021.046]

2.1.3.2.3.2 195°C Tests

One sample of each of the four fuel types was oxidized in a dry-air atmosphere at 195°C. In each case, the sample consisted of fragments that had been crushed and sieved to a Tyler mesh size of –12/+24 (roughly 0.7 to 1.7 mm). Figure 2.1.3.2-10 shows the change in the O/M ratio as a function of time for these four samples. With the exception of the Turkey Point fuel, which had been previously oxidized for 28,868 hr at 110°C to a bulk O/M of 2.009, all of the samples were as-irradiated and assumed to have an O/M of 2.00. The ATM-105 sample was freshly crushed for this test; the ATM-104 and ATM-106 samples were from powder stored for 3 yr prior to the start of this test. Again, it appears that a plateau in the range of O/M 2.35 to 2.40 had been reached, and mass increase was continuing to occur at the end of the measurements.
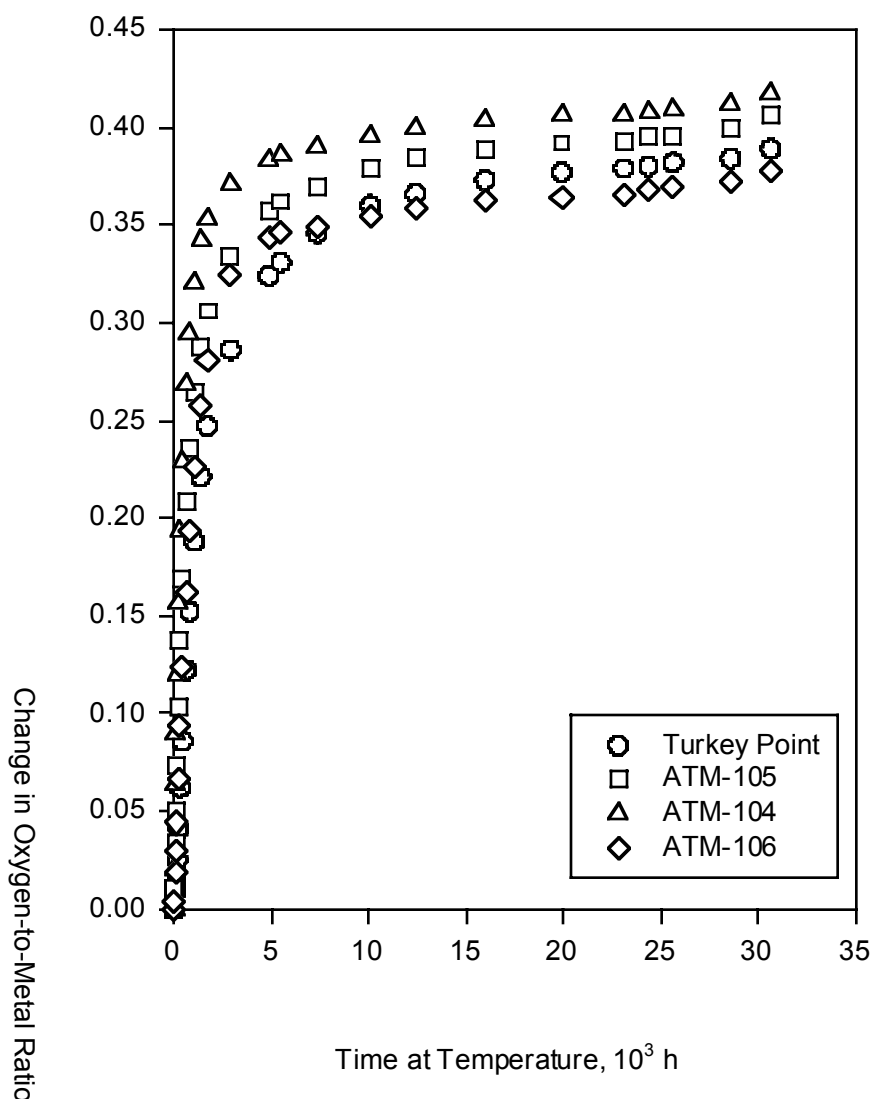
Figure 2.1.3.2-10 Oxidation behavior of crushed LWR spent-fuel fragments in a 195°C dry-bath [LL980608251021.046]

2.1.3.2.3.3 255°C Test

In 1993, a dry-bath test at 255°C was initiated. This test contained 11 samples, 7 of which each consisted of approximately 5 g of spent fuel fragments, with the remaining 4 samples consisting of approximately 5 g each of crushed fuel fragments. The seven samples were as follows:

- One sample each of ATM-104 and ATM-105 from as-irradiated (no prior oxidation) fuel fragments
- One each of Turkey Point (110°C for 28,868 hr to O/M ~2.004) and ATM-106 (110°C for 525 hr to O/M ~2.000) that had been very slightly oxidized at low temperature
- One each of Turkey Point (175°C for 43,945 hr to O/M ~2.395), ATM-105 (175°C for 34,420 hr to O/M ~2.422), and ATM-104 (176°C for 15,671 hr to O/M ~2.395) from fragments that had been oxidized to an O/M ratio near the plateau at 175°C

Figure 2.1.3.2-11 is a plot of the oxidation curves for the as-irradiated and slightly pre-oxidized samples. Unlike the previous data of Einziger and Strain (1986), in which the plateau at 250°C existed for almost 10,000 hr, none of these samples exhibited the typical plateau behavior. The lack of an observable plateau for these samples, which started with an O/M <2.005, is in marked contrast to the behavior of the Turkey Point and ATM-105 samples that had been pre-oxidized to an O/M ratio near the plateau at lower temperatures before being oxidized at 255°C.
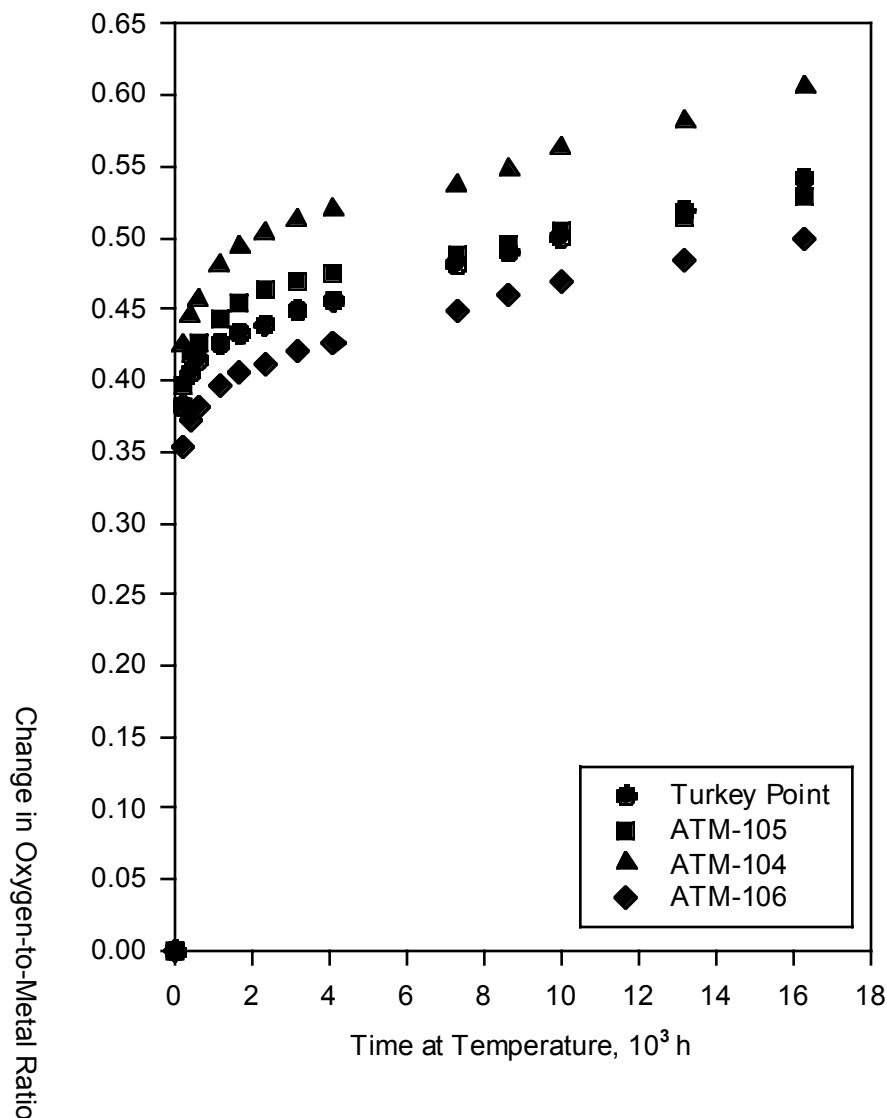
Figure 2.1.3.2-11 Oxidation behavior of as-irradiated LWR spent-fuel fragments in a 255°C dry-bath [LL980608251021.046]

The open symbols in Figure 2.1.3.2-12 represent the samples that had been pre-oxidized. The previously oxidized samples of Turkey Point and ATM-105 fuel clearly exhibited plateau behavior, although the duration was much less than that expected based on the previous Einziger data (Einziger and Strain, 1986).
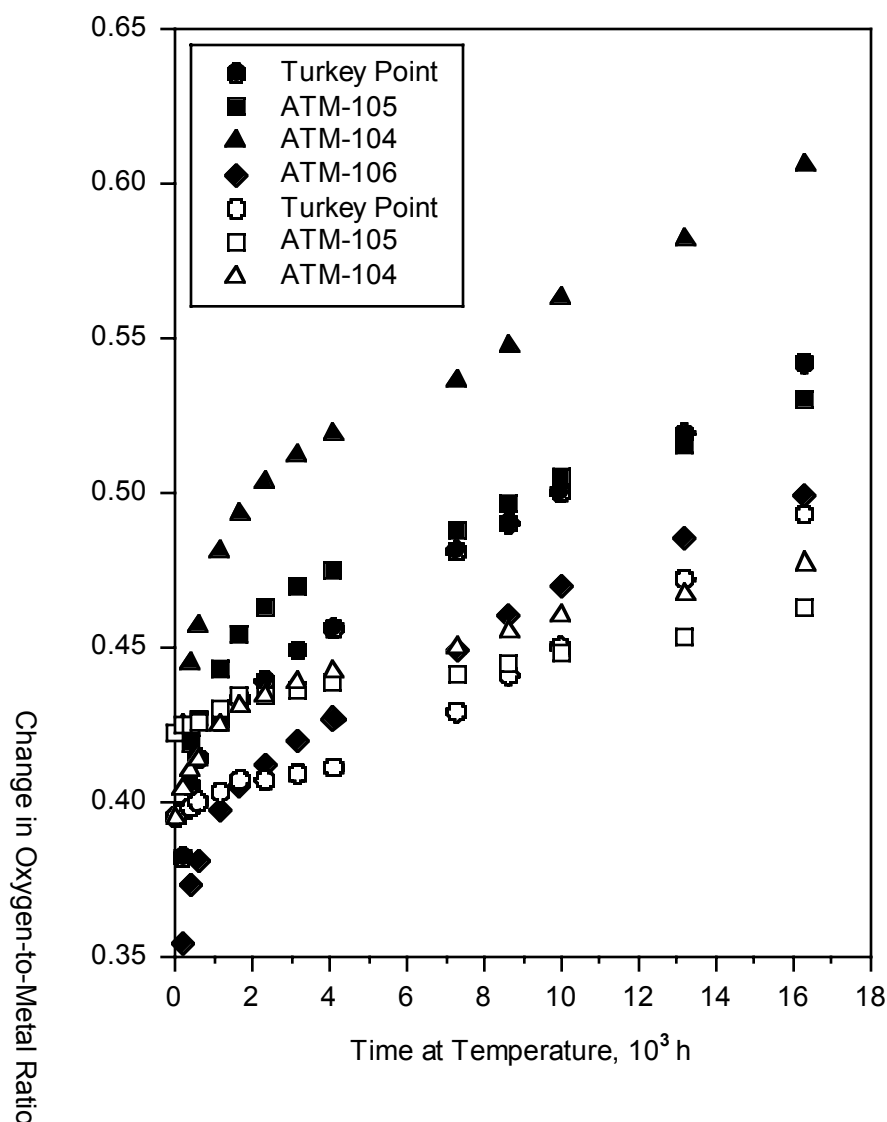
Figure 2.1.3.2-12 Oxidation behavior of as-irradiated and pre-oxidized (open symbols) LWR spent-fuel fragments in a 255°C dry-air bath [LL980608251021.046]

The ATM-104 pre-oxidized sample, on the other hand, had no observable plateau. All samples did, however, begin to oxidize at about the same rate of change in O/M ratio after approximately 4000 hr. (No interim weighings to determine mass increase were performed between 4095 and 7281 hr). Figure 2.1.3.2-13 is a plot of the oxidation curves for the four different Turkey Point fuels oxidized in the 255°C dry-bath test. Again, it is clear that the sample oxidized at a lower temperature to an O/M ratio of about 2.4 prior to oxidation at 255°C exhibited a plateau (open circles), whereas the as-irradiated or only slightly pre-oxidized samples (closed symbols) exhibited no plateau. It is also clear that the crushed fragments increased in mass much more quickly than did the intact fragments because of the much larger surface area exposed.

XRD of the samples oxidized in the 255°C dry-bath with an O/M ratio as high as 2.56 has detected U$_4$O$_9$ with only minor U$_3$O$_8$ formation, even though the two Turkey Point samples and one of the ATM-105 samples had formed significant amounts of powder. A Turkey Point

sample of crushed fragments also oxidized at 255°C had obtained a bulk O/M ratio of 2.62; still the only phase identified by XRD was U$_4$O$_9$. The lack of observable U$_3$O$_8$ at these relatively high O/M ratios is in contrast to the TGA studies in which U$_3$O$_8$ has been identified in samples oxidized at 283°C to an O/M as low as 2.49.
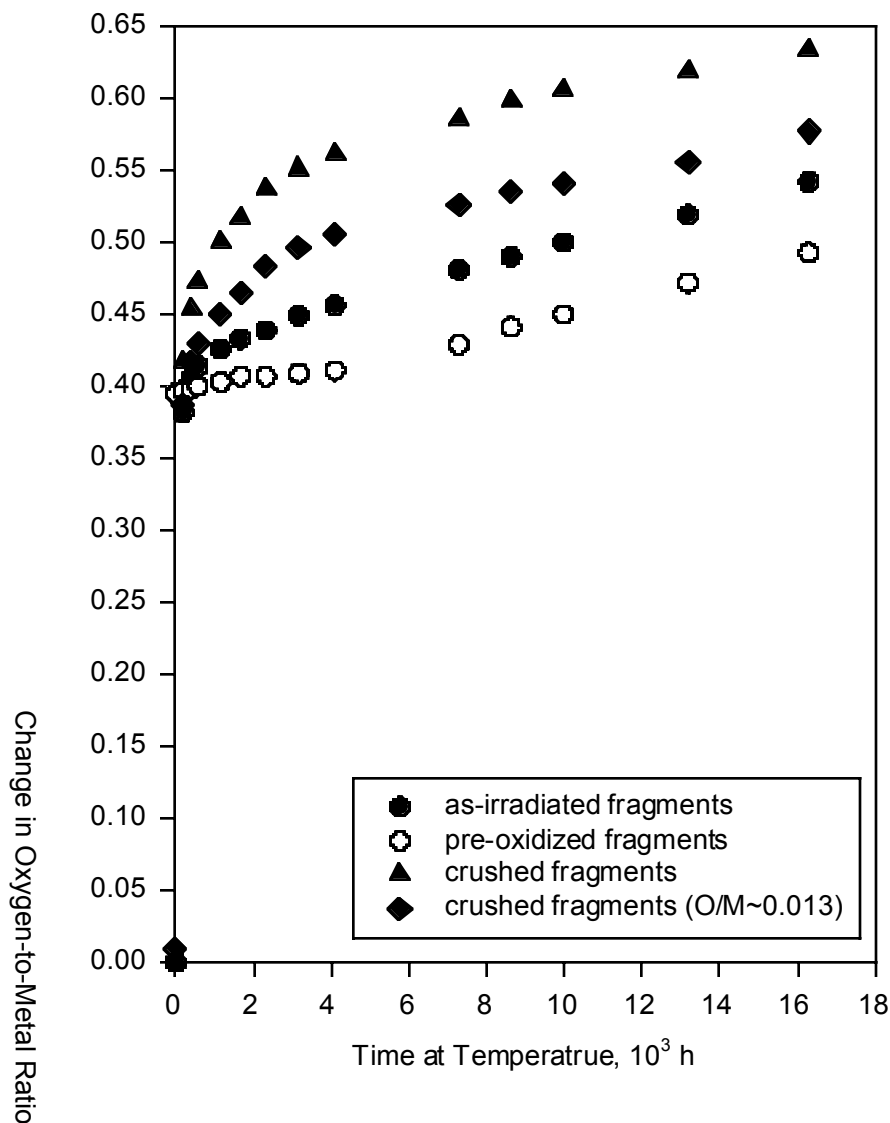
Figure 2.1.3.2-13 Oxidation behavior of Turkey Point fuel in a 255°C dry-bath [LL980608251021.046]

2.1.3.2.4 Quantitative XRD Results

A quantitative XRD analysis of spent-fuel samples oxidized in the dry-baths and having average O/M ratios ranging from 2.40 to 2.61 was conducted by Larry Thomas of Pacific Northwest National Laboratory (PNNL) (Einziger et al., 1995) by combining known quantities of fuel and a reference material (in this case, Al$_2$O$_3$). Using the integrated peak intensities, with the knowledge of the amount of material present, it was possible to determine the weight fractions of each phase present.

Figure 2.1.3.2-14 is a plot of the peak intensity of the U$_4$O$_9$ (UO$_{2.4}$) peak when normalized to the Al$_2$O$_3$ standard and corrected for the fuel to Al$_2$O$_3$ weight ratio of each sample. It is clear that, as the O/M ratio increases, the amount of UO$_{2.4}$ present decreases. There is also a corresponding broadening of the X-ray peak. Because no other phases are present, it is clear that the UO$_{2.4}$ is being transformed into a phase that is amorphous to XRD, meaning it is either a nanocrystalline phase or is truly amorphous. Analysis of 10 oxidized samples resulted in an average O/M of 2.70±0.08 for this "amorphous" phase. A truly amorphous phase would not be expected to have such a constant O/M. Because the calculated O/M ratio is very similar to that of U$_3$O$_8$, it is believed that oxidation of spent fuel beyond UO$_{2.4}$ at temperatures ≤255°C results in U$_3$O$_8$ formation, but in a nanocrystalline state that is not readily detected by XRD. This is in agreement with the findings of Hoekstra et al. (1961), who have shown that U$_3$O$_8$ formed below about 250°C may be poorly crystalline.
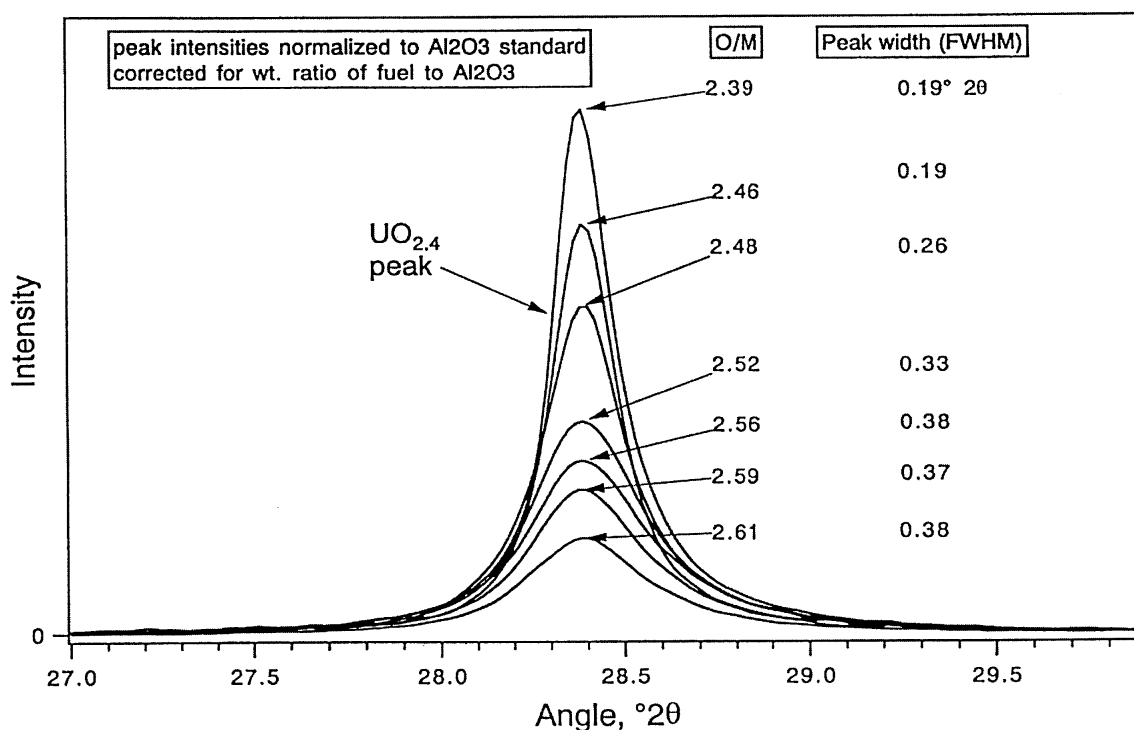
Figure 2.1.3.2-14 Quantitative XRD analysis of oxidized LWR spent fuel

2.1.3.2.5 References

ASTM (1990). "Standard Test Method for Atom Percent Fission in Uranium and Plutonium Fuel (Neodymium-148 Method)" (Standard E 321) *Annual Book of ASTM Standards, Vol. 12.02*. Philadelphia, PA: American Society for Testing and Materials.

Einziger , R.E., and R.V. Strain (1986). "Behavior of Breached Pressurized Water-Reactor Spent-Fuel Rods in an Air Atmosphere Between 250°C and 360°C." *Nucl. Technol.* **75**(1):82–95. [238325]

Einziger, R.E., L.E. Thomas, and B.D. Hanson (1995). *Oxidation of Spent LWR Fuel, FY 95 Year end Report.* (MOL212 and MOL213 combined interim report). Richland, WA: Pacific Northwest National Laboratory. [MOL.19960611.0215]

Einziger, R.E., L.E. Thomas, H.C. Buchanan, and R. B. Stout (1992). "Oxidation of Spent Fuel in Air at 175 to 195°C," *J. Nucl. Mat.* **190**:53–60. [MOL.19980213.0585]

Guenther, R.J., D.E. Blahnik, T.K. Campbell, U.P. Jenquin, J.E. Mendel, L.E. Thomas, and C.K. Thornhill (1991a). *Characterization of Spent Fuel Approved Testing Material-ATM-105.* (PNNL-5109-105) Richland, WA: Pacific Northwest National Laboratory. [NNA.19911217.0014]

Guenther, R.J., D.E. Blahnik, U.P. Jenquin, J.E. Mendel, L.E. Thomas, and C.K. Thornhill (1991b). *Characterization of Spent Fuel Approved Testing Material- ATM-104.* (PNNL-5109-104) Richland, WA: Pacific Northwest National Laboratory. [NNA.19911218.0073]

Guenther, R.J., D.E. Blahnik, and N.J. Wildung (1994). *Radiochemical Analyses of Several Spent Fuel Approved Testing Materials.* (PNL-10113) Richland, WA: Pacific Northwest Laboratory.

Hanson, B.D. (1998). *The Burnup Dependence of Light Water Reactor Spent Fuel Oxidation.* (PNNL-11929) Richland, WA: Pacific Northwest National Laboratory. [238459]

Hoekstra, H.R., A. Santoro, and S. Siegel (1961). "The Low Temperature Oxidation of UO$_2$ and U$_4$O$_9$." *J. Inorg. Nucl. Chem.* **18**:166–178.

Section 2.1.3.2 Appendix
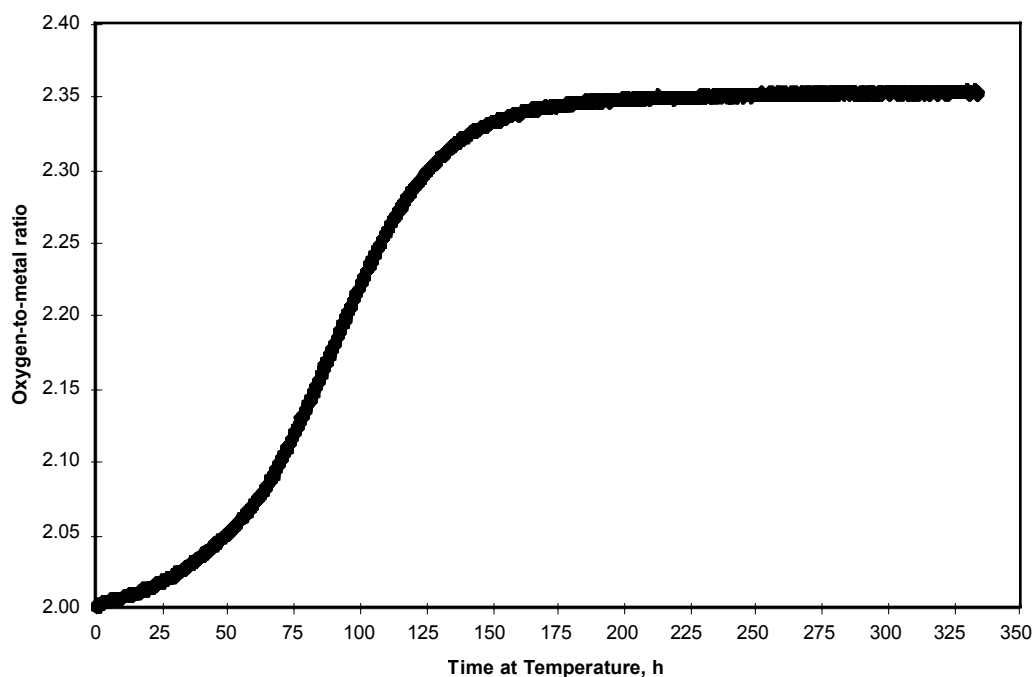
Figure 2.1.3.2-A-1   **Sample of unirradiated UO$_2$ with 8 wt% Gd^{203} oxidized at 283°C [LL980601851021.044]**
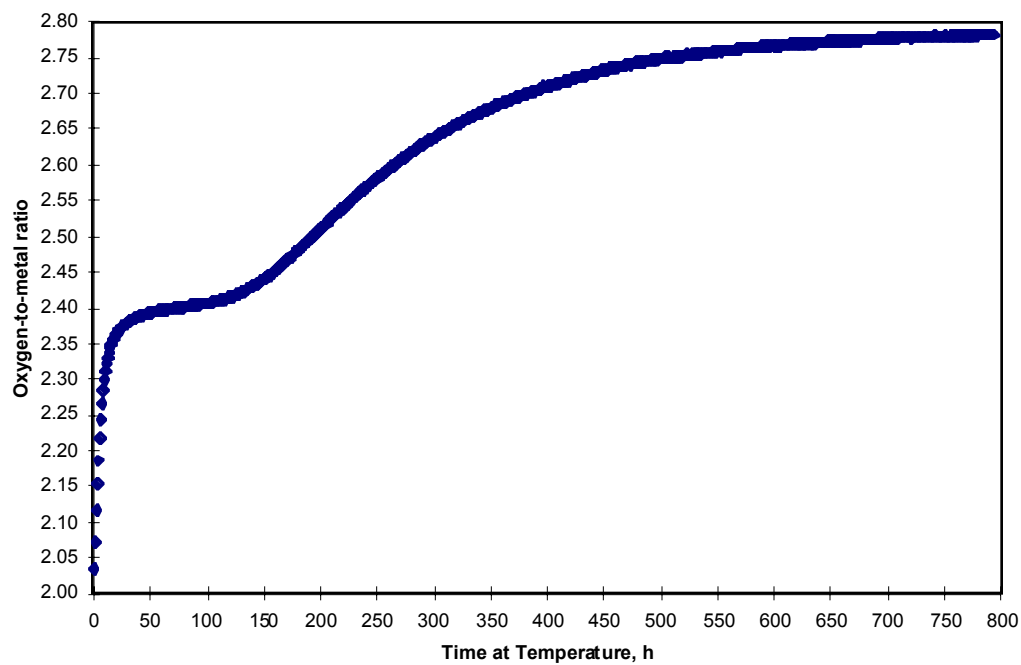
Figure 2.1.3.2-A-2   **Sample of 105-01 oxidized at 283°C [LL980601851021.044]**
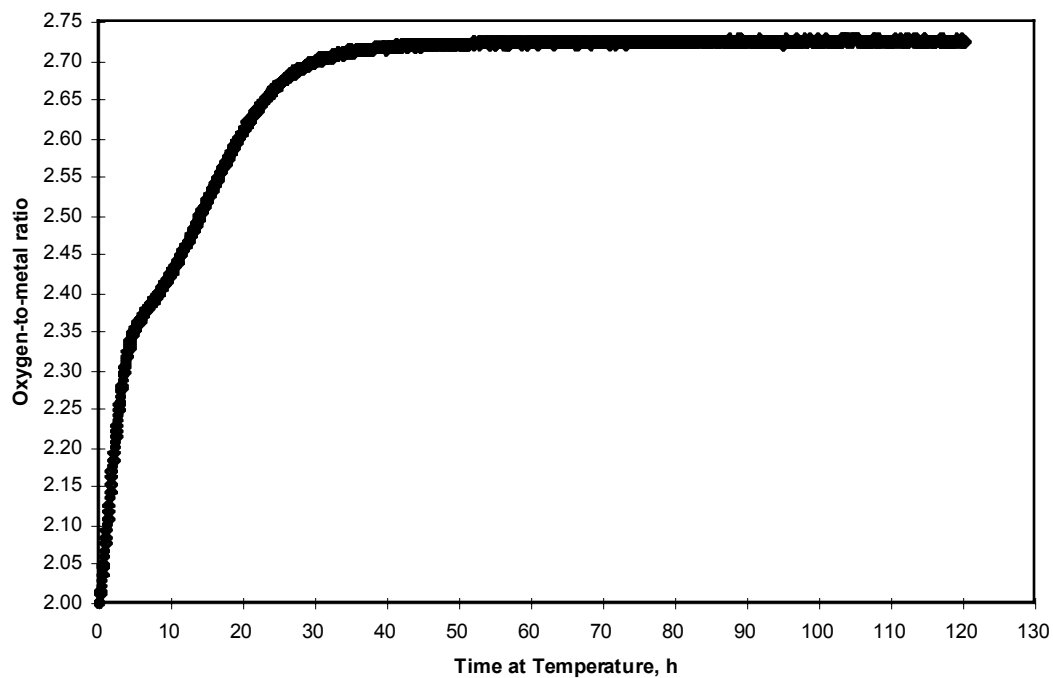
Figure 2.1.3.2-A-3   Sample 105-02 oxidized at 325°C [LL980601851021.044]
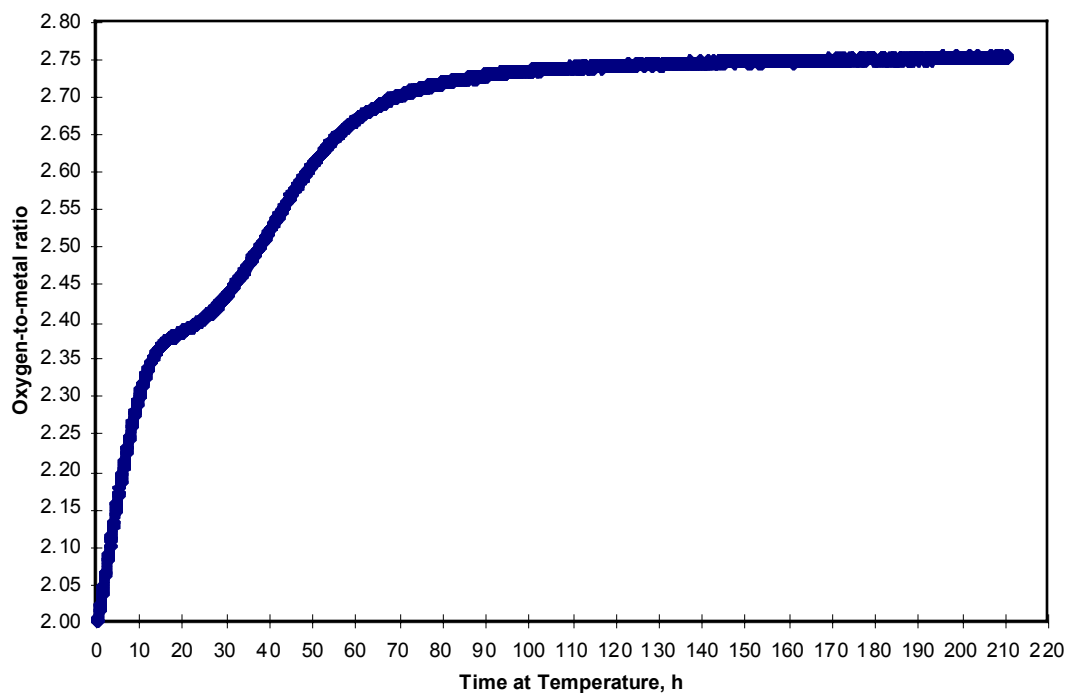
Figure 2.1.3.2-A-4   Sample 105-03 oxidized at 305°C [LL980601851021.044]
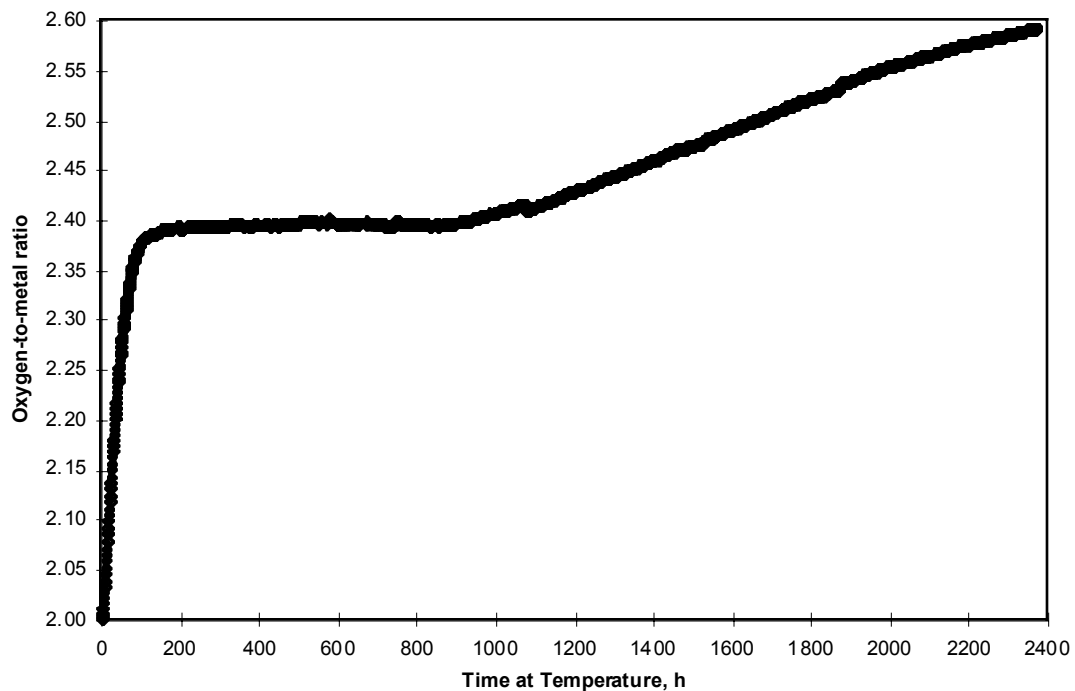
Figure 2.1.3.2-A-5 Sample 105-04 oxidized at 270°C [LL980601851021.044]
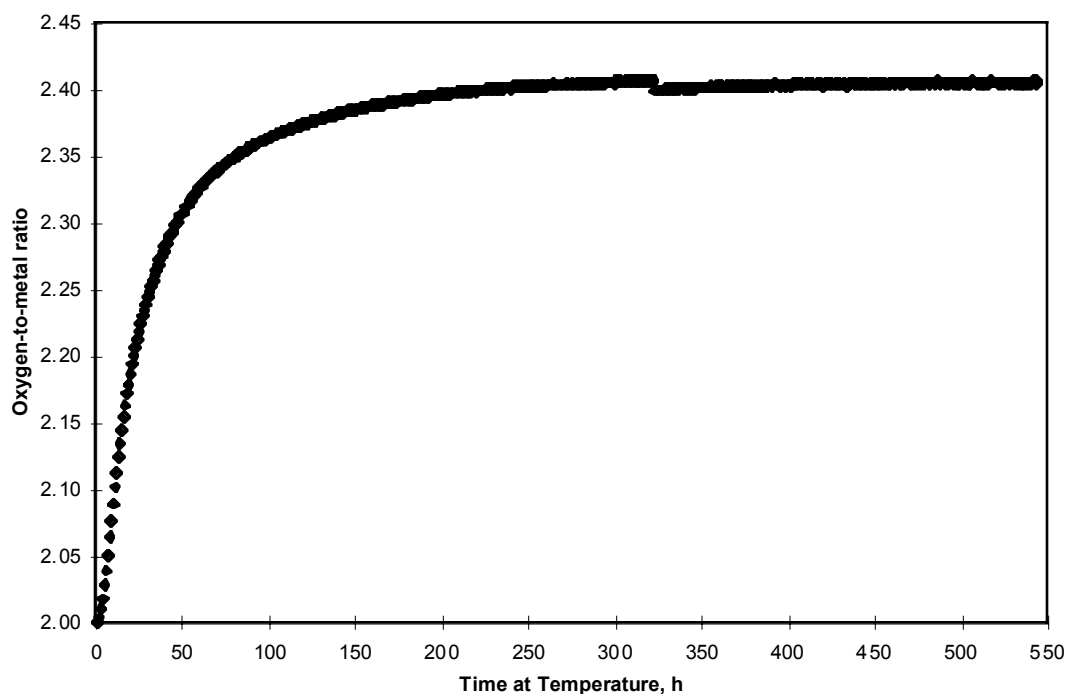
Figure 2.1.3.2-A-6 Sample 105-05 oxidized at 255°C [LL980601851021.044]
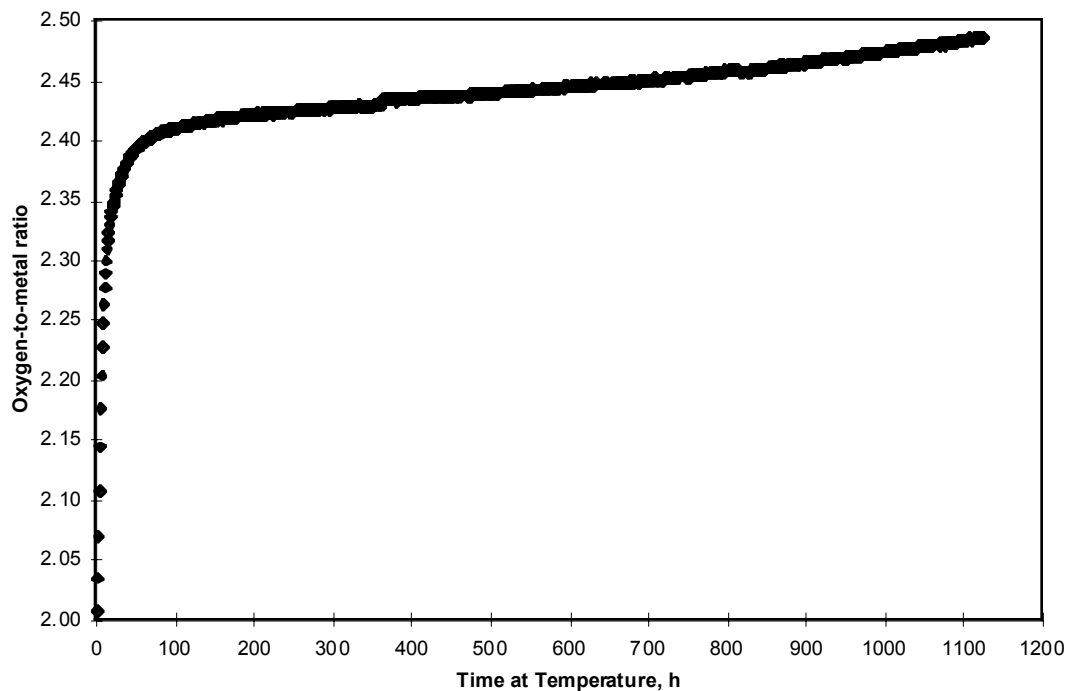
Figure 2.1.3.2-A-7   Sample 105-06 oxidized at 283°C [LL980601851021.044]
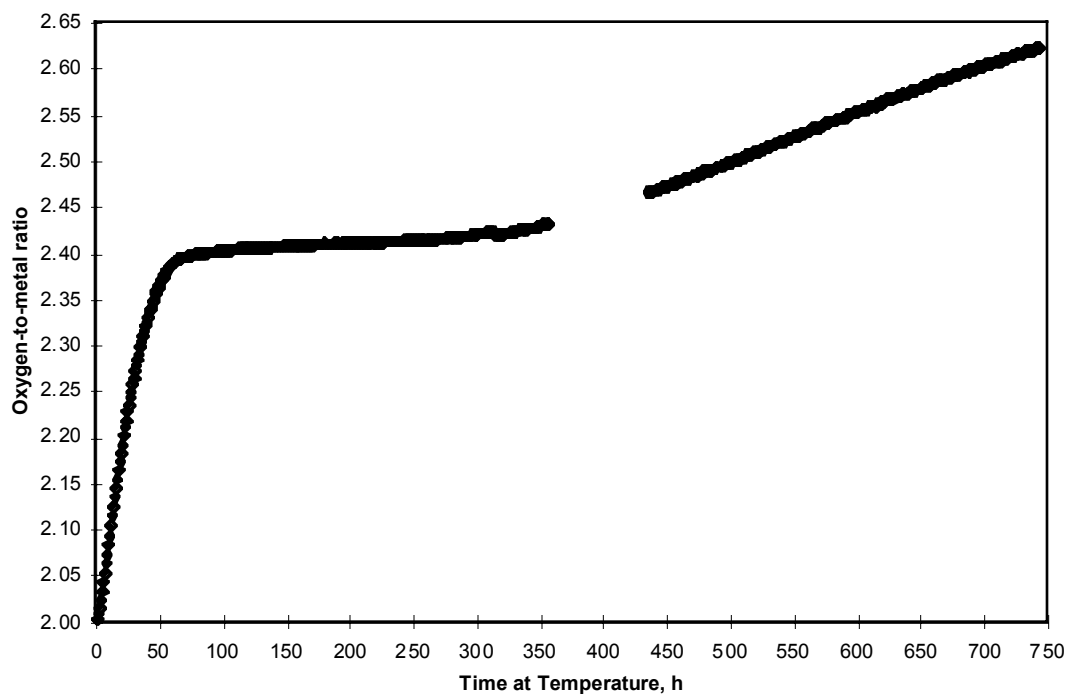
Figure 2.1.3.2-A-8   Sample 105-07 oxidized at 283°C [LL980601851021.044]
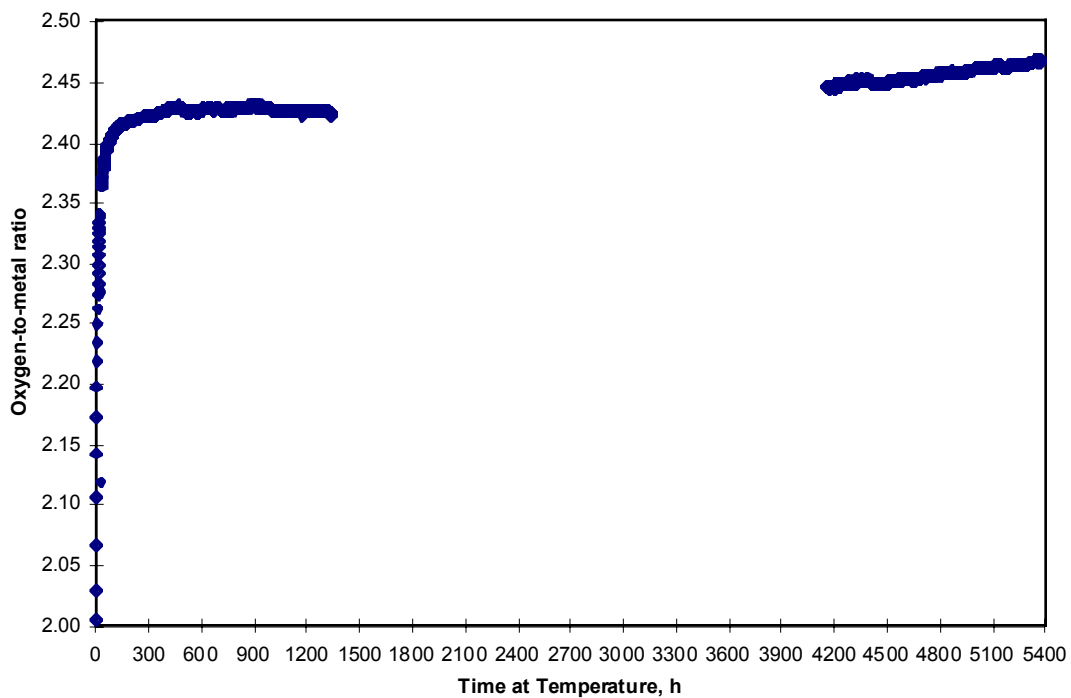
Figure 2.1.3.2-A-9   **Sample 105-08 oxidized at 283°C [LL980601851021.044]**
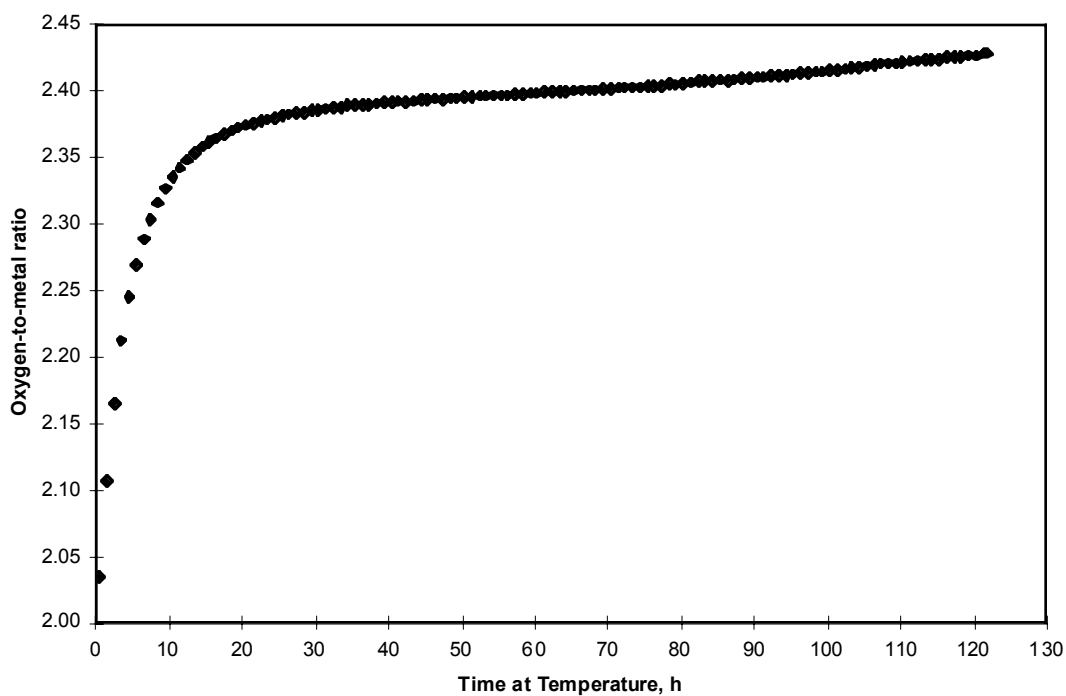
Figure 2.1.3.2-A-10   **Sample 105-09 oxidized at 305°C [LL980601851021.044]**
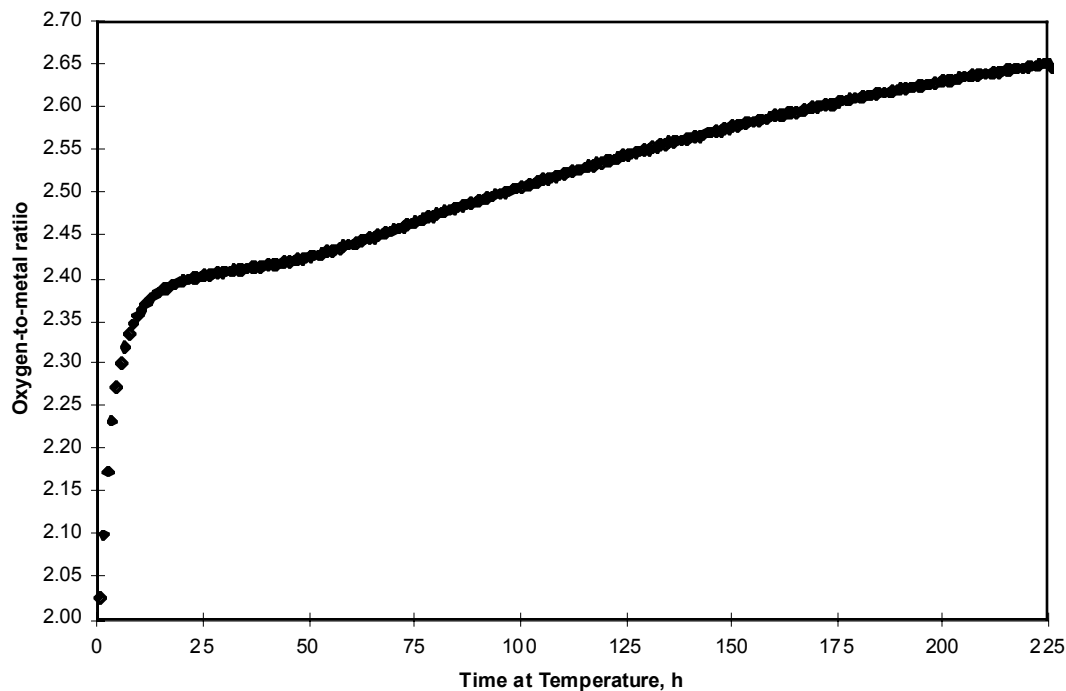
Figure 2.1.3.2-A-11   Sample 105-10 oxidized at 305°C [LL980601851021.044]
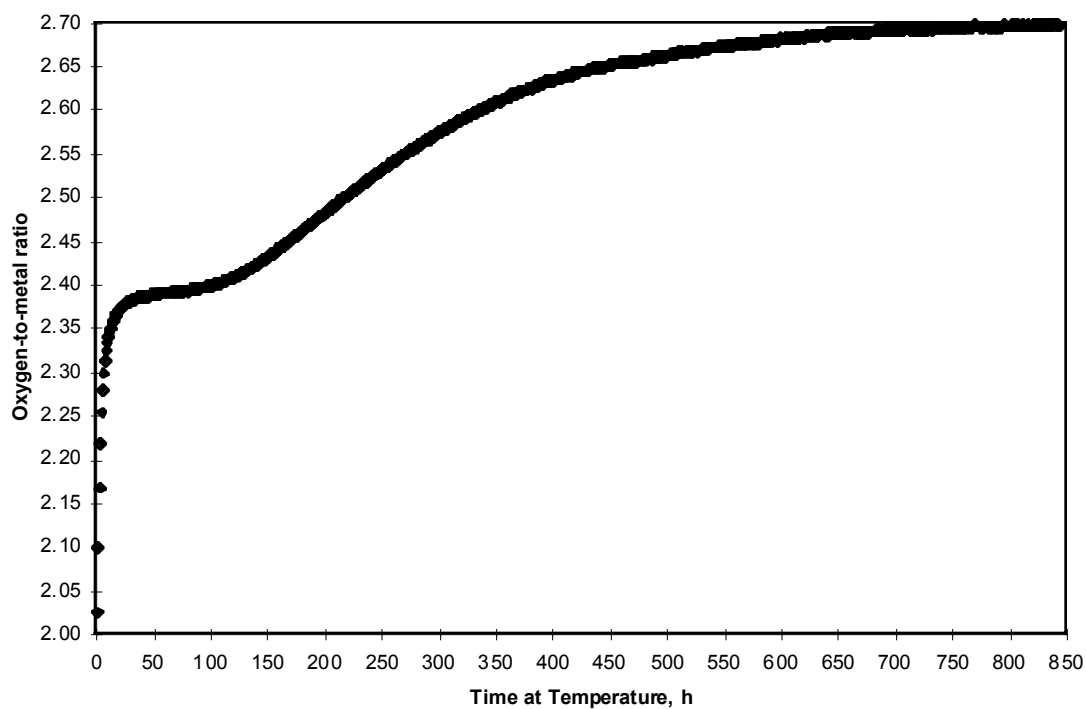
Figure 2.1.3.2-A-12   Sample 105-11 oxidized at 305°C [LL980601851021.044]
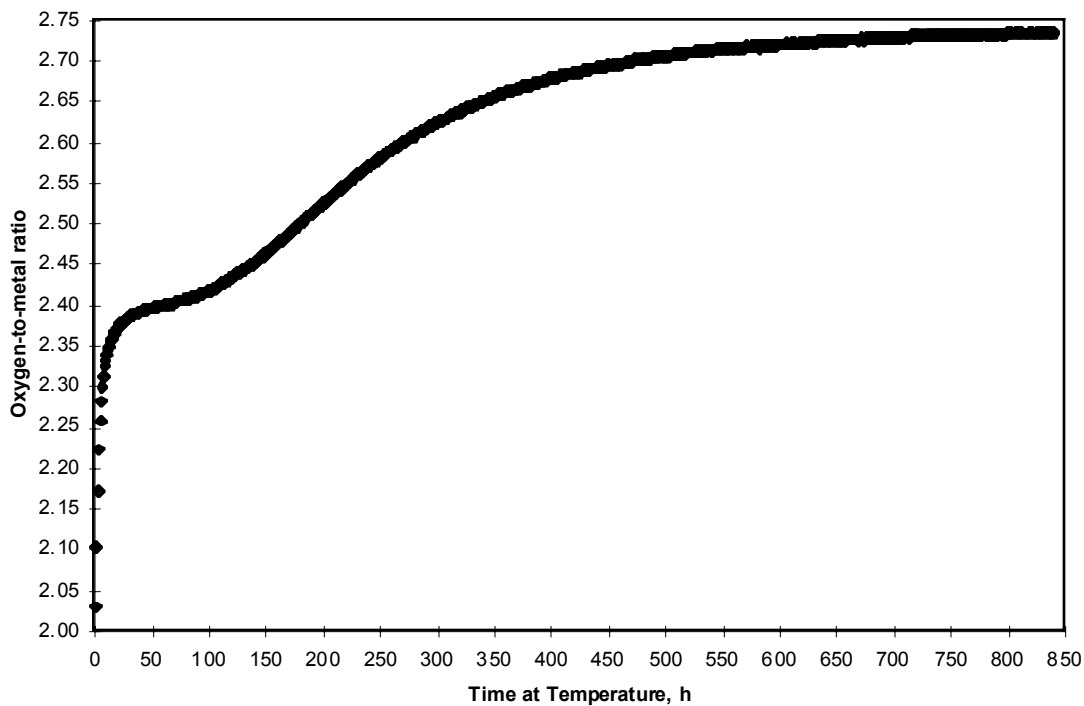
Figure 2.1.3.2-A-13   Sample 105-12 oxidized at 305°C [LL980601851021.044]
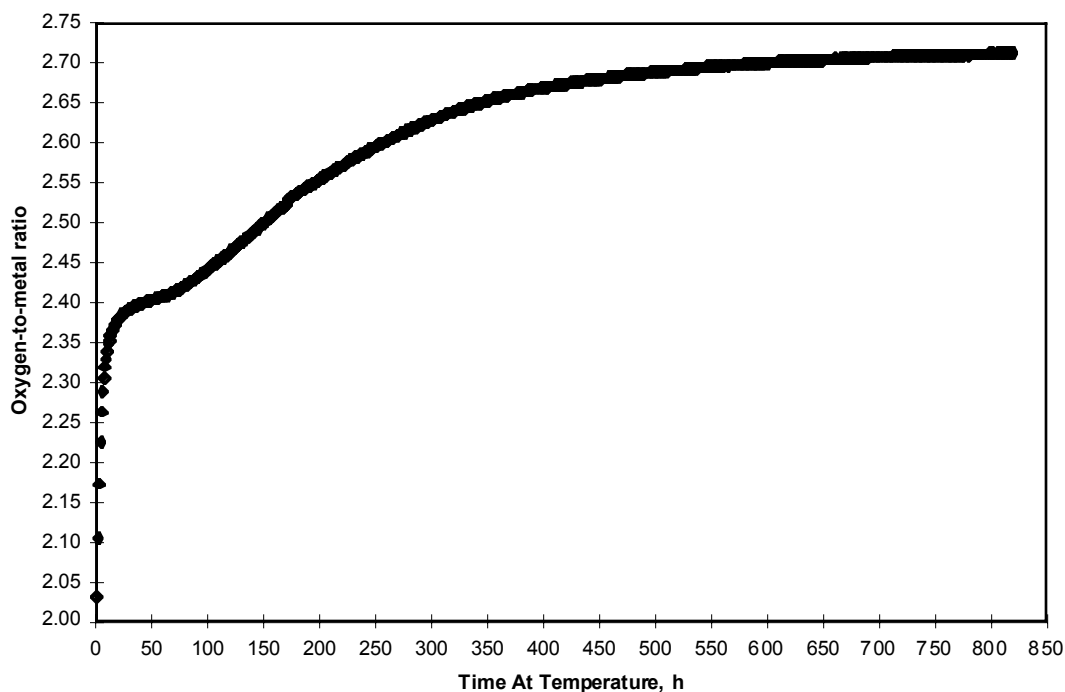
Figure 2.1.3.2-A-14   Sample 105-13 oxidized at 305°C [LL980601851021.044]
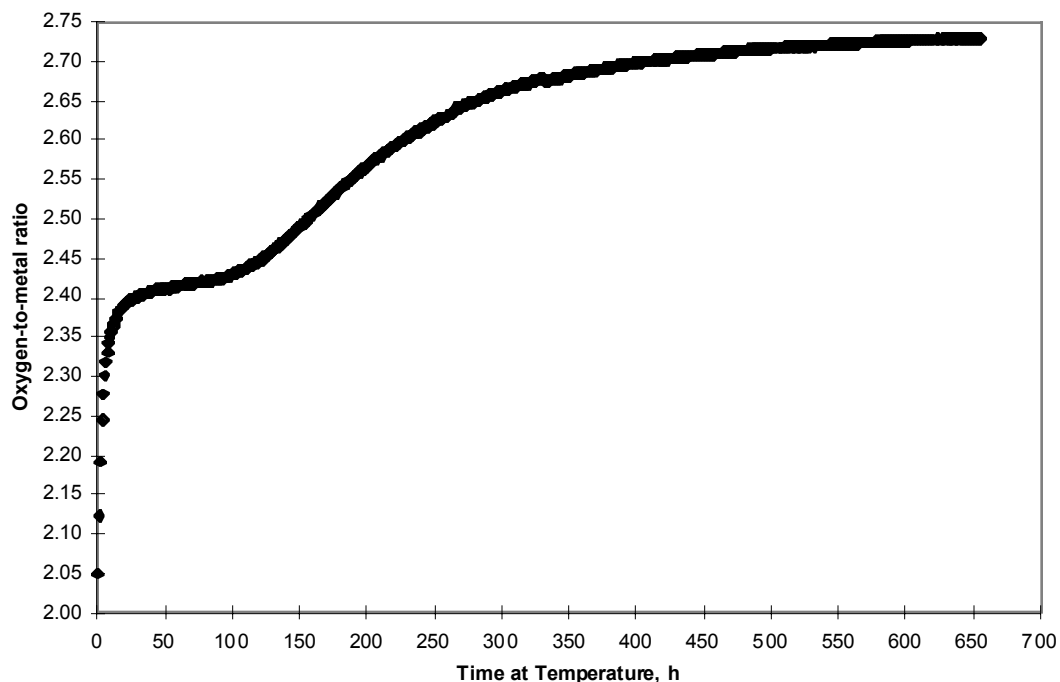
Figure 2.1.3.2-A-15   Sample 105-14 oxidized at 305°C [LL980601851021.044]
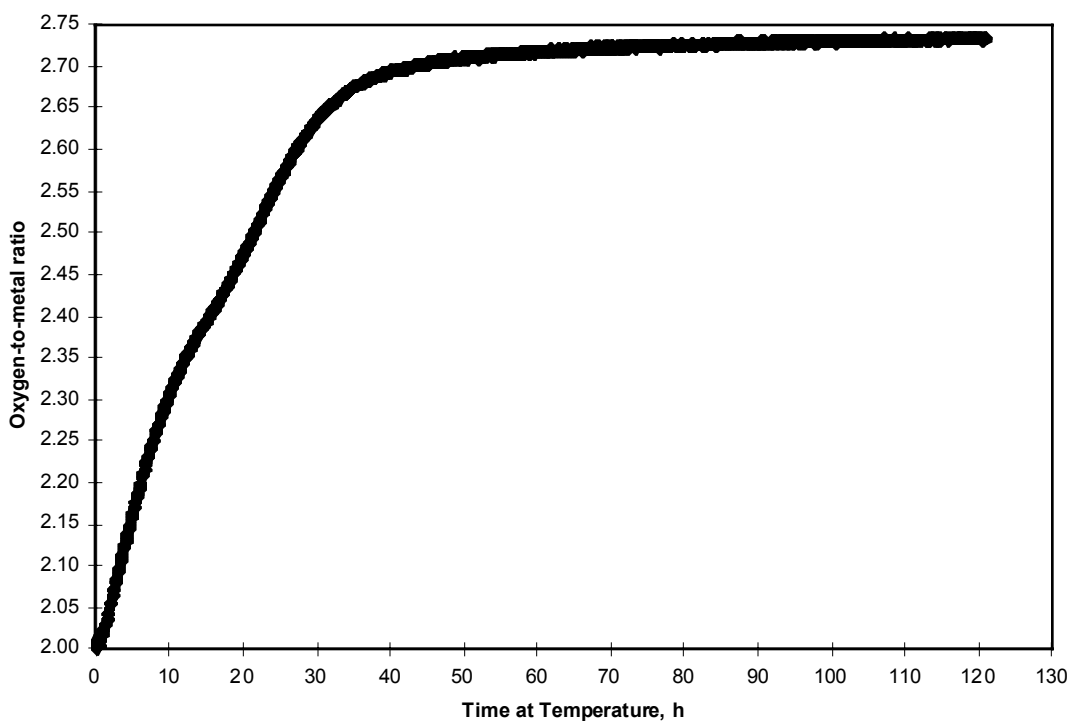
Figure 2.1.3.2-A-16   Sample 105-15 oxidized at 305°C [LL980601851021.044]
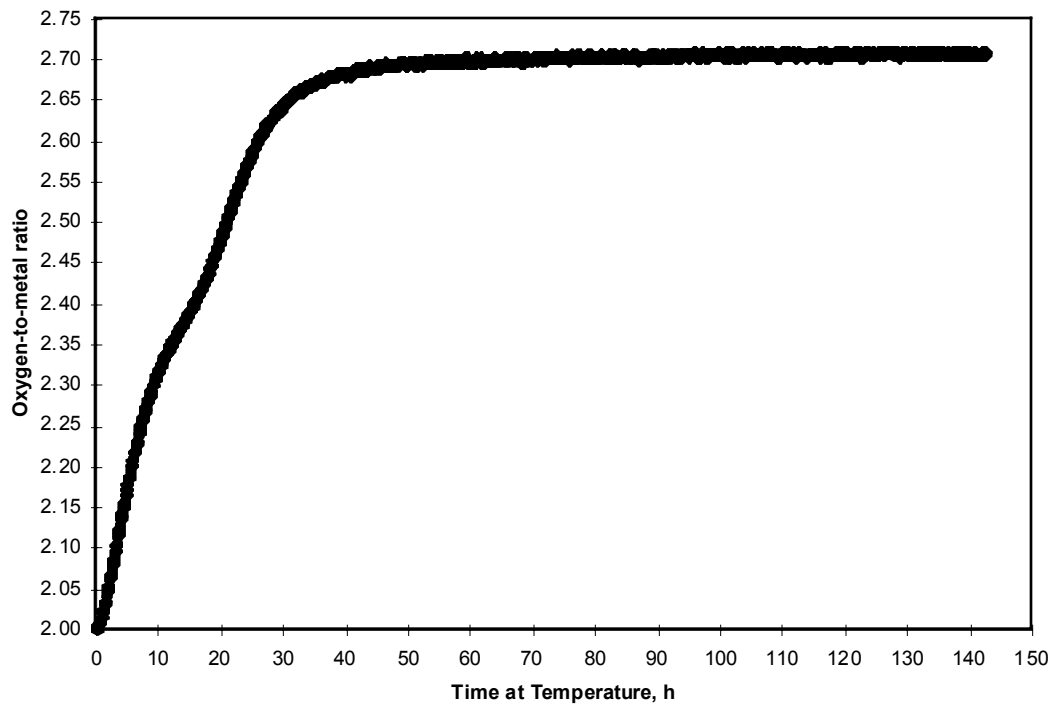
Figure 2.1.3.2-A-17   Sample 105-16 oxidized at 305°C [LL980601851021.044]
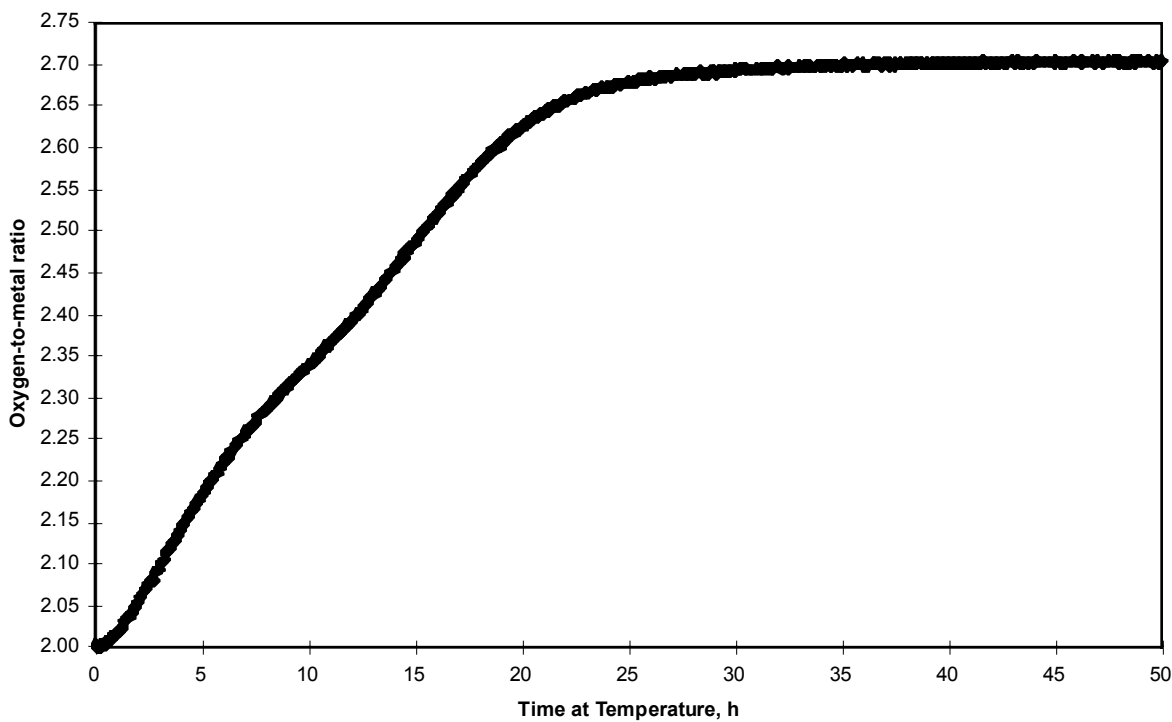
Figure 2.1.3.2-A-18   Sample 105-17 oxidized at 305°C [LL980601851021.044]
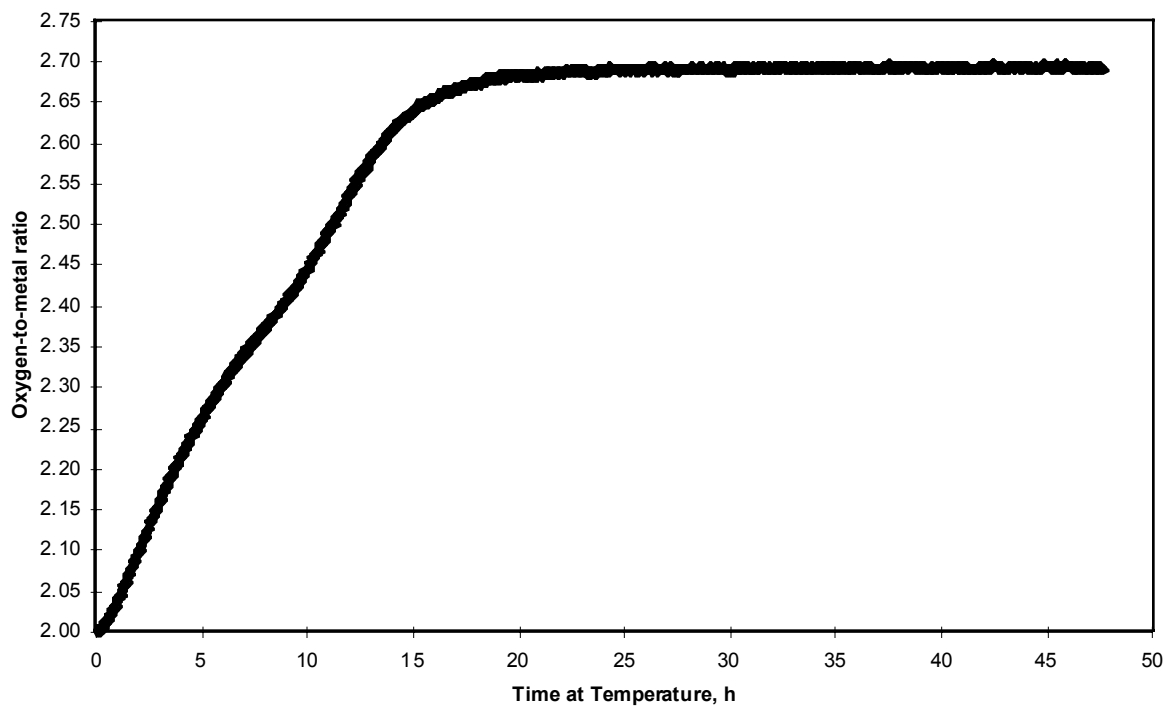
Figure 2.1.3.2-A-19   Sample 105-18 oxidized at 305°C [LL980601851021.044]
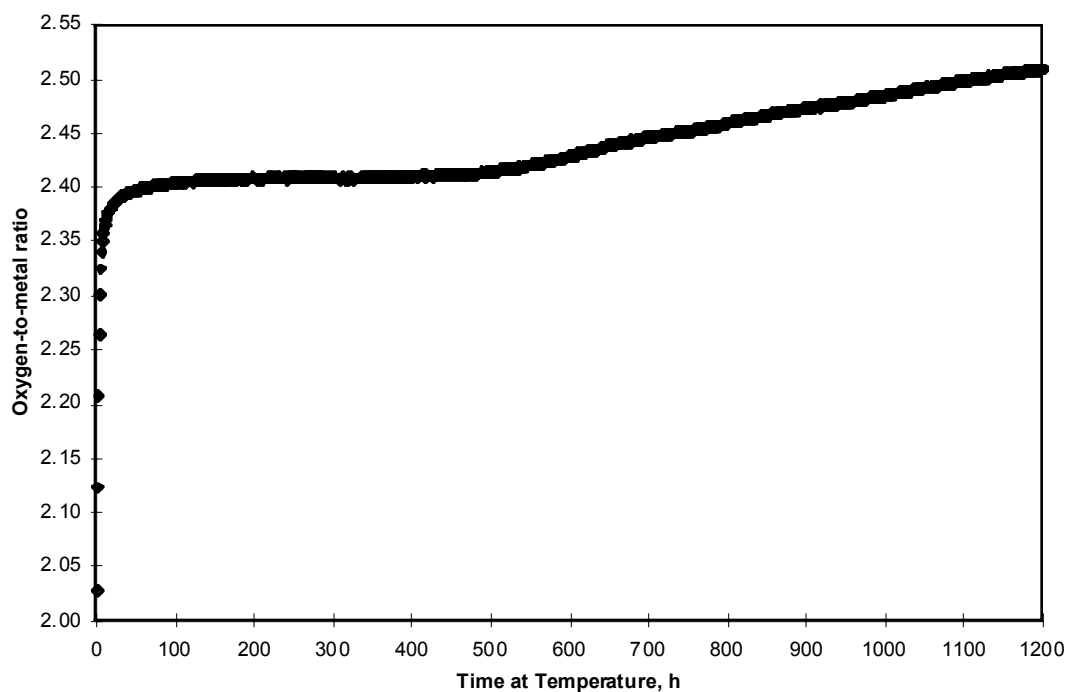
Figure 2.1.3.2-A-20   Sample 104-01 oxidized at 305°C [LL980601851021.044]
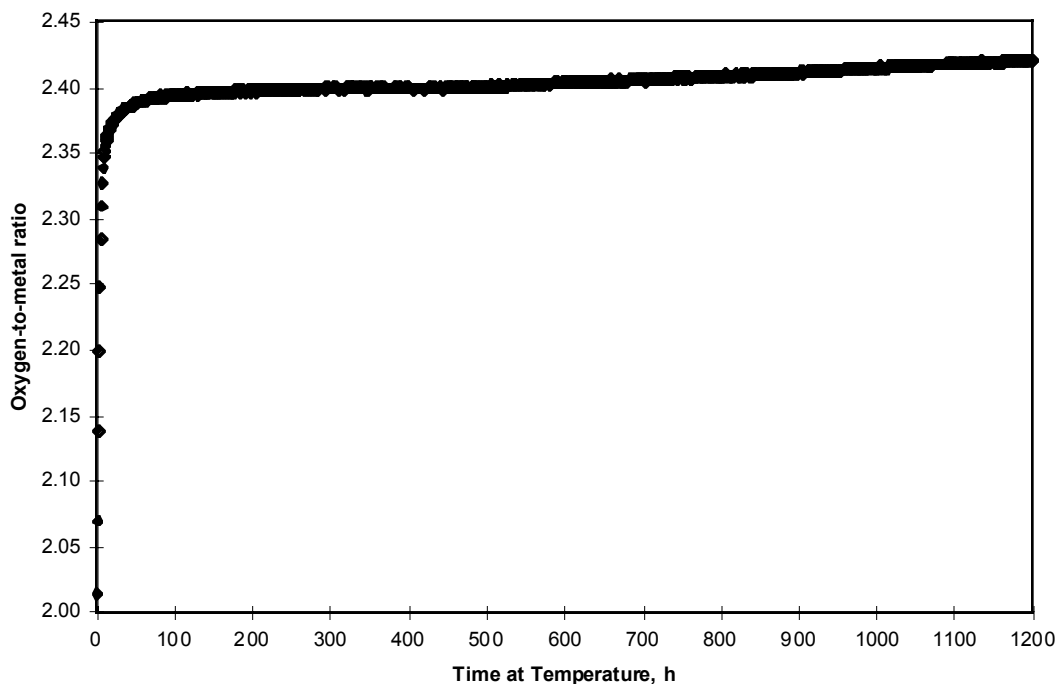
Figure 2.1.3.2-A-21   Sample 104-02 oxidized at 305°C [LL980601851021.044]
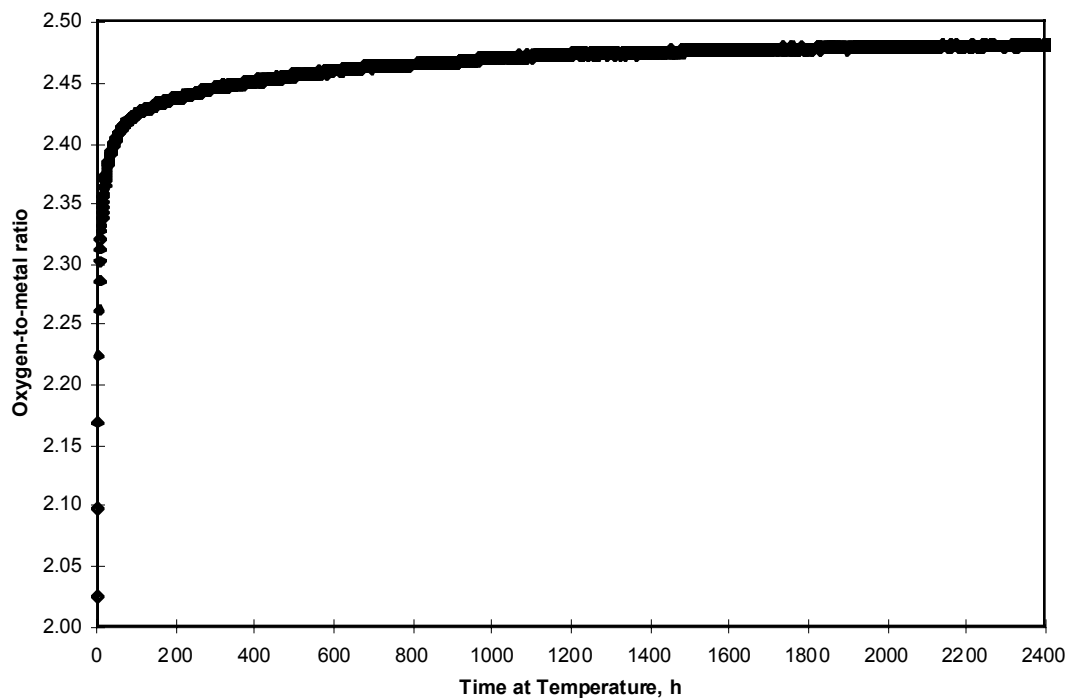
Figure 2.1.3.2-A-22   Sample 108-01 oxidized at 3-5°C [LL980601851021.044]
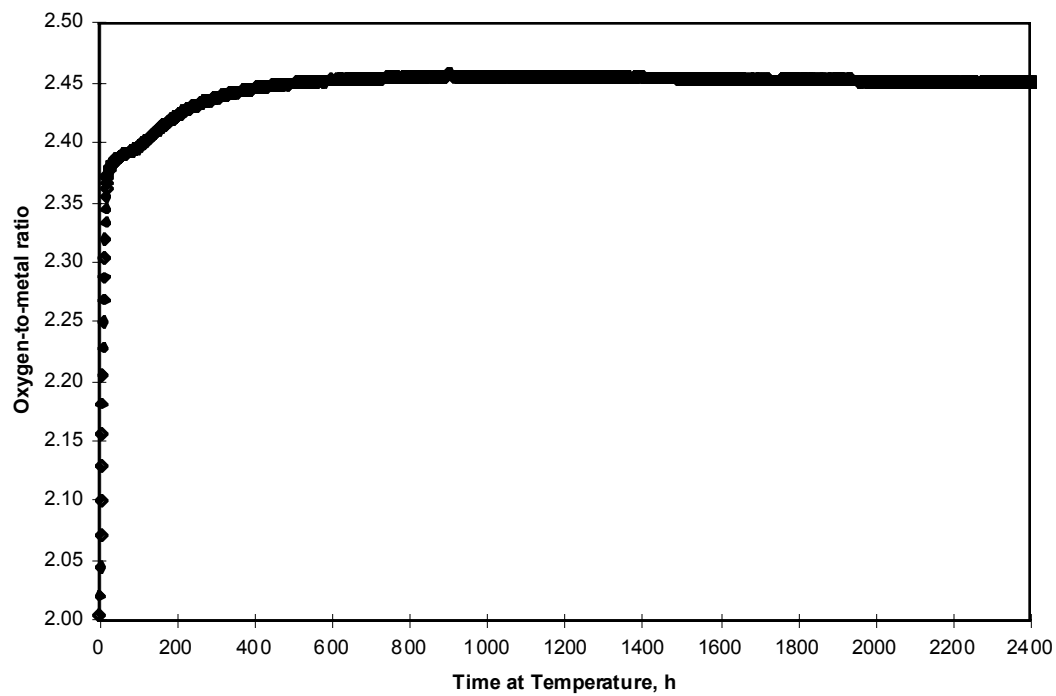
Figure 2.1.3.2-A-23   Sample 108-02 oxidized at 305*C [LL980601851021.044]

2.1.3.3 Gaseous Radionuclide Release from Cladding
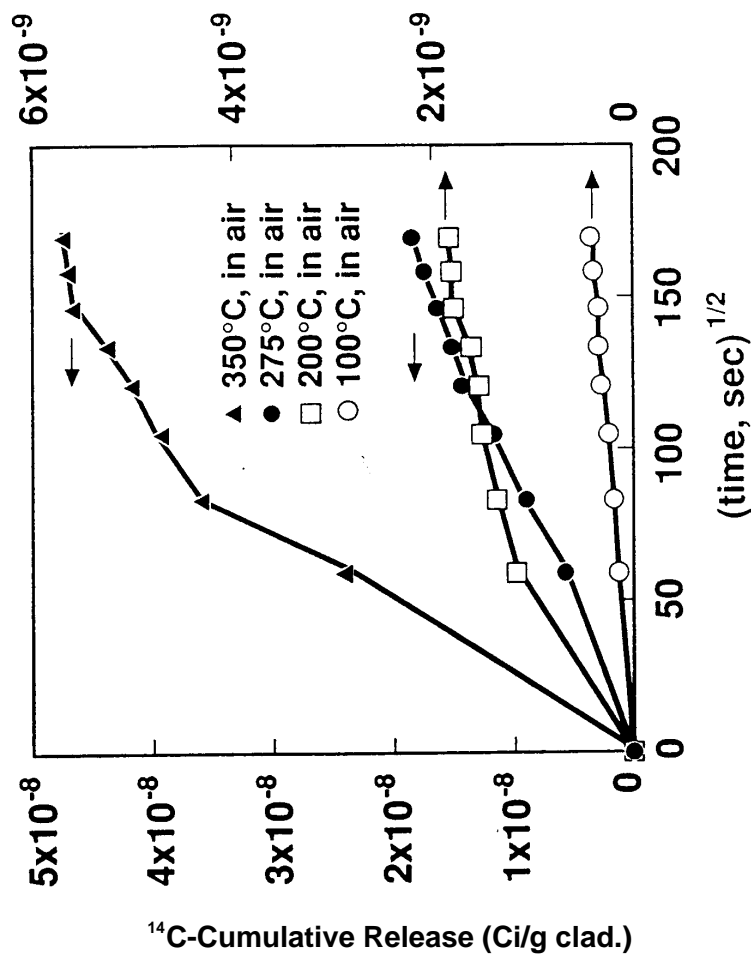
PWR fuel with oxide thickness ~12 to 20 μm and burnup ~27 to 30 MWd/kg HM.

Figure 2.1.3.3-1   Constant temperature tests, thick oxide (Figure ? from H. D. Smith, *Spent Fuel Cladding Degradation,* presented to the Nuclear Waste Technical Review Board, August, 1990.)

¹⁴C-Cumulative Release (Ci/g clad.)

PWR fuel with oxide thickness ~12 to 20 μm and burnup ~27 to 30 MWd/kg HM.
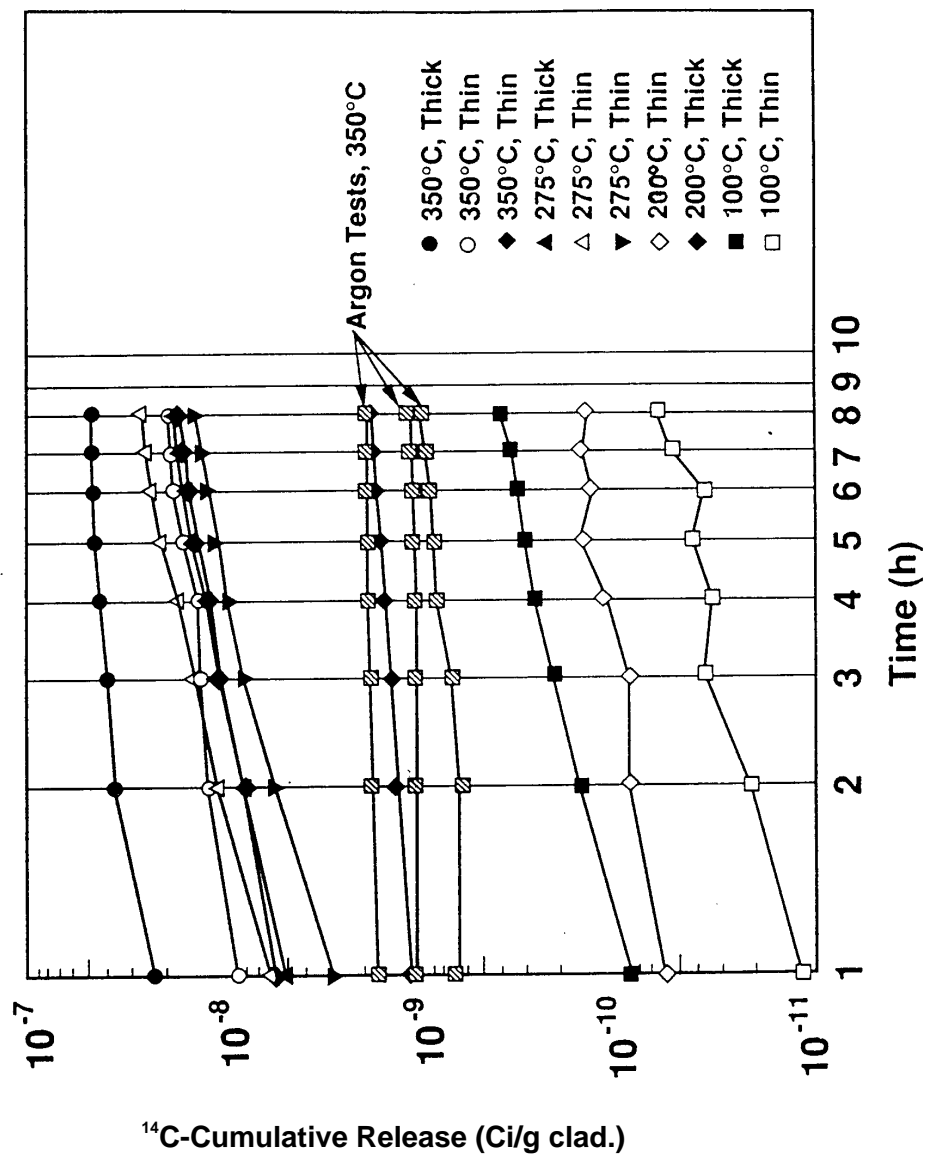
Figure 2.1.3.3-2 Observed ¹⁴C release from Zircaloy-4 spent fuel cladding (Figure ? from H. D. Smith, *Spent Fuel Cladding Degradation,* presented to the Nuclear Waste Technical Review Board, August, 1990.)
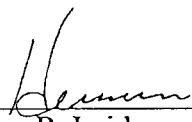
2.1.3.4 Gaseous Radionuclide Release from UO₂ Fuel

We have an equation that describes the fission gas release curves presented at the "Status and Future Directions of Spent Fuel ATM Acquisition and Characterization" by **(?)** C. E. Beyer of the MCC at PNL in March 28-29, 1989. The equation is good for burn-up $\geq$ 20 MWd/kgM and for fission gas releases $\leq$ 60%.

This plot is shown in one of the attached figures. The added curves in the second figure are those calculated for burn-ups of 30, 50 and 60 MWd/kgM, using the equation

$$\log_{10} [\text{fractional release}] = \frac{13}{8} \log_{1 \cup} - \quad -\text{up (MWd/kgM)}] - \frac{4420}{T(K)}$$

This expression overestimates the release above 60% according to the MCC curves. The points superimposed on the 20 and 40 MWd/kgM curves are calculated according to the equation and show that the fit to the MCC curves is quite good.

Herman R. Leider
Physical Chemistry Section
Chemistry & Materials Science Dept.

Attachments

Percent of Fission Gas Release
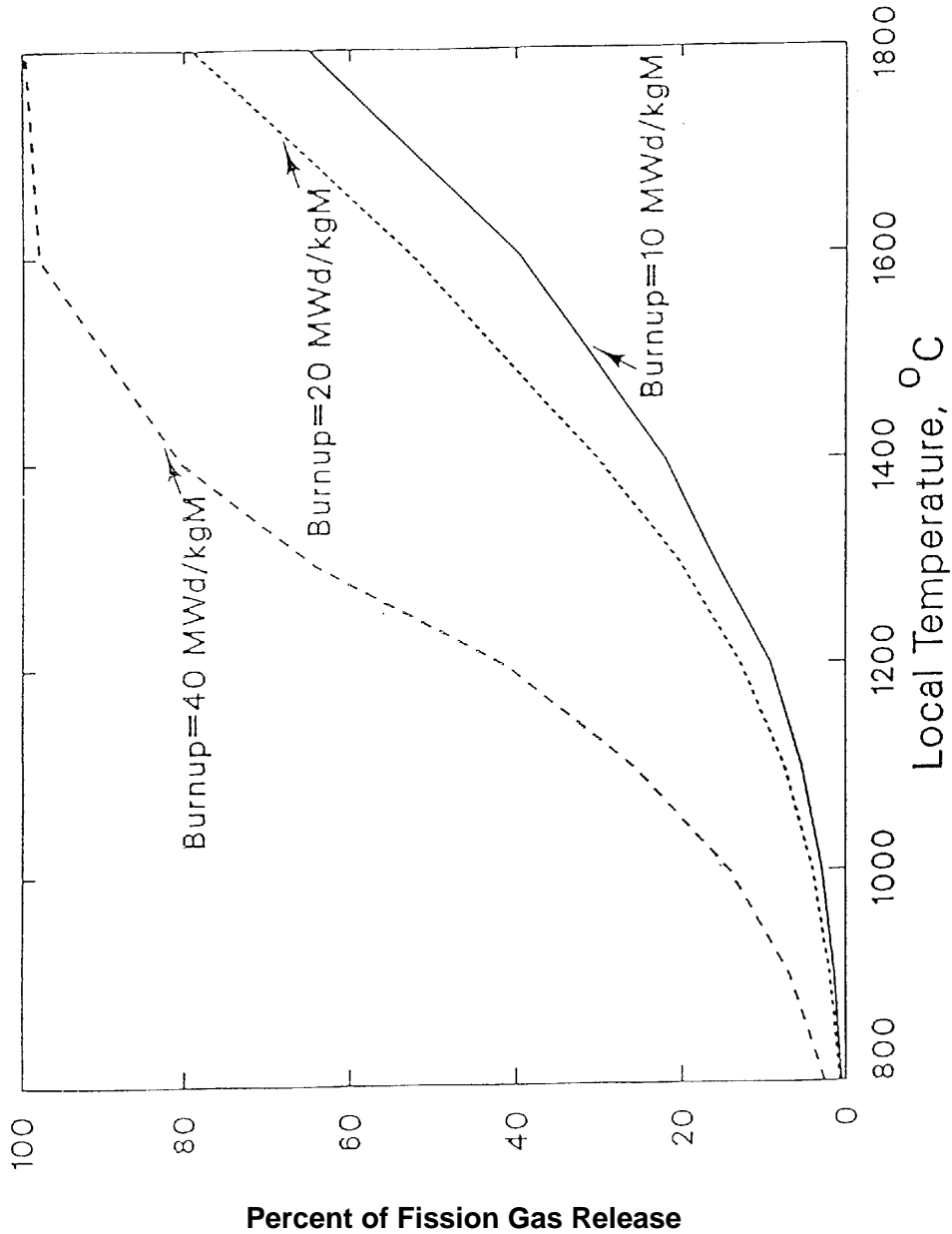
Figure 2.1.3.4-1   **Percent of fission gas release versus local temperature (Figure ?
from C.E. Beyer, in *Status and Future Direction of Spent Fuel
ATM Acquisition and Characterization,* meeting in Richland,
Washington, March, 1989.)**

Percent of Fission Gas Release
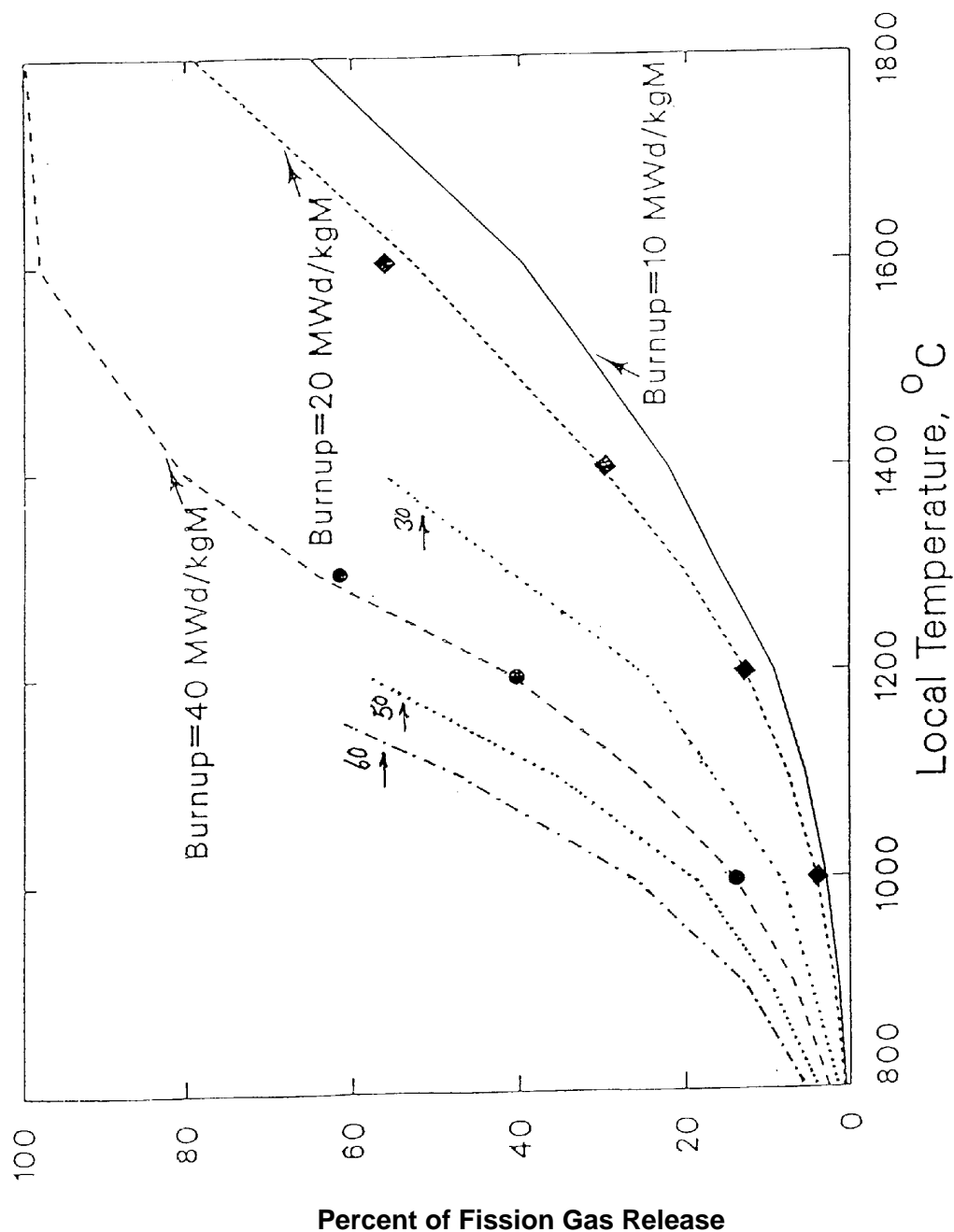
Figure 2.1.3.4-2   Percent of fission gas release versus local temperature (Figure ? C.E. Beyer, in *Status and Future Direction of Spent Fuel ATM Acquisition and Characterization,* meeting in Richland, Washington, March, 1989)
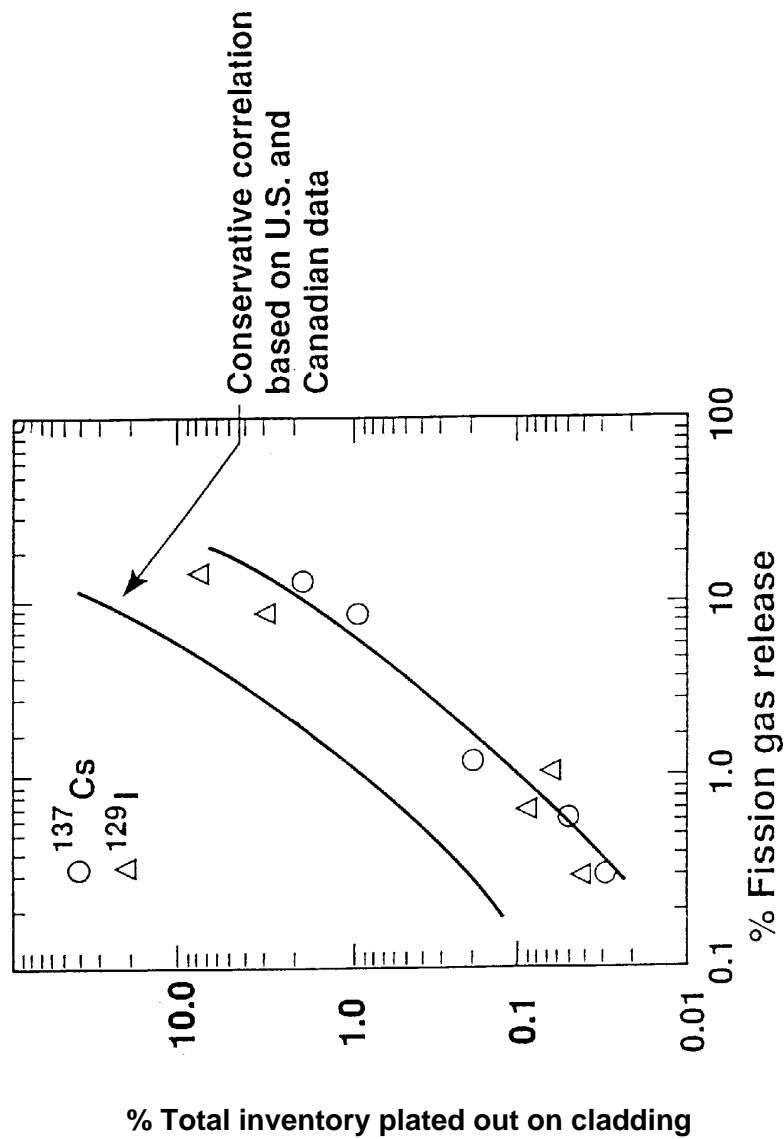
Figure 2.1.3.4-3 Method of correlating gap and grain boundary
inventory with rod-average fission gas release
(from R.B. Stout, *Spent Fuel Characteristics
Overview,* presented to the Nuclear Waste Technical
Review Board, August, 1990)
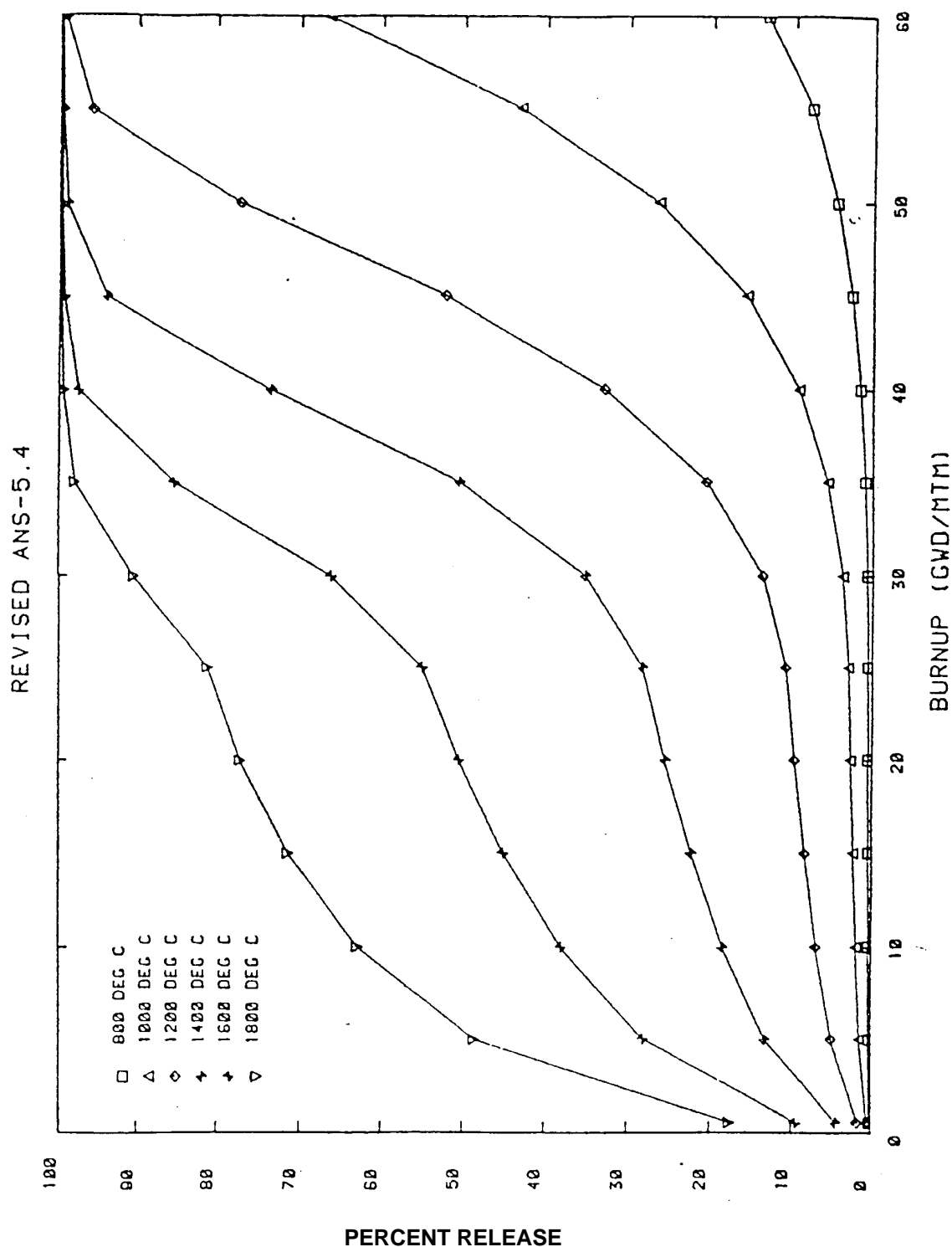
Figure 2.1.3.4-4 Revised ANS 5.4 model predictions at isothermal temperatures as a function of burnup. (Figure 1 from C.E. Beyer, in *Status and Future Direction of Spent Fuel ATM Acquisition and Characterization,* meeting in Richland, Washington, March, 1989)

2.1.3.5 Dissolution Radionuclide Release from UO$_2$ Fuel

2.1.3.5.1 Introduction

The long-term effects of the interactions between spent fuel, as a radioactive waste form, and groundwaters must be anticipated to safely dispose of spent fuel in an underground repository. Spent-fuel dissolution and subsequent transport processes in groundwater are generally considered to be the main routes by which radionuclides could be released from a geological repository. Laboratory testing of the behavior of spent fuel under the conditions expected in a repository provides the information necessary to determine the magnitude of the potential radionuclide source term at the boundary of the fuel's cladding. Dissolution (leach) and solubility tests of spent fuel and uranium dioxide (UO$_2$) are the most important data-collection activities in spent-fuel waste-form testing. All work in these activities is done within the controls of an approved quality assurance (QA) program.

The testing is done under conditions identified by modeling Activity D-20-50 as most important in calculating release rates. Any scenarios to be used as the basis for long-term modeling are being tested to the extent possible on a laboratory scale. Spent fuel with characteristics spanning the ranges identified in Activity D-20-50 will be tested. In addition, oxidized fuel produced under Activity D-20-45 will be tested. The three dissolution activities have been separated, based on the different technical techniques involved in conducting saturated (semi-static), flow-through and unsaturated (drip) tests. The solubility tests with actinide isotopes will provide concentration limits, speciation, and potential colloidal formation for a range of compositions of groundwater that may contact the waste forms at various temperatures. The key outputs from these activities are the dissolution rate of irradiated fuel, the release rates of radionuclides from spent fuel, and the solution chemistry of water in contact with spent fuel.

Because UO$_2$ is the primary constituent of spent nuclear fuel, the dissolution of the UO$_2$ spent-fuel matrix is regarded as a necessary first step for release of about 98% of the radioactive fission products contained within the UO$_2$ matrix. The intrinsic UO$_2$ dissolution rate sets an upper bound on the aqueous radionuclide release rate, even if the fuel is substantially degraded by other processes such as oxidation. If the fuel is substantially degraded to other oxidation states, the fuels' dissolution responses also must be provided. The release rate is reduced for the solubility-limited actinides (U, Np, Pu, and Am), which account for most of the long-lived radioactivity in spent fuel when colloids are not present. In scenarios for the potential Yucca Mountain repository, it is assumed that the cladding has failed, and water as vapor or liquid contacts the fuel. Drip tests that simulate the unsaturated and oxidizing conditions expected at Yucca Mountain are in progress to evaluate the long-term behavior of spent nuclear fuel.

There have been many investigations of the dissolution of UO$_2$, spent fuel, and uraninite (a naturally occurring UO$_2$ mineral) in aqueous solutions, under both reducing and oxidizing conditions and as a function of various other environmental variables. Several reviews have been written, the most recent being by Grambow (1989) and McKenzie (1992). Important variables considered in the reviewed investigations included pH, temperature, oxygen fugacity, carbonate/bicarbonate concentrations, and fuel attributes. The data vary because of the differences in experimental purpose and methods, the diverse history of the fuel samples, the formation of secondary phases during the tests, the complexity of the solution and the surface chemistry of UO$_2$, and the surface area measurements of the test specimens.

The following material summarizes the available Yucca Mountain Site Characterization Project (YMP) spent-fuel and unirradiated-uranium-oxide dissolution data.

2.1.3.5.2 Saturated (Static) Dissolution Tests

The Series 1 tests described (Wilson, 1984) were the first of several tests planned at Pacific Northwest National Laboratory (PNNL) to characterize potential radionuclide release from and behavior of spent fuel stored under YMP-proposed conditions. In the Series 1 tests, specimens prepared from Turkey Point Reactor Unit 3 fuel were tested in deionized distilled water in unsealed, fused silica vessels under ambient hot-cell air and temperature[1] conditions. Four specimen configurations were tested:

1. Undefected fuel-rod segments with watertight end fittings
2. Fuel-rod segments containing small (~200 μm diameter) laser-drilled holes through the cladding and with watertight end fittings
3. Fuel-rod segments with machined slits through the cladding and watertight end fittings
4. Bare fuel particles removed from the cladding plus the cladding hulls

A "semi-static" test procedure was developed in which periodic solution samples were taken with the sample volume replenished with fresh deionized distilled water. Cycle 1 of the Series 1 tests was started during July 1983 and was 240 days in duration. At the end of the first cycle, the tests were sampled, the vessels stripped in 8 $\underline{M}$ HNO$_3$, and the specimens restarted in fresh deionized distilled water for a second cycle. Cycle 2 of the Series 1 tests was terminated at 128 days in July 1984. A cycle is a testing period in which samples are taken at its conclusion and the test vessels are stripped and cleaned or replaced. Samples may have also been cleaned before starting another cycle.

The Series 2 tests (Wilson, 1990b) were similar to the Series 1 tests except for the following:

- The Series 2 tests were run in YMP (Nevada Nuclear Waste Site Investigations [NNWSI]) reference J-13 well water.
- Each of the four specimen configurations was duplicated using both the Turkey Point Reactor and H. B. Robinson Reactor pressurized-water reactor (PWR) spent fuels.
- A vessel and specimen rinse procedure was added to the cycle termination procedures.

Filtration of the collected rinse solution provided solids residues that were later examined for secondary-phase formation. Cycle 1 of the Series 2 tests was started in June 1984. All eight Series 2 specimens were run for a second cycle. The 2 bare fuel specimens were continued for Cycles 3, 4, and 5. Cycle 5 of the Series 2 bare fuel tests was terminated in June 1987 for a total 5-cycle testing time of ~34 mos.

The Series 3 tests (Wilson, 1990b) were run for three cycles during the same approximate time period as were Cycles 3, 4, and 5 of the Series 2 tests. The Series 3 tests were run in sealed. stainless-steel vessels and used the same four-specimen configurations used in Series 1 and Series 2 Cycles 1 and 2. Five specimens: one each of the four configurations using H. B. Robinson (HBR) reactor fuel (plus an additional bare-fuel specimen using Turkey Point (TP)

---

[1] Hot cell temperature range is approximately 21°C to 28°C, depending on time of year and time of day. An average value of 25°C was assumed for these ambient temperature tests (Wilson, 1990a).

reactor fuel) were tested at 85°C; a sixth specimen (HBR bare fuel) was run at 25°C. Two additional scoping tests using preoxidized bare fuel specimens in Series-2-type silica vessels were started in August 1986. The Series 1 and 2 tests were originally entitled "Cladding Containment Credit Tests." All of the test series were later referred to as "Spent-Fuel Dissolution Tests."

2.1.3.5.2.1 Series 1 Summary

Measured releases were compared to the 10 CFR 60 inventory maximum annual release rate requirement of l0^{-5} of l000-yr inventory per year. Total measured release and total measured release as a fraction of inventory $\times 10^5$ are summarized in Table 2.1.3.5-1. The principal observations and conclusions from these spent-fuel leaching tests are summarized as follows:

- Within the probable accuracy of total release measurements and specimen inventory calculations, the actinides U, Pu, Am, and Cm appear to have been released congruently.

- Limited data suggest that ^{237}Np may have been preferentially released rather than being congruently released with other actinides as expected. However, these data are too limited to be conclusive. Inaccuracies in ORIGEN-2 -calculated ^{237}Np inventory and radiochemical analysis could also account for those results.

- A fractional release of cesium on the order of the fractional fission-gas release was observed for the bare-fuel, slit-defect, and holes-defect tests. Additional preferential cesium release, possibly from grain boundary inventory, was also noted in the second run (cycle) on these specimens.

- Observed fractional ^{99}Tc release ranged from one order of magnitude greater relative to the actinides in the bare-fuel test to almost three orders of magnitude greater fractional release relative to the actinides in the holes-defect test.

- For the actinides U, Pu, Am, and Cm, approximately two orders of magnitude less total fractional release was measured in the slit-defect test relative to the bare-fuel test. An additional approximate one order of magnitude reduction in actinide release was observed in the holes-defect test relative to the slit-defect test.

- Apparent uranium saturation occurred at ~1 ppb in all tests. Uranium in excess of a few ppb was removed by 18 Å filtration. Most of the U, Am, and Cm in solution samples from the bare-fuel test was removed by filtration.

- Grain-boundary dissolution appeared to be a major source of release. Preferential release of ^{99}Tc is likely a result of its segregation to the grain boundaries. Grain boundaries in the spent fuel are relatively wide and easily resolved by scanning electron microscopy (SEM). Grain boundaries in unirradiated UO$_2$ are tight and not resolvable on a fracture surface by SEM.

- Spent-fuel leaching behavior, as well as other chemical and mechanical behavior, is influenced by microstructural phenomena such as localized segregation of some elements to the grain boundaries. The extent of localized radionuclide segregation is influenced by irradiation temperature and may be correlated to fission-gas release. Additional segregation of radionuclides into more easily leached phases could possibly occur if the fuel structure is degraded by oxidation during long-term repository storage.

Table 2.1.3.5-1   Total measured release as a fraction of inventory ($\times 10^5$)[a] for Series 1 [LL980710651021.049]

Component	Bare Fuel	Slit Defect	Holes Defect	Undefected
Uranium (µg)	28.0	0.078	<0.041	<0.018
	(9510)	(28)	(<14)	(<6.6)
$^{239+240}$Pu (nCi)	28.0	0.341	0.069	0.027
	(7940)	(104)	(20)	(8)
^{241}Am (nCi)	21.7	0.208	<0.030	<0.011
	(12,604)	(130)	(<18.6)	(<6.4)
^{244}Cm (nCi)	30.0	0.76	0.039	0.008
	(13,300)	(362)	(18.1)	(<3.9
^{237}Np[b] (nCi)	54	2.2	—	—
	(4.73)	(0.2)	—	—
^{137}Cs (nCi)	300[c]	142.1	85.6	0.041
	(1.94x10^6)	(3.94x10^6)	(2.33x10^6)	(1.1x10^3)
^{99}Tc[d] (nCi)	230	12.1	<6.7	—
	(900)	(51)	(<28)	—

[a]   Total measured release given in parentheses; sum of both cycles.
[b] ^{237}Np includes only vessel strip from initial and second runs (cycles) and final solution from second run (cycle).
[c]   Estimate based on maximum ^{137}Cs activities measured in solution.
[d] ^{99}Tc includes only final solution in a vessel strip from initial and second runs (cycle).

2.1.3.5.2.2 Series 2 Summary

Radionuclide releases were measured from PWR spent-fuel specimens tested in YMP (NNWSI) J-13 well water (see Table 2.1.3.5-2) in unsealed, fused silica vessels under ambient hot-cell air conditions (~25°C). Two bare-fuel specimens were tested: one prepared from a rod irradiated in the HBR Unit 2 reactor and the other from a rod irradiated in the TP Unit 3 reactor. Both fuels were low-gas release and moderate burnup. The specimen particle size range (2 to 3 mm) was that which occurs in the fuel as a result of thermal cracking. A semi-static test method was used in which the specimens were tested for multiple cycles starting in fresh J-13 water. Periodic water samples were taken during each cycle with the sample volume (~l0% of test solution) being replenished with fresh J-13 water. The specimens were tested for 5 cycles for a total time of 34 months.

Table 2.1.3.5-2   J-13 well-water analysis [LL980710651021.049]

Component	Concentration (μg/ml)	Component	Concentration (μg/ml)
Li	0.042	Si	27.0
Na	43.9	F	2.2
K	5.11	Cl	6.9
Ca	12.5	NO$_3$	9.6
Mg	1.92	SO$_4$	18.7
S r	0.035	HCO$_3$	125.3
Al	0.012	—	—
Fe	0.006	pH	7.6

- Series 2 actinide concentrations appeared to rapidly reach steady-state levels during each test cycle. Concentrations of Pu, Am, and Cm were dependent on filtration, with Am and Cm concentrations being affected the most by filtration; this suggests that these elements may have formed colloids. Approximate steady-state concentrations of actinide elements indicated in 0.4-µm-filtered-solution samples are as follows:

  U — 4×10^{-6} to 8×10^{-6} $\underline{M}$ (1 to 2 ppm)

  Pu — 8.8×10^{-10} to 4.4×10^{-9} $\underline{M}$ (20 to l00 pCi/mL $^{239+240}$Pu)

  Am— ~1.5×10^{-10} $\underline{M}$ (~l00 pCi/mL ^{241}Am)

  Cm — ~2.6×10^{-12} $\underline{M}$ (~50 pCi/mL ^{244}Cm)

  Np — 2.4×10^{-9} $\underline{M}$ (0.4 pCi/mL ^{237}Np)

- Actinide releases as a result of water transport should be several orders of magnitude lower than the NRC l0 CFR 60.113 release limits (10^{-5} of l000-yr inventory per year) if actinide concentrations (true solution plus colloids) in the repository do not greatly exceed the steady-state concentrations measured in 0.4-µm filtered samples. Assuming a water flux through the repository of 20 L per yr per waste package containing 3140 kg of spent-fuel saturates at the actinide elemental concentrations given previously, the following annual fractional releases are calculated based on l000-yr inventories for 33 megawatt days/kgM burnup PWR fuel:

  U — (8×10^{-6} M), 1.4×10^{-8} per yr

  Pu — (4×10^{-9} M), ~1×10^{-9} per yr

  Am — ~8×10^{-10} per yr

  Cm — ~1×10^{-8} per yr

  Np — ~3×10^{-9} per yr

- Gap inventory ^{137}Cs releases of about 0.7% of inventory in the HBR test and about 0.2% of inventory in the TP test were measured at the start of Cycle 1. Smaller initial Cycle 1 releases on the order of 10^{-4} of inventory were measured for ^{129}I and ^{99}Tc.

- Fission product nuclides ^{137}Cs, ^{90}Sr, ^{99}Tc, and ^{129}I were continuously released with time and did not reach saturation in solution. The continuous-release rates of these soluble nuclides were relatively constant during Cycles 3, 4, and 5. During Cycle 5, the release

rate for both ^{90}Sr and ^{129}I was about 5.5×10^{-5} of inventory per yr in both HBR and TP tests. Marginally higher continuous-release rates on the order of 1×10^{-4} of inventory per yr were measured for ^{137}Cs and ^{99}Tc.

- The degree to which the soluble nuclides (^{137}Cs, ^{90}Sr, ^{99}Tc, and ^{129}I) were preferentially released relative to the amount of congruent dissolution of the UO$_2$ matrix phase was not quantitatively measured. However, the near-congruent release of soluble nuclides in later test cycles and the inventory ratios of these nuclides to that of uranium in initial solution samples from the later cycles (a ratio of about 2.5 for ^{137}Cs) suggest that the fractional-release rates for these nuclides may not have greatly exceeded the matrix dissolution rate. Based on these data, a matrix dissolution rate of about 4×10^{-5} per yr appears to be a reasonable estimate for the 2- to 3-mm fuel particles tested.

- The present data suggesting fuel-matrix dissolution rates greater than 10^{-5} per yr imply that demonstrating l0 CFR 60.113 compliance for soluble nuclides will involve considerations other than the durability of the spent-fuel waste form—e.g., scenarios for low-probability water contact, a distribution of cladding/container failures over time, or very low migration rates. In time, fuel degradation resulting from oxidation and grain-boundary dissolution (increasing surface area) may increase the matrix-dissolution rate. Upper limits for degraded-fuel matrix-dissolution rates are yet to be determined.

- Comparison to the Series 3 tests (sealed vessels) indicated that most of the ^{14}C released in the Series 2 tests was lost to the atmosphere as CO$_2$ and not measured. The ^{14}C was preferentially released in the Series 3 tests at about 1% of its measured inventory in HBR fuel samples. As an activation product derived partially from nitrogen impurities, evaluation of ^{14}C release relative to l0 CFR 60.113 is complicated because its inventory and distribution in fuel are not well characterized.

- The quantities of precipitated, secondary-phase material observed in filter residues were significantly less than those observed in the 85°C Series 3 tests. UO$_2$ and calcite were the only phases confirmed by X-ray powder diffractometry (XRD) examination of a cycle-termination rinse filter, with a tentative indication of haiweeite based on a single line in the XRD pattern. Amorphous-appearing, silicon-containing phases were also observed by SEM on the rinse filters, and silicon-containing flocs were observed on filters used to filter solution samples. With the possible exception of haiweeite for uranium, phases controlling the solubility of actinide nuclides were not identified.

2.1.3.5.2.3 Series 3 Summary

Specimens prepared from PWR fuel rod segments were tested in sealed, stainless-steel vessels in Nevada Test Site J-13 well water at 85°C and 25°C. The test matrix included three specimens of bare-fuel particles plus cladding hulls, two fuel-rod segments with artificially defected cladding and watertight end fittings, and an undefected fuel-rod section with watertight end fittings. Periodic solution samples were taken during test cycles with thesample volumes replenished with fresh J-13 water. Test cycles were periodically terminated and the specimens restarted in fresh J-13 water. The specimens were run for 3 cycles for a total test duration of 15 mos.

Actinide concentrations (U, Pu, Am, Cm, and Np) peaked early in Cycle 1 of the bare-fuel tests and then declined to steady-state levels. Isotopes of Pu and Am account for approximately 98% of the activity in spent fuel at 1000 yr. Actinide concentrations rapidly reached stable steady-state values during Cycles 2 and 3. Steady-state activities on the order of 100 pCi/mL were measured for $^{239+240}$Pu, ^{241}Am, and ^{244}Cm at 25°C, and much lower

activities on the order of 1 pCi/mL were measured for these radionuclides at 85°C. Even using the higher 25°C values, the steady-state concentrations indicated for all of the actinide elements were at least three orders of magnitude below those required to meet the Nuclear Regulatory Commission (NRC) 10 CFR 60.113 controlled-release requirements for any realistic water-flow rate through the repository. Calcium-uranium-silicate phases that may have contributed to the control of U concentrations were identified in the 85°C tests. Secondary phases controlling Np, Pu, Am, and Cm concentrations were not identified.

Concentrations of the more soluble fission-product and activation-product radionuclides generally tended to increase continuously with time. An exception was ^{90}Sr, which tended to reach maximum concentrations in the 85°C tests. Continuous release rates measured for ^{99}Tc, ^{137}Cs, and ^{129}I were generally in the range of 10^{-4} to 10^{-3} of inventory per yr, but the rate for ^{129}I was lower at 25°C. Preferential release of ^{14}C continued through all three test cycles for a total release of about 1% of the ^{14}C specimen inventory. Comparison of ^{14}C releases in tests conducted in sealed and unsealed vessels indicated that ^{14}C was released to the atmosphere, most likely as CO$_2$. Although soluble radionuclides were released at rates in excess of the NRC limit of 10^{-5} of inventory per yr in the current tests, additional data are needed to predict long-term release rates.

The following conclusions and observations are made based on the results of the YMP (NNWSI) Series 3 Spent-Fuel Dissolution Tests:

- Actinide concentrations (U, Pu, Am, Cm, and Np) generally appeared to reach steady-state levels in all three test cycles of the bare-fuel tests. Control of actinide concentrations at stable levels in solution was attributed to the achievement of a steady-state between fuel dissolution and secondary-phase formation or other mechanisms such as sorption.

- Uranium-bearing secondary phases were found in significant amounts in filter (18 Angstrom) residues from the 85°C bare-fuel tests. Formation of the calcium-uranium-silicate phase uranophane was confirmed, and haiweeite was tentatively identified. A possible indication of soddyite formation was also found in one of the filter residues. Secondary phases controlling Pu, Am, Cm, and Np concentrations were not identified.

- Pu, Am, and Cm activities measured in solution samples from the 85°C bare-fuel tests were from two to three orders of magnitude lower than those measured in unfiltered and 0.4 μm filtered samples from the 25°C test. Slightly lower U concentrations were also measured at 85°C in Cycles 2 and 3. Lower actinide concentrations at 85°C are attributed to faster kinetics for formation of solubility-limiting secondary phases at the higher 85°C temperature. Np activities showed no significant dependence on temperature or filtration.

- Pu, Am, and Cm activities measured in 18Å filtered samples from the 25°C bare-fuel test were less than those measured in unfiltered and 0.4-μm filtered samples; this suggests that these elements were present as colloids in this test. The effects of filtration were generally greater for Am and Cm than for Pu. Notable reductions in Am and Cm activities also occurred with 0.4 μm filtration in the 85°C bare-fuel tests.

- Steady-state actinide concentrations measured in 0.4-μm filtered samples from the 25°C bare-fuel test were at least three orders of magnitude below those necessary to meet the NRC 10 CFR 60.113 controlled-release requirements, based on reasonable assumed water-flow rates through a repository. This result is of particular significance

because Pu and Am isotopes account for ~98% of the activity in spent fuel at 1000 yr, and eventual Pu and Am concentrations may be lower than those measured in 0.4-µm filtered samples from the 25°C tests.

- Measured U concentrations were consistent with those predicted by the EQ3/6 geochemical modeling code for precipitation of soddyite. Good agreement between measured and predicted concentration was obtained for Np, based on equilibration with NpO$_2$ at 25°C when the oxygen fugacity in the simulation was set at 10^{-12} bars. A broad range of concentrations that bracketed the measured values was predicted for Pu, depending on the assumed oxygen fugacity and concentration-controlling phase. Measured Am concentrations were less than predicted, based on data for equilibration with Am(OH)CO$_3$ or Am(OH)$_3$.

- Actinide fractional releases from the bare-fuel tests were much greater than in the slit-defect or hole-defects tests. Actinide releases from the slit-defect test were somewhat greater than in the hole-defects test, with most of the difference accounted for in the Cycle 1 acid strip samples. Actinide releases in the hole-defects test were not significantly different than those measured in the undefected test.

- The radionuclides ^{137}Cs, ^{90}Sr, ^{99}Tc, ^{129}I, and ^{14}C were continuously released in the bare-fuel tests at rates exceeding 10^{-5} of inventory per yr. Of these radionuclides, only ^{90}Sr showed significant indications that its concentration was limited by solubility. Cesium-137 showed the greatest fractional release during Cycle 1, while ^{14}C showed the greatest fractional release during Cycles 2 and 3.

- Iodine-129 release was much greater at 85°C than at 25°C. Comparison of the Series 3 test results to those from the Series 2 tests gave no indication that ^{129}I had been lost as I$_2$ from the unsealed, Series 2 vessels. The ^{129}I release in the slit-defect test was equivalent to that in the bare-fuel test, but ^{129}I released in the hole-defects test was not significantly greater than that in the undefected test.

- Comparison of ^{14}C solution activity data measured in the sealed, Series 3 tests to that measured in the unsealed, Series 2 tests indicated that most of the ^{14}C released in the Series 2 tests was probably lost to the atmosphere as ^{14}CO$_2$. The TP fuel appeared to have a much greater ^{14}C inventory (or gap inventory) than did the HBR fuel on which fuel and cladding ^{14}C inventory was radiochemically determined.

- Long-term release rates for soluble nuclides were uncertain. The relative contributions of fuel-matrix dissolution, versus preferential release from locations such as grain boundaries where soluble nuclides may be concentrated, was not determined. Preferential release would likely decrease as the inventory of soluble nuclides on exposed grain boundaries is depleted.

- A vessel-corrosion anomaly occurred during Cycle 1 of the 85°C HBR bare-fuel test. The most significant effects associated with the apparent vessel corrosion were 1) U concentration dropped to about 10 ppb, and 2) ^{99}Tc activity dropped to less than detectable. These effects are attributed to removal of U and Tc by coprecipitation with or sorption on iron-bearing precipitates or to reduction of the soluble UO$_2^{2+}$ and TcO$_4^-$ species as a result of redox coupling with Fe^0 to Fe^{2+}/Fe^{3+} reactions.

- Ca, Mg, Si, and HCO$_3^-$ precipitated from solution during all 85°C tests cycles, while the chemistry of the starting J-13 well water remained essentially unchanged during the 25°C test. In addition to the calcium-uranium-silicate phases observed in the two 85°C bare-fuel tests, scale formation was observed at the waterline in all of the 85°C tests. The SEM–energy-dispersive spectrometry (EDS) examinations suggest that calcite, SiO$_2$ (possibly as a gel), and possibly dolomite were formed during the 85°C

tests. A portion of the released ^{14}C is likely to be incorporated in the carbonate phases. A portion of the released ^{90}Sr is also likely to be incorporated in secondary phases, possibly as a partial substitute for Ca.

2.1.3.5.2.4 Summary of "Semi-Static" Unsaturated Tests and Geochemical Modeling

The following summary was extracted from Wilson and Bruton (1989). The full text of that paper is attached to this section as Addendum 1. Laboratory testing and geochemical simulation of the dissolution of spent fuel under conditions selected for relevance to the proposed Yucca Mountain repository have resulted in the following conclusions:

- Radionuclides of interest in spent fuel appear to fall into three categories of potential release mechanisms: 1) radionuclides whose release appears to be controlled by concentration-limiting mechanisms, 2) more highly soluble radionuclides, and 3) radionuclides that are released in the vapor phase (principally C-14).

- The principal radionuclides whose releases appear to be controlled by concentration-limiting mechanisms are the actinides U, Np, Pu, Am, and Cm. Steady-state concentrations measured for these actinide elements are at least three orders of magnitude lower than those required to meet NRC release limits, based on conservative estimates of water fluxes through the repository. This result is of particular significance because isotopes of Pu and Am account for about 98% of the activity in spent fuel at l000 yr. However, results from geochemical modeling suggest that steady-state concentrations may vary significantly with time because of changes in solution composition and the identity of precipitating phases.

- Good agreement between measured and predicted concentrations was obtained for Np based on equilibration with NpO$_2$ at 25°C when the oxygen fugacity in the simulation was set at 10^{-12} bars. A broad range of solubilities that bracketed the measured values was predicted for Pu depending on the assumed oxygen fugacity and solubility-controlling phase. Measured Am concentrations were less than predicted, based on data for equilibration with Am(OH)CO$_3$ and Am(OH)$_3$.

- Dissolution rates for soluble radionuclides (^{137}Cs, ^{90}Sr, ^{99}Tc and ^{129}I) exceeding 10^{-5} of specimen inventory per year were measured during the laboratory tests. The implications of these data relative to long-term release of soluble radionuclides from a failed waste package (WP) are uncertain. The degree to which these radionuclides were preferentially released from grain boundaries where they may have concentrated during irradiation was not determined. Preferential release could be expected to provide a lesser contribution overtime as exposed grain boundary inventories are depleted. However, physical degradation of the fuel over time from exposure to the oxidizing repository environment may result in accelerated release of soluble nuclides.

- Additional work is required to identify solid phases that control actinide concentrations and to acquire reliable thermodynamic data on these phases for use in geochemical modeling. In this regard, identification of any stable, suspended phases that can be transported by water movement is also important. In addition, there is a need for a better understanding of the potential release of soluble and volatile radionuclides, which may initially depend on preferential release from gap and grain boundary inventories, but may ultimately depend on the rate of fuel degradation by oxidation or other processes in the postcontainment repository environment.

2.1.3.5.3 Flow-Through Dissolution Tests

The purpose of the work reported here is to examine the systematic effect of temperature and important water-chemistry variables on the dissolution rates of the UO$_2$ matrix phase in both unirradiated UO$_2$ and spent fuel. The dissolution rates of the higher oxidation states of uranium, U$_4$O$_{9+x}$, U$_3$O$_8$ and UO$_3 \cdot x$H$_2$O are also reported because of their likely presence in spent fuel placed in a repository. Unirradiated UO$_{2+x}$ represents reactor fuel with no burnup. The data sets obtained at equivalent conditions allow a direct comparison of UO$_{2+x}$ and spent-fuel dissolution rates and provide insight into the effect of fuel burnup. Additional data at higher spent-fuel burnup are needed to model the effect of burnup over the range of spent-fuel inventory.

The exact chemistry of groundwater in an underground repository is not certain, but groundwater has typical constituents such as carbonates, sulfates, chlorides, silicates, and calcium. Water taken from wells near Yucca Mountain contains all of these ions and has a pH near 8. Of the anions commonly found in groundwater, carbonate is considered to be the most aggressive towards UO$_2$ and, as such, is a conservative surrogate for all anions in groundwater.

As mentioned in Section 2.1.3.5.1,, there have been many investigations of the dissolution of UO$_2$, spent fuel, and uraninite in aqueous solutions under both reducing and oxidizing conditions and as a function of various other environmental variables (Grambow, 1989). Important variables considered in the investigations included pH, temperature, oxygen fugacity, carbonate/bicarbonate concentrations, and fuel attributes. These same variables were used in the flow-through experiments reported here.

The data obtained from the tests described here can be used to 1) identify important parameters that control the dissolution rates of the UO$_2$-matrix phase of spent fuel, 2) estimate bounding values for UO$_2$ and spent-fuel matrix dissolution rates, and 3) develop a release model for radionuclides from spent fuel that will be used in waste-package design and in performance assessment.

The intrinsic dissolution rates of UO$_{2+x}$ and spent fuel were determined by using a single-pass, flow-through method that was used successfully in the study of the dissolution kinetics of glass and other minerals (Knauss et al., 1989; 1990). The advantage of the single-pass, flow-through technique is that flow rates and specimen size can be controlled so that the UO$_2$ dissolves under conditions that are far from solution saturation (no precipitation of dissolved products). Under such conditions, the steady-state dissolution rates are directly proportional to the effective surface area of the specimen. Thus, the dependence of UO$_2$ dissolution kinetics on pH, temperature, oxygen, and carbonate/bicarbonate concentrations can be evaluated.

To test for nonlinear effects of the four variables on the uranium dissolution rate from UO$_2$ and spent fuel, experiments at three different values of each variable were required. The chosen settings were pH = 8, 9, 10; temperatures of 25°, 50°, and 75°C; oxygen partial pressures of 0.002, 0.02, and 0.2 atm; and total carbonate concentrations of 0.2, 2, and 20 millimol/L. Because carbonate solutions are natural pH buffers, total carbonate concentration and pH could be tested independently by varying the carbonate/bicarbonate and CO$_2$ gas ratios. A statistical experimental-design approach was used to select the experiments to be performed and to reduce the number of required experiments. A model including nonlinear effects and interactions of all 4 variables has at least 15 terms, thus requiring a minimum design of 17 experiments with 2 degrees of freedom or redundancy.

A set of experiments was selected to examine systematically the effects of temperature (25–75°C), dissolved oxygen (0.002–0.2 atm overpressure), pH (8–10), and carbonate concentrations (0.2–20 millimol/L) on UO_2 and spent-fuel dissolution (Steward and Gray, 1994). Similar sets of experiments at atmospheric oxygen partial pressure were conducted on U_3O_8 and $UO_3 \cdot xH_2O$ to measure the effect of higher oxidation states on dissolution. The high temperature in all experiments was limited to 75°C, because temperatures nearer to 100°C induce experimental difficulties in an aqueous, flow-through system. The carbonate concentrations bracketed the typical groundwater concentration of about 1–2 millimol/L. The oxygen pressure represented the atmospheric value and down two orders of magnitude to a minimally oxidizing atmosphere. The pH covered a value typical of groundwaters (pH = 8) to very alkaline conditions. In the basic region, carbon dioxide dissolved in water, CO_2 (aq), occurs mostly as carbonate/bicarbonate species. Therefore, carbonate/bicarbonate concentrations were fixed by adding sodium carbonate and bicarbonate to those basic buffer solutions, and the partial pressure of CO_2 in the gas phase above them was kept at the values calculated for stability. The spent fuel used in the PNNL tests was ATM-103, a PWR fuel with a burnup of 30 MWd/kgM and a fission gas release of 0.25%. The UO_2 specimens used at Lawrence Livermore National Laboratory (LLNL) were about 1 cm across and consisted of large crystallites containing dislocation substructures (i.e., low-angle grain boundaries).

Table 2.1.3.5-3 provides a list of the spent fuels used in the flow-through dissolution and other tests.

Table 2.1.3.5-3   Spent-fuel test materials [LL980711051031.048]

Reactor Type	Fuel	Rod	Peak Burnup (MWd/kgM)	Fission Gas Release (%)
PWR	ATM-103	MLA-098	30	0.25
PWR	ATM-104	MKP-109	44	1.1
BWR	ATM-105	ADD-2974	31	0.59
BWR	ATM-105	ADD-2966	34	7.9
PWR	ATM-106	NBD-095	43	7.4
PWR	ATM-106	NBD-107	46	1
PWR	ATM-106	NBD-131	50	18

2.1.3.5.3.1 Flow-Through Test Results

The results of the combined uranium dioxide and ATM-103 spent-fuel test matrices (Steward and Gray, 1994) are given in Table 2.1.3.5-4. Two different averages of the ATM-103 spent fuel and UO_2 data were calculated. The first was for 20% oxygen (air), and the second was for all tests where the conditions were nominally identical. For both averages, the UO_2 rates were about three times higher than the spent fuel rates. There is a clear difference in the way the two materials responded to changes in oxygen concentration, which may be a result of radiolysis-produced oxidants. Uranium dioxide dissolves significantly faster at the aggressive condition of high temperature, oxygen, and carbonate. Aside from oxygen concentration, both spent-fuel and UO_2 dissolution rates were most dependent on temperature, with a lesser dependence on carbonate concentration. Changes in pH had the least effect on the dissolution rates of both materials.

Additional spent-fuel data are available for specific fuels and conditions (Gray and Wilson, 1995; Gray, 1996; Gray, 1998). These 11 dissolution rates of unoxidized higher burnup

fuels are listed in Table 2.1.3.5-4a. The combined 53 dissolution rates from Tables 2.1.3.5-4 and 4a are used in the most recent intrinsic dissolution model of Section 3.4.2.

Table 2.1.3.5-4   Test parameters and results for spent fuel (ATM-103) and UO$_2$ dissolution tests[a] [LL980601551021.042]

Run No.	Temp. (°C)	Carbonate[b] (mmol/L)	Oxygen[c] %	pH[d]	U Dissolution Rate (mgU/m^2·day)	
					Spent Fuel (ATM-103)	UO$_2$
1	50	2	20	9.0	6.34	
2	50	2	20	9.0	7.05	
3	50	2	20	9.0	5.07	
4	22/25	20	20	8.0/8.7	3.45	2.42
5	74/75	20	20	10.0/10.3	14.2	77.4
6	74/75	0.2	20	8.0/9.1	8.60	10.9
7	21/25	0.2	20	10.0/9.0	0.63	2.55
8	22/25	20	20	9.0/9.4	2.83	6.72
9	22/25	2	20	10.0/9.3	2.04	9.34
10	27/26	0.2	2	8.0/7.8	1.79	0.12
11	78/75	0.2	2	10.0/9.7	1.49	9.21
12	25/26	20	2	10.0/10.1	2.05	1.87
13	77/75	20	2	8.0/8.5	2.89	5.11
14	23/25	20	0.3/0.2	8.0/8.0	2.83	0.22
15	74/75	20	0.3/0.2	10.0/9.8	0.69	5.61
16	78/75	0.2	0.3/0.2	8.0/8.7	1.98	0.51
17	19/26	0.2	0.3/0.2	10.0/9.3	0.51	0.23
18	50/50	20	0.3/0.2	10.0/9.9	1.04	4.60
19	21/26	2	0.3/0.2	9.0/9.0	1.87	1.52
20	75	20	2	10.0	4.75	
21	50	2	2	8.9		12.3
22	50	2	2	8.8		7.96
23	50	2	2	8.9		10.4
24	75	0.2	20	9.5		6.48
25	75	2	20	9.6		23.3
26	75	20	20	8.5		54.0
Average	Runs 4–9				5.29	18.2
Average	Runs 4–19				3.08	8.57

[a]   Numbers separated by a "/" are data for spent fuel and UO$_2$ respectively (SF/UO$_2$)
[b]   Made up using appropriate amounts of Na$_2$CO$_3$ and NaHCO$_3$
[c]   Percent of oxygen in sparge gas
[d]   Measured at room temperature. For spent fuel, the measured values were within $\pm$0.1 unit of the nominal values listed.

Table 2.1.3.5-4a   Additional spent-fuel flow-through dissolution tests at atmospheric oxygen (20%) [LL980704251021.045; LL980711051031.048]

Fuel	Rod	Burnup (MWd/kgM)	Intrinsic Dissolution Rates [mgU/(m^2·day)]				
			pH = 8 2×10^{-2} M Total Carbonate		pH = 8 2×10^{-4} M Total Carbonate		pH = 9 2×10^{-3} M Total Carbonate
			25°C	75°C	25°C	75°C	50°C
ATM-104	MKP-109	44	3.5[a]				
ATM-105	ADD-2974	31	4.0[a]	9.1[a]	2.6[a]	11[b]	6.6[b]
ATM-106	NBD-131	50	1.5				
ATM-106	NBD-131	50	3.8[c]	6.9[c]	2.9[c]	9.5[c]	

[a]   These values were revised in Gray, 1998.
[b]   These values from Gray, 1996.
[c]   These values were added in Gray, 1998.

The dependence of UO$_{2+x}$ dissolution kinetics on pH, temperature, time, and carbon dioxide/carbonate/bicarbonate concentrations was also investigated (Steward and Mones, 1997). All experiments in this higher-oxide test series were run at 20% oxygen buffer solution overpressure or 8 ppm dissolved oxygen. The flow-through tests were carried out in basic buffer solutions (pH of 8–10). The chemical composition of the solutions provided concentrations and dissolution-rate data useful in developing kinetic models for UO$_2$ matrix dissolution of spent fuel and for use in the waste-package design. The intrinsic dissolution rate obtained from these data is expected to be an upper-bound dissolution response for high pH water chemistries. Again, in order to test for nonlinear effects, experiments at three different values of each quantitative or continuous variable were required. Tests were done at three temperatures (25°, 50°, and 75°C), three carbonate/bicarbonate concentrations (2×10^{-4} to 2×10^{-2} mol/L), and three pH values (8, 9, and 10) using an arbitrary flow rate (>100 mL/day) for the two compounds U$_3$O$_8$ and UO$_3$·xH$_2$O.

Dehydrated schoepite, UO$_3$·xH$_2$O, was used in the UO$_3$ runs. It is easy to produce and is more stable than either the dihydrate or anhydrous form of uranium trioxide. Approximately 20 grams of UO$_3$·xH$_2$O were prepared via an aqueous hydrolysis of uranyl acetate, UO$_2$(Ac)$_2$, a procedure that took place over several days. The U$_3$O$_8$ in use is National Bureau of Standards (NBS) Standard Reference Material (SRM) 750b. It can also be produced by heating the dehydrated schoepite in air. Both U$_3$O$_8$ and UO$_3$·xH$_2$O samples were powders because of the synthetic routes available for each. U$_3$O$_8$ is the most stable of the uranium oxides and is easily produced by the well-known method of heating a uranium compound, UO$_2$ in this case, to several hundred degrees centigrade in air. Surface areas of both materials were measured via the traditional Brunauer–Emmett–Teller (BET) method using xenon gas. The resulting surface area for the U$_3$O$_8$ is 0.18±0.02 m^2/g and 0.31± 0.04 m^2/g for the UO$_3$·xH$_2$O. Particle-size distributions were also determined by means of sedimentation techniques. The median particle size for the U$_3$O$_8$ powder was 2.1 μm with a 25–75 percentile range of 1.0 to 2.8 μm. The median particle size for the UO$_3$·xH$_2$O powder was 4.1 μm with a 25–75 percentile range of 2.5 to 5.5 μm.

Table 2.1.3.5-5 lists the uranium dissolution rates for the three oxides UO$_2$, U$_3$O$_8$ and UO$_3$·xH$_2$O that were measured at LLNL under atmospheric oxygen conditions. The two new, room-temperature UO$_2$ results were measured at a pH of 10 and 2 x 10^{-4} molar total carbonate and a pH of 10 at 2 x 10^{-2} molar total carbonate. These were recently acquired so that there would be a full set of eight measurements at the extreme conditions (a full-factorial linear experimental design) for each oxide. Previously obtained results for spent fuel (ATM-103) are listed at equivalent conditions. To facilitate comparisons of the dissolution rates and variable effects, the results for the eight experimental conditions at the high and low values of each variable are grouped together at the beginning of the table (Part 1). They are grouped first by pH, then by carbonate concentration, and finally by temperature. The results at intermediate conditions are listed last as Part 2 in Table 2.1.3.5-5, using the same grouping scheme.

As shown in Table 2.1.3.5-5, Part 1, the oxide state had, by far, the strongest effect on the uranium-dissolution rate. The rate increased significantly in going from UO$_2$ to U$_3$O$_8$ and dramatically from U$_3$O$_8$ to UO$_3$·xH$_2$O. Increasing carbonate concentrations increased the dissolution rates of U$_3$O$_8$ and UO$_3$·xH$_2$O, as shown previously with UO$_2$. An increase in U$_3$O$_8$ dissolution rate with increasing temperature was also seen. A similar temperature effect on UO$_3$·xH$_2$O was not apparent, which may be due to the rapid UO$_3$·xH$_2$O dissolution. Raising the temperature to 75°C from room temperature increased the dissolution rate by a factor of 2 to 4 for the two higher oxides. As with the UO$_2$ results, alkaline pH did not have a significant role in changing the dissolution rate of the higher oxides. However, the detailed dependence on temperature and carbonate concentrations was not visually well demonstrated. Because pH shows little correlation, a surface plot for dissolution rate in three dimensions would better depict the effects of carbonate concentration and temperature.

The data in Table 2.1.3.5-5 indicate that, with the higher oxides, unlike UO$_2$, carbonate seems to affect the dissolution rate to a greater extent than does temperature. The enhancement is particularly strong at the highest carbonate concentration.

Because U$_3$O$_8$ has both U(IV) and U(VI) valence states, its dissolution rates might be expected to be between that of UO$_2$ and UO$_3$·xH$_2$O, particularly as carbonate concentrations increase. That does not seem to be the case with the present data. The data indicate that alkaline pH is the least significant factor in dissolution of spent fuel or any of the uranium oxides under the alkaline conditions of these experiments. Changes in alkaline pH produced almost random changes in dissolution rates in this and previous data sets.

Table 2.1.3.5-5, Part 1   Comparison of dissolution rates at bounding conditions [ll961210151021.027]

pH	Carbonate (mol/L)	Oxygen (atm)	Temp (°C)	Dissolution Rate (mgU/(m²·day))			
				ATM-103 Spent Fuel	UO$_2$	U$_3$O$_8$	UO$_3$·xH$_2$O
8	0.0002	0.2	25		3.87	~5	~100
8	0.0002	0.2	50		5.4		
8	0.0002	0.2	75	8.6	10.9	~6	>200
8	0.02	0.2	25	3.45	2.42	18.8	~700
8	0.02	0.2	50		38.3		
8	0.02	0.2	75		54	~150	>1500

pH	Carbonate (mol/L)	Oxygen (atm)	Temp (°C)	Dissolution Rate (mgU/(m^2·day))			
				ATM-103 Spent Fuel	UO$_2$	U$_3$O$_8$	UO$_3$·xH$_2$O
10	0.0002	0.2	25	0.63	2.55	0.8	>100
10	0.0002	0.2	50		3.1		
10	0.0002	0.2	75		6.48	~3	>150
10	0.02	0.2	25		20.1	21.1	~200
10	0.02	0.2	50		25.8		
10	0.02	0.2	75	14.2	77.4	~200	>1000

Table 2.1.3.5-5, Part 2   Comparison of dissolution rates at intermediate conditions [ll961210151021.027]

pH	Carbonate (mol/L)	Oxygen (atm)	Temp (°C)	Dissolution Rate (mgU/(m^2·day))			
				ATM-103 Spent Fuel	UO$_2$	U$_3$O$_8$	UO$_3$·xH$_2$O
8	0.002	0.2	25			~10	
8	0.002	0.2	50			~10	
9	0.0002	0.2	25			1.26	
9	0.0002	0.2	75			~4	
9	0.002	0.2	25				~120
9	0.002	0.2	50	6.1	11.7		
9	0.002	0.2	75		23.3		>20
9	0.02	0.2	25	2.83	6.72	8.33	>1500
9	0.02	0.2	50			>100	
10	0.002	0.2	25	2.04	9.34		

2.1.3.5.3.2 Dissolution Rates of Oxidized Spent Fuel and Additional Tests With Unirradiated Uranium Oxides

Uranium dissolution rates were measured on crushed, unirradiated UO$_2$ fuel pellet samples under oxidizing conditions using the flow-through test method (Wilson and Gray, 1990). Water compositions included J-13 well water, deionized distilled water (DIW), and variations on the J-13 water composition selected to measure the effects of various J-13 water components on UO$_2$ dissolution rates. Dissolution rates at 25°C in air-equilibrated DIW were 1–2 mgU/(m^2·day). Calcium (15 µg/ml as CaCl$_2$ and CaNO$_3$) and silicon (30 µg/ml as silicic acid) were sequentially added to the DIW, resulting in an order of magnitude decrease in uranium dissolution rate. Adding NaHCO$_3$ in concentrations similar to J-13 water (170 µg/ml) to this calcium- and silicon-containing DIW increased the uranium dissolution rate by almost two orders of magnitude.

Results from flow-through dissolution tests with oxidized specimens of spent fuel and unirradiated U$_3$O$_7$ and U$_3$O$_8$ have been published (Gray and Thomas, 1992; Gray et al., 1993; and Gray and Thomas, 1994. Therefore, only highlights are discussed here, together with some details that were not included in these publications (Gray and Wilson, 1995).

Dissolution rates of spent fuels oxidized to U$_4$O$_{9+x}$ currently have been measured for three spent fuels; ATM-104, ATM-105, and ATM-106. The surface-area normalized-dissolution rate of oxidized fuel grains was little or no higher than unoxidized (UO$_2$) grains for ATM-105. Oxidized ATM-106 fuel grains dissolved somewhat faster than did unoxidized grains, but the difference still was a factor of only about five.

Note that the test conditions for ATM-105 were different from those used with the ATM-104 and ATM-106 fuels (see Table 2.1.3.5-6). This precludes a direct comparison between ATM-105 and the other two fuels. However, the purpose of the tests in each case was to compare results for oxidized versus unoxidized specimens, not for comparisons among different fuels. The tests with ATM-105 were conducted first, and a decision was made after that to change the conditions for future tests. This test condition (2×10^{-2} M total carbonate, pH =8, 25°C, atmospheric oxygen partial pressure), which will be included in most future testing to allow a wider variety of direct comparisons among different fuels, was used for the oxidized and unoxidized specimens of ATM-104 and ATM-106 fuels.

Oxidation has the potential to change spent-fuel dissolution rates in two ways: it could change the intrinsic dissolution rates; it could increase the dissolution rate of fuel particles by making the grain boundaries more accessible to the water, thereby increasing the effective surface area.

Table 2.1.3.5-6 shows that the intrinsic dissolution rates of ATM-104 and ATM-105 (data obtained using grain specimens) were not significantly affected by oxidation, but there was a modest increase in the intrinsic dissolution rate of ATM-106 fuel grains. Secondly, oxidation left the dissolution rate of ATM-105 particles unchanged, which implies that the depth of water penetration into the grain boundaries was unchanged by the oxidation.

Table 2.1.3.5-6   **Dissolution rate (mgU·m^{-2}·d^{-1}) and estimated grain boundary penetration of unoxidized (UO$_2$) and oxidized (U$_4$O$_{9+x}$) spent fuel [LL980711051031.048]**

Fuel	Rod	Unoxidized			Oxidized		
		Grains	Particles	GBP[a]	Grains	Particles	GBP[a]
ATM-104[b]	MKP-109	3.4	33	4–6	3.5	166	~100
ATM-106[b]	NBD-131	1.5	25	6–9	8.2	241	12–18
ATM-105[c]	ADD-2974	6.6	25	2–3	7.4	28	2–3

[a]   Grain boundary penetration: estimate of depth of water penetration into the grain boundaries (number of grain layers)
[b] 2×10^{-2} M total carbonate, pH =8, 25°C, atmospheric oxygen partial pressure
[c] 2×10^{-3} M total carbonate, pH =9, 50°C, atmospheric oxygen partial pressure

In contrast to its effect on the ATM-105 particles, oxidation had a marked effect on the dissolution rates of ATM-104 and ATM-106 particles. This effect can be attributed to opening of the grain boundaries by the oxidation, which allows greater water penetration, thereby increasing the effective surface area available for reaction with the water. So great was this effect with ATM-104 that the water appears to have penetrated the entire volume of grain

boundaries throughout the particles. This is evident from the estimated depth of water penetration (~100 grain layers) multiplied by the grain size (~12 μm), which leads to a penetration depth that is well over half the particle diameters (700 to 1700 μm).

Because replicate tests have not been run, it is not possible to say whether the three different fuels in Table 2.1.3.5-6 really respond differently to oxidation and subsequent reaction with water or if the observed differences were simply sample-to-sample variations. However, the data do suggest that oxidation up to the U$_4$O$_{9+x}$ stage does not have a large effect on intrinsic dissolution rates (the largest increase was a factor of <6). Data for some of the particle specimens also suggest that this degree of oxidation may markedly increase dissolution rates of relatively intact fuel rods by opening the grain boundaries and thereby increasing the effective surface area that is available for contact by water. From a disposal viewpoint, this is the more important consideration.

When ATM-106 fuel was oxidized to U$_3$O$_8$, its surface-area normalized-dissolution rate was about 10 times faster than unoxidized ATM-106 fuel grains and about twice as fast as ATM-106 fuel grains oxidized to U$_4$O$_{9+x}$. A more important effect of oxidation to U$_3$O$_8$ was the very large increase in surface area compared to the particles used to prepare the U$_3$O$_8$. This resulted in a fractional dissolution rate (rate per unit specimen weight) of U$_3$O$_8$ equal to 150 times that of the unoxidized particles.

At atmospheric O$_2$ overpressure, the intrinsic dissolution rate of unirradiated U$_3$O$_7$ (~3 mgU/(m^2·day)) was similar to UO$_2$ (~2.5 mgU/(m^2·day)), and the intrinsic dissolution rate of unirradiated U$_3$O$_8$ (~10-15 mgU/(m^2·day)) was about three to five times that of UO$_2$. At an O$_2$ overpressure of 0.003 atm, the intrinsic dissolution rate of the U$_3$O$_7$ was two to three times that of UO$_2$ (0.5-1 mgU/(m^2·day)). These estimates are based on single experiments with each oxide at each condition.

In summary, for each test conducted with oxidized spent fuel or unirradiated U$_3$O$_7$ or U$_3$O$_8$, the intrinsic dissolution rate of the oxidized material was only moderately higher than that of the unoxidized (UO$_2$) material. The largest difference was a factor of 10 with spent fuel U$_3$O$_8$. This difference seems relatively small when one considers that the surface of UO$_2$ must first oxidize to a stoichiometry equivalent to approximately UO$_{2.33}$ before significant dissolution of U, as U(VI) species, can occur. These observations suggest that initial surface oxidation is not involved in a rate-limiting step of the UO$_2$ oxidation/dissolution mechanism.

A major reason for conducting dissolution tests with spent fuel oxidized to U$_3$O$_8$ was to determine whether the inter- and intragranular cracks produced by the oxidation would lead to high initial dissolution rates of soluble radionuclides. Therefore, 100% of the test-column effluent was collected and analyzed for each of the first two days. During the first day (29 h), 16.2% of the total ^{137}Cs inventory dissolved compared with 4.5% of the U; thus the excess of ^{137}Cs over U was about 12%, which represents the amount exposed by oxidation-induced cracking and grain-boundary opening. Nearly congruent dissolution of ^{137}Cs and U was observed during the second and subsequent days.

Because the fuel particles were washed before they were oxidized to U$_3$O$_8$, the ^{137}Cs associated with the gap inventory would have been removed. Also, the ^{137}Cs inventory associated with grain boundaries of this fuel was only about 1% of the total ^{137}Cs inventory. Therefore, of the 12% excess of ^{137}Cs over U cited previously, only 1% could have come from oxidation-induced opening of the grain boundaries. The remaining 11% had to originate from oxidation-induced cracking of the grain interiors. This confirms speculation that oxidation to U$_3$O$_8$ might expose a relatively large fraction of the ^{137}Cs inventory to water where it could be readily dissolved, at least for this one type of spent fuel (ATM-106).

2.1.3.5.3.3 Flow-through Studies of Dissolution Rates of Unirradiated Uranium Oxides and Spent Fuel Performed Outside the Yucca Mountain Site Characterization Project (Non-Qualified Studies)

There are a number of uranium oxide and spent fuel dissolution studies in the literature. Grambow (1989) and McKenzie (1992) provide reviews of the literature prior to 1992. There are three more recent reports of particular interest for flow-through dissolution data. De Pablo (1997) performed flow-through studies of UO$_2$ dissolution in brine solutions as a function of both temperature and carbonate concentration at atmospheric oxygen. Tait and Luht (1997) recently published a report summarizing UO$_2$ and spent-fuel flow-through dissolution studies performed over an extended period of time at Atomic Energy of Canada, Limited, Whiteshell Laboratories. Acidic and alkaline dissolution of UO$_2$ under reducing conditions at room temperature were reported by Bruno et al. (1991). These data can be used for comparison with dissolution models developed for performance assessment.

2.1.3.5.4 Unsaturated Dissolution Tests

This section summarizes work reported in Bates et al. (1995) and Finn et al. (1997). In scenarios for the potential Yucca Mountain repository, it is assumed that the cladding has failed, and water as vapor or liquid has contacted the fuel. Drip tests that simulate the unsaturated and oxidizing conditions expected at Yucca Mountain are in progress to evaluate the long-term behavior of spent nuclear fuel. The purpose of the experiments is to determine if the rate of fuel alteration affects the release rate[2] of different radionuclides under unsaturated conditions. The results from the drip tests are used to monitor the reaction rate of the fuel, the formation of alteration phases, the corresponding release rates for individual radionuclides, and the solution chemistry. The information from these tests can be used to estimate the magnitude of the potential radionuclide source term at the exterior of the fuel cladding and the changes that can be expected in water chemistry due to groundwater interaction with the spent fuel.

The reaction of UO$_2$ and spent nuclear fuel samples was examined in unsaturated drip tests that simulate an environment that may be expected for spent fuel in the unsaturated/oxidizing environment of the potential Yucca Mountain nuclear waste repository. The reaction of both UO$_2$ and spent fuel in these tests, results in the formation of alteration phases similar to minerals observed during the oxidative dissolution of uraninite in natural geologic systems. Overall reaction pathways for both UO$_2$ and spent fuel appear to be controlled by a combination of sample corrosion, precipitation kinetics of alteration phases, and leachant composition.

2.1.3.5.4.1 UO$_2$ Reactions Through 12 Years of Testing

The present unsaturated drip tests are being conducted with unirradiated UO$_2$, as a surrogate for spent fuel, using EJ-13 water at 90°C. Direct testing of spent fuel is difficult because of its high level of radioactivity. While these experiments cannot mimic spent-fuel behavior completely, the reaction processes operating during the corrosion of spent fuel and UO$_2$ should be similar because spent fuel contains >95% UO$_2$. The gross corrosion processes

---

[2] In these unsaturated tests, radionuclide release means the quantity of those elements that go into solution as dissolved or colloidal species or precipitate on the container walls. The quantity of sample that initially dissolves and reprecipitates on the sample or sampleholders is not measured or included in the mass-release totals.

in the UO$_2$ experiments should be relevant to spent-fuel behavior, especially with respect to the identification of secondary alteration products and modes of waste-form degradation. More specifically, these tests examine the dissolution behavior of the UO$_2$ pellets, identify long-term mineral paragenesis in the alteration phases, identify parameters that control the release of uranium from the UO$_2$ pellets, and serve as a pilot study for similar tests with spent nuclear fuel.

The experimental apparatus and materials used to conduct these tests have been described previously (Wronkiewicz et al., 1991; 1992) and are only briefly summarized here. The samples were fabricated and pressed sintered from a uranium oxide powder with a natural isotopic abundance of uranium and an oxygen/metal ratio of 2.000 ± 0.002. An analysis of the samples indicated <70 ppm total contaminants, of which Cl (10 ppm), Th (15-ppm), and Fe (20 ppm) were the major contributors.

The UO$_2$ samples were placed into 0.38-mm-thick Zircaloy™-4 metal tubes that had been cut to accommodate the lengths of the various sample configurations. Pellets were exposed on their upper and lower surfaces, with their sides enclosed by the Zircaloy™. Several sample configurations were used to assess the effect of surface/volume (S/V) ratios on the dissolution of UO$_2$ (Table 2.1.3.5-7). These configurations included the following:

1. A stack of eleven 13.9 mm-diameter by 1.8 mm-thick wafered pellets (experiments 1 and 2)
2. Crushed _60- to +80-mesh grains sandwiched between an upper and lower wafer of the dimensions of the first assembly (experiments 3 and 4)
3. A stack of three 13.9 mm-diameter by 10 mm-thick pellets (experiments 5 through 8)

Uranium release from the UO$_2$ samples, listed in Table 2.1.3.5-7 and Table 2.1.3.5-8, was rapid from 1 to 2 yr of testing, followed by relatively low rates of release over the 2- to 10-yr period (Wronkiewicz et al., 1996). The rapid release period could be correlated with an episode of preferential corrosion along UO$_2$ grain boundaries and subsequent spallation of micrometer-to-submicrometer-sized UO$_{2+x}$ particles (where $0 \leq x \leq 0.25$) from the sample surfaces. Electron microscopy and optical examinations of the altered samples revealed a reaction front that penetrated into the UO$_2$ samples an average of 2 to 4 grains (~10 to 20 μm) ahead of the exposed external sample surface, but varied from regions with little visible corrosion to regions where penetration occurred to a depth of approximately 10 grains. This corrosion occurred preferentially along the grain boundaries between the original press-sintered granules making up the UO$_2$ pellets (Figure 2.1.3.5-1a). The formation of a dense mat of alteration phases in the longer-term tests enveloped the loosened UO$_2$ grains (Figure 2.1.3.5-1b), reducing particulate spallation and lowering uranium-release rates.
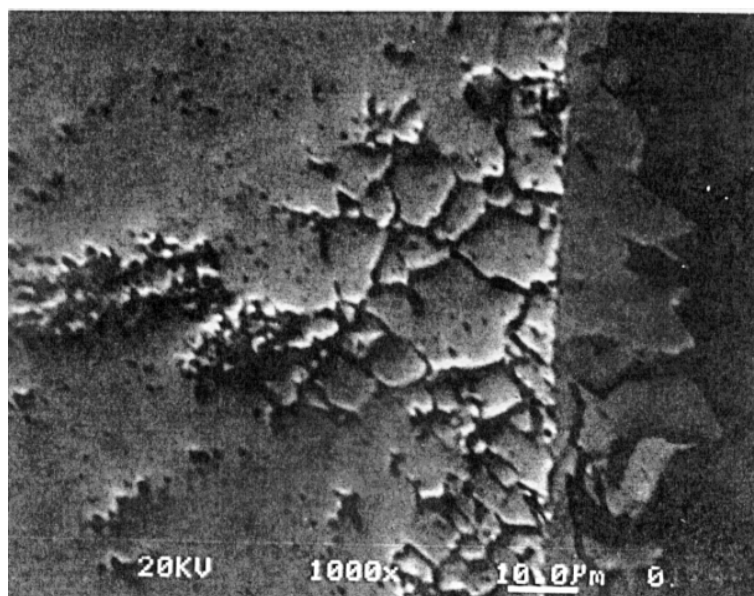
(a)
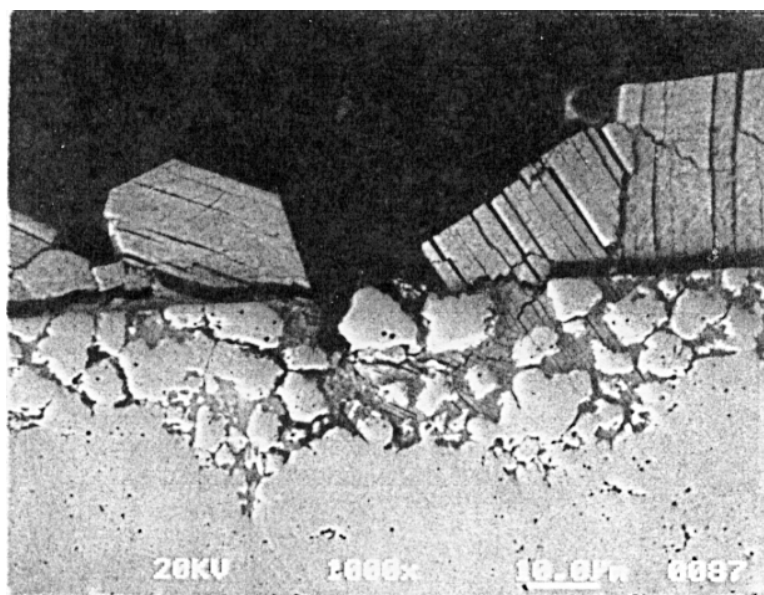
(b)

Figure 2.1.3.5-1   **Scanning electron photomicrographs of cross-sectioned corroded UO$_2$ pellet samples:**

(a) Open porosity resulting from penetrative intergrannular corrosion along pellet sides from the 3.5-yr sample. Surface phase (gray color) is dehydrated schoepite. (b) Precipitation of compreignacide on top surface of the 8-yr sample. Note the continuation of crystal delamination planes into the open porous region of the sample and the encapsulation of the residual UO$_{2+x}$ surface grains by the alteration phases.

Uranium-release rates vary, as determined using unfiltered solutions from the 2- to 10-yr period, but were generally between 0.1 and 0.3 mg/m^2·day. An analysis of the size-fractioned release patterns during this period indicates that the majority (86 to 97%) of the released

uranium was sorbed or precipitated on the walls of the stainless-steel test vessel and the Teflon™ support stand. Between 1 and 12% (U) was present as >5 nm-sized particles suspended in the leachate, whereas less than 2% of the total uranium passed through a filter with a 5-nm pore size. This latter fraction corresponds to a uranium concentration of 4×10^{-6} M in the leachate at the bottom of the test vessel.

An SEM examination of the cross-sectioned samples indicated that the vast majority of the uranium released from the dissolving samples was deposited on the surface of the UO$_2$ pellets and Zircaloy™ cladding as alteration phases. The quantity of uranium incorporated in these phases was calculated by estimating the volume of material precipitated on the sample surface, the relative proportions of each alteration phase, and the molar proportion of uranium contained in each alteration phase and multiplying the calculated volume of each alteration phase by its respective density. Preliminary calculations for sample PMP8U-2 (Table 2.1.3.5-9), which reacted for 8 yr, indicate that ~80 mg of uranium was incorporated into the alteration phases deposited on the sample or Zircaloy™ surfaces, an amount that far exceeds the 5 mg released (as recovered in the acid strip component).

2.1.3.5 Dissolution Radionuclide Release from UO$_2$ Fuel

Table 2.1.3.5-7   Total uranium release in unsaturated tests with UO$_2$ samples[a] [LL980710651021.049]

Elapsed Time (wks)	Sample #1 Sol. Vol. (mL)	Sample #1 U Release (μg)	Sample #1 Cum. U Release (μg)	Sample #2 Sol. Vol. (mL)	Sample #2 U Release (μg)	Sample #2 Cum. U Release (μg)	Sample #3 Sol. Vol. (mL)	Sample #3 U Release (μg)	Sample #3 Cum. U Release (μg)	Sample #4 Sol. Vol. (mL)	Sample #4 U Release (μg)	Sample #4 Cum. U Release (μg)
8.0	0.84	26.2	26.2	0.81	11	11	0.78	0.28	0.28	0.81	2.7	2.7
13.0	0.19	21.6	47.8	0.64	25.7	36.7	0.58	5.88	6.16	0.64	7.7	10.4
19.6	0.77	449	497	1.01	388	425	0.79	71.3	77.5	0.83	9.2	19.6
26.0	0.78	264	761	0.93	201	626	0.78	126	204	0.81	9.7	29.3
32.6	0.67	129	890	0.81	56.2	682	0.75	88.8	293	0.75	193	222
39.0	0.64	74.5	965	0.83	38.3	721	0.82	31.1	324	0.81	113	336
45.6	0.66	1001	1966	0.66	46.9	768	0.85	195	518	0.63	624	959
52.0	0.74	2159	4125	0.80	1446	2214	0.83	131	649	0.25	967	1927
78.0	3.21	274	4398	2.63	1494	3708	3.42	266	915	1.57	1401	3328
105	3.03	168	4566	3.40	105	3812	3.31	139	1053			
134	3.29	145	4711	3.65	69.6	3882	3.52	50.8	1104	Terminated after		
157	2.58	124	4836	3.22	174	4056	3.06	287	1391	78 weeks		
183	2.77	164	4999	3.41	73.9	4130	3.26	172	1563			
211				2.09	193	4323	3.32	250	1813			
238	Terminated after			1.87	71.6	4394	2.38	97.7	1911			
291	183 weeks			5.43	38.1	4432	6.14	106	2017			
358				6.70	266	4698	8.15	424	2441			
417				4.47	325	5023	5.88	301	2742			
469							4.24	298	3040			
521				Terminated after			3.54	288	3328			
				417 weeks			Ongoing					
Drip Rate	0.075 mL/3.5 days			0.075 mL/3.5 days			0.075 mL/3.5 days			0.075 mL/3.5 days		
Configuration	11 disks			11 disks			Crushed UO$_2$			Crushed UO$_2$		
Sample Wt (g)	29.52			29.17			19.86			18.26		
Sample SA (m^2)	40.7			40.6			486			467		
Sample Vol. (m^3)	2.83			2.80			2.21			2.14		

Elapsed Time (wks)	Sample #1			Sample #2			Sample #3			Sample #4		
	Sol. Vol. (mL)	U Release (μg)	Cum. U Release (μg)	Sol. Vol. (mL)	U Release (μg)	Cum. U Release (μg)	Sol. Vol. (mL)	U Release (μg)	Cum. U Release (μg)	Sol. Vol. (mL)	U Release (μg)	Cum. U Release (μg)
8.0	0.75	2.85	2.85	0.87	2.61	2.61						
13.0	0.58	1.22	4.07	0.66	2.95	5.56	0.30	1.06	1.06	0.35	0.88	0.88
19.6	0.85	109	113	0.78	30.4	36.0						
26.0	0.76	36.1	150	0.77	41.9	77.9	0.67	302	303	0.51	525	526
32.6	0.77	33.8	183	0.70	799	876						
39.0	0.77	19.4	203	0.76	1391	2267		95.3	398	0.34	247	772
45.6	1.07	322	524	0.43	55.7	2323						
52.0	0.92	72.7	597	0.22	593	2916	0.39	665	1063	0.63	264	1036
78.0	3.62	103	700	2.95	3710	6626	0.72	1075	2138	0.78	5948	6984
105	3.41	47.8	748	3.14	389	7015	0.52	225	2363	0.37	2107	9091
134	3.35	69.3	817				0.13	79.3	2442	0.51	10324	19415
157	1.54	58.2	876	6.52	450	7465	0.64	113	2555			
183	1.24	31.1	907	3.48	85.0	7550	1.05	106	2661	Terminated after		
211				1.16	424	7974	2.53	110	2771	117 Weeks		
238	Terminated after			2.37	56.0	8030	0.61	11.9	2783			
291	183 weeks			6.09	76.2	8106	1.50	14.4	2797			
358				7.79	97.0	8203	2.28	42.8	2840			
417				5.98	162.0	8365	1.88	56.8	2897			
469				4.80	198.0	8562	1.58	159.0	3056			
521				4.06	356	8918 Ongoing	1.31	57.6	3114 Ongoing			
Drip Rate	0.075 mL/3.5 days			0.075 mL/3.5 days			0.0375 mL/7 days			0.0375 mL/7 days		
Configuration	3 Pellets			3 Pellets			3 Pellets			3 Pellets		
Sample Wt (g)	47.96			48.36			47.60			47.77		
Sample SA (m²)	22.1			22.2			21.9			22.1		
Sample Vol. (m³)	4.54			4.58			4.48			4.54		

[a] Values represent total uranium released from sample, excluding portion that reprecipitates on the UO$_2$-Zircaloy™ assembly. Solution volumes determined by weight differences measured between the beginning and the end of each sampling period. Terminated and ongoing tests are indicated. Blanks indicate no analysis performed. Horizontal bars separate per annum intervals. Water-injection schedule and sample configuration explained in the text. All experiments were conducted at 90°C. Uranium determinations made from collected and acid strip solution of the test vessels.

Table 2.1.3.5-8   Normalized release rate for UO$_2$ samples in unsaturated tests [LL980710651021.049]

	Pellet Surface Area (m^2)	Normalized Periodic Release (mg/m^2/day)	Sampling Period (weeks)	Normalized Cumulative Release (mg/m^2/day)	Elapsed Time (weeks)		Pellet Surface Area (m^2)	Normalized Periodic Release (mg/m^2/day)	Sampling Period (weeks)	Normalized Cumulative Release (mg/m^2/day)	Elapsed Time (weeks)
PMP8U-1	0.00407	0.11515	8.0	0.11515	8.0	PMP8U-3	0.0486	0.00010	8.0	0.00010	8.0
		0.15133	5.0	0.12907	13.0			0.00345	5.0	0.00139	13.0
		2.39978	6.6	0.89150	19.6			0.03190	6.6	0.01163	19.6
		1.43969	6.4	1.02704	26.0			0.05775	6.4	0.02304	26.0
		0.69075	6.6	0.95919	32.6			0.03974	6.6	0.02641	32.6
		0.40672	6.4	0.86812	39.0			0.01424	6.4	0.02440	39.0
		5.34723	6.6	1.51401	45.6			0.08706	6.6	0.03344	45.6
		11.79066	6.4	2.78448	52.0			0.05976	6.4	0.03669	52.0
		0.36943	26.0	1.97946	78.0			0.03005	26.0	0.03488	78.0
		0.22085	26.7	1.53081	104.7			0.01525	26.7	0.02957	104.7
		0.17635	28.9	1.23819	133.6			0.00518	28.9	0.02430	133.6
		0.18940	23.0	1.08413	156.6			0.03672	23.0	0.02613	156.6
		0.22096	26.0	0.96120	182.6			0.01940	26.0	0.02517	182.6
								0.02624	28.0	0.02531	210.6
PMP8U-2	0.00406	0.04848	8.0	0.04848	8.0			0.01064	27.0	0.02364	237.6
		0.18103	5.0	0.09946	13.0			0.00588	53.0	0.02040	290.6
		2.07823	6.6	0.76386	19.6			0.01852	67.4	0.02005	357.9
		1.10180	6.4	0.84742	26.0			0.01490	59.6	0.01932	417.3
		0.30067	6.6	0.73711	32.6			0.01683	52.0	0.01904	469.3
		0.20958	6.4	0.65016	39.0			0.01627	52.0	0.01877	521.6
		0.25122	6.6	0.59263	45.6						
		7.91338	6.4	1.49767	52.0	PMP8U-4	0.0467	0.00103	8.0	0.00103	8.0
		2.02146	26.0	1.67227	78.0			0.00472	5.0	0.00245	13.0
		0.13801	26.7	1.28085	104.7			0.00428	6.6	0.00306	19.6
		0.08484	28.9	1.02246	133.6			0.00460	6.4	0.00344	26.0
		0.26617	23.0	0.91136	156.6			0.08988	6.6	0.02088	32.6
		0.10003	26.0	0.79582	182.6			0.05387	6.4	0.02632	39.0
		0.24244	28.0	0.72224	210.6			0.29037	6.6	0.06440	45.6
		0.09331	27.0	0.65076	237.6			0.46036	6.4	0.11335	52.0

Pellet Surface Area (m²)	Normalized Periodic Release (mg/m²/day)	Sampling Period (weeks)	Normalized Cumulative Release (mg/m²/day)	Elapsed Time (weeks)	Pellet Surface Area (m²)	Normalized Periodic Release (mg/m²/day)	Sampling Period (weeks)	Normalized Cumulative Release (mg/m²/day)	Elapsed Time (weeks)
	0.10003	26.0	0.79582	182.6		0.05387	6.4	0.02632	39.0
	0.24244	28.0	0.72224	210.6		0.29037	6.6	0.06440	45.6
	0.09331	27.0	0.65076	237.6		0.46036	6.4	0.11335	52.0
	0.02532	53.0	0.53668	290.6		0.16478	26.0	0.13049	78.0
	0.13910	67.4	0.46191	357.9					
	0.19262	59.6	0.42358	417.3					
PMP8U-5	0.02300	8.0	0.02300	8.0	PMP8U-7	0.00531	13.0	0.00531	13.0
0.00221	0.01579	5.0	0.02023	13.0	0.00219	1.51479	13.0	0.76005	26.0
	1.07652	6.6	0.37490	19.6		0.47826	13.0	0.66612	39.0
	0.36278	6.4	0.37190	26.0		3.33593	13.0	1.33357	52.0
	0.33216	6.6	0.36388	32.6		2.69632	26.0	1.78782	78.0
	0.19496	6.4	0.33604	39.0		0.54993	26.7	1.47201	104.7
	3.16443	6.6	0.74389	45.6		0.17935	28.9	1.19274	133.6
	0.73091	6.4	0.74229	52.0		0.32024	23.0	1.06458	156.6
	0.25635	26.0	0.58031	78.0		0.26570	26.0	0.95081	182.6
	0.11571	26.7	0.46178	104.7		0.25592	28.0	0.85841	210.6
	0.15513	28.9	0.39553	133.6		0.02882	27.0	0.76413	237.6
	0.16365	23.0	0.36147	156.6		0.01768	53.0	0.62797	290.6
	0.07739	26.0	0.32101	182.6		0.04146	67.4	0.51768	357.9
						0.06239	59.6	0.45286	417.3
PMP8U-6	0.02097	8.0	0.02097	8.0		0.19973	52.0	0.42481	469.3
0.00222	0.03793	5.0	0.02749	13.0		0.07223	52.0	0.38964	521.6
	0.29806	6.6	0.11834	19.6					
	0.41986	6.4	0.19289	26.0	PMP8U-8	0.00435	13.0	0.00435	13.0
	7.81982	6.6	1.73166	32.6	0.00221	2.61075	13.0	1.30755	26.0
	13.92192	6.4	3.74104	39.0		1.22607	13.0	1.28039	39.0
	0.54592	6.6	3.28030	45.6		1.31096	13.0	1.28803	52.0
	5.93649	6.4	3.60868	52.0		14.78857	26.0	5.78821	78.0
	9.18176	26.0	5.46637	78.0		5.09921	26.7	5.61244	104.7
	0.93702	26.7	4.31086	104.7		56.28545	11.9	10.76668	116.6
	0.55796	51.9	3.06788	156.6					

2.1.3.5 Dissolution Radionuclide Release from UO$_2$ Fuel

Pellet Surface Area (m^2)	Normalized Periodic Release (mg/m^2/day)	Sampling Period (weeks)	Normalized Cumulative Release (mg/m^2/day)	Elapsed Time (weeks)	Pellet Surface Area (m^2)	Normalized Periodic Release (mg/m^2/day)	Sampling Period (weeks)	Normalized Cumulative Release (mg/m^2/day)	Elapsed Time (weeks)
	0.21048	26.0	2.66096	182.6					
	0.97387	28.0	2.43663	210.6					
	0.13339	27.0	2.17486	237.6					
	0.09252	53.0	1.79505	290.6					
	0.09274	67.4	1.47492	357.9					
	0.17528	59.6	1.28991	417.3					
	0.24509	52.0	1.17413	469.3					
	0.44016	52.0	1.10091	521.6					

Pellet surface area determined by geometric calculation.

Table 2.1.3.5-9 Fractional distribution of uranium from unsaturated drip tests with UO_2 and spent fuel (values in mg and total percentage in parentheses) [LL980710651021.049]

Test	Acid Strip	Alteration Phases	Grain Boundary Corroded	Unaffected Region	Initial Sample Weight
8-yr UO_2	5.0 (0.02%)	80 (0.3%)	780 (3.0%)	24,844 (96.6%)	25,709
Spent fuel[a]	ND[c]	180 (2.3%)	All visible	None	8,000
Spent Fuel[b]	250 (acid strip + alteration phases) (3.1%)		ND	ND	8,000

[a] Fractions determined from measured cross-sections of alteration layers
[b] Fractions determined from Tc release
[c] ND = not determined

Reaction of UO_2 pellets occurs primarily along boundaries between the original press-sintered UO_2 grains. Most of the dissolved uranium reprecipitated into alteration products on the sample surfaces. A significant portion of the uranium was released as particulate matter. Both colloidal-sized uranyl silicates and UO_{2+x} particles were observed in the filtered residues from the tests. The observed alteration-phase paragenesis mimics that of natural uraninite alteration under oxidizing conditions (e.g., the Nopal I deposit in Mexico). Both the natural and experimental systems display the following mineral paragenetic sequence: $UO_2 \Rightarrow$ uranyl oxide hydrates $\Rightarrow$ alkali- and alkaline-earth uranyl oxide hydrates $\Rightarrow$ uranyl silicates $\Rightarrow$ alkali- and alkaline-earth uranyl silicates + palygorskite clay (Table 2.1.3.5-10).

The alkali- and alkaline-earth uranyl silicates appear to be the long-term solubility-limiting phases for uranium in the UO_2 tests and the uranium deposits at Nopal. This similarity suggests that the present experiments and the analogous reactions at Nopal may simulate the long-term reaction progress of spent UO_2 fuel following disposal at the proposed Yucca Mountain repository.

Table 2.1.3.5-10   Summary of UO_2 alteration phases [LL980710651021.049]

Uranyl-Oxide Hydrates	
Schoepite (meta-schoepite)	$UO_3 \cdot 2H_2O$
Dehydrated Schoepite	$UO_3 \cdot (0.8\text{-}1.0H_2O)$
Compreignacite	$(Na,K)_2[(UO_2)_6O_4(OH)_6] \cdot 8H_2O$
Becquerelite	$Ca[(UO_2)_6O_4(OH)_6] \cdot 8H_2O$
Uranyl Silicate Hydrate	
Soddyite	$(UO_2)_2SiO_4 \cdot 2H_2O$
Uranyl Alkaline Silicate Hydrates	
β-Uranophane	$Ca(UO_2)_2(SiO_3OH)_2(H_2O)_5$
Boltwoodite	$K_2(UO_2)(SiO_3OH)(H_2O)$

Uranyl Alkaline Silicate Hydrates (continued)	
Na-Boltwoodite	(Na,K)(UO$_2$)(SiO$_3$OH)(H$_2$O)
Sklodowskite	Mg(UO$_2$)$_2$(SiO$_3$OH)(H$_2$O)$_4$
Non-Uranyl Phases	
Palygorskite	(Mg,Al$_{0.12-0.66}$)$_5$(Si,Al$_{0.12-0.66}$)$_8$O$_{20}$ (OH)$_5$·4H$_2$O
Fe-Oxides	
Ti-Oxides	
Amorphouse Silica	

2.1.3.5.4.2 Spent Nuclear Fuel Reactions After 3.7 Years

Radionuclide Release from Spent Fuel

Samples of two pressurized-water-reactor fuels, ATM-103 (Guenther et al., 1988a) and ATM-106 (Guenther, 1988b), with burnups of 30 and 45 MWd/kg U, respectively, are used in these ongoing unsaturated drip tests with EJ-13 water at 90°C. See Finn et al. (1994) and Bates et al. (1995) for a detailed description of the experimental apparatus and conditions of the unsaturated drip tests. Alteration of the spent fuel was noted on a microscopic scale after 60 days of reaction and on a macroscopic scale after 748 days of reaction. During the almost three years of testing, concurrent release of radionuclides was also noted. The magnitude of the radionuclide release in these tests was a function of several parameters, including time. The following preliminary conclusions are drawn from release results for the first 581 days of reaction.

Congruent release of the radionuclides with ^{238}U was not noted during the first 581 days of reaction. An exception was the release of the transuranics ^{239}Pu, ^{237}Np, and ^{241}Am from the ATM-106 fuel. The ^{238}U release fractions were much lower than those for ^{99}Tc, ^{129}I, ^{90}Sr, and ^{137}Cs. Because there was, after 748 days of reaction, macroscopic evidence for the formation of alteration products, the release results may indicate that the fuel matrix dissolved congruently under the conditions of the test; however, because of the low water inventory in the drip tests, many of the radionuclides were reprecipitated on the fuel or on the Zircaloy™ fuel holder. Only those isotopes with very high solubilities in acidic solutions (the pHs in these tests) were found in the leachate collected in the test vessel.

The different release fractions observed for the different radioisotopes suggest that the four fission products (Cs, Sr, Tc, and I) were affected differently by the conditions in these tests. The possible parameters included water chemistry (e.g., acidic pH). The cumulative and 581-day-interval ^{90}Sr release fractions were comparable to the ^{137}Cs release fractions for both fuels. For the ATM-103 fuel, the ^{99}Tc release fractions were two orders of magnitude larger than the ^{137}Cs release fractions. These large ^{99}Tc release fractions may be associated with rapid aqueous oxidation and dissolution of this fuel. The cumulative ^{129}I release fractions were two orders of magnitude larger than the ^{137}Cs release fractions for both fuels. Release in the earlier reaction intervals, which had the highest ^{129}I release fractions, may be dominated by release from the gap and grain boundaries. Later release fractions may be dominated by release from the UO$_2$ matrix. The large fractional releases for ^{99}Tc may then reflect actual matrix dissolution under the conditions present in the unsaturated tests. These results would

suggest that uranium release fractions do not reflect matrix dissolution for low water-volume flow rates, which are typical of unsaturated testing conditions, nor the release fraction of highly soluble species. This observation may impact some of the assumptions made concerning the magnitude of the source term in performance assessment studies.

Colloidal species containing americium and plutonium have been found in the leachate of the drip tests. These results suggest that significant quantities of colloids can form and may provide a mode of transport for the transuranics. Therefore, the incorporation of colloidal transport in performance assessment models is needed to ensure that the models have conservative transport limits.

The total extent of the spent-fuel reaction is difficult to determine because the amount of material incorporated into precipitated alteration products or adsorbed on the Zircaloy™ holder or on the spent-fuel fragments has not been measured. However, the following terms are defined to aid in comparing and interpreting the data:

- "Interval release fraction" is the ratio of the sum for each test interval of the amount of radionuclide in the leachate and in the acid strip divided by the amount of radionuclide in the spent fuel sample.
- The "cumulative release fraction" is the sum of the individual interval release fractions.
- "Release rate" is the ratio of an interval release fraction divided by the days in the interval. (This definition assumes that all of the fuel surface area has reacted in a given time interval.)

The fractional release behavior of the radionuclides for high-drip rate, low-drip rate and vapor tests are listed in Tables 2.1.3.5-11 through 2.1.3.5-13 (Finn et al., 1996). Table 2.1.3.5-11 lists the interval-release fractions for the high-drip rate tests. Table 2.1.3.5-12 lists the cumulative release fractions after 1.6, 2.5, and 3.1 yr of reaction for the high-drip rate tests. Table 2.1.3.5-13 compares the cumulative release fractions for the high-drip, low-drip, and vapor tests at 1.6 and 2.5 yr, respectively, and the cumulative release fraction for a "semistatic" saturated test. These tables are similar to the later tables 2.1.3.5-16, 2.1.3.5-17, 2.1.3.5-19, and 2.1.3.5-20, which focus only on the release of the ε-phase constituents.

Table 2.1.3.5-11   Interval-release fractions for the high-drip-rate tests [LL980710651021.049]

Time (yr)	I-129	Tc-99	Mo-97	Sr-90	Cs-137	U-238	Pu-239
ATM-103							
0.2	8E-3	2E-3	1E-5	2E-3	5E-4	3E-5	4E-6
0.3	4E-3	3E-3	2E-4	7E-4	8E-4	2E-5	2E-6
0.7	7E-3	2E-3	9E-5	5E-5	2E-4	5E-6	1E-6
1.3	3E-4	7E-3	2E-4	1E-4	9E-5	9E-6	2E-6
1.6	3E-4	8E-3	1E-3	3E-5	2E-4	2E-5	3E-7
2.0	1E-4	1E-3	4E-4	4E-6	1E-4	2E-6	2E-8
2.5	2E-4	2E-3	3E-4	2E-5	1E-4	8E-7	1E-8
3.1	3E-4	5E-3	1E-2	1E-5	2E-3	3E-6	6E-7

2.1.3.5 Dissolution Radionuclide Release from UO$_2$ Fuel

Time (yr)	I-129	Tc-99	Mo-97	Sr-90	Cs-137	U-238	Pu-239
ATM-106							
0.2	2E-3	0	0	9E-8	3E-8	1E-9	3E-10
0.3	1E-2	1E-5	6E-6	5E-5	4E-5	2E-5	2E-5
ATM-106							
0.7	2E-2	1E-4	6E-4	4E-4	2E-3	2E-4	1E-4
1.3	2E-4	6E-5	9E-6	1E-5	1E-3	8E-6	8E-6
1.6	6E-4	1E-3	3E-4	3E-5	1E-4	1E-6	3E-8
2.0	4E-4	4E-3	9E-5	9E-6	3E-4	1E-7	8E-9
2.5	8E-4	4E-3	9E-5	8E-6	2E-4	3E-7	4E-8
3.1	6E-4	8E-3	8E-4	5E-6	6E-4	3E-7	2E-8

Table 2.1.3.5-12 Comparison of cumulative release fractions after 1.6, 2.5, and 3.1 yr reaction—high-drip-rate tests [LL980710651021.049]

	I-129	Tc-99	Mo-97	Sr-90	Cs-137	U-238	Pu-239
1.6 Yr Reaction							
ATM-103	2e-2	2e-2	2e-3	3e-3	2e-3	9E-5	1E-5
ATM-106	4E-2	2e-3	8e-4	5e-4	3e-3	2E-4	1E-4
2.5 Yr Reaction							
ATM-103	2e-2	2e-2	3e-3	3e-3	2e-3	9E-5	1E-5
ATM-106	4e-2	1e-2	1e-3	5e-4	3e-3	2E-4	1E-4
3.1 Yr Reaction							
ATM-103	2e-2	3e-2	1e-2	3e-3	4e-3	9E-5	1E-5
ATM-106	4e-2	2e-2	2e-3	5e-4	4e-3	2E-4	1E-4

Table 2.1.3.5-13 Comparison of cumulative release fractions[a] for high-drip, low-drip, and vapor tests after 1.6 and 2.5 years of reaction and those for "semistatic" tests [LL980710651021.049]

	High Drip		Low Drip		Vapor		Semistatic[c]	
Reaction Time: 1.6 yr[b]								
Fuel ATM#	103	106	103	106	103	106	TP	101
[99]Tc	2E-2	2E-3	9E-5	9E-5	2E-6	8E-7	5E-4	2E-4
[137]Cs	2E-3	3E-3	2E-5	1E-6	1E-7	4E-6	5E-3	1E-2
[238]U	9E-5	2E-4	4E-6	2E-5	6E-8	4E-7	1E-4	1E-4
[239]Pu	1E-5	1E-4	2E-5	2E-5	2E-7	3E-7	1E-4	1E-4
[237]Np	1E-3	1E-4	4E-5	5E-5	7E-7	5E-7	1E-4	1E-4
[241]Am	3E-3	3E-4	4E-4	1E-4	3E-6	6E-7	1E-4	2E-4

	High Drip		Low Drip		Vapor	
Reaction Time: 2.5 yr						
Fuel	**103**	**106**	**103**	**106**	**103**	**106**
^{99}Tc	2E-2	1E-2	1E-4	1E-4	6E-5	2E-6
^{137}Cs	2E-3	3E-3	2E-5	3E-6	1E-6	4E-6
^{238}U	9E-5	2E-4	4E-6	2E-5	5E-7	4E-7
^{239}Pu	1E-5	1E-4	2E-5	2E-5	9E-7	3E-7
^{237}Np	1E-3	1E-4	4E-5	5E-5	1E-6	5E-7
^{241}Am	3E-3	3E-4	4E-4	1E-4	4E-6	6E-7

a   The error bars for ^{137}Cs are ± 0.5% and are ±50% for the actinides.
b   A reaction time of 1.6 yr is comparable to the total length of Wilson's tests.
c   Three cycles (460 d) at 85°C for Turkey Point (TP) fuel, 27 (MWd)/kg U, and a fission
     gas release of 0.3%; and two cycles (360 d) for ATM-101 fuel, 30 (MWd)/kg U, and a
     fission gas release of 0.2% (Wilson and Gray, 1990)

Corrosion of the ε-Phase

Particles of corroded spent fuel from the ATM-103 test were selected for analysis with electron microscopy (Finn et al., 1997). Several interesting features were observed in this sample. Particles of a molybdenum-technetium-ruthenium (Mo-Tc-Ru) phase (ε-phase) were found within the spent-fuel grain. The particles were extremely small: approximately 20–50 nm in diameter. Some appeared weathered; on the whole, however, they appeared uniform. The composition of many of the particles did not match that reported by Thomas et al. (Thomas and Guenther, 1989; Thomas and Charlot, 1990; Thomas et al., 1992) during analytical electron microscopy (AEM) characterization of the ATM-103. Quantitative analysis by Thomas et al. (Thomas and Guenther, 1989; Thomas and Charlot, 1990; Thomas et al., 1992) of the transition metals in the ε-particles agreed with the fission product ratio for these elements in ATM-103. This result supports the contention that all the transition metals partition to the ε-phases. The Tc and Mo appeared suppressed relative to Ru and Pd, suggesting that the phases may have reacted.

Two types of ε-ruthenium phase were found in the fuel; this, again, is consistent with the work of Thomas et al. (Thomas and Guenther 1989; Thomas and Charlot, 1990; Thomas et al., 1992) (see Table 2.1.3.5-14); however, the palladium (Pd)-rich phase may be described as α-Pd(Ru,Rh) phase based on tertiary plots by (Kleykamp et al., 1985). The ε-ruthenium phase is the accepted transition metal phase described by Thomas and Guenther (1989). The ratio of Mo/(Ru+Pd) has been used to allow comparison of all particles observed. This ratio is one in uncorroded ATM-103 calculated using the ORIGEN-2 code. Thomas and Guenther have also obtained this value in their analyses. In the particles found in the vapor test exposed to a corroding environment for 49 mos, this ratio was found to be much lower for many of the analyzed particles. However, in comparison to the particles found in the ATM-103 high-drip test, ε-ruthenium phases retained more Mo in the vapor tests (see Table 2.1.3.5-18). This indicates that the 4d-metal phases examined exhibited preferential removal of Mo during the corrosion tests. This partial corrosion of the ε-phases may provide some insight into the local oxidative conditions. The observed behavior is in agreement with the relative nobility of the 4d metals.

For comparison of quantification methods, results from Thomas and Charlot (1990) and from the ATM-103 high-drip test fuel fragments are shown in Table 2.1.3.5-15. Thomas and Charlot (1990) performed semi-quantitative energy-dispersive spectroscopy (EDS) analyses of transition metals in the ε-phases. Table 2.1.3.5-15 also presents recent quantification of ε-phases with electron-energy-loss spectroscopy (EELS) and EDS. In the high-drip sample, it was more difficult to find evidence of corrosion of ε-ruthenium phases because all appeared to be equally modified from the more typical composition. The "Pu-rich region" in Table 2.1.3.5-15 refers to a region in the ATM-103 fuel that had higher levels of Pu than did most other portions of the fuel.

Evidence for the partial corrosion of the ε-phase supports the use of Tc as a marker element for spent-fuel dissolution. However, there are still questions regarding the role of intra- and intergranular ε-particles. Further analysis of thin sections of corroded fuel will be necessary to understand the possible differences.

Table 2.1.3.5-14   Composition of ε-phase (elements in wt%) ATM-103 vapor hydration results [LL980710551022.012]

Element	Calculated[a]	Pd-Rich Particles			
Mo	44	29	30	30	
Tc	11	9	12	11	
Ru	28	40	30	30	
Rh	—	—	—	—	—
Pd	17	22	28	28	~100
Mo/(Ru+Pd)	0.98	0.47	0.51	0.52	—
		Ru-Rich Particles			
Mo		29	26	33	27
Tc		17	15	12	0
Ru		33	42	55	73
Rh		—	—		—
Pd		22	17		—
Mo/(Ru+Pd)		0.53	0.44	0.60	0.36

[a]   Calculated from Guenther et al. (1989) in ATM-103 and normalized without Rh
[b]   Pd not analyzed in this case.

Table 2.1.3.5-15   Composition of ε-phase (elements in wt%) ATM-103 high-drip results [LL980710551022.012]

Element	Calculated[a]	Unreacted Phase[b]	Edge Region	Pit Region	Pu-Rich Region[c]
Mo	41.2	40	12.3	16.6	15.2
Tc	9.6	10	5.0	10.1	3.9
Ru	27.5	25	41.7	44.8	45.1
Rh	5.5	10	7.5	17.6	9.8
Pd	16.0	15	32.6	10.8	26.1
Mo/(Pd+Ru)	0.95	1.0	0.16	0.30	0.21

[a]   Calculated from Guenther et al. (1989) from ORIGEN2 code for 30 MWd/kgM at 15 yr
[b]   Semiquantitative EDS analysis by Thomas and Charlot (1990)
[c]   Quantification of EELS was performed using a 100 eV window and the oscillator strength values calculated from a Dirac-Foch model by Ahn et al. (1989).

This section examines the reaction of the ε-phase in high-drip-rate tests in the leachate for the first 3.1 yr of reaction. Table 2.1.3.5-16 provides a summary of the release behavior of the five elements in the ε-phase (Tc, Mo, Ru, Rh, and Pd) for tests with ATM-103 for successive reaction intervals. Similar information for the ATM-106 test is shown in Table 2.1.3.5-17. The information includes the following:

- Released mass (μg) for the isotope of each element with minimal interference from other elements
- Total released mass of each element, based on the isotope measured and the element's isotopic distribution
- Calculated mass of elements from the ε-phases that reacted, based on the ⁹⁹Tc release and the distribution of each element in the ε-phase
- Amount of each element that was not released, based on the difference between the material released (column 2) and that calculated to have reacted (column 3)

The isotope ⁹⁹Tc was the dominant element released from ATM-103 and ATM-106 at each reaction interval. Ten percent of the Mo and only trace amounts of Rh, Ru, and Pd were detected in the leachate.

Microtomed samples of reacted fuel were examined to determine if ε-phase particles (Ru-Mo-Tc-Rh-Pd) were being oxidized as proposed (Finn et al., 1996). Table 2.1.3.5-18, as a superset of Table 2.1.3.5-15, shows the distribution of the five elements in unreacted fuel and the ratio Mo/(Ru+Pd), which can range from 0.9 to 1.5, depending on fission yield or the (Guenther et al., 1988a) distribution found in unreacted fuel (Guenther, 1988b). To determine if the ε-phase particles had reacted in both the ATM-103 high-drip-rate and the vapor tests, the Mo/(Ru+Pd) mass ratio was measured in reacted particles, as was the change in the relative masses of the five elements in the ε-phase particles.

In Table 2.1.3.5-19, the cumulative release fractions for ⁹⁹Tc, ²³⁸U, and ²³⁹Pu, as well as for ¹³⁷Cs and ⁹⁷Mo, are shown for several cumulative reaction times. Table 2.1.3.5-19 illustrates the following points:

- After 3.7 yr of reaction, the cumulative ⁹⁹Tc release fractions for the two fuels are similar: 3% of the total inventory for ATM-103 and 2% for ATM-106.

- For the ATM-103 fuel, the ^{97}Mo cumulative release fraction after 3.7 yr of reaction is similar to the ^{99}Tc cumulative release fraction; however, for the ATM-106 fuel, the ^{97}Mo release fraction is only 10% of the ^{99}Tc release fraction. Thus, some of the Mo appears to be held up in the ATM-106 test; however, at 4.1 yr of reaction, the Mo and Tc release fractions appear comparable (data analysis is still in progress).

- The ^{137}Cs cumulative release fractions for the two fuels are similar, but are only 10-20% of the cumulative ^{99}Tc release fraction. It appears that most ^{137}Cs is held up. An alteration product that can incorporate both Cs and Mo is $(Cs_{0.9}Ba_{0.55})[(UO_2)_5(MoO_2)O_4(OH)_6] \cdot 6H_2O$ (Buck et al., 1997). The formation of this alteration product could account for the hold up of ^{137}Cs and Mo relative to ^{99}Tc, especially in the ATM-106 test prior to 4.1 yr of reaction.

- Prior to the first 1.6 yr of reaction, both fuels had a large ^{238}U release fraction; thereafter, most (99.9%) of the reacted uranium remained on the fuel surface in alteration products based on the difference in release fractions between ^{99}Tc and U, the visual appearance of the fuel, and the weight gain measured.

- Prior to the first 1.6 yr of reaction, both fuels had a ^{239}Pu release fraction that was equivalent to 10–40% of the U release fraction. At longer reaction times, most of the Pu was held up.

The reaction suggested by the leachate data for both fuels is one in which there is a continuous release of ^{99}Tc over 4 yr of reaction, which consists of at least 0.3% of the total inventory in each 6-mo interval. The U release effectively ceases after about a year, but uranium is incorporated into alteration products that form on the surface of the fuel. Alteration-phase formation increases after 1.6 yr of reaction, but the ^{99}Tc release does not increase. The ^{99}Tc release fraction can be used to calculate the uranium release fraction and, thus, the mass of uranium that has reacted. This value can be compared to the amount of sodium and silicon removed from the dripped EJ-13 water. In addition, the mass gain for the reacted spent fuel can be compared to the expected increase in mass due to the formation of alteration products. These data are summarized in Table 2.1.3.5-20 for the two fuels after 3.1 yr of reaction. (Units of moles are used for simplicity in comparing the different elements.)

In Table 2.1.3.5-21, the cumulative release fractions for ^{99}Tc, ^{97}Mo, ^{137}Cs, ^{238}U, and ^{239}Pu for the ATM-106 low-drip-rate test after 2.5 yr of reaction and 3.1 yr of reaction are compared. At the longer time, the fuel fragments were immersed in EJ-13 for 10 min to determine if reaction had occurred but insufficient liquid were present for transport of the released radionuclides. After immersion, the ^{99}Tc release fraction increased two orders of magnitude, yielding a total release of ~1%, which is comparable to the cumulative release in the high-drip-rate test after 3.7 yr of 3%. Nearly all of the ^{99}Tc release after immersion (93%) is in the leachate, as is most of the ^{97}Mo release. From 90 to 100% of the ^{137}Cs, ^{238}U, and ^{239}Pu release in the 3.1-yr interval is sorbed on the stainless steel. The sorption behavior on stainless steel is not surprising for the actinides, but was not expected for cesium.

The large fractional release after a short immersion in EJ-13 suggests that the fraction of fuel reacted is underrepresented by the ^{99}Tc release in the low-drip-rate tests and that most of the reacted radionuclides are present on the fuel surface. If this hypothesis is true, a potential exists for large radionuclide bursts during episodic water flow if fracture flow occurs after a large portion of the spent fuel has reacted with low volumes of standing water or with water vapor for extended periods. This is different than with the normal steady-state film flow.

The fission product Tc, owing to its high solubility and general tendency not to become incorporated into alteration phases, is being used as a marker element for calculating the corrosion rate of spent nuclear fuel in the ongoing drip tests. Based on the preceding discussion, the Tc marker may be appropriate, at least for low-burnup fuels. However, previous studies have suggested that the ε-phase is highly insoluble and that, therefore, the observed leached Tc must originate from grain-boundary regions in the fuel.

Fission product segregation and precipitation in low burnup light-water reactor (LWR) fuels can only be effectively studied with AEM because these features, which are characteristic of these types of spent nuclear fuel, can only be probed with a high-spatial–resolution instrument. As limited transport of fission products occurred in the fuel, the features observed in one series of spent nuclear fuel grains are most likely representative of the entire material.

Table 2.1.3.5-16   Disposition of elements in ε-phase for selected reactive intervals—ATM-103 high-drip-rate test [LL980710551022.012]

Isotope	Measured[a] Released Element[b] (µg)	Calculated Released Element[c] (µg)	Calculated Amount Reacted (µg)	Element[d] Retained (mass %)
0.3-Yr Reaction				
^{99}Tc	20	20	20	—
^{97}Mo	0.9	4	50	93
^{101}Ru	0.02	0.07	50	100
^{103}Rh	0.6	0.6	7	92
^{105}Pd	0.04	0.1	0.5	75
0.8-Yr Reaction				
^{99}Tc	10	10	10	—
^{97}Mo	0.05	2	30	94
^{101}Ru	6E-5	2E-4	40	100
^{103}Rh	0.06	0.06	5	99
^{105}Pd	ND[e]	ND	0.3	100
1.6-Yr Reaction				
^{99}Tc	40	40	40	—
^{97}Mo	8	30	100	77
^{101}Ru	2E-3	7E-3	200	100
^{103}Rh	0.02	0.02	20	100
^{105}Pd	2E-3	9E-3	1	100
2.1-Yr Reaction				
^{99}Tc	5	5	5	—
^{97}Mo	2	10	20	44
^{101}Ru	8E-5	2E-4	20	100
^{103}Rh	7E-3	7E-3	3	100
^{105}Pd	8E-3	0.03	0.2	83

2.1.3.5 Dissolution Radionuclide Release from UO_2 Fuel

Isotope	Measured[a] Released Element[b] (μg)	Calculated Released Element[c] (μg)	Calculated Amount Reacted (μg)	Element[d] Retained (mass %)
2.5-Yr Reaction				
^{99}Tc	10	10	10	—
^{97}Mo	1	6	30	82
^{101}Ru	6E-4	2E-3	30	100
^{103}Rh	0.02	0.02	5	100
^{105}Pd	5E-3	0.02	0.3	94

a   Measured mass in leachate. Values were rounded to one significant figure.
b   The isotopic distribution for each element and the mass of the measured isotope were used to determine the total mass released.

c   For ATM-103, the wt%s in the ε-phase are (Guenther, 1998a): Tc(11.8); Mo(39.9); Ru(42.3); Rh(5.6); Pd(0.4). The released ^{99}Tc was the basis for the reacted amount of a given element.

d   This is the minimum amount retained and is based on ^{99}Tc and its wt% in the ε-phase.
e   ND = not detected

Table 2.1.3.5-17   Disposition of elements in ε-phase for selected reactive intervals—ATM-106 high-drip–rate test [LL980710551022.012]

Isotope	Measured[a] Released Element[b] (μg)	Calculated Released Element[c] (μg)	Calculated Amount Reacted (μg)	Element[d] Retained (mass %)
0.3 Yr Reaction				
^{99}Tc	0.07	0.07	0.07	—
^{97}Mo	0.05	0.2	0.2	4
^{101}Ru	0.03	0.1	0.2	50
^{103}Rh	0.1	0.1	0.04	Xs[e]
^{105}Pd	0.04	0.2	0.1	XS
0.8 Yr Reaction				
^{99}Tc	0.9	0.9	0.9	—
^{97}Mo	4	20	3	XS
^{101}Ru	0.02	0.05	3	83
^{103}Rh	0.02	0.02	0.4	50
^{105}Pd	ND[f]	ND	2	100
1.3 Yr Reaction				
^{99}Tc	0.4	0.4	0.4	—
^{97}Mo	0.08	0.3	1	70
^{101}Ru	8E-3	0.03	1	97
^{103}Rh	0.03	0.03	0.2	85
^{105}Pd	0.03	0.1	0.8	87

Isotope	Measured[a] Released Element[b] (μg)	Calculated Released Element[c] (μg)	Calculated Amount Reacted (μg)	Element[d] Retained (mass %)
1.6 Yr Reaction				
^{99}Tc	10	10	10	—
^{97}Mo	2	9	40	77
^{101}Ru	6E-4	2E-3	30	100
^{103}Rh	4E-3	4E-3	5	100
^{105}Pd	ND	ND	20	100
2.1 Yr Reaction				
^{99}Tc	30	30	30	—
^{97}Mo	0.07	3	105	97
^{101}Ru	1E-3	3E-3	90	100
^{103}Rh	6E-3	6E-3	15	100
^{105}Pd	3E-3	0.01	60	100
2.5 Yr Reaction				
^{99}Tc	30	30	30	—
^{97}Mo	0.07	3	105	100
2.5 Yr Reaction				
^{101}Ru	1E-4	3E-4	90	100
^{103}Rh	0.01	0.01	15	100
^{105}Pd	5E-3	0.02	60	100

a   Measured mass in leachate. Values were rounded to one significant figure.

b   The isotopic distribution for each element and the mass of the isotope that was measured were used to determine the total mass released.

c   The wt% for ATM-106 (Thomas et al., 1992) for the ε-phase were: Tc(10); Mo(35); Ru(30); Rh(5); Pd(20). The released ^{99}Tc mass was the basis for the amount of a given element that reacted.

d   This is the minimum amount retained and is based on ^{99}Tc and its wt% in the ε-phase.

e   XS = excess measured

f   ND = not detected

Table 2.1.3.5-18 Composition of reacted ε-phase particles in ATM-103 tests (elements in wt%) [LL980710551022.012]

Unreacted Particles			
Element	Fission Yield	Grain Boundary (Guenther et al., 1988b)	Grain (I-1) (Guenther et al., 1988b)
Mo	40	39.9	52
Tc	10	11.8	8
Ru	30	42.3	23
Rh	5	5.6	6
Pd	15	0.4	12
Mo/(Ru+Pd)	0.9	0.9	1.5

2.1.3.5 Dissolution Radionuclide Release from UO$_2$ Fuel

High-Drip-Rate Test after 3.7 Years of Reaction			
Element	**Edge Region**	**Pit Region**	**Pu-Rich[b] Region**
Mo	12	17	15
Tc	5	10	4
Ru	42	45	45
Rh	8	18	10
Pd	33	11	26
Mo/(Ru+Pd)	0.2	0.3	0.2

Vapor Test after 4.1 Years of Reaction					
Element	**Sample 1**	**Sample 2**	**Sample 3**	**Sample 4**	**Sample 5**
Mo	29	30	30	29	26
Tc	9	12	11	17	15
Ru	40	30	30	33	42
Rh	—	—	—	—	—
Pd	22	28	28	22	17
Mo/(Ru+Pd)	0.5	0.5	0.5	0.5	0.4

a   This is the average distribution in the fuel.
b   Quantification of EELS was done using a 100 eV window and the oscillator strength values calculated from a Dirac-Foch model.

Table 2.1.3.5-19 Cumulative release fractions[a] for the high-drip–rate tests [LL980710551022.012]

Time (yr)	^{99}Tc	^{97}Mo	^{137}Cs	^{238}U	^{239}Pu
1.6 Yr of Reaction					
ATM-103	2.1E-2[b]	1.9E-3	1.8E-3	8.6E-5	9.8E-6
ATM-106	1.6E-3	8.5E-4	3.0E-3	1.8E-4	1.4E-4
2.5 Yr of Reaction					
ATM-103	2.4E-2	2.6E-3	2.0E-3	9.0E-5	9.9E-6
ATM-106	9.6E-3	1.0E-3	3.4E-3	1.8E-4	1.4E-4
3.1 Yr of Reaction					
ATM-103	2.9E-2	1.4E-2	3.7E-3	9.2E-5	1.0E-5
ATM-106	1.7E-2	8.E-3	4.0E-3	1.8E-4	1.4E-4
3.7 Yr of Reaction					
ATM-103	3.0E-2	1.6E-2	4.7E-3	9.3E-5	1.0E-5
ATM-106	2.0E-2	2.1E-3	5.0E-3	1.8E-4	1.4E-4

a   Cumulative release fractions have been rounded to two significant figures.
b   The unit E-2 is 1 x10^{-2}.

Table 2.1.3.5-20 High-drip–rate tests—alteration products after 3.1 yr of reaction [LL980710551022.012]

Species	Na-Boltwoodite[c] (mol)	Dehydrated Schoepite[d] (mol)	Excess[e] (mol)	Total (mol)	Calculated[a] Weight-UO_2 (g)	Measured[b] Weight Gain (g)
ATM-106					0.07	0.06
U	2.9E-4	6E-5	1E-4	4.5E-4		
Si	2.9E-4	—	—	2.9E-4		
Na	2.9E-4	—	6E-4	8.9E-4		
ATM-103					0.07	0.05
U	2.7E-4	2E-4	2.9E-4	8E-4		
Si	2.7E-4	—	—	2.7E-4		
Na	2.7E-4	—	5E-5	3.2E-4		

[a]   Difference between sum of masses of alteration products and the original fuel's UO_2

[b]   Difference between original fuel weight and that after 3.1 yr of reaction. The weight gain for the interval between 2.5 and 3.1 yr was estimated as the average over the previous 2.5 yr: 0.01 g/0.5 yr for ATM-106 and 0.007 g/0.5 yr for ATM-103. Weights when water was retained were not used.

[c]   Formula: $Na[(UO_2)(SiO_3OH)] \cdot H_2O$. This was the major alteration product from XRD; the silicon was assumed to be primarily in this product. The total moles of U are based on the ^{99}Tc release fraction.

[d]   Formula: $UO_3 \cdot 0.8\ H_2O$. This was identified in the vapor test.

[e]   The moles listed are the differences from the total moles. The excess may result from uncertainty in the analyses of Na and U in solution and U unaccounted for during solids analysis

Table 2.1.3.5-21 Release fractions for the ATM-106 low-drip–rate test after 3.1 yr of reaction and immersion for 10 min in EJ-13 [LL980710551022.012]

Radionuclide	Cumulative Interval		
	2.5 yr	3.1 yr	3.1 yr
^{99}Tc	1.0E-4	9.4E-3	9.4E-3
^{97}Mo	1.2E-4	1.1E-3	9.7E-4
^{137}Cs	3.3E-6	4.9E-4	4.9E-4
^{238}U	1.8E-5	1.6E-4	1.4E-4
^{239}Pu	2.4E-5	2.0E-4	1.8E-4

Evidence for Plutonium Segregation

During the AEM examination of corroded ATM-103 from both the vapor and high-drip tests, regions were found that possessed anomalously high concentrations of plutonium. The plutonium enrichment levels in these regions far exceeded those reported in the uncorroded fuels (Thomas and Guenther, 1989; Thomas and Charlot, 1990; Thomas et al., 1992). EDS indicated significant levels of Zr and Ru in this region. Zirconium is a fission product, and the fuel cladding is a zirconium alloy. Zirconium is also the major component in the sample retainer of the test apparatus. It is possible that reaction might occur at the fuel's edge where pellets are in contact with the Zr-bearing cladding. However, the levels of Pu in these regions are generally suppressed, owing to the high burnup. Also, these regions exhibit high levels of fission products such as rare earths. The EELS analysis indicated anomalously low

concentrations of rare earths. Therefore, the enriched Pu regions are most likely produced during oxidative corrosion. This may also suggest that Pu is not readily incorporated into uranyl phases. Burns et al. (1997) speculate that substitution of Pu^{6+} and Pu^{4+} for U^{6+} may occur in uranyl oxide hydrates and uranyl silicates.

Alteration Phases

Combined optical, SEM, EDS, and XRD examinations of samples taken from tests being performed on the two ATM fuels indicated that the rate at which groundwater contacts the fuel samples may be the most important single factor determining the alteration-phases that form as spent UO$_2$ fuel corrodes in a humid, oxidizing environment (Finn et al., 1997). The three tests (high-drip–rate, low-drip–rate, and vapor) show several similarities, including corroded grain boundaries, dissolution of fuel grains, and precipitation of U^{6+}-phases (Table 2.1.3.5-22). The vapor tests display the simplest assemblage of alteration products; only U and the radionuclides in the fuel dissolve into the thin film of water in contact with the fuel surfaces. The most abundant phase identified in the vapor tests is probably dehydrated schoepite, $(UO_2)O_{0.25-x}(OH)_{1.5+2x}$ ($0 \leq x \leq 0.15$).

The drip tests display more chemically complex alteration phases, owing to the interaction of the fuel with EJ-13 water (rather than water vapor only). The most abundant elements in EJ-13 water are Na and S; not surprisingly, the most abundant alteration products in the high-drip–rate tests are Na- and Si-bearing U^{6+} phases. Other U^{6+} phases are also present, including metaschoepite and β-uranophane, indicating the importance of additional minor phases and elements to the overall corrosion process.

An important observation at this stage is that the time-dependent evolution of the alteration-phase assemblage appears to be strongly dependent on the rate at which the EJ-13 water contacts the spent fuel. Fuel samples exposed to the higher drip-rates (nominally 10 times higher than that of the low-drip–rate tests) display a comparatively simple phase assemblage consisting of two uranophane-group silicates, β-uranophane and Na-boltwoodite (Table 2.1.3.5-22). In contrast, the sample from the low-drip–rate test displays a more complex alteration-phase assemblage, with four or five phases identified (Table 2.1.3.5-22). It is likely that the simpler phase assemblage in the high-drip–rate tests reflects higher overall reaction progress for the spent fuel in these tests. Also, samples from the first sampling periods were not taken, and it is possible that the early phases formed but were not detected.

Another important observation concerns the identification of uranyl oxy-hydroxides in the vapor-hydration tests. The precipitation of dehydrated schoepite and metaschoepite in these tests indicates that the film of water that forms on the fuel surface is sufficiently corrosive to dissolve the fuel and form a thin corrosion rind of alteration products. Such a water film is likely present in the drip tests as well during those intervals that EJ-13 water is not being dripped onto the fuel. It seems likely that the corrosion processes important in the vapor tests remain important in the drip tests. Dehydrated schoepite and/or metaschoepite may continue to form in the drip tests between water injections. If these phases are present when contacted by EJ-13 water, they may be at least as susceptible to dissolution and/or replacement as the unoxidized fuel. The degree to which this may be important is unknown at this time.

The mechanism by which the fuel has reacted during these tests is important, although there is only limited information available at this time. Most striking is that the fuel in the high-drip–rate test on sample ATM-103 has dissolved along a uniform front that has penetrated from the outer surface into the spent-fuel fragments. This "through-fragment"

dissolution has proceeded without regard to existing grain boundaries. The replacement of the fuel by Na-boltwoodite at the fuel surface may also be self-accelerating. Through-fragment dissolution appears to be an important mechanism by which the fuel is reacting in the high-drip–rate tests. Of course, the dissolution of the fuel along grain boundaries is also important in the high-drip–rate tests. This is especially evident from the extent to which the grain boundaries in one fragment of ATM-103 had been opened, resulting in a friable fragment that decomposed during sample handling.

Additional grains and fragments of reacted fuel are being examined to understand more fully the corrosion and alteration processes, including grain-boundary penetration by water, changes in the reactive surface area, and the distribution of radionuclides between the alteration phases and the EJ-13 water.

Table 2.1.3.5-22 Alteration Phases Identified by SEM or XRD from ATM Test Samples [LL980710551022.012]

Phase	Formula	Test
metaschoepite (?)	$UO_3 \cdot 2H_2O$ (?)	ATM-103 (LDR) ATM-103 (vapor) ATM-106 (vapor)
dehydrated schoepite	$(UO_2)O_{0.25-x}(OH)_{1.5+2x}$ ($0 \leq x \leq 0.15$)	ATM-103 (LDR) (?) ATM-103 (vapor) ATM-106 (vapor)
unidentified Na-UOH	$(Na,K)[(UO_2)_3O_2(OH)_3](H_2O)$ (?)	ATM-103 (LDR)
soddyite	$(UO_2)_2SiO_4(H_2O)_2$	ATM-103 (LDR)
β-uranophane	$Ca(UO_2)_2(SiO_3OH)_2(H_2O)_5$	ATM-103 (HDR)
Na-boltwoodite	$(Na,K)(UO_2)(SiO_3OH)(H_2O)$	ATM-103 (LDR) ATM-103 (HDR) ATM-106 (HDR)

(?) indicates a tentative identification or an uncertain formula
LDR = low-drip–rate test; HDR = high-drip–rate test

Two fragments of reacted spent fuel were examined by SEM: ATM-103 and ATM-106. Based on crystal morphology, chemical composition as determined by EDS and XRD, the most abundant alteration product of spent fuel after 3.7 yr of reaction is Na-boltwoodite, $(Na,K)(UO_2)(SiO_3OH)(H_2O)$. Additional minor phases have been detected by AEM and XRD analyses, the most abundant of which is β-uranophane, $Ca(UO_2)_2(SiO_3OH)_2(H_2O)_5$ (~10 vol.%); however, Na-boltwoodite makes up more than ~80 vol.% of the alteration products identified (a Cs-Mo-uranyl phase was found on the Zircaloy™ stand removed from the test vessel at 1.8 yr).

Figure 2.1.3.5-2 shows a cross-section through a fragment of the ATM-103 fuel. This is the only fragment studied as of July 1997, and final conclusions must be based on a representative number of fragments. Nevertheless, the SEM image shows the fuel (brightest region), in which the grain boundaries are readily visible. Gaps of approximately 0.5 μm or less are visible between the fuel grains. No alteration phases between the grain boundaries have been detected, and Si is not evident from EDS analyses at the grain boundaries; this indicates that dissolved Si is depleted in fluids penetrating the grain boundaries, possibly due to the formation of uranyl silicates on the outer surface of the fuel.

Surrounding the fuel is an alteration layer consisting of predominantly Na-boltwoodite. The thickness of the layer varies but is approximately 20–40 µm. This Na-boltwoodite layer consists of two regions that differ in appearance: a dense layer, approximately 10 µm thick closest to the fuel surface, and a much less dense outer layer, 10–30 µm thick. No difference in composition is evident between the two layers using EDS. Near the outer edge of the denser (inner) layer is an interface (arrow, Figure 2.1.3.5-2b) defined by a gap (dark band) that lies approximately 10 µm above the fuel surface and 2-3µm below the outer edge of the dense layer. Just below this interface, crystals of Na-boltwoodite have formed more or less perpendicular to the fuel surface; whereas, above this interface, Na-boltwoodite forms a dense mat of crystals subparallel to the fuel surface. Above these flat-lying crystals is the low-density outer layer. The inner, dense layer may represent a region where the spent fuel has been replaced isovolumetrically by the Na-boltwoodite, but this hypothesis requires verification. The different densities of the two layers are manifested as different colors under optical examination: the inner layer is dark yellow, and the outer layer is pale yellow to white. The inner layer is attached strongly to the adjacent fuel grains, whereas the outer layer is not.

Neptunium Incorporation in Alteration Phases

AEM analysis of the dehydrated schoepite with EELS indicates the presence of Np. Examinations of cross-sections of the corroded fuel grains and alteration products indicate that it is unlikely that the occurrence of Np is due to sorption on the dehydrated schoepite; however, this mechanism cannot be totally excluded for retention of Np in an alteration phase.

Np was observed with EELS in three samples of dehydrated schoepite that were taken from different regions of the corroded fuel pellets. The U:Np ratio was estimated to be between 1:0.003 and 1:0.006, based on 5 analyses. In the dehydrated schoepite (UO$_3$·0.8H$_2$O), where Np was detected, this ratio corresponds to one Np atom for every 250 unit cells of UO$_3$·0.8H$_2$O or about 550 ppm. The U:Np ratio in the ATM-103 fuel is 1:0.0005, taken from calculated values reported by Guenther et al. (Guenther, 1988b) for ATM 103 at 35 MWd/kgM after 15 yr. The estimated U:Np ratio in the alteration phase indicates that a large proportion of the Np has entered into the phase. Owing to the scarcity of water on the fuel surface in the vapor tests, only a small amount of water was able to flow into the steel collection vessel positioned at the bottom of the test apparatus. Under these conditions, it might be expected that the highly soluble elements would become concentrated enough in the thin film of water to precipitate secondary phases. The absence of Pu and Am in the dehydrated schoepite supports the contention that mainly Np and U were mobilized during the corrosion process and were incorporated into a secondary phase. There may be a suggestion of some Np in a uranyl silicate phase; however, the levels are at, or below, the detection limits for the instrument.

2.1.3.5.4.3 Discussion

The interface indicated in Figure 2.1.3.5-2b is interpreted as corresponding to the position of the surface of the original fuel fragment. Na-boltwoodite precipitated on the fuel surface, forming a mat of flat-lying crystals; as the fuel dissolved, Na-boltwoodite replaced the fuel as the surface dissolved. There is approximately a four-fold volume increase between cubic UO$_2$ and monoclinic Na-boltwoodite, so that (at most) one-quarter of the U in the replaced outer fuel layer is incorporated in the Na-boltwoodite within the replacement layer. The remaining three-quarters of the U was transported out of the replaced region, where much of it

precipitated as Na-boltwoodite making up the outer, less-dense layer. However, Na-boltwoodite is not sufficiently dense to contain all the U that was lost from the reacted layer. Based on an estimate of the density of the Na-boltwoodite depicted in Figure 2.1.3.5-2a, the outer layer probably contains only about one-half of the U lost from the reacted layer (i.e., ~38% of the reacted uranium). Some U is adsorbed on the vessel walls and is associated with the retainer, and there may be a build-up of alteration phases elsewhere in the test vessel.

There appears to have been extensive dissolution along grain boundaries, as evident from the friable nature of the fuel fragment when removed from the test vessel and from the wide gaps between grains (Figure 2.1.3.5-2) (the expansion of the gaps between grains is enhanced by the oxidation of UO$_2$ to UO$_{2.25}$, but this cannot account fully for the observed widths of the gaps). However, dissolution along grain boundaries appears to be limited compared to the "through-fragment" dissolution of the UO$_2$ fragments, as indicated by the lack of embayment at grain-boundaries (Figure 2.1.3.5-2). The replacement of the fuel proceeded uniformly inward from the original outer surface (arrow in Figure 2.1.3.5-2b) without regard to grain boundaries. Thus, the through-fragment dissolution of the UO$_2$ fuel matrix may predominate over grain-boundary–enhanced dissolution at this stage of reaction and has resulted in the replacement of spent fuel by (predominantly) Na-boltwoodite. Note, however, that the volume of fuel reacted along grain boundaries within the fuel grains may be quite large compared to a uniform ~10 μm-thick replacement layer (see subsequent text).
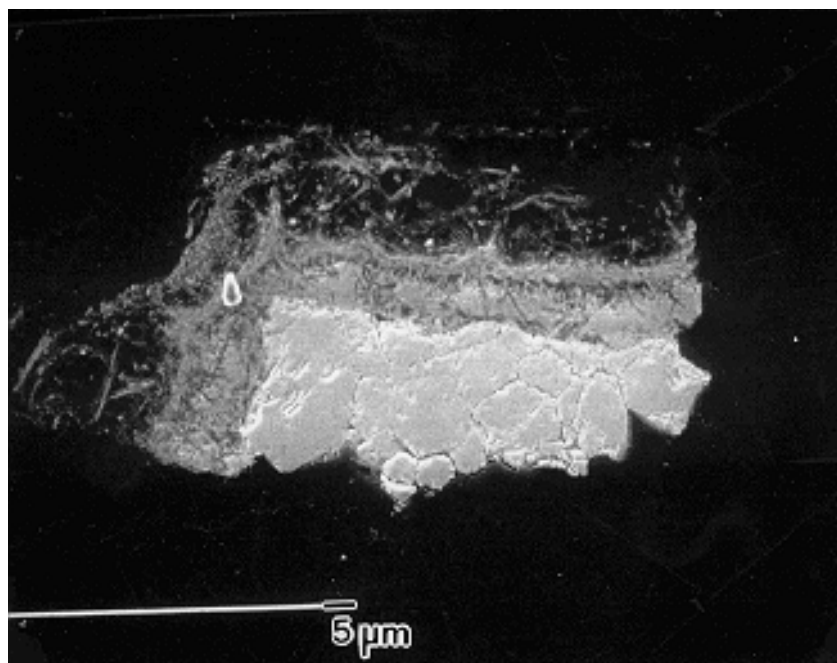
(a)
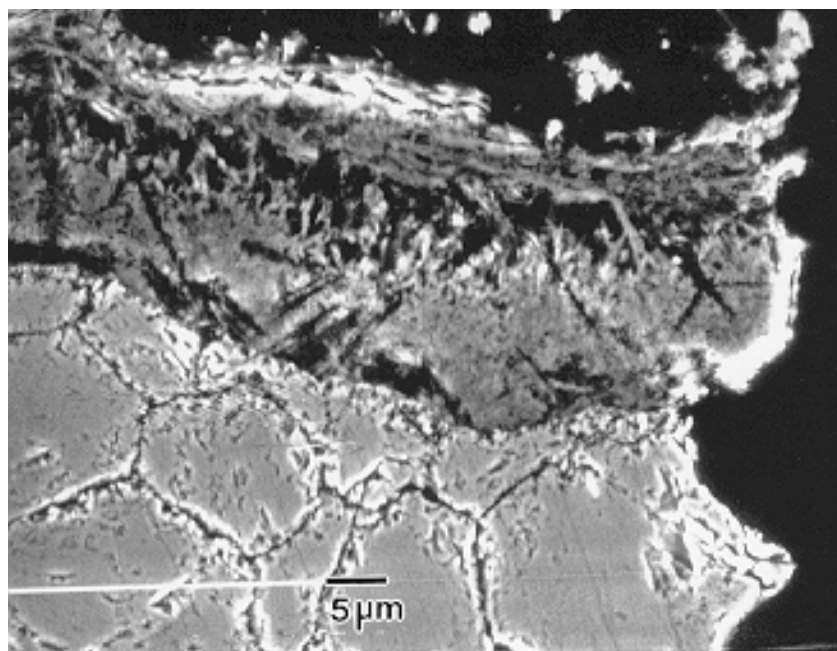
(b)

Figure 2.1.3.5-2   ATM-103 sample (HDR, 3.7 reaction) SEM micrographs of polished
section through the contact between fuel grains and corrosion rind:
(a) Particle showing both corrosion layers and the adjacent fuel grains;
(b) magnified view of particle shown in (a), illustrating details of the
dense inner layer of Na-boltwoodite.

The (simplified) reaction for the oxidative dissolution of the UO$_2$ fuel can be written as

$$UO_2 + 2H^+ + 1/2O_2 \Rightarrow UO_2^{2+} + H_2O \qquad\qquad 2.1.3.5\text{-}1$$

The precipitation of Na-boltwoodite is

$$UO_2^{2+} + H_4SiO_4 + Na^+ + H_2O \Rightarrow Na(UO_2)(SiO_3OH)(H_2O) + 3H^+ \qquad 2.1.3.5\text{-}2$$
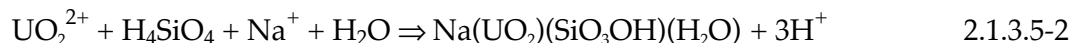
Thus the *net* reaction for the replacement of the UO$_2$ fuel by Na-boltwoodite is

$$UO_2 + H_4SiO_4 + Na^+ + 1/2O_2 \Rightarrow Na(UO_2)(SiO_3OH)(H_2O) + H^+ \qquad 2.1.3.5\text{-}3$$
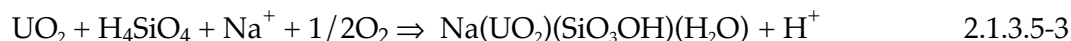
The last reaction (which is not an equilibrium expression) shows that, as Na- and Si-rich EJ-13 water is added to the system (i.e., to react with the UO$_2$ fuel) and/or H$^+$ is removed (due to flowing water and/or reaction with fuel via the first reaction), the replacement reaction proceeds to the right, provided that a sufficient supply of oxidants is available. In fact, an abundant supply of oxidants is likely available because of the effects of radiolysis and O$_2$ in the reaction vessel atmosphere.

2.1.3.5.4.4 Summary

The retention of fission products and actinides cannot be predicted quantitatively at this time without further examination of additional grains and fragments of reacted fuel to obtain a better understanding of the grain-boundary penetration and the increase of surface area and the distribution of radionuclides between reacted phases and solution. While these studies suggest that the alteration phases will incorporate a large proportion of the radionuclides that have been released from dissolved spent fuel and that such a process may act as a significant mechanism for retarding the migration of radionuclides from the WP, synergistic effects among the waste form, and parameters affecting its corrosion, and other components of the repository must be taken into account before using the present data in predicting the fate of radionuclides in a repository.

2.1.3.5.5 References

Ahn, C. C., D. H. Pearson, P. Rez, and B. Fultz (1989). "EELS white line intensities calculated for the 3d and 4d metals." In proceedings from 47th Annual Meeting of Electron Microscopy Society of America. G. W. Bailey (Ed.). pp. 388–389.

Bates, J. K., J. A. Fortner, P. A. Finn, D. J. Wronkiewicz, J. C. Hoh, J. W. Emery, E. C. Buck, and S. F. Wolf (1995). Yucca Mountain Project—Argonne National Laboratory, Annual Progress Report, FY 1995. (ANL-95/xx; YMP Milestone 209) Argonne, IL: Argonne National Laboratory [MOL.19960620.0123]

Bruno, J., I, Casas, and I. Puigdomenech (1991). "The Kinetics of Dissolution of UO$_2$ Under Reducing Conditions and the Influence of an Oxidized Surface Layer (UO$_{2+x}$): Application of a Continuous Flow-Through Reactor." *Geochim. Cosmochim. Acta* **55**(3):647–658. [NNA.19910821.0004]

Buck, E. C., D. J. Wronkiewicz, P. A. Finn, and J. K. Bates (1997) "A New Uranyl Oxide Hydrate Alteration Phase Derived from Spent Fuel Corrosion." *J. Nucl. Mater.* **249**:70. [MOL.19980107.0446]

Burns, P. C., R. C. Ewing, and M. L. Miller (1997). "Incorporation Mechanisms of Actinide Elements into the Structures of U^{6+} phases formed during the Oxidation of Spent Nuclear Fuel." *J. Nucl. Mater.* **245:**1. [235501]

de Pablo, J., I. Casas, J. Giménez, M. Molera, and M. E. Torrero (1997). "Effect of Temperature and Bicarbonate Concentration on the Kinetics of UO$_2$(s) Dissolution Under Oxidizing Conditions." In proceedings from Material Research Society Symposia. **465**:535–542.

Finn, P. A., E. C. Buck, M. Gong, J. C. Hoh, J. W. Emery, L.D. Hafenrichter, and J. K. Bates (1994). "Colloidal products and actinide species in leachate from spent nuclear fuel." *Radiochim. Acta* **66/67**:189. [238493]

Finn, P. A., J. C. Hoh, S. F. Wolf, M. T. Surchik, E. C. Buck, and J. K. Bates (1996). Spent fuel reaction: The behavior of the ε-phase over 3.1 years." In proceedings from Material Research Society Symposia. **465**:527–534. [MOL.19970121.0095]

Finn, P. A., D. J. Wronkiewicz, R. J. Finch, J. C. Hoh, J. W. Emery, E. C. Buck, J. A. Fortner, S. F. Wolf, L. A. Neimark, and J. K. Bates (1997). *Yucca Mountain Project—Argonne National Laboratory, Annual Progress Report, FY 1997.* (ANL-98/12) Argonne, IL: Argonne National Laboratory. [MOL.19980818.0230]

Grambow, B. (1989). *Spent Fuel Dissolution and Oxidation. An Evaluation of Literature Data.* (SKB Technical Report 89-13) Stockholm, Sweden: Swedish Nuclear Fuel and Waste Management Co. [NNA.18981013.0094]

Gray, W. J., and L. E. Thomas (1992). "Dissolution Rates of As-Received and Partially Oxidized Spent Fuel." In proceedings from Third International High-Level Radioactive Waste Management Conference. La Grange Park, IL: American Nuclear Society, Inc. pp. 1458–1464. [NNA.19920204.0037]

Gray, W. J., L. E. Thomas, and R. E. Einziger (1993). "Effects of Air Oxidation on the Dissolution Rate of LWR Spent Fuel." In proceedings from Scientific Basis for Nuclear Waste Management XVI. C. G. Interrante and R. T. Pabalan 294 [Eds.]. Pittsburgh, PA: Materials Research Society. pp. 47–54. [236035]

Gray, W. J., and L. E. Thomas (1994). "Initial Results from Dissolution Testing of Various Air-Oxidized Spent Fuels." In proceedings from Scientific Basis for Nuclear Waste Management XVII. Barkatt and R. A. Van Konynenburg (Eds.) Pittsburgh, PA: Materials Research Society **333A:**391–398. [NNA.19940204.0108]

Gray, W. J., and C.N. Wilson (1995). *Spent Fuel Dissolution Studies FY1991 to 1994.* (PNL-10540) Richland, WA: Pacific Northwest National Laboratory. [MOL.19960802.0045]

Gray, W. J. (1996). *FY 1996 Letter Report on Spent Fuel Dissolution Studies.* (Informal YMP Status Report) Richland, WA: Pacific Northwest National Laboratory. [MOL.19970114.0282]

Gray, W. J. (1998). *Letter Report on Spent Fuel Dissolution Rates as a Function of Burnup and Water Chemistry.* (Informal YMP Status Report, PNNL-11895) Richland, WA: Pacific Northwest National Laboratory.

Guenther, R. J., D. E. Blattnik, T. K. Campbell, U. P. Jenquin, J. E. Mendel, L. E. Thomas, and C. K. Thornhill (1988a). *Characterization of Spent Fuel Approved Testing Material—ATM-103.* (PNL-5109-103) Richland, WA: Pacific Northwest Laboratory. [NNA.19911017.0104]

Guenther, R. J., D. E. Blattnik, T. K. Campbell, U. P. Jenquin, J. E. Mendel, L. E. Thomas, and C. K. Thornhill (1988b). *Characterization of Spent Fuel Approved Testing Material—ATM-106.* (PNL-5109-106) Richland, WA: Pacific Northwest Laboratory. [NNA.19911017.0105]

Kleykamp, H., J. O. Paschoal, R. Pejsa, and F. Thommler (1985). "Composition and Structure of Fission Product Precipitates in Irradiated Oxide Fuels: Correlation with Phase Studies in the Mo-Ru-Rh-Pd and BaO$_2$-UO$_2$-ZrO$_2$-MoO$_2$ Systems," *J. Nucl. Mater.* **130:**426–433.

Knauss, K. G., and T. J. Wolery (1989). Muscovite dissolution kinetics as a function of pH and time at 70°C." *Geochim. Cosmochim. Acta.* **53**(7):1493–1501.

Knauss, K. G., W. L. Bourcier, K. D. McKeegan, C. I. Merabacher, S. N. Nguyen, F. J. Ryerson, D. K. Smith, H. C. Weed, and L. Newton (1990). "Dissolution kinetics of a simple analogue nuclear waste glass as a function of pH, time, and temperature." In proceedings from Materials Research Society: Scientific Basis for Nuclear Waste Management XIII. **176:**371. [NNA.19900320.0195]

McKenzie, W. F. (1992). *UO$_2$ Dissolution Rates: A Review.* (UCRL-ID-111663) Livermore, CA: Lawrence Livermore National Laboratory.

Steward, S. A., and W. J. Gray (1994). "Comparison of Uranium Dissolution Rates from Spent Fuel and Uranium Dioxide." In proceedings from Fifth Annual Intl. High-Level Radionuclide Waste Management Conference. Las Vegas, NV: May 22–26, 1994. **4:**2602–2608. (Also UCRL-JC-115355 for Lawrence Livermore National Laboratory, Livermore, CA). [210933]

Steward, S. A., and E. T. Mones (1997). "Comparison and Modeling of Aqueous Dissolution Rates of Various Uranium Oxides." In proceedings from Materials Research Society Fall Meeting: Scientific Basis for Nuclear Waste Management XX. W. J. Gray and I. R. Triay (Eds.). Boston, MA: December 2–6, 1996. **465** 557–564. Also UCRL-JC-124602 (1996) for Lawrence Livermore National Laboratory, Livermore, CA. [MOL.19971210.0278]

Tait, J. C., and J. L. Luht (1997). *Dissolution Rates of Uranium from Unirradiated and Uranium and Radionuclides from Used CANDU Fuel Using the Single-Pass Flow-Through Apparatus.* (06819-REP-01200-0006 R00) Atomic Energy of Canada, Ltd., Whiteshell Laboratories, and Ontario Hydro.

Thomas, L. E., and R. J. Guenther (1989). "Characterization of low-gas-release LWR fuels by transmission electron microscopy." In proceedings from Mater. Res. Soc. **127:**293–300. [NNA.19910326.0091]

Thomas, L. E., and L. A. Charlot (1990). "Analytical Electron Microscopy of Light-Water Reactor Fuels." *Ceram. Trans.* **9:**397–407.

Thomas, L. E., C. E. Beyer, and L. A. Charlot (1992). "Microstructural analysis of LWR spent fuels at high burnup." *J. Nucl. Mater.* **188**:80–89. [MOL.19980326.0383]

Wilson, C.N. (1984). *Results from NNWSI Series 1 Spent Fuel Leach Tests.* (HEDL-TME 84-30) Richland, WA: Hanford Engineering Development Laboratory. [NNA.900216.0070]

Wilson, C.N. (1990a). *Results from NNWSI Series 2 Spent Fuel Dissolution Tests.* (PNL-7169) Richland, WA: Pacific Northwest National Laboratory. [200816]

Wilson, C.N. (1990b). *Results from NNWSI Series 3 Spent Fuel Dissolution Tests.* (PNL-7170) Richland, WA: Pacific Northwest National Laboratory. [NNA.199000814.0048]

Wilson, C.N., and C. J. Bruton (1989). "Studies on Spent Fuel Dissolution Behavior Under Yucca Mountain Repository Conditions." *Ceramic Transactions*. In proceedings from Nuclear Waste Mgt. III. G. B. Mellinger (Ed.) Westerville, OH. **9:**423–442. [NNA.19891106.0260]

Wilson, C.N., and W. J. Gray (1990). "Effects of Water Composition on the Dissolution Rate of UO$_2$ Under Oxidizing Conditions." In proceedings from First International High-Level Radioactive Waste Management Topical Meeting. La Grange Park, IL: American Nuclear Society, Inc. pp. 1431–1436. [MOL.19980324.0145]

Wronkiewicz, D. J., J. K. Bates, T. J. Gerding, E. Veleckis, and B. S. Tani (1991). *Leaching action of EJ-13 water on unirradiated UO$_2$ surfaces under unsaturated conditions at 90°C: Interim Report.* (ANL-91/11) Argonne, IL: Argonne National Laboratory. [NNA.19910314.0091]

Wronkiewicz, D. J., J. K. Bates, T. J. Gerding, E. Veleckis, and B. S. Tani (1992). "Uranium Release and Secondary Phase Formation During Unsaturated Testing of UO$_2$ at 90°C." *J. Nucl. Mater.* **190:** 107–127. [MOL.19980314.0091]

Wronkiewicz, D. J., J. K. Bates, S. F. Wolf, and E. C. Buck (1996). "Ten-Year Results From Unsaturated Drip Tests With UO$_2$ at 90°C: Implications for the Corrosion of Spent Nuclear Fuel." *J. Nucl. Mater.* **238:** 78–95. [MOL.19971218.0965]

STUDIES ON SPENT FUEL DISSOLUTION BEHAVIOR*
UNDER YUCCA MOUNTAIN REPOSITORY CONDITIONS

C. N. Wilson
Pacific Northwest Laboratory

C. J. Bruton
Lawrence Livermore National Laboratory

ABSTRACT

Nuclide concentrations measured in laboratory tests with PWR spent fuel specimens in Nevada Test Site J-13 well water are compared to equilibrium concentrations calculated using the EQ3/6 geochemical modeling code. Actinide concentrations in the laboratory tests reach steady-state values lower than those required to meet Nuclear Regulatory Commission (NRC) release limits. Differences between measured and calculated actinide concentrations are discussed in terms of the effects of temperature (25°C to 90°C), sample filtration, oxygen fugacity, secondary phase precipitation, and the thermodynamic data in use. The concentrations of fission product radionuclides in the laboratory tests tend to increase continuously with time, in contrast to the behavior of the actinides.

1.0   INTRODUCTION

The Yucca Mountain Project of the U. S. Department of Energy is studying the potential dissolution and radionuclide release behavior of spent fuel in a candidate repository site at Yucca Mountain, Nevada. The repository horizon under study lies in the unsaturated zone 200 to 400 meters above the water table. With the exception of C-14, which may migrate in a vapor phase,[1] and possibly I-129, the majority of long-lived radionuclides present in spent nuclear fuel will be transported from a failed waste package in the repository via dissolution or suspension in water in the absence of a major geological event such as volcanism.

*This material also is important in understanding Section 3.4.

[1] Published in Ceramic Transactions, V-9, pp. 423-442. Nuclear Waste Mgt. III, G. B. Mellinger, ed. Westerville, Ohio, 1990.

Spent fuel will not be contacted by liquid water infiltrating the rock until several hundred years after disposal when the repository has cooled to below the 95°C boiling temperature of water at the repository elevation. The potential dissolution behavior of spent fuel during the repository post-thermal period is being studied using geochemical models and laboratory tests with actual spent fuel specimens.* Selected initial results from these studies are discussed in the present paper.

2.0   LABORATORY TESTS

Three spent fuel dissolution test series have been conducted in laboratory hot cells using spent fuel specimens of various configurations. Results from the Series 2 and Series 3 tests with bare fuel particles are discussed in the present paper. The Series 2 tests used unsealed fused silica test vellels and were run for five cycles in air at ambient hot cell temperature (25°C). The Series 3 tests used sealed stainless steel vessels and were run for three cycles at 25°C and 85°C. Each test cycle was started in fresh Nevada Test Site J-13 well water and was about six months in duration. Periodic solution samples were taken during each test cycle and the sample volume was replenished with fresh J-13 water. Five bare fuel specimens tested in these two tests series are identified in Table 1 and the test configurations are shown in Figure 1. Additional information on the laboratory tests is provided in references 3 and 4.

2.1   Actinide Results

Actinide concentrations (U, Np, Pu, Am and Cm) measured in solution samples rapidly reached maximum levels during the first test cycle and then generally dropped to lower steady-state levels in later test cycles. The concentrations of uranium and the activities of Pu-239+240 and Am-241 measured in 0.4 mm filtered solution samples are plotted in Figure 2. The initial concentration peaks are attributed to dissolution of more readily soluble UO_{2+x} oxidized phases present initially of the fuel particle surfaces, and to kinetic factors limiting the nucleation and growth of secondary phases that may ultimately control actinide concentrations at lower levels.

Table 1. Bare Fuel Test Identification

identification	Description	Starting Fuel Wt. (g)
HBR-2-25	Series 2, H.B. Robinson Fuel, 25°C	83.10
TP-2-25	Series 2, Turkey Point Fuel, 25°C	27.21
HBR-3-25	Series 3, H.B. Robinson Fuel, 25°C	80.70
HBR-3-85	Series 3, H.B. Robinson Fuel, 85°C	85.55
TP-3-85	Series 3, Turkey Point Fuel, 85°C	86.17

Uranium (U) concentrations at 25°C were lower in the Series 3 tests than in the Series 2 tests, and with the exception of the Cycle 1 data, U concentrations in the 85°C Series 3 tests were lower than those in the 25°C tests. The very low U concentrations measured during Cycle 1 of the HBR-3-85 test were attributed to a vessel corrosion anomaly. In the later cycles of the Series 2 tests, U concentrations tended to stabilize at steady-state levels of about 1 to 2 µg/ml. In Cycles 2 and 3 of the Series 3 tests, U concentrations stabilized at about 0.3 µg/ml at 25°C and about 0.15 µg/ml at 85°C. Precipitated crystals of the calcium-uranium-silicates, uranophane (Figure 3) and haiweeite, and possibly the uranium-silicate soddyite, were found on filters used to filter cycle termination rinse solutions from both 85°C tests. Phase identifications were based on examinations by X-ray diffraction and microanalysis in the SEM.[4] Secondary phases controlling actinide concentrations other than U were not found.

The 0.4 µm filtered Pu-239+240 solution activities measured in Cycles 2 through 5 of the TP-2-25 test generally ranged from about 100 to 200 pCi/ml (Figure 2). Activities as low as about 20 pCi/ml were measured in the HBR-2-25 test. During Cycles 2 and 3 of the HBR-3-25 test, activities varied from about 60 to 1 00 pCi/ml. A value of 100 pCi/ml, which corresponds to a Pu concentration of about 4.4×10^{-9} $\underline{M}$ ($\underline{M}$ = molarity), would appear to be a reasonable estimate of steady-state Pu-239+240 activities in 0.4 µm filtered solutions in the 25°C. Significantly lower activities on the order of 1 pCi/ml were measured in the 85°C tests. The lower activities at 85°C may result from enhanced nucleation and growth of secondary phases at the higher temperature that limit pU concentration.
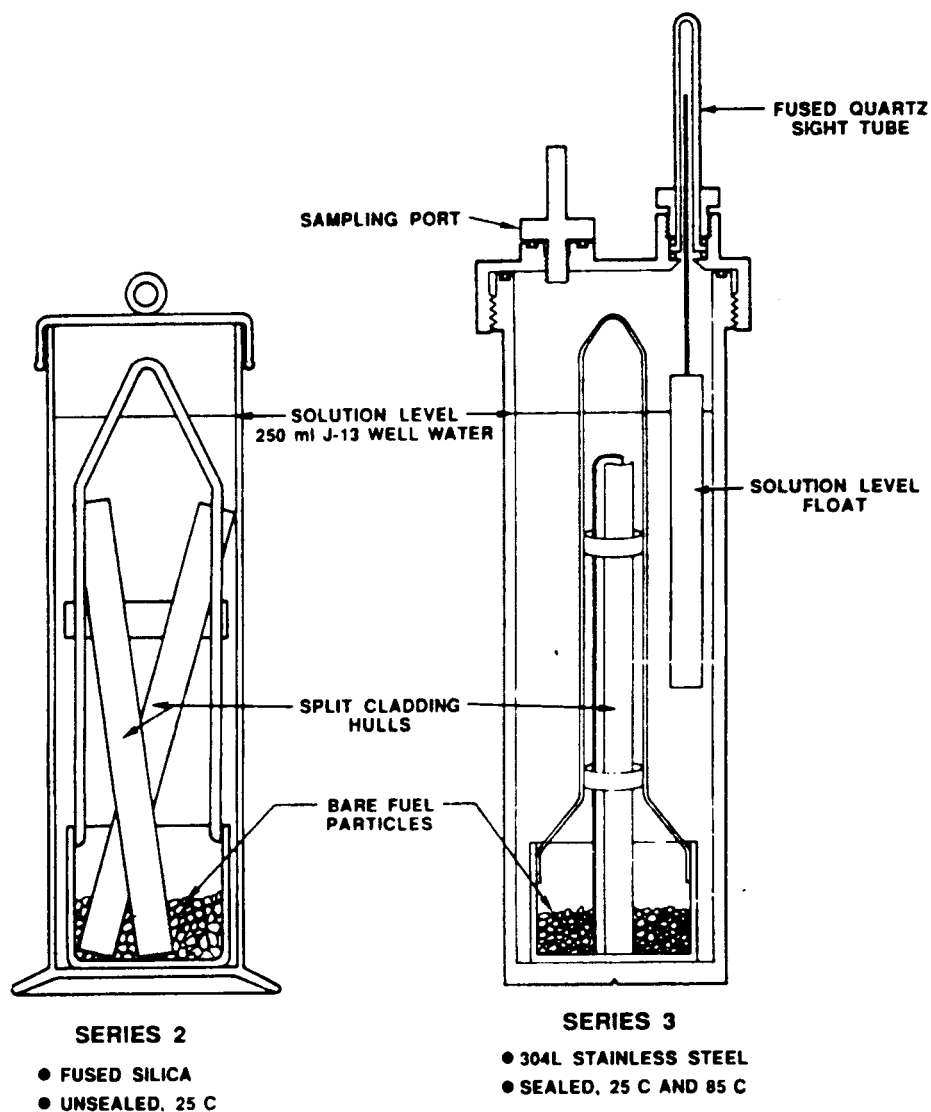
Figure 1. Test Configurations for the Series 2 and Series 3 Bare Fuel Dissolution Tests.

Selected solution samples were centrifuged through membrane filters that provide an estimated filtration size of approximately 2 nm.* Filtering to 2 nm caused Pu-239+240 activities to decrease by about 20 to 40%. No significant differences between 0.4 μm filtered sample data are considered the most significant relative to radionuclide release because larger particles probably would not be transported by water, whereas colloidal particles greater than 2 nm may remain in stable suspension and be transported by water movement.

Table 2. J-13 Well Water Analysis[2]

Component	Concentration (μg/ml)	Component	Concentration (μg/ml)
Li	0.042	Si	27.0
Na	43.9	F	2.2
K	5.11	Cl	6.9
Ca	12.5	NO_3	9.6
Mg	1.92	SO_4	18.7
Sr	0.035	HCO_3	125.3
Al	0.012		
Fe	0.006	pH	7.6

Steady-state Am-241 activities on the order of 100 pCi/ml, corresponding to Am concentrations of about 1.5×10^{-10} $\underline{M}$, were measured in 0.4 μm filtered samples during cycles 2 and 3 of the TP-2-25 and HBR-3-25 tests. The 100 pCi/ml value would appear to be a conservative estimate for Am-241 activity at steady-state and 25°C considering that activities on the order of 10 pCi/ml were measured during Cycles 2, 4 and 5 of the HBR-2-25 test. Much lower 0.4 μm filtered Am-241 activities of about 0.3 pCi/ml were measured during Cycles 2 and 3 of the two 85°C tests. The effects of both 0.4 μm and 2 nm filtration were in general greater for Am-241 than for Pu-239+240. Association of Am with an apparent suspended phase is suggested by unfiltered data from the 85°C tests plotted as dashed lines in Figure 2, and by a relatively large fraction of 0.4 μm filtered Am-241 activity removed by 2 nm filtration (not shown). Cm-244 activity measured in most samples was similar to that measured for Am-241 in each of the tests. However, Cm-244 alpha decays with an 18-year half-life to Pu-240 and will not be present during the repository post-thermal period.

Measured Np-237 activities in most samples were generally not much greater than the detection limit of 0.1 pCi/ml and were below detection limits in several samples. Measured Np-237 activities showed very little dependence on temperature, vessel type or sample filtration. Following initially higher values at the beginning of Cycle l, Np-237 activities generally ranged from 0.1 to 0.5 pCi/ml.

---

*Amicon Corporation Model CF-25 centrifuge membrane cone filter
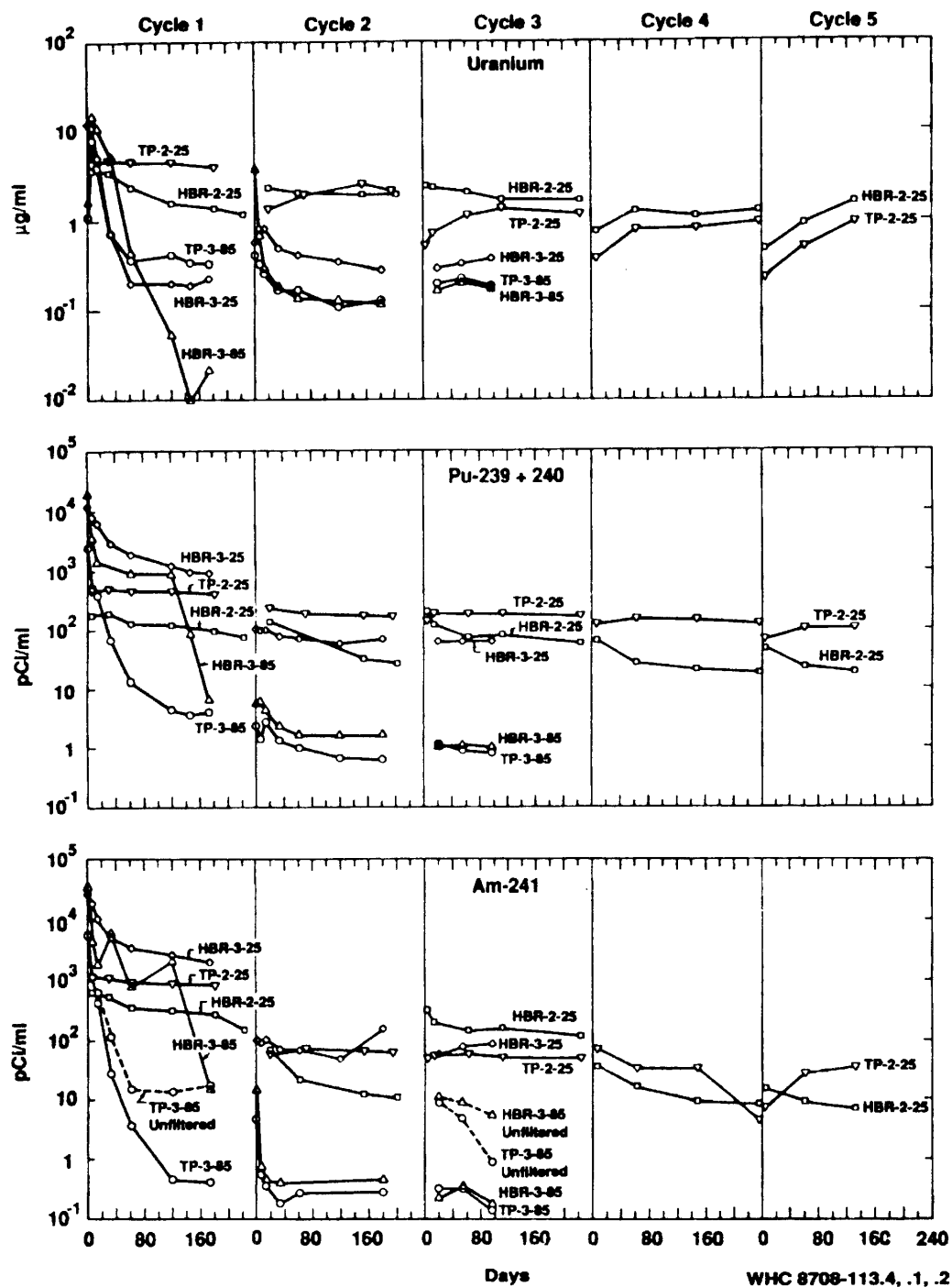
Figure 2. Uranium Concentrations (top), Pu-239+240 Activities (center), and Am-241
Activities (bottom); Measured in 0.4 μm Filtered Solution Samples.
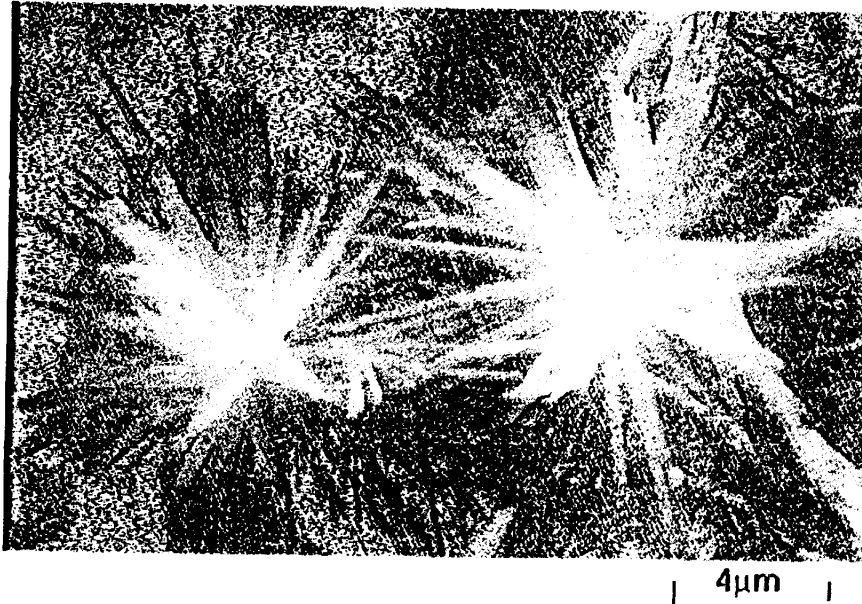
Figure 3. Acicular crystals of Uranophane formed on spent fuel grains in the 85°Series 3 tests.

2.2   Fission Product Results

Specimen inventory fractions of the fission product radionuclides Cs-137, Sr-90, Tc-99, and I-129 measured in solution are plotted in Figure 4 for the HBR-2-25 and HBR-3-85 tests. Each data point represents the fraction of the ORIGEN-2 calculated specimen inventory in solution on the sample data plus the inventory fraction calculated to have been removed in previous samples from the test cycle. During Cycle 1 of the HBR-3-85 test, Tc-99 fell to below detectable levels as a result of the corrosion anomaly that occurred in this test. Cycle 1 Cs-137 gap inventory release was about 0.7% from the HBR fuel and is therefore off-scale in Figure 4. Sr-90 was not measured during Cycle 1 of the Series 2 tests, and appeared to be limited by association with an unknown precipitated phase in the 85°C tests.

The inventory fractions of Cs-137, Sr-90, Tc-99 and I-129 in solution increased continuously with time, with the exception of the anomalous precipitation of Tc-99 in Cycle 1 of the HBR-3-85 test and the limit on Sr-90 activity in solution at 85°C. The continuous release rates of the fission products in units of inventory fraction per year are given in Figure 4 for the final cycle of the two tests. Because the actual quantity of fuel matrix dissolution and precipitation of actinides was not measured, it is not known to what degree the continuous fission product release resulted form preferential leaching of grain boundaries where fission products were thought to concentrate during irradiation. Whether as a result of increased matrix dissolution or increased grain boundary leaching, the soluble fission product release rate is greater in the later test cycles at the higher temperature.
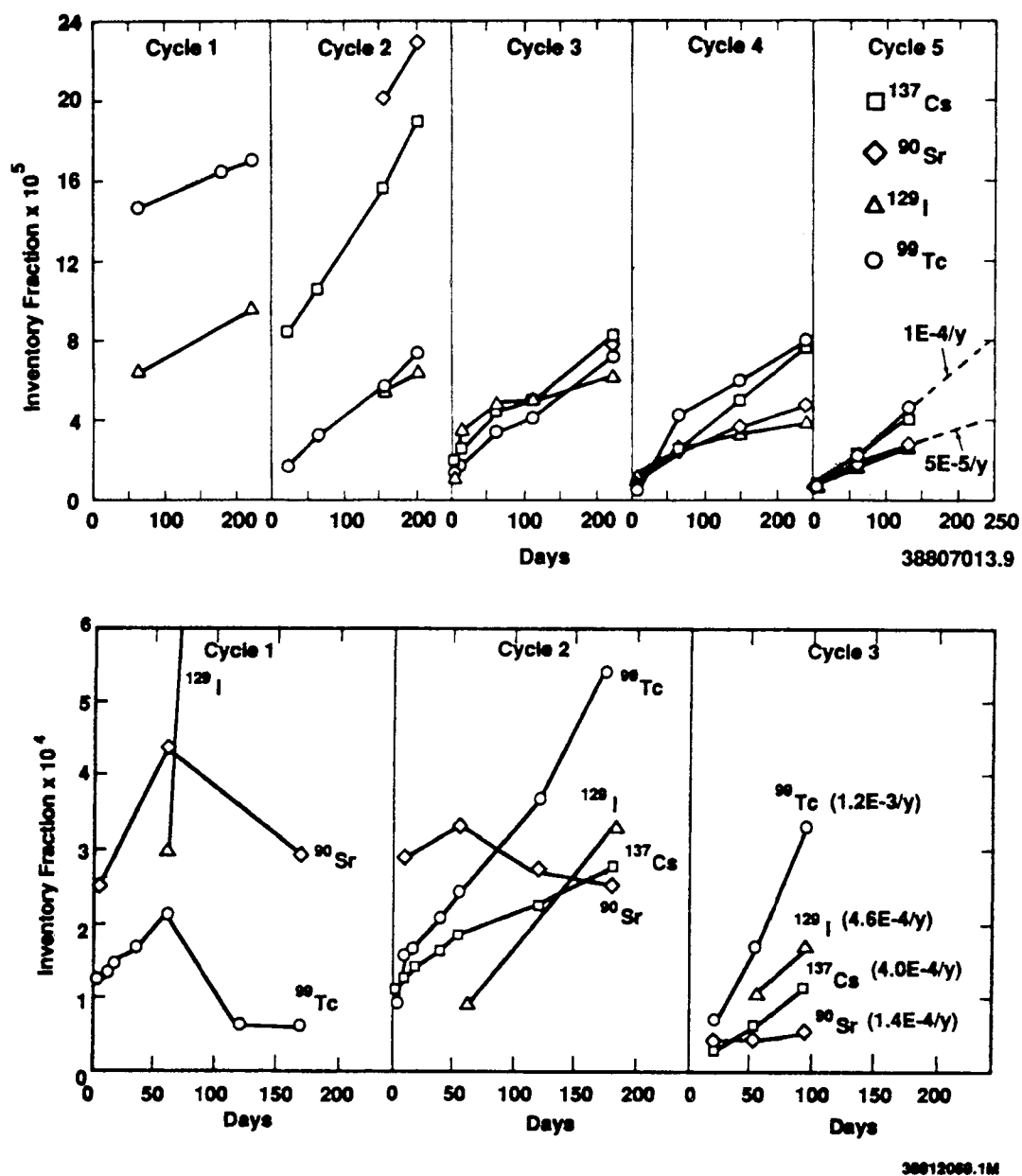
Figure 4. Inventory Fractions of Cs-137, Sr-90, Tc-99 and I-129 Measured in Solution in the HBR-2-25 Test (top) and in the HBR-3-85 Test (bottom). Approximate annual fractional release rates are listed for each nuclide during the last cycle plotted.

3.0   GEOCHEMICAL MODELING

3.1   Actinide Concentrations in Solution

Spent fuel dissolution in J-13 well water was simulated using the geochemical modeling code EQ3/6[5] to determine whether steady-state actinide concentrations measured in the tests could be related to the precipitation of actinide-bearing solids. Version 3245 of the EQ3/6 code and version 327OR13 of the supporting thermodynamic database were used to simulate spent fuel dissolution at 25°C and 90°C assuming atmospheric CO_2 gas fugacity and two different 0_2 gas fugacities of $10^{-0.7}$ (atmospheric) and 10^{-12} bars (see later discussion). The simulation process is described in more detail elsewhere.[6] The computer simulations yield: 1) the sequence of solids that precipitate and sequester elements released during spent fuel dissolution, and 2) the corresponding elemental concentrations in solution. Approximate steady-state actinide concentrations measured at 25°C and 85°C in the Series 3 laboratory tests were compared in Table 3 to concentrations of actinides in equilibrium with the listed solids as calculated in the EQ3/6 simulations. Comparisons of simulation results with experimental results are being used to determine the adequacy of the thermodynamic database and to identify additional aqueous species and minerals for which data are needed.

Table 3. Comparison of Measured and Predicted Actinide
Concentrations (log M)
(New runs have not been completed) May 22, 1993 RBS)

	Measured[a]		EO3/6[b] 25°C		90°C		
Actinide	-25°C	85°C	-0.7	-12.0	-0.7	-12.0	Phase
U	-5.9	-6.2	-7.2/-7.0*	-7.1/6.9	-8,8.-7.6	-8.5/-7/5	H
			-7.0/-6.9	-6.9/-6/8	-7/6	-7.5	H + S
			-6.9/-4.3	-6.8/-4.2	-7.6/-6.0	-7.5/-5.9	S
			-4.3	-4.2	-6.0	-5.9	S + Sch
			-4.2	-4.1	-6.0/-5.8	-5.8/-5.6	Sch
Np	-8.9	-9.1	-6.2	-9.0	-5.2	-8.0	NpO_2
Pu	-8.4	-10.4	-12.4	-13.8	-11.9	-14.6	PuO_2
			-4.3	-5.7	-4.2	-6.9	$Pu(OH)_4$
Am	-9.8	-12.3	-8.3	-8.3	--	--	$Am(OH)CO_3$
			--	--	-8.4	-8.4	$Am(OH)_3$
Cm	-11.3	-14.3			Cm not in thermodynamic data base		

(a) Series 3 tests, 0.4 µm filtered.
(b) At oxygen fugacities log f_{02} = -0.7 (atmospheric) and log f_{02} = -12.0 with solubility control by precipitated secondary phases as listed. H = haiweeite; S = soddyite; Sch = schospite. All phases are in crystalline state except $Pu(OH)_4$ which is amorphous.
*-7.2/-7.0- refers to a range in concentration from -7.2 to -7.0.

Uranium (U) concentrations in the simulations vary as a function of the secondary U-bearing precipitates. The following sequence of mineral assemblages are predicted to precipitate and sequester U as increasing amounts of spent fuel dissolve: haiweeite, haiweeite plus soddyite, soddyite, soddyite plus schoepite, and schoepite. The relative compositions of these phases and of U-bearing phases that were observed in residues from the 85°C laboratory tests are shown in Figure 5. Unique, and steadily increasing, concentrations of U in solution are related to each mineral assemblage. The concentration of U varies not only as the precipitates vary, but also during the precipitation of a single mineral, such as soddyite, because of changes in the pH and overall chemical characteristics of the fluid. As previously discussed, uranophane, haiweeite, and possibly soddyite were found in the 85°C Series 3 tests. Unfortunately, reliable thermodynamic data for uranophane were not available, which complicates comparison of the laboratory test results to the calculated solutibility limits. Haiweeite, aCa-U-silicate like uranophane, is predicated to precipitate at U concentrations that are lower than the measured steady-state values. In the absence of data for uranophane, the experimental concentrations of U would appear to be consistent with the precipitation of soddyite at both 25°C and 90°C in the simulations.
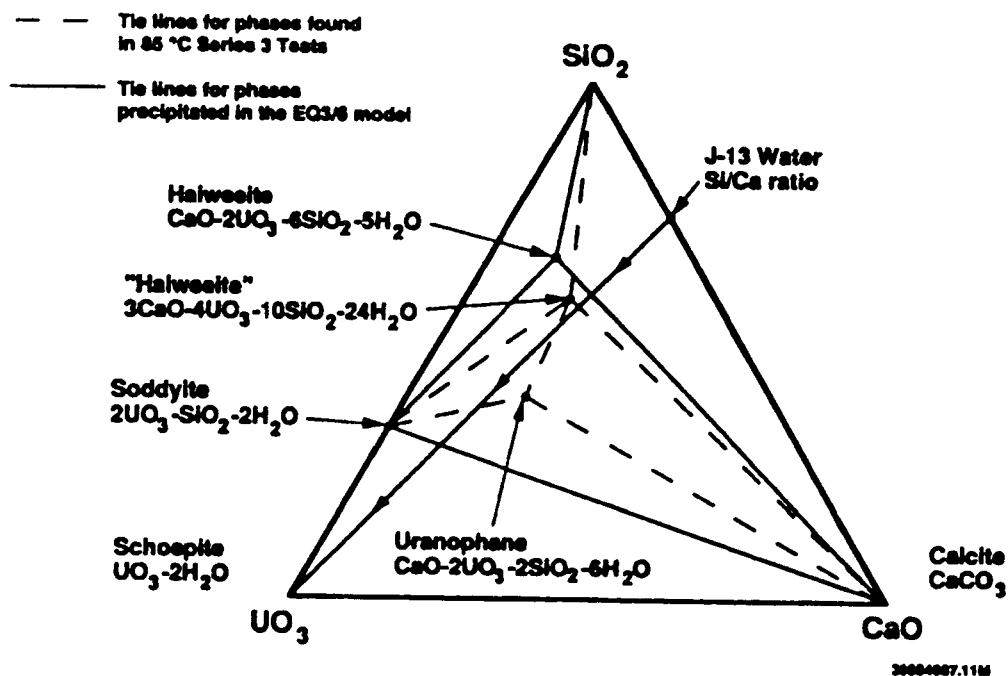
Figure 5.   **Relative Compositions (mole %) of U-bearing Phases
Indicated as Controlling U Concentration in the EQ3/6 Simulation and for
which Indications were Observed in the 85°C Series 3 Tests.**

Neptunium concentration is controlled by equilibrium with NpO_2 in the simulations. However, the predicted concentration of Np is highly dependent on solution Eh and pH .[7] The O_2 fugacity in the simulations was reduced from $10^{-0.7}$ bars to 10^{-12} bars in order to produce good agreement between the measured and predicted concentrations of Np at 25°C. An O_2 fugacity of 10^{-12} bars may correspond to conditions at the fuel surface in an otherwise oxygenated system (i.e., contains an air cap) that is poorly buffered. Eh was not measured during the laboratory tests, and redox equilibrium may not have been established among the various species and phases within the sealed stainless steel vessels. An oxygen fugacity of 10^{-12} bars over-estimates Np concentration at 90°C, however, because the experimental data do not reflect predicted increases in Np concentration with temperature. The thermodynamic data for Np and other actinides must, consequently, be critically evaluated at elevated temperature.

Significant differences exist between measured and predicted Pu and Am concentrations in Table 3. Measured Am concentrations may have been lower than those predicted because of Am removal from solution by phases such as lanthanide precipitates that were not accounted for in the E03/6 simulations. Another possible mechanism controlling Am concentration not accounted for in the simulation may have been sorption. Although $Am(OH)CO_3$ is predicted to control Am concentration at 25°C and $Am(OH)_3$ precipitates at 90°C, the Am concentration in equilibrium with both phases is about the same.

Predicted Pu concentrations in equilibrium with crystalline PuO_2 at both temperatures and oxygen fugacities are much lower than those measured. Pu concentrations measured at 25°C are similar to those reported by Rai and Ryan,[8] who measured the solubility of PuO_2 and hydrous $PuO_2 \cdot xH_2O$ in water for periods of up to 1300 days at 25°C. At a pH of 8, which was the extrapolated lower limit of their data and the approximate pH in the Series 2 and 3 tests, they reported that Pu concentrations ranged from about $10^{-7.4}$ $\underline{M}$, where amorphous $PuO_2 \cdot xH_2O$ was thought to control concentration, down to about 10^{-9} $\underline{M}$ where aging of the amorphous material produced a more (but incompletely) crystalline PuO_2 that was thought to control concentration. Concentrations of Pu in equilibrium with amorphous $Pu(OH)_4$ calculated in recognition of the fact that an amorphous or less crystalline phase is more likely to precipitate than crystalline PuO_2, are listed in Table 3. Measured Pu concentrations would be expected to fall between the equilibrium concentrations for PuO_2 and $Pu(OH)_4$, becoming closer to PuO_2 with aging. Equilibrium with amorphous $Pu(OH_4)$ and crystalline PuO_2 at O_2 fugacities of $10^{-0.7}$ and 10^{-12} bars yields predicted Pu concentrations that bracket measured results at both 25°C and 85°C.

3.2   Sources of Discrepancy Between Measured and Predicted Results

Discrepancies between measured and predicted concentrations are to be expected considering database limitations and uncertainty in the interpretation of measured apparent steady-state actinide concentrations. Care must be taken in interpreting the 90°C simulation results because insufficient data exist to accurately calculate the temperature-dependence of the thermodynamic properties of many radionuclide-bearing solids and solution species. The 3270 thermodynamic data basis constantly updated through inclusion of new and revised thermodynamic data and the selection of a consistent set of aqueous complexes for reach chemical element. Puigdomenech and Bruno[9] have constructed a thermodynamic database for U minerals and aqueous species that they showed to be in reasonable agreement with available experimental solubility data in systems in which U is complexed by OH- and CO_3. The 3270 database contains many of the same aqueous species and minerals, but Puigdomenech and Bruno have included recent data for aqueous uranyl hydroxides from Lemire[10] which are not yet in the EQ3/6 database. Future plans include a critical evaluation of simulations of spent fuel dissolution made using the Puigdomenech and Bruno U database, and comparison with simulations made using the latest version of the EQ3/6 database. Inclusion of standard Nuclear Energy Agency (NEA) data for U minerals and species will also help to standardize future databases.

Until the U database is better established, calculated U concentrations must be recognized as preliminary and speculative. Simulation results can be used as a vehicle for identifying geochemical trends and studying the interactions between solid precipitation and elemental concentrations in solution. Seemingly small changes in the thermodynamic database can have potentially large impacts on predictions. For example, U concentrations calculated to be in equilibrium with schoepite using version 3270 of the E03/6 database are radically lower than those predicted in 1987[6] using an older database. The species $(U_2)_3(OH)_7$ - and $(UO_2)_2(OH)_3CO_3$ - were omitted from version 3270 of the EQ3/6 database because their validity was questioned. $UO_2(CO_3)_2^{-2}$ and $UO_2(CO_3)_3^{-4}$ were left as the only dominant U species in solution throughout the EQ3/6 simulations. U concentrations accordingly remain lower during U mineral precipitation. Future work must address the sensitivity of the results to variations in thermodynamic data and the choice of a self-consistent set of aqueous species for elements of interest.

Comparisons between experimental results and predictions in Table 3 are predicated on the assumption that the listed solid phases precipitate from solution and control the solution composition. Except for some U-bearing minerals, no minerals containing radionuclides have been identified in the laboratory tests. Detection and characterization of actinide-bearing secondary phases may be difficult because of the extremely small masses of these actinides involved. Precipitates limiting actinide concentrations in the laboratory tests may

also be amorphous, colloidal, or in some other less-than-perfect crystalline state. For instance, Rai and Ryan" observed that early Pu precipitates tend to be hydrated oxides which undergo aging to more crystalline solids. The concentrations of the affected actinides would, therefore, gradually decrease as aging progresses.

The chemistry of trivalent Am and Cm can be expected to be almost identical to that of the light lanthanide fission product elements which are present in much greater concentrations in spent fuel than are Am and Cm. Am and Cm may, therefore, be present in dilute solid solution with secondary phases formed by the lanthanides, which would result in lower measured solution concentrations than predicted for Am based on equilibration with $Am(OH)CO_3$ or $Am(OH)_3$. Pu and Np, and possibly Am and Cm, may also have been incorporated at low concentrations in solid solution with the U-bearing precipitates or other secondary phases. Efforts are planned to separate crystals of uranophane from test residues and to perform radiochemical analyses of these crystals to check for incorporation of other radionuclides. Sorption of actinides on colloids or other surfaces such as the fuel or test hardware may also control solution concentrations, but the impact or sorption was not considered in the simulations. Other factors, such as local variations in redox potential, may also contribute to differences between measured and predicted solubilities.

As it is not currently reasonable to expect a geochemical model to predict accurately the effects of all potential concentration-controlling processes over thousands of years, we hope to use modeling predictions to establish upper limits, or conservative estimates, of radionuclide concentrations over time. Lower limits to radionuclide concentrations imposed by solid precipitation are also of interest, however, as a baseline for further calculations, and because radionuclide concentrations may be expected to approach the lower limits over extended time periods. Accordingly, we assume in this paper that the actinide concentrations are controlled by the most stable and insoluble precipitates for which data are available. The consequences of precipitation of progressively less stable precipitates will be explored in future calculations, and upper limits of radionuclide concentrations controlled by solid precipitation will be estimated. In the case of Pu, for example, we have begun to explore the upper limits to Pu concentration as controlled by the precipitation of amorphous $Pu(OH)_4$. Comparison of modeling results with experimental results helps to identify phenomena which may revise our estimates of concentration limits. Processes such as sorption and aging of solids to forms of increasing crystallinity tend to lower element concentrations in solution, and increase the conservative nature of our estimates. However, consideration of colloid formation and colloid migration with the fluid phase may lead to an increase in our estimates of mobile concentrations over those made considering precipitation phenomena alone.

4.0   RADIONUCLIDE RELEASES

Annual actinide releases per failed waste package were calculated assuming that water flowing at a rate of 20 1/yr per waste package transports the actinides at the approximate concentrations measured at steady-state in Cycles 2 and 3 of the HBR-3-25 test. Each waste package was assumed to contain 3140 kg of fuel with an average burnup of approximately 33,000 MWd/MTM. The logarithms of the waste package 1000-year inventory fractions transported annually for each actinide under such conditions is given in Table 4. These releases are at least three orders of magnitude lower than the Nuclear Regulatory Commission (NRC) requirement in 10 CRF 60.113[11] that annual radionuclide releases during the post-containment period shall not exceed one part in 100,000 of the 1000-year inventories. The calculated annual release results would appear to be particularly encouraging for Pu and Am because isotopes of these two actinide elements account for about 98% of the total activity present in spent fuel at 1000 years. These values may be conservative in that they are based on the higher steady-state Pu and Am concentrations measured at 25°C and assume a conservative (high) estimate of the water flux through the repository. The calculated releases do, however, assume maintenance of steady values for actinide concentrations over time, whereas the geochemical simulations suggest that actinide concentrations, and U concentrations in particular, may vary with time. Confidence in such release predictions will be greatly increased when the chemical mechanisms of solubility control are identified and successfully modeled.

Table 4. Annual Actinide Releases as a Fraction of the 1000-Year
Inventories Based on HBR-3-25 Test Date

Actinide	Concentration Log(M)	Log (Release)*
U	-5.9	-8.6
Np	-8.9	-8.8
Pu	-8.4	-9.0
Am	-9.8	-9.1

*Assumes water flow rate of 20 1/yr per waste package transporting actinides at the indicated concentrations. Each waste package is assumed to contain 3140 kg of 33,000 MWd/MTM burnup PWR fuel.

Measured activities of the more soluble fission product radionuclides Cs-137, Sr-90, Tc-99 and I-129 continuously increase in solution at rates generally corresponding to annual release rates in the range of 10^{-4} to 10^{-3} of specimen inventory per year (Figure 4). These release rates imply a problem in meeting the NRC10^{-5} annual fractional release limit for the more soluble radionuclides if the waste form alone is expecting to carry the burden of compliance in the unanticipated case of large quantities of water contacting the waste. However, there are two factors that make these release rates uncertain. First, the degree to which these radionuclides are preferentially released from grain boundaries where they may be concentrated during irradiation has not yet been determined. Preferential release could be expected to provide a lesser contribution over time as exposed grain boundary inventories are depleted and release rates approach the congruent fuel matrix dissolution rate. A second factor is the extent to which the fuel may be degraded over time by exposure to the repository environment. Degradation of the fuel as a result of oxidation to higher oxygen stoichiometries such as U_3O_8, or as a result of preferential grain boundary dissolution, may cause increases in surface area and increased rates of nuclide dissolution from grain boundaries and from the fuel matrix over time.

Flow-through tests in which uranium minerals do not precipitate are being developed to measure the degree to which soluble nuclides are preferentially released during the initial phases of fuel dissolution. Dissolution tests using spent fuel specimens that have been degraded by slow, low-temperature oxidation are also planned. Results from these tests should provide a better understanding of potential long-term releases of the soluble and volatile radionuclides. Additional characterization of potential release of C-14 is important because it is soluble as bicarbonate and could also be released in the vapor phase as CO_2.

5.0   CONCLUSIONS

Laboratory testing and geochemical simulation of the dissolution of spent fuel under conditions selected for relevance to the proposed Yucca Mountain repository have resulted in the following conclusions.

1.   Radionuclides of interest in spent fuel appear to fall into three categories of potential release mechanisms: 1) radionuclides whose release appears to be controlled by concentration-limiting mechanisms, 2) more highly soluble radionuclides, and 3) radionuclides that are released in the vapor phase (principally C-14).

2.   The principal radionuclides whose releases appear to be controlled by concentration-limiting mechanisms are the actinides U, Np, Pu, Am and Cm.

Steady-state concentrations measured for these actinide elements are at least three orders of magnitude lower than those required to meet NRC release limits based on conservative estimates of water fluxes through the repository. This result is of particular significance because isotopes of Pu and Am account for about 98% of the activity in spent fuel at l000 years. However, results from geochemical modeling suggest that steady-state concentrations may vary significantly with time because of changes in solution composition and the identity of precipitating phases.

3. Good agreement between measured and predicted concentrations was obtained for Np based on equilibration with NpO_2 at 25°C when the oxygen fugacity in the simulation was set at 10^{-12} bars. A broad range of solubilities that bracketed the measured values were predicted for Pu depending upon the assumed oxygen fugacity and solubility-controlling phase. Measured Am concentrations were less than predicted based on data for equilibration with $Am(OH)CO_3$ and $Am(OH)_3$.

4. Dissolution rates for soluble radionuclides (Cs-137, Sr-90, Tc-99 and I-129) exceeding 10^{-5} of specimen inventory per year were measured during the laboratory tests. The implications of these data relative to long-term release of soluble radionuclides from a failed waste package are uncertain. The degree to which these radionuclides were preferentially released from grain boundaries where they may have concentrated during irradiation was not determined. Preferential release could be expected to provide a lesser contribution overtime as exposed grain boundary inventories are depleted. However, physical degradation of the fuel over time from exposure to the oxidizing repository environment may result in accelerated release of soluble nuclides.

5. Additional work is required to identify solid phases that control actinide concentrations, and to acquire reliable thermodynamic data on these phases for use in geochemical modeling. In this regard, identification of any stable suspended phases that can be transported by water movement is also important. In addition, we must better understand the potential release of soluble and volatile radionuclides, which may initially depend on preferential release from gap and grain boundary inventories, but may ultimately depend on the rate of fuel degradation by oxidation or other processes in the postcontainment repository environment.

REFERENCES

1. R. A. Van Konynenburg, C. F. Smith, H. W. Culham and C. H. Otto Jr., "Behavior of Carbon-14 in Waste Packages for Spent Fuel in a Repository in Tuff," Scientific Basis for Nuclear Waste Management VIII, C. M. Jantzen, J. A. Stone and R. C. Ewing, eds., Materials Research Soc., Pittsburgh, PA, 44:405-412 (1985). [NNA.19900320.0150]

2. J. M. Delany, Reaction of Topopah Spring Tuff with J-13 Water: A Geochemical Modeling Approach Using the EQ3/6 Reaction Path Code, Lawrence Livermore National Laboratory, UCRL-53631 (1985). [HQS.19880517.2419]

3. C. N. Wilson, Results from Cycles 1 and 2 of NNWSI Series 2 Spent Fuel Dissolution Tests, Hanford Engineering Development Laboratory, HEDL-TME 85-22 (1987). [HQS.19980517.2581]

4. C. N. Wilson, "Summary Results from the Series 2 and Series 3 NNWSI Bare Fuel Dissolution Tests," Scientific Basis for Nuclear Waste Management IX, M. J. Apted and R. E. Westerman, eds. Materials Research Soc., Pittsburgh, PA, 112:473-483 (1987). [NNA.19871009.0010]

5. T. J. Wolery, Calculation of Chemical Equilibrium Between Aqueous Solution and Minerals: The EQ3/6 Software Package, Lawrence Livermore National Laboratory, UCRL-52658 (1979). [HQS.19880517.2586]

6. C. J. Bruton and H. F. Shaw, "Geochemical Simulation of Reaction Between Spent Fuel Waste Form and J-13 Water at 25°C and 90°C," Scientific Basis for Nuclear Waste Management IX, M. J. Apted and R. E. Westerman, eds. Materials Research Soc., Pittsburgh, PA, 112:485-494 (1987). [NNA.19891228.0519]

7. R. J. Lemire, An Assessment of the Thermodynamic Behavior of Neptunium in Water and Model Groundwater from 25°C to 150°C, Atomic Energy of Canada Limited, Whiteshell Nucl. Res. Estbl. AECL-7817 (1984). [NNA.19900320.0149]

8. D. Rai and J. L. Ryan "Crystallinity and Solubility of PU(IV) Oxide and Hydrous Oxide in Aged Aqueous Suspensions, "Radiochem. Acta, 30:213~-216 (1982). [NNA.19900306.0013]

9. I. Puigdomenech and J. Bruno, Modelling Uranium Solubilities in Aqueous Solutions: Validation of Thermodynamic Data Base for the EQ3/6 Geochemical Codes, SKB technical report 88-21 (1988). [NNA.19980425.0186]

10. R. J. Lemire, Effects of High Ionic Strength Groundwaters on Calculated Equilibrium Concentrations in the Uranium-Water System, Atomic Energy of Canada Limited, Whiteshell Nucl. Res. Estbi. AECL-9549 (1988).

11. Code of Federal Regulations, "Disposal of High-Level Radioactive Wastes in Geological Repositories - Licensing Procedures, Title 10, Ch. 1, Pt. 60, Sec. 60.113 (1983).

LAWRENCE LIVERMORE NATIONAL LABORATORY

LLYMP9101029   WBS 1.2.2.3.1.1
 January 22, 1991   QA

SEPDB Administrator
Sandia National Laboratory
Organization 6310
P.O. Box 5800
Albuquerque NM 87185

Subject: Submission of Data to the SEPDB

Attached are a Technical Data Information Form (TDIF) and associated data for inclusion in the SEPDB. These
data are taken from two reports:

1)   C.N. Wilson, "Results from Cycles 1 and 2 of NNWSI Series 2 Dissolution Tests." HEDLTME85-22, May
      1987.

2)   C.N. Wilson, "Results from the NNWSI Series 3 Spent Fuel Dissolution Tests," PNL-7170, June 1990.

The pertinent solubility data taken after "steady-state" was reached are given in Table 1. In cases where several
values from different samples with different geometries and different bumup histories were shown, the most
conservative upper value is indicated. Since we don't know the cause of the scatter, it is prudent to assume the
worst case, pending a better understanding of the spread in the steady-state solubilities. Where filtered and
unfiltered values were available, the filtered dam were used because solubility is the information desired.

Table 2 indicates the specific source for each data value.

For slow flow of water over the spent fuel, the solubility can be used to determine the mass of each
radionuclide dissolved as a function of time. Given solubilities, C, a flow rate of water contacting
the spent fuel, Φ, and a time, t, over which dissolution occurs, the total amount of any nuclide, i, dissolved and
transported, M_i, is given by

$$M_i = C_i \, \Phi \, t$$

Please contact Mike Revelli of my staff at FTS 532-1982 for further information.

                                        L. J. Jardine
                                        LLNL Technical Project Officer
                                         for the Yucca Mountain Project

LJJ/JB.jw

Attachments

c: C. Newbury, YMPO

Table 1. Solubility Data, Ci

Species	Upper Limit Steady-State Concentration (µg/ml)	
	25°C	85°C
U	≤ 5	$\leq$ 0.5
$^{239+240}$Pu	$\leq 5 \times 10^{-3}$	$\leq$ 6×10^{-5}
^{241}Am	$\leq 3 \times 10^{-4}$	$\leq$ 1.5×10^{-7}
^{244}CM	$\leq 1.2 \times 10^{-4}$	$\leq$ 2.4×10^{-9}
^{237}Np	$\leq 4 \times 10^{-4}$	$\leq$ 1.4×10^{-3}

Only data for the solubility limited species are listed in the above table.

Table 2. Solubility Data Sources

Species	References	
	25°C	85°C
U	Ref. 1, Fig. 5	Ref. 2, Fig. 3.1
$^{239+240}$Pu	Ref. 1, Fig. 6	Ref. 2, Fig. 3.12
^{241}AM	Ref. 1, Fig. 7	Ref. 2, Fig. 3.15
^{244}CM	Ref. 1, Fig. 8	Ref. 2, Fig. 3.18
^{237}Np	Ref. 2, Fig. 3.20	Ref. 2, Fig. 3.20

Conversion factors from pCi to μg taken from Ref. 2, Table A.l.

The following describes data and an analysis procedure to obtain the release rate time response for a fully wetted mass of spent fuel dissolving without solubility limitations in water. The description is from an LLNL report UCRL-ID-107289 published in December, 1991.

Waste package analysts and designers have to understand the long term dissolution of waste form in groundwater to safely dispose of high level nuclear waste in an underground repository. The dissolution and transport processes in groundwater flow are generally considered to be the main route by which radionuclides could be released to the biosphere from a geological repository.

Many researchers have investigated the dissolution of UO_2, spent fuel and uraninite (a naturally occurring UO_2 mineral) in aqueous solutions, under either reducing or oxidizing conditions, and as a function of various other environmental variables. Experimental data on the dissolution rates of UO_2, spent fuel and uraninite have been reviewed by Arnell and Langmuir,[1] Parks and Pohl,[2] Bruno et al,[3] and most recently by Grambow.[4]

Important variables considered in the many investigations were pH, temperature, oxygen fugacity, carbonate/bicarbonate concentrations and other reacting media. The dissolution data are very scattered, and vary as much as six orders of magnitudes.[4] The dependence of the dissolution rates of UO_2, spent fuel and uraninite on these variables is not clear because of uncertainties regarding redox chemistry of uranium in solutions and in solid phases, secondary-phase formation, and surface area measurement. In addition, the previous studies were conducted under experimental conditions which were either inadequately controlled or which simulated complex repositorial conditions. The results of such studies are difficult to interpret. Several of these researchers have developed equations to correlate dissolution rates as a function of relevant variables.[5-8] However, none of the rate laws is universal, and inconsistencies or incompatibilities among the proposed laws are common.

Data indicate that UO_2 is easily oxidized to U_4O_9 and U_3O_7 in an air[9,10] and can be further oxidized to either U_4O_8[9,10,11] or schoepite, $UO_3 \cdot 2H_2O$.[12] The UO_2 surface oxidation may lead to higher leach rates because of possibly higher dissolution rates of U_3O_7, U_4O_8 or schoepite relative to that of UO_2[4] because of the increase of surface area of the fuels due to surface cracking.

Discussion

We are estimating a source term for liberation of radionuclides from spent fuel
dissolving under conditions of temperature and water composition related to those
anticipated for a potential repository at Yucca Mountain. This is done in the same spirit as
estimates that have been made for repositories in Germany[13] and Sweden.[14] It is implicit in
the following treatment that fission products are dissolved congruently with the UO_2 fuel
matrix, except for those volatile species that have partially vaporized and that fraction that
has migrated to near-surface grain boundaries and are possibly dissolved independent of
the matrix dissolution. Most fission products and higher actinides are distributed
throughout the UO_2 matrix, however.

Recent measurements on UO_2[15] and spent fuel (SF)[16] under comparable conditions have
provided dissolution rates for UO_2 between 25°C and 85°C in waters of various
composition and for SF in deionized water (DIW) at 25°C. These experiments were done in
contact with air. The results are shown in Figures 1 and 2. The rate of dissolution of SF in
DIW at 25°C is $1.2\text{-}1.7 \times 10^{-12}$ g cm^{-2} sec^{-1} This is similar to the rate for UO_2 in DIW at 25°C at
-5×10^{-12} g cm^{-2} sec^{-1}. Given the great variability in other reported values[4] this is reasonable
agreement. In fact, the observed dissolution rate for SF at 25°C is about the same as that of
UO_2 in (DIW + Ca + Si), a simulation of ground water.[14]

A model for dissolution is used in which the dissolution front propagates linearly in
time, much like a recently published model for the advance of the oxidation front during
oxidation Of UO_2 and spent fuel.[16-19] This implies that the particle geometry is retained. We
can describe the change in characteristic dimension of a SF particle (a sort of "radius"), X as
follows:

$$\mathbf{X(t)} = \mathbf{X_0} - \left(\frac{\mathbf{Q}}{\rho}\right)\mathbf{t,} \tag{1}$$

where   X(t) = the characteristic dimension as a function of time
                X_0 = the original dimension (half of the actual size)
                t   = time
                Q = dissolution rate per unit area
                ρ = density

The time for complete dissolution of a particle of original size X_o is then

$$\mathbf{t_\infty = \frac{X_0 r}{Q}} \qquad\qquad (2)$$

This dissolution time is proportional to size, of course, and for an ensemble of particles of different sizes, t_∞ for the ensemble is that for the largest particle.

Some data are available on the size distribution of spent fuel fragments. These data are given for two different fuels but the distributions are quite similar. The aggregate of these two sets of data can be adequately described by the simplified distribution shown in Table I.

Table I

Approximate Size (cm) $(2X_o)$	Weight (Volume Fraction
0.15	.02
0.25	.14
0.35	.29
0.50	.38
0.70	.17

Using the relationship of equation (1), we can calculate the time to dissolve a given weight (volume) fraction of an amount of SF as a function of time. For generality, we treat time as the dimensionless quantity t/t_∞ with t_∞ defined above. This is shown in Figure 3 for the size distribution given in Table I*, and also for a single size with $X_o = 0.35$ cm. Here V_o and $V(t)$ are the original volume of a particle and its volume at arbitrary time, respectively. The volume is proportional to the characteristic dimension

$$V_o = kX_o{}^3 \text{ and } V(t) = kX^3(t)$$

where k is a constant depending on shape. Since geometry is retained, as noted above,

---

*Each size was calculated separately and the time responses were added together.

$$\frac{V(t)}{Vo} = \left(\frac{X(t)}{Xo}\right)^3 = 1 - 3\left(\frac{Q}{X_o\rho}\right)t + 3\left(\frac{Q}{X_o\rho}\right)^2 t^2 - \left(\frac{Q}{X_o\rho}\right)^3 t^3, \tag{3}$$

$$\frac{d\left(\frac{V(t)}{V_o}\right)}{dt}$$

and the dissolution rate is -

Initially, i.e., $t \rightarrow 0$

$$\text{Rate } (t=0) = 3\left(\frac{Q}{X_o\rho}\right)$$

and the extrapolated time for total dissolution is

$$t_\infty^* = \frac{X_o\rho}{3Q}$$

In Figure 4 we show that the rate of dissolution relative to the initial rate varies with time for both the system with $X_o = 0.35$ cm and for the distribution of Table I.

The measured dissolution rate for UO_2[15] and spent fuel[16] allow us to calculate actual times for dissolution. As is evident from Figure 3, the overall dissolution rate is greatest at early time and approaches zero as t_∞ is approached; therefore, as a conservative approximation, we have also calculated the total dissolution time extrapolated from the initial rate, t_∞^*. These times calculated for the size distribution in Table I are given in Table II. The actual dissolution rates are derived from the bottom curve in Figure 1. We chose this curve as most representative of the expected ground water. The rate equation used is

$$Q(t)(\text{gcm}^{-2}\text{ sec}^{-1} = 6.43\text{x}10^{-9}\text{ex} - \left(\frac{4740}{RT(K)}\right) \text{ (R is in cal/mole K)} \tag{5}$$

Table II

Temperature (°C) t_∞^*	Dissolution Time (years) t_∞
258.0 x 10³	5.5 x 10⁴
852.2 x 10³	1.5 x 10⁴

<u>Conclusions</u>

These times are calculated for the case of bare fuel immersed in unlimited quantities of flowing water at flow rates sufficient to prevent any species from forming a saturated solution. Nonetheless, this estimate provides a "core" value on which to apply "credits" corresponding to features of realistic repository performance such as frequency of cladding and container failure, actual amounts of ground water and various transport rates, etc. Of course, this "core" estimate is based on only one particular dissolution rate, as is discussed above. Future measurements of dissolution rate may change this value considerably. The estimates presented here ignore the possibility that grain boundary dissolution behaves differently than bulk SF dissolution.

Dissolution tests are now under way that are designed to define the mechanism of the dissolution process Of UO_2 and SF in terms of oxidizing potential, temperature, pH and other water composition variables generally appropriate to a potential repository at Yucca Mountain. When these tests are completed, considerably more realistic estimates will be possible. These tests will also clarify the contribution of radionuclides from grain boundaries to the total dissolution rate.[16]
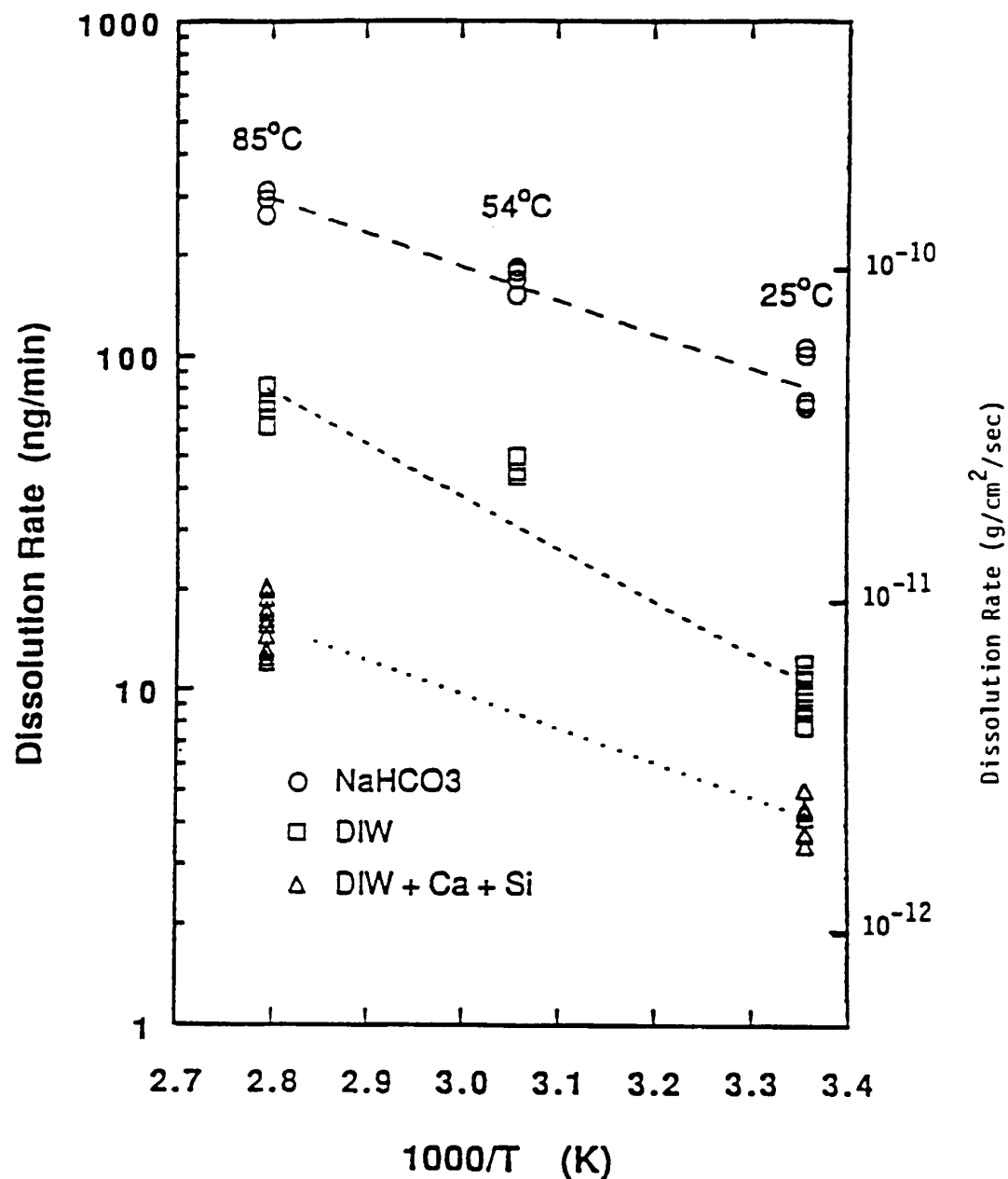
Figure 1. Arrhenius plots of the dissolution rate of UO_2 in waters of various composition.

ATM—105 in DIW
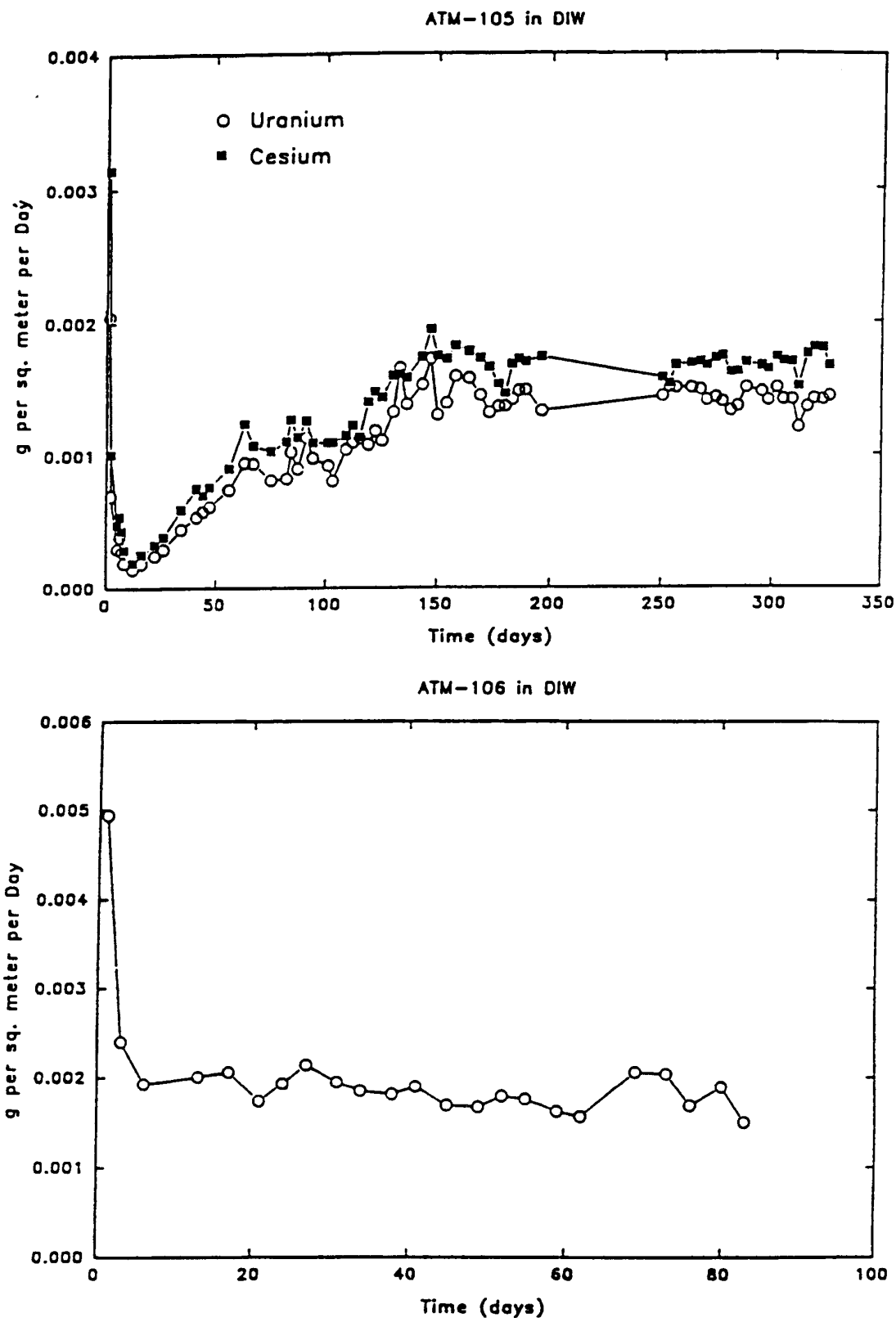

ATM—106 in DIW

Figure 2. The approach to steady-state of the dissolution rate of two spent fuel
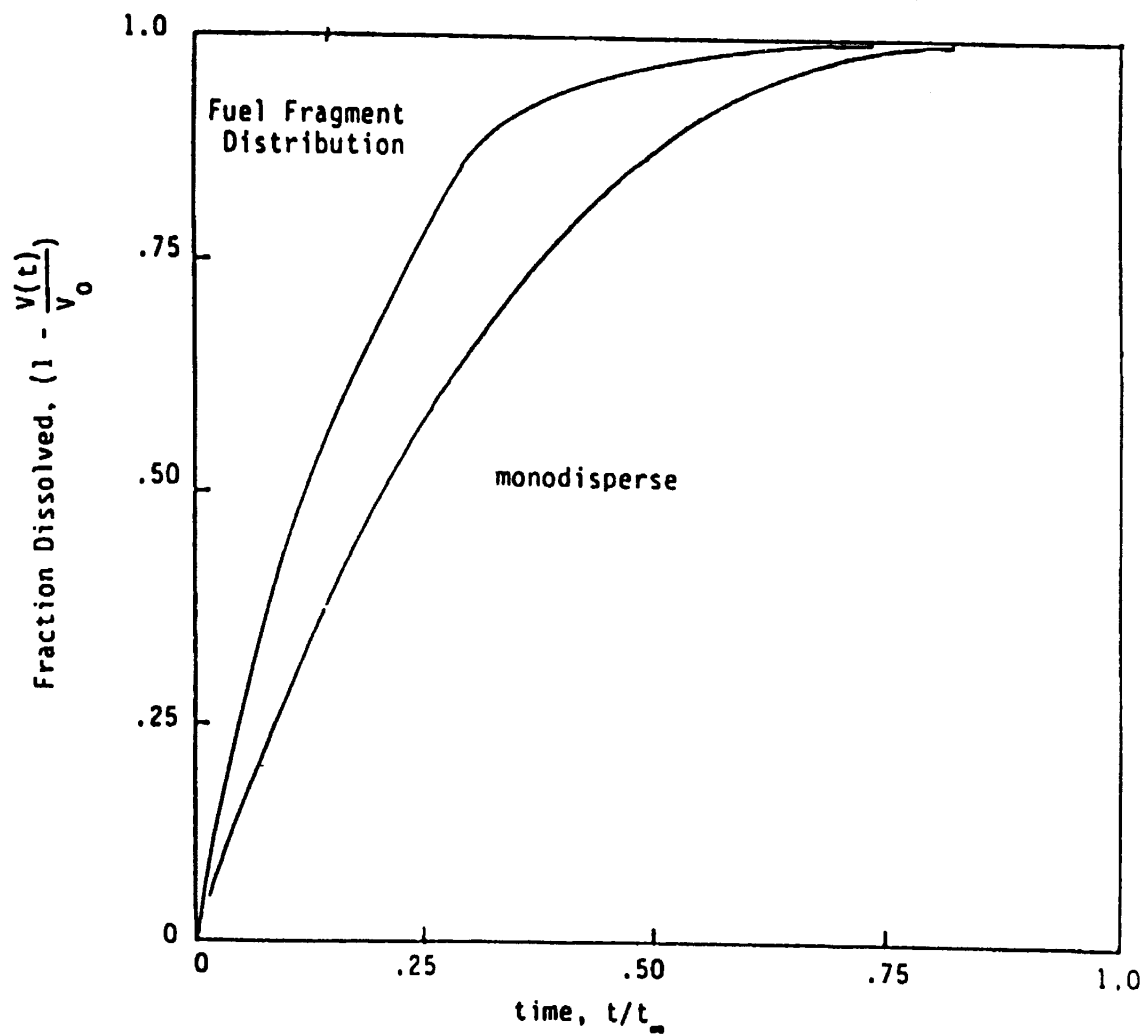samples.' Experiments were done at 25°C using deionized water (DIW).

Figure 3. Calculation of the fractional dissolution in terms of dimensionless time, according to equation (3). Monodisperse refers to a single particle size.
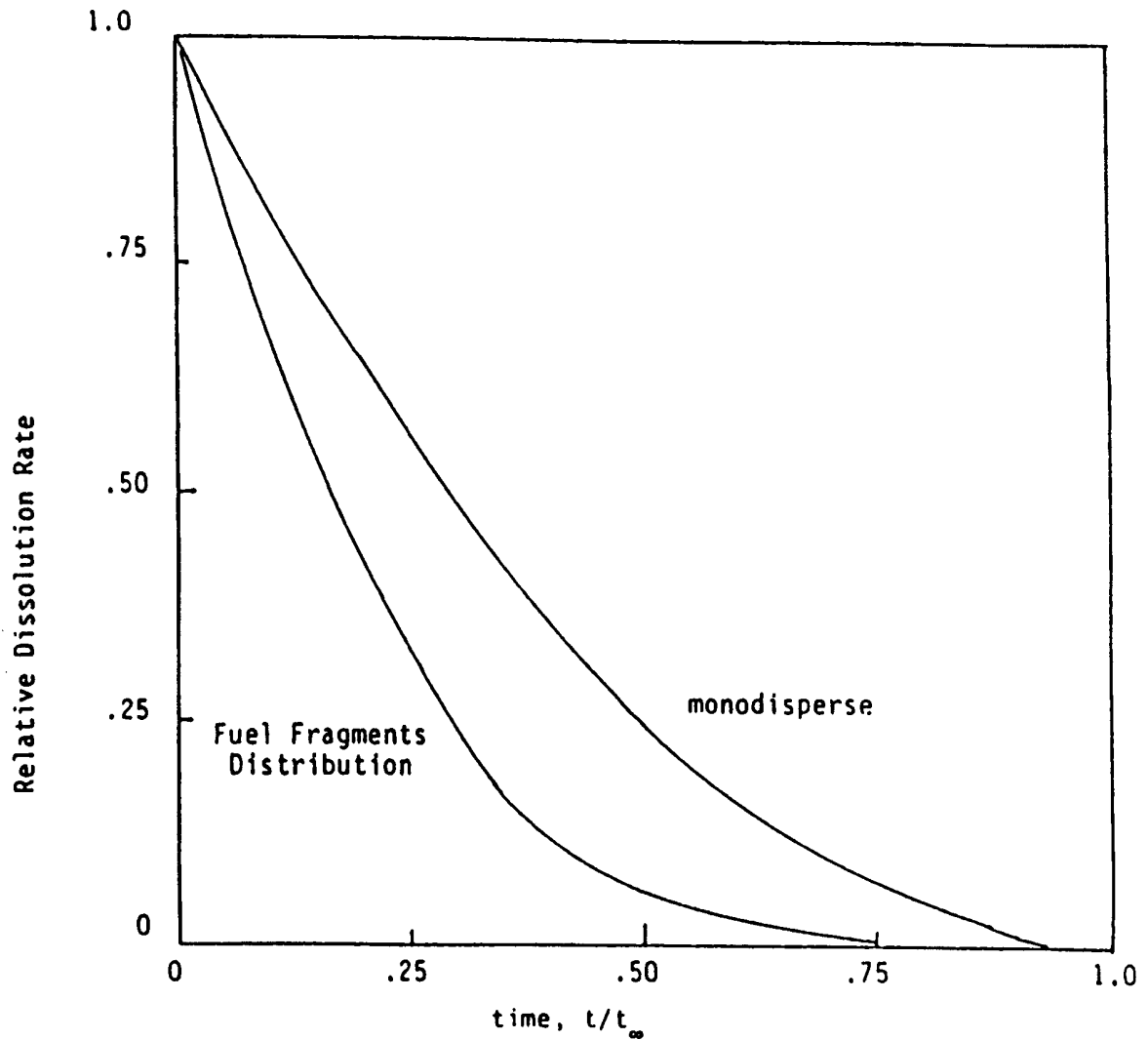
Figure 4. Evolution of the normalized dissolution rate with time as the particle size decreases, according to equation (3).

References

1.   Amell, A. R., and Langmuir, D., "Factors Influencing the Solution Rate of Uranium Dioxide Under Conditions Applicable to in-Situ Leaching", Bureau of Mines Open File Report 84-79, U.S. Department of the Interior - Bureau of Mines, (1978). (Readily Available)

2.   Parks, G. A., and Pohl, D. C., "Hydrothermal Solubility of Uraninite", Geochiin. Cosmochim. Acta $\underline{52}$ 863 (1988). NNA.910821.0003

3.   Bruno, J., Casas, I., and Puigdomenech, I., "The Kinetics of Dissolution of $UO_2(s)$ Under Reducing Conditions", Radiochimica Acta $\underline{44/45}$, 11 (1988). NNA.910821.0004

4.   Grambow, B., "Spent Fuel Dissolution and Oxidation. An Evaluation of Literature Data", SKB Technical Report 89-13 (1989). NNA.891013.0094

5.   Grandstaff, D. E., "A Kinetic Study of the Dissolution of Uraninite", Econ. Geo. $\underline{71}$ 1493, (1976). NNA.911025.0061

6.   Schortmann, W. E. and De Sesa, M. A., "Kinetics of the Dissolution of Uranium Dioxide in Carbonate-Bicarbonate Solutions", Proc. 2nd International United Nations Conference Peaceful Uses of Atomic Energy, United Nations, Geneva, $\underline{3}$, 333 (1958). NNA.910821.0005

7.   Pearson, R. L, and Wadsworth, M. E., "A Kinetic Study of the Dissolution of UO_2 in Carbonate Solution", Trans. Metal Sor. AIME $\underline{212}$, 294 (1958). NNA.910821.0006

8.   Habashi, F., and Thurston, G. A., "Kinetics and Mechanisms of the Dissolution of Uranium Dioxide", Energ. Nucl. $\underline{14}$. $\underline{238}$ (1967). NNA.910821.0007

9.   Aronson, S., "Oxidation and Corrosion of Uranium Dioxide in Uranium Dioxide: Properties and Nuclear Applications", J. Belle, ed., United States Atomic Energy Commission, 377 (1961). NNA.9110234.0060

10. Einziger, R. E., "Test Plan for Long-Term, Low-Temperature Oxidation of BWR Spent Fuel", PNL-6427, Pacific Northwest Laboratory, (1988). NNA.890224.0045

11. Aronson, S., Oxidation of UO_2 in Water Containing Oxygen", Bettis Tech. Rev., Westinghouse Atomic Powu Div., Report WAPD-BT-10, 93 (1958). NNA.91IM5.0062

12. Wadsten, T., "The Oxidation of Polycrystalline Uranium Dioxide in Air at Room Temperature", T. Nucl. Mat. 64, 315 (1977). (Readily Available)

13. Wvertz, R. and Ellinger, M., "Source Term for the Activity Release from a Repository for Spent LWR Fuel', Mat. Res. Soc. Symp. Proc 50, 393 (1985). (Readily Available).

14. Gray, W. and Wilson, C., "Effects of Water Composition and Temperature on the Dissolution Rate of UO_2' presented at 1990 Spent Fuel Workshop, Gull Harbor, Manitoba, Canada (1990). NNA.910821.0008

15. Gray, W., and Strachan, D., "Spent Fuel Grain Boundary Inventory and Testing the Congruency of UO_2 Matrix Dissolution of Spent Fuel", presented at the 1990 Spent Fuel Workshop, Gull Harbor, Manitoba, Canada (1990). NNA.910821.0009

16. Stout, R. B, Shaw, H. F. and Einziger, R. E., "Statistical Model for Grain Boundary and Grain Volume Oxidation Kinetics in UO_2 Spent Fuel", Lawrence Livermore National Laboratory UCRL-100859, September 1989. NNA.891031.0015

17. Stout, R. B., Kansa, E., Buchanan, H. C., Einziger, R. E. and Thomas, L. E., "Spent Fuel Waste Form Characteristics: Grain and Fragment Size Statistical Dependence for Oxidation Studies", Lawrence Livermore National Laboratory, UCRL-104932, December 1990. (Readily Available)

18. Stout, R. B. et al, "Spent Fuel Waste Form Characteristics: Grain and Fragment Size Statistical Dependence for Dissolution Response", Lawrence Livermore National Laboratory Report UCRL-104931, December 1990. (Readily Available)

19. Van Luik, A. E, et al, "Spent Nuclear Fuel as a Waste Form for Geologic Disposal: Assessment and Recommendations on Data and Modeling Needs, Pacific Northwest Laboratory Report, PNL-6329 (UC-70), September 1987. [HQS.1988.0105.0020]

2.1.3.6 Soluble-Precipitated/Colloidal Species

Table 2.1.3.6-1 **Phases identified on reacted UO_2 surface (Table II from J. K. Bates,** *Identification of Secondary Phases Formed During Unsaturated Reaction of UO_2 with EJ-13 Water,* **Materials Research Society Symposium proceedings 176, 499 [1990])**

Phase	Formula	Appearance
Schoepite	$UO_3 \cdot 2H_2O$	Dark yellow crystals
Dehydrated Schoepite	$UO_3 \cdot 0.8H_2O$	Yellow crystals with reflective face
Compreignacite	$K_2U_6O_{19} \cdot 11H_2O$	Yellow crystals
Uranophane	$Ca(UO_2)_2(SiO_3)_2(OH)_2 \cdot 5H_2O$	Fine white needles
Boltwoodite	$K(H_3O)UO_2(SiO_4) \cdot nH_2O$	Yellow crystals
Sklodowskite	$Mg(UO_2)_2(SiO_3OH)_2 \cdot 5H_2O$	Fine needles
Becquerelite	$CaU_6O_{19} \cdot 10H_2O$	Dark yellow crystals
Fluoropolymer	Not determined	White feathers

Table 2.1.3.6-2 **No title (Table 2 from C.J. Bruton,** *Solubility Controls on Radionuclide Concentrations in Solution: Preliminary Results for U, Np, Pu, and Am,* **LLNL draft report, November, 1990)**

U		
	Concentration	
Solid	mg/l	molality (moles/kg)
Haiweeite $Ca(UO_2)_2Si_6O_{15} \cdot 5H_2O$	0.1641E–3	0.6893E–9
Soddyite $(UO_2)_2SiO_4 \cdot 2H_2O$	0.015	0.6096E–7
Sklodowskite $Mg(H_3O)_2(UO_2)_2-(SiO_4)_2 \cdot 4H_2O$	11.05	0.4642E–4
$CaUO_4$	12.59	0.5289E–4
Schoepite $UO_3 \cdot 2H_2O$	38.90	0.1634E–3
$UO_2(OH)_2(beta)$	56.73	0.2383E–3
Uranophane $Ca(UO_2)_2(SiO_3)_2(OH)_2$	142.48	0.5986E–03

Table 2.1.3.6-3   No title (Table 3 from C.J. Bruton, *Solubility Controls on Radionuclide Concentrations in Solution: Preliminary Results for U, Np, Pu, and Am*, LLNL draft report, November, 1990)

Np		
	Concentration	
Solid	mg/l	molality (moles/kg)
NpO_2	0.59	0.2468E–5
$NpO_2(OH)(am)$	129.39	0.5459E–3
$NaNpO_2CO_3 \cdot 3.5H_2O$	139.99	0.5906E–3
am = amorphous		

Table 2.1.3.6-4   No title (Table 4 from C.J. Bruton, *Solubility Controls on Radionuclide Concentrations in Solution: Preliminary Results for U, Np, Pu, and Am*, LLNL draft report, November, 1990)

Pu		
	Concentration	
Solid	mg/l	molality (moles/kg)
PuO_2	0.39E–6	0.1612E–11
$PuO_2(OH)_2$	0.015	0.6204E–7
$Pu(OH)_4$	27.97	0.1146E–3

Table 2.1.3.6-5   No title (Table 5 from C.J. Bruton, *Solubility Controls on Radionuclide Concentrations in Solution: Preliminary Results for U, Np, Pu, and Am*, LLNL draft report, November, 1990)

Am		
	Concentration	
Solid	mg/l	molality (moles/kg)
$AmOHCO_3$	0.0041	0.1696E–7
$Am(OH)_3$	8.42	0.3464E–4
$Am(OH)_3(am)$	158.66	0.6529E–3

Figure 2.1.3.6-1 **U concentration vs. pH in J-13 water (Figure from C.J. Bruton,** *Solubility Controls on Radionuclide Concentrations in Solution: Preliminary Results for U, Np, Pu, and Am*, **LLNL draft report, November, 1990)**

Figure 2.1.3.6-2   U concentrations vs. pH in J-13 water (U-bearing solids)
(Figure from C.J. Bruton, *Solubility Controls on Radionuclide*
Concentrations in Solution: Preliminary Results for U,
***Np, Pu, and Am*, LLNL draft report, November, 1990)**

εh, volts

Figure 2.1.3.6-3 **GETSOL: Mon July 30 13:11:24 1990 (Figure from C.J. Bruton,** *Solubility Controls on Radionuclide Concentrations in Solution: Preliminary Results for U, Np, Pu, and Am*, **LLNL draft report, November, 1990)**
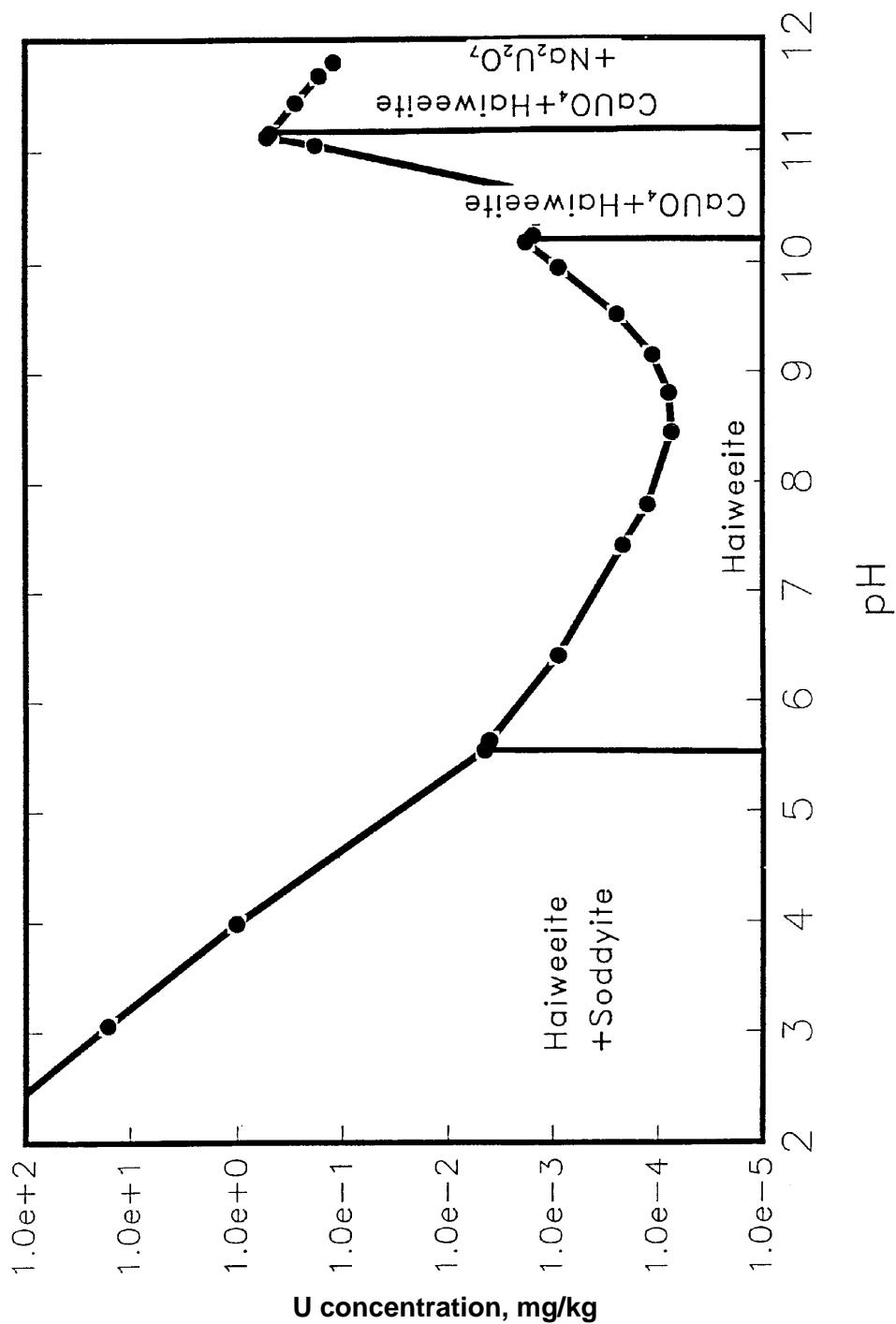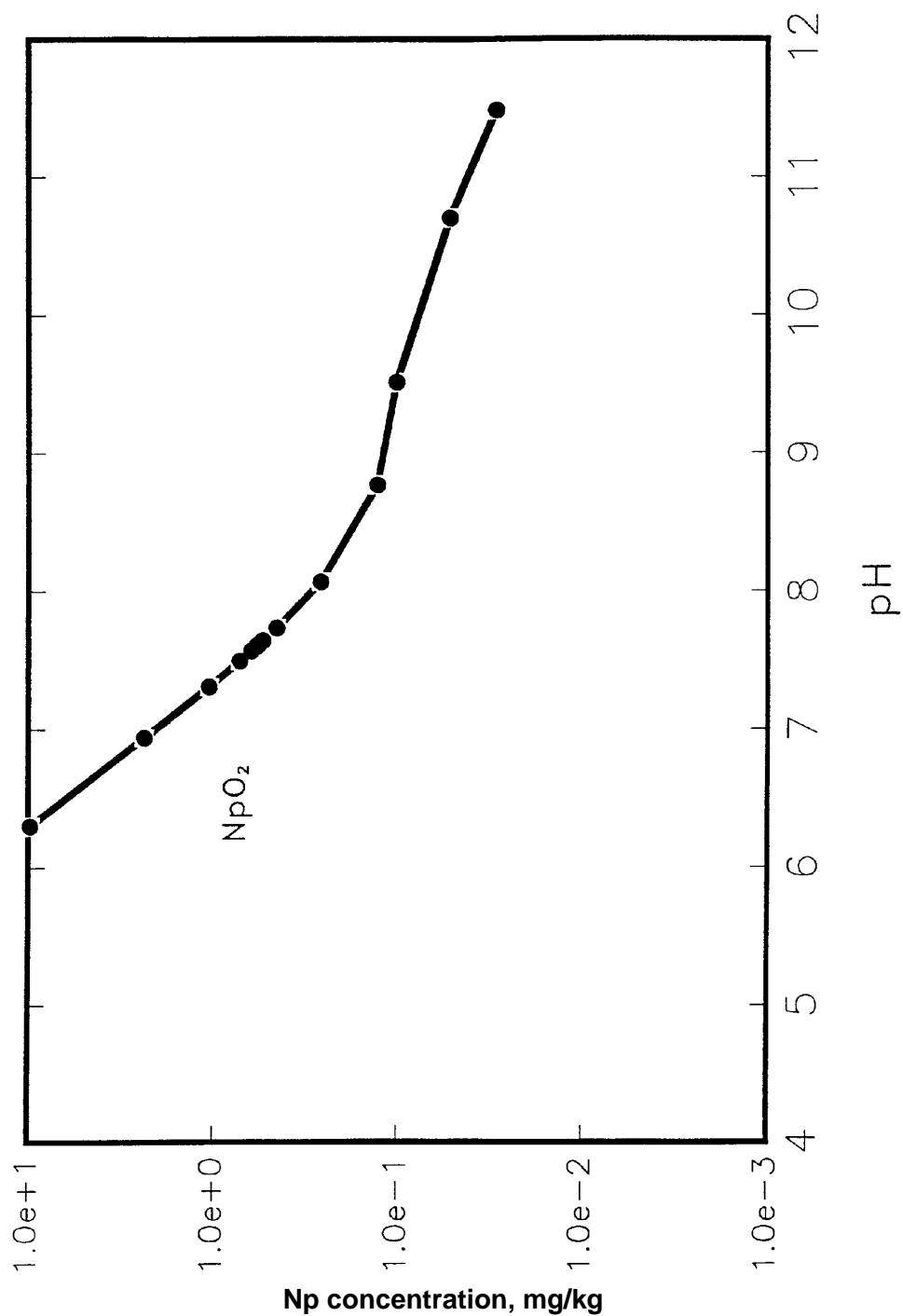
Figure 2.1.3.6-4   Np concentration vs. pH in J-13 water (Figure from C.J. Bruton, *Solubility Controls on Radionuclide Concentrations in Solution: Preliminary Results for U, Np, Pu, and Am***, LLNL draft report, November, 1990)**
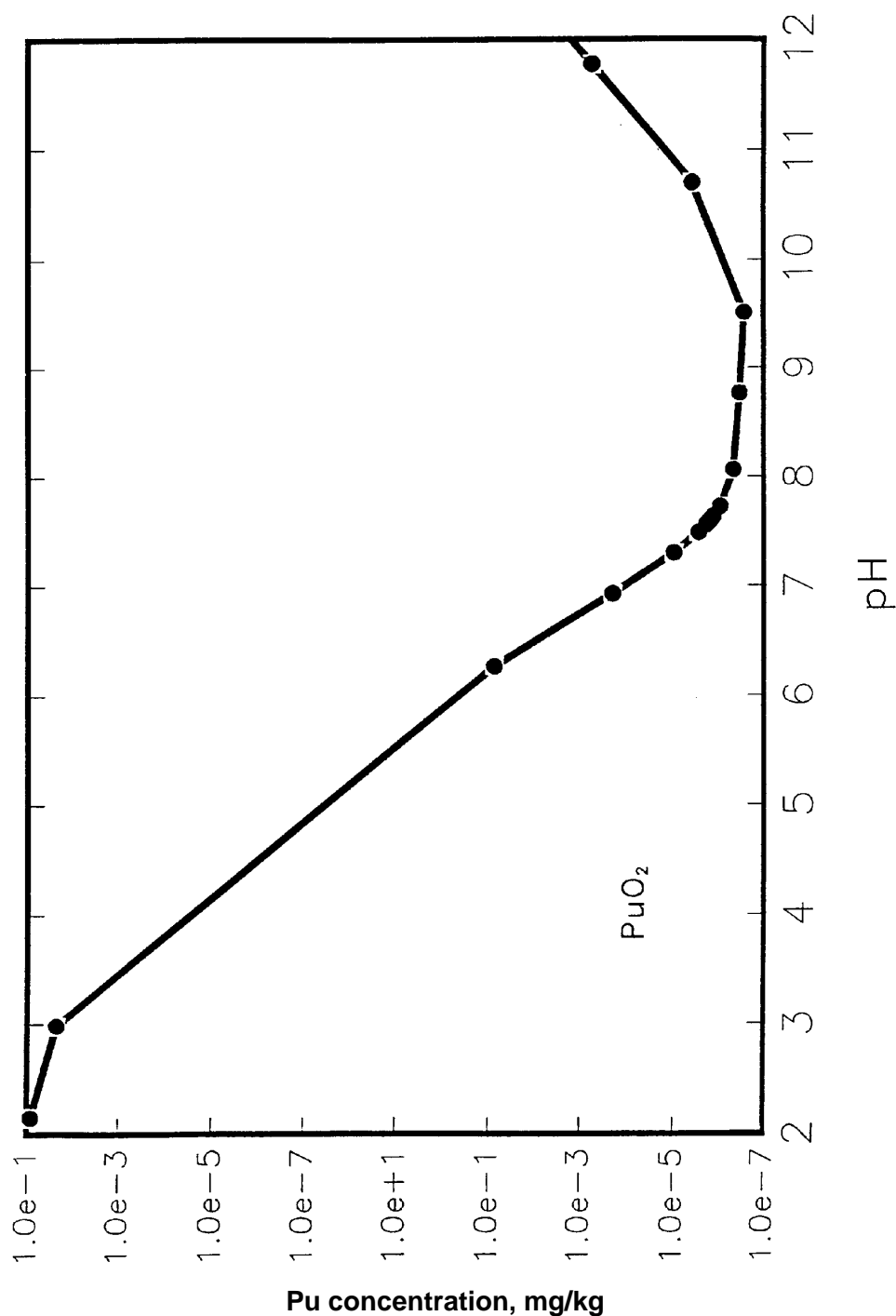
Figure 2.1.3.6-5   Pu concentration vs. pH in J-13 water (PuO₂) (Figure from C.J. Bruton, *Solubility Controls on Radionuclide Concentrations in Solution: Preliminary Results for U, Np, Pu, and Am*, LLNL draft report, November, 1990)
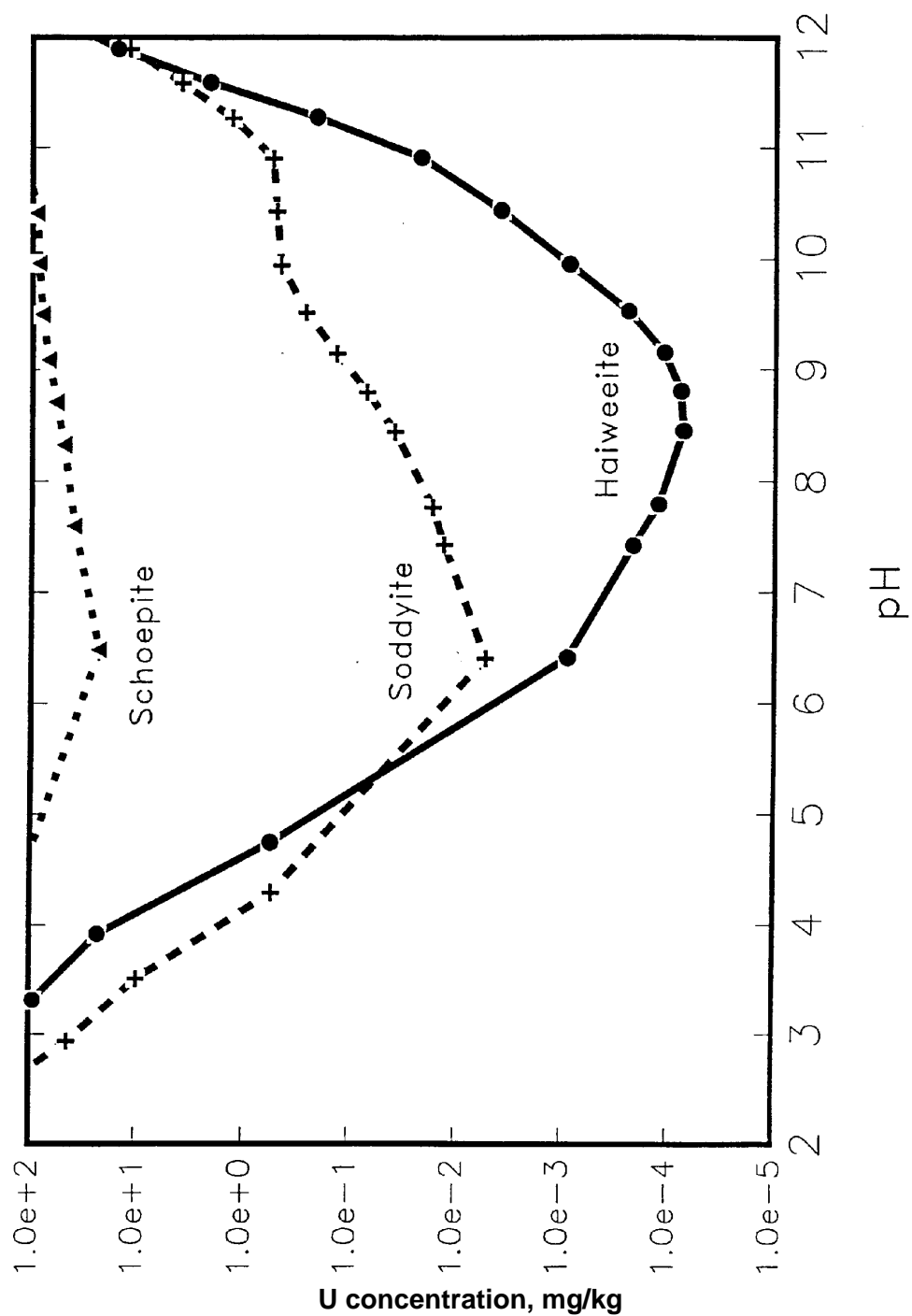
Pu concentration, mg/kg
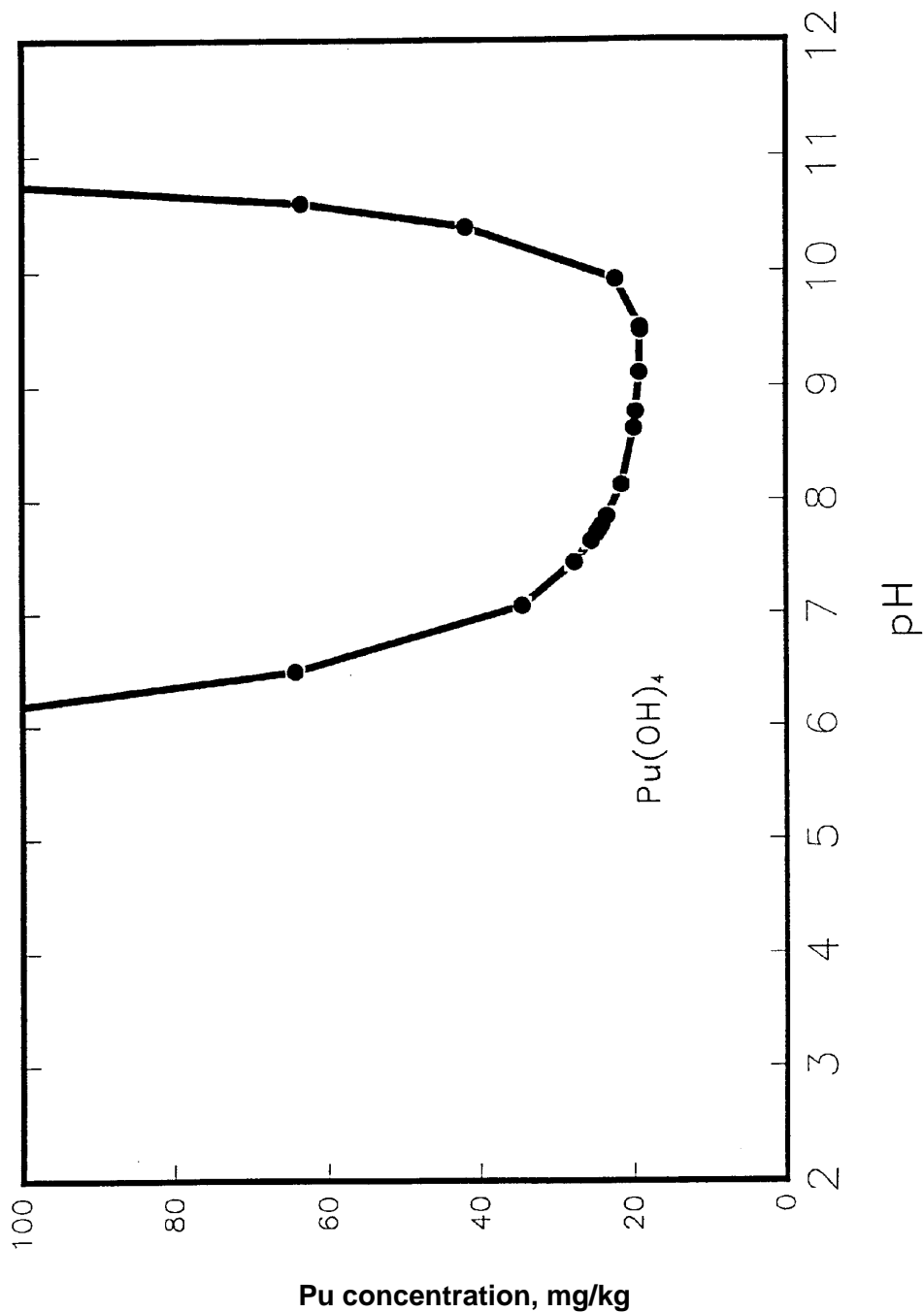
**Figure 2.1.3.6-6   Pu concentration vs. pH in J-13 water (Pu(OH)$_4$)
(Figure from C.J. Bruton, *Solubility Controls on
Radionuclide Concentrations in Solution: Preliminary
Results for U, Np, Pu, and Am*, LLNL draft report,
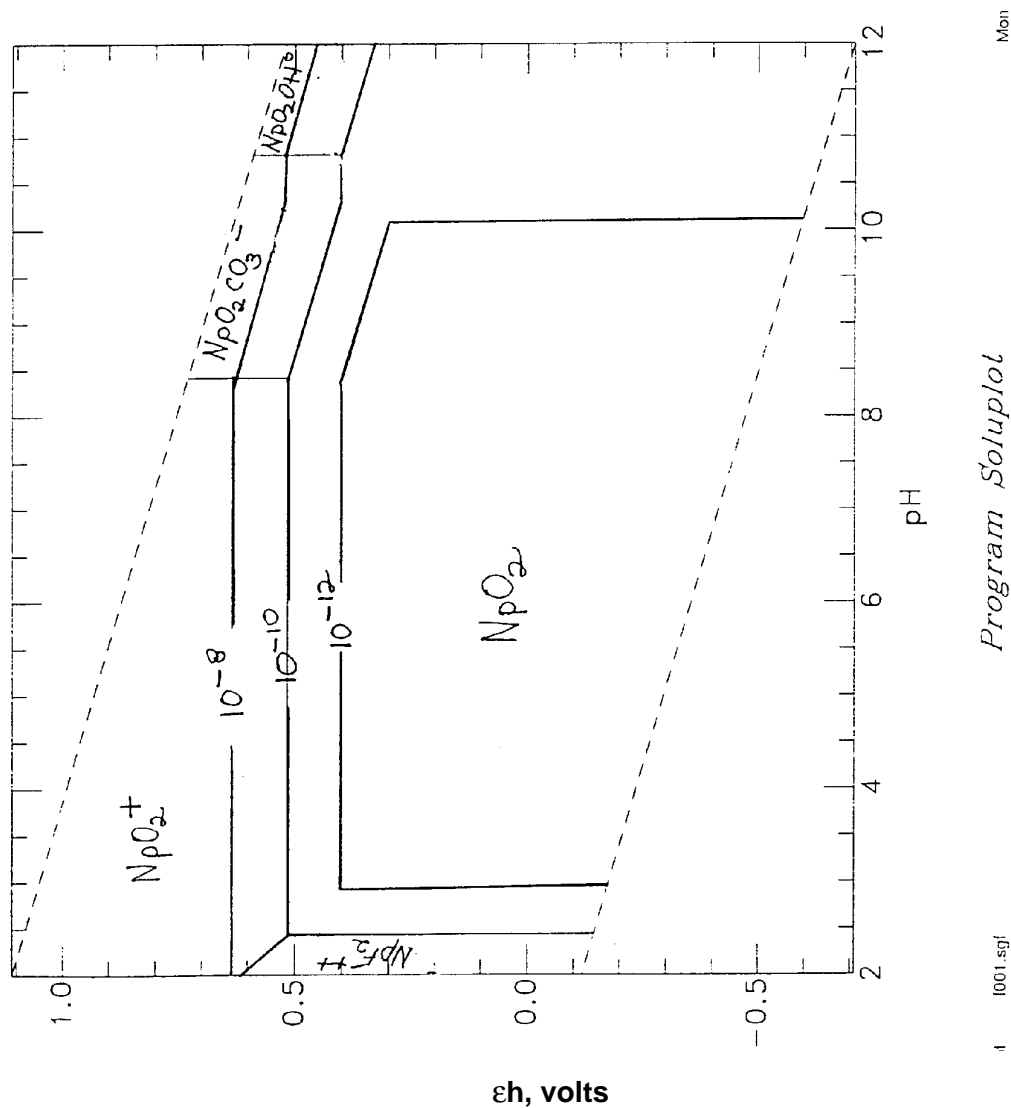November, 1990)**
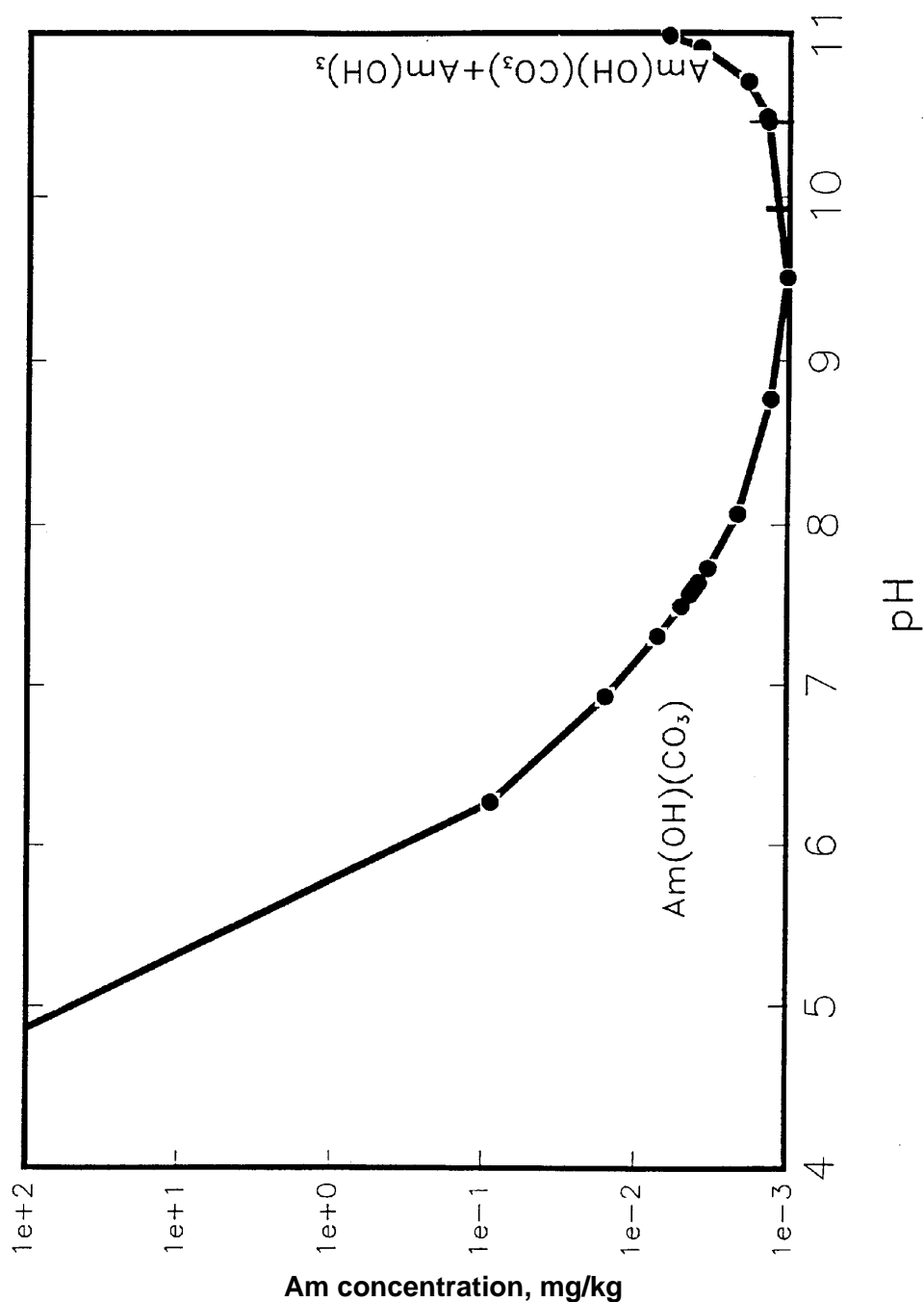
Figure 2.1.3.6-7   Am concentration vs. pH in J-13 water (Figure from C.J. Bruton, *Solubility Controls on Radionuclide Concentrations in Solution: Preliminary Results for U, Np, Pu, and Am*, LLNL draft report, November, 1990)
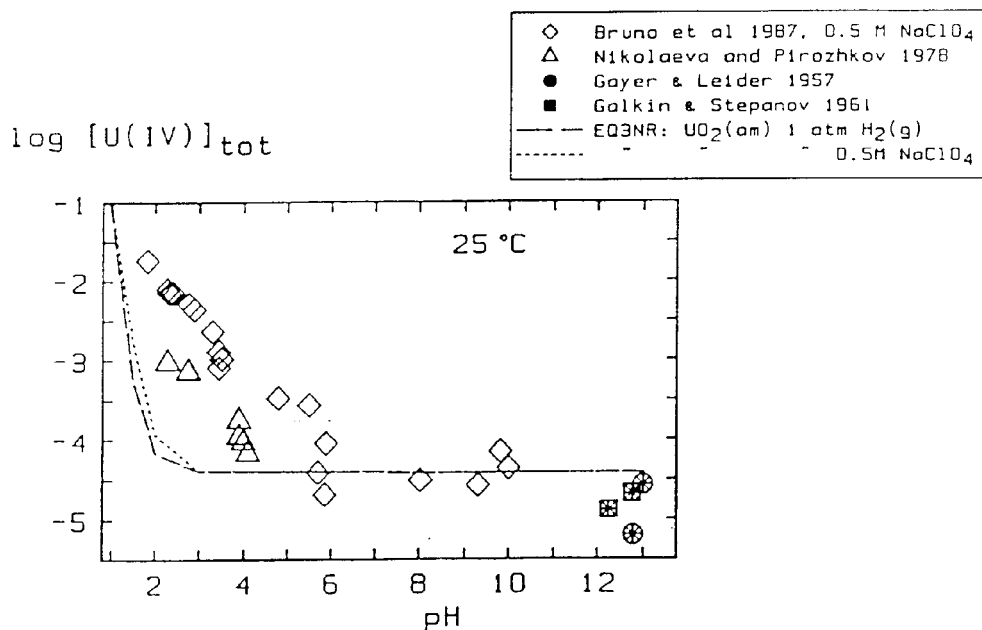
Figure 2.1.3.6-8 The solubility of UO$_2$ (am) (both in diluted solutions and in 0.5 M NaClO$_4$) as a function of pH at 25°C (Figure 5.12 from I. Puigdomenech and J. Bruno, *Modeling Uranium Solubilities in Aqueous Solutions: Validation of a Thermodynamic Data Base for the EQ3/6 Geochemical Codes,* SKB technical report 88-21, October 1988)
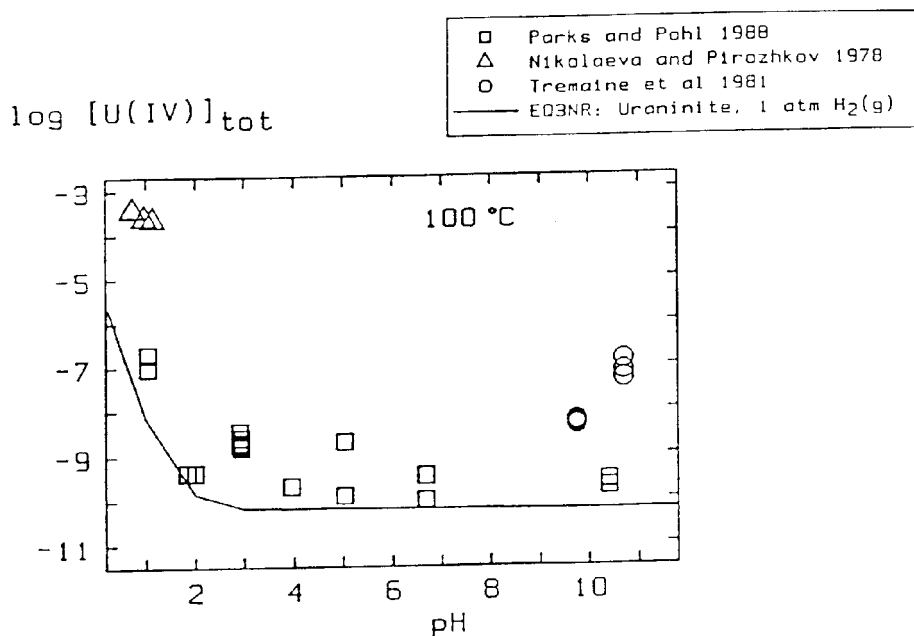
Figure 2.1.3.6-9 The solubility of crystalline UO$_2$ (s) versus pH at 100°C (Figure 5.14 from I. Puigdomenech and J. Bruno, *Modeling Uranium Solubilities in Aqueous Solutions: Validation of a Thermodynamic Data Base for the EQ3/6 Geochemical Codes,* SKB technical report 88-21, October 1988)
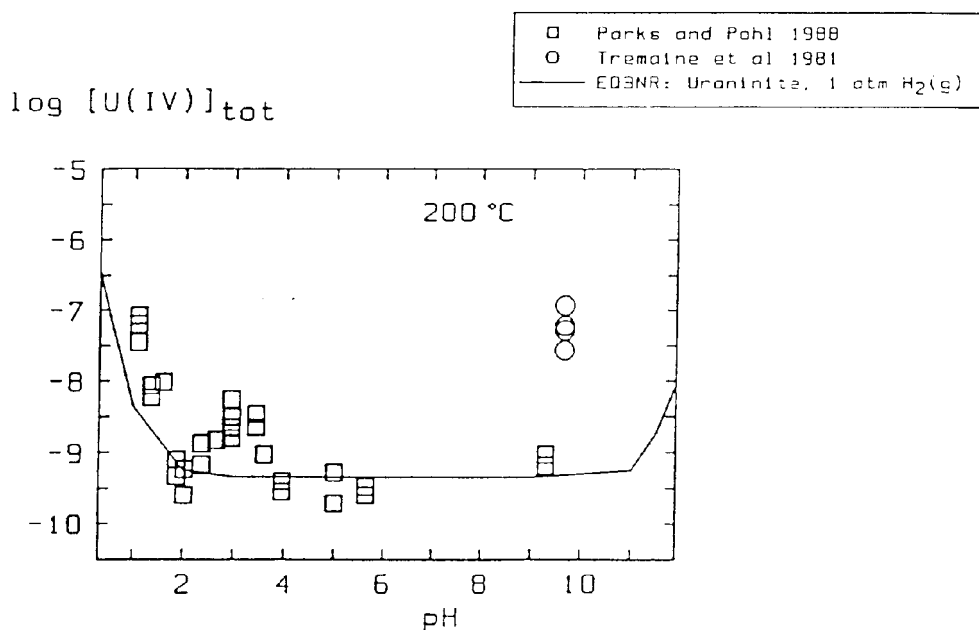
Figure 2.1.3.6-10 The solubility of crystalline UO$_2$ (s) versus pH at 200°C (Figure 5.15 from I. Puigdomenech and J. Bruno, *Modeling Uranium Solubilities in Aqueous Solutions: Validation of a Thermodynamic Data Base for the EQ3/6 Geochemical Codes,* SKB technical report 88-21, October 1988)
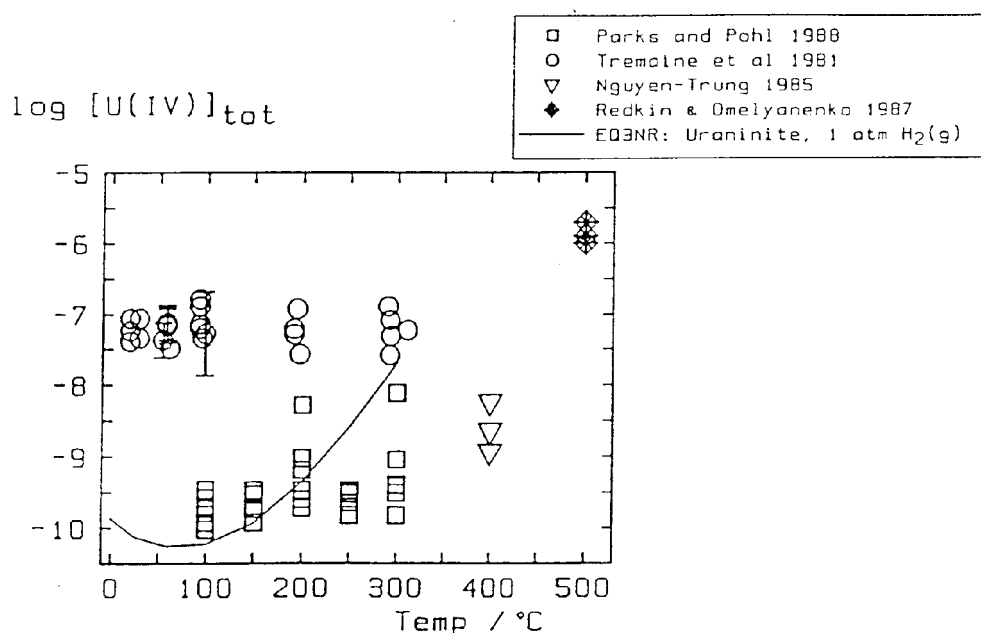
Figure 2.1.3.6-11 The calculated solubility of crystalline UO$_2$ (s) in water at 1 atm H$_2$(g) versus T, compared with experimental literature values (for UO$_2$ (c) solubility either in water or in diluted solutions of pH>5) (Figure 5.16 from I. Puigdomenech and J. Bruno, *Modeling Uranium Solubilities in Aqueous Solutions: Validation of a Thermodynamic Data Base for the EQ3/6 Geochemical Codes,* SKB technical report 88-21, October 1988)
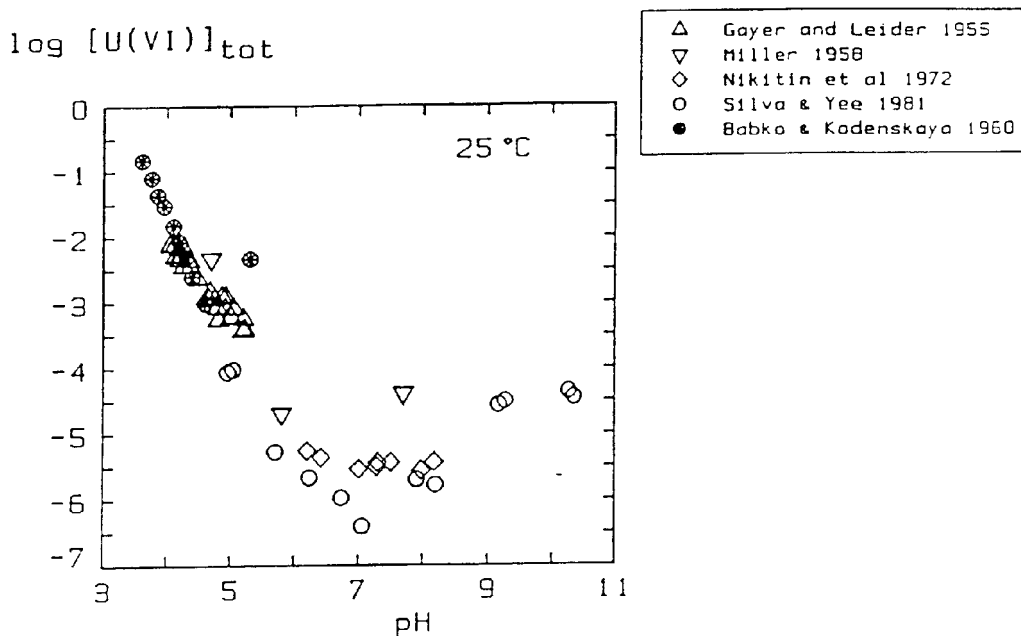
Figure 2.1.3.6-12 Some of the experimental literature data for the solubility of U(VI) hydroxide as a function of pH at 25°C (Figure 2.2 from I. Puigdomenech and J. Bruno, *Modeling Uranium Solubilities in Aqueous Solutions: Validation of a Thermodynamic Data Base for the EQ3/6 Geochemical Codes,* SKB technical report 88-21, October 1988)
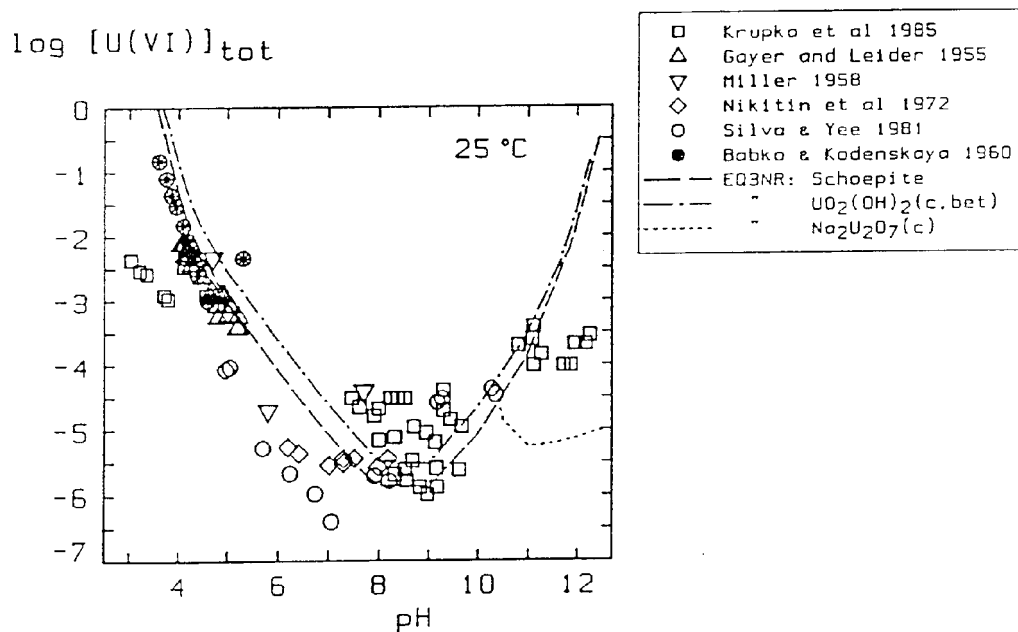
Figure 2.1.3.6-13 The solubility at 25°C of UO_2 $(OH)_2$ (c), schoepite and $Na_2U_2O_7$(c) as a function of pH (Figure 5.1 from I. Puigdomenech and J. Bruno, *Modeling Uranium Solubilities in Aqueous Solutions: Validation of a Thermodynamic Data Base for the EQ3/6 Geochemical Codes,* SKB technical report 88-21, October 1988)
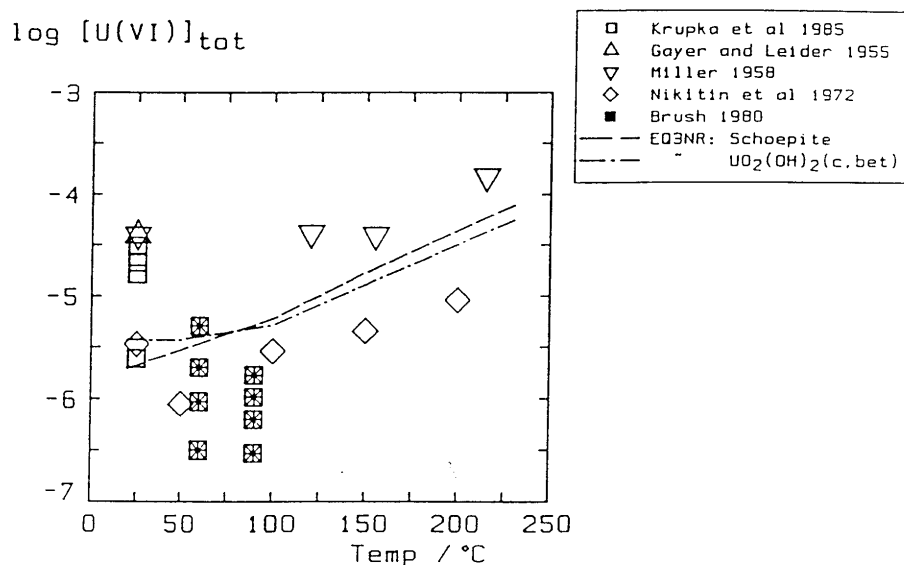
Figure 2.1.3.6-14 The calculated solubility of schoepite and UO$_2$ (OH)$_2$(c) in water as a function of T, compared with experimental values in the pH range 7 to 8 (Figure 5.6 from I. Puigdomenech and J. Bruno, *Modeling Uranium Solubilities in Aqueous Solutions: Validation of a Thermodynamic Data Base for the EQ3/6 Geochemical Codes,* SKB technical report 88-21, October 1988)
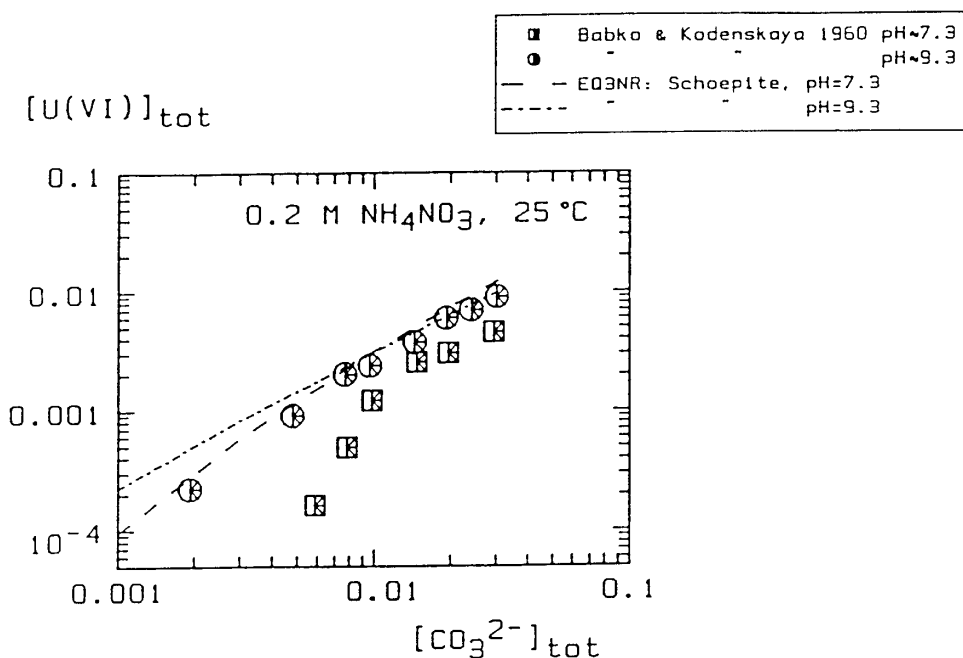
Figure 2.1.3.6-15 The solubility at 25°C of schoepite and as a function of carbonate concentration in 0.2 M NH$_4$NO$_3$ (Figure 5.4 from I. Puigdomenech and J. Bruno, *Modeling Uranium Solubilities in Aqueous Solutions: Validation of a Thermodynamic Data Base for the EQ3/6 Geochemical Codes,* SKB technical report 88-21, October 1988)
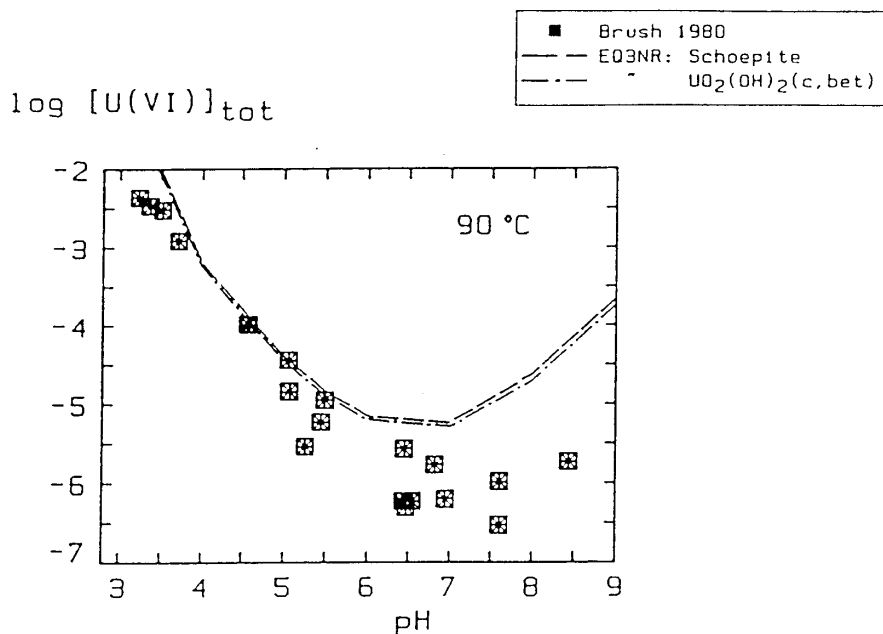
Figure 2.1.3.6-16 The solubility at 90°C of $UO_2(OH)_2$(c) as a function of pH (Figure 5.5 from I. Puigdomenech and J. Bruno, *Modeling Uranium Solubilities in Aqueous Solutions: Validation of a Thermodynamic Data Base for the EQ3/6 Geochemical Codes,* SKB technical report 88-21, October 1988)
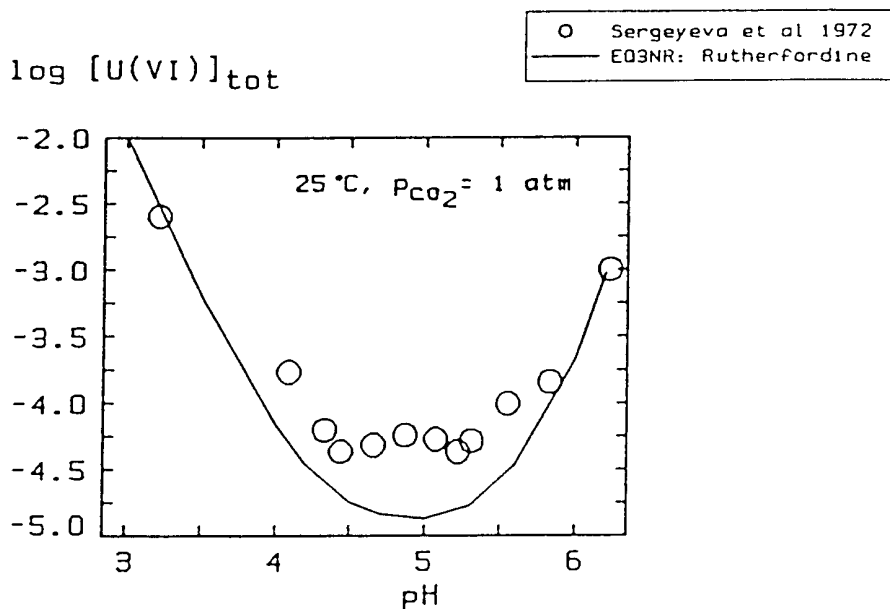

Figure 2.1.3.6-17 The solubility of rutherfordine ($UO_2\ CO_3$ (c)) in dilute solutions as a function of pH at p_{co2} = 1 atm and 25°C (Figure 5.7 from I. Puigdomenech and J. Bruno, *Modeling Uranium Solubilities in Aqueous Solutions: Validation of a Thermodynamic Data Base for the EQ3/6 Geochemical Codes,* SKB technical report 88-21, October 1988)

log $[U(VI)]_{tot}$
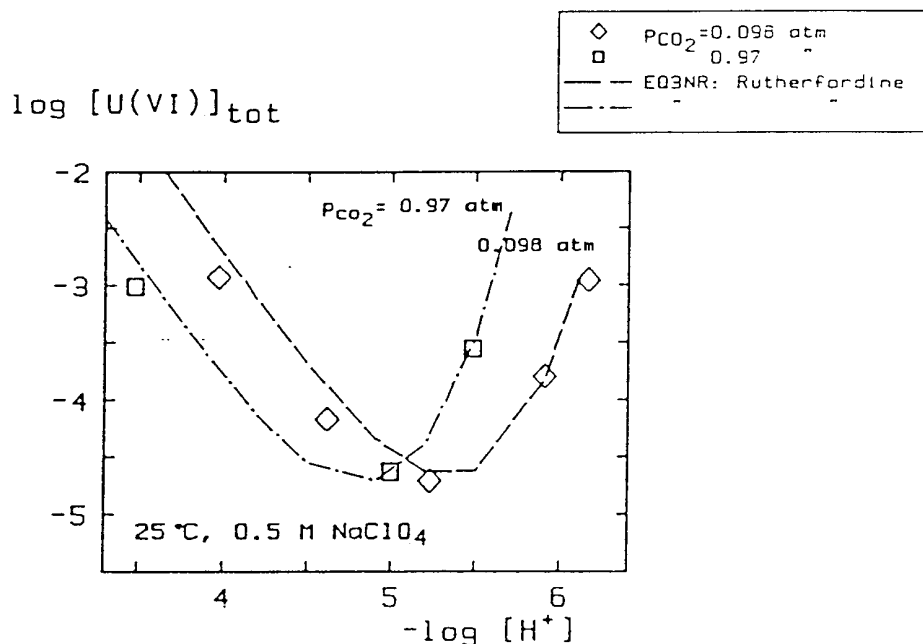
Figure 2.1.3.6-18 The solubility of rutherfordine ($UO_2 CO_3$ (c)) in 0.5 M $NaCIO_4$ solutions as a function of pH at 25°C and p_{co2} = 0.97 and 0.98 atm (Figure 5.8 from I. Puigdomenech and J. Bruno, *Modeling Uranium Solubilities in Aqueous Solutions: Validation of a Thermodynamic Data Base for the EQ3/6 Geochemical Codes,* SKB technical report 88-21, October 1988)

log $[U(VI)]_{tot}$
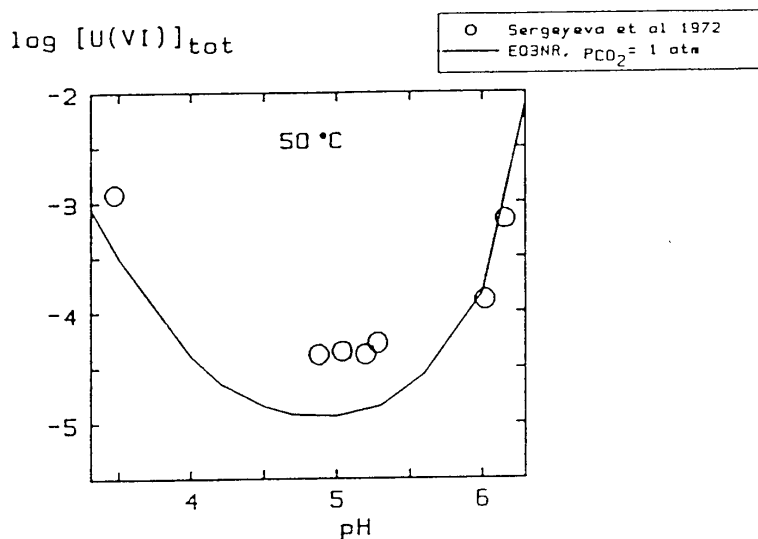
Figure 2.1.3.6-19 The solubility of rutherfordine ($UO_2 CO_3$ (c)) in dilute solutions as a function of pH at p_{co2} = 1 atm and 50°C (Figure 5.10 from I. Puigdomenech and J. Bruno, *Modeling Uranium Solubilities in Aqueous Solutions: Validation of a Thermodynamic Data Base for the EQ3/6 Geochemical Codes,* SKB technical report 88-21, October 1988)
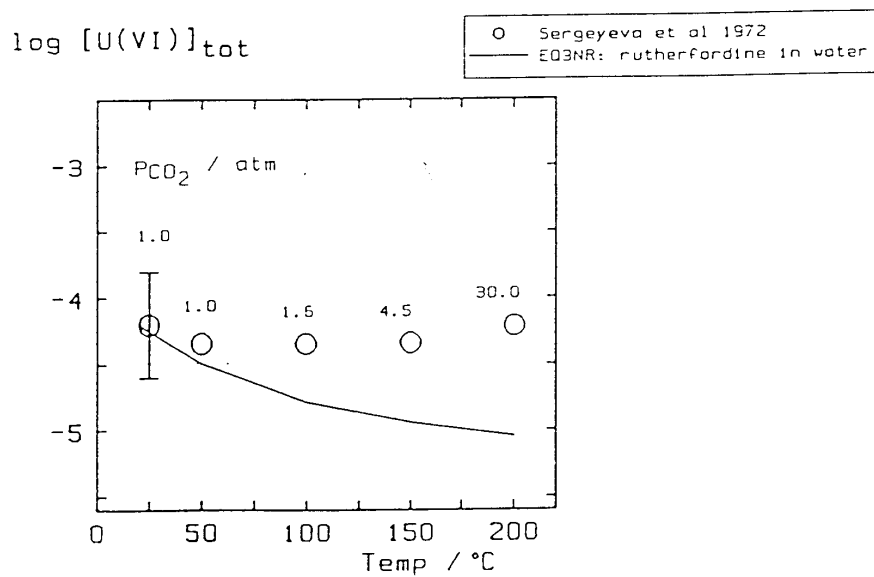
Figure 2.1.3.6-20 The calculated solubility of rutherfordine ($UO_2\,CO_3$ (c)) in water as a function of temperature at the given values for the partial pressure of CO_2 (g) (p_{co2}) compared with experimental results of Sergeyeva et al (1972) (Figure 5.11 from I. Puigdomenech and J. Bruno, *Modeling Uranium Solubilities in Aqueous Solutions: Validation of a Thermodynamic Data Base for the EQ3/6 Geochemical Codes,* SKB technical report 88-21, October 1988)

	Pu 25°C	Pu 85°C	Am 25°C	Am 85°C	Cm 25°C	Cm 85°C	U 25°C	U 85°C	Np 25°C	Np 85°C
Fraction in Solution	.25	.25	.05	.01	.05	.01	1	1	1	1
Fraction as Colloid	.75	.75	.95	.99	.95	.99	0	0	0	0

Figure 2.1.3.6-21 Colloid formation in Actinides (Figure from C.N. Wilson, *Indications for the Formation of Pu, Am, and Cm Colloids in Semi-Static Spent Fuel Dissolution Tests,* **presented at the 1990 Spent Fuel Workshop, September, 1990)**
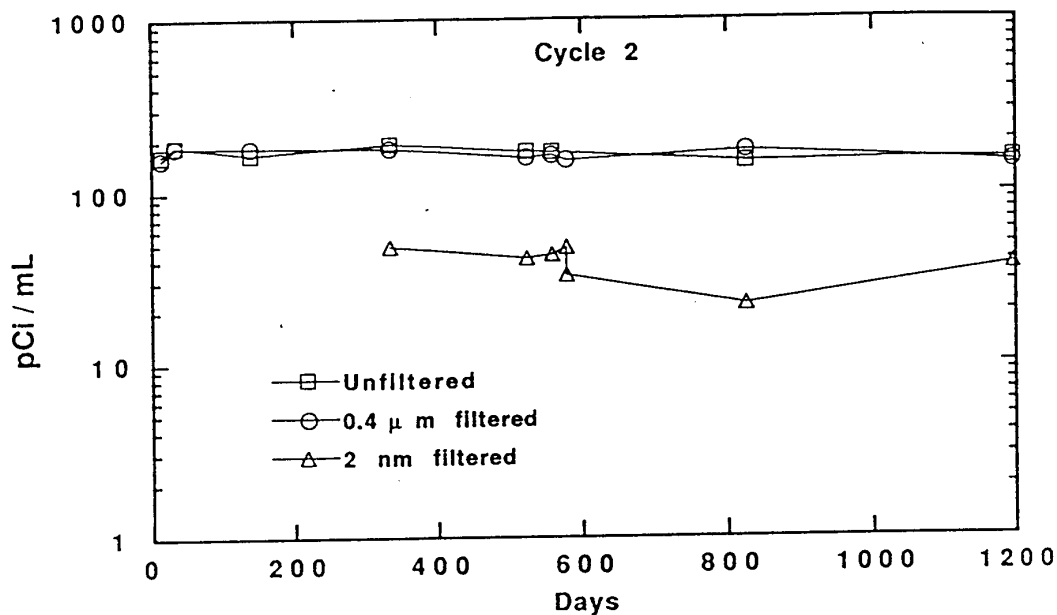
Figure 2.1.3.6-22 [239 + 240]Pu activities in O/M = 2.21 test (25°C) (Figure from C.N. Wilson, *Indications for the Formation of Pu, Am, and Cm Colloids in Semi-Static Spent Fuel Dissolution Tests,* presented at the 1990 Spent Fuel Workshop, September, 1990)
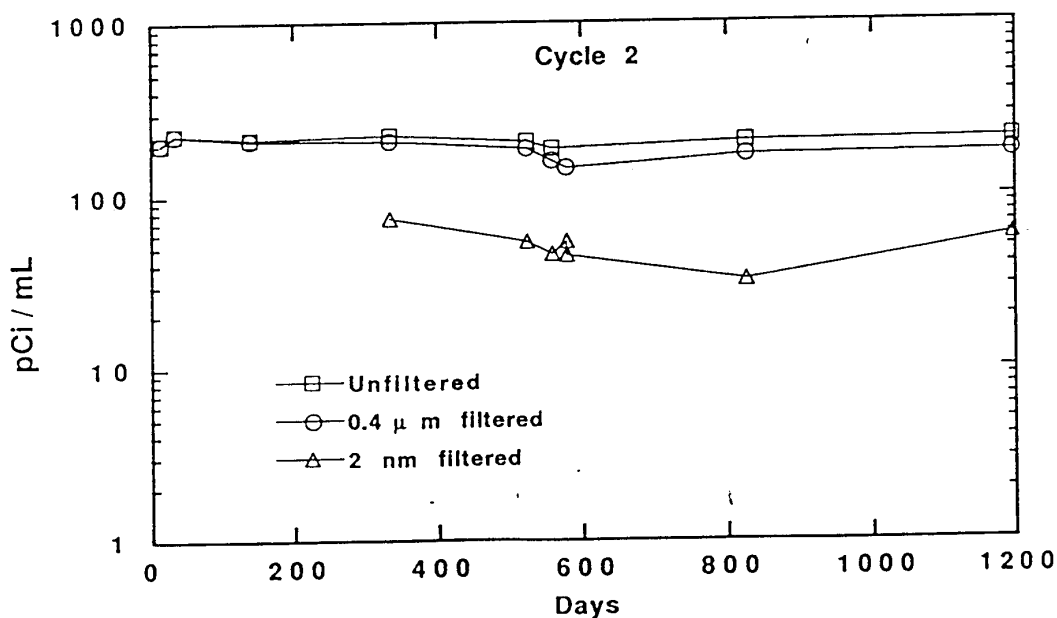
Figure 2.1.3.6-23 [239 + 240]Pu activities in O/M = 2.33 test (25°C) (Figure from C.N. Wilson, *Indications for the Formation of Pu, Am, and Cm Colloids in Semi-Static Spent Fuel Dissolution Tests,* presented at the 1990 Spent Fuel Workshop, September, 1990)
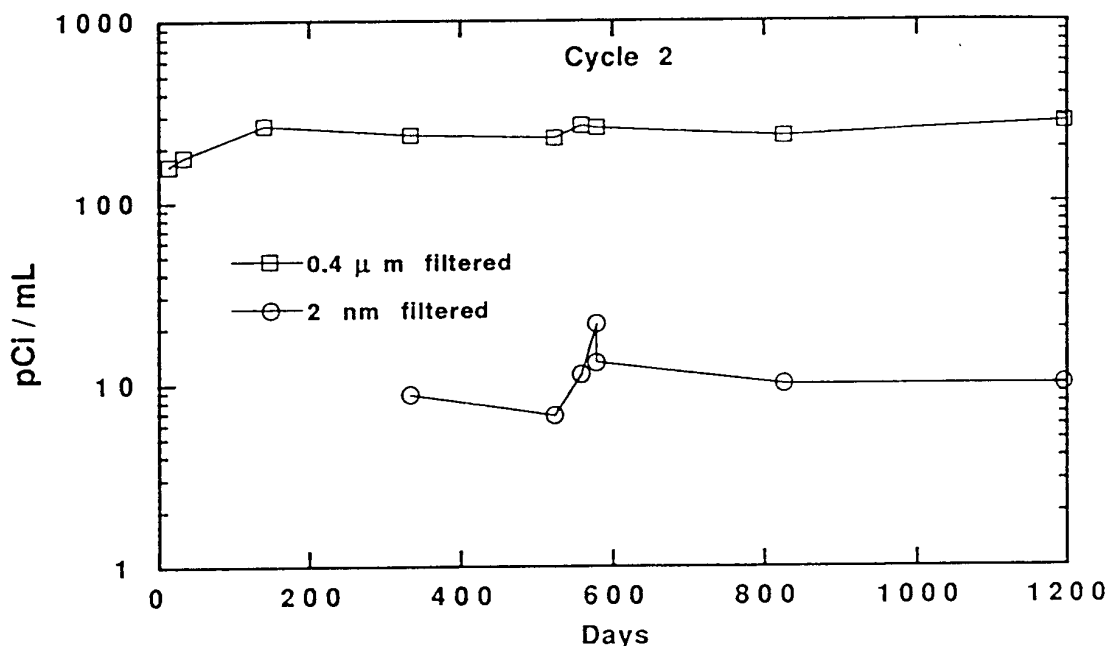
Figure 2.1.3.6-24 [241]**Am activities in O/M = 2.21 test (25°C) (Figure from C.N. Wilson,** *Indications for the Formation of Pu, Am, and Cm Colloids in Semi-Static Spent Fuel Dissolution Tests,* **presented at the 1990 Spent Fuel Workshop, September, 1990)**
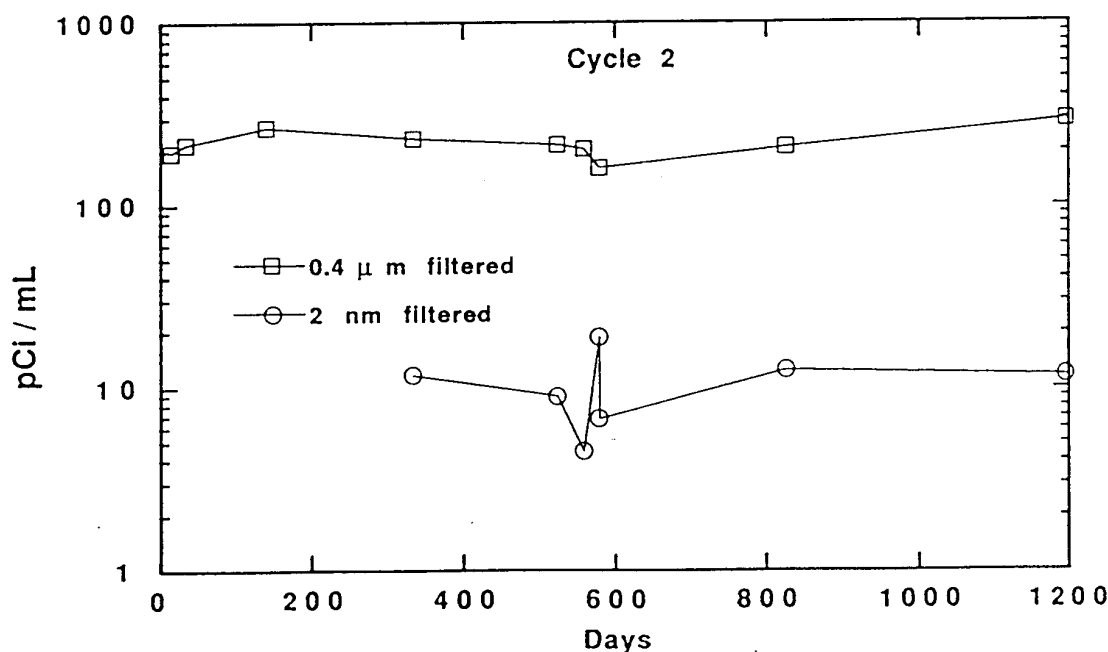
Figure 2.1.3.6-25 [241]**Am activities in O/M = 2.33 test (25°C) (Figure from C.N. Wilson,** *Indications for the Formation of Pu, Am, and Cm Colloids in Semi-Static Spent Fuel Dissolution Tests,* **presented at the 1990 Spent Fuel Workshop, September, 1990)**
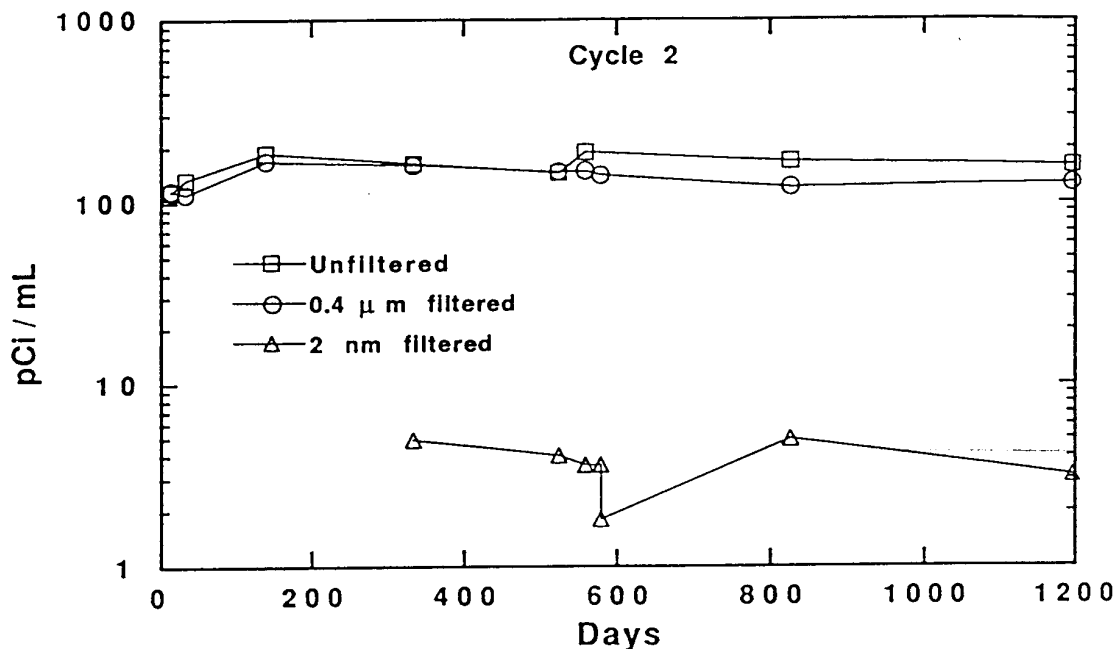
Figure 2.1.3.6-26 [244]Cm activities in O/M = 2.21 test (25°C) (Figure from C.N. Wilson, *Indications for the Formation of Pu, Am, and Cm Colloids in Semi-Static Spent Fuel Dissolution Tests,* presented at the 1990 Spent Fuel Workshop, September, 1990)
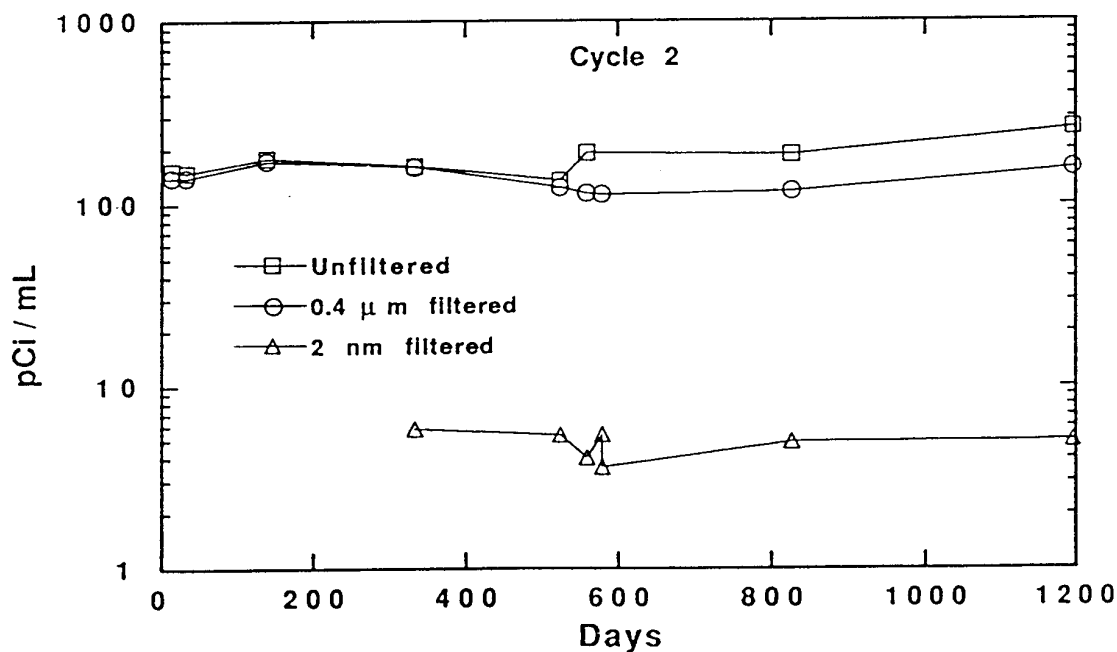
Figure 2.1.3.6-27 [244]Cm activities in O/M = 2.33 test (25°C) (Figure from C.N. Wilson, *Indications for the Formation of Pu, Am, and Cm Colloids in Semi-Static Spent Fuel Dissolution Tests,* presented at the 1990 Spent Fuel Workshop, September, 1990)
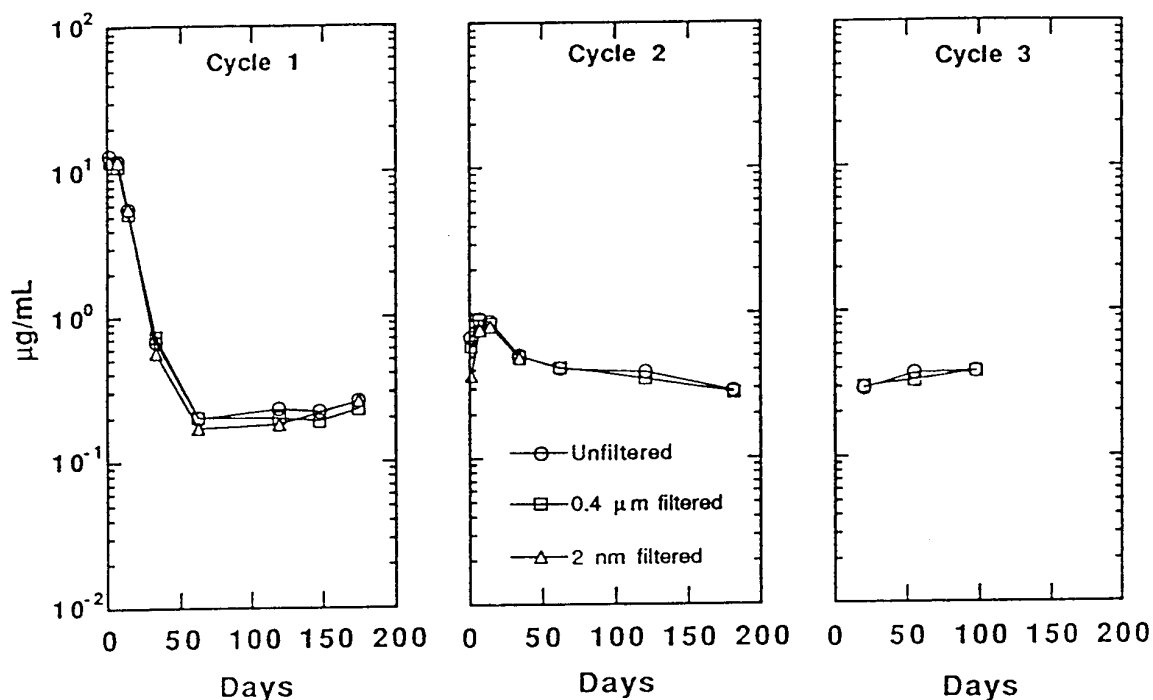
Figure 2.1.3.6-28 U, TP fuel, 25°C (Figure from C.N. Wilson, *Indications for the Formation of Pu, Am, and Cm Colloids in Semi-Static Spent Fuel Dissolution Tests,* **presented at the 1990 Spent Fuel Workshop, September, 1990)**
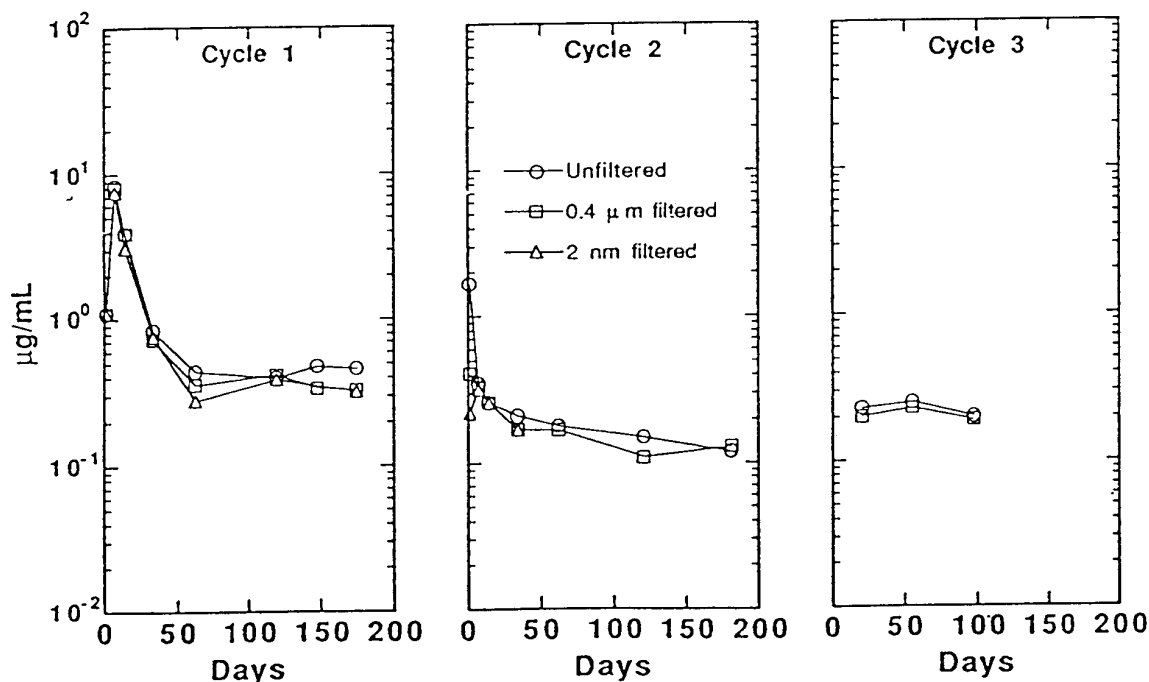
Figure 2.1.3.6-29 U, TP fuel, 85°C (Figure from C.N. Wilson, *Indications for the Formation of Pu, Am, and Cm Colloids in Semi-Static Spent Fuel Dissolution Tests,* **presented at the 1990 Spent Fuel Workshop, September, 1990)**
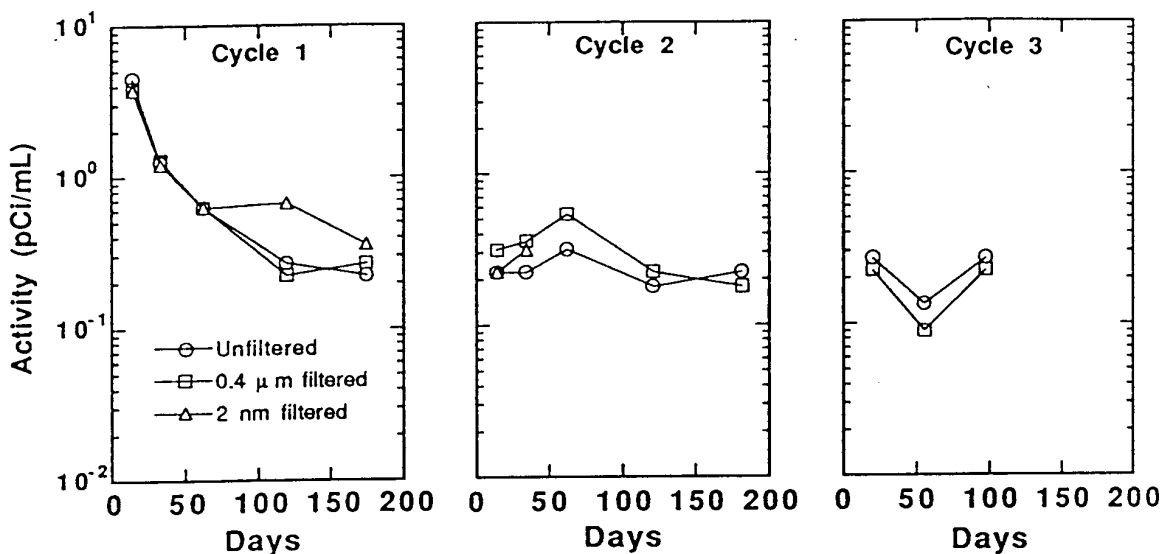
Figure 2.1.3.6-30 ^{237}Np, HBR fuel, 25°C (Figure from C.N. Wilson, *Indications for the Formation of Pu, Am, and Cm Colloids in Semi-Static Spent Fuel Dissolution Tests,* presented at the 1990 Spent Fuel Workshop, September, 1990)
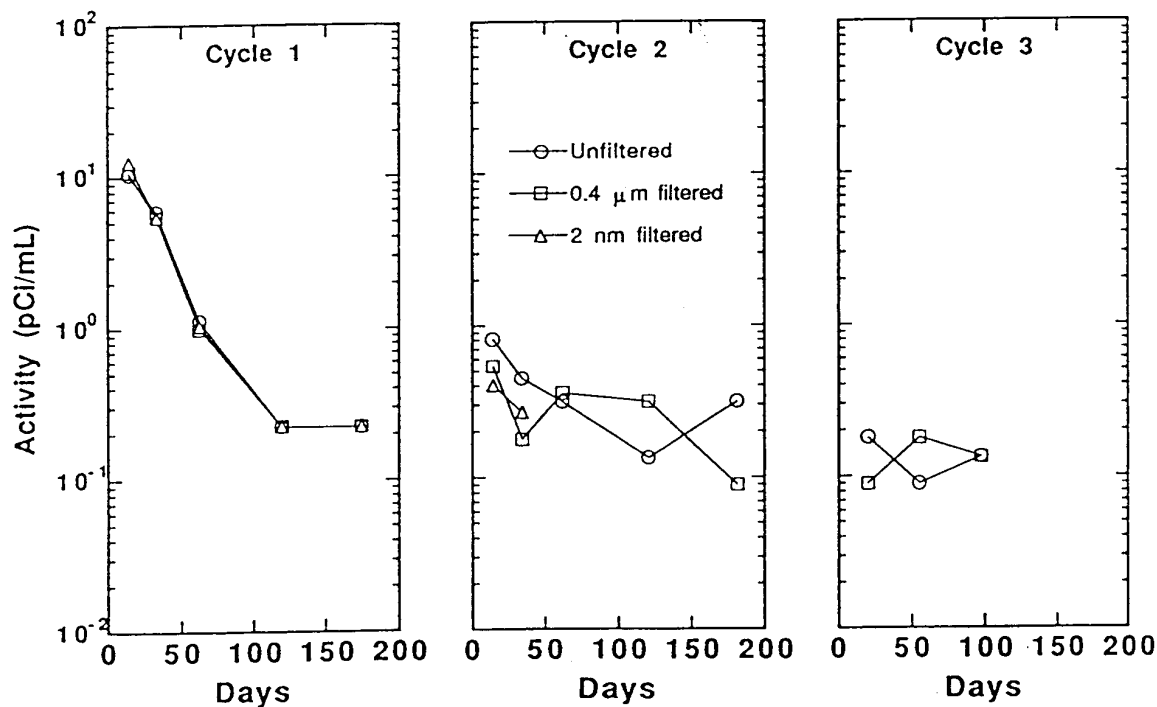
Figure 2.1.3.6-31 ^{237}Np, HBR fuel, 85°C. (Figure from C.N. Wilson, *Indications for the Formation of Pu, Am, and Cm Colloids in Semi-Static Spent Fuel Dissolution Tests,* presented at the 1990 Spent Fuel Workshop, September, 1990)
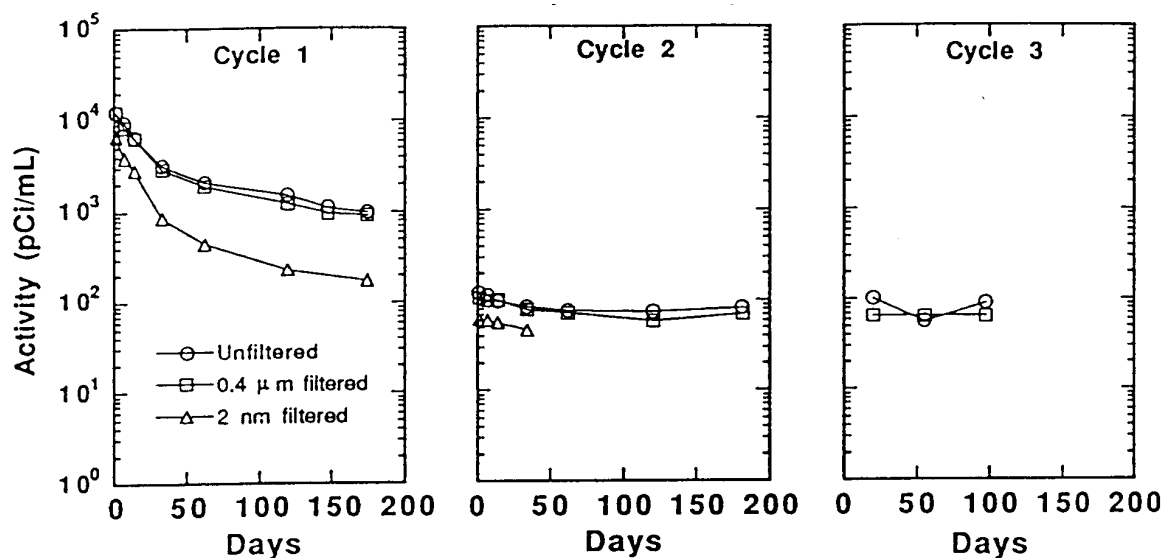
Figure 2.1.3.6-32 $^{239+240}$Pu, HBR fuel, 25°C (Figure from C.N. Wilson, *Indications for the Formation of Pu, Am, and Cm Colloids in Semi-Static Spent Fuel Dissolution Tests,* presented at the 1990 Spent Fuel Workshop, September, 1990)
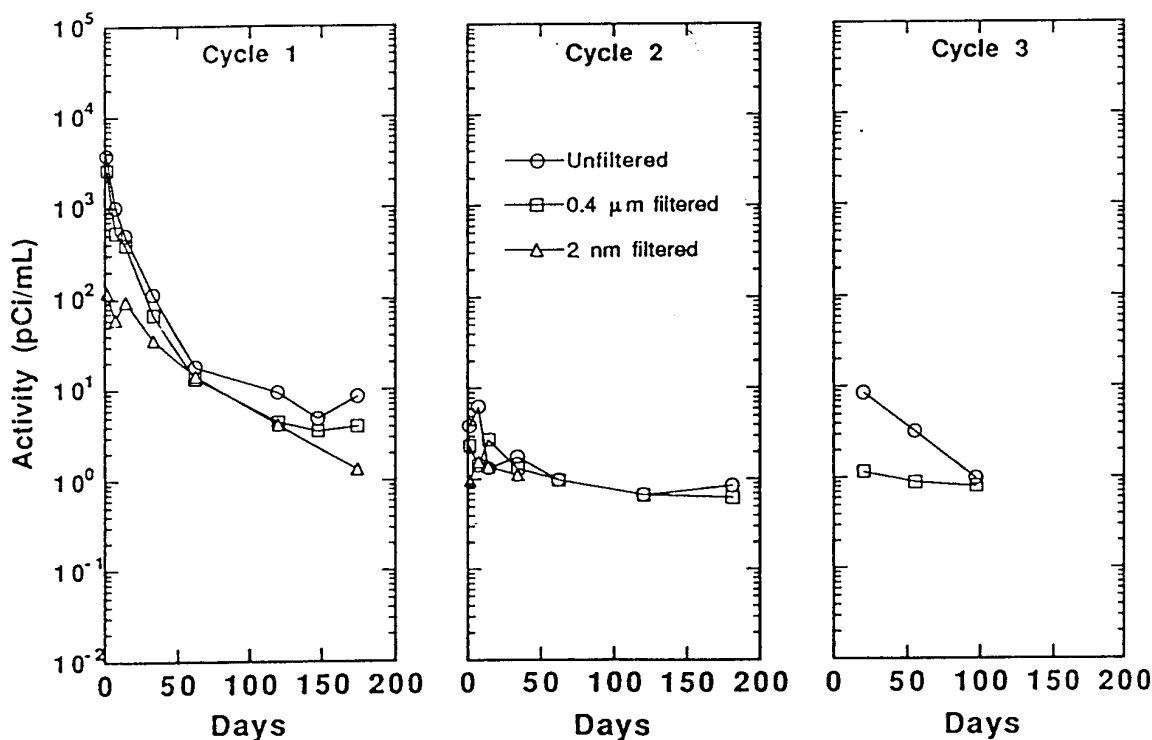
Figure 2.1.3.6-33 $^{239+240}$Pu, TP fuel, 85°C (Figure from C.N. Wilson, *Indications for the Formation of Pu, Am, and Cm Colloids in Semi-Static Spent Fuel Dissolution Tests,* presented at the 1990 Spent Fuel Workshop, September, 1990)
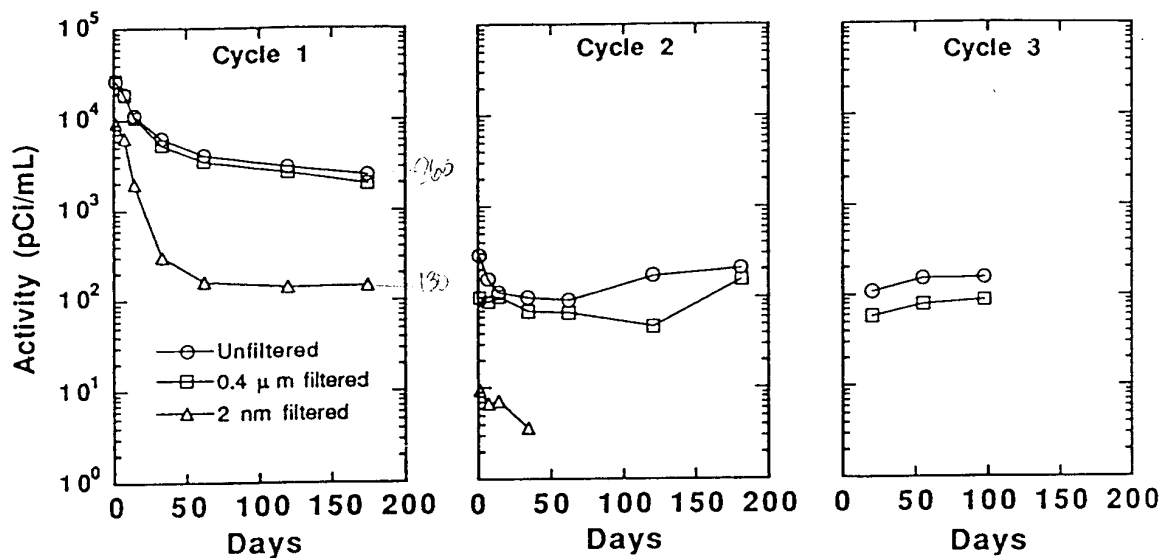
Figure 2.1.3.6-34 [241]Am, HBR fuel, 25°C (Figure from C.N. Wilson, *Indications for the Formation of Pu, Am, and Cm Colloids in Semi-Static Spent Fuel Dissolution Tests,* presented at the 1990 Spent Fuel Workshop, September, 1990)
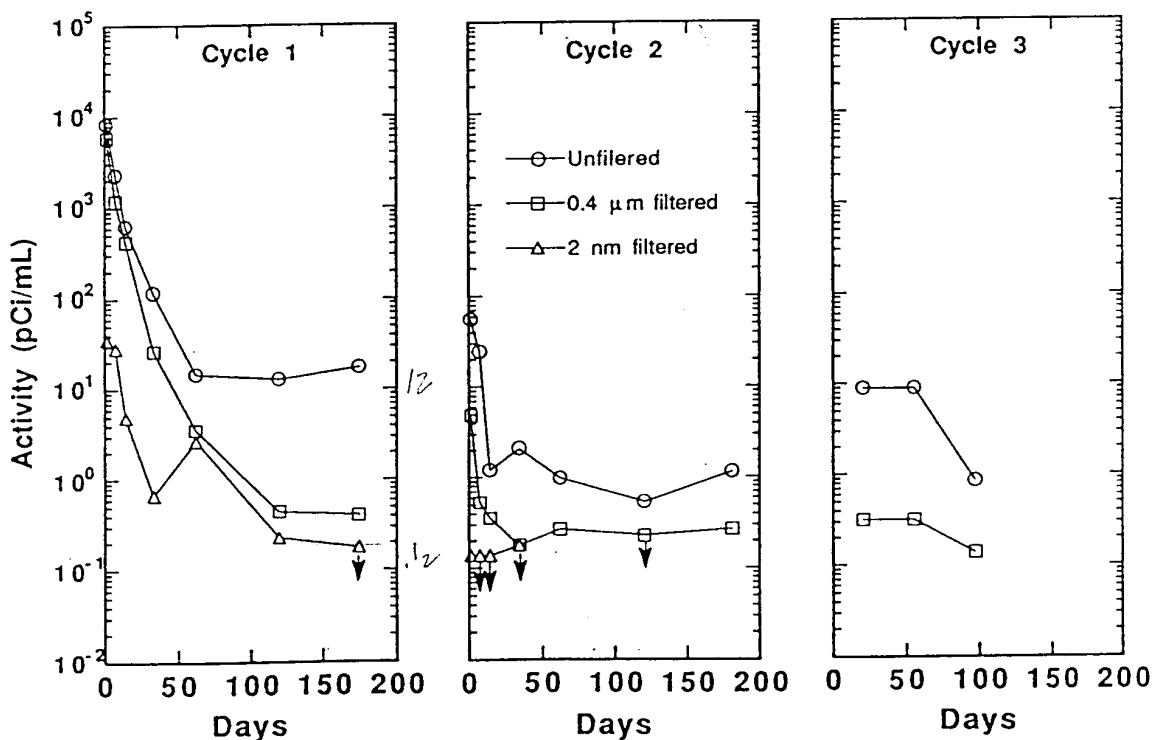
Figure 2.1.3.6-35 [241]Am, TP fuel, 85°C (Figure from C.N. Wilson, *Indications for the Formation of Pu, Am, and Cm Colloids in Semi-Static Spent Fuel Dissolution Tests,* presented at the 1990 Spent Fuel Workshop, September, 1990)
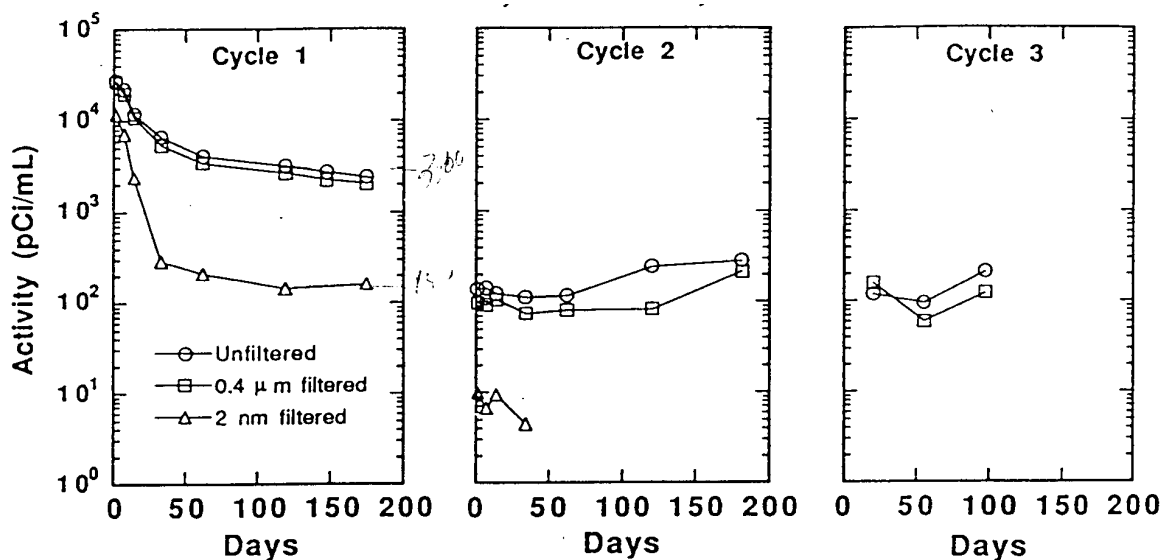
Figure 2.1.3.6-36 ^{244}Cm, HBR fuel, 25°C (Figure from C.N. Wilson, *Indications for the Formation of Pu, Am, and Cm Colloids in Semi-Static Spent Fuel Dissolution Tests,* presented at the 1990 Spent Fuel Workshop, September, 1990)
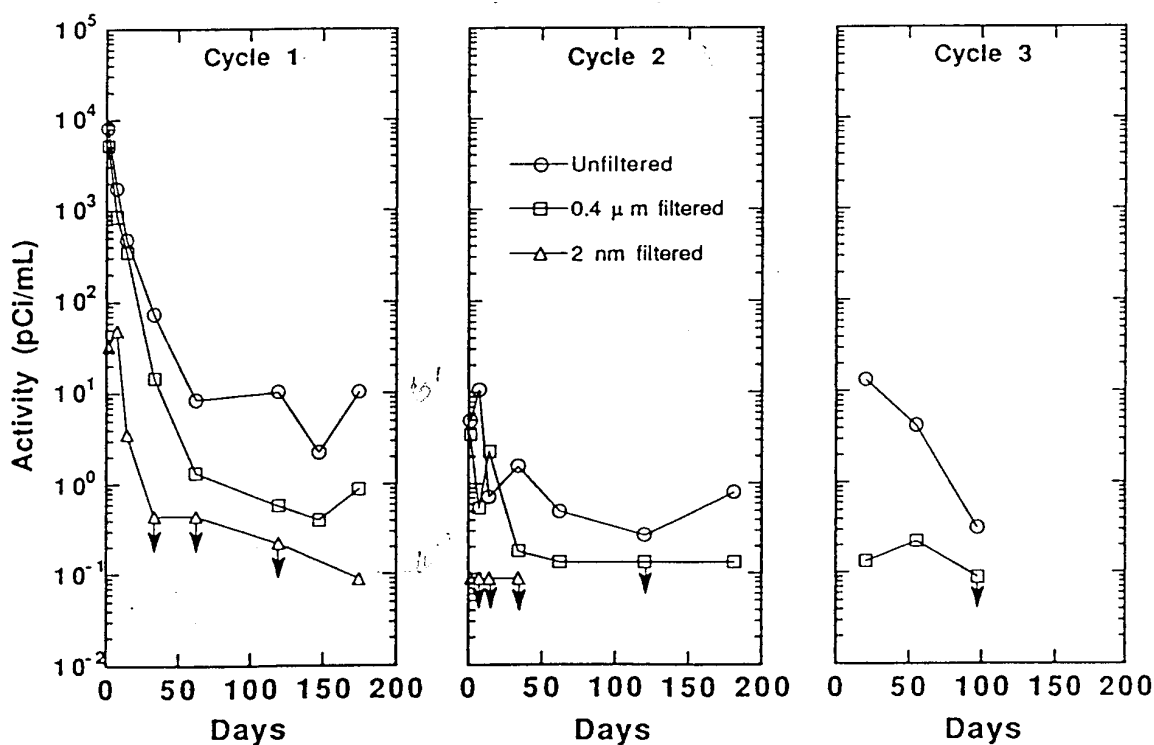
Figure 2.1.3.6-37 ^{244}Cm, TP fuel, 85°C (Figure from C.N. Wilson, *Indications for the Formation of Pu, Am, and Cm Colloids in Semi-Static Spent Fuel Dissolution Tests,* presented at the 1990 Spent Fuel Workshop, September, 1990)

2.1.3.7 Radionuclide Release from Hardware

Table 2.1.3.7-1   Variation of radioactivity (Ci/MTIHM) for significant activation- and fission-product nuclides as a function of time since discharge from a 60,000-MWd/MTIHM PWR (includes all structural material) (Table 3.5 from J.W. Roddy, H.C. Claiborne, R.C. Ashline, P.T. Johnson, and B.T. Rhyne, *Physical and Decay Characteristics of Commercial LWR Spent Fuels*, ORNL/TM-9591/V.1, October, 1985)

	Time since discharge (years)					
Isotope[a]	1.0E+0	1.0E+1	1.0E+2	1.0E+3	1.0E+4	1.0E+5
H-3[b]	1.17E+3	7.09E+2	4.54E+0	–	–	–
C-14[c]	2.44E+0	2.44E+0	2.41E+0	2.16E+0	7.27E-1	–
Mn-54[c]	4.59E+2	–	–	–	–	–
Fe-55[c]	5.24E+3	4.76E+2	–	–	–	–
Co-58[c]	2.13E+2	–	–	–	–	–
Co-60[c]	9.54E+3	2.92E+3	–	–	–	–
Ni-59[c]	6.40E+0	6.40E+0	6.39E+0	6.34E+0	5.87E+0	2.69E+0
Ni-63[c]	1.05E+3	9.83E+2	4.98E+2	–	–	–
Zn-65[c]	4.78E+1	–	–	–	–	–
Se-79	–	–	–	–	6.45E-1	2.47E-1
Kr-85	1.34E+4	7.48E+3	2.22E+1	–	–	–
Sr-89	4.53E+3	–	–	–	–	–
Sr-90	1.14E+5	9.16E+4	1.08E+4	–	–	–
Y-90	1.14E+5	9.16E+4	1.08E+4	–	–	–
Y-91	1.22E+4	–	–	–	–	–
Zr-93[b]	3.32E+0	3.32E+0	3.32E+0	3.32E+0	3.30E+0	3.17E+0
Zr-95[b]	2.93E+4	–	–	–	–	–
Nb-93m[b]	–	–	3.14E+0	3.15E+0	3.14E+0	3.01E+0
Nb-94[c]	–	–	–	2.18E+0	1.61E+0	7.43E-2
Nb-95[b]	6.59E+4	–	–	–	–	–
Tc-99	2.11E+1	2.11E+1	2.11E+1	2.10E+1	2.04E+1	1.52E+1
Ru-103	2.84E+3	–	–	–	–	–
Ru-106	3.84E+5	7.88E+2	–	–	–	–
Rh-106	3.84E+5	7.88E+2	–	–	–	–
Pd-107	–	–	–	2.43E-1	2.43E-1	2.41E-1
Ag-110m	3.72E+3	–	–	–	–	–
Sn-119m[b]	2.47E+3	–	–	–	–	–
Sn-126	1.47E+0	1.47E+0	1.47E+0	1.46E+0	1.37E+0	7.35E-1
Sb-125[b]	1.80E+4	1.89E+3	–	–	–	–
Sb-126	–	–	–	2.04E-1	1.92E-1	1.03E-1
Sb-126m	–	–	–	1.46E+0	1.37E+0	7.35E-1
Te-125m[b]	4.38E+3	4.62E+2	–	–	–	–
I-129	5.68E-2	5.68E-2	5.68E-2	5.68E-2	5.68E-2	5.66E-2
Cs-134	2.62E+5	1.27E+4	–	–	–	–
Cs-135	–	–	–	7.66E-1	7.64E-1	7.43E-1
Cs-137	1.78E+5	1.44E+5	1.80E+4	–	–	–
Ba-137m	1.68E+5	1.37E+5	1.71E+4	–	–	–
Ce-144	4.29E+5	1.42E+2	–	–	–	–
Pr-144	4.29E+5	1.42E+2	–	–	–	–
Pr-144m	5.14E+3	1.70E+0	–	–	–	–
Pm-147	9.39E+4	8.71E+3	–	–	–	–
Sm-151	5.30E+2	4.95E+2	2.47E+2	2.42E-1	–	–
Eu-154	2.33E+4	1.13E+4	7.99E+0	–	–	–
Eu-155	1.42E+4	4.05E+3	–	–	–	–
OTHER	7.55E+3	2.29E+2	1.22E+1	2.40E+0	9.89E-1	7.63E-2
SUBTOTAL						
A.P.[d]	2.59E+4	4.79E+3	5.11E+2	1.18E+1	8.71E+0	3.24E+0
F.P.[e]	2.75E+6	5.14E+5	5.70E+4	3.22E+1	3.10E+1	2.38E+1
TOTAL	2.79E+6	5.18E+5	5.75E+4	4.40E+1	3.98E+1	2.71E+1

[a]Nuclides contributing >0.1% are listed.

[b]Both activation and fission products contribute to this nuclide.

[c]Only activation products contribute to this nuclide.

[d]A.P. = Activation products.

[e]F.P. = Fission products.

Table 2.1.3.7-2 Variation of radioactivity (Ci/MTIHM) for significant activation- and fission-product nuclides as a function of time since discharge from a 33,000-MWd/MTIHM PWR (includes all structural material) (Table 3.6 from J.W. Roddy, H.C. Claiborne, R.C. Ashline, P.T. Johnson, and B.T. Rhyne, *Physical and Decay Characteristics of Commercial LWR Spent Fuels*, ORNL/TM-9591/V.1, October, 1985)

Isotope[a]	Time since discharge (years)					
	1.0E+0	1.0E+1	1.0E+2	1.0E+3	1.0E+4	1.0E+5
H-3[b]	7.69E+2	4.64E+2	2.97E+0	–	–	–
C-14[c]	1.55E+0	1.55E+0	1.53E+0	1.38E+0	4.63E-1	–
Mn-54[c]	3.91E+2	–	–	–	–	–
Fe-55[c]	4.28E+3	3.89E+2	–	–	–	–
Co-58[c]	1.92E+2	–	–	–	–	–
Co-60[c]	6.97E+3	2.12E+3	–	–	–	–
Ni-59[c]	5.15E+0	5.15E+0	5.15E+0	5.11E+0	4.72E+0	2.17E+0
Ni-63[c]	6.97E+2	6.52E+2	3.31E+2	3.76E-1	–	–
Zn-65[c]	4.72E+1	–	–	–	–	–
Se-79	–	–	–	–	3.67E-1	1.41E-1
Kr-85	8.69E+3	4.85E+3	1.44E+1	–	–	–
Sr-89	5.72E+3	–	–	–	–	–
Sr-90	7.08E+4	5.72E+4	6.71E+3	–	–	–
Y-90	7.08E+4	5.72E+4	6.71E+3	–	–	–
Y-91	1.49E+4	–	–	–	–	–
Zr-93[b]	1.93E+0	1.93E+0	1.93E+0	1.93E+0	1.92E+0	1.84E+0
Zr-95[b]	3.14E+4	–	–	–	–	–
Nb-93m[b]	–	–	–	1.83E+0	1.83E+0	1.75E+0
Nb-94[c]	–	–	–	1.24E+0	9.10E-1	4.21E-2
Nb-95[b]	7.07E+4	–	–	–	–	–
Tc-99	1.31E+1	1.31E+1	1.30E+1	1.30E+1	1.26E+1	9.43E+0
Ru-103	2.59E+3	–	–	–	–	–
Ru-106	2.68E+5	5.50E+2	–	–	–	–
Rh-106	2.68E+5	5.50E+2	–	–	–	–
Pd-107	–	–	–	1.12E-1	1.12E-1	1.11E-1
Ag-110m	1.52E+3	–	–	–	–	–
Sn-119m[b]	2.14E+3	–	–	–	–	–
Sn-126	7.76E-1	7.76E-1	7.76E-1	7.71E-1	7.24E-1	3.88E-1
Sb-125[b]	1.22E+4	1.29E+3	–	–	–	–
Sb-126	–	–	–	1.08E-1	1.01E-1	5.44E-2
Sb-126m	–	–	–	7.71E-1	7.24E-1	3.88E-1
Te-125m[b]	2.98E+3	3.14E+2	–	–	–	–
I-129	3.15E-2	3.15E-2	3.15E-2	3.15E-2	3.15E-2	3.14E-2
Cs-134	1.08E+5	5.22E+3	–	–	–	–
Cs-135	–	–	–	3.45E-1	3.44E-1	3.35E-1
Cs-137	1.01E+5	8.21E+4	1.03E+4	–	–	–
Ba-137m	9.56E+4	7.77E+4	9.71E+3	–	–	–
Ce-144	4.51E+5	1.49E+2	–	–	–	–
Pr-144	4.51E+5	1.49E+2	–	–	–	–
Pr-144m	5.41E+3	1.79E+0	–	–	–	–
Pm-147	1.02E+5	9.48E+3	–	–	–	–
Sm-151	3.55E+2	3.31E+2	1.66E+2	1.62E-1	–	–
Eu-154	9.69E+3	4.69E+3	3.32E+0	–	–	–
Eu-155	5.62E+3	1.60E+3	–	–	–	–
OTHER	6.81E+3	3.80E+1	8.70E+0	9.90E-1	6.70E-2	5.60E-2
SUBTOTAL						
A.P.[d]	1.95E+4	3.48E+3	3.40E+2	8.38E+0	6.36E+0	2.46E+0
F.P.[e]	2.16E+6	3.04E+5	3.36E+4	1.92E+1	1.86E+1	1.42E+1
TOTAL	2.18E+6	3.07E+5	3.39E+4	2.76E+1	2.49E+1	1.67E+1

[a] Nuclides contributing >0.1% are listed.

[b] Both activation and fission products contribute to this nuclide.

[c] Only activation products contribute to this nuclide.

[d] A.P. = Activation products.

[e] F.P. = Fission products.

Table 2.1.3.7-3   Variation of radioactivity (Ci/MTIHM) for significant activation- and fission-product nuclides as a function of time since discharge from a 40,000-MWd/MTIHM BWR (includes all structural material) (Table 3.7 from J.W. Roddy, H.C. Claiborne, R.C. Ashline, P.T. Johnson, and B.T. Rhyne, *Physical and Decay Characteristics of Commercial LWR Spent Fuels,* ORNL/TM-9591/V.1, October, 1985)

Isotope[a]	Time since discharge (years)					
	1.0E+0	1.0E+1	1.0E+2	1.0E+3	1.0E+4	1.0E+5
H-3[b]	8.43E+2[a]	5.09E+2	3.26E+0	–	–	–
C-14[c]	2.05E+0	2.05E+0	2.02E+0	1.82E+0	6.11E-1	–
Mn-54[c]	1.49E+2	–	–	–	–	–
Fe-55[c]	2.54E+3	2.31E+2	–	–	–	–
Co-58[c]	3.75E+1	–	–	–	–	–
Co-60[c]	2.62E+3	8.01E+2	–	–	–	–
Ni-59[c]	1.39E+0	1.39E+0	1.39E+0	1.38E+0	1.27E+0	5.84E-1
Ni-63[c]	2.08E+2	1.94E+2	9.84E+1	–	–	–
Zn-65[c]	3.56E+1	–	–	–	–	–
Se-79	–	–	–	4.80E-1	4.36E-1	1.67E-1
Kr-85	9.52E+3	5.32E+3	1.58E+1	–	–	–
Sr-89	3.59E+3	–	–	–	–	–
Sr-90	8.20E+4	6.62E+4	7.77E+3	–	–	–
Y-90	8.20E+4	6.62E+4	7.77E+3	–	–	–
Y-91	9.41E+3	–	–	–	–	–
Zr-93[b]	2.56E+0	2.56E+0	2.56E+0	2.56E+0	2.55E+0	2.45E+0
Zr-95[b]	2.18E+4	–	–	–	–	–
Nb-93m[b]	–	–	–	2.44E+0	2.43E+0	2.33E+0
Nb-95[b]	4.89E+4	–	–	–	–	–
Tc-99	1.56E+1	1.56E+1	1.56E+1	1.56E+1	1.51E+1	1.13E+1
Ru-103	1.86E+3	–	–	–	–	–
Ru-106	2.28E+5	4.67E+2	–	–	–	–
Rh-106	2.28E+5	4.67E+2	–	–	–	–
Pd-107	–	–	–	1.40E-1	1.40E-1	1.39E-1
Ag-110m	1.63E+3	–	–	–	–	–
Sn-119m[b]	3.83E+3	–	–	–	–	–
Sn-126	8.88E-1	8.88E-1	8.87E-1	8.82E-1	8.28E-1	4.44E-1
Sb-125[b]	1.25E+4	1.31E+3	–	–	–	–
Sb-126	–	–	–	1.24E-1	1.16E-1	6.22E-2
Sb-126m	–	–	–	8.82E-1	8.28E-1	4.44E-1
Te-125m[b]	3.04E+3	3.20E+2	–	–	–	–
I-129	3.73E-2	3.73E-2	3.73E-2	3.73E-2	3.73E-2	3.72E-2
Cs-134	1.27E+5	6.15E+3	–	–	–	–
Cs-135	–	–	–	5.66E-1	5.64E-1	5.49E-1
Cs-137	1.19E+5	9.66E+4	1.21E+4	–	–	–
Ba-137m	1.12E+5	9.14E+4	1.14E+4	–	–	–
Ce-144	3.06E+5	1.01E+2	–	–	–	–
Pr-144	3.06E+5	1.01E+2	–	–	–	–
Pr-144m	3.67E+3	–	–	–	–	–
Pm-147	8.80E+4	8.20E+3	–	–	–	–
Sm-151	3.80E+2	3.55E+2	1.78E+2	1.73E-1	–	–
Eu-154[b]	1.30E+4	6.31E+3	4.42E+0	–	–	–
Eu-155[b]	7.46E+3	2.12E+3	–	–	–	–
OTHER	4.95E+3	2.15E+1	3.52E+1	2.12E-1	8.14E-2	2.10E-2
SUBTOTAL						
A.P.[d]	1.94E+4	1.84E+3	1.04E+2	4.15E+0	2.71E+0	1.35E+0
F.P.[e]	1.81E+6	3.52E+5	3.93E+4	2.30E+1	2.22E+1	1.71E+1
TOTAL	1.83E+6	3.53E+5	3.94E+4	2.72E+1	2.50E+1	1.85E+1

[a]Nuclides contributing >0.1% are listed.
[b]Both activation and fission products contribute to this nuclide.
[c]Only activation products contribute to this nuclide.
[d]A.P. = Activation products.
[e]F.P. = Fission products.

Table 2.1.3.7-4 Variation of radioactivity (Ci/MTIHM) for significant activation- and fission-product nuclides as a function of time since discharge from a 27,500-MWd/MTIHM BWR (includes all structural material) (Table 3.8 from J.W. Roddy, H.C. Claiborne, R.C. Ashline, P.T. Johnson, and B.T. Rhyne, *Physical and Decay Characteristics of Commercial LWR Spent Fuels*, ORNL/TM-9591/V.1, October, 1985)

Isotope[a]	Time since discharge (years)					
	1.0E+0	1.0E+1	1.0E+2	1.0E+3	1.0E+4	1.0E+5
H-3[b]	6.63E+2	4.00E+2	2.56E+0	–	–	–
C-14[c]	1.53E+0	1.53E+0	1.52E+0	1.36E+0	4.57E-1	–
Mn-54[c]	1.45E+2	–	–	–	–	–
Fe-55[c]	2.23E+3	2.02E+2	–	–	–	–
Co-58[c]	3.71E+1	–	–	–	–	–
Co-60[c]	2.18E+3	6.66E+2	–	–	–	–
Ni-59[c]	1.07E+0	1.07E+0	1.07E+0	1.06E+0	9.82E-1	4.50E-1
Ni-63[c]	1.57E+2	1.47E+2	7.47E+1	–	–	–
Zn-65[c]	3.51E+1	–	–	–	–	–
Se-79	–	–	–	3.34E-1	3.04E-1	1.16E-1
Kr-85	7.02E+3	3.92E+3	1.16E+1	–	–	–
Sr-89	3.90E+3	–	–	–	–	–
Sr-90	5.82E+4	4.70E+4	5.52E+3	–	–	–
Y-90	5.82E+4	4.70E+4	5.52E+3	–	–	–
Y-91	1.01E+4	–	–	–	–	–
Zr-93[b]	1.80E+0	1.80E+0	1.80E+0	1.80E+0	1.80E+0	1.72E+0
Zr-95[b]	2.24E+4	–	–	–	–	–
Nb-93m[b]	–	–	–	1.71E+0	1.71E+0	1.64E+0
Nb-95[b]	5.04E+4	–	–	–	–	–
Tc-99	1.11E+1	1.11E+1	1.11E+1	1.11E+1	1.08E+1	8.04E+0
Ru-103	1.81E+3	–	–	–	–	–
Ru-106	1.97E+5	4.04E+2	–	–	–	–
Rh-106	1.97E+5	4.04E+2	–	–	–	–
Pd-107	–	–	–	9.46E-2	9.45E-2	9.36E-2
Ag-110m	1.05E+3	–	–	–	–	–
Sn-119m[b]	3.77E+3	–	–	–	–	–
Sn-126	6.25E-1	6.24E-1	6.24E-1	6.20E-1	5.83E-1	3.12E-1
Sb-125[b]	1.05E+4	1.10E+3	–	–	–	–
Sb-126	–	–	–	8.68E-2	8.16E-2	4.37E-2
Sb-126m	–	–	–	6.20E-1	5.83E-1	3.12E-1
Te-125m[b]	2.56E+3	2.69E+2	–	–	–	–
I-129	2.64E-2	2.64E-2	2.64E-2	2.64E-2	2.64E-2	2.63E-2
Cs-134	7.65E+4	3.71E+3	–	–	–	–
Cs-135	–	–	–	3.59E-1	3.58E-1	3.49E-1
Cs-137	8.37E+4	6.80E+4	8.49E+3	–	–	–
Ba-137m	7.91E+4	6.43E+4	8.03E+3	–	–	–
Ce-144	3.10E+5	1.02E+2	–	–	–	–
Pr-144	3.10E+5	1.02E+2	–	–	–	–
Pr-144m	3.72E+3	1.23E+0	–	–	–	–
Pm-147	8.68E+4	8.05E+3	–	–	–	–
Sm-151	3.20E+2	2.98E+2	1.49E+2	1.46E-1	–	–
Eu-154[b]	7.63E+3	3.70E+3	2.61E+0	–	–	–
Eu-155[b]	4.49E+3	1.28E+3	–	–	–	–
OTHER	5.82E+3	9.30E+1	–	1.53E-1	5.40E-2	4.16E-2
SUBTOTAL						
A.P.[d]	1.81E+4	1.58E+3	7.92E+1	3.14E+0	2.06E+0	1.02E+0
F.P.[e]	1.58E+6	2.50E+5	2.78E+4	1.63E+1	1.57E+1	1.21E+1
TOTAL	1.60E+6	2.51E+5	2.78E+4	1.94E+1	1.78E+1	1.31E+1

[a]Nuclides contributing >than 0.1% are listed.

[b]Both activation and fission products contribute to this nuclide.

[c]Only activation products contribute to this nuclide.

[d]A.P. = Activation products.

[e]F.P. = Fission products.

Figure 2.1.3.7-1   Radioactivity from irradiated grid spacers, springs, braze, end pieces, and miscellaneous SS-304 for a PWR (Figure 4.1 from J.W. Roddy, H.C. Claiborne, R.C. Ashline, P.T. Johnson, and B.T. Rhyne, *Physical and Decay Characteristics of Commercial LWR Spent Fuels,* ORNL/TM-9591/V.1, October, 1985)
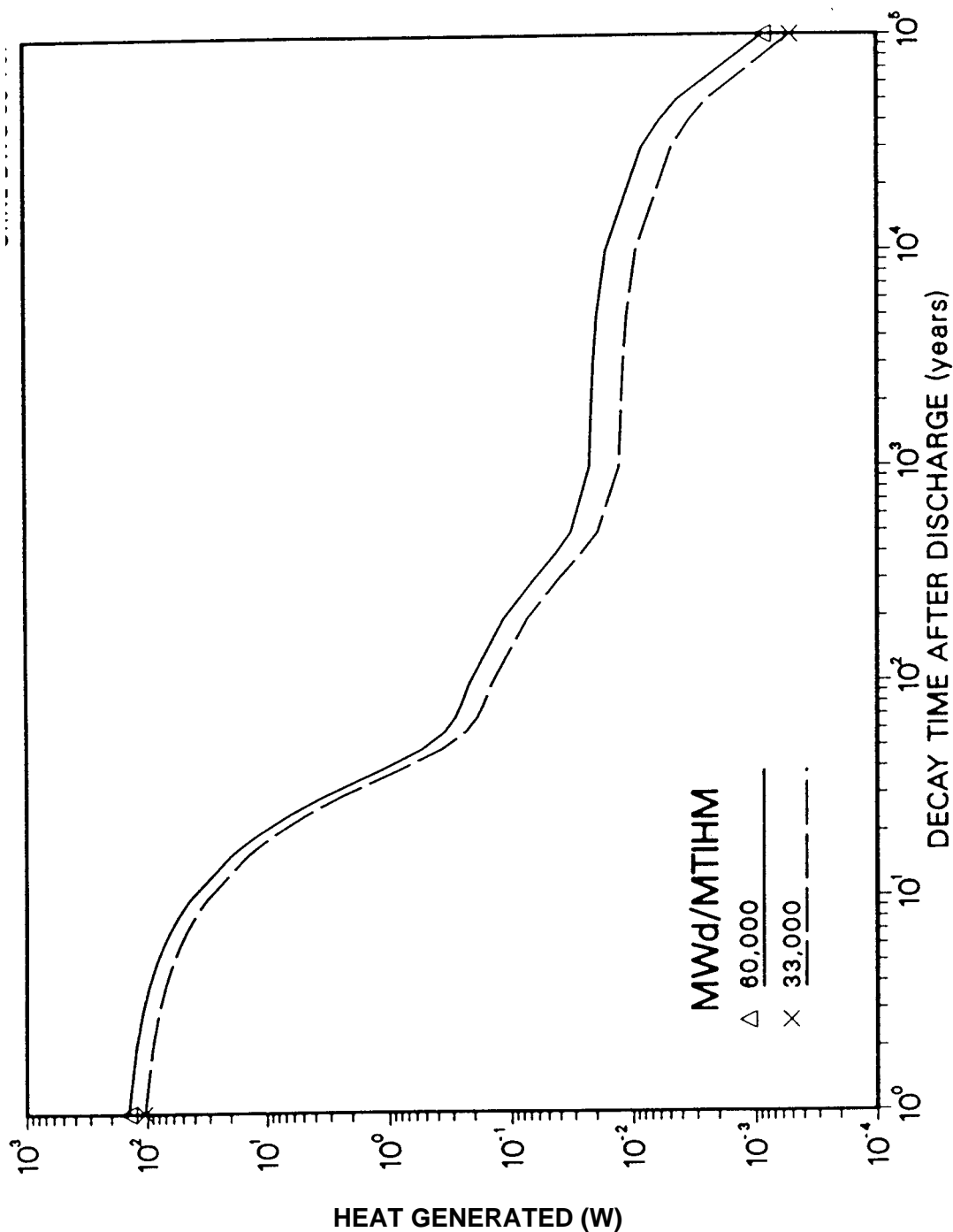
Figure 2.1.3.7-2   Heat generated from irradiated grid spacers, springs, braze, end pieces, and miscellaneous SS-304 for a PWR (Figure 4.2 from J.W. Roddy, H.C. Claiborne, R.C. Ashline, P.T. Johnson, and B.T. Rhyne, *Physical and Decay Characteristics of Commercial LWR Spent Fuels,* **ORNL/TM-9591/V.1, October, 1985)**
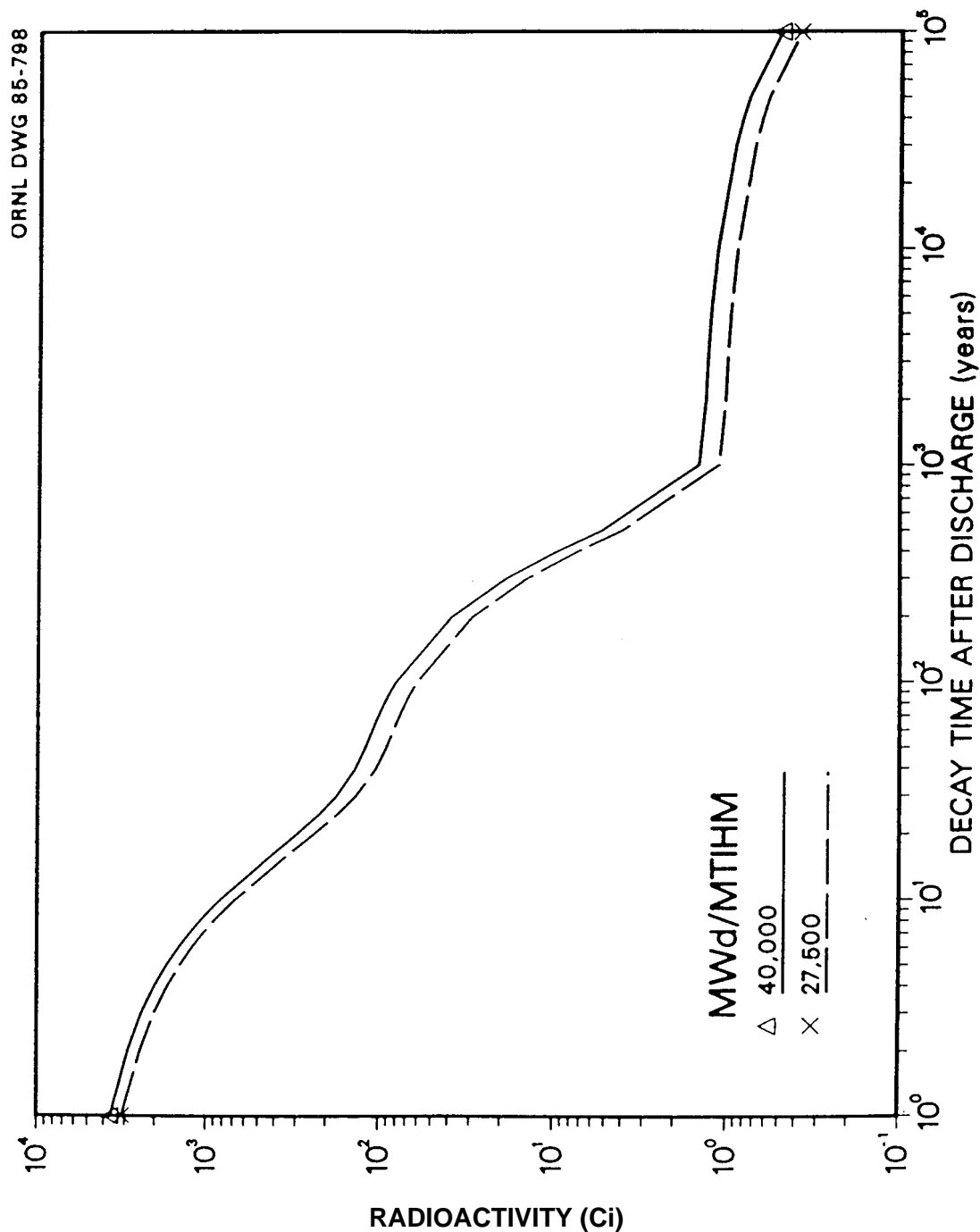
Figure 2.1.3.7-3   Radioactivity from irradiated grid spacers, springs, and end pieces
for a BWR (Figure 4.3 from J.W. Roddy, H.C. Claiborne, R.C. Ashline,
P.T. Johnson, and B.T. Rhyne, *Physical and Decay Characteristics of
Commercial LWR Spent Fuels,* ORNL/TM-9591/V.1, October, 1985)
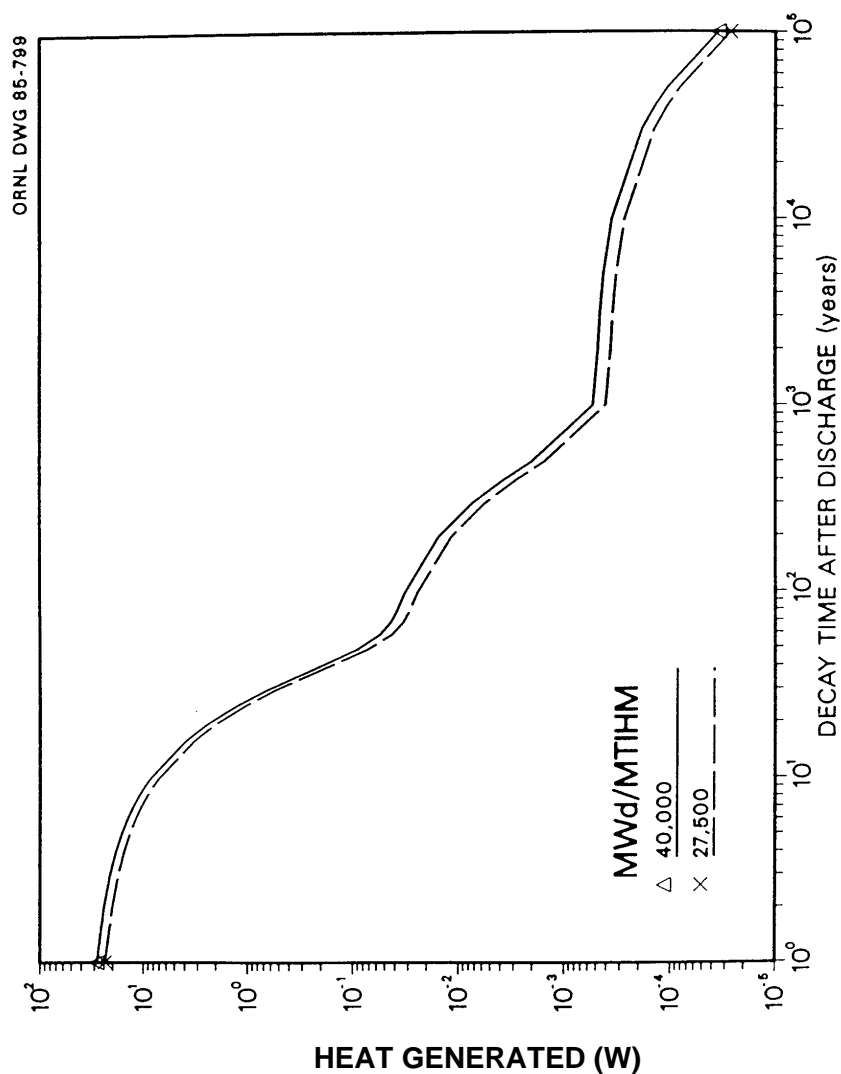
Figure 2.1.3.7-4   Heat generated from irradiated grid spacers, springs, and end pieces for a BWR (Figure 4.4 from J.W. Roddy, H.C. Claiborne, R.C. Ashline, P.T. Johnson, and B.T. Rhyne, *Physical and Decay Characteristics of Commercial LWR Spent Fuels,* **ORNL/TM-9591/V.1, October, 1985)**
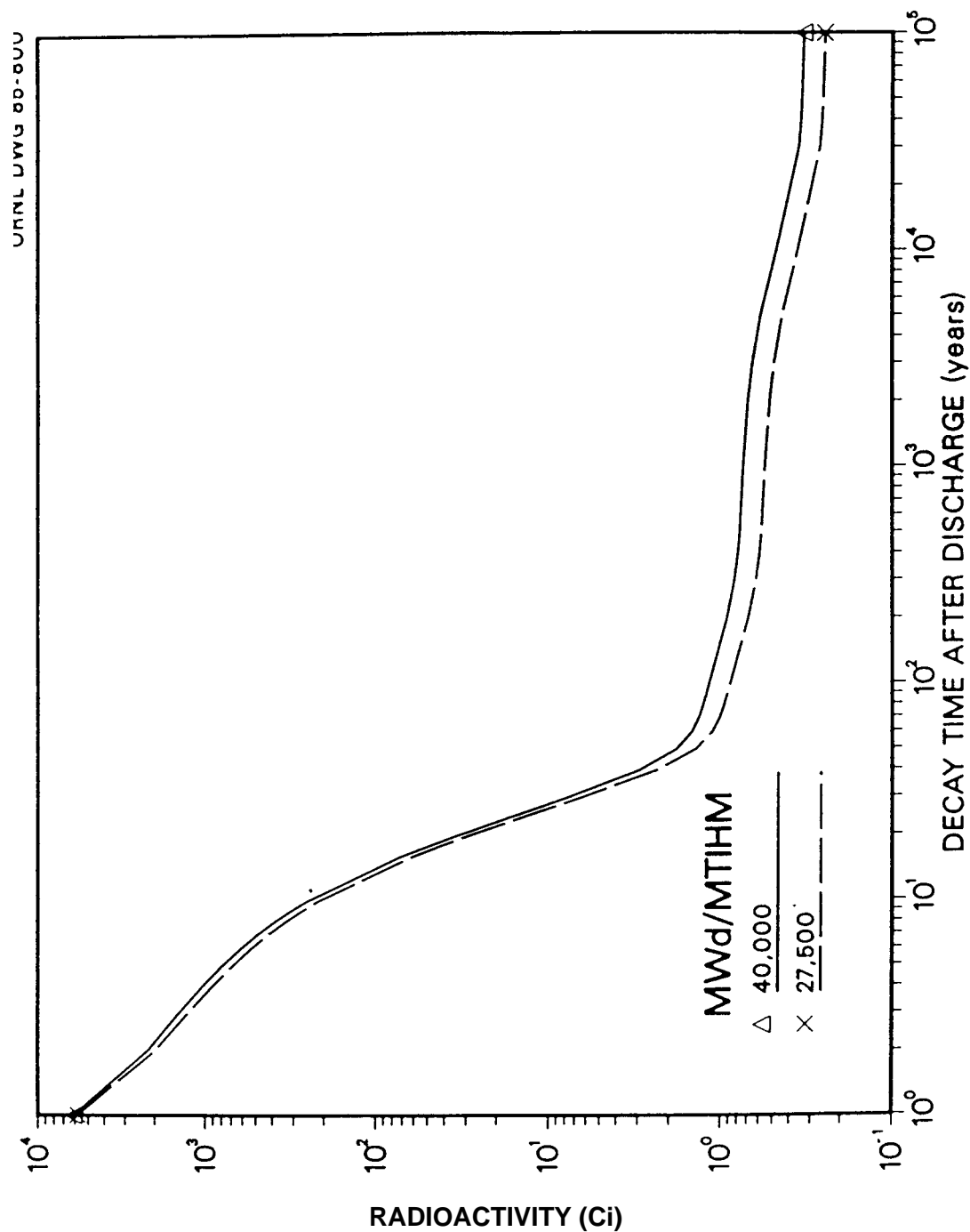
Figure 2.1.3.7-5   Radioactivity from irradiated fuel channels from a BWR (Figure 4.5 from J.W. Roddy, H.C. Claiborne, R.C. Ashline, P.T. Johnson, and B.T. Rhyne, *Physical and Decay Characteristics of Commercial LWR Spent Fuels,* **ORNL/TM-9591/V.1, October, 1985)**
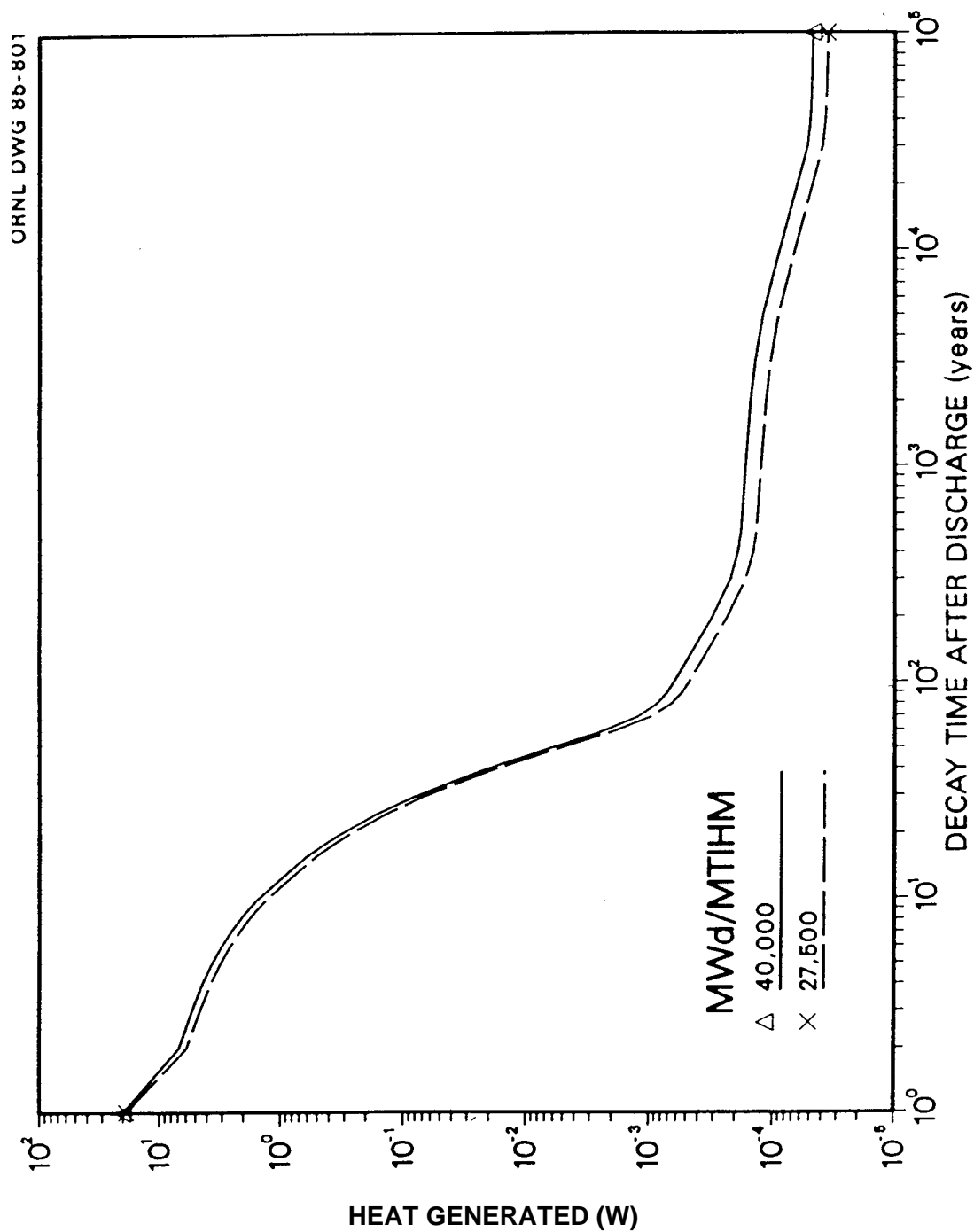
Figure 2.1.3.7-6   Heat generated from irradiated fuel channels from a BWR (Figure 4.6 from J.W. Roddy, H.C. Claiborne, R.C. Ashline, P.T. Johnson, and B.T. Rhyne, *Physical and Decay Characteristics of Commercial LWR Spent Fuels,* **ORNL/TM-9591/V.1, October, 1985)**

1. Parameter of Principal Interest

Leaching rates from activated spent fuel hardware.

2. Test Conditions and Other Qualifying Data

The basis of the estimate of the number and type of fuel assemblies is the 1989 EIA's no new orders case (ref.1 is the annual estimate based on data through 1988: the report incorporating the 1989 data has not yet been published). The no new orders case uses data provided by the utilities on the RW-859 annual report. The projected number of fuel assemblies assumes that the reactors run to their anticipated end of life and are then shutdown. Fuel assemblies are assumed to be discharged on a routine basis, and the type of assemblies are assumed to be the type currently in use, unless information has been provided by the utilities to the contrary. The projection does not account for future design changes that are inevitable. For example, the predominant fuel type for boiling water reactors (BWRs) is currently an 8X8 configuration. Fuel assemblies with 9X9 and 10X10 configurations are being marketed and are expected to constitute a significant portion of the BWR fuel in the future. This, and other similar situations, are not accounted for in these estimates. Additionally, higher burnup of fuels is expected in the future. This would decrease the number of assemblies requiring disposal. This unknown is one of the greatest sources of uncertainty.

The mass and composition of the fuel assemblies was taken from ref.2. The distribution of materials in the core was also obtained from that report. This distribution was necessary in order to account for differing activation levels in the core (e.g. top end fittings vs. material in the active core). A small number of assemblies are not included in these estimates. They include some of the very odd fuel, such as West 15X16, that constitutes less than 1% of the manufacturers projected production.

Estimates of the numbers of non-fuel bearing components were taken from ref.3. Table 4-1 of that report provided estimates of the number of NFBC requiring disposal. Currently, efforts are underway to better define these estimates, but the results of that work will not be available until FY91. The estimates used in this report will likely prove to be

A.T. Luksic, Battelle, PNL Letter Report LLYMP 9104248

conservative. Estimates of the masses and compositions of the non-fuel bearing components was compiled using data in ref.2, 4, & 5.

The activation of the hardware was estimated using the ORIGEN2 computer code, and incorporating the appropriate scaling factors from ref.2. PWR hardware was activated to a burnup of 33,000 MWD/MTU and BWR to 27,500 MWD/MTU. These values reflect the average burnup expected from these fuel types. Non-fuel bearing components used fluxes commensurate with those burnups, but for component specific residence times. ORIGEN2 was then used to decay the radionuclides out to one million years. The results of these calculations were folded with the material quantities estimated above, and total inventories, as a function of time were developed. These are provided in the attached tables.

Surface area estimates were developed based on detailed measurements of a number of available hardware components. These included both top and bottom end fittings of a GE 8X8 BWR, West 14X14 PWR (top only), West 17X17 PWR, and CE 14X14 PWR. Measurements of grid spacers for these assembly types were also made. These represent a large fraction of the fuel assembly types that were considered. The results of these measurements were used to infer surface areas of fuel assembly types that were not available for measurements. An example of this is the surface area of a West 15X15 assembly. From drawings in ref.2, it can be seen that a 15X15 assembly is similar to a 14X14 assembly with an extra row of fuel pins added to two sides. To estimate the surface area of the end fittings and grid spacers, the measured values from the 14X14 are scaled up by a factor of (15*15)/(14*14). For the guide tubes, the surface area of a single guide tube multiplied by the actual number in each fuel type is used (i.e. 20 in the 15X15 vs. 16 in the 14X14).

In evaluating the leaching of radionuclides from the hardware, the thickness of the materials is important. Though this data was not part of the scope of work, some generalizations can be made that should prove helpful. The end fittings are the most massive pieces. They are generally cast stainless steel, and their thickness varies between 1/8" to 5/8" in individual pieces. Grid spacers, made either of Inconel or Zircaloy, are thin pieces of sheet metal. The thickness of the individual strips are approximately 0.025" in the samples we have measured. The guide tubes, mostly Zircaloy but some stainless steel, are only slightly thicker, at about 0.035" - 0.045". Overall, the bulk of the Zircaloy and Inconel are relatively

A.T. Luksic, Battelle, PNL Letter Report LLYMP 9104248

thin. Leaching and/or corrosion would occur from both sides of the material. Given the high surface to volume ratio for the bulk of the Zircaloy and Inconel, a higher percentage of their inventory would be expected to be released earlier than the stainless steel end fittings. Leaching from the guide tubes and grid spacers would occur twice as fast as from the fuel cladding, because the grid spacers and guide tubes will corrode and leach from both sides.

Table IV provides the total inventory of actinides and transuranics for the no new orders case that can be used as a comparison to the results in Tables II-A through II-J for the spent fuel hardware and Tables III-A through III-J7 for the non-fuel bearing components. Overall, the number of curies associated with the actinides and transuranics is several orders of magnitude more than the activation products.

List of Tables

Table I	Repository Hardware Inventory Characteristics
Table II-A	Radioactivity At Discharge in Spent Fuel Hardware
Table II-B	100 Year Radioactivity in Spent Fuel Hardware
Table II-C	200 Year Radioactivity in Spent Fuel Hardware
Table II-D	500 Year Radioactivity in Spent Fuel Hardware
Table II-E	1,000 Year Radioactivity in Spent Fuel Hardware
Table II-F	2,000 Year Radioactivity in Spent Fuel Hardware
Table II-G	5,000 Year Radioactivity in Spent Fuel Hardware
Table II-H	10,000 Year Radioactivity in Spent Fuel Hardware
Table II-I	100,000 Year Radioactivity in Spent Fuel Hardware
Table II-J	1 Million Year Radioactivity in Spent Fuel Hardware
Table III-A	Radioactivity At Discharge in Non-Fuel Bearing Components
Table III-B	100 Year Radioactivity in Non-Fuel Bearing Components
Table III-C	200 Year Radioactivity in Non-Fuel Bearing Components
Table III-D	500 Year Radioactivity in Non-Fuel Bearing Components
Table III-E	1,000 Year Radioactivity in Non-Fuel Bearing Components
Table III-F	2,000 Year Radioactivity in Non-Fuel Bearing Components
Table III-G	5,000 Year Radioactivity in Non-Fuel Bearing Components
Table III-H	10,000 Year Radioactivity in Non-Fuel Bearing Components
Table III-I	100,000 Year Radioactivity in Non-Fuel Bearing Components
Table III-J	1 Million Year Radioactivity in Non-Fuel Bearing Components
Table IV	Spent Fuel Activity Inventory

A.T. Luksic, Battelle, PNL Letter Report LLYMP 9104248

Table 2.1.3.7-5   Repository hardware inventory characteristics (Table I from A.T. Luksic, Battelle, PNL Letter Report, LLYMP 9104248)

MATERIAL	Stainless Steel	Inconel	Zircaloy
Surface Area (M^2)	652,000	1,480,000	400,000
Weight (MT)	3,260	750	6,800
Total Activity At Discharge (Ci)	3,130,000	17,600,000	14,000,000
Total Activity 100 Years (Ci)	1,490,000	8,410,000	7,740
Total Activity 200 Years (Ci)	720,000	4,050,000	6,140
Total Activity 500 Years (Ci)	105,000	587,000	5,210
Total Activity 1,000 Years (Ci)	34,300	190,000	4,980
Total Activity 2,000 Years (Ci)	31,300	177,000	4,680
Total Activity 5,000 Years (Ci)	27,800	167,000	3,960
Total Activity 10,000 Years (Ci)	23,900	152,000	3,190
Total Activity 100,000 Years (Ci)	9,270	54,800	1,980
Total Activity 1 Million Years (Ci)	5	25	1,290

Table 2.1.3.7-6   Radioactivity at discharge in spent fuel hardware (Table II-A from A.T. Luksic, Battelle, PNL Letter Report LLYMP 9104248)

Ci

Isotope	SS	Inc	Zr-4	Total
BE 10	1.43E-03	0.00E+00	0.00E+00	1.43E-03
C 14	1.22E+04	1.18E+04	2.85E+03	2.68E+04
CL 36	1.09E+01	1.05E+01	4.14E+01	6.28E+01
NI 59	2.20E+04	1.27E+05	1.91E+01	1.49E+05
CO 60	0.00E+00	0.00E+00	1.93E+06	1.93E+06
NI 63	3.10E+06	1.75E+07	2.73E+03	2.06E+07
SR 90	0.00E+00	0.00E+00	1.04E+01	1.04E+01
Y 90	0.00E+00	0.00E+00	1.20E+07	1.20E+07
ZR 93	0.00E+00	2.75E-01	1.03E+03	1.03E+03
NB 93M	0.00E+00	1.82E-02	6.84E+01	6.84E+01
NB 94	8.62E+01	4.56E+04	3.91E+02	4.61E+04
MO 93	0.00E+00	8.98E+02	0.00E+00	8.98E+02
TC 99	0.00E+00	4.80E+01	0.00E+00	4.80E+01
SN121M	0.00E+00	0.00E+00	4.67E+03	4.67E+03
Total	3.13E+06	1.76E+07	1.40E+07	3.48E+07

Table 2.1.3.7-7   100 year radioactivity in spent fuel hardware (Table II-B from A.T. Luksic, Battelle, PNL Letter Report LLYMP 9104248)

Ci

Isotope	SS	Inc	Zr-4	Total
BE 10	1.43E-03	0.00E+00	0.00E+00	1.43E-03
C 14	1.20E+04	1.16E+04	2.82E+03	2.64E+04
CL 36	1.09E+01	1.05E+01	4.14E+01	6.28E+01
NI 59	2.20E+04	1.27E+05	1.91E+01	1.49E+05
CO 60	0.00E+00	0.00E+00	3.73E+00	3.73E+00
NI 63	1.46E+06	8.22E+06	1.29E+03	9.68E+06
SR 90	0.00E+00	0.00E+00	9.66E-01	9.66E-01
Y 90	0.00E+00	0.00E+00	9.66E-01	9.66E-01
ZR 93	0.00E+00	2.75E-01	1.03E+03	1.03E+03
NB 93M	0.00E+00	2.59E-01	9.77E+02	9.77E+02
NB 94	8.59E+01	4.55E+04	3.90E+02	4.59E+04
MO 93	0.00E+00	8.80E+02	0.00E+00	8.80E+02
TC 99	0.00E+00	4.82E+01	0.00E+00	4.82E+01
SN121M	0.00E+00	0.00E+00	1.17E+03	1.17E+03
Total	1.49E+06	8.41E+06	7.74E+03	9.91E+06

Table 2.1.3.7-8   200 year radioactivity in spent fuel hardware (Table II-C from A.T. Luksic, Battelle, PNL Letter Report LLYMP 9104248)

Ci

Isotope	SS	Inc	Zr-4	Total
BE 10	1.43E-03	0.00E+00	0.00E+00	1.43E-03
C 14	1.19E+04	1.15E+04	2.78E+03	2.61E+04
CL 36	1.09E+01	1.05E+01	4.14E+01	6.28E+01
NI 59	2.20E+04	1.27E+05	1.91E+01	1.49E+05
CO 60	0.00E+00	0.00E+00	7.24E-06	7.24E-06
NI 63	6.86E+05	3.87E+06	6.06E+02	4.56E+06
SR 90	0.00E+00	0.00E+00	8.94E-02	8.94E-02
Y 90	0.00E+00	0.00E+00	8.94E-02	8.94E-02
ZR 93	0.00E+00	2.75E-01	1.03E+03	1.03E+03
NB 93M	0.00E+00	2.61E-01	9.82E+02	9.82E+02
NB 94	8.57E+01	4.53E+04	3.89E+02	4.58E+04
MO 93	0.00E+00	8.63E+02	0.00E+00	8.63E+02
TC 99	0.00E+00	4.82E+01	0.00E+00	4.82E+01
SN121M	0.00E+00	0.00E+00	2.91E+02	2.91E+02
Total	7.20E+05	4.05E+06	6.14E+03	4.78E+06

Table 2.1.3.7-9   500 year radioactivity in spent fuel hardware (Table II-D from A.T. Luksic, Battelle, PNL Letter Report LLYMP 9104248)

Ci

Isotope	SS	Inc	Zr-4	Total
BE 10	1.43E-03	0.00E+00	0.00E+00	1.43E-03
C 14	1.15E+04	1.11E+04	2.68E+03	2.52E+04
CL 36	1.09E+01	1.05E+01	4.14E+01	6.28E+01
NI 59	2.19E+04	1.26E+05	1.90E+01	1.48E+05
CO 60	0.00E+00	0.00E+00	0.00E+00	0.00E+00
NI 63	7.16E+04	4.04E+05	6.32E+01	4.75E+05
SR 90	0.00E+00	0.00E+00	7.08E-05	7.08E-05
Y 90	0.00E+00	0.00E+00	7.08E-05	7.08E-05
ZR 93	0.00E+00	2.75E-01	1.03E+03	1.03E+03
NB 93M	0.00E+00	2.61E-01	9.82E+02	9.82E+02
NB 94	8.48E+01	4.49E+04	3.85E+02	4.53E+04
MO 93	0.00E+00	8.13E+02	0.00E+00	8.13E+02
TC 99	0.00E+00	4.81E+01	0.00E+00	4.81E+01
SN121M	0.00E+00	0.00E+00	4.54E+00	4.54E+00
Total	1.05E+05	5.87E+05	5.21E+03	6.97E+05

Table 2.1.3.7-10   1000 year radioactivity in spent fuel hardware (Table
II-E from A.T. Luksic, Battelle, PNL Letter Report
LLYMP 9104248)

Ci

Isotope	SS	Inc	Zr-4	Total
BE 10	1.43E-03	0.00E+00	0.00E+00	1.43E-03
C 14	1.08E+04	1.04E+04	2.53E+03	2.37E+04
CL 36	1.09E+01	1.05E+01	4.13E+01	6.27E+01
NI 59	2.18E+04	1.26E+05	1.89E+01	1.47E+05
CO 60	0.00E+00	0.00E+00	0.00E+00	0.00E+00
NI 63	1.66E+03	9.33E+03	1.46E+00	1.10E+04
SR 90	0.00E+00	0.00E+00	4.80E-10	4.80E-10
Y 90	0.00E+00	0.00E+00	4.80E-10	4.80E-10
ZR 93	0.00E+00	2.75E-01	1.03E+03	1.03E+03
NB 93M	0.00E+00	2.61E-01	.82E+02	9.82E+02
NB 94	8.33E+01	4.41E+04	3.78E+02	4.46E+04
MO 93	0.00E+00	7.37E+02	0.00E+00	7.37E+02
TC 99	0.00E+00	4.81E+01	0.00E+00	4.81E+01
SN121M	0.00E+00	0.00E+00	4.42E-03	4.42E-03
Total	3.43E+04	1.90E+05	4.98E+03	2.30E+05

Table 2.1.3.7-11   2000 year radioactivity in spent fuel hardware (Table
II-F from A.T. Luksic, Battelle, PNL Letter Report
LLYMP 9104248)

Ci

Isotope	SS	Inc	Zr-4	Total
BE 10	1.43E-03	0.00E+00	0.00E+00	1.43E-03
C 14	9.55E+03	9.23E+03	2.24E+03	2.10E+04
CL 36	1.09E+01	1.05E+01	4.12E+01	6.25E+01
NI 59	2.16E+04	1.25E+05	1.88E+01	1.46E+05
CO 60	0.00E+00	0.00E+00	0.00E+00	0.00E+00
NI 63	8.85E-01	4.99E+00	7.81E-04	5.87E+00
SR 90	0.00E+00	0.00E+00	0.00E+00	0.00E+00
Y 90	0.00E+00	0.00E+00	0.00E+00	0.00E+00
ZR 93	0.00E+00	2.74E-01	1.03E+03	1.03E+03
NB 93M	0.00E+00	2.61E-01	9.81E+02	9.82E+02
NB 94	8.05E+01	4.26E+04	3.66E+02	4.31E+04
MO 93	0.00E+00	6.04E+02	0.00E+00	6.04E+02
TC 99	0.00E+00	4.79E+01	0.00E+00	4.79E+01
SN121M	0.00E+00	0.00E+00	4.18E-09	4.18E-09
Total	3.13E+04	1.77E+05	4.68E+03	2.13E+05

Table 2.1.3.7-12 5000 year radioactivity in spent fuel hardware (Table
II-G from A.T. Luksic, Battelle, PNL Letter Report
LLYMP 9104248)

Ci

Isotope	SS	Inc	Zr-4	Total
BE 10	1.43E-03	0.00E+00	0.00E+00	1.43E-03
C 14	6.64E+03	6.42E+03	1.56E+03	1.46E+04
CL 36	1.08E+01	1.04E+01	4.09E+01	6.21E+01
NI 59	2.11E+04	1.21E+05	1.83E+01	1.42E+05
CO 60	0.00E+00	0.00E+00	0.00E+00	0.00E+00
NI 63	1.35E-10	7.62E-10	1.19E-13	8.97E-10
SR 90	0.00E+00	0.00E+00	0.00E+00	0.00E+00
Y 90	0.00E+00	0.00E+00	0.00E+00	0.00E+00
ZR 93	0.00E+00	2.74E-01	1.03E+03	1.03E+03
NB 93M	0.00E+00	2.60E-01	9.80E+02	9.80E+02
NB 94	7.27E+01	3.85E+04	3.30E+02	3.89E+04
MO 93	0.00E+00	3.33E+02	0.00E+00	3.33E+02
TC 99	0.00E+00	4.74E+01	0.00E+00	4.74E+01
SN121M	0.00E+00	0.00E+00	0.00E+00	0.00E+00
Total	2.78E+04	1.67E+05	3.96E+03	1.98E+05

Table 2.1.3.7-13 10,000 year radioactivity in spent fuel hardware (Table
II-H from A.T. Luksic, Battelle, PNL Letter Report
LLYMP 9104248)

Ci

Isotope	SS	Inc	Zr-4	Total
BE 10	1.42E-03	0.00E+00	0.00E+00	1.42E-03
C 14	3.63E+03	3.51E+03	8.50E+02	7.98E+03
CL 36	1.07E+01	1.03E+01	4.05E+01	6.14E+01
NI 59	2.02E+04	1.16E+05	1.75E+01	1.36E+05
CO 60	0.00E+00	0.00E+00	0.00E+00	0.00E+00
NI 63	0.00E+00	0.00E+00	0.00E+00	0.00E+00
SR 90	0.00E+00	0.00E+00	0.00E+00	0.00E+00
Y 90	0.00E+00	0.00E+00	0.00E+00	0.00E+00
ZR 93	0.00E+00	2.73E-01	1.03E+03	1.03E+03
NB 93M	0.00E+00	2.60E-01	9.78E+02	9.78E+02
NB 94	6.13E+01	3.24E+04	2.78E+02	3.28E+04
MO 93	0.00E+00	1.24E+02	0.00E+00	1.24E+02
TC 99	0.00E+00	4.67E+01	0.00E+00	4.67E+01
SN121M	0.00E+00	0.00E+00	0.00E+00	0.00E+00
Total	2.39E+04	1.52E+05	3.19E+03	1.79E+05

Table 2.1.3.7-14   100,000 year radioactivity in spent fuel hardware (Table
II-I from A.T. Luksic, Battelle, PNL Letter Report
LLYMP 9104248)

Ci

Isotope	SS	Inc	Zr-4	Total
BE 10	1.37E-03	0.00E+00	0.00E+00	1.37E-03
C 14	6.77E-02	6.55E-02	1.59E-02	1.49E-01
CL 36	8.67E+00	8.35E+00	3.29E+01	4.99E+01
NI 59	9.25E+03	5.33E+04	8.03E+00	6.26E+04
CO 60	0.00E+00	0.00E+00	0.00E+00	0.00E+00
NI 63	0.00E+00	0.00E+00	0.00E+00	0.00E+00
SR 90	0.00E+00	0.00E+00	0.00E+00	0.00E+00
Y 90	0.00E+00	0.00E+00	0.00E+00	0.00E+00
ZR 93	0.00E+00	2.62E-01	9.88E+02	9.88E+02
NB 93M	0.00E+00	2.49E-01	9.39E+02	9.39E+02
NB 94	2.84E+00	1.50E+03	1.29E+01	1.52E+03
MO 93	0.00E+00	2.23E-06	0.00E+00	2.23E-06
TC 99	0.00E+00	3.48E+01	0.00E+00	3.48E+01
SN121M	0.00E+00	0.00E+00	0.00E+00	0.00E+00
Total	9.27E+03	5.48E+04	1.98E+03	6.61E+04

Table 2.1.3.7-15   1 million year radioactivity in spent fuel hardware (Table
II-J from A.T. Luksic, Battelle, PNL Letter Report
LLYMP 9104248)

Ci

Isotope	SS	Inc	Zr-4	Total
BE 10	9.26E-04	0.00E+00	0.00E+00	9.26E-04
C 14	0.00E+00	0.00E+00	0.00E+00	0.00E+00
CL 36	1.09E+00	1.05E+00	4.14E+00	6.28E+00
NI 59	3.80E+00	2.19E+01	3.30E-03	2.57E+01
CO 60	0.00E+00	0.00E+00	0.00E+00	0.00E+00
NI 63	0.00E+00	0.00E+00	0.00E+00	0.00E+00
SR 90	0.00E+00	0.00E+00	0.00E+00	0.00E+00
Y 90	0.00E+00	0.00E+00	0.00E+00	0.00E+00
ZR 93	0.00E+00	1.75E-01	6.57E+02	6.57E+02
NB 93M	0.00E+00	1.66E-01	6.24E+02	6.24E+02
NB 94	1.28E-13	6.76E-11	5.80E-13	6.83E-11
MO 93	0.00E+00	0.00E+00	0.00E+00	0.00E+00
TC 99	0.00E+00	1.86E+00	0.00E+00	1.86E+00
SN121M	0.00E+00	0.00E+00	0.00E+00	0.00E+00
Total	4.89E+00	2.51E+01	1.29E+03	1.32E+03

Table 2.1.3.7-16   Radioactivity at discharge in non-fuel bearing components
(Table III-A from A.T. Luksic, Battelle, PNL Letter Report
LLYMP 9104248)

Ci

Isotope	SS	Inc	Zr-4	Total
BE 10	1.31E-06	0.00E+00	0.00E+00	1.31E-06
C 14	1.21E+01	3.89E+02	7.03E+03	7.43E+03
CL 36	1.09E-02	3.47E-01	1.03E+02	1.04E+02
NI 59	2.12E+01	4.21E+03	4.30E+01	4.28E+03
CO 60	0.00E+00	0.00E+00	4.83E+06	4.83E+06
NI 63	3.08E+03	5.75E+05	6.75E+03	5.85E+05
SR 90	0.00E+00	0.00E+00	0.00E+00	0.00E+00
Y 90	0.00E+00	0.00E+00	0.00E+00	0.00E+00
ZR 93	0.00E+00	9.36E-03	2.77E+03	2.77E+03
NB 93M	0.00E+00	6.19E-04	1.85E+02	1.85E+02
NB 94	8.64E-02	1.51E+03	9.96E+02	2.51E+03
MO 93	0.00E+00	2.99E+01	0.00E+00	2.99E+01
TC 99	0.00E+00	1.24E+00	0.00E+00	1.24E+00
SN121M	0.00E+00	0.00E+00	1.16E+04	1.16E+04
Total	3.11E+03	5.81E+05	4.86E+06	5.44E+06

Table 2.1.3.7-17   100 year radioactivity in non-fuel bearing components
(Table III-B from A.T. Luksic, Battelle, PNL Letter
Report LLYMP 9104248)

Ci

Isotope	SS	Inc	Zr-4	Total
BE 10	1.31E-06	0.00E+00	0.00E+00	1.31E-06
C 14	1.19E+01	3.84E+02	6.94E+03	7.34E+03
CL 36	1.09E-02	3.47E-01	1.03E+02	1.04E+02
NI 59	2.12E+01	4.21E+03	4.29E+01	4.27E+03
CO 60	0.00E+00	0.00E+00	9.35E+00	9.35E+00
NI 63	1.45E+03	2.71E+05	3.18E+03	2.75E+05
SR 90	0.00E+00	0.00E+00	0.00E+00	0.00E+00
Y 90	0.00E+00	0.00E+00	0.00E+00	0.00E+00
ZR 93	0.00E+00	9.36E-03	2.77E+03	2.77E+03
NB 93M	0.00E+00	8.84E-03	2.62E+03	2.62E+03
NB 94	8.61E-02	1.51E+03	9.92E+02	2.50E+03
MO 93	0.00E+00	2.93E+01	0.00E+00	2.93E+01
TC 99	0.00E+00	1.25E+00	0.00E+00	1.25E+00
SN121M	0.00E+00	0.00E+00	2.91E+03	2.91E+03
Total	1.48E+03	2.77E+05	1.96E+04	2.98E+05

Table 2.1.3.7-18 200 year radioactivity in non-fuel bearing components
(Table III-C from A.T. Luksic, Battelle, PNL Letter
Report LLYMP 9104248)

Ci

Isotope	SS	Inc	Zr-4	Total
BE 10	1.31E-06	0.00E+00	0.00E+00	1.31E-06
C 14	1.18E+01	3.79E+02	6.86E+03	7.25E+03
CL 36	1.09E-02	3.47E-01	1.03E+02	1.04E+02
NI 59	2.12E+01	4.21E+03	4.29E+01	4.27E+03
CO 60	0.00E+00	0.00E+00	1.81E-05	1.81E-05
NI 63	6.83E+02	1.27E+05	1.50E+03	1.30E+05
SR 90	0.00E+00	0.00E+00	0.00E+00	0.00E+00
Y 90	0.00E+00	0.00E+00	0.00E+00	0.00E+00
ZR 93	0.00E+00	9.35E-03	2.77E+03	2.77E+03
NB 93M	0.00E+00	8.89E-03	2.63E+03	2.63E+03
NB 94	8.58E-02	1.50E+03	9.89E+02	2.49E+03
MO 93	0.00E+00	2.87E+01	0.00E+00	2.87E+01
TC 99	0.00E+00	1.25E+00	0.00E+00	1.25E+00
SN121M	0.00E+00	0.00E+00	7.27E+02	7.27E+02
Total	7.16E+02	1.34E+05	1.56E+04	1.50E+05

Table 2.1.3.7-19 500 year radioactivity in non-fuel bearing components
(Table III-D from A.T. Luksic, Battelle, PNL Letter
Report LLYMP 9104248)

Ci

Isotope	SS	Inc	Zr-4	Total
BE 10	1.31E-06	0.00E+00	0.00E+00	1.31E-06
C 14	1.14E+01	3.66E+02	6.62E+03	7.00E+03
CL 36	1.08E-02	3.47E-01	1.03E+02	1.04E+02
NI 59	2.11E+01	4.20E+03	4.28E+01	4.26E+03
CO 60	0.00E+00	0.00E+00	0.00E+00	0.00E+00
NI 63	7.12E+01	1.33E+04	1.56E+02	1.35E+04
SR 90	0.00E+00	0.00E+00	0.00E+00	0.00E+00
Y 90	0.00E+00	0.00E+00	0.00E+00	0.00E+00
ZR 93	0.00E+00	9.35E-03	2.77E+03	2.77E+03
NB 93M	0.00E+00	8.89E-03	2.63E+03	2.63E+03
NB 94	8.49E-02	1.49E+03	9.79E+02	2.47E+03
MO 93	0.00E+00	2.71E+01	0.00E+00	2.71E+01
TC 99	0.00E+00	1.24E+00	0.00E+00	1.24E+00
SN121M	0.00E+00	0.00E+00	1.13E+01	1.13E+01
Total	1.04E+02	1.94E+04	1.33E+04	3.28E+04

Table 2.1.3.7-20   1,000 year radioactivity in non-fuel bearing components
(Table III-E from A.T. Luksic, Battelle, PNL Letter Report
LLYMP 9104248)

Ci

Isotope	SS	Inc	Zr-4	Total
BE 10	1.31E-06	0.00E+00	0.00E+00	1.31E-06
C 14	1.07E+01	3.44E+02	6.23E+03	6.58E+03
CL 36	1.08E-02	3.46E-01	1.03E+02	1.03E+02
NI 59	2.10E+01	4.18E+03	4.26E+01	4.24E+03
CO 60	0.00E+00	0.00E+00	0.00E+00	0.00E+00
NI 63	1.65E+00	3.07E+02	3.61E+00	3.12E+02
SR 90	0.00E+00	0.00E+00	0.00E+00	0.00E+00
Y 90	0.00E+00	0.00E+00	0.00E+00	0.00E+00
ZR 93	0.00E+00	9.35E-03	2.77E+03	2.77E+03
NB 93M	0.00E+00	8.88E-03	2.63E+03	2.63E+03
NB 94	8.35E-02	1.46E+03	9.63E+02	2.43E+03
MO 93	0.00E+00	2.45E+01	0.00E+00	2.45E+01
TC 99	0.00E+00	1.24E+00	0.00E+00	1.24E+00
SN121M	0.00E+00	0.00E+00	1.10E-02	1.10E-02
Total	3.35E+01	6.32E+03	1.27E+04	1.91E+04

Table 2.1.3.7-21   2,000 year radioactivity in non-fuel bearing components
(Table III-F from A.T. Luksic, Battelle, PNL Letter Report
LLYMP 9104248)

Ci

Isotope	SS	Inc	Zr-4	Total
BE 10	1.31E-06	0.00E+00	0.00E+00	1.31E-06
C 14	9.47E+00	3.05E+02	5.52E+03	5.83E+03
CL 36	1.08E-02	3.46E-01	1.03E+02	1.03E+02
NI 59	2.09E+01	4.14E+03	4.22E+01	4.20E+03
CO 60	0.00E+00	0.00E+00	0.00E+00	0.00E+00
NI 63	8.80E-04	1.64E-01	1.93E-03	1.67E-01
SR 90	0.00E+00	0.00E+00	0.00E+00	0.00E+00
Y 90	0.00E+00	0.00E+00	0.00E+00	0.00E+00
ZR 93	0.00E+00	9.35E-03	2.77E+03	2.77E+03
NB 93M	0.00E+00	8.88E-03	2.63E+03	2.63E+03
NB 94	8.07E-02	1.41E+03	9.30E+02	2.34E+03
MO 93	0.00E+00	2.01E+01	0.00E+00	2.01E+01
TC 99	0.00E+00	1.24E+00	0.00E+00	1.24E+00
SN121M	0.00E+00	0.00E+00	1.04E-08	1.04E-08
Total	3.04E+01	5.88E+03	1.20E+04	1.79E+04

Table 2.1.3.7-22 5,000 year radioactivity in non-fuel bearing components
(Table III-G from A.T. Luksic, Battelle, PNL Letter Report
LLYMP 9104248)

Ci

Isotope	SS	Inc	Zr-4	Total
BE 10	1.31E-06	0.00E+00	0.00E+00	1.31E-06
C 14	6.59E+00	2.12E+02	3.84E+03	4.06E+03
CL 36	1.07E-02	3.43E-01	1.02E+02	1.03E+02
NI 59	2.03E+01	4.03E+03	4.11E+01	4.10E+03
CO 60	0.00E+00	0.00E+00	0.00E+00	0.00E+00
NI 63	1.34E-13	2.51E-11	2.95E-13	2.55E-11
SR 90	0.00E+00	0.00E+00	0.00E+00	0.00E+00
Y 90	0.00E+00	0.00E+00	0.00E+00	0.00E+00
ZR 93	0.00E+00	9.33E-03	2.76E+03	2.76E+03
NB 93M	0.00E+00	8.87E-03	2.62E+03	2.62E+03
NB 94	7.28E-02	1.28E+03	8.40E+02	2.12E+03
MO 93	0.00E+00	1.11E+01	0.00E+00	1.11E+01
TC 99	0.00E+00	1.23E+00	0.00E+00	1.23E+00
SN121M	0.00E+00	0.00E+00	0.00E+00	0.00E+00
Total	2.70E+01	5.54E+03	1.02E+04	1.58E+04

Table 2.1.3.7-23 10,000 year radioactivity in non-fuel bearing components
(Table III-H from A.T. Luksic, Battelle, PNL Letter Report
LLYMP 9104248)

Ci

Isotope	SS	Inc	Zr-4	Total
BE 10	1.30E-06	0.00E+00	0.00E+00	1.30E-06
C 14	3.60E+00	1.16E+02	2.10E+03	2.22E+03
CL 36	1.06E-02	3.39E-01	1.01E+02	1.01E+02
NI 59	1.95E+01	3.86E+03	3.94E+01	3.92E+03
CO 60	0.00E+00	0.00E+00	0.00E+00	0.00E+00
NI 63	0.00E+00	0.00E+00	0.00E+00	0.00E+00
SR 90	0.00E+00	0.00E+00	0.00E+00	0.00E+00
Y 90	0.00E+00	0.00E+00	0.00E+00	0.00E+00
ZR 93	0.00E+00	9.31E-03	2.76E+03	2.76E+03
NB 93M	0.00E+00	8.85E-03	2.62E+03	2.62E+03
NB 94	6.14E-02	1.08E+03	7.08E+02	1.78E+03
MO 93	0.00E+00	4.12E+00	0.00E+00	4.12E+00
TC 99	0.00E+00	1.21E+00	0.00E+00	1.21E+00
SN121M	0.00E+00	0.00E+00	0.00E+00	0.00E+00
Total	2.31E+01	5.06E+03	8.32E+03	1.34E+04

Table 2.1.3.7-24   100,000 year radioactivity in non-fuel bearing components
(Table III-I from A.T. Luksic, Battelle, PNL Letter Report
LLYMP 9104248)

Ci

Isotope	SS	Inc	Zr-4	Total
BE 10	1.25E-06	0.00E+00	0.00E+00	1.25E-06
C 14	6.72E-05	2.16E-03	3.91E-02	4.14E-02
CL 36	8.63E-03	2.76E-01	8.21E+01	8.24E+01
NI 59	8.93E+00	1.77E+03	1.81E+01	1.80E+03
CO 60	0.00E+00	0.00E+00	0.00E+00	0.00E+00
NI 63	0.00E+00	0.00E+00	0.00E+00	0.00E+00
SR 90	0.00E+00	0.00E+00	0.00E+00	0.00E+00
Y 90	0.00E+00	0.00E+00	0.00E+00	0.00E+00
ZR 93	0.00E+00	8.94E-03	2.65E+03	2.65E+03
NB 93M	0.00E+00	8.50E-03	2.51E+03	2.51E+03
NB 94	2.84E-03	4.98E+01	3.28E+01	8.25E+01
MO 93	0.00E+00	7.42E-08	0.00E+00	7.42E-08
TC 99	0.00E+00	9.00E-01	0.00E+00	9.00E-01
SN121M	0.00E+00	0.00E+00	0.00E+00	0.00E+00
Total	8.94E+00	1.82E+03	5.29E+03	7.13E+03

Table 2.1.3.7-25   1 million year radioactivity in non-fuel bearing components
(Table III-J from A.T. Luksic, Battelle, PNL Letter Report
LLYMP 9104248)

Ci

Isotope	SS	Inc	Zr-4	Total
BE 10	8.50E-07	0.00E+00	0.00E+00	8.50E-07
C 14	0.00E+00	0.00E+00	0.00E+00	0.00E+00
CL 36	1.09E-03	3.47E-02	1.03E+01	1.04E+01
NI 59	3.66E-03	7.27E-01	7.42E-03	7.39E-01
CO 60	0.00E+00	0.00E+00	0.00E+00	0.00E+00
NI 63	0.00E+00	0.00E+00	0.00E+00	0.00E+00
SR 90	0.00E+00	0.00E+00	0.00E+00	0.00E+00
Y 90	0.00E+00	0.00E+00	0.00E+00	0.00E+00
ZR 93	0.00E+00	5.95E-03	1.76E+03	1.76E+03
NB 93M	0.00E+00	5.65E-03	1.67E+03	1.67E+03
NB 94	1.28E-16	2.24E-12	1.48E-12	3.72E-12
MO 93	0.00E+00	0.00E+00	0.00E+00	0.00E+00
TC 99	0.00E+00	4.81E-02	0.00E+00	4.81E-02
SN121M	0.00E+00	0.00E+00	0.00E+00	0.00E+00
Total	4.75E-03	8.22E-01	3.44E+03	3.44E+03

Table 2.1.3.7-26   Spent fuel activity inventory (Table IV from A.T. Luksic, Battelle, PNL Letter Report LLYMP 9104248)

CI

Time	PWR	BWR	Total
Discharge	9.94E+12	4.06E+12	1.40E+13
100 Years	2.27E+09	9.31E+08	3.20E+09
200 Years	4.47E+08	1.88E+08	6.35E+08
500 Years	1.64E+08	7.25E+07	2.37E+08
1,000 Years	9.75E+07	4.33E+07	1.41E+08
2,000 Years	5.40E+07	2.41E+07	7.81E+07
5,000 Years	3.57E+07	1.60E+07	5.17E+07
10,000 Years	2.59E+07	1.17E+07	3.76E+07
100,000 Years	2.64E+06	1.14E+06	3.78E+06
1 Million Yrs	1.08E+06	4.67E+05	1.54E+06

References

1 SR/CNEAF/90-01, **Spent Nuclear Fuel Discharges from U.S. Reactors 1988**, prepared by the Energy Information Administration, U.S. Department of Energy, March 1990.

2 DOE/RW-0184, **Characteristics of Spent Fuel, High-Level Waste, and Other Radioactive Wastes Which May Require Long-Term Isolation**, prepared by Oak Ridge National Laboratory, December 1987.

3 ORNL/Sub/86-SA094/8, **Acceptance of Non-Fuel Assembly Hardware by the Federal Waste Management System**, prepared by E.R. Johnson Associates,Inc., March 1990.

4 PNL-6046, **Spent Fuel Disassembly Hardware and Other Non-Fuel Bearing Components: Characterization, Disposal Cost Estimates, and Proposed Repository Acceptance Criteria**, A.T. Luksic, et al, October 1986

5 PNL-6906, **Spent Fuel Assembly Hardware: Characterization and 10CFR61 Classification for Waste Disposal**, A.T. Luksic, et al, June 1989.

A.T. Luksic, Battelle, PNL Letter Report LLYMP 9104248

2.2 Glass Waste Form

The glass form is the most probably disposal form for the various High-Level Wastes (HLW) other than Spent Fuel. HLW originates from domestic fuel reprocessing plants, both commercial and defense related.

2.2.1 Radionuclide Content

2.2.1.1 Present Inventory

ORNL DWG 90-8260

HLW
COMMERCIAL
0.04%

LLW
COMMERCIAL
29.7%

SF*
0.17%

TRU
5.6%

LLW
DOE
56.2%

HLW
DOE
8.3%

WASTE	CUBIC METERS
HLW	
A) Commercial	1.88E+03
B) DOE	3.79E+06
Total HLW	3.81E+06
LLW	
A) Commercial	1.35E+06
B) DOE	2.56E+06
Total LLW	3.91E+06
TRU Waste	2.62E+06
SF*	7.92E+03
TOTAL	4.55E+06
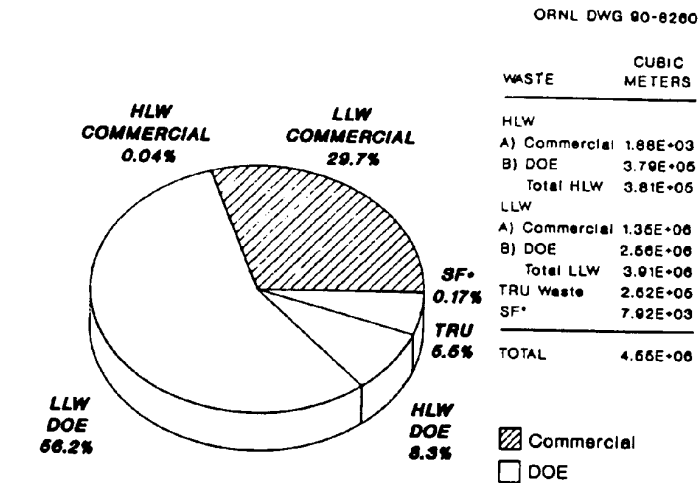
⊞ Commercial
☐ DOE

*Includes spacing between fuel assembly rods.
Does not Include DOE spent fuel to be reprocessed.

Figure 2.2.1.1-1 Volumes of commercial and DOE wastes and spent fuel accumulated through 1989 (Figure 0.1 from *Integrated Data Base for 1990: U.S. Spent Fuel and Radioactive Waste Inventories, Projections, and Characteristics.* USDOE/RW-0006 Rev. 6, October 1990)

ORNL DWG 90-8261

HLW
COMMERCIAL
0.1%

HLW
DOE
5.0%

TRU
0.02%

SF*
94.8%

LLW
DOE
0.06%

LLW
COMMERCIAL
0.02%

WASTE	CURIES
HLW	
A) Commercial	2.79E+07
B) DOE	1.08E+09
Total HLW	1.11E+09
LLW	
A) Commercial	5.28E+06
B) DOE	1.36E+07
Total LLW	1.91E+07
TRU Waste	3.67E+06
SF*	2.07E+10
TOTAL	2.18E+10
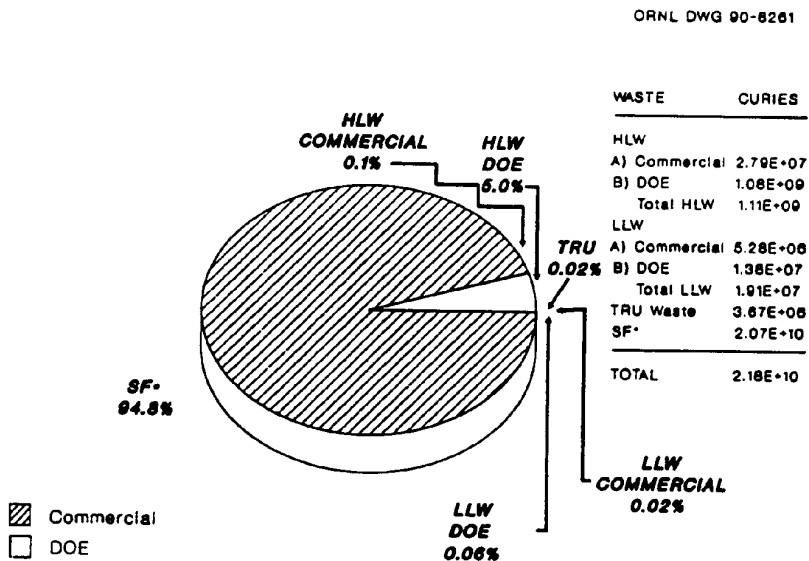
⊞ Commercial
☐ DOE

*Does not Include DOE spent fuel to be reprocessed.

Figure 2.2.1.1-2 Radioactivities of commercial and DOE wastes and spent fuel accumulated through 1989 (Figure 0.2 from *Integrated Data Base for 1990: U.S. Spent Fuel and Radioactive Waste Inventories, Projections, and Characteristics.* USDOE/RW-0006 Rev. 6, October 1990)

Table 2.2.1.1-1   Dimensions, weights, and radioactivity of canisters (Table 6.2 from K.J. Notz, T.D. Welch, R.S. Moore, and W.J. Reich, *Preliminary Waste Form Characteristics*, ORNL-TM-11681 [draft] September, 1990)

	West Valley Demonstration Project	Savannah River Site	Hanford Site	Idaho Nat'l Engineering Laboratory
Outside diameter, cm	61	61	61	61
Overall height, cm	300	300	300	300
Material	SS	SS	SS	SS
Wall thickness, mm	3.4	9.5	9.5	9.5
Weights (kg) Canister Glass or ceramic Total	252 1900 2152	500 1682 2182	500 1650 2150	500 1825 2325
Curies per canister[a]	114,700	234,400	298,000[b]	109,000
Watts per canister[a]	342	709	869[c]	339

[a]aThese are estimated maximum values from ORIGEN2 calculations based on radionuclide compositions supplied by the sites. Curies and watts shown are at time of filling the canister, except for West Valley Demonstration Project where the values shown are for the start of year 1992. For West Valley Demonstration Project, maximum values are assumed to be 110% of average values, and average values are based on the Revision 7 mass balance (Crocker 1989a). Maximum values for the defense sites do not necessarily represent initial operations.

[b]Based on Mitchell and Nelson 1988, maximum case.

[c]Based on ORIGEN2 calculations using Mitchell and Nelson maximum case.

Table 2.2.1.1-2   West Valley demonstration project. High-level waste form and canister characteristics.[a] (Table 6.3 from K.J. Notz, T.D. Welch, R.S. Moore, and W.J. Reich, *Preliminary Waste Form Characteristics,* ORNL-TM-11681 [draft] September, 1990)

Waste form	Borosilicate glass in sealed canister
Canister material	Stainless steel type 304L
Borosilicate glass density, g/cm^3 at 25°C	2.7

Weights per canister:

Empty canister, kg	234
Cover, kg	18
Borosilicate glass, kg	1,900
Total loaded weight, kg	2,152

Canister dimensions:

Outside diameter, cm	61
Height overall, cm	300
Wall thickness, cm	0.34

Radionuclide content, curies per canister (1992)[b]

Average	104,300
Maximum[c]	114,700

Thermal power, watts per canister (1992)[b]

Average	311
Maximum[c]	342

[a]Source: Crocker 1989a and ORNL calculations based on Rev. 7 mass balance.
[b]Quantities shown are at 85% fill. Curies and watts per canister are for the start of year 1992.
[c]Maximum activity is assumed to be 110% of average.

Table 2.2.1.1-3   Savannah River site. High-level waste form and canister characteristics.[a] (Table 6.4 from K.J. Notz, T.D. Welch, R.S. Moore, and W.J. Reich, *Preliminary Waste Form Characteristics*, ORNL-TM-11681 [draft] September, 1990)

	Canister 85% fill
Canister inside volume, m^3	0.736
Glass volume at average fill temperature (see note b), m^3	0.626
Glass density at average fill temperature (see note b), g/cm^3	2.69
Glass weight, kg	1,682
Canister weight, kg	500
Gross weight, kg	2,182
Total activity, curies	234,000[c]
Decay heat, watts	690[c]

[a]Sources: DWPF Basic Data Report, DPSP 80-1033, Rev. 91, April 1985

[b]The average fill temperature (i.e. the average temperature of the glass upon completion of filling to 85% of canister volume) is 825°C. The glass volume per canister when cooled to 25°C is about 0.59 m^3 . The density of the glass is about 2.69 g/cm3 at 825°C and 2.85 g/cm^3 at 25°C (SRP 1987).

[c]These figures are the ones given in DPSP 80-1033, Rev. 91. The corresponding figures calculated by ORIGEN2 are 234,400 Ci and 709W, as shown in Table 3.3.4. Activity and decay heat (thermal power) are at the time of filling the canister and are based on the maximum case, i.e. 5-yr old sludge and 15-yr old supernate.

Table 2.2.1.1-4   Hanford site. High-level waste form and canister characteristics.[a] (Table 6.5 from K.J. Notz, T.D. Welch, R.S. Moore, and W.J. Reich, *Preliminary Waste Form Characteristics,* ORNL-TM-11681 [draft] September, 1990)

Waste form	Borosilicate glass in sealed steel canister
Canister material	Type 304L stainless steel
Weights per canister	
Empty canister, kg	500
Borosilicate glass, kg	<u>1650</u>
Total loaded weight, kg	2150
Canister dimensions	
Outside diameter, cm	61
Height overall, cm	300
Wall thickness, cm	0.95
Inside volume, m^3	0.736
Glass volume at average fill temperature, m^3	0.626[b]
Radionuclide content, curies per canister[c]	
Nominal	137,000
Maximum	298,000
Thermal power, watts per canister[c]	
Nominal	389
Maximum	869

[a]Sources: Wolfe 1985, White 1986, Mitchell and Nelson 1988.

[b]Canister is filled to 85% of volume at average fill temperature of 825°C.

[c]All values shown are based on NCAW reference feed (neutralized current acid waste) with 25% wt waste oxide in glass. Activities and thermal power are at time of filling canister. Range of values shown is from Mitchell and Nelson 1988 in which estimated activities and radionuclide compositions were given for two NCAW feeds referred to as nominal and maximum. Radionuclide compositions are shown in Table 3.4.4.

Table 2.2.1.1-5   Idaho National Engineering Laboratory. High level waste form and canister characteristics.[a] (Table 6.6 from K.J. Notz, T.D. Welch, R.S. Moore, and W.J. Reich, *Preliminary Waste Form Characteristics,* ORNL-TM-11681 [draft] September, 1990)

Waste form	Glass-ceramic blocks in sealed canister
Canister material	Stainless steel type 304L
Glass-ceramic density, g/cm^3	3.2
Weights per canister:	
Empty canister, kg	500
Glass-ceramic, kg	1825
Total loaded weight, kg	2325
Waste loading in glass-ceramic, wt%	70[b]
Glass-ceramic volume per canister, m^3	0.57[b]
Canister dimensions:	
Outside diameter, cm.	61
Height overall, cm.	300
Wall thickness, cm.	0.95
Radionuclide content, curies/canister	108,900[c]
Heat generation rate, watts/canister	339[c]

[a]Based on the following assumptions:
    1. Glass-ceramic form is chosen for HLW immobilization. The term "glass-ceramic" denotes an immobilized waste form consisting of a glass phase dispersed in a ceramic phase.
    2. Canister load is equivalent to 1277 kg calcine.
    3. Calcine is 3 years old at time of immobilization.
    4. Canister is similar in dimensions to DWPF canister.
    5. Radionuclide content of calcine is as shown in IDO-10105 (see Table 3.5.3).

[b]Reference: Berreth 1987.

[c]At time of immobilization. Quantities shown are estimated maximum values; average values are expected to be considerably less.

2.2.1.2 Projected Inventory

Figure 2.2.1.2-1   Projections of annual volume additions for various wastes and spent fuel—DOE and commercial fuel cycle (Figure 0.3 from *Integrated Data Base for 1990: U.S. Spent Fuel and Radioactive Waste Inventories, Projections, and Characteristics.* USDOE/RW-0006 Rev. 6, October 1990)
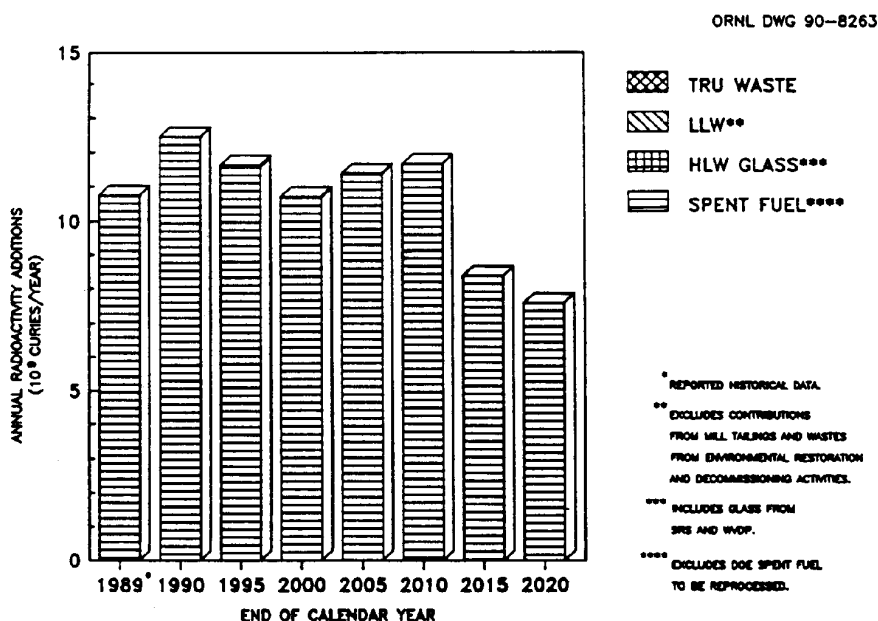
Figure 2.2.1.2-2   Projections of annual radioactivity additions for various wastes and spent fuel—DOE and commercial fuel cycle (Figure 0.4 from *Integrated Data Base for 1990: U.S. Spent Fuel and Radioactive Waste Inventories, Projections, and Characteristics.* USDOE/RW-0006 Rev. 6, October 1990)

ORNL DWG 90-8264
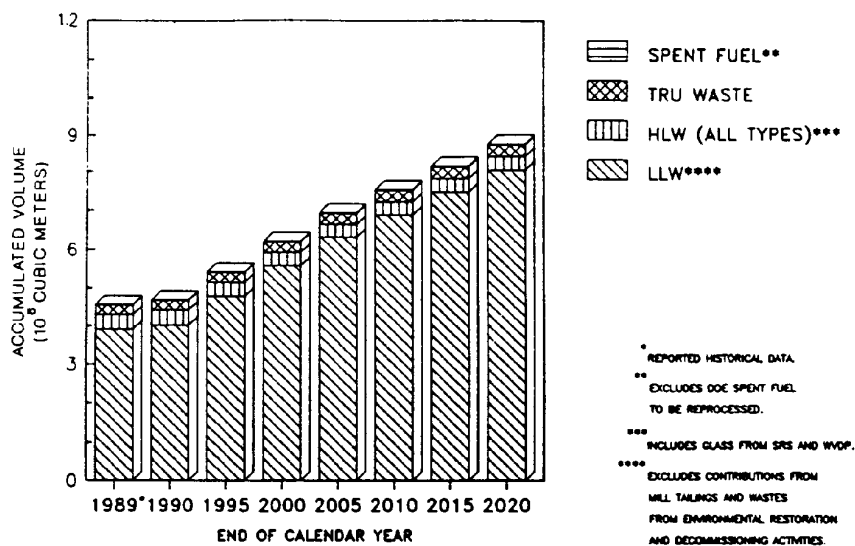
Figure 2.2.1.2-3 **Projections of accumulated volumes for various wastes and spent fuel—DOE and commercial fuel cycle (Figure 0.5 from *Integrated Data Base for 1990: U.S. Spent Fuel and Radioactive Waste Inventories, Projections, and Characteristics*. USDOE/RW-0006 Rev. 6, October 1990)**
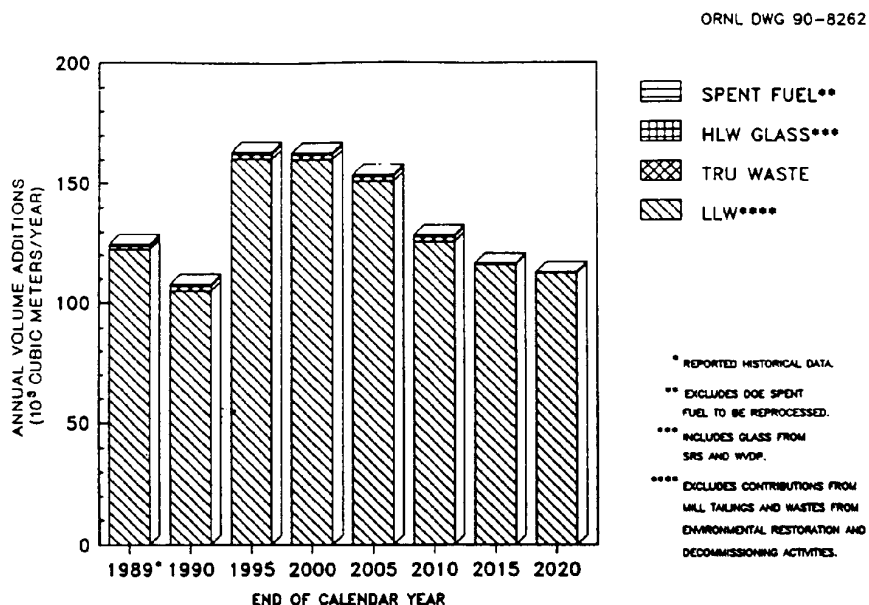
ORNL DWG 90-8265
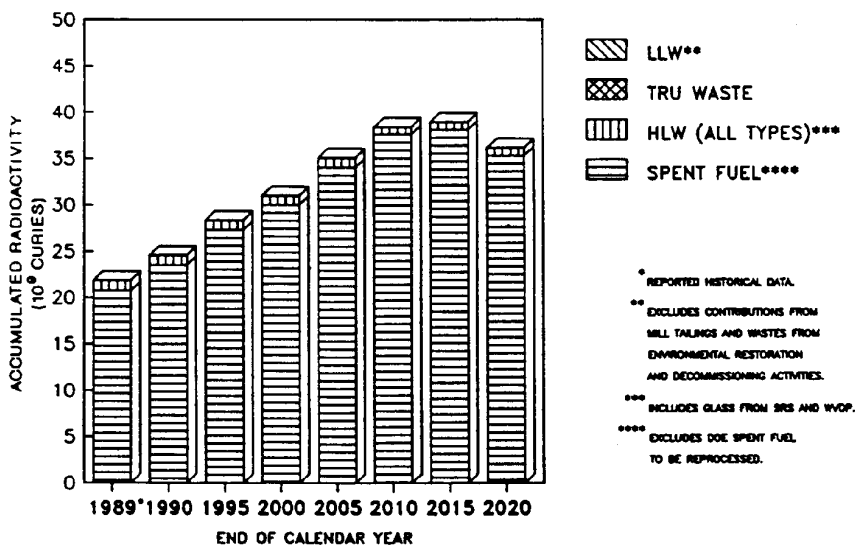
Figure 2.2.1.2-4 **Projections of accumulated radioactivity for various wastes and spent fuel—DOE and commercial fuel cycle (Figure 0.6 from *Integrated Data Base for 1990: U.S. Spent Fuel and Radioactive Waste Inventories, Projections, and Characteristics*. USDOE/RW-0006 Rev. 6, October 1990)**

Table 2.2.1.2-1   Projected annual number of canisters of immobilized HLW produced at each site.[a,b] (Table 6.7 from K.J. Notz, T.D. Welch, R.S. Moore, and W.J. Reich, *Preliminary Waste Form Characteristics,* ORNL-TM-11681 [draft] September, 1990)

Calendar year	WVDP	SRS	Hanford	INEL	Total
1989	0	0	0	0	0
1990	0	0	0	0	0
1991	0	0	0	0	0
1992	0	136	0	0	136
1993	25	308	0	0	333
1994	200	376	0	0	576
1995	50	410	0	0	460
1996	0	410	0	0	410
1997	0	383	0	0	383
1998	0	369	0	0	369
1999	0	369	0	0	369
2000	0	342	240	0	582
2001	0	342	370	0	712
2002	0	342	345	0	687
2003	0	342	185	0	527
2004	0	302	370	0	672
2005	0	273	370	0	643
2006	0	273	80	0	353
2007	0	273	0	0	273
2008	0	32	0	0	32
2009	0	0	0	0	0
2010	0	0	0	0	0
2011	0	0	0	0	0
2012	0	0	0	500	500
2013	0	0	0	600	600
2014	0	0	0	700	700
2015	0	0	0	1000	1000
2016	0	0	0	1000	1000
2017	0	0	0	1000	1000
2018	0	0	0	1000	1000
2019	0	0	0	1000	1000
2020	0	0	0	1000	1000
Total	275	5282	1960	7800	15,317

[a]Sources: WVDP - Crocker 1989, 1989a, 1990
            SRS - Garvin 1990
            HANF - Turner 1990
            INEL - Berreth 1990
[b]For assumptions used in compiling this table see Table 3.1.4. This table represents the 1990 Base Case for this report. Canisters produced after 2020 are not included here. Canister production figures represent most likely estimates rather than maximum potential.

Figure 2.2.1.2-5   Annual canister production for each site (Figure 6.1 from K.J. Notz,
T.D. Welch, R.S. Moore, and W.J. Reich, *Preliminary Waste Form
Characteristics,* ORNL-TM-11681 [draft] September, 1990)
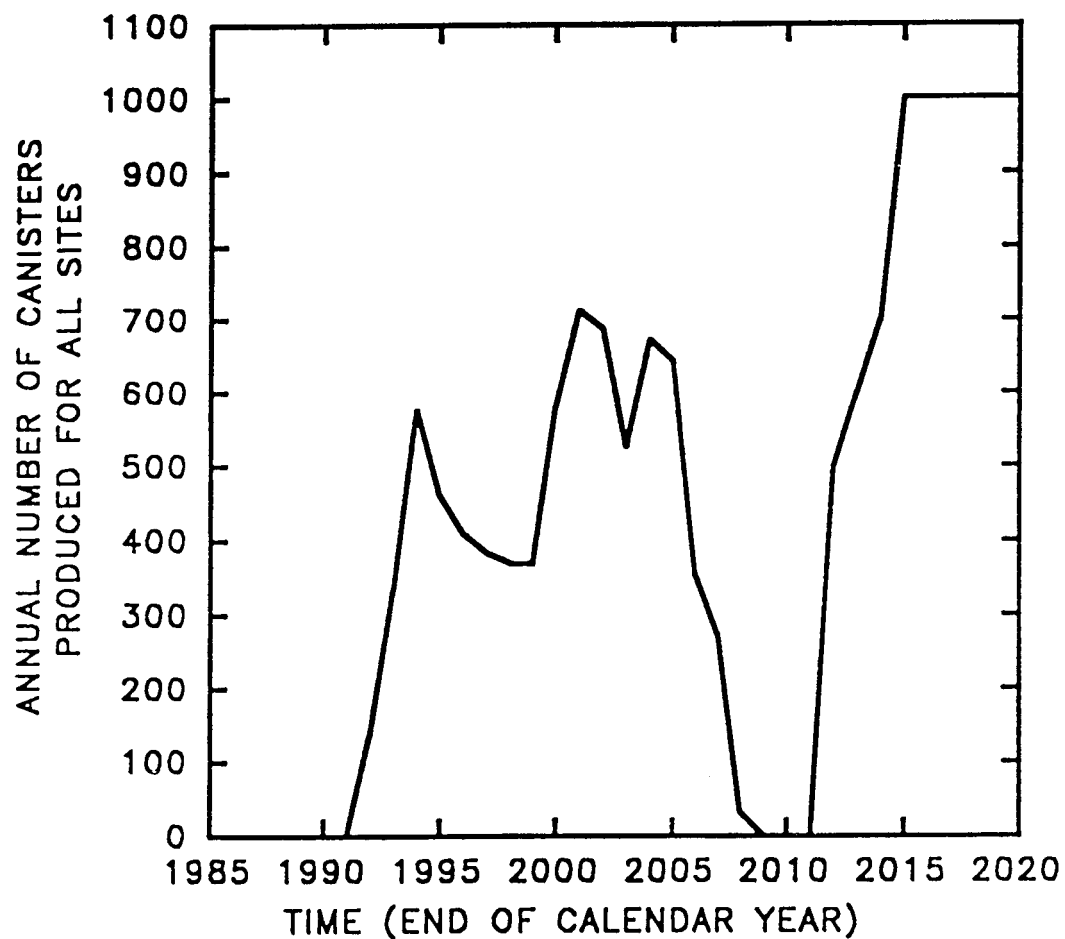
Figure 2.2.1.2-6   Total annual canister production (Figure 6.2 from K.J. Notz, T.D. Welch, R.S. Moore, and W.J. Reich, *Preliminary Waste Form Characteristics,* ORNL-TM-11681 [draft] September, 1990)

Table 2.2.1.2-2   Projected cumulative production of canisters of immobilized HLW at each site.[a,b] (Table 6.8 from K.J. Notz, T.D. Welch, R.S. Moore, and W.J. Reich, *Preliminary Waste Form Characteristics,* ORNL-TM-11681 [draft] September, 1990)

Calendar year	WVDP	SRP	Hanford	INEL	Total
1989	0	0	0	0	0
1990	0	0	0	0	0
1991	0	0	0	0	0
1992	0	136	0	0	136
1993	25	444	0	0	469
1994	225	820	0	0	1045
1995	275	1230	0	0	1505
1996	275	1640	0	0	1915
1997	275	2023	0	0	2298
1998	275	2392	0	0	2667
1999	275	2761	0	0	3036
2000	275	3103	240	0	3618
2001	275	3445	610	0	4330
2002	275	3787	955	0	5017
2003	275	4129	1140	0	5544
2004	275	4431	1510	0	6216
2005	275	4704	1880	0	6859
2006	275	4977	1960	0	7212
2007	275	5250	1960	0	7485
2008	275	5282	1960	0	7517
2009	275	5282	1960	0	7517
2010	275	5282	1960	0	7517
2011	275	5282	1960	0	7517
2012	275	5282	1960	500	8017
2013	275	5282	1960	1100	8617
2014	275	5282	1960	1800	9317
2015	275	5282	1960	2800	10317
2016	275	5282	1960	3800	11317
2017	275	5282	1960	4800	12317
2018	275	5282	1960	5800	13317
2019	275	5282	1960	6800	14317
2020	275	5282	1960	7800	15317

[a]Sources: WVDP - Crocker 1989, 1989a, 1990.
              SRS - Garvin 1990.
              HANF - Turner 1990.
              INEL - Berreth 1990.

[b]For assumptions used in compiling this table see Table 3.1.4. This table represents the 1990 Base Case for this report. Canisters produced after 2020 are not included here. Canister production figures represent most likely estimates rather than maximum potential.
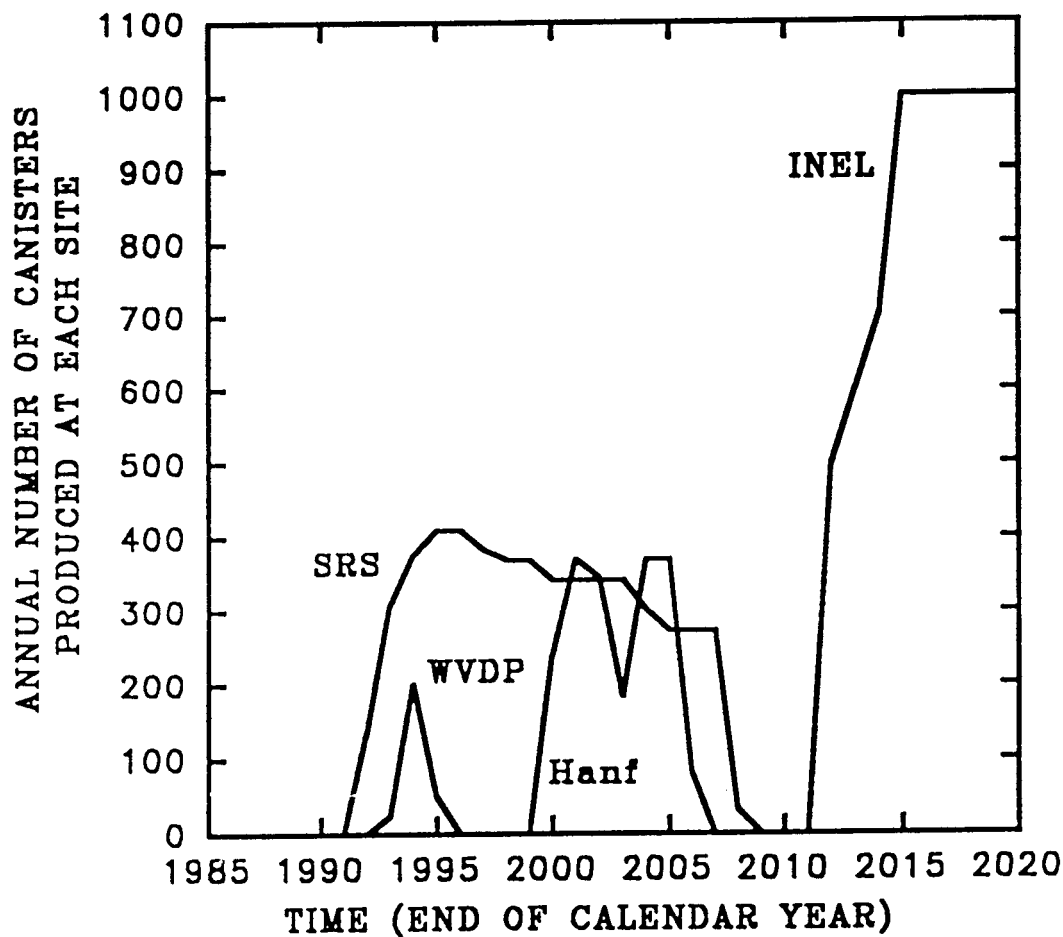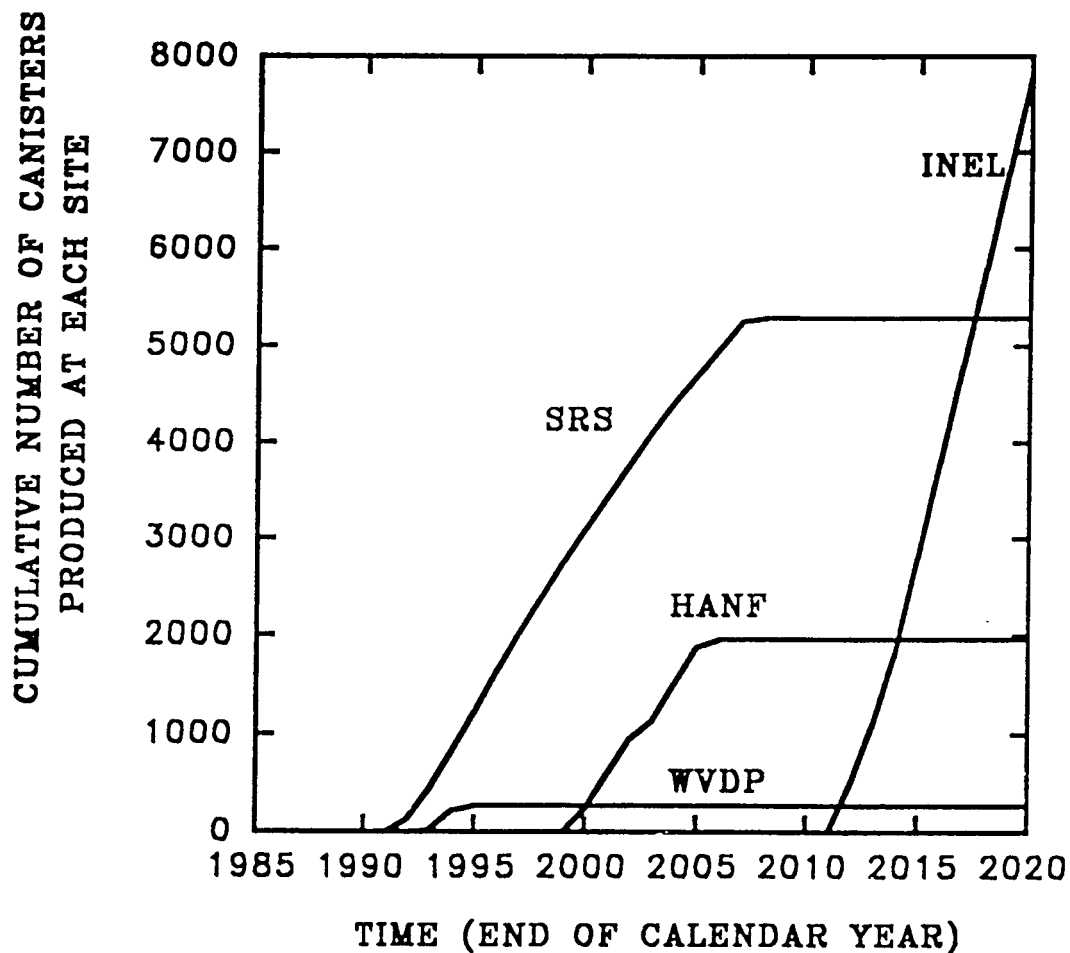
Figure 2.2.1.2-7   Cumulative canister production for each site (Figure 6.3 from K.J. Notz, T.D. Welch, R.S. Moore, and W.J. Reich, *Preliminary Waste Form Characteristics,* ORNL-TM-11681 [draft] September, 1990)
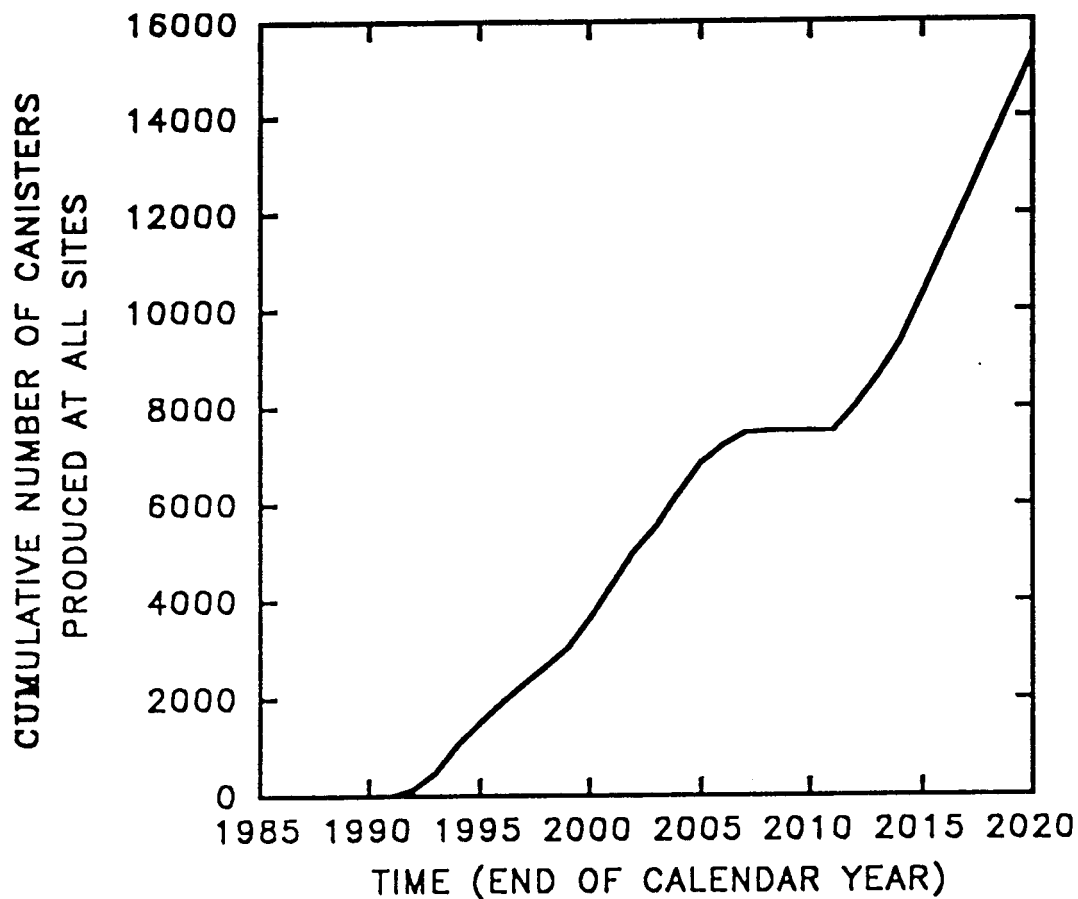
Figure 2.2.1.2-8 Cumulative canister production for all sites (Figure 6.4 from K.J. Notz, T.D. Welch, R.S. Moore, and W.J. Reich, *Preliminary Waste Form Characteristics,* ORNL-TM-11681 [draft] September, 1990)

2.2.1.3 Radioactivity and Decay Heat vs. Time

Figure 2.2.1.3-1 Radioactivity and thermal power for canister (Figure 6.5 from K.J. Notz, T.D. Welch, R.S. Moore, and W.J. Reich, *Preliminary Waste Form Characteristics*, ORNL-TM-11681 [draft] September, 1990)

Table 2.2.1.3-1   West Valley demonstration project. Calculated radioactivity and thermal power per HLW canister.[a] (Table 6.9 from K.J. Notz, T.D. Welch, R.S. Moore, and W.J. Reich, *Preliminary Waste Form Characteristics,* ORNL-TM-11681 [draft] September, 1990)

Decay time after 1990, years	Average radioactivity per canister (Ci)	Average thermal power per canister (W)
0	109,600	326
1	106,900	319
2	104,300	311
5	97,080	290
10	86,230	258
15	76,660	230
20	68,180	205
30	53,970	164
50	33,890	105
100	10,730	37
200	1,260	8.9
300	291	5.4
350	202	4.8
500	128	3.7
1,000	63	1.9
1,050	60	1.8
2,000	26.7	0.70
5,000	15.8	0.33
10,000	13.2	0.26
20,000	10.3	0.18
50,000	6.8	0.08
100,000	5.2	0.04
500,000	3.8	0.04
1,000,000	3.1	0.03

[a]Calculations made with ORIGEN2 code based on data supplied by WVDP (Crocker 1989). Canister contains 1900 kg of HLW glass. Initial time point (0 years) is at the start of year 1990. The material balance used by WVDP for this case (Revision 7, October 1989) shows 484,000 kg of total glass and a total radioactivity of 27.9 x 10[e] Ci at the start of year 1990 in the HLW to be vitrified. Data are for the average canister and do not take into account possible variations in melter feed and fill level.

WEST VALLEY DEMONSTRATION PROJECT

Figure 2.2.1.3-2   Radioactivity and thermal power per canister (Figure 6.6 from K.J. Notz, T.D. Welch, R.S. Moore, and W.J. Reich, *Preliminary Waste Form Characteristics,* ORNL-TM-11681 [draft] September, 1990)

Table 2.2.1.3-2   Savannah River site. Calculated radioactivity and thermal power per HLW canister.[a] (Table 6.10 from K.J. Notz, T.D. Welch, R.S. Moore, and W.J. Reich, *Preliminary Waste Form Characteristics,* ORNL-TM-11681 [draft] September, 1990)

| Decay time, years[b]	Radioactivity per canister (Ci)[c]	Thermal power per canister (W)[c]
0	234,400	709
1	208,500	627
2	193,800	586
5	169,300	527
10	145,800	467
15	128,400	418
20	113,900	374
30	90,000	301
50	56,500	198
100	17,900	75
200	2,100	17
300	390	7.2
350	227	5.2
500	95	2.7
1,000	42	1.1
1,050	41	1.1
2,000	29	0.72
5,000	24	0.54
10,000	20	0.43
20,000	16	0.30
50,000	11	0.16
100,000	9.2	0.11
500,000	4.8	0.05
1,000,000	2.4	0.02

[a]Based on 5-yr cooled sludge and 15-yr cooled supernate. Calculations made by ORIGEN2 code based on data supplied by SRS (Basic Data Report, DPSP-80-1033, Rev. 91, April 1985). Canister is filled to 85% of capacity and contains 1682 kg of glass.

[b]Years after vitrification.

[c]Radioactivity and thermal power include contributions of actinides and activation products as well as fission products.
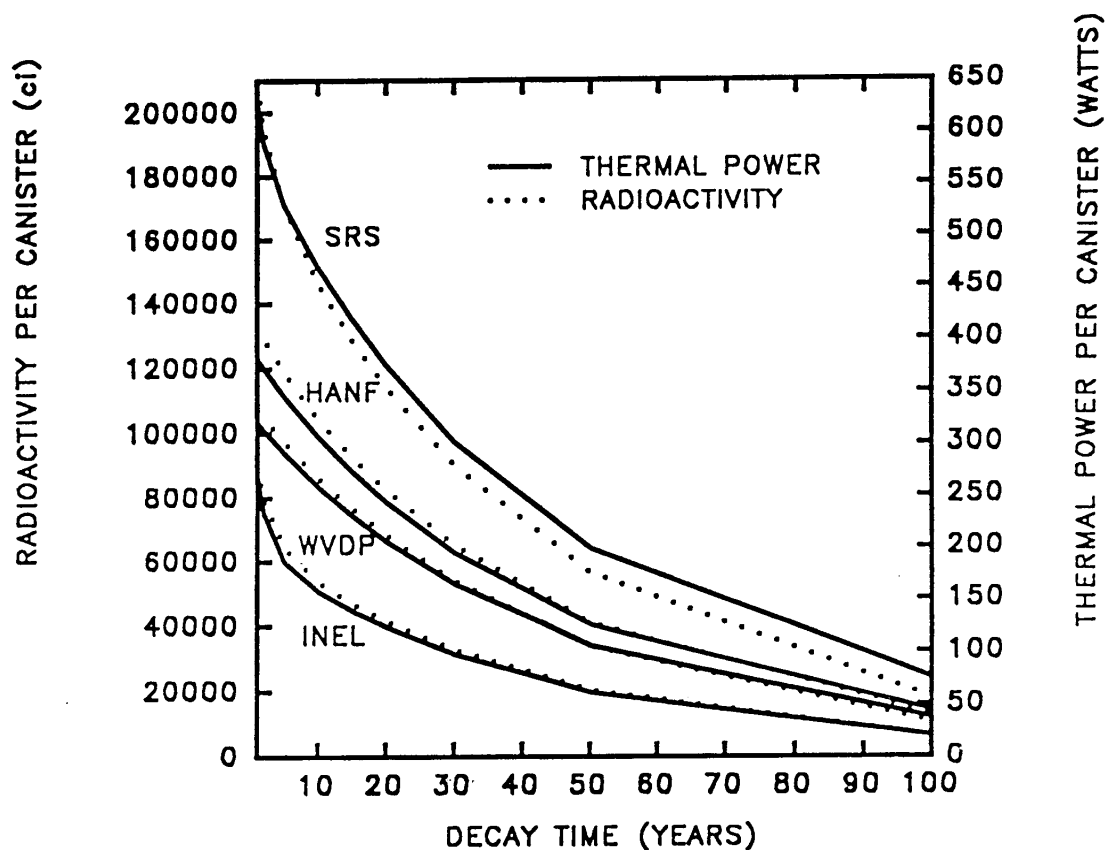
SAVANNAH RIVER SITE

Figure 2.2.1.3-3   Radioactivity and thermal power per canister (Figure 6.7 from K.J. Notz, T.D. Welch, R.S. Moore, and W.J. Reich, *Preliminary Waste Form Characteristics*, ORNL-TM-11681 [draft] September, 1990)

Table 2.2.1.3-3   Hanford site. Calculated radioactivity and thermal power per HLW canister.[a] (Table 6.11 from K.J. Notz, T.D. Welch, R.S. Moore, and W.J. Reich, *Preliminary Waste Form Characteristics,* ORNL-TM-11681 [draft] September, 1990)

Decay time, years[b]	Radioactivity per canister (Ci)		Thermal power per canister (W)	
	Nominal	Maximum	Nominal	Maximum
0	136,900	298,300	389	869
1	132,600	243,600	380	683
2	128,500	214,600	370	595
5	118,200	177,100	344	502
10	104,200	149,400	306	439
15	92,500	131,000	273	391
20	82,300	116,100	243	349
30	65,200	91,900	194	279
50	41,000	57,800	125	181
100	13,100	18,500	44	67
200	1,570	2,310	10	19
300	375	621	6.2	12
350	260	454	5.6	11
500	157	295	4.3	8.7
1,000	70	133	2.0	3.9
1,050	66	123	1.8	3.6
2,000	24	39	0.44	0.86
5,000	12	16	0.06	0.08
10,000	12	15	0.05	0.06
20,000	11	14	0.04	0.05
50,000	10	13	0.03	0.04
100,000	9.2	12	0.03	0.04
500,000	5.3	7.0	0.05	0.07
1,000,000	3.6	4.9	0.04	0.07

[a]Calculations made by ORIGEN2 code based on data supplied by HANF (Mitchell and Nelson 1988). Canister is filled to 85% of capacity and contains 1650 kg of HLW glass made from neutralized current acid waste (NCAW). Data are shown for two cases, the nominal case and the maximum case. The maximum case is based on a 21-month cooling time from fuel reprocessing to HWVP.

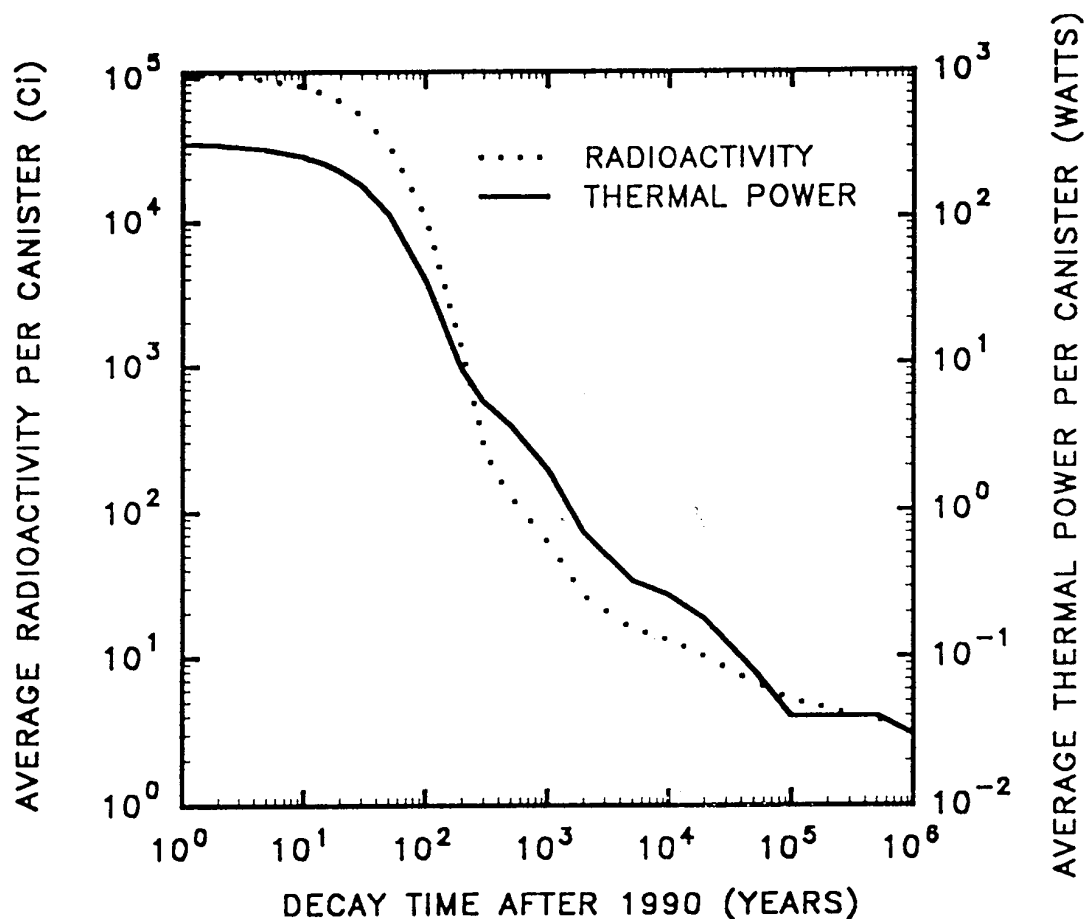[b]Years after vitrification.

HANFORD SITE

Figure 2.2.1.3-4   Radioactivity and thermal power per canister (Figure 6.8 from K.J. Notz,
T.D. Welch, R.S. Moore, and W.J. Reich, *Preliminary Waste Form
Characteristics,* ORNL-TM-11681 [draft] September, 1990)

Table 2.2.1.3-4   Idaho National Engineering Laboratory. Calculated radioactivity and thermal power per HLW canister.[a] (Table 6.12 from K.J. Notz, T.D. Welch, R.S. Moore, and W.J. Reich, *Preliminary Waste Form Characteristics,* ORNL-TM-11681 [draft] September, 1990)

Decay time after immobilization, years	Total radioactivity per canister (Ci)	Total thermal power per canister (W)
0	108,900	339
1	89,400	267
2	78,600	230
5	64,100	185
10	53,600	157
15	46,900	138
20	41,500	123
30	32,800	97
50	20,500	61
100	6,430	20
200	680	2.6
300	98	0.67
350	48	0.45
500	16	0.24
1,000	7.2	0.11
1,050	7.0	0.10
2,000	5.6	0.06
5,000	5.0	0.04
10,000	4.6	0.033
20,000	4.2	0.023
50,000	3.6	0.012
100,000	3.1	0.008
500,000	1.4	0.003
1,000,000	0.71	0.001

[a]Results of ORIGEN2 calculations based on glass-ceramic form, assuming 1277 kg of calcine per canister (1825 kg of glass-ceramic per canister), with the initial radionuclide composition shown in Table 3.5.3.
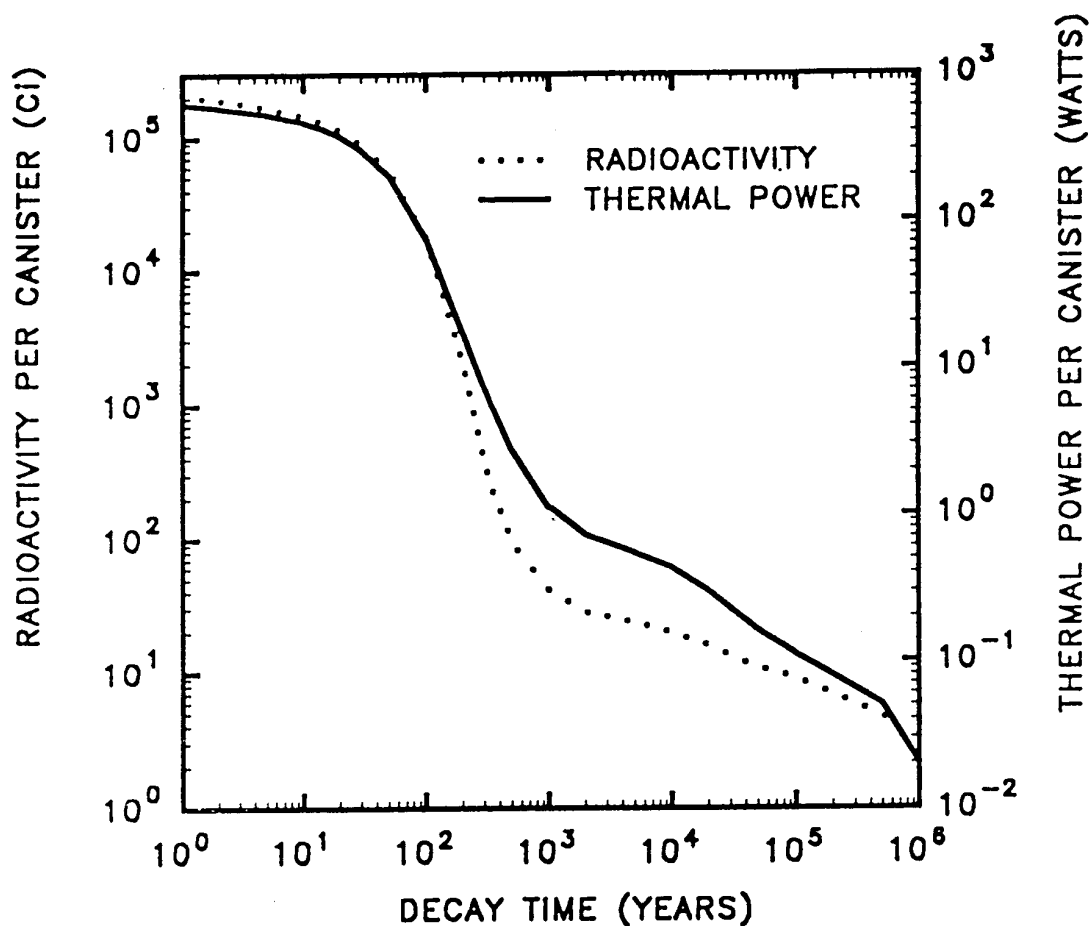
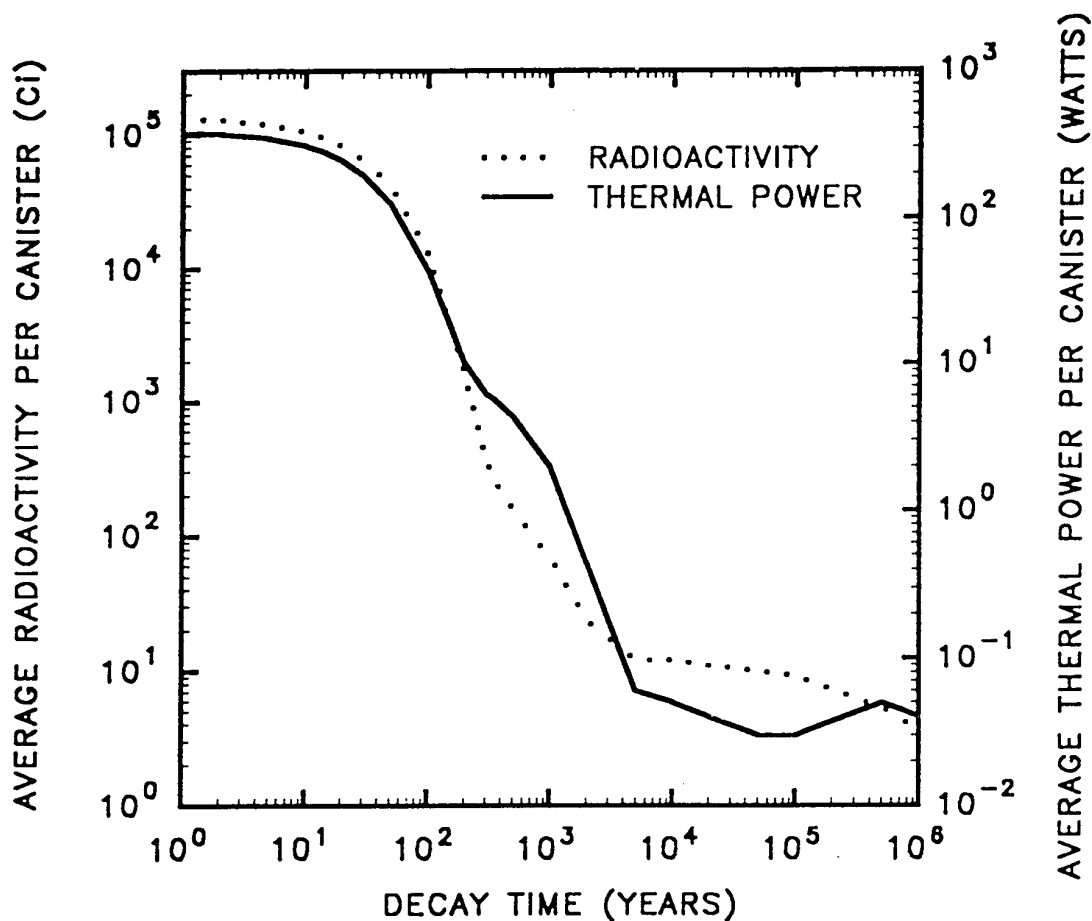# IDAHO NATIONAL ENGINEERING LAB
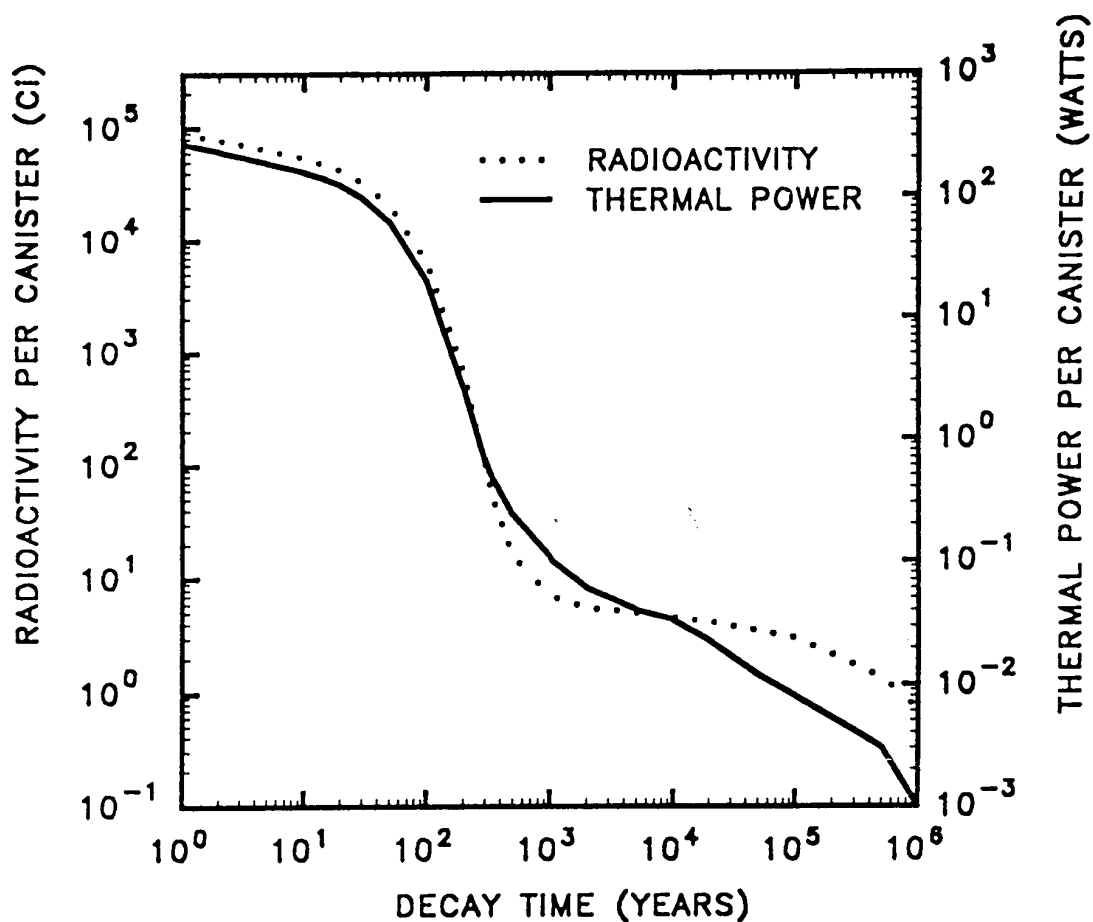

Figure 2.2.1.3-5 Radioactivity and thermal power per canister (Figure 6.9 from K.J. Notz, T.D. Welch, R.S. Moore, and W.J. Reich, *Preliminary Waste Form Characteristics,* ORNL-TM-11681 [draft] September, 1990)

2.2.1.4 Glass Species Composition Statistics

Table 2.2.1.4-1   Radioisotope composition of West Valley Demonstration Project vitrified high-level waste.[a] (Table 6.13 from K.J. Notz, T.D. Welch, R.S. Moore, and W.J. Reich, *Preliminary Waste Form Characteristics,* ORNL-TM-11681 [draft] September, 1990)

Radioisotope	Grams/canister	Curies/canister	Watts/canister
Fe-55	0.1104E-02	0.2760E+01	0.9313E-04
Co-60	0.2679E-02	0.3030E+01	0.4666E-01
Ni-59	0.5491E+01	0.4160E+00	0.1650E-04
Ni-63	0.4895E+00	0.3020E+02	0.3039E-02
Se-79	0.1980E+00	0.1380E-01	0.3431E-05
Sr-90	0.1928E+03	0.2630E+05	0.3048E+02
Y-90	0.4833E-01	0.2630E+05	0.1456E+03
Zr-93	0.4257E+03	0.1070E+01	0.1242E-03
Nb-93m	0.2529E-02	0.7150E+00	0.1265E-03
Tc-99	0.2524E+02	0.4280E+00	0.2144E-03
Ru-106	0.1655E-04	0.5540E-01	0.3290E-05
Rh-106	0.1556E-10	0.5540E-01	0.5307E-03
Pd-107	0.8416E+02	0.4330E-01	0.2563E-05
Cd-113m	0.3845E-01	0.8340E+01	0.1402E-01
Sn-121m	0.1160E-02	0.6860E-01	0.1373E-03
Sn-126	0.1441E+02	0.4090E+00	0.5095E-03
Sb-125	0.2769E-01	0.2860E+02	0.8929E-01
Sb-126	0.6852E-06	0.5730E-01	0.1057E-02
Sb-126m	0.5206E-08	0.4090E+00	0.5201E-02
Te-125m	0.3885E-03	0.7000E+01	0.5876E-02
Cs-134	0.1569E-01	0.2030E+02	0.2063E+00
Cs-135	0.5505E+03	0.6340E+00	0.2113E-03
Cs-137	0.3252E+03	0.2830E+05	0.3126E+02
Ba-137m	0.4981E-04	0.2680E+05	0.1051E+03
Ce-144	0.8023E-06	0.2560E-02	0.1696E-05
Pr-144	0.3387E-10	0.2560E-02	0.1879E-04
Pm-146	0.9566E-04	0.4260E-01	0.2146E-03
Pm-147	0.3721E+00	0.3450E+03	0.1236E+00
Sm-151	0.1258E+02	0.3310E+03	0.3876E-01
Eu-152	0.8267E-02	0.1430E+01	0.1080E-01
Eu-154	0.1389E+01	0.3750E+03	0.3350E+01
Eu-155	0.2014E+00	0.9370E+02	0.6806E-01
Tl-207	0.1690E-09	0.3220E-01	0.9444E-04
Tl-208	0.4312E-10	0.1270E-01	0.2985E-03
Pb-209	0.1815E-09	0.8250E-03	0.9475E-06
Pb-211	0.1308E-08	0.3230E-01	0.9666E-04
Pb-212	0.2540E-07	0.3530E-01	0.6712E-04
Bi-211	0.7718E-10	0.3230E-01	0.1287E-02
Bi-212	0.2409E-08	0.3530E-01	0.5995E-03
Bi-213	0.4265E-10	0.8250E-03	0.3464E-05
Po-212	0.1274E-18	0.2260E-01	0.1196E-02
Po-213	0.6231E-19	0.7860E-03	0.3972E-04
Po-215	0.1095E-14	0.3230E-01	0.1440E-02
Po-216	0.1013E-12	0.3530E-01	0.1443E-02
At-217	0.5124E-15	0.8250E-03	0.3516E-04
Rn-219	0.2482E-11	0.3230E-01	0.1339E-02
Rn-220	0.3826E-10	0.3530E-01	0.1339E-02
Fr-221	0.4653E-11	0.8250E-03	0.3180E-04
Fr-223	0.1117E-10	0.4320E-03	0.1120E-05
Ra-223	0.6306E-06	0.3230E-01	0.1149E-02

Table 2.2.1.4-1   (continued)

Radioisotope	Grams/canister	Curies/canister	Watts/canister
Ra-224	0.2216E-06	0.3530E-01	0.1210E-02
Ra-225	0.2104E-07	0.8250E-03	0.5778E-06
Ra-228	0.2550E-04	0.5970E-02	0.4595E-06
Ac-225	0.1421E-07	0.8250E-03	0.2878E-04
Ac-227	0.4464E-05	0.3230E-03	0.1562E-06
Ac-228	0.2662E-08	0.5970E-02	0.5153E-04
Th-227	0.1034E-05	0.3180E-01	0.1159E-02
Th-228	0.4306E-04	0.3530E-01	0.1153E-02
Th-229	0.3877E-02	0.8250E-03	0.2521E-04
Th-230	0.1169E-01	0.2360E-03	0.6670E-05
Th-231	0.6657E-09	0.3540E-03	0.1984E-06
Th-232	0.5880E+05	0.6450E-02	0.1559E-03
Th-234	0.1356E-06	0.3140E-02	0.1271E-05
Pa-231	0.1264E+01	0.5970E-01	0.1796E-02
Pa-233	0.4422E-05	0.9180E-01	0.2081E-03
Pa-234m	0.4571E-11	0.3140E-02	0.1550E-04
U-232	0.1270E-02	0.2720E-01	0.8721E-03
U-233	0.3666E+01	0.3550E-01	0.1031E-02
U-234	0.2640E+01	0.1650E-01	0.4746E-03
U-235	0.1637E+03	0.3540E-03	0.9259E-05
U-236	0.1700E+02	0.1100E-02	0.2976E-04
U-238	0.9337E+04	0.3140E-02	0.7954E-04
Np-236	0.2823E+01	0.3720E-01	0.7494E-04
Np-237	0.1302E+03	0.9180E-01	0.2802E-02
Np-239	0.5861E-05	0.1360E+01	0.3283E-02
Pu-236	0.6209E-05	0.3300E-02	0.1147E-03
Pu-238	0.1904E+01	0.3260E+02	0.1079E+01
Pu-239	0.1028E+03	0.6390E+01	0.1967E+00
Pu-240	0.2053E+02	0.4680E+01	0.1455E+00
Pu-241	0.3076E+01	0.3170E+03	0.9815E-02
Pu-242	0.1668E+01	0.6370E-02	0.1879E-03
Am-241	0.6117E+02	0.2100E+03	0.6967E+01
Am-242	0.1435E-05	0.1160E+01	0.1315E-02
Am-242m	0.1204E+00	0.1170E+01	0.4616E-03
Am-243	0.6820E+01	0.1360E+01	0.4366E-01
Cm-242	0.2912E-03	0.9630E+00	0.3544E-01
Cm-243	0.1021E-01	0.5270E+00	0.1931E-01
Cm-244	0.3707E+00	0.3000E+02	0.1048E+01
Cm-245	0.2015E-01	0.3460E-02	0.1147E-03
Cm-246	0.1279E-02	0.3930E-03	0.1285E-04
Total	0.7029E+05	0.1096E+06	0.3260E+03

[a]Calculated from data in WVDP Mass Balance, Revision 7 (Crocker 1989). This is based on 484,000 kg of total glass and 1900 kg of glass per canister, and represents the average canister composition. Radioactivity shown is as of the start of year 1990.

Table 2.2.1.4-2   Savannah River site. Radioisotope content per HLW canister.[a] (Table 6.14 from K.J. Notz, T.D. Welch, R.S. Moore, and W.J. Reich, *Preliminary Waste Form Characteristics,* ORNL-TM-11681 [draft] September, 1990)

	Isotope	Curies/canister	Grams/canister
1	Cr-51	0.9312E-16	0.1008E-20
2	Co-60	0.1699E+03	0.1502E+00
3	Ni-59	0.2397E-01	0.3163E+00
4	Ni-63	0.2975E+01	0.4824E-01
5	Tl-208	0.1128E-02	0.3829E-11
6	U-232	0.1339E-01	0.6256E-03
7	U-233	0.1584E-05	0.1636E-03
8	U-234	0.3428E-01	0.5485E+01
9	U-235	0.1573E-03	0.7278E+02
10	U-236	0.1128E-02	0.1742E+02
11	U-238	0.1050E-01	0.3122E+05
12	Np-236	0.1744E-07	0.1323E-05
13	Np-237	0.8904E-02	0.1263E+02
14	Pu-236	0.1221E+00	0.2297E-03
15	Pu-237	0.8941E-11	0.7401E-15
16	Pu-238	0.1484E+04	0.8667E+02
17	Pu-239	0.1291E+02	0.2076E+03
18	Pu-240	0.8681E+01	0.3809E+02
19	Pu-241	0.1670E+04	0.1620E+02
20	Pu-242	0.1224E-01	0.3206E+01
21	Am-241	0.1102E+02	0.3210E+01
22	Am-242	0.1436E-01	0.1776E-07
23	Am-242m	0.1447E-01	0.1488E-02
24	Am-243	0.5788E-02	0.2902E-01
25	Cm-242	0.3495E-01	0.1057E-04
26	Cm-243	0.5565E-02	0.1078E-03
27	Cm-244	0.1076E+03	0.1329E+01
28	Cm-245	0.6715E-05	0.3910E-04
29	Cm-246	0.5342E-06	0.1739E-05
30	Cm-247	0.6604E-12	0.7116E-08
31	Cm-248	0.6864E-12	0.1614E-09
32	Se-79	0.1699E+00	0.2439E+01
33	Rb-87	0.8719E-06	0.9961E+01
34	Sr-89	0.4267E-04	0.1470E-08
35	Sr-90	0.4675E+05	0.3426E+03
36	Y-90	0.4786E+05	0.8795E-01
37	Y-91	0.7568E-03	0.3085E-07
38	Zr-93	0.1117E+01	0.4443E+03

Table 2.2.1.4-2   (continued)

	Isotope	Curies/canister	Grams/canister
39	Zr-95	0.1005E-01	0.4680E-06
40	Nb-94	0.9646E-04	0.5147E-03
41	Nb-95	0.2115E-01	0.5407E-06
42	Nb-95m	0.1247E-03	0.3272E-09
43	Tc-99	0.3079E+01	0.1816E+03
44	Ru-103	0.1684E-07	0.5217E-12
45	Ru-106	0.2252E+04	0.6729E+00
46	Rh-103m	0.1636E-07	0.5028E-15
47	Rh-106	0.2259E+04	0.6346E-06
48	Pd-107	0.1473E-01	0.2863E+02
49	Ag-110m	0.1258E+00	0.2647E-04
50	Cd-113	0.5009E-13	0.1472E+00
51	Cd-115m	0.1213E-08	0.4763E-13
52	Sn-121m	0.7902E-01	0.1336E-02
53	Sn-123	0.2549E+00	0.3101E-04
54	Sn-126	0.4415E+00	0.1556E+02
55	Sb-124	0.7123E-07	0.4071E-11
56	Sb-125	0.8496E+03	0.8226E+00
57	Sb-126	0.6159E-01	0.7365E-06
58	Sb-126m	0.4415E+00	0.5619E-08
59	Te-125m	0.2760E+03	0.1532E-01
60	Te-127	0.1202E+00	0.4555E-07
61	Te-127m	0.1228E+00	0.1302E-04
62	Te-129	0.3053E-11	0.1457E-18
63	Te-129m	0.4749E-11	0.1576E-15
64	Cs-134	0.3372E+03	0.2606E+00
65	Cs-135	0.9943E-01	0.8633E+02
66	Cs-136	0.7828E-39	0.1068E-43
67	Cs-137	0.4341E+05	0.4989E+03
68	Ba-136m	0.8607E-38	0.3195E-49
69	Ba-137m	0.4155E+05	0.7724E-04
70	Ba-140	0.1024E-35	0.1404E-40
71	La-140	0.4304E-36	0.7734E-42
72	Ce-141	0.3591E-10	0.1260E-14
73	Ce-142	0.9609E-05	0.4005E+03
74	Ce-144	0.9869E+04	0.3093E+01
75	Pr-143	0.1198E-33	0.1780E-38
76	Pr-144	0.9869E+04	0.1306E-03
77	Pr-144m	0.1187E+03	0.6545E-06

Table 2.2.1.4-2   (continued)

	Isotope	Curies/canister	Grams/canister
78	Nd-144	0.4860E-09	0.4110E+03
79	Nd-147	0.1261E-43	0.1570E-48
80	Pm-147	0.2419E+05	0.2609E+02
81	Pm-148	0.6975E-10	0.4243E-15
82	Pm-148m	0.1009E-08	0.4722E-13
83	Sm-147	0.2000E-05	0.8796E+02
84	Sm-148	0.5788E-11	0.1916E+02
85	Sm-149	0.1781E-11	0.7420E+01
86	Sm-151	0.2478E+03	0.9418E+01
87	Eu-152	0.3688E+01	0.2132E-01
88	Eu-154	0.6196E+03	0.2295E+01
89	Eu-155	0.4749E+03	0.1021E+01
90	Eu-156	0.5231E-31	0.9489E-36
91	Tb-160	0.1120E-05	0.9923E-10
	Total	0.2344E+06	0.3427E+05

[a]Quantities shown are for sludge + supernate glass and are based on the DWPF Basic Data Report, DPSP 80-1033, Rev. 91, April 1985, assuming sludge aged an average of 5 years and supernate aged an average of 15 years, with a canister load of 3710 lb of glass (1682 kg). Radionuclide contents are at time of filling canister.

Table 2.2.1.4-3 Hanford site. Radioisotope content per HLW canister (NCAW glass).[a] (Table 6.15 from K.J. Notz, T.D. Welch, R.S. Moore, and W.J. Reich, *Preliminary Waste Form Characteristics,* ORNL-TM-11681 [draft] September, 1990)

Isotope	Curies/canister		Grams/canister	
	Nominal	Maximum	Nominal	Maximum
Fe-55	1.80E+01	1.41E+02	7.20E-03	5.64E-02
Ni-59	1.09E-01	1.36E-01	1.44E+00	1.80E+00
Co-60	1.50E+00	4.29E+00	1.33E-03	3.79E-03
Ni-63	1.21E+01	1.57E+01	1.96E-01	2.54E-01
Se-79	3.15E-03	3.90E-03	4.52E-02	5.60E-02
Sr-89	5.35E-13	6.52E-02	1.84E-17	2.24E-06
Sr-90	2.98E+04	4.18E+04	2.18E+02	3.06E+02
Y-90	2.98E+04	4.18E+04	5.48E-02	7.68E-02
Y-91	1.38E-10	7.26E-01	5.63E-15	2.96E-05
Nb-93m	6.16E-01	5.77E-01	2.18E-03	2.04E-03
Zr-93	1.05E+00	1.29E+00	4.18E+02	5.13E+02
Zr-95	2.92E-09	2.76E+00	1.36E-13	1.28E-04
Nb-95	6.73E-09	5.67E+00	1.72E-13	1.45E-04
Tc-99	7.51E+00	9.35E+00	4.43E+02	5.51E+02
Ru-103	3.37E-18	2.98E-04	1.04E-22	9.23E-09
Rh-103m	3.04E-18	2.69E-04	9.34E-26	8.27E-12
Ru-106	4.18E+01	4.99E+03	1.25E-02	1.49E+00
Rh-106	4.18E+01	4.99E+03	1.17E-08	1.40E-06
Pd-107	3.02E-02	4.07E-02	5.87E+01	7.91E+01
Ag-110m	2.22E-03	1.59E+00	4.67E-07	3.35E-04
Cd-113m	8.53E+00	1.46E+01	3.93E-02	6.73E-02
In-113m	1.01E-07	2.52E-02	6.04E-15	1.51E-09
Sn-113	1.01E-07	2.52E-02	1.01E-11	2.51E-06
Cd-115m	3.20E-18	8.78E-06	1.26E-22	3.45E-10
Sn-119m	6.80E-03	5.42E+00	1.52E-06	1.21E-03
Sn-121m	7.76E-02	1.06E-01	1.31E-03	1.79E-03
Sn-123	3.65E-05	2.89E+00	4.44E-09	3.52E-04
Sn-126	3.65E-01	4.60E-01	1.29E+01	1.62E+01
Sb-124	1.15E-14	3.50E-05	6.57E-19	2.00E-09
Sb-126	5.10E-02	6.48E-02	6.10E-07	7.75E-07
Sb-126m	3.65E-01	4.60E-01	4.65E-09	5.86E-09
Sb-125	2.54E+02	1.76E+03	2.46E-01	1.70E+00
Te-125m	6.20E+01	4.29E+02	3.44E-03	2.38E-02
Te-127	6.55E-06	2.95E+00	2.48E-12	1.12E-06
Te-127m	6.66E-06	3.00E+00	7.06E-10	3.18E-04
Te-129	3.14E-23	3.75E-07	1.49E-30	1.79E-14
Te-129m	4.82E-23	5.77E-07	1.60E-27	1.91E-11
I-129	1.29E-05	1.63E-05	7.31E-02	9.23E-02

Table 2.2.1.4-3   (continued)

Isotope	Curies/canister		Grams/canister	
	Nominal	Maximum	Nominal	Maximum
Cs-134	9.31E+01	1.20E+03	7.19E-02	9.27E-01
Cs-135	2.02E-01	2.51E-01	1.75E+02	2.18E+02
Cs-137	3.61E+04	5.10E+04	4.15E+02	5.86E+02
Ba-137m	3.40E+04	4.82E+04	6.32E-05	8.96E-05
Ce-141	2.93E-22	1.13E-05	1.03E-26	3.97E-10
Ce-144	8.00E+01	2.98E+04	2.51E-02	9.34E+00
Pr-144	8.00E+01	2.98E+04	1.06E-06	3.94E-04
Pr-144m	9.60E-01	3.58E+02	5.29E-09	1.97E-06
Pm-147	5.21E+03	3.97E+04	5.62E+00	4.28E+01
Pm-148m	6.23E-19	1.32E-05	2.92E-23	6.18E-10
Sm-151	6.98E+02	8.36E+02	2.65E+01	3.18E+01
Eu-152	1.40E-00	2.74E+00	8.09E-03	1.58E-02
Gd-153	1.35E-05	1.15E-02	3.83E-09	3.26E-06
Eu-154	1.45E+02	3.36E+02	5.37E-01	1.24E+00
Eu-155	1.37E+02	4.11E+02	2.94E-01	8.83E-01
Tb-160	9.49E-13	1.10E-04	8.41E-17	9.74E-09
U-234	4.57E-03	4.82E-03	7.31E-01	7.71E-01
U-235	1.91E-04	1.97E-04	8.83E+01	9.11E+01
U-236	4.21E-04	4.75E-04	6.51E+00	7.34E+00
U-238	3.51E-03	3.72E-03	1.04E+04	1.11E+04
Np-237	1.56E-01	1.99E-01	2.21E+02	2.82E+02
Pu-238	4.43E-01	7.68E-01	2.59E-02	4.48E-02
Pu-239	1.17E+00	1.41E+00	1.88E+01	2.27E+01
Pu-240	3.93E-01	5.42E-01	1.72E+00	2.38E+00
Pu-241	1.26E+01	2.58E+01	1.22E-01	2.50E-01
Pu-242	7.61E-05	1.31E-04	1.99E-02	3.43E-02
Am-241	2.84E+02	5.77E+02	8.27E+01	1.68E+02
Am-242	2.21E-01	4.14E-01	2.73E-07	5.12E-07
Am-243	3.79E-02	6.76E-02	1.90E-01	3.39E-01
Cm-242	1.82E-01	4.99E-01	5.50E-05	1.51E-04
Cm-244	5.03E+00	1.25E+01	6.22E-02	1.54E-01
Total	1.37E+05	2.98E+05	1.26E+04	1.40E+04

[a]This table identifies the nominal and maximum activity of HWVP canisters at the time of vitrification. The maximum is principally based on close-coupling the final accumulated tank of NCAW (21 mo. from fuel discharge to HWVP). The overall waste loading is 0.031 kg non-volatile oxides/l (0.26 lb non-volatile oxides/gal) of feed. Canister contains 1650 kg of HLW glass (85% fill). Source: Mitchell and Nelson 1988.

Table 2.2.1.4-4   Idaho National Engineering Laboratory. Radioisotope content per HLW canister.[a] (Table 6.16 from K.J. Notz, T.D. Welch, R.S. Moore, and W.J. Reich, *Preliminary Waste Form Characteristics,* ORNL-TM-11681 [draft] September, 1990)

	Isotope	Curies/canister	Grams/canister
1	Se-79	0.8173E-01	0.1173E+01
2	Rb-87	0.4597E-05	0.5252E+02
3	Sr-90	0.1660E+05	0.1217E+03
4	Y-90	0.1660E+05	0.3051E-01
5	Zr-93	0.3959E+00	0.1575E+03
6	Nb-93M	0.9577E-01	0.3387E-03
7	Tc-99	0.2682E+01	0.1582E+03
8	Ru-106	0.1239E+04	0.3701E+00
9	Rh-106	0.1239E+04	0.3479E-06
10	Pd-107	0.2554E-02	0.4965E+01
11	Sn-126	0.4086E-01	0.1440E+01
12	Sb-126M	0.4086E-01	0.5201E-09
13	Sb-126	0.4086E-01	0.4887E-06
14	Cs-134	0.4214E+04	0.3256E+01
15	Cs-135	0.9577E-01	0.8316E+02
16	Cs-137	0.1660E+05	0.1908E+03
17	Ba-137M	0.1532E+05	0.2848E-04
18	Ce-144	0.1047E+05	0.3282E+01
19	Pr-144	0.1047E+05	0.1386E-03
20	Pm-147	0.1532E+05	0.1653E+02
21	Sm-151	0.2171E+03	0.8250E+01
22	Eu-154	0.2299E+03	0.8513E+00
23	U-233	0.1532E-08	0.1583E-06
24	U-234	0.5491E-06	0.8785E-04
25	U-235	0.2299E-05	0.1063E+01
26	U-236	0.1277E-04	0.1973E+00
27	U-237	0.6130E-08	0.7507E-13
28	U-238	0.1277E-10	0.3797E-04
29	Np-237	0.6130E-04	0.8693E-01
30	Pu-238	0.8939E+02	0.5221E+01
31	Pu-239	0.8939E+00	0.1437E+02
32	Pu-240	0.8300E+00	0.3642E+01
33	Pu-241	0.2043E+03	0.1983E+01
34	Pu-242	0.2299E-02	0.6018E+00
35	Am-241	0.1162E+01	0.3385E+00
36	Am-243	0.1060E-01	0.5315E-01
37	Cm-242	0.8300E+00	0.2510E-03
38	Cm-244	0.6640E+00	0.8201E-02
Total		0.1088E+06	0.8315E+03

[a] Quantities are at time of filling canister and are based on 3-yr old calcine immobilized in glass-ceramic with a load of 1277 kg of calcine per canister (1825 kg of glass-ceramic per canister). Based on IDO-10105 (1982) and Berreth 1986.

Table 2.2.1.4-5   West Valley demonstration project. Chemical composition of reference HLW glass.[a] (Table 6.17 from K.J. Notz, T.D. Welch, R.S. Moore, and W.J. Reich, *Preliminary Waste Form Characteristics,* ORNL-TM-11681 [draft] September, 1990)

Component	Nominal composition (wt%)	Range (wt%)	
AgO	0.0001	-	-
Al$_2$O$_3$	2.8295	1.19	7.15
AmO$_2$	0.0073	-	-
BaO	0.0540	0.04	0.08
B$_2$O$_3$	9.9516	9.33	10.66
CaO	0.5993	0.39	0.93
CdO	0.0003	-	-
CeO$_2$	0.0670	0.04	0.10
CmO$_2$	0.0001	-	-
CoO	0.0002	-	-
Cr$_2$O$_3$	0.3112	0.21	0.48
Cs$_2$O	0.0826	0.05	0.13
CuO	0.0001	-	-
Eu$_2$O$_3$	0.0014	-	-
Fe$_2$O$_3$	12.1570	8.32	18.50
Gd$_2$O$_3$	0.0003	-	-
In$_2$O$_3$	0.0001	-	-
K$_2$O	3.5733	3.36	3.84
La$_2$O$_3$	0.0337	0.02	0.05
Li$_2$O	3.0315	2.84	3.25
MgO	1.3032	1.22	1.39
MnO$_2$	1.3107	0.84	1.96
MoO$_3$	0.0088	-	0.01
NaCl	0.0183	0.01	0.03
NaF	0.0013	-	-
Na$_2$O	10.9340	10.25	11.71
Nd$_2$O$_3$	0.1209	0.08	0.19
NiO	0.3358	0.22	0.52
NpO$_2$	0.0224	0.01	0.03
P$_2$O$_5$	2.5084	0.21	3.16
PdO	0.0062	-	-
Pm$_2$O$_3$	0.0003	-	-
Pr$_6$O$_{11}$	0.0321	0.02	0.05
PuO$_2$	0.0076	-	-
Rb$_2$O	0.0005	-	-

Table 2.2.1.4-5   (continued)

RhO$_2$	0.0136	0.01	0.02
RuO$_2$	0.0759	0.05	0.12
SO$_3$	0.2164	0.14	0.33
Sb$_2$O$_3$	0.0001	-	-
SeO$_2$	0.0005	-	-
SiO$_2$	44.8770	42.08	48.10
Sm$_2$O$_3$	0.0267	0.02	0.04
SnO$_2$	0.0006	-	-
SrO	0.0269	0.02	0.04
Tc$_2$O$_7$	0.0021	-	-
ThO$_2$	3.5844	1.83	6.56
TeO$_2$	0.0028	-	-
TiO$_2$	0.9800	0.92	1.05
UO$_2$	0.5605	0.37	0.87
Y$_2$O$_3$	0.0177	0.01	0.03
ZnO	0.0010	-	-
ZrO$_2$	0.2943	0.19	0.45
Other	0.0084	-	-
Total	100.0000		

[a]Source: Eisenstatt 1986. Reference glass composition is WV-205.

Table 2.2.1.4-6   Savannah River site. Chemical composition of HLW glass.[a] (Table 6.18 from K.J. Notz, T.D. Welch, R.S. Moore, and W.J. Reich, *Preliminary Waste Form Characteristics,* ORNL-TM-11681 [draft] September, 1990)

Component	Water free wt %
Ag	0.05
Al_2O_3	3.96
B_2O_3	10.28
$BaSO_4$	0.14
$Ca_3(PO_4)_2$	0.07
CaO	0.85
$CaSO_4$	0.08
Cr_2O_3	0.12
Cs_2O	0.08
CuO	0.19
Fe_2O_3	7.04
FeO	3.12
K_2O	3.58
Li_2O	3.16
MgO	1.36
MnO	2.00
Na_2O	11.00
Na_2SO_4	0.36
NaCl	0.19
NaF	0.07
NiO	0.93
PbS	0.07
SiO_2	45.57
ThO_2	0.21
TiO_2	0.99
U_3O_8	2.20
Zeolite	1.67
ZnO	0.08
Others	0.58
Total	100.00

[a]Source: Baxter 1988.

Table 2.2.1.4-7   Hanford site. Chemical compositions of HWVP reference HLW (NCAW), substituted NCAW, frit, and borosilicate glass.[a] (Table 6.19 from K.J. Notz, T.D. Welch, R.S. Moore, and W.J. Reich, *Preliminary Waste Form Characteristics,* ORNL-TM-11681 [draft] September, 1990)

Component	Reference NCAW waste composition wt %	Substituted NCAW waste composition[b] wt %	Frit composition wt %	Glass composition wt %
SiO_2	2.9	3.0	67.25	51.3
B_2O_3	0.0	0.0	12.75	9.6
Na_2O	10.5	10.7	10.25	10.4
Li_2O	0.0	0.0	5.0	3.8
CaO	0.3	0.3	3.75	2.9
MgO	0.2	0.3	1.0	0.8
Fe_2O_3	44.0	44.4	--	11.1
Al_2O_3	17.0	17.2	--	4.3
Cr_2O_3	5.3	5.3	--	1.3
ZrO_2	2.3	2.4	--	0.6
NiO	2.3	2.4	--	0.6
La_2O_3	2.2	2.2	--	0.6
SO_4	1.8	1.8	--	0.4
Nd_2O_3	1.7	2.1	--	0.5
MoO_3	1.2	1.2	--	0.3
F	1.2	1.2	--	0.3
CuO	0.6	0.6	--	0.1
$TOCc$	0.6	0.6	--	--
MnO_2	0.6	0.7	--	0.2
CeO_2	0.6	0.7	--	0.2
RuO_2	0.6	0.6	--	0.1
U_3O_8	0.6	Sub Nd	--	--
Cs_2O	0.4	1.0	--	0.2
BaO	0.4	0.4	--	0.1
SrO	0.4	0.4	--	0.1
Pr_6O_{11}	0.4	0.4	--	0.2
Tc_2O_7	0.4	Sub Mn	--	--
Rb_2O	0.2	Sub Cs	--	--
Y_2O_3	0.2	0.2	--	0.04
Sm_2O_3	0.2	0.2	--	0.04
PdO	0.2	Del	--	--
Rh_2O_3	0.2	Del	--	--
NpO_2	0.1	Sub Ce	--	--
TeO_2	0.1	Del	--	--
Pm_2O_3	0.1	Sub Nd	--	--
BeO	0.1	Sub Mg	--	--
SeO_2	0.03	Del	--	--
SnO_2	0.02	Del	--	--
CdO	0.02	Del	--	--

Table 2.2.1.4-7   (continued)

Component	Reference NCAW waste composition wt %	Substituted NCAW waste composition[b] wt %	Frit composition wt %	Glass composition wt %
Eu$_2$O$_3$	0.02	Sub Nd	--	--
PuO$_2$	0.02	Sub Ce	--	--
Am$_2$O$_3$	0.02	Sub Nd	--	--
P$_2$O$_5$	0.02	Del	--	--
Ag$_2$O	0.01	Del	--	--
Nb$_2$O$_5$	0.01	Sub Mo	--	--
Gd$_2$O$_5$	0.01	0.01	--	0.003
Ta$_2$O	0.01	Del	--	--
TiO$_2$	0.01	Del	--	--
Total	100	100	100	100

[a]Source: Mitchell 1986. Reference glass is HW-39. Data given are for a waste oxide loading of 25 wt% and are based on approximately 4-year old waste.

[b]Components marked sub were substituted as indicated. Components marked Del were deleted. TOC = total organic carbon

Table 2.2.1.4-8   Compositions of typical ceramic-based waste forms developed for immobilization of INSL calcined HLW.[a] (Table 6.20 from K.J. Notz, T.D. Welch, R.S. Moore, and W.J. Reich, *Preliminary Waste Form Characteristics,* ORNL-TM-11681 [draft] September, 1990)

Formulation number	SiO_2 (wt %)	Na_2O (wt %)	Li_2O (wt %)	B_2O_3 (wt %)	Waste (wt %)
12	8.6	1.1	0.5	2.6	87.2
11	16.0	0.0	0.0	1.4	82.6
17	30.3	0.0	0.0	2.3	67.5
6	28.6	2.1	0.9	3.5	64.9
1	14.2	2.6	1.2	1.7	80.3

[a]Source: Baker 1986.

Table 2.2.1.4-9   Typical composition of INEL calcine waste.[b] (Table 6.21 from K.J. Notz, T.D. Welch, R.S. Moore, and W.J. Reich, *Preliminary Waste Form Characteristics,* ORNL-TM-11681 [draft] September, 1990)

Component	Type of Calcine and Composition (wt%)			
	Alumina	Zirconia	Fluorinel	Zirconia-Sodium
Al_2O_3	82-95	13-17	6	12-14
Na_2O	1-3	---	---	0-5
ZrO_2	---	21-27	23	20-26
CaF_2	---	50-56	56	48-53
Ca	---	2-4	4	2-4
NO_3	5-9	0.5-2	0.5-2	0.5-4
B_2O_3	0.5-2	3-4	4	3-4
CdO	---	---	6	---
Fission Products and Actinides	<1	<1	<1	<1

[b]   Source: Staples 1986.

MAJOR GLASS COMPONENTS weight %	CONSTITUENT SLUDGE TYPE						
	Blend[d]	Batch 1	Batch 2	Batch 3	Batch 4	HM	Purex[w]
Al_2O_3	3.98	4.87	4.46	3.25	3.32	7.08	2.89
B_2O_3	8.01	7.69	7.70	7.69	8.11	6.94	10.21
$BaSO_4$	0.27	0.22	0.24	0.26	0.38	0.18	0.29
CaO	0.97	1.17	1.00	0.93	0.83	1.00	1.02
$CaSO_4$	0.077	0.12	0.11	0.10	0.0034	trace	0.12
Cr_2O_3	0.12	0.10	0.12	0.13	0.14	0.086	0.14
CuO	0.44	0.40	0.41	0.40	0.46	0.25	0.42
Fe_2O_3	10.41	12.52	10.61	11.16	11.32	7.38	12.74
Group A[a]	0.14	0.099	0.14	0.10	0.20	0.20	0.078
Group B[b]	0.36	0.22	0.44	0.25	0.60	0.89	0.084
K_2O	3.86	3.49	3.50	3.47	3.99	2.14	3.58
Li_2O	4.40	4.42	4.42	4.42	4.32	4.62	3.12
MgO	1.35	1.36	1.35	1.35	1.38	1.45	1.33
MnO	2.03	2.06	1.62	1.81	3.08	2.07	1.99
Na_2O	8.73	8.62	8.61	8.51	8.88	8.17	12.14
Na_2SO_4	0.10	0.10	0.12	0.096	0.13	0.14	0.12
$NaCl$	0.19	0.31	0.23	0.22	0.090	0.093	0.26
NiO	0.89	0.75	0.90	1.07	1.09	0.40	1.21
SiO_2	50.20	49.81	50.17	49.98	49.29	54.39	44.56
ThO_2	0.19	0.36	0.63	0.77	0.24	0.55	0.011
TiO_2	0.90	0.66	0.67	0.66	1.02	0.55	0.65
U_3O_8	2.14	0.53	2.30	3.16	0.79	1.01	2.89
Total	99.76	99.88	99.75	99.79	99.66	99.59	99.85

a Group A: semi-volatile radionuclides (Se, Te, Rb, Mo, Tc)

b Group B: nonvolatile radionuclides (e.g., Sm, Sn, Co, Np, Am, Cm)

d The "Blend" is the current DWPF design-basis glass

w The "Purex" glass is a possible "worst-case" composition

Figure 2.2.1.4-6   Projected DWPF waste glass compositions (Figure from M. J. Plodinec, *Defense Waste Processing Facility High Level Waste Qualification Activities,* presented to the Nuclear Waste Technical Review Board, August, 1990)
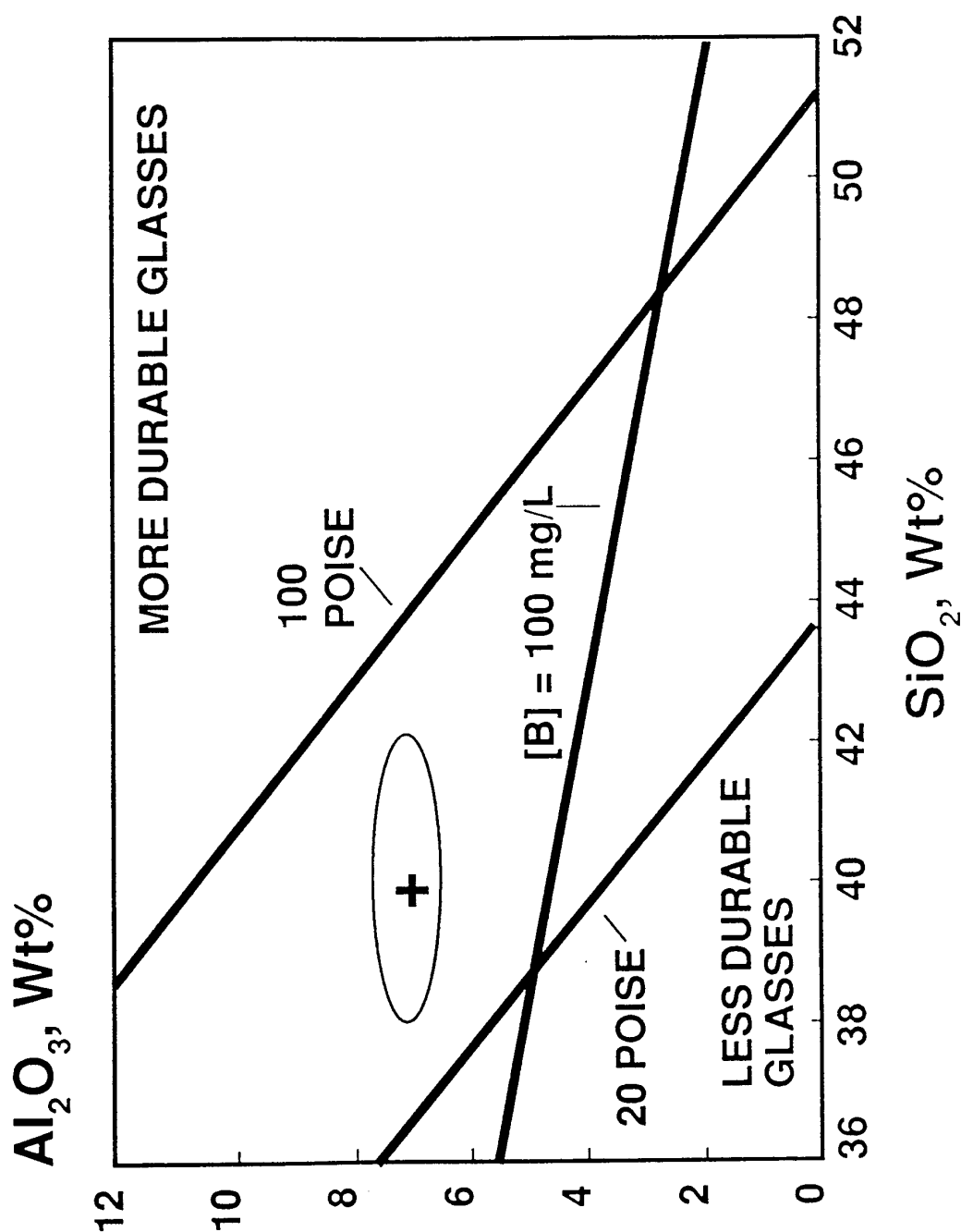
Figure 2.2.1.4-7 Acceptable glasses (Figure from R. A. Palmer, *West Valley Demonstration Project High Level Waste Qualification Activities,* presented to the Nuclear Waste Technical Review Board, August, 1990)

GLASS OXIDES	COMPOSITION (WT. %)	LOWER BOUND	UPPER BOUND
Si	43.1	38.0	45.0
Al	6.2	5.0	10.0
Fe	12.2	10.0	16.0
B	10.9	6.9	13.0
Na+K+Li	17.8	12.0	20.0
P	2.4	0.5	4.0
Mn	1.0	0.1	2.0

Figure 2.2.1.4-8 Durable glass region (Figure from R. A. Palmer, *West Valley Demonstration Project High Level Waste Qualification Activities,* presented to the Nuclear Waste Technical Review Board, August, 1990)

### *2.2.1.5 Fracture/Fragmentation Studies*

Summary of Effects of Fracturing on Reactive Surface Area of Borosilicate
Glass Waste Form

This section documents the recommended values of glass surface area to be used in estimating glass alteration rates in the total system performance assessment–viability assessment (TSPA-VA) modeling work.

Background

The reactive surface area of glass in a defense waste processing facility (DWPF) pour canister is increased above its simple geometric value through two processes (Wicks, 1985):

- **Thermal Fracturing**—As the waste glass cools after pouring, thermal gradients induce stresses that cause the glass to crack. Figure 2.2.1.5-1 shows the relative increase in actual surface area over the geometric surface area as a function of cooling rate. The faster the glass cools, the larger the surface area due to cracking. For typical cooling rates for the DWPF, the factor is approximately 10 to 15 (Smith and Baxter, 1981; Baxter, 1983). The glass area also is increased a minor amount due to production of fines generated during thermal cracking. These fines do not appear to contribute significantly to total surface area and, based on leaching studies of cracked glasses (Perez and Westsik, 1980) and on measurements of fines generated (Ross and Mendel, 1979), these fines can be ignored.

- **Impact Cracking**—If the glass canister is impacted by being dropped or experiencing a collision, the glass will crack (Smith and Ross, 1975). Figure 2.1.1.5-2 shows the increase in surface area, again expressed as a fraction of initial (geometric) surface area, as a function of collision velocity. At an impact velocity of 117 ft per sec (80 mph), the glass surface area is increased by a factor of about 40.
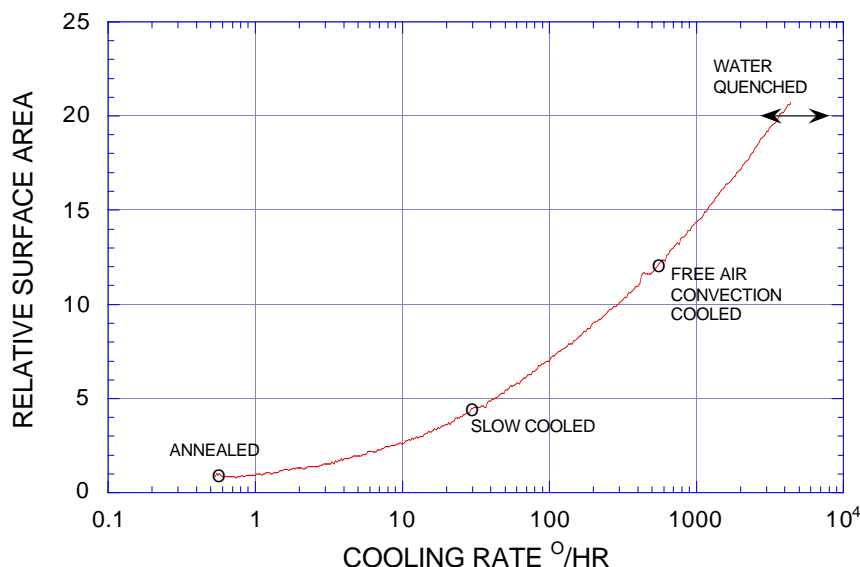
Figure 2.2.1.5-1   Area increase of thermally shocked, simulated nuclear waste glass; values are relative to geometric area of glass cylinder with no surface roughness (data from Ross and Mendel, 1979)
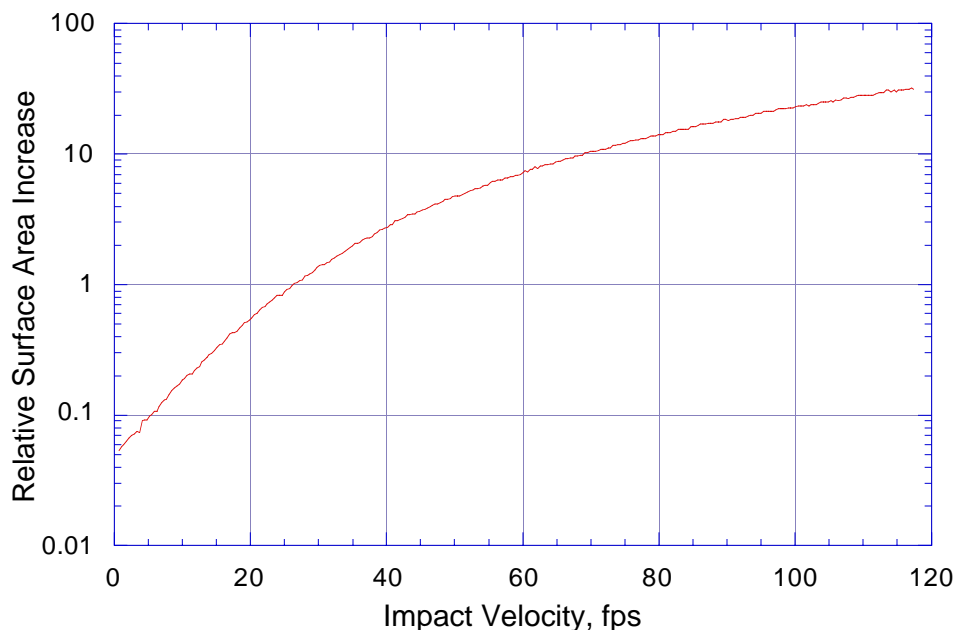
Figure 2.2.1.5-2   Impact effects on surface area for simulated commercial waste glass (from Smith and Ross, 1975)

For both types of cracking, the actual increase in glass reaction rate is actually less than proportional to the increase in surface area (Perez and Westsik, 1980). Presumably this is due to a combination of restricted water mobility through tight cracks, solution saturation effects, and swelling due to precipitation of hydrous alteration phases. Generally, a factor of 10 increase in surface area gives only a factor of 3 to 5 times faster reaction rate in a static leach test (Wicks, 1985.

Recommendation

Based on these data, a conservative surface area value of roughly 21 times geometric area for typical DWPF glass, which is approximately 20% smaller than the value used in calculations in Section 3.5.1 of this report, is recommended To obtain this value, one assumes 1% of all canisters suffer severe damage during transit so that their surface areas are increased a factor of 40 times above the normal value of air-cooled glass. For every 100 canisters, the one damaged canister has a surface area of $40 \times 15 = 600$ times geometric, and the other 99 have surface areas of 15 times geometric. The total surface area is

$$40 \times 15 \times 1 \text{ (damaged)} + 15 \times 99 \text{ (undamaged)} = 2085/100 = 20.85 \text{ times}$$

No credit is given for the lack of scaling between observed increase in surface area and a lessor increase in glass reaction rate.

A typical, filled canister of SRL-202 glass has approximately 1680 kg of glass with a density of 2.7 g/cm^3. The volume of the glass log is therefore $1,680,000/2.7 = 622,000$ cm^3. The inside diameter of the canister is approximately 60 cm. Therefore the glass cylinder has a height of

$\Pi r^2 \times$ height = volume

height = 622,000 c^{m3} / _900 c^{m2} = 220 cm

with total surface area

$2\ \Pi r^2 + 2\Pi r \times$ length = 5,655 + 41,469 = 47,124 cm^2 = 4.7 m^2

Therefore an average DWPF glass canister has a surface area of $21 \times 4.7 = 99$ m^2.

References

Baxter, R. G. (1983). Description of Defense Waste Processing Facility Reference Waste Form and Container. Aiken, SC: Savannah River Site. [210286]

Perez, J. M., and J. H. Westsik (1980). "Effects of Cracks on Glass Leaching." In proceedings from ORNL Conference on Leachability of Radioactive Solids. Oak Ridge, TN: Oak Ridge National Laboratory. p. 35.

Ross, W. A., and J. E. Mendel (1979). *Annual Report on the Development and Characterization of Solidified Waste Forms for High-Level Wastes.* Richland, WA: Pacific Northwest National Laboratory.

Smith, P. K.. and C. A. Baxter (1981). *Fracture During Cooling of Cast Borosilicate Glass Containing Nuclear Wastes.* Aiken, SC: Savannah River Laboratory. [238536]

Smith, T. H., and W. A. Ross (1975). *Impact Testing of Simulated High-Level Waste Glass in Canisters.* Richland, WA: Pacific Northwest National Laboratory. [238924]

Wicks, G. (1985). "Nuclear waste glasses." *Treatise on Materials Science and Technology.* **26:**57–117. New York, NY: Academic Press. [238484]

2.2.2 Repository Response

2.2.2.1 Gaseous Release from Glass

Internal pressure within the canister is due to the accumulation of helium from alpha emission of transuranic nuclides. A DWPF canister filled with waste glass produces about 0.32 cm3 of helium per year at 40°C. The helium produced is assumed to diffuse through the glass into the void space above the solid glass surface. At the end of 1,000 years, the 103-liter void space pressure has increased by only 0.05 psi. This negligible pressure buildup is of no concern in waste package design. For the case of a canister filled to 25.3 ft3 (733 L), the 23-liter void space pressure would increase by 0.2 psi.

(Baxter, R. G., Defense Waste Form Processing Facility Waste Form and Canister Description, DuPont SRL Report DP-1606, p.17, (December, 1988).

2.2.2.2 Dissolution Radionuclide Release from Glass

2.2.2.2.1   Radionuclide Release Data From Unsaturated Tests

2.2.2.2.1.1 Data Description

The N2 and N3 unsaturated (drip) tests have been in progress at Argonne National Laboratory since February 1986 and July 1987, respectively. Drip tests are designed to replicate the synergistic interactions between waste glass, repository groundwater, water vapor, and sensitized 304L stainless steel in the proposed Yucca Mountain repository.

The tests using actinide- and technetium-doped Savannah River Laboratory (SRL) 165 glass, are termed the N2 Test Series. Tests with a West Valley Demonstration Project former reference glass (ATM-10) have been in progress and are termed the N3 Test Series. The information provided here includes long-term data relevant to glass reaction under conditions anticipated for an unsaturated repository. While SRL-165 glass is no longer the reference glass to be used for the defense waste-processing facility (DWPF), it does represent a glass within the production envelope, and the tests provide information that can be used for the following:

- Model validation
- Investigation of reaction mechanisms
- Evaluation of synergistic effects
- Form of radionuclide release
- Glass reaction rates over long time periods under repository service conditions

Measurements obtained from each test series include the rate of glass reaction and radionuclide release as a function of time, a description of the distribution of radionuclides in solution (i.e., dissolved in solution, associated with colloidal material, or sorbed onto metal components of the test), and monitoring of the interactions among the various components in the test. Ultimately, the Yucca Mountain Site Characterization Project (YMP) plans to use the results from these tests to validate source terms of models used in waste-package-performance assessment codes.

In the unsaturated tests, 0.075 mL (about 3 drops) of tuff-equilibrated groundwater from the J-13 well near Yucca Mountain (termed EJ-13 water) is dripped every 3.5 days onto the simulated waste package (WP) in a sealed stainless-steel test vessel. Additional air is injected into the test vessel with the water. The simulated waste-package assemblage (WPA) used in the tests consists of a cylindrical monolith of waste glass, approximately 16 mm diameter and 20 mm high, contacted on the top and bottom by two perforated retainer plates made from sensitized 304L stainless steel; these are held in place by two wire posts, also made from 304L stainless steel. The entire test apparatus is enclosed in a 90°C oven, except when samples are taken and observations made.

Details of the unsaturated test procedure are given elsewhere (Bates and Gerding, 1990; ANL, 1996). Each ongoing test series consists of three identically prepared WPAs, each in its own test vessel, and a blank (empty test vessel). Water drips down the sides of the glass and accumulates at the bottom of the WPA. Eventually the water drips from the WPA to the bottom of the vessel. When the drip tests are sampled (currently at 26-wk intervals), the WPA

is examined visually to qualitatively ascertain the degree of reaction, including evidence of alteration-phase formation and possible spalling of the alteration phases and clay layer. After observation, the WPA is transferred to a fresh test vessel, the test solution is removed for analysis, and the just-used vessel is acid-stripped to determine sorbed species.

The compositions of the glasses used in the N2 and N3 tests are given in Table 2.2.2.2-1. The approximate composition, for the most concentrated elements, of the groundwater (EJ-13) used in the tests is given in Table 2.2.2.2-2.

Table 2.2.2.2-1   Compositions, in oxide-weight percentage, of glasses used in the N2 and N3 tests [LL980710651021.049; LL980710551022.012]

Oxide	N2 Tests SRL 165[a]	N3 Tests ATM-10[b]
Al_2O_3	4.08	6.65
AmO_2	0.00091	0.0064
B_2O_3	6.76	9.17
BaO	0.06	0.045
CaO	1.62	0.60
CeO_2	<0.05	0.072
Cr_2O_3	<0.01	0.253
CsO_2	0.072	0.062
Fe_2O_3	11.74	11.5
K_2O	0.19	3.34
La_2O_3	<0.05	0.025
Li_2O	4.18	2.88
MgO	0.70	1.15
MnO_2	2.79	1.29
Na_2O	10.85	10.5
Nd_2O_3	<0.05	0.168
NiO	0.85	0.296
NpO_2	0.0283	0.021
P_2O_5	0.29	2.34
PuO_2	0.048	0.0081
RhO_2	—	0.012
RuO_2	—	0.061
SO_3	—	0.31
SiO_2	52.86	45.8
SrO	0.11	0.025
Tc_2O_7	0.02	0.0031
ThO_2	—	3.29
TiO_2	0.14	0.858

Oxide	N2 Tests SRL 165[a]	N3 Tests ATM-10[b]
UO$_2$	1.25	0.527
Y$_2$O$_3$	—	0.017
ZrO$_2$	0.66	0.247

[a]   From Bates and Gerding (1990), except as noted
[b]   From ANL (1996)

Table 2.2.2.2-2   Typical composition of the EJ-13 water used in the N2 and N3 tests [LL980710551022.012]

Element	Concentration (mg/L)
Al	0.7
B	0.2
Ca	6.6
Fe	<0.1
K	7
Mg	0.15
Li	0.04
Na	53
Si	40
F$^-$	3
Cl$^-$	10
NO$_2^-$	<1
NO$_3^-$	11
SO$_4^-$	23
HCO$_3^{2-}$	100
total carbon	25
organic carbon	7

The pH of EJ-13 water is ~8.6.
Other cations are < 0.1mg/L.

2.2.2.2.2 Results

2.2.2.2.2.1 Solution Cation Analyses

In the following discussion, the solution collected in the test vessel that had contacted the WP during the course of the test is designated as the vessel rinse, and the solution that results from soaking the vessel with acidified water is called the acid strip. As the glass reacts, material is released from the glass either truly dissolved in solution or as particulate material. The solution is also in contact with the pre-sensitized, 304L, stainless-steel retainer during the reaction process, so the analysis of the solution collected in the bottom of the test vessel represents all the material that is transported from the glass and the glass retainer. The

solution is analyzed for its constituent parts, as described previously, but all the material analyzed in the test solution is considered to have been released from the glass/stainless-steel assembly.

A comparison of behaviors among elements present in widely different concentrations in the glass is best made by examination of the *normalized releases*. The normalized release rate is $N_i = M_i/(\Delta t\, c_i\, A)$, where M_i is the measured mass of element i in the leachate solution, c_i is its element fraction in the source glass, Δt is the time interval between tests, and A is the surface area of the glass monolith (1.36×10^{-3} m²). However, the use of such a normalization process in the drip tests averages the three types of water contact that occur: humid air, dripping water, and standing water.

2.2.2.2.2.2 Elements in the N2 Solution

Figure 2.2.2.2-1 shows the total cumulative mass release of lithium and boron in the vessel rinse from the N2 tests into solution as a function of time. The term "release" is used throughout this section to indicate elements that have left the WPA and are dissolved in solution, suspended as colloids, or sorbed onto the test vessel. The release of these elements is an important gauge of the glass corrosion because they are not expected to form secondary phases, are not major components of the EJ-13, and are not present in the steel.

Negligible amounts of lithium and boron are measured in the acid strip solutions. Normalized release rates for these elements appear in Figure 2.2.2.2-2. Note also the nearly identical behavior of these two elements, an indication that they are remaining in solution (dissolved) and are released from the glass congruently. Further note that, while the data from the three replicate samples in the test may differ, the N2-10 sample releases both lithium and boron at the fastest rate, while the N2-9 sample releases both elements at the slowest rate (not including N2-11, which was a blank test). The differences in measured reaction rate are real and are reflections of the reproducibility of this type of test over a 10-yr period. The composition of the unfiltered N2-10 vessel-rinse test solution from the June 17, 1996, sampling, which includes plutonium and americium contributions from colloids, appears in Table 2.2.2.2-3.
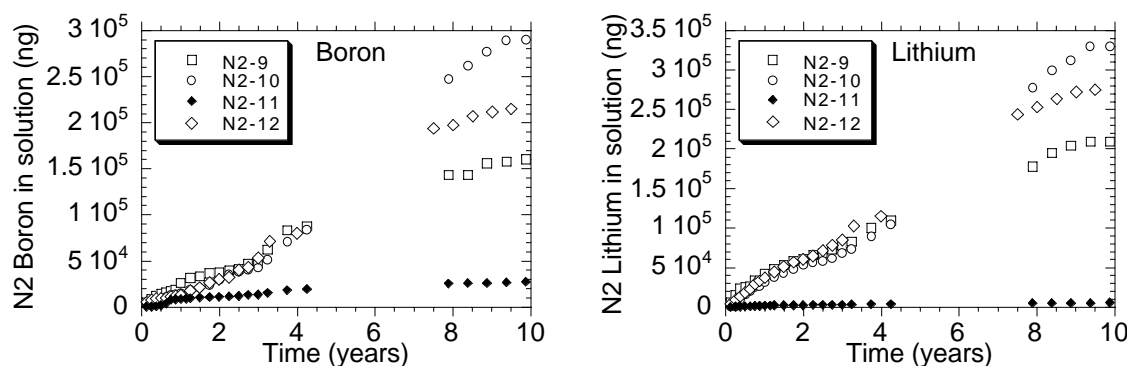
Figure 2.2.2.2-1   Cumulative release of boron and lithium from the N2 tests as a function of elapsed time. Note the increased release rate, relative to the other tests, from N2-10. The test N2-11 is a blank test, and the release data from the N2-11 test are upper bounds because of detection limits. [LL980913251031.060]
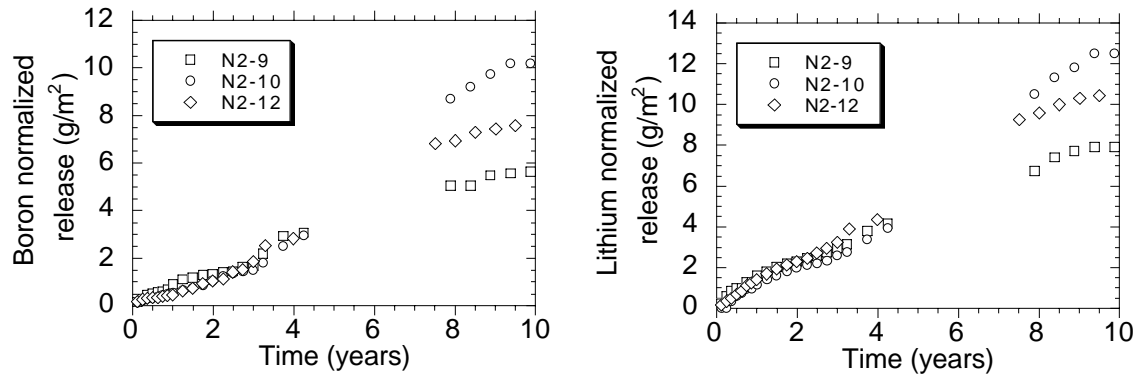
Figure 2.2.2.2-2 Normalized cumulative release of boron and lithium from the N2 tests as a function of elapsed time. Note the increased release rate, relative to the other tests, from N2-10 (note also that the normalized releases of these elements are in excellent agreement) [LL980913251031.060]

Table 2.2.2.2-3 Composition of the unfiltered test solution collected from N2-10 on June 17, 1996 (these values are typical of what has been observed in the N2 series over the past 3 yr) [LL980710551022.012]

Concentration (μg/mL)						
Li	B	Na	Al	Si	K	Ca
31200	6300	329000	10300	153000	54600	17500
Concentration (μg/mL)						
Cr	Fe	Ni	U	Np	Pu	Am
1800	30500	6500	2040	35	63	1.0

Uranium release from the N2 tests appears in Figure 2.2.2.2-3. Note that the uranium normalized release is about half (or less) that of lithium and boron (Figure 2.2.2.2-2) and that the N2-10 test appears to be releasing uranium at a much higher rate than did the other two. These plots do not include uranium from the acid strip of the test vessel, which has only been measured since the December 1993 sampling; extrapolating from present trends, the acid strip data would add about 30% to the observed release of uranium and are included in the normalized uranium release rates of Table 2.2.2.2-4. From Table 2.2.2.2-4, it is apparent that the normalized uranium release from N2-10 is approximately the same as the normalized lithium or boron release, whereas the N2-9 and 12 are releasing uranium somewhat more slowly. A release mechanism by solution-born colloids is proposed later in this section as a likely explanation of such variations among samples.
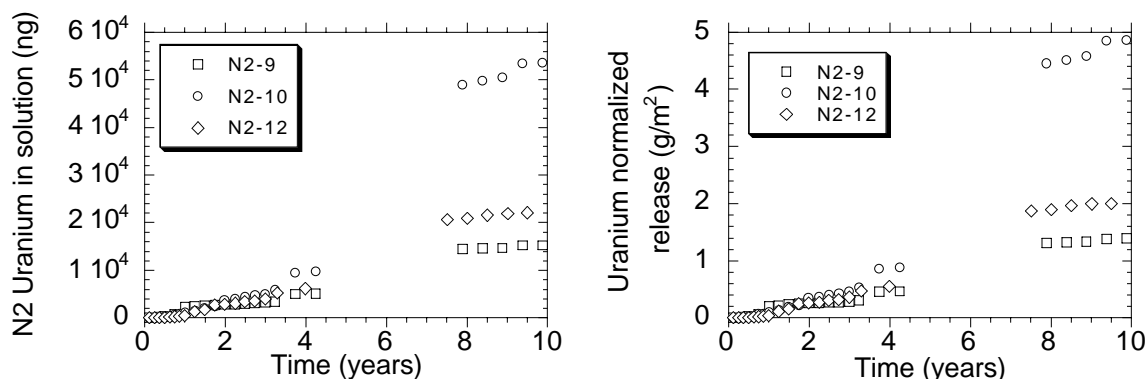
Figure 2.2.2.2-3 **Cumulative uranium release from the N2 tests as a function of time (left, total mass release; right, normalized release) [LL980913251031.060]**

Table 2.2.2.2-4 **Normalized release rates over the latest 2.5-yr period for selected elements from the N2 tests series[a] [LL980710551022.012]**

Normalized Release Rates [b] ($g\ m^{-2}\ day^{-1}$)					
Test Series	**Li**	**B**	**U**	**Np**	**Pu**	**Am**
N2-9	1.6×10^{-3}	0.9×10^{-3}	4.0×10^{-4}	1.0×10^{-4}	3.0×10^{-5}	4.4×10^{-5}
N2-10	2.8×10^{-3}	2.2×10^{-3}	1.3×10^{-3}	3.4×10^{-3}	1.4×10^{-3}	1.4×10^{-3}
N2-12	1.7×10^{-3}	1.1×10^{-3}	3.2×10^{-4}	4.0×10^{-4}	0.8×10^{-4}	0.9×10^{-5}
Average	2.1×10^{-3}	1.4×10^{-3}	6.7×10^{-4}	1.6×10^{-3}	4.8×10^{-4}	5.0×10^{-4}

[a]   The rates include data from the period December 1993 through December 1995. The above rates are for vessel rinse only, except for the rates for U, Pu, and Am, which include the acid strip.

[b]   Error is approximately ±30% for each of the above rates. These rates reflect the latest glass composition analysis by ICP-MS (Table 2.2.2-1).

The elements in the acid strip solution (except for the actinides plus iron, nickel, and chromium from the stainless-steel test vessel itself) are present at very low amounts relative to the vessel rinse solution. Neptunium, plutonium, and americium in the acid strip have been monitored by high-resolution alpha spectroscopy since the tests were initiated. Uranium levels in the acid strip were not measurable by the alpha spectroscopy procedure and have only recently become available with the inductively coupled plasma–mass spectroscopy ICP-M S data.

The release of the transuranic elements Np, Pu, and AM into solution is plotted in Figures 2.2.2.2-4 and 2.2.2.2-5 for the N2 test series. Np is highly soluble and does not sorb substantially onto the stainless steel, a fact confirmed by measurements of the acid strip solutions. The reported values for Np, like those of Li and B, thus include only the vessel rinse. Pu and Am, on the other hand, are known to sorb onto the stainless steel (from which the test vessel is made) and may also be incorporated into the clay layer and alteration phases (Bates et al., 1992; Fortner et al., 1995; Fortner et al., 1997). The Pu and Am data in the figures

represent a sum of the vessel rinse and acid strip results, where there are comparable contributions from each. Typically, 60 to 70% of the Pu and Am is from the vessel rinse, with the remaining 30 to 40% from the acid strip.
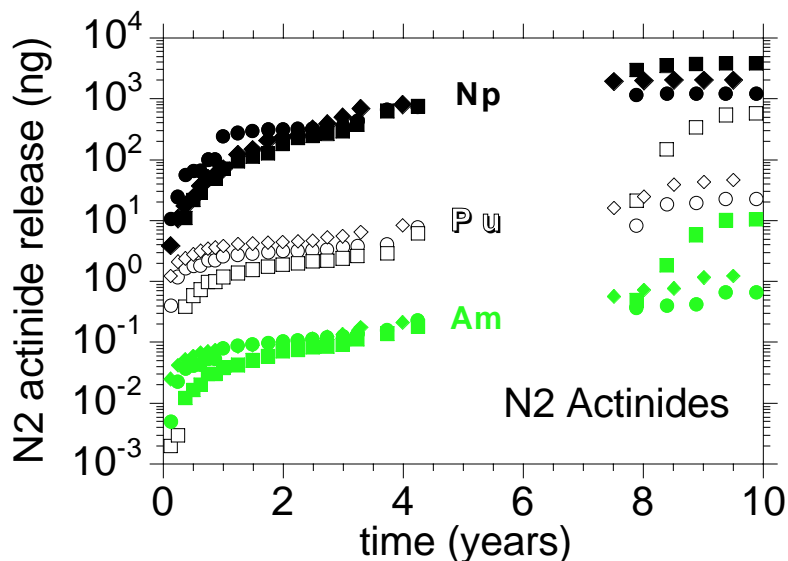
Figure 2.2.2.2-4   Cumulative mass releases for the transuranic elements neptunium, plutonium, and americium from the N2 Tests: N2-9 (circles), N2-10 (rectangles) and N2-12 (diamonds) [LL980913251031.060]
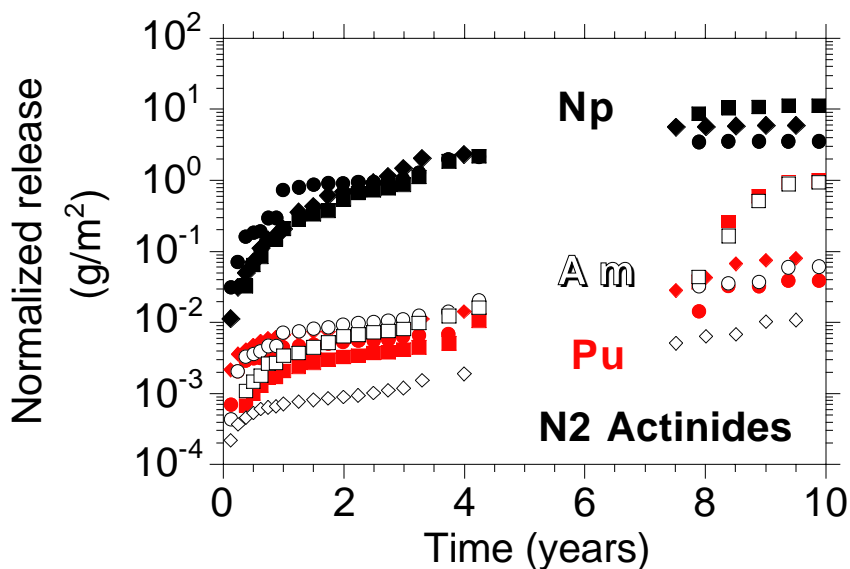
Figure 2.2.2.2-5   Normalized actinide release from the N2 tests: N2-9 (circles), N2-10 (rectangles), and N2-12 (diamonds). Note the retention of Am and Pu relative to Np. [LL980913251031.060]

The sharp increases in Pu and Am release rates seen in some of the latest data are a result of some actinide-bearing secondary phases spalling off the glass and appearing in the test solution. These increases are correlated with the visual observations, where the N2-10 test is

observed to undergo the greatest (of the N2 series tests) corrosion of the metal and spalling of clay from the glass into the test solution. A comparison of the normalized releases of B, Np, Pu, and Am appears in Figure 2.2.2.2-6. For the first eight years, the release of the soluble B and Np was more than two orders of magnitude greater than that of the relatively insoluble Pu and Am. During the latest two years, the release rate of the Pu and Am has nearly equaled that of the soluble elements (Table 2.2.2.2-4). Note that the Np release does not experience the recent jumps observed for Pu and Am, but continues smoothly as do the Li and B releases. This is consistent with the clay alteration layer being depleted in these elements; their release is thus unaffected by the spalling of the clay. Continued spalling of the clay may ultimately cause the normalized release of Pu and Am (as solution-born solid phases) to approach that of the Li and B. These lower rates are due to incorporation of elements into secondary phases, many of which remain attached to the WPA. The spalling off of these phases is then what controls the release of the incorporated elements from the glass. These spalled-off phases may become suspended in solution as colloids. The role of colloidal solids in solution is also reflected in the sequential filtering data, where substantial Pu and Am often appear on the filters and are removed from the filtered solution. Recent use of ultracentrifugation filtration has shown that nearly 100% of the Np is recovered in the filtered solution from the N2 tests, whereas less than 10% of the Pu and Am pass.

A more detailed analysis of the filtered solutions will be prepared as more data are compiled and analyzed. The masses of truly dissolved actinides from the N2-12 test sampled December 18, 1995, appear in Table 2.2.2.2-5. It is clear from these data (and others) that little of the Np in solution is associated with undissolved solids, whereas a majority of the Am and Pu are incorporated into p¥articulates and colloids. Examples of solid phases observed from the N2 test components appear in Table 2.2.2.2-6.
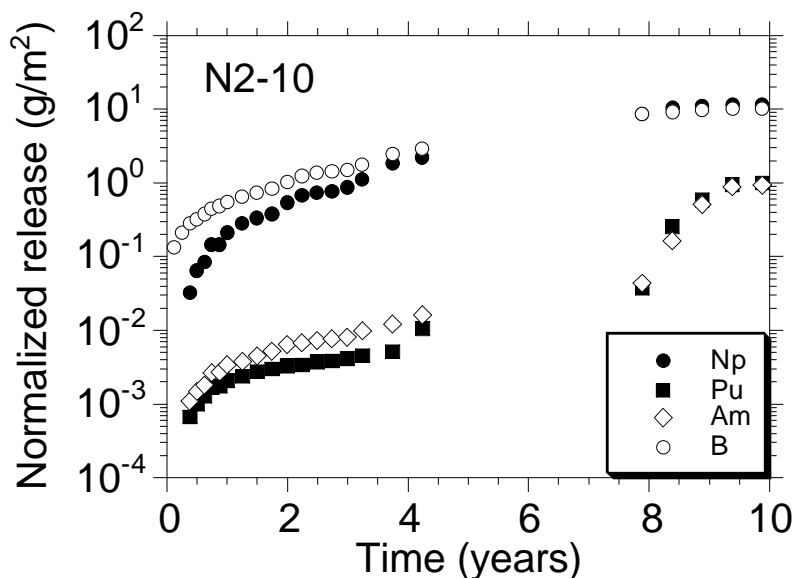
Figure 2.2.2.2-6 **Normalized release of Np, B, Am, and Pu from a single test series, N2-10, which displayed evidence of excessive clay spallation. Note the sudden increase in release of the insoluble elements Pu and Am without an accompanying disruption in the release of the more soluble Np and B. This is likely due to the release of the Am and Pu as solids (colloids or larger particulates), potentially leading to near-congruent release of elements. [LL980913251031.060]**

Table 2.2.2.2-5 **Comparison of transuranic content in unfiltered and ultracentrifuge-filtered solutions from the N2-12 test sampled December 18, 1995 (the solution volume recovered was 1.42 mL) [LL980710551022.012]**

Element in Solution (ng)					
Np (Unfiltered)	Np (Filtered)	Pu (Unfiltered)	Pu (Filtered)	Am (Unfiltered)	Am (Filtered)
5.1	5.2[a]	0.844	0.002	0.0115	0.0003

[a] The recovery of more than 100% of the Np is an artifact of statistical error.

Table 2.2.2.2-6 **Alteration phases identified on N2 solid components (from Bates and Gerding, 1990)**

Phase	Nominal Composition	comments
Ferrihydrate	$5Fe_2O_3 \cdot 9H_2O$	
Iron oxyhydroxide	$FeOOH$	
Sodium feldspar	$NaAlSi_3O_8$	Precipitate
Cristobalite	SiO_2	Precipitate
Orthoclase	$KAlSi_3O_8$	Precipitate
Smectite clay	Layered aluminosilicate with interlayer Fe and Mg	Variable composition

2.2.2.2.2.3 Elements in the N3 solution

The cumulative release of B and Li from the N3 tests appears in Figure 2.2.2.2-7, with normalized release plotted in Figure 2.2.2.2-8. As with the N2 tests, the normalized release of these elements is nearly identical with each test in the N3 series, consistent with congruent dissolution of the glass and complete solubility of the Li and B under the test conditions.
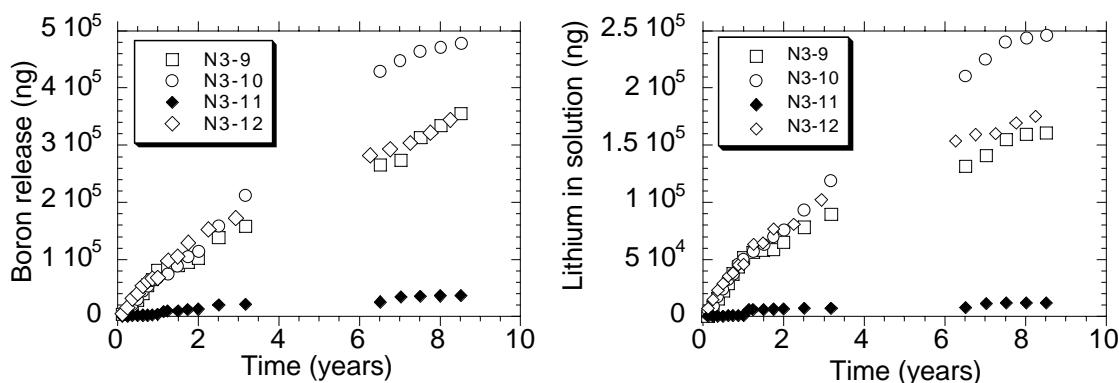
Figure 2.2.2.2-7 **Cumulative release of B and Li from the N3 tests as a function of elapsed time. The test N3-11 is a blank test, and the release data from the N3-11 test are upper bounds due to detection limits. [LL980913251031.060]**
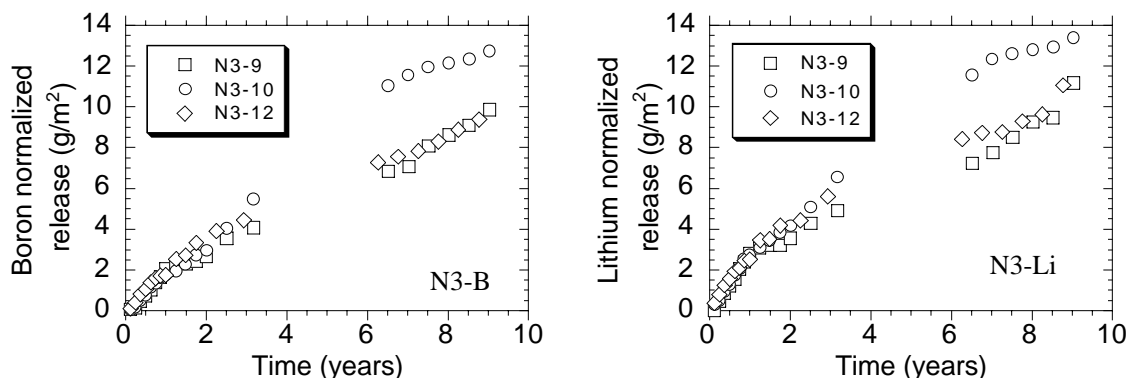
Figure 2.2.2.2-8   **Normalized cumulative release of B and Li from the N3 tests as a function of elapsed time. Note also that the normalized releases of these elements are in excellent agreement with one another. [LL980913251031.060]**

Transuranic release appears in Figures 2.2.2.2-9 and 2.2.2.2-10 as total mass release and normalized release, respectively. From these figures, it is apparent that the release rate for Pu and Am has increased by a factor of nearly two during the past two years, but still remains well below the release for the soluble elements (Table 2.2.2.2-7), rather than jumping by an order of magnitude, as was observed in the N2-10 test.
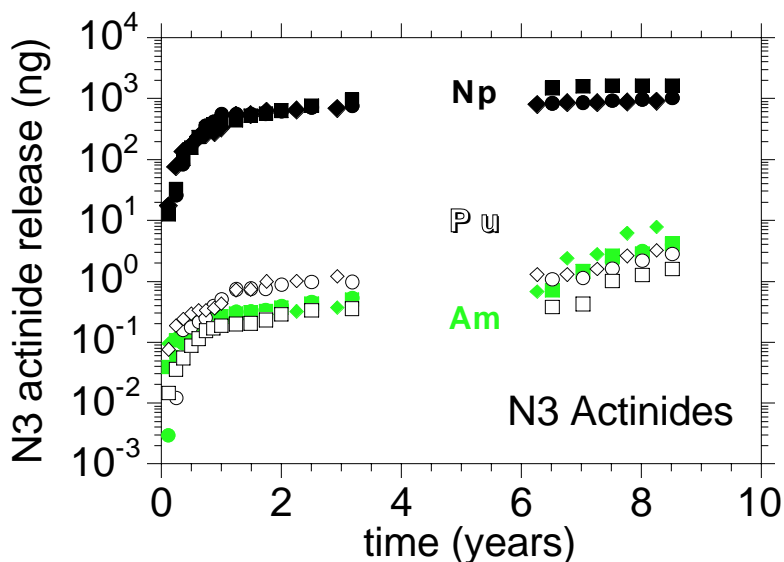
Figure 2.2.2.2-9   **Cumulative mass releases for the transuranic elements Np, Pu, and Am from the N3 Tests: N3-9 (circles), N3-10 (rectangles), and N3-12 (diamonds). [LL980913251031.060]**

Figure 2.2.2.2-10 **Normalized actinide release from the N3 tests:**
N3-9 (circles), N3-10 (rectangles), and N3-12
(diamonds). Note the retention of Am and
Pu relative to Np. [LL980913251031.060]

Table 2.2.2.2-7 **Normalized release rates over the latest 2.5-yr period for selected elements**
from the N3 tests series[a]

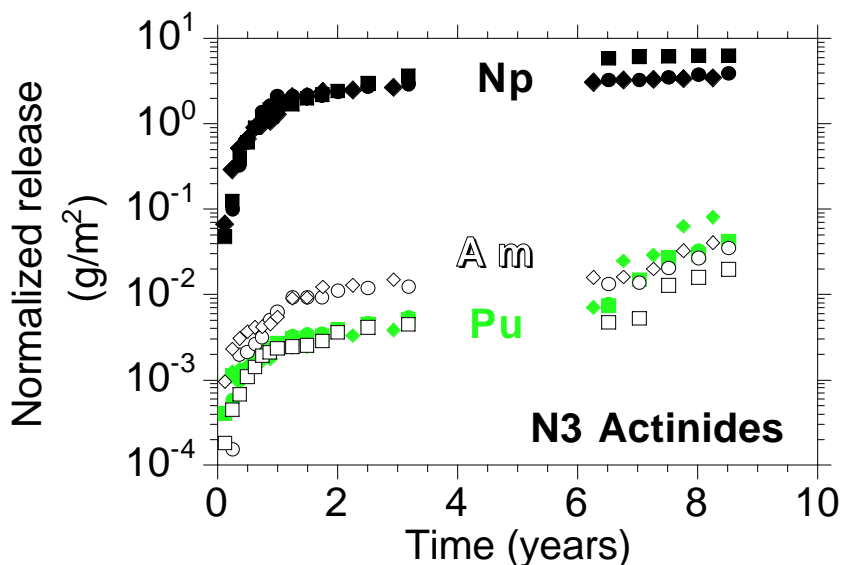| Normalized Release Rates[b] (g m^{-2} day^{-1})							
Test Series	Li	B	Th	U	Np	Pu	Am
N3-9	4.0×10^{-3}	3.4×10^{-3}	1.3×10^{-5}	2.6×10^{-4}	9.6×10^{-4}	4.7×10^{-5}	3.0×10^{-5}
N3-10	1.8×10^{-3}	1.7×10^{-3}	2.1×10^{-5}	4.3×10^{-4}	6.6×10^{-4}	4.7×10^{-5}	2.2×10^{-5}
N3-12	2.6×10^{-3}	2.3×10^{-3}	1.1×10^{-5}	3.7×10^{-4}	4.9×10^{-4}	1.0×10^{-4}	3.6×10^{-5}
Average	2.8×10^{-3}	2.5×10^{-3}	1.5×10^{-5}	3.5×10^{-4}	7.0×10^{-4}	6.5×10^{-5}	3.0×10^{-5}

[a] The rates include data from the period January 1994 through July 1996. The rates are for vessel rinse only, except the rates for Th, U, Pu, and Am, which include the acid strip.

[b] Error is approximately ±30% for each of the rates.

The West Valley-type glass used in the N3 tests is unusual in that it contains a large amount, relative to most other waste glasses, of the actinide element Th. This element is found to concentrate in alteration phases (Fortner and Bates, 1996; Bates et al., 1992, Fortner et al., 1995). The N3 tests continue to release Th at the relatively low rate of 1.5 (±0.5) x10^{-5} g/(m^2 day), about 100 time less than the normalized release rates for B and Li (Table 2.2.2.2-7). This low release rate suggests that the Th alteration phases are mostly remaining with the test WPA, although they have been observed in colloidal particles from the test solution phases (Fortner and Bates, 1996; Bates et al., 1992). Alteration phases observed on components from the N3 test series are summarized in Table 2.2.2.2-8.

Table 2.2.2.2-8   Summary of alteration phases noted on the N3 surfaces (Fortner et al., 1997)

Phase	Location	Identification	Comments
Smectite clays	A layer on all glass surfaces. Spalled fragments located sporadically on 304L retainer components	Energy-dispersive spectroscopy (EDS), electron diffraction, lattice imaging	A ubiquitous layer that grew with test duration. The more advanced growths displayed a "backbone" structure.
Brockite (CaThPO$_4$)	Copious amounts found on most glass surfaces. Clusters found on most 304L retainer surfaces, except those of shortest test duration.	EDS, electron diffraction, electron-energy-loss spectroscopy (EELS)	Appeared to form as separate crystallites in or on outer layer of clay. Entrained rare earth elements, U, and probably transuranics. This phase was amorphous or partly amorphized.
Uranium silicates	Very sparsely located on glass and 304L retainer surfaces. Were possibly more likely to be observed where 304L retainer interacted with glass.	EDS	Positive phase identification of these rarely encountered crystallites was not possible; they did not appear in any Auger electron microscopy (AEM) samples.
Iron silicates, iron silicate hydrates, and iron oxyhydrates	In some cases, iron-rich layers grew on glass where it contacted 304L retainer. Separate material and crystals found on most glass and 304L retainer surfaces.	EDS, electron diffraction	Electron diffraction generally found these materials to be amorphous. Fayalite was identified in one instance by electron diffraction.
Thorium titanium iron silicate	Appeared to precipitate colloidally between glass and clay layer or in other regions of restricted water flow	EDS, EELS	This material was amorphous and grew as wisps that were usually mixed with the clay. The clay appeared to serve as a barrier, trapping this material between the glass and the clay "backbone."
Zeolites	Rarely encountered (possibly artifacts).	EDS, electron diffraction	Only two instances observed; once in the scanning electron microscopy (SEM) (N3#8 glass top) and once in the AEM (N3#3 glass bottom). Electron diffraction identified the later as a member of the heulandite subgroup.
Amorphous silica	Occasional white surface particulates	EDS, EELS, electron diffraction (as diffuse rings)	The conditions that, for silica rather than clay formation, are unknown

2.2.2.2.3 References

ANL (1996). *NNWSI Unsaturated Test Procedure.* (NNWSI-05-011, Rev. 4) Argonne IL: Argonne National Laboratory, Chemical Technology Division.

Bates, J. K., and T. J. Gerding (1990). *Application of the NNWSI Unsaturated Test Method to Actinide Doped SRL 165 Type Glass.* (ANL-89/24) Argonne, IL: Argonne National Laboratory Report. [NNA.19891213.0188]

Bates, J. K., J. P. Bradley, A. Teetsov, C. R. Bradley, and M. Buchholtz ten-Brink (1992). "Colloid formation during waste form reaction: Implications for nuclear waste-disposal. *Science* **256**(5057):649–651. [MOL.19980326.0392]

Fortner, J. A., and J. K. Bates (1996). "Long-Term Results from Unsaturated Durability Testing of Actinide-Doped DWPF and WVDP Waste Glasses." In proceedings from *Mat. Res. Soc.* **412**:205–211. [MOL.19960418.0084]

Fortner J. A., T. J. Gerding, and J. K. Bates (1995). "Long-Term Test Results from a West Valley Actinide-Doped Reference Glass," in "Environmental Issues and Waste Management Technologies in the Ceramic and Nuclear Industries." V. Jain and R. Palmer (Eds.).*Ceramic Trans.* **61:** 455–462.

Fortner J. A., J. K. Bates, and T. J. Gerding (1997). *Analysis of Components from Drip Tests with ATM-10 Glass.* (ANL-96/16) Argonne, IL: Argonne National Laboratory.

2.2.2.3 Soluble-Precipitated/Colloidal Species

2.2.2.3.1 Colloidal Particle Analysis of Unsaturated Tests

2.2.2.3.1.1 Colloidal Particle Analyses

Small samples (~5µl) of the N2 and N3 unsaturated-drip–test fluids have been wicked through a porous or "holey" carbon-transmission electron-microscope grid to allow Auger electron microscopy (AEM) examination of suspended particles. In both the N2 and N3 tests, the majority of colloidal particles observed by AEM have been either a smectite-type clay or a variety of iron-silicates. Both clays and iron silicates can sorb actinides, and thus these colloids represent potential transport mechanisms for insoluble elements.

As stated in Sections 2.2.2.2.1 and 2.2.2.2-2, more than 90% of the Pu and Am in solution from the N2 and N3 tests appears to be associated with particulate matter that will not pass through a 1-µm filter. In the N2 tests, both the clay and iron-silicate colloids are sometimes observed to contain small amounts of U. U is also observed on occasion in the clays and iron-silicates from the N3 tests; Th is generally detected only in an alteration phase such as brockite (Fortner and Bates, 1996; Bates et al., 1992; Fortner et al., 1995) and not in the clay itself (see Table 2.2.2.2-8 and discussion).

2.2.2.3.1.2 Summary

Drip tests designed to replicate the synergistic interactions among waste glass, repository groundwater, water vapor, and sensitized 304L stainless steel in the proposed Yucca Mountain repository have been in progress for with actinide-doped glasses more than 10 yr. The N2 test series on defense waste-processing facility (DWPF) -type glass has clearly demonstrated the importance of alteration phases in controlling actinide release from the corroding waste glass. These alteration phases may be spalled from the glass surface, releasing the actinides as solution-borne colloids and particulates. Unusual actinide-containing phases, several of which have been identified, formed on waste glass from the West Valley Demonstration Project (WVDP) in the N3 tests. As with the N2 tests, actinides in the N3 tests were initially retained in the alteration phases; they were later released by layer spallation as glass corrosion progressed. This alteration/spallation process effectively results in near-congruent release of elements from the glass, irrespective of their solubilities.

2.2.2.3.1.3 Ongoing Work

The N2 and N3 tests will continue, and updates of data and interpretations will be made in reports and publications in refereed journals. Detailed analysis of the sequentially filtered solution data and AEM examination of colloids will be performed. Because it appears from recent data that the spallation rate is increasing for actinide-bearing phases from the waste package test assembly, the role of colloidal particles in controlling release rates is expected to become correspondingly more important. An example of data now available but previously unpublished include Tc release, which is available for sample periods since 1993. Total mass-release rates for Tc from the N2 and N3 tests appear in Table 2.2.2.3-1.

Table 2.2.2.3-1   Release rates over the latest
                    2.5-yr period for Tc from the
                    N2 and N3 tests series
                    [LL980710551022.012]

Test Series	Tc Release Rate (ng year^{-1})
N2-9	2.9
N2-10	25
N2-12	15
N3-9	15
N3-10	3.3
N3-12	16

2.2.2.3.2 References

Bates, J. K., J. P. Bradley, A. Teetsov, C. R. Bradley, and M. Buchholtz ten-Brink (1992). "Colloid formation during waste from reaction: Implications for nuclear waster-disposal." *Science* **256**(5057):649–651. [MOL.19980326.0392]

Fortner, J. A., and J. K. Bates (1996). "Long-Term Results from Unsaturated Durability Testing of Actinide-Doped DWPF and WVDP Waste Glasses." In proceedings from *Mat. Res. Soc.* **412**:205–211. [MOL.19960418.0084]

Fortner J. A., T. J. Gerding, and J. K. Bates (1995). "Long-Term Test Results from a West Valley Actinide-Doped Reference Glass," in "Environmental Issues and Waste Management Technologies in the Ceramic and Nuclear Industries." V. Jain and R. Palmer (Eds.).*Ceramic Trans.* **61:** 455–462.

2.3 Special Cases Waste Forms

Waste Forms that may require special handling or may require special processing or containerizing.

2.3.1 Damaged Spent Fuel

Table 2.3.1-1   Typical fuel assembly parameters* (Table J-11.1 from Partial List of Fuel Assemblies considered for Rod Consolidation from RFP No. DE-RP07-86ID12618.)

VENDOR	GE 8x8 R	GE 8x8	GE 7x7	ENC 8x8	ENC 15x15	W 17x17	W 15x15	W 14x14	C-E 16x16	C-E 14x14	B&W 17x17	B&W 15x15
Fuel Rod Array	8x8 R	8x8	7x7	8x8	15x15	17x17	15x15	14x14	16x16	14x14	17x17	15x15
Reactor Type	BWR	BWR	BWR	BWR	PWR	PWR	PWR	PWR	PWR	PWR	PWR	PWR
Assemblies per Core	560	560	764	560	193	193	193	121	177	217	205	177
Fuel Rod Locations Per Assembly	64	64	49	64	225	289	225	196	256	196	289	225
Fuel Rods Per Assembly	62	63	49	60	204	264	204	179	236	176	264	208
Empty Locations Per Assembly	2	1	NONE	4	21	25	21	17	5	5	25	17
Rod Pitch, mm (in.)	16.3 (0.640)	16.3 (0.640)	18.7 (0.738)	16.3 (0.642)	14.3 (0.563)	12.6 (0.496)	14.3 (0.563)	14.1 (0.556)	12.9 (0.5063)	14.7 (0.580)	12.7 (0.501)	14.4 (0.568)
System Pressure, MPa (psia)	7.14 (1035)	7.14 (1035)	7.14 (1035)	7.14 (1035)	15.5 (2250)	15.5 (2250)	15.5 (2250)	15.5 (2250)	15.5 (2250)	15.5 (2250)	15.5 (2250)	15.2 (2200)
Core Average Power Density, kW/liter	49.15	50.51	50.732	40.57	98.1	104.7	98.1	95.6	96.4	78.5	107.3	91.4
Average LHGR, kW/M (kW/ft)	17.7 (5.38)	17.9 (5.45)	23.1 (7.049)	15.2 (4.63)	22.0 (6.70)	17.8 (5.44)	22.0 (6.70)	20.3 (6.20)	17.5 (5.34)	20.0 (6.09)	18.8 (5.73)	20.3 (6.20)
Axial Peak LHGR, in an Average Rod, W/M (kW/ft)	21.24 (6.99)	21.48 (7.09)	27.72 (9.16)	18.24 (6.02)	26.40 (8.04)	21.36 (6.53)	26.40 (8.04)	24.36 (7.44)	21.00 (6.41)	24.00 (7.31)	22.57 (6.88)	24.41 (7.44)
Max. Peak LHGR, kW/M (kW/ft)	44.0 (13.4)	44.0 (13.4)	60.2 (18.35)	47.6 (14.5)	51.9 (15.83)	44.6 (13.6)	61.7 (18.8)	56.8 (17.3)	42.7 (13.0)	53.5 (16.3)	49.9 (15.20)	53.0 (16.16)
Max. Fuel Temp., °C (°F)	1890 (3435)	1830 (3325)	2440 (4430)	2040 (3700)	2200 (3997)	1870 (3400)	2340 (4250)	2260 (4100)	1880 (3420)	2140 (3890)	2090 (4155)	2340 (4245)
Core Average Enrichment, wt% 235U	1.99	1.80	2.19	2.65	3.02	2.60	2.80	2.90	2.36	2.35	2.67	3.00
Max. Local Exposure, MWd/MTU GJ/kgU	45,000 3888	40,000 3456	40,000 3456	35,000 3024	47,500 4104	50,000 4320	50,000 4320	50,000 4320	55,000 4752	50,000 4320	55,000 4752	55,000 4752
Cladding Material	Zry-2	Zry-2	Zry-2	Zry-2	Zry-4	Zry-4	Zry-4	Zry-4	Zry-4	Zry-4	Zry-4	Zry-4

Table 2.3.1-1   (Continued)

VENDOR	B&W	B&W	C-E	C-E	W	W	W	ENC	ENC	GE	GE	GE
Fuel Rod Length, m (in.)	3.904 (153.688)	3.864 (152.125)	3.71 (145.9)	4.09 (161.02)	3.87 (152.36)	3.80 (149.7)	3.85 (151.6)	3.86 (152.0)	3.99 (156.92)	4.09 (161.1)	4.09 (161.1)	4.20 (185.4)
Active Fuel Height, m (in.)	3.602 (141.8)	3.632 (143)	3.47 (136.7)	3.81 (150)	3.66 (144)	3.66 (144)	3.65 (143.7)	3.66 (144)	3.66 (144)	3.66 (144)	3.71 (146)	3.81 (150)
Plenum Length, m (in.)	0.298 (11.27)	0.242 (9.52)	0.22 (8.5)	0.25 (10.00)	0.18 (6.99)	0.21 (8.2)	0.16 (6.3)	0.17 (6.8)	0.27 (10.63)	0.41 (16.0)	0.36 (14.0)	0.25 (10.0)
Fuel Rod OD, mm (in.)	10.922 (0.430)	9.627 (0.379)	11.18 (0.440)	9.70 (0.382)	10.72 (0.422)	10.72 (0.422)	9.50 (0.374)	10.77 (0.424)	12.74 (0.5015)	14.30 (0.563)	12.52 (0.493)	12.27 (0.483)
Cladding ID, mm (in.)	9.576 (0.377)	8.407 (0.331)	9.86 (0.388)	8.43 (0.332)	9.48 (0.3734)	9.48 (0.3734)	8.36 (0.329)	9.25 (0.364)	10.91 (0.4295)	12.68 (0.499)	10.80 (0.425)	10.64 (0.419)
Cladding Thickness, mm (in.)	0.673 (0.0265)	0.610 (0.0240)	0.660 (0.026)	0.635 (0.025)	0.617 (0.0243)	0.617 (0.0243)	0.572 (0.0225)	0.762 (0.030)	0.914 (0.036)	0.813 (0.032)	0.864 (0.034)	0.813 (0.032)
Diametral Gap, micron (mil)	213.4 (8.4)	198.1 (7.8)	216 (8.5)	178 (7.0)	190 (7.5)	190 (7.5)	165 (6.5)	190 (7.5)	254 (10.0)	305 (12.0)	229 (9.0)	229 (9.0)
Fuel Pellet Diameter, mm (in.)	9.362 (0.3686)	8.209 (0.3232)	9.64 (0.3795)	8.26 (0.325)	9.29 (0.3659)	9.29 (0.3659)	8.19 (0.3225)	9.06 (0.3565)	10.66 (0.4195)	12.37 (0.487)	10.57 (0.416)	10.41 (0.410)
Fuel Pellet Length, mm (in.)	15.240 (0.600)	9.525 (0.375)	16.51 (0.650)	9.91 (0.390)	15.24 (0.600)	15.24 (0.600)	13.46 (0.530)	6.93 (0.273)	8.13 (0.320)	12.70 (0.500)	10.67 (0.420)	10.41 (0.410)
Fuel Pellet Density, %TD	95	95	94.75	95	94	95	95	94	95	95	95	95

Table 2.3.1-2   Historical quantities of spent fuel by Assembly Class (reproduced from the LWR Quantities Data Base) (Table 3.1 from K.J. Notz, T.D. Welch, R.S. Moore, and W.J. Reich, *Preliminary Waste Form Characteristics,* ORNL-TM-11681 [draft] September, 1990)

LWR QUANTITIES DATABASE
Historical Data
Discharged Assemblies by Assembly Class

ASSEMBLY CLASS	FUEL ASSEMBLIES	FUEL RODS	DEFECTIVE ASSEMBLIES	AVERAGE BURNUP (MWd/MT)	TOTAL WEIGHT (MT)	AVERAGE INITIAL ENRICH.
B&W 15 X 15	3,564	740K	67	28,004	1654.8	2.815
CE 14 X 14	3,329	551K	6	29591	1271.5	2.865
CE 16 X 16	1,231	238K	23	24884	512.5	2.554
CE 16 X 16 SYSTEM 80	188	41K	0	17699	78.8	2.137
GE BWR/2,3	14,809	827K	1478	21493	2762.1	2.384
GE BWR/4-6	20,470	1,194K	949	21233	3795.0	2.307
WE 14 X 14	2,949	520K	80	32309	1146.1	3.150
WE 15 X 15	5,557	1,133K	132	30127	2507.2	2.926
WE 17 X 17	5,873	1,552K	100	27835	2670.1	2.833
Big Rock Point	315	29K	52	19339	41.6	3.490
Dresden-1	891	32K	159	16227	90.8	2.166
Ft. Calhoun	426	73K	0	30549	154.0	2.912
Haddam Neck	734	150K	43	31320	303.2	3.819
Humboldt Bay	390	15K	1	14936	28.9	2.351
Indian Point	160	28K	0	16715	30.6	4.111
Lacrosse	333	33K	104	14708	38.0	3.727
Palisades	597	126K	21	22720	239.3	2.640
St. Lucie-2	236	84K	0	23626	88.9	2.347
San Onofre-1	468	53K	7	29029	171.4	3.792
Yankee Rowe	417	102K	0	28285	100.6	3.949
— GRAND TOTALS	62,749	7,521K	3222	25950	17606.6	2.718

Table 2.3.1-3 Defective BWR fuels by assembly class and fuel design.[1] (Table 5.5 from K.J. Notz, T.D. Welch, R.S. Moore, and W.J. Reich, *Preliminary Waste Form Characteristics,* ORNL-TM-11681 [draft] September, 1990)

Fuel Design	GE BWR/2,3 (9 reactors)			GE BWR/4,5,6 (28 reactors)		
	Discharged Assemblies	Defective Assemblies	Percent Defective	Discharged Assemblies	Defective Assemblies	Percent Defective
GE Model 2 7 X 7 Fuel	6719	1469	21.90	1142	385	33.70
GE Model 3 Improved 7 X 7 Fuel	394	7	1.78	4936	130	2.63
GE Model 4 Original 8 X 8 Fuel	3876	1	0.03	3571	185	5.18
GE Model 5 8 X 8 Retrofit Fuel	792	1	0.13	3455	104	3.01
GE Prepressurized Fuel	1836	0	0.00	6591	144	2.18
GE Barrier Fuel	248	0	0.00	775	1	0.13
ANF 7 X 7 Fuel	260	0	0.00	None Used	Not Applicable	Not Applicable
ANF 8 X 8 Fuel	684	0	0.00	Not Yet Discharged	Not Applicable	Not Applicable

1. R. S. Moore, K. J. Notz, and C. G. Lawson, Classification of LWR Defective Fuel Data, Oak Ridge National Laboratory, June 1990, paper to be given at Spectrum '90 and published in the proceedings of September 1990.

Table 2.3.1-4 Defective Westinghouse PWR fuels by assembly class and fuel design.[1] (Table 5.6 from K.J. Notz, T.D. Welch, R.S. Moore, and W.J. Reich, *Preliminary Waste Form Characteristics,* ORNL-TM-11681 [draft] September, 1990)

Fuel Design	WE 14 X 14 (6 reactors)			WE 15 X 15 (10 reactors)			WE 17 X 17 (33 reactors)		
	Discharged Assemblies	Defective Assemblies	Percent Defective	Discharged Assemblies	Defective Assemblies	Percent Defective	Discharged Assemblies	Defective Assemblies	Percent Defective
WE Standard	592	1	0.2	1457	103	7.1	None Used	Not Applicable	Not Applicable
WE LOPAR	1409	77	5.5	3087	16	0.5	5102	99	1.9
WE OFA	88	1	1.1	266	1	0.4	628	1	0.2
WE VANTAGE 5	Not Yet Discharged	Not Applicable	Not Applicable	Not Yet Discharged	Not Applicable	Not Applicable	4	0	0.0
ANF for WE	559	0	0.0	743	12	1.6	139	0	0.0
ANF TOPROD	299	1	0.3	None Used	Not Applicable	Not Applicable	None Used	Not Applicable	Not Applicable

1 R. S. Moore, K. J. Notz, and C. G. Lawson, Classification of LWR Defective Fuel Data, Oak Ridge National Laboratory, June 1990, paper to be given at Spectrum '90 and published in the proceedings of September 1990.

Figure 2.3.1-1   **Fuel rod failures in PWR plants.**[13] **(Figure 9a from R.E. Woodley,** *The Characteristics of Spent LWR Fuel Relevant to its Storage in Geologic Repositories,* **HEDL-TME 83-28, October, 1983)**
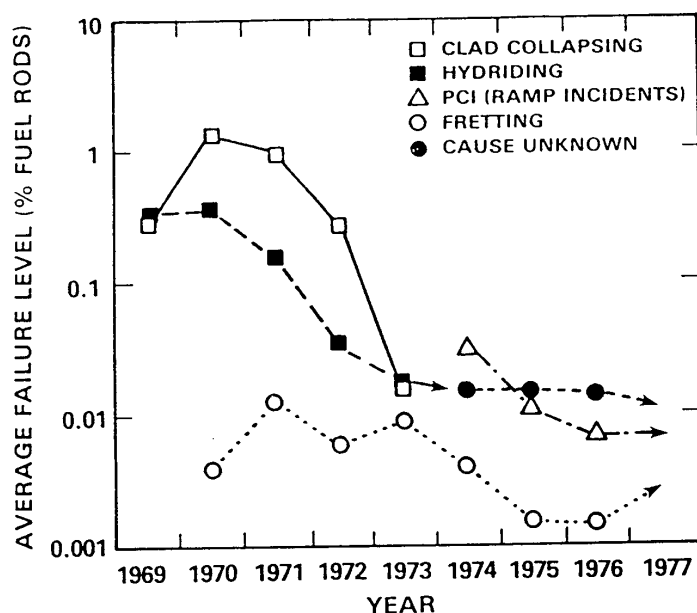

Figure 2.3.1-2   **Fuel rod failures in BWR plants.**[13] **(Figure 9b from R.E. Woodley,** *The Characteristics of Spent LWR Fuel Relevant to its Storage in Geologic Repositories,* **HEDL-TME 83-28, October, 1983)**
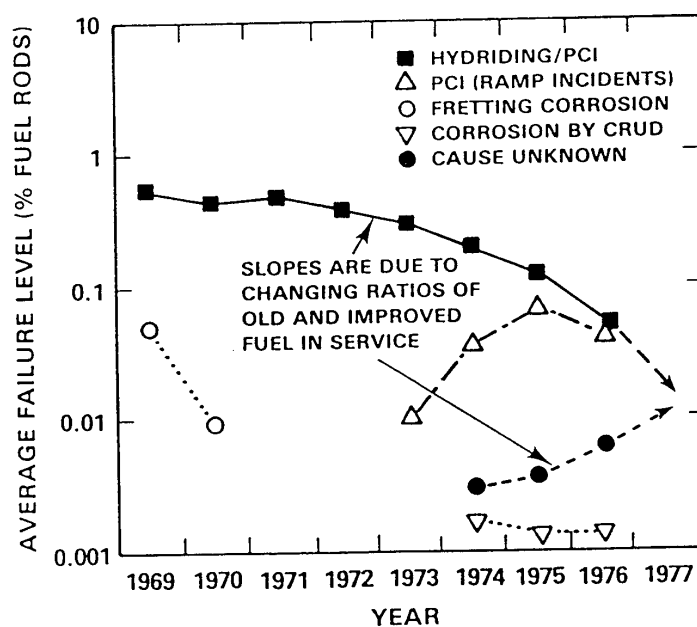
2.3.2 Non-LWR Spent Fuel

Table 2.3.2-1   Number of research and test reactors in each fuel type category (Table 7-1 from K.J. Notz, T.D. Welch, R.S. Moore, and W.J. Reich, *Preliminary Waste Form Characteristics,* ORNL-TM-11681 [draft] September, 1990)

Fuel type	University/ educational	Private research and test	Government- owned (DOE)	Government- owned (non-DOE)
MTR-plate type, U-Al alloy, high enrichment	15	2	14	1
TRIGA (U-Zr hydride fuel)	16	4	2	3
UO_2-polyethylene disks or blocks	4	0	0	0
PULSTAR and other low-enriched pin type	3	2	0	0
Liquid fuels (aqueous solutions)	0	0	1	0
U-Mo alloy, high-enriched (93.2%)	0	0	4	2
FFTF (UO_2- PuO_2)	0	0	1	0
Miscellaneous	0	0	26	0
Totals	38	6	48	6

Table 2.3.2-2   Summary of non-LWR spent fuels (Table 7-2 from K.J. Notz, T.D. Welch, R.S. Moore, and W.J. Reich, *Preliminary Waste Form Characteristics, ORNL-TM-11681 [draft] September, 1990)*

	Estimated quantities		
Reactor or site	End of 1989	Annual rate	End of 2020
HTGR Reactors			
Fort St. Vrain (elements)	732	0[a]	2214[b]
Peach Bottom I			
Core I (elements)	819	0	819
Core II (elements)	820	0	820
Research and Test Reactors[c]			
MTR Plate	--	-	20,000[d]
TRIGA	--	-	4,500
UO$_2$/Polyethylene	--	-	87
PULSTAR	--	-	170
FFTF (assemblies)	170	30-45	677[e]
Miscellaneous (kg HM)[g]			
ANL West	311		
Babcock & Wilcox	88		
Battelle-PNL	2,348		
HEDL	263[h]		
INEL	39,508[i]		
LANL	38		
ORNL	1,254		
SRS	19,110		

[a]Reactor was shut down in 1989. No further refueling is expected.

[b]Includes final discharge of full core.

[c]Total through 2020, including fuels in reactors at that time. Quantities shown are numbers of individual fuel elements, except for the FFTF.

[d]This is expected to be reprocessed and disposed of as defense HLW.

[e]Through year 2003; does not include final core discharge.

[g]Reported as kg of heavy metal (U plus Pu plus Th). Data are from Integrated Data Base for 1990.

[h]Includes some FFTF and TRIGA fuels.

[i]Not including Shippingport LWBR fuel (982 kg U, mostly U-233, and 56,167 kg Th), 17 Turkey Point 3 assemblies and 69 VEPCO assemblies being used for dry consolidation testing, HTGR fuel, Pulstar and TRIGA fuel, and TMI-2 spent fuel and core debris.

Table 2.3.2-3   Estimated number of canisters required for repository
                 disposal of various non-LWR and special LWR spent fuels[a]
                 (Table 7-5 from K.J. Notz, T.D. Welch, R.S. Moore, and
                 W.J. Reich, *Preliminary Waste Form Characteristics,*
                 ORNL-TM-11681 [draft] September, 1990)

| | Number of fuel assemblies | | Estimated fuel assemblies per canister | Estimated number of canisters required |
	In storage, 1988	Total as of year 2020[b]		
24-in. diam x 12 ft canisters				
Fort St. Vrain	732	2214	4	554
Peach Bottom-1	1639	1639	12	138
TRIGA	800	4500	112	40
PULSTAR	24	170	48	4
CEUSP material	401[c]	401[c]	24	17
Fermi-1 blanket	510	510	12	43
Elk River	188	188	12	16
EBWR	300	300	24	13
Canned fuel at B&W	58[d]	58[d]	24	3
Saxton	14[e]	14[e]		4
Other	-	-	-	60[f]
Total	4,666	9,994		892
28-in. diam x 15 ft canisters				
VEPCO	69	69	48[g]	15
Turkey Point	20	20	4	5
Dresden 1	20	20	8	3
Shippingport LWBR	65	65	1	65
TMI-2 (estimated)	-	-		350
Other	-	-	-	40[f]
Total	174	174		478
Total number of canisters				1,370

[a]Only the major non-LWR and special LWR fuels are listed. An allowance is included for minor fuels not specifically listed.

[b]Reloads and in-core fuel are included in totals.

[c]CEUSP material is stored in 3.5-in. diameter x 24 in. cans; numbers shown are numbers of cans.

[d]There are 58 cans of LWR fuel at B&W, Lynchburg. Cans are 4.25-in. diameter x 33 in. long.

[e]Quantities shown are numbers of cans.

[f]An allowance is included here for fuels not specifically listed.

[g]Some of these assemblies have been compacted.

Table 2.3.2-4   Radioactivity and decay heat of Fort St. Vrain spent fuel per MTIHM (Table 7-6 from K.J. Notz, T.D. Welch, R.S. Moore, and W.J. Reich, *Preliminary Waste Form Characteristics,* ORNL-TM-11681 [draft] September, 1990)

Time after discharge, years	Radioactivity (Ci/MTIHM)	Decay heat (W/MTIHM)
1	3.36E06	1.0E04
10	9.82E05	2.5E03
100	1.17E05	4.0E02
1,000	4.42E02	1.5E01
10,000	1.22E03	3.0E01
100,000	1.40E03	3.0E01
1,000,000	6.17E01	2.0E00

Table 2.3.2-5   Estimated radioactivity and decay heat per canister of Fort St. Vrain fuel (Table 7-7 from K.J. Notz, T.D. Welch, R.S. Moore, and W.J. Reich, *Preliminary Waste Form Characteristics,* ORNL-TM-11681 [draft] September, 1990)

Time after discharge, years	Radioactivity (Ci/canister)	Decay heat W/canister
1	75,600	225
10	22,000	56
100	2,600	9
1,000	10	0.3
10,000	27	0.7
100,000	32	0.7
1,000,000	1.4	0.05

Table 2.3.2-6   Estimated radioactivity and decay heat per canister of
FLIP TRIGA fuel (Table 7-8 from K.J. Notz, T.D. Welch,
R.S. Moore, and W.J. Reich, *Preliminary Waste Form
Characteristics,* ORNL-TM-11681 [draft] September, 1990)

Time after discharge (years)	Radioactivity (Ci/canister)	Decay heat (W/canister)
1	9.0E04	380
5	2.0E04	100
10	1.5E04	80
100	1.6E03	40
1,000	68	2
10,000	9	0.5
100,000	1	0.04
1,000,000	0.16	0.02

Table 2.3.2-7   Estimated radioactivity and decay heat per canister of
PULSTAR fuel (Table 7-9 from K.J. Notz, T.D. Welch,
R.S. Moore, and W.J. Reich, *Preliminary Waste Form
Characteristics,* ORNL-TM-11681 [draft] September, 1990)

Time after discharge (years)	Radioactivity (Ci/canister)	Decay heat (W/canister)
1	1.7E05	750
10	3.0E04	82
100	3.0E03	21
1,000	140	4
10,000	35	1
100,000	4	0.08
1,000,000	0.4	0.04

**Table 2.3.2-8   Projected volumes of miscellaneous wastes[a] (Table 7-10
from K.J. Notz, T.D. Welch, R.S. Moore, and W.J. Reich,
Preliminary Waste Form Characteristics, ORNL-TM-11681
[draft] September, 1990)**

	Estimated total in 2020 (m³)	Est. annual rate in 2020 (m³)
OCRWM-generated TRU waste	600[b]	60-260[c]
Commercial TRU waste West Valley decommissioning	300	0
Other decommissioning	680	TBD
Abnormal reactor operations	70[d]	10-30
Industrial/institutional	TBD	10-40
Reactor decommissioning	15060[e]	46[f]
Radioisotope capsules	500[g]	0
Routine reactor operations[h]	8,000	15[b]
Totals	11,710	282-532

[a]Data are given in m³. One 2-ft by 12-ft canister holds about 1 m³. "TBD" means to be determined.

[b]Depends on startup date for these facilities; 2010 was assumed.

[c]From dry rod consolidation. The upper limit is a conservative (high) estimate of HEPA filter usage.

[d]Quantity estimated based on two abnormal reactor operations (at Oyster Creek and TMI-2).

[e]Assumes 65 have been decommissioned.

[f]Assumes 2 per year.

[g]Assumes that 90% of existing capsules are packages in canisters by 1995; later packaging would result in fewer canisters because of the decreased thermal output per capsule.

[h]Based on estimated quantity of 3 m³ per GW(e)-yr being GTCC, and an EIA projection of 52 GW(e) installed capacity in 2020 (no new orders case).

Table 2.3.2-9   Volumes and activities of decommissioned LWR activated metals[a]
(Table 7-11 from K.J. Notz, T.D. Welch, R.S. Moore, and W.J. Reich,
Preliminary Waste Form Characteristics, ORNL-TM-11681 [draft]
September, 1990)

Component	Constr.[b] Material	Disposal Volume[c] (m^3)	Activity (Ci)	Disposal Concentration (Ci/m^3)
Reference BWR:				
Steam separator assembly	S	10	9,600	960
Fuel support pieces	S	5	700	140
Control rods and in-core				
instruments	S	15	189,000	12,600
Control rod guide tubes	S	4	100	25
Jet pump assemblies	S	14	20,000	1,429
Top fuel guide	S	24	30,000	1,254
Core support plate	S	11	650	59
Core shroud	S	47	6,300,000	134,043
Reactor vessel wall	C	8	2,160	270
Total		138	6,552,310	
Reference PWR:				
Pressure vessel				
cylindrical wall	C	108	19,170	178
Vessel head	C	57	<10	0.18
Vessel bottom	C	57	<10	0.18
Upper core				
support assembly	S	11	<10	0.91
Upper support columns	S	11	<100	9.1
Upper core barrel	S	6	<1,000	167
Upper core grid plate	S	14	24,310	1,736
Guide tubes	S	17	<100	6
Lower core barrel	S	91	651,000	7,154
Thermal shields	S	17	146,000	8,594
Core shroud	S	11	3,431,100	311,909
Lower grid plate	S	14	553,400	39,529
Lower support columns	S	3	10,000	333
Lower core forging	S	31	2,500	81
Miscellaneous internals	S	23	2,000	87
Reactor cavity liner	S	14	<10	0.7
Total		485	4,840,820	

a   *Source*: Oztunali 1986.

b   Construction material symbols: S – stainless steel, C – carbon steel.

c   Disposal volumes include the disposal container after the activated metal
components have been cut into manageable pieces.

Table 2.3.2-10   Radioactivity and thermal power of canisters within strontium
and cesium capsules[a] (Table 7-12 from K.J. Notz, T.D. Welch,
R.S. Moore, and W.J. Reich, *Preliminary Waste Form Characteristics,*
ORNL-TM-11681 [draft] September, 1990)

Decay time (years)	Strontium canister (4 capsules)		Cesium canister (4 capsules)	
	Curies	Watts	Curies	Watts
0	412,400	1,380	371,000	918
5	366,300	1,230	330,000	817
10	325,200	1,090	294,000	727
20	256,300	860	233,000	577
50	125,500	420	117,000	290
100	38,200	128	36,800	91
200	3,530	12	3,650	9
300	327	1.1	360	0.9
1,000	1.9E-05	6.4E-08	3.4E-05	8.4E-08

[a]Based on ORIGEN2 calculations. Radioactivity and thermal power
include the contributions of the daughter isotopes Y-90 and Ba-137M.
Starting point for decay time is December 1985. The assumed thermal
limits at a decay time of 10 years are 1,170 W/canister for Sr capsules
and 800 W/canister for Cs capsules (Coony 1987).

Table 2.3.2-11   Average properties of LWR spent fuel (Table 8-1 from K.J.
Notz, T.D. Welch, R.S. Moore, and W.J. Reich, *Preliminary
Waste Form Characteristics,* ORNL-TM-11681 [draft]
September, 1990)

BWR Spent Fuel Average Properties:	Historical	Projected	Total
Burnup (GWd/MTU)	21	33	30
Enrichment (%)	2.3	3.2	3.0
Discharged (year)	1981	2007	2001
Thermal Power (W/MT)			
in 2010 (over 5 years old)	–	--	
in 2020 (over 5 years old)	–	--	
in 2050 (all fuel)	–	--	

PWR Spent Fuel Average Properties:	Historical	Projected	Total
Burnup (GWd/MTU)	29	42	39
Enrichment (%)	2.9	3.9	3.7
Discharged (year)	1982	2007	2002
Thermal Power (W/MT)			
in 2010 (over 5 years old)	--	–	
in 2020 (over 5 years old)	--	--	
in 2050 (all fuel)	--	--	

Table 2.3.2-12   No title (from R.E. Woodley, *The Characteristics of Spent
LWR Fuel Relevant to its Storage in Geologic Repositories.*
HEDL-TME 83-28, Oct. 1983)

Major Contributors	Est. Canisters
HTGRs	
Fort St. Vrain	554
Peach Bottom-1	138
Degraded LWR Fuel	
TMI-2	350
Other Contributors	
Shippingport LWBR	65
Fermi-1 Blanket	43
TRIGA	40
All Others	245